



## City Research Online

### City, University of London Institutional Repository

---

**Citation:** Cook, A. H. (1995). The joining of new to old dental amalgam. (Unpublished Doctoral thesis, City, University of London)

This is the accepted version of the paper.

This version of the publication may differ from the final published version.

---

**Permanent repository link:** <https://openaccess.city.ac.uk/id/eprint/29384/>

**Link to published version:**

**Copyright:** City Research Online aims to make research outputs of City, University of London available to a wider audience. Copyright and Moral Rights remain with the author(s) and/or copyright holders. URLs from City Research Online may be freely distributed and linked to.

**Reuse:** Copies of full items can be used for personal research or study, educational, or not-for-profit purposes without prior permission or charge. Provided that the authors, title and full bibliographic details are credited, a hyperlink and/or URL is given for the original metadata page and the content is not changed in any way.

**THE JOINING OF NEW TO OLD DENTAL AMALGAM**

by

**ALLAN HAMILTON COOK**

BDS (U. Lond.), LDS RCS (Eng.)

A dissertation submitted to  
City University  
as part of the requirement  
for the degree of  
Doctor of Philosophy

June 1995

Department of Mechanical Engineering & Aeronautics  
City University  
London EC1V 0HB

## Contents

Contents . . . . .	2
List of Tables . . . . .	6
List of Figures . . . . .	8
List of Plates . . . . .	9
Acknowledgements . . . . .	12
Declaration . . . . .	13
Abstract . . . . .	14
List of abbreviations . . . . .	15
Dedication . . . . .	16
Chapter 1. Introduction . . . . .	17
Chapter 2. Dental amalgam . . . . .	21
2.1 Definition . . . . .	21
2.2 Manufacture of dental amalgam alloy . . . . .	21
2.3 Use of dental amalgam . . . . .	22
2.4 Standard specifications for amalgam alloys . . . . .	24
2.5 Setting reactions of dental amalgam . . . . .	28
2.5.1 Conventional amalgams . . . . .	29
2.5.2 High copper admixed amalgams . . . . .	29
2.5.3 High copper single composition amalgams . . . . .	30
2.5.4 Longer term changes . . . . .	31
Chapter 3. Review of the literature on the amalgam to amalgam bond . . . . .	32
3.1 Work reporting strong joints . . . . .	33
3.2 Age of repaired parent amalgam . . . . .	36
3.3 Mercury treatments . . . . .	38
3.4 Amalgam alloy type . . . . .	40
3.5 Location of fracture in joined samples . . . . .	41
3.6 Structure of the joint . . . . .	41
3.7 Clinical repair of dental amalgam . . . . .	43
3.8 Corrosion . . . . .	45
3.9 Unusual preparation or test procedures . . . . .	47
Chapter 4. Experimental Equipment and Method . . . . .	49
4.1 Amalgamators . . . . .	49
4.1.1 The Dentomat 2 amalgamator . . . . .	49
4.1.2 The Silamat amalgamator . . . . .	50
4.2 The test specimens . . . . .	51
4.2.1 The moulds for test specimens . . . . .	52
4.2.1.1 The British Standard mould . . . . .	52
4.2.1.2 The split mould . . . . .	52
4.2.1.2.1 Plugs . . . . .	55
4.3 The equipment for condensation . . . . .	55
4.3.1 Weights . . . . .	56
4.3.2 Vibration . . . . .	58
4.3.3 Pistons . . . . .	61
4.3.3.1 Lower piston . . . . .	61
4.3.3.2 Upper pistons for use with the weights . . . . .	61
4.3.3.2.1 B.S. piston . . . . .	61
4.3.3.2.2 Bevelled piston . . . . .	61

4.3.3.3	Pistons used for vibrational condensation of amalgam	62
4.3.3.3.1	Flat ended pistons	63
4.3.3.3.2	Shaped ended pistons	63
4.3.3.4	Pistons used for condensation of amalgam at the joint	64
4.3.3.4.1	RI piston	64
4.3.3.4.2	SRI piston	64
4.3.3.4.3	Paddle piston	64
4.4	Procedures for the Preparation of Test Samples	68
4.4.0.1	The quantity of mix used	68
4.4.1	Condensation procedure: deadweight method	69
4.4.2	Condensation procedure: vibration assisted methods	70
4.4.2.1	Manipulation and division of amalgam mix	70
4.4.2.2	Condensation of one-piece specimens using vibration	70
4.4.2.3	Condensation when using "cut-cone" or "dome" pistons	71
4.4.3	Manufacture of two-piece specimens	72
4.4.3.1	Marking of the joint interface	72
4.4.3.2	End preparation of parent amalgam for joining	72
4.4.3.3	Measurement for location in 3 point bend	73
4.4.3.4	Placement of parent amalgam samples in mould for joining	77
4.4.3.5	Condensation of the addition part of joined amalgam	77
4.4.3.6	Adjustment of the depth of the "paddle"	78
4.4.4	Notes on specimen preparation	78
4.4.4.1	Temperature of preparation, storage and test	78
4.4.4.2	Timing	79
4.4.4.3	Storage of specimens prior to test	79
4.4.4.4	Photography after fracture	79
4.4.4.5	Long term storage of specimens	79
4.4.4.6	Mercury hygiene	80
4.5	Testing procedures	80
4.5.1	The compression testing machines	80
4.5.2	The 3-point bend testing apparatus	80
4.5.3	Location of samples in the 3 point loading apparatus	81
4.5.4	The test to fracture	82
4.5.5	Notched samples	85
4.5.5.1	The notching procedure	85
4.5.5.2	The location of the notch	85
4.6	Metallography	87
4.6.1	Preparation of Samples for Microstructure Examination	87
4.6.1.1	Mounting Materials	87
4.6.1.2	Pre-mounting procedure	88
4.6.1.2.1	Intact samples	88
4.6.1.2.2	Fractured samples	88
4.6.1.3	Mounting	88
4.6.1.4	Grinding	88
4.6.1.5	Polishing	88
4.6.1.5.1	First polish	88
4.6.1.5.2	Second polish	89
4.6.1.6	Etching	89
4.6.2	Optical microscopy	89
4.7	Statistical analysis of the results	90
4.7.1	Descriptive statistics	90
4.7.2	The tests for normality	91
4.7.3	The tests for differences between data sets	91
4.7.3.1	Student's t-test	92
4.7.3.2	Analysis of variance	92
4.7.3.3	Non-parametric tests	93
4.7.4	Graphical presentation of the results	93
4.7.4.1	Scatter plots	93
4.7.4.2	Cumulative frequency of force to fracture	93
4.7.5	Examination of the numbers failing in the parent, joint or addition	94

Chapter 5.	The materials used . . . . .	95
5.1	Mercury . . . . .	95
5.2	Amalgam Alloys . . . . .	95
5.2.1	Chemical composition of amalgam alloys used in this study . . . . .	96
5.2.2	Amalgam alloys supplied as loose powder . . . . .	97
5.2.3	Amalgam alloys supplied precapsulated with mercury . . . . .	97
Chapter 6.	Results and analysis . . . . .	104
6.1	Statistical analysis of results . . . . .	105
6.1.1	The tests for normality . . . . .	105
6.2	Preliminary work . . . . .	106
6.2.1	Use of a rectangular mould . . . . .	106
6.2.2	Use of a cylindrical steel mould . . . . .	107
6.3	Preliminary experiments using the split mould . . . . .	108
6.3.1	Condensation of joined samples by weights . . . . .	108
6.3.2	Condensation of joined samples by vibration . . . . .	109
6.3.3	Marking of the joint interface . . . . .	110
6.4	Preparation of joined samples: deadweighted parents . . . . .	111
6.4.1	Comparison of Batch 1 with one-piece Batches 2 and 3 . . . . .	114
6.4.2	Opening the mould after 30 minutes or 7 days . . . . .	114
6.4.3	Duralloy capsules and conventional Amalgam M . . . . .	118
6.4.4	One-piece Batches 8 and 9 . . . . .	122
6.4.5	Sample diameter . . . . .	122
6.4.6	Review of the initial experiments: Sets 1 (joined), 2 and 3 (one-piece) . . . . .	123
6.5	Preparation of joined samples: parents condensed by vibration . . . . .	130
6.5.1	Addition condensed using the flat ended piston for 2s: Set 4 . . . . .	131
6.5.2	Addition condensed using the RI piston for 2s: Set 5 . . . . .	132
6.5.3	Addition condensed using the RI piston for 10s: Batch 15 . . . . .	135
6.5.4	Opening the mould 5 minutes after completion of batch condensation . . . . .	135
6.5.4.1	Deadweighted addition: Batch 19 . . . . .	136
6.5.4.2	Addition condensed for 2s by RI piston: Batch 20 . . . . .	137
6.6	Preparation of joined samples: increased vibration time . . . . .	139
6.6.1	Addition condensed using the RI piston for 10s: Set 7 . . . . .	140
6.6.2	Addition condensed using the flat ended piston for 10s: Set 8 . . . . .	141
6.6.3	Addition condensed using the flat ended piston for 2s: Batch 23 . . . . .	141
6.6.4	"Gramophone groove" end preparation: Set 9 . . . . .	143
6.6.5	Use of the Spiral rubbing-in (SRI) piston: Batch 29 . . . . .	147
6.6.6	Increased duration of vibration for one-piece samples: Batch 27 . . . . .	148
6.7	Preparation and test of one-piece samples . . . . .	149
6.7.1	Testing immediately after removal from 37°C storage oven . . . . .	149
6.7.2	Use of a new flat ended condensing piston . . . . .	150
6.7.3	Use of three separate amalgam mixes . . . . .	152
6.7.3.1	Divided or undivided mix: new or old flat piston . . . . .	153
6.7.3.2	Duration of vibration using divided mixes . . . . .	156
6.7.4	Use of Duralloy high copper alloy . . . . .	157
6.7.4.1	Condensation using the cut cone piston . . . . .	157
6.7.4.2	Effect of delayed condensation . . . . .	159
6.8	Microstructure of joined and repaired amalgams . . . . .	160
6.8.1	Laboratory prepared joined sample A1.9 . . . . .	162
6.8.2	Retrieved clinical amalgam addition restoration . . . . .	162
6.9	Development of joined sample preparation procedures using the Paddle . . . . .	165
6.9.1	Preliminary work using Duralloy: Batches 53, 54 and 55 . . . . .	165
6.9.1.1	Flexural strength tests . . . . .	166
6.9.1.2	Microstructure . . . . .	169
6.9.2	Further work using Aristaloy 21 . . . . .	170
6.9.2.1	One-piece samples . . . . .	170
6.9.2.2	Extended application . . . . .	171
6.9.2.3	Number of turns . . . . .	174
6.9.2.4	Height setting . . . . .	174
6.9.2.5	Delayed condensation of the first increment . . . . .	175
6.9.2.6	Pooled results: Sets 11 and 22 . . . . .	176

6.9.2.7	Review of development	177
6.9.2.8	Mode of condensation and inversion of the parent	179
6.10	Preparation of joined samples: further work using Veraloy	180
6.10.1	Addition condensed using the RI piston, flat piston or weights	180
6.10.2	Delayed condensation of the first increment after paddle use	180
6.10.3	Mode of condensation and inversion of the parent	181
6.10.3.1	Deadweight: non-inverted Set 12; inverted Set 13	181
6.10.3.2	Dome piston: non-inverted Set 14; inverted Set 15	182
6.10.3.3	Pooled and subdivided results from Sets 12 to 15	187
6.10.4	One-piece samples	187
6.10.5	Further considerations: sample length and weight	188
6.10.5.1	One-piece samples	188
6.10.5.2	Joined samples	191
6.10.5.3	Homogeneity of samples from different lumens of the mould	192
6.10.5.3.1	Mean force to fracture	192
6.10.5.3.2	Parent sample length	193
6.10.5.3.3	Parent sample weight	193
6.10.5.3.4	Addition parts	193
6.11	Joined samples from amalgam alloys supplied in capsules	195
6.11.1	Force to fracture	196
6.11.2	Sample length and weight	205
6.12	Retest of Amalgam M	206
6.12.1	Joined samples: Batches 118 to 121	206
6.12.2	One-piece Batches 122 to 125	207
6.13	Re-assembled fractured samples	213
6.13.1	Re-examination of Duralloy joined samples	213
6.13.2	Notched parent: loaded addition	216
6.13.2.1	Veraloy and Aristaloy	220
6.13.2.2	Duralloy specimen M11	225
6.13.2.3	Dispersalloy specimen N10	229
6.13.2.4	Dispersalloy specimen M3	232
6.13.2.5	Tytin specimen N3	234
6.13.2.6	Amalcap SAS specimen M9	238
6.13.2.7	Amalcap specimens P4 and P2	244
6.13.3	Notched joint: loaded parent	249
6.13.3.1	Amalcap specimen P6	250
6.13.3.2	Tytin specimen P20	253
6.13.4	Other notched samples	253
6.13.4.1	Dispersalloy	256
6.13.4.2	Amalgam M	260
Chapter 7.	Discussion	263
7.1	Sample preparation and test	264
7.2	The nature of the joint	270
7.3	Conclusions and the relation of this work to dental practice	276
7.4	Further work	280
7.5	Originality of this work	282
7.6	The contribution to knowledge	284
7.7	Conclusions	286
References and Bibliography		287
Appendix 1.	Raw data for test results	296
Appendix 2.	Descriptive statistics of force to fracture for Batches	302
Appendix 3.	Descriptive statistics of force to fracture for Sets	304
Appendix 4.	Length and weight of samples (Batches 94 to 125)	305
Appendix 5.	Statistics for sample failure location	310
Appendix 6.	Published work	311
Appendix 7.	Published correspondence	317

## List of Tables

<b>Table 1.</b> Permitted limits of alloy composition to BS 2938: 1961. . . . .	24
<b>Table 2.</b> Permitted limits of alloy composition (by weight) to BS 2938: 1985. . . . .	26
<b>Table 3.</b> Permitted limits of alloy composition to BS EN 21559: 1992. . . . .	26
<b>Table 4.</b> Schedule for condensation of amalgam by the two thrust deadweight method. . . . .	69
<b>Table 5.</b> Schedule for vibrational condensation of one piece samples and the parent parts of samples to be joined. . . . .	71
<b>Table 6.</b> The Standard Paddle Procedure: schedule for vibrational condensation of the addition part of joined samples using the "paddle". . . . .	78
<b>Table 7.</b> The etchants used. . . . .	89
<b>Table 8.</b> The chemical composition (by weight) of the amalgam alloys used. . . . .	96
<b>Table 9.</b> Amalgam alloys supplied as loose powder. . . . .	97
<b>Table 10.</b> Amalgam alloys supplied precapsulated with mercury. . . . .	98
<b>Table 11.</b> Force to fracture statistics of Sets 1, 2 and 3 (Newtons). . . . .	125
<b>Table 12.</b> Confidence intervals for differences in mean force to fracture between Sets 1, 2 and 3 and results of two sample t-testing. . . . .	125
<b>Table 13.</b> Force to fracture statistics (Newtons) of Sets 2, 3 and Set 1 which was divided into groups where the fracture originated in the Parent or Joint. . . . .	126
<b>Table 14.</b> Confidence intervals for difference in mean force to fracture between Sets 2, 3, and Set 1 Parents and Joints and results of two sample t-testing. . . . .	126
<b>Table 15.</b> Force to fracture statistics for Sets 4, 5 and 6 (Newtons). . . . .	133
<b>Table 16.</b> Confidence interval for difference in mean force to fracture between Sets 4, 5 and 6 and results of two sample t-testing. . . . .	133
<b>Table 17.</b> Force to fracture statistics for Set 5 and Batch 20 (Newtons). . . . .	138
<b>Table 18.</b> Force to fracture statistics for Sets 6, 7 and 8 (Newtons). . . . .	142
<b>Table 19.</b> Confidence intervals for differences in mean force to fracture between Sets 6, 7 and 8 and results of two sample t-testing. . . . .	142
<b>Table 20.</b> Force to fracture statistics for Sets 1, 7 and 9 (Newtons). . . . .	145
<b>Table 21.</b> Confidence intervals for differences in mean force to fracture between Sets 1, 7 and 9 and results of two sample t-testing. . . . .	145
<b>Table 22.</b> Force to fracture statistics in Newtons for Batch 27 (one-piece) and Sets 7 and 9 which were pooled and divided into Parent and Joint subgroups according to location of fracture origin. . . . .	146
<b>Table 23.</b> Force to fracture statistics in Newtons of Batches 32 to 41. . . . .	153
<b>Table 24.</b> Preparation procedures and force to fracture results for Batches 62 to 87. Aristaloy 21. . . . .	172
<b>Table 25.</b> Force to fracture statistics in Newtons of Sets 11 and 22 (Aristaloy 21), which were pooled and subdivided according to the location of fracture origin (Parent, Joint or Addition). . . . .	178
<b>Table 26.</b> Confidence intervals for differences in mean force to fracture between the Parent, Joint and Addition subgroups of pooled Sets 11 and 22 (Aristaloy 21) and results of two sample t-testing. . . . .	178
<b>Table 27.</b> Preparation procedures and force to fracture results for Batches 88 to 108. Veraloy. . . . .	184
<b>Table 28.</b> Force to fracture statistics of Veraloy Sets 12 to 15 (Newtons). . . . .	185
<b>Table 29.</b> Confidence intervals for differences in mean force to fracture between Set 14 and Sets 12, 13 and 15 and results of two sample t-testing. . . . .	185
<b>Table 30.</b> Force to fracture statistics in Newtons of one-piece Sets 16 and 17 and Veraloy joined samples grouped according to location of fracture origin. . . . .	186
<b>Table 31.</b> Confidence intervals for differences in mean force to fracture and results of t-testing for the pooled results from Sets 12 to 15 (Veraloy), which were grouped according to the location of the fracture origin. . . . .	186
<b>Table 32.</b> Descriptive statistics of the lengths and weights of Veraloy one-piece samples: Set 16: DW condensation; Set 17: Vibrated condensation. . . . .	189
<b>Table 33.</b> Descriptive statistics of the lengths and weights of the parts of the Veraloy samples in Sets 12 and 13 (DW parents), Sets 14 and 15 (Dome vibrated parents) and the pooled data from all addition parts of Sets 12 to 15. . . . .	190
<b>Table 34.</b> Force to fracture statistics in Newtons of joined samples prepared from pre-capsulated amalgam alloys. . . . .	203

<b>Table 35.</b> Confidence intervals for differences in mean force to fracture and results of t-testing for Tytin and joined specimens prepared from different pre-capsulated alloys. . . . .	203
<b>Table 36.</b> Preparation procedures and force to fracture results for joined Batches 118 to 121 and one-piece Batches 122 to 125. Amalgam M. . . . .	208
<b>Table 37.</b> Force to fracture statistics for Sets 23, 24 and 25 (Newtons). . . . .	209
<b>Table 38.</b> Confidence intervals for differences in mean force to fracture between Sets 23, 24 and 25 and results of two sample t-testing. . . . .	209

## List of Figures

<b>Figure 1.</b> The dimensions in mm of the cylindrical test specimens. . . . .	51
<b>Figure 2.</b> British Standard mould for dental amalgam specimens. . . . .	53
<b>Figure 3.</b> The Split Mould. The dimensions are in mm. . . . .	53
<b>Figure 4.</b> The split mould, bevelled piston and BS spacer No 2. . . . .	62
<b>Figure 5.</b> Diagram of the paddle condensation piston with the split mould ready for condensation of the addition amalgam to the parent amalgam which is in place in the mould. The dimensions are in mm. . . . .	66
<b>Figure 6.</b> Diagram of the 3 point loading apparatus. . . . .	82
<b>Figure 7.</b> Diagram of the joined amalgam specimen in place in the 3 point bending apparatus. . . . .	83
<b>Figure 8.</b> The position of the notched specimens in the test apparatus. (a) notch to parent; (b) notch to addition. . . . .	86
<b>Figure 9.</b> Force to fracture for Batches 1 to 9. . . . .	112
<b>Figure 10.</b> Instron test machine moving paper pen chart. . . . .	113
<b>Figure 11.</b> Cumulative frequencies of force to fracture for Sets 1, 2 and 3. . . . .	125
<b>Figure 12.</b> Cumulative frequencies of force to fracture for Sets 1, 2 and 3 where Set 1 has been divided into subgroups according to the location of fracture origin. . . . .	126
<b>Figure 13.</b> Force to fracture for Batches 10 to 20. The parent parts were condensed using a flat piston under vibration for 2s on each of four portions. . . . .	131
<b>Figure 14.</b> Cumulative frequencies of force to fracture for Sets 4, 5 and 6. . . . .	133
<b>Figure 15.</b> Cumulative frequencies of force to fracture for Set 5 and Batch 20. The numbers below the data points for Batch 20 refer to the sample hole in the split mould used for specimen preparation. . . . .	138
<b>Figure 16.</b> Force to fracture for Batches 21 to 30. The four parent increments were condensed for 2,2,4,10s respectively. . . . .	140
<b>Figure 17.</b> Cumulative frequencies of force to fracture for Sets 6, 7 and 8. . . . .	142
<b>Figure 18.</b> Cumulative frequencies of force to fracture for Sets 1, 7 and 9. . . . .	145
<b>Figure 19.</b> Cumulative frequencies of force to fracture of Batch 27 (One-piece) and Sets 7 and 9 which were pooled and divided into Parent and Joint subgroups according to location of fracture origin. . . . .	146
<b>Figure 20.</b> Force to fracture for Batches 32 to 41. Amalgam M. . . . .	153
<b>Figure 21.</b> Force to fracture Batch 46 to 55. Duralloy. Batches 48 to 53 were condensed using the cut cone piston. . . . .	158
<b>Figure 22.</b> Force to fracture for Batches 62 to 87. Aristaloy 21. . . . .	173
<b>Figure 23.</b> Cumulative frequencies of force to fracture for Sets 11 and 22 which were pooled and subdivided according to location of fracture origin. . . . .	178
<b>Figure 24.</b> Force to fracture for Batch 88 to 108. Veraloy. . . . .	183
<b>Figure 25.</b> Cumulative frequencies of force to fracture for Sets 12, 13, 14 and 15 (Veraloy) where the preparation of the parent parts was varied. . . . .	185
<b>Figure 26.</b> Cumulative frequencies of force to fracture for Veraloy Sets 16 and 17 (one-piece) and joined samples in Sets 12 to 15 which were pooled and grouped according to the location of fracture origin. . . . .	186
<b>Figure 27.</b> Graph of length vs weight of Veraloy one-piece samples: Set 16: DW condensation; Set 17: Vibrated condensation. . . . .	189
<b>Figure 28.</b> Graph of length vs weight of parts of Veraloy samples: DW parents; Dome vibrated parents and all additions. . . . .	190
<b>Figure 29.</b> Force to fracture Batch 109 to 117. Pre-capsulated amalgams. . . . .	196
<b>Figure 30.</b> Cumulative frequencies of force to fracture for joined samples prepared from pre-capsulated amalgam alloys. . . . .	203
<b>Figure 31.</b> A to F. Graphs of weights and lengths of the parent parts and added to samples from encapsulated amalgams. . . . .	204
<b>Figure 32.</b> Force to fracture for Batches 118 to 125. Amalgam M. . . . .	208
<b>Figure 33.</b> Cumulative frequencies of force to fracture for Sets 23, 24 and 25. . . . .	209

## List of Plates

<b>Plate 1.</b> The Dentomat 2 and Silamat amalgamators with the dental amalgam alloys and precapsulated materials used in this study. . . . .	51
<b>Plate 2.</b> The British Standard mould, holder, pistons and spacers. . . . .	54
<b>Plate 3.</b> The split mould, pistons, support blocks and spacer. . . . .	54
<b>Plate 4.</b> The Desoutter weight bearing assembly. . . . .	56
<b>Plate 5.</b> Condensation of amalgam in the split mould (first thrust of the two thrust deadweight method). . . . .	57
<b>Plate 6.</b> Pressing a joined sample from the inverted split mould. . . . .	57
<b>Plate 7.</b> The Burgess vibration tool in place in the split mould. . . . .	59
<b>Plate 8.</b> The Burgess engraving tool fitted with a flat ended piston. A standard engraving point with the split retaining ring is inset. . . . .	60
<b>Plate 9.</b> The disassembled modified chuck of the Burgess engraving tool. . . . .	60
<b>Plate 10.</b> The pistons used for vibrational condensation of amalgam. From left to right: "brand new" flat; new flat; old flat; cut cone; dome. . . . .	63
<b>Plate 11.</b> End views of the pistons used for condensation of amalgam at the joint. From left to right: "brand new" RI; used RI; SRI; Paddle piston. . . . .	65
<b>Plate 12.</b> Side views of the shaped condensation pistons. . . . .	65
<b>Plate 13.</b> The "paddle" piston with depth adjustment mechanism. . . . .	67
<b>Plate 14.</b> The mix was divided on the Widger and fed into the split mould. . . . .	71
<b>Plate 15.</b> End preparation of the parent amalgam sample. . . . .	74
<b>Plate 16.</b> Radial score marks in the end-prepared parent amalgam. . . . .	74
<b>Plate 17.</b> The disassembled drill chuck used in end preparation. . . . .	75
<b>Plate 18.</b> Measurement of the sample using ball attachment micrometer. . . . .	75
<b>Plate 19.</b> Placement of parent amalgam samples in the split mould. . . . .	76
<b>Plate 20.</b> Adjustment of the depth of the "paddle". . . . .	76
<b>Plate 21.</b> The disassembled 3 point loading apparatus. . . . .	83
<b>Plate 22.</b> The test area of the 3 point loading apparatus. . . . .	84
<b>Plate 23.</b> A joined amalgam sample positioned for 3 point loading test. . . . .	84
<b>Plate 24.</b> The Hounsfield notching machine. . . . .	86
<b>Plate 25.</b> The notching procedure on a joined amalgam sample. . . . .	87
<b>Plate 26.</b> Amalgam M conventional alloy powder. (x900) . . . . .	99
<b>Plate 27.</b> Duralloy powder. (x225) . . . . .	100
<b>Plate 28.</b> Aristaloy 21 powder. (x225) . . . . .	100
<b>Plate 29.</b> Veraloy powder. (x225) . . . . .	101
<b>Plate 30.</b> Amalcap SAS Non gamma 2 powder. (x225) . . . . .	101
<b>Plate 31.</b> Dispersalloy powder. (x225) . . . . .	102
<b>Plate 32.</b> Tytin powder. (x225) . . . . .	102
<b>Plate 33.</b> Matticap Fine 68 powder. (x225) . . . . .	103
<b>Plate 34.</b> ANA 2000 alloy powder. (x225) . . . . .	103
<b>Plate 35.</b> Surface porosity in the addition after condensation by weights. . . . .	109
<b>Plate 36.</b> Batch 1 after fracture. (x3) Mean force to fracture: 339N. . . . .	111
<b>Plate 37.</b> Batch 4: removed from the mould 30 mins after tenth sample. (x3) Mean force to fracture: 371N. . . . .	116
<b>Plate 38.</b> Batch 5: left in the mould for 7 days. (x3) Mean force to fracture: 377N. . . . .	116
<b>Plate 39.</b> Fractured surfaces of specimen 4.3. (x18) . . . . .	117
<b>Plate 40.</b> Fractured surfaces of specimen 4.6. (x18) . . . . .	117
<b>Plate 41.</b> Batch 6. Duralloy (capsules). (x3) Mean force to fracture: 282N. . . . .	121
<b>Plate 42.</b> Batch 7. Amalgam M. (x3) Mean force to fracture: 301N. . . . .	121
<b>Plate 43.</b> Batch 14: 2s RI piston. Mean force to fracture: 332N (x3) . . . . .	134
<b>Plate 44.</b> Batch 15: 10s RI piston. Mean force to fracture: 321N (x3) . . . . .	134
<b>Plate 45.</b> Fractured end surfaces of specimen 19.3 (x18) . . . . .	137
<b>Plate 46.</b> "Gramophone groove" end preparation. (x18) . . . . .	144
<b>Plate 47.</b> Batch 29. Prepared using the SRI piston. . . . .	144
<b>Plate 48.</b> A rim of less granular material was visible on the fracture surface when failure occurred between increments condensed using the old flat piston. . . . .	151

Plate 49. Specimen A1.7. The curved interface between increments condensed by vibration using the old flat piston for 10s. (x110) . . . . .	151
Plate 50. Batch 32 after fracture: deadweighted condensation. . . . .	154
Plate 51. Batch 33 after fracture: condensed using the "old flat" piston. . . . .	154
Plate 52. Batch 34 after fracture: condensed using the "new flat" piston. . . . .	155
Plate 53. Batch 37 after fracture: 3 separate undivided doses. . . . .	156
Plate 54. Fracture surfaces of Duralloy Batch 48. . . . .	159
Plate 55. Macroscopic appearance of polished specimen A1.9. . . . .	160
Plate 56. Microstructure sample A1.9. Bright field. (x110) . . . . .	161
Plate 57. Microstructure sample A1.9. Dark field. (x110) . . . . .	161
Plate 58. Macrostructure of a retrieved clinical sample. (x18) . . . . .	163
Plate 59. Microstructure at the occlusal surface of the clinical sample. Unetched. (x110) . . . . .	164
Plate 60. Microstructure of clinical sample. (x110) The parent material is at the bottom of the frame. . . . .	164
Plate 61. Microstructure of clinical sample. (x225) . . . . .	165
Plate 62. Duralloy Batch 54 after fracture. Mean force to fracture: 198N. . . . .	167
Plate 63. Duralloy Batch 55 after fracture. Mean force to fracture: 202N. . . . .	167
Plate 64. Microstructure of Duralloy specimen A5.2. (Cut cone). (x110) . . . . .	168
Plate 65. Duralloy specimen A5.4. Three turns given to the paddle. (x110) . . . . .	168
Plate 66. Duralloy specimen A5.5. Six turns given to the paddle. (x225) . . . . .	169
Plate 67. Batch 112: Tytin. . . . .	198
Plate 68. Batch 109: Aristaloy 21. . . . .	198
Plate 69. Batch 114: Matticap Fine 68. . . . .	199
Plate 70. Batch 117: ANA 2000. . . . .	199
Plate 71. Batch 116: Amalcap SAS. . . . .	200
Plate 72. Batch 110: Dispersalloy. . . . .	200
Plate 73. Amalgam M Batch 119 after fracture. . . . .	210
Plate 74. Amalgam M Batch 118 after fracture. . . . .	210
Plate 75. Amalgam M Batch 120 after fracture. . . . .	211
Plate 76. Amalgam M Batch 121 after fracture. . . . .	211
Plate 77. Polished section of Duralloy specimen 54.2 after fracture. The fracture terminated at the lower edge of the sample. (x225) . . . . .	214
Plate 78. Microstructure of Duralloy specimen 54.2. Dark field illumination. The fracture traversed the joint, passing through a spherical residual alloy particle in the parent. (x900) . . . . .	214
Plate 79. Microstructure of Duralloy specimen 54.2. Bright field illumination. The fracture traversed the joint interface. (x900) . . . . .	215
Plate 80. Dispersalloy sample R5 after fracture where the parent part was notched. (x18) . . . . .	218
Plate 81. The indentation of the central loading roller in Amalcap SAS sample P4. The load was applied to the addition 0.2mm offset from the joint. (x18) . . . . .	218
Plate 82. Joined samples M1 to M8 after notching. . . . .	219
Plate 83. Joined samples M9 to M16 after notching. . . . .	219
Plate 84. Joined samples N1 to N10 after notching. . . . .	220
Plate 85. Veraloy specimen M15. Fracture surfaces. (x18) . . . . .	221
Plate 86. Veraloy specimen M15. (x18) Polished microstructure surface. Unetched. . . . .	221
Plate 87. Veraloy specimen M15. (x900) Microstructure of fracture transition area. . . . .	222
Plate 88. Aristaloy 21 specimen N7. (x18) Polished microstructure surface. Unetched. . . . .	223
Plate 89. Aristaloy 21 specimen N7. (x900) Microstructure of fracture transition area. . . . .	224
Plate 90. Duralloy specimen M11. Fracture surfaces. (x18) . . . . .	225
Plate 91. Duralloy specimen M11. Microstructure. (x110) . . . . .	226
Plate 92. Duralloy specimen M11. (x225) Lower part of Plate 91 above. . . . .	226
Plate 93. Duralloy specimen M11. Bright field. (x900) . . . . .	227

<b>Plate 94.</b> Duralloy specimen M11. Dark field. (x900) . . . . .	228
<b>Plate 95.</b> Dispersalloy specimen N10. Fractured surfaces. (x18) . . . . .	229
<b>Plate 96.</b> Dispersalloy specimen N10. (x110) . . . . .	230
<b>Plate 97.</b> Dispersalloy specimen N10. (x225) . . . . .	230
<b>Plate 98.</b> Dispersalloy specimen N10. (x900) . . . . .	231
<b>Plate 99.</b> Dispersalloy specimen M3. Fractured surfaces. (x18) . . . . .	232
<b>Plate 100.</b> Dispersalloy specimen M3. (x225)	
Transition zone: upper part. . . . .	233
<b>Plate 101.</b> Dispersalloy specimen M3. (x225)	
Transition zone: lower part. . . . .	233
<b>Plate 102.</b> Tytin specimen N3. Fractured end surfaces. (x18) . . . . .	235
<b>Plate 103.</b> Tytin specimen N3. (x225)	
The fracture traversed the joint. . . . .	235
<b>Plate 104.</b> Tytin specimen N3. (x900)	
Transition area where the fracture traversed the joint. . . . .	236
<b>Plate 105.</b> Tytin specimen N3. (x110)	
Composite micrograph of the joint and fracture path.	
The fracture traversed the joint about 0.5mm from the top. . . . .	237
<b>Plate 106.</b> Amalcap SAS specimen M9. Fractured surfaces. (x18) . . . . .	239
<b>Plate 107.</b> Amalcap SAS specimen M9. (x225)	
Central part of the specimen where the fracture deviated from the joint. . . . .	239
<b>Plate 108.</b> Amalcap specimen M9. (x110)	
Composite micrograph of the joint and fracture zone. . . . .	240
<b>Plate 109.</b> Amalcap specimen M9. (x900)	
Lower transition zone. . . . .	241
<b>Plate 110.</b> Amalcap specimen M9. (x720)	
Upper transition zone. . . . .	242
<b>Plate 111.</b> Amalcap specimen M9. (x720)	
Upper transition zone. Dark field illumination. . . . .	243
<b>Plate 112.</b> Amalcap SAS specimen P4. (x110)	
The fracture path was similar to that of specimen M9 (Plate 108). . . . .	245
<b>Plate 113.</b> Amalcap SAS specimen P2. (x225)	
The fracture path traversed the joint from the parent to addition amalgam. . . . .	246
<b>Plate 114.</b> Amalcap SAS specimen P2. (x900)	
The fracture path traversed the joint. . . . .	247
<b>Plate 115.</b> Amalcap SAS specimen P2. (x900)	
The fracture path departed from the region of the joint. . . . .	248
<b>Plate 116.</b> Amalcap SAS specimen P6. Fractured surfaces. (x18) . . . . .	250
<b>Plate 117.</b> Amalcap SAS specimen P6. (x225)	
The notched part of the sample. . . . .	251
<b>Plate 118.</b> Amalcap specimen P6. Centre of Plate 117. (x900)	
The fracture path was in the parent to the left of the cut spherical particle identifying the joint. . . . .	251
<b>Plate 119.</b> Amalcap specimen P6. (x900)	
Departure of the fracture from the joint. . . . .	252
<b>Plate 120.</b> Tytin specimen P20. Fractured end surfaces. (x18) . . . . .	254
<b>Plate 121.</b> Tytin specimen P20. (x900)	
The fracture originated at the notch adjacent to the joint. . . . .	254
<b>Plate 122.</b> Tytin specimen P20. (x900)	
The fracture departed from the joint. . . . .	255
<b>Plate 123.</b> Dispersalloy sample R6. Composite micrograph. (x110)	
The fracture reached the joint interface about 0.6mm from the lower surface. . . . .	257
<b>Plate 124.</b> Dispersalloy sample R6. (x225) . . . . .	258
<b>Plate 125.</b> Dispersalloy sample R6. (x900)	
The zone where the fracture reached the joint interface. . . . .	259
<b>Plate 126.</b> Dispersalloy Batch R after notching and test. . . . .	260
<b>Plate 127.</b> Batch T. Notched samples.	
Amalgam M, Tytin, Aristaloy 21 and Dispersalloy. . . . .	261
<b>Plate 128.</b> Amalgam M microstructure sample S20. (x225) . . . . .	261

## Acknowledgements

I should like to express my thanks to the many people who have encouraged and assisted me during this research study.

At City University, I thank Professor G.T.S. Done, the former Head of Department, for the provision of the facilities which made the study possible and his staff for the contributions they have made. I thank the present Head of Department, Professor A.R.D. Thorley without whose encouragement I might never have started the project.

I thank my supervisor Mr Roy Vipond for his continued guidance, tolerance and constructive criticism since starting.

I am most indebted to Dr John D.R. Walker for his kindness and expert advice and to his technical assistants, Ms Shammi Chaudhry and Mr Martin Young for their cooperation in the Dental Test Centre.

I greatly appreciate the practical advice of Mr Rod Stokes especially in the design of the Three Point Loading Apparatus. I would particularly acknowledge Mr E.E. James and Professor D.L. McDiarmid for their most helpful discussions on the bending and fracture of beams.

I am grateful to Professor H.P. Wynn for his help and advice regarding the statistical analysis of the results.

In other academic institutions, I thank my former teacher Professor N.E. Waters who first sparked my academic interest in this subject and Dr D. Brown of The United Medical and Dental Schools, Guy's Hospital for their help and advice.

I would record my appreciation of the many dentists and patients who have shown confidence in my unorthodox technique of amalgam repair and of those authors across the world with whom I have corresponded.

I am grateful to Dr Jill Davies and Dr Wagdy Youssef for their encouragement and support and to Dr Len Aw and Dr S.M. Dunne for their helpful criticism of the manuscript.

I am indebted to Degussa Ltd for their generous donation of a Dentomat 2 amalgamator, amalgam alloy and mercury and to Mr Don Clark of Engelhard Sales Ltd who kindly supplied some of the amalgam alloys used.

Lastly, I acknowledge those dental colleagues whose continued scepticism has inspired me to complete this work.

## **Declaration**

I grant powers of discretion to the University Librarian to allow this thesis to be copied in whole or in part without further reference to me. This permission covers only single copies made for study purposes, subject to normal conditions of acknowledgement.

## Abstract

The objective of this work was to manufacture and examine dental amalgam samples joined by the addition of new to old material.

Cylindrical samples 4mm in diameter were prepared from commercial dental amalgam alloys in a split mould. The end surface of the old amalgam was abraded, the sample replaced in the mould and fresh amalgam condensed using experimental vibration techniques developed during the study. Samples were subsequently fractured using 3 point loading.

Although there was considerable scatter in the force to fracture, several experimental procedures produced samples which did not break at the joint. The force to fracture these joined samples generally exceeded that for one-piece samples condensed in a manner similar to that prescribed in BS 2938: 1985.

Notches were machined adjacent to the joint in a selection of joined samples and the central load roller of the 3 point test rig was located opposite. Most fractures commenced at the notch, traversed the joint interface and terminated at the point of applied load. For samples notched at the joint and offset loaded, the fracture path departed from the joint at about halfway. This indicated that the joint was not the weak link in the samples.

The location of the joint was revealed in the microstructure when the parent alloy contained spherical particles: these were cut by the end preparation procedure. Reassembled notched samples after fracture showed the crack to traverse or follow and then depart from the joint. An incomplete copper-tin reaction layer was also seen at the joint on cut spherical silver-copper particles in high copper admixed amalgam.

The range of amalgam alloys which were prepared and tested and where the joint was not weak included conventional, high copper single composition spherical and lathe cut, blended, hybrid and admixed types.

## List of abbreviations

DW	Deadweight; condensation of amalgam using a static load
SPP	Standard paddle condensation procedure
RI	Rubbing-in piston
SRI	Spiral rubbing-in piston
pdl	paddle special condensation piston
6xpdI	6 turns of the vibrating paddle condensation piston
4x2s	condensation for 2s on each division of four portions of a mix
6x2s	condensation for 2s on each division of six portions of a mix
Ag	Silver
Cu	Copper
Hg	Mercury
Sn	Tin
HCA	High copper admixed amalgam alloy
HCSC	High copper single composition amalgam alloy
AmM	Amalgam M
DUR	Duralloy
A21	Aristaloy 21
VER	Veraloy
DISP	Dispersalloy
ANA	ANA 2000
TYT	Tytin
ACAP	Amalcap SAS
MCAP	Matticap Fine 68
A.D.A.	American Dental Association
BS	British Standard
ANOVA	Analysis of variance
COV	Coefficient of variation
F	Ratio of between group to within group variances
t	The difference between means divided by its standard error
p	Probability
=	equal to
<	less than
>	greater than
<i>et al</i>	and other authors
mm	millimetres
$\mu\text{m}$	micrometres
MPa	Mega-Pascals
N	Newtons

**Dedication**

**To my parents**

**Phyllis Mary Cook A.A.Dip., A.R.I.B.A.**

**1916 – 1991**

**Herbert Frederick Cook M.A. (Oxon.)**

**1913 – 1991**

## Chapter 1. Introduction

The author's interest in the repair of dental amalgam started in about 1971 when he was a recently graduated dentist in general practice. A patient for whom he had placed a large amalgam filling in an upper second premolar tooth about two weeks previously returned with the palatal cusp having fractured. The standard treatment procedure in such cases was removal of the filling and placement of a new amalgam restoration with one or more dentine pins to aid retention. This was done and critical examination revealed several faults in the resultant restoration which had not been present in the filling which had been removed. The areas of contact with the adjacent teeth were somewhat deficient on the side where the cusp had been lost. Difficulty had been experienced in carving the occlusal (biting) surface to the correct contours and there were excesses of amalgam at the gingival (gum) margins.

A short time later, a small part of the occlusal surface of the amalgam filling in his own lower right first molar tooth broke away but no decay was present. The generally accepted view on repair was that the bond was a source of weakness and that repair of fractured amalgam was a hazardous procedure (Skinner and Phillips, 1967). It was, however, acknowledged that extensive amalgam restorations were repaired, becoming "patched with amalgam" (Messing and Ray, 1972) but this was not orthodox treatment. In long-term reviews, repair or resurfacing was not considered as a possibility: amalgam restorations either survived or had been replaced (Osborne *et al*, 1991). Deteriorations in surface/edge (marginal) quality of fillings over time were assessed in five categories by Redit analysis (Mahler *et al*, 1970) but later work included a sixth category "requiring replacement" (Mahler *et al*, 1973).

Each time a dental restoration is replaced, further tooth substance is inevitably removed. Restorations become progressively more extensive and therefore

difficult for the dentist to achieve results of high quality. In work which post-dates the clinical events reported in this chapter, it was shown that the resulting larger restorations have a shorter life expectancy (Elderton, 1977) and more marginal deterioration (Berry *et al*, 1981). Eventually it may become impossible to restore the tooth. If repair rather than replacement of a faulty restoration were possible then more elaborate restorative procedures or tooth extraction might be deferred during the patient's lifetime.

One of the author's teachers at The Royal Dental Hospital of London School of Dental Surgery (Kirk, 1962) reported that repaired amalgam did not always break at the joint under tensile testing. The work was not publicised widely: even the Head of Department was unaware of its existence (Pickard, 1993).

The author decided to attempt an experimental repair on his own tooth, carrying out the work himself by observation in a mirror. The amalgam fracture surface was freshened using a steel bur in a conventional speed handpiece and the debris washed away with a water-air spray. A small portion of fresh amalgam mix was applied using an air driven vibration instrument (mechanical condenser) and further small increments added to restore the filling to its original surface form. The author's hypothesis was that mercury in the new mix might react with residual silver-tin alloy particles in the old filling in the same manner as occurs in the normal amalgam setting reaction. Objectives during condensation were to wet the prepared surface with mercury which is present in the new amalgam paste and to minimise the occurrence of voids at the new-old amalgam interface. Otherwise, mercury would not react with the old amalgam resulting in joint weakness and failure of the repair. The repair remained in his mouth for about twenty three years.

A short time later, another patient attended with the palatal cusp of an upper first premolar tooth having fractured leaving a clinically satisfactory mesio-

occluso-distal amalgam restoration in place. It was decided to attempt an amalgam repair in the first instance on the grounds that if this was successful, the patient would have been saved from a relatively unpleasant and difficult restorative procedure. If the repair failed then conventional treatment (a large pinned amalgam restoration or crown) would be carried out which could be difficult to achieve successfully in the mouth as indicated above. There was little to be lost by making the attempt to bond an amalgam cusp to the existing restoration. The exposed amalgam surface was prepared using a diamond bur in an air turbine handpiece and a small inverted cone bur used to make undercut pits in the original amalgam. Using the mechanical condenser, a small portion of new amalgam mix was rubbed against the freshly prepared surface and a cusp built up freehand in small increments. A matrix band which is required by conventional techniques to support the amalgam during condensation was not used. The occlusal surface of the cusp was kept clear of the opposing teeth. When the patient was next seen, the repair appeared to be satisfactory, giving encouragement to the view that it might be possible to effect amalgam repair without significant loss of strength.

The repair technique became modified in the light of experience over the following years and it became the author's usual treatment for fractured cusps where appearance was not an important consideration. Eventually, it was discovered through conversation with colleagues that no-one else had tried a similar procedure so photographs of some completed cases were collected and a short lecture prepared to demonstrate the process. This was first presented at University College Hospital Dental School in November 1979 and published in *Dental Update* (Cook, 1981a; Appendix 6) where the clinical case described in the paragraph above is shown after eight years service.

Publication of the technique was met with derision in some quarters and with encouragement in others by dentists who had tried the method and found it

to be useful. A correspondent to Dental Update (Dwyer, 1981; Appendix 7) presumed that the article was intended for publication on April 1st and felt that its content was totally irrelevant to modern dentistry. Another colleague described the article as being of limited interest because it was unscientific. The author decided to attempt to validate his method for amalgam repair. Laboratory facilities were available to post-graduate students, so with the encouragement of Dr (now Professor) David Thorley, the author applied for a part-time place at the Department of Mechanical Engineering, City University.

The objectives of this research study were to devise laboratory methods for the preparation of joined dental amalgam specimens including procedures which simulated the author's clinical technique; for testing the strength or integrity of the joint; and to consider reasons for variations in the strength of bond and microstructure obtained. The author's clinical technique is applied to the repair of mature amalgam and the fracture of joined samples in this study was carried out (with few exceptions) seven days after joining to seven day old parents. Since there is controversy regarding the strength of amalgam joints to immature parent materials and that in the author's experience repairs to recently condensed amalgams are unreliable these are not part of this study. Only the direct metal to metal joint was tested: use of intermediate adhesives and bonding resins are not considered.

Dental amalgam alloys and their reactions with mercury are briefly described in Chapter 2 of this thesis and the literature on the new to old amalgam joint or bond is reviewed in Chapter 3. The experimental equipment and methods used are described in Chapter 4 and the materials used are reported in Chapter 5. Chapter 6 reports the results of the experimental programme together with analysis supporting the evolution of the methods used to study joint strength. Finally, the results are reviewed and assessed in Chapter 7 including comparisons with previously published work.

## **Chapter 2. Dental amalgam**

This chapter defines the dental amalgam alloy and briefly describes its manufacture, preparation and use. National specifications for the chemical compositions of dental amalgam alloys and their setting reactions are described.

### **2.1 Definition**

An alloy for dental amalgam is defined as an alloy in fine particles, composed mainly of silver, tin and copper, which, when mixed with mercury, produces a dental amalgam (BS EN 21559: 1992).

### **2.2 Manufacture of dental amalgam alloy**

Dental amalgam alloys are dispensed to dentists in the form of powder which may be of irregular or approximately spherical particle shape. They are manufactured by melting together the required quantities of pure metals. The molten metal may be either cast into an ingot or atomised by spraying into a cold inert atmosphere. The "as-cast" ingot has a dendritic structure which is inhomogeneous in its chemical composition. It is therefore subjected to a homogenising anneal before comminution into irregular shaped particles in a lathe or milling machine. The particles may be treated by ball milling, washing in acid or further heat treatment.

The particle size of both lathe cut and atomised alloys is determined by the manufacturer. Amalgam alloys may consist of particles manufactured from the same melt or from mixtures of alloys of differing composition and/or particle shape.

### 2.3 Use of dental amalgam

Dental amalgams are produced ready for use by mixing together the recommended proportions of amalgam alloy powder and mercury. The mixing procedure is known as trituration. Although historically this was done by hand using a mortar and pestle, rubber finger-stall and by mulling in the palm, such procedures are obsolete. Machines, known as amalgamators, are used almost universally by dentists for the trituration of amalgam.

After mixing, the amalgam is introduced into the dental cavity in portions where it is worked or pressed by a technique known as condensation. This adapts the amalgam to the cavity floor and walls, removes excess mercury from the mix and ideally minimises the formation of voids or porosity. The cavity is over-filled and the surface mercury rich layer is removed. The exterior of the amalgam is shaped to the desired surface contours, smoothed and left to harden or set.

In the laboratory, steel moulds are used for the preparation of test specimens. Close fitting steel pistons are used to confine the amalgam mix within the mould under pressure while allowing excess liquid mercury to escape. The freshly condensed sample may be pressed immediately from the cylindrical ejector-type mould; or, if a split mould is used, the sample may be removed after initial setting has occurred.

Weakness results if more than about 55% mercury by weight is present in the set amalgam (Shwartz and Phillips, 1956). Trituration by hand with a mortar and pestle required an excess of mercury in the mix (about 8 parts of mercury to 5 parts alloy) which was subsequently removed by squeezing in a cloth prior to condensation. These procedures were susceptible to operator variation. By the use of a mechanical amalgamator, the initial mercury content

of the mix was reduced to 50% or less eliminating the need for the squeeze procedure prior to condensation (Eames, 1959).

It is possible to reduce the mercury content of the mix to the detriment of the mechanical properties of the restoration. Use of an overly dry mixture produced layering, porosity and weakness in the restoration (Mahler and Mitchem, 1965). Jørgensen *et al* (1966) proposed a "wet" technique where a 1/4mm thick layer of mercury rich amalgam remained on the surface and promoted good coherence between layers. The cavity was overfilled and any undesirable excess mercury was eliminated by removal of the surface layer during carving to establish the desired surface contours. The resulting specimens were less porous and stronger than those prepared by the traditional and Eames techniques. A 1% increase in mercury content led to a moderate reduction in crushing strength but a 1% increase in porosity resulted in an essential reduction in strength. Eames (1967) found that for a fast setting alloy, a ratio of 52% mercury in the mix adapted better to the mould than the 50% mix, particularly when low condensation pressures were used. Wetter mixes moved more readily into the angles of the mould and a 48% mercury mix or large increments adapted badly.

There has been controversy regarding surface treatment of the newly placed restoration. Use of a burnisher was held to bring excess mercury to the margins which were weakened and more susceptible to tarnish and corrosion (Phillips, 1953). This may have applied to amalgams triturated by hand but for mechanically amalgamated alloys burnishing led to better adaptation, markedly reduced porosity and the proportion of residual alloy in the restoration margins was also increased (Kanai, 1966). When fully set, any excess amalgam should be removed, the bite re-adjusted if necessary and finally the restoration polished to reduce adherence of bacterial plaque and corrosion.

## 2.4 Standard specifications for amalgam alloys

Chemical composition standards for dental amalgam alloys have been modified during the last three decades. The British Standard Specification for Dental Amalgam Alloy (silver-tin) BS 2938: 1961 prescribed composition limits which are shown in Table 1.

Metal	Content % (by weight)
Silver	65 min.
Tin	29 max.
Copper	6 max.
Zinc	2 max.
Mercury	3 max.

**Table 1.** Permitted limits of alloy composition to BS 2938: 1961.

Other elements were permitted to replace or in addition to the copper, zinc or mercury provided that the composition was approved by the British Standards Institution. Evidence was required to show that these elements were safe for use in the mouth.

It is well recognised that excessive expansion of amalgam may occur after setting if zinc-containing amalgams become contaminated with water before or during manipulation of the mix. BS 2938: 1961 stated that if the alloy contained zinc "in sufficient quantity to cause gaseous dissociation of water" the following precaution was to be printed in type larger than that in the body of the instructions:

"The alloy contains zinc and the amalgam made therefrom will show excessive corrosion and expansion if moisture is introduced during mixing and packing. Therefore, the amalgam should not be mullled in or touched with the bare hands, condensed in a wet cavity or contaminated with moisture in any manner."

More recently published standards have required similar warnings to be given in zinc containing alloys. In 1977, the Revised American Dental Association Specification No. 1 for alloy for dental amalgam considered an alloy to contain zinc if the content was higher than 0.01%. The main constituents were silver and tin. Gold, copper, zinc and mercury could be used in amounts less than the silver or tin content. If other elements were used the manufacturer was required to list the chemical composition.

The British Standard for Dental Amalgam Alloys BS 2938: 1985 classified amalgam alloys into three types according to composition and methods of preparation. All alloys complied with the permitted limits of composition in Table 2. Amalgam alloys containing less than 6% copper were described as Type I conventional alloys. Amalgam M and Matticap Fine 68 are examples of conventional amalgam alloys which were used in this study.

Type II alloys were high copper dispersion alloys having a copper content above 6% achieved by mixing particles of differing compositions - usually conventional silver-tin based alloy with particles of a high copper content alloy such as silver-copper eutectic. Alloys of this type may be referred to as high copper admixed or HCA alloys. Dispersalloy and Amalcap SAS are examples of this alloy type.

Type III alloys contained over 6% copper, achieved by the addition of larger amounts of copper to the melt so that all of the copper was initially in solution. Type III alloys may be referred to as high copper single composition or HCSC alloys. In amalgam alloys of this type, extra copper is substituted for silver. They may be relatively high in silver content with about 12% copper (for example, Tytin), or with reduced silver content (less than 50%), and extra high copper (more than 20%). Aristaloy 21, Veraloy and ANA2000 containing about 24% copper are examples of the latter alloy type.

Type	Silver	Tin	Copper		Zinc	Indium	Mercury
	min. %	max. %	max. %	min. %	max. %	max. %	max. %
I	65	29	6	-	2	-	3
II	60	25	25	6	2	-	3
III	40	32	30	6	2	5	3

**Table 2.** Permitted limits of alloy composition (by weight) to BS 2938: 1985.

Alloy types were not classified in the British Standard Specification for Alloys for Dental Amalgam BS EN 21559: 1992. The manufacturer was required to describe the particle shapes and to list all elements present in greater concentration than 0.1% by weight. Certain chemical composition limits were prescribed which are listed in Table 3. However, metals other than those specified in Table 3 were permitted to replace parts of tin and copper provided that the manufacturer presented adequate evidence to show that the alloy was safe to use in the mouth.

Metal	Content % (by weight)
Silver	40 min.
Tin	32 max.
Copper	30 max.
Zinc	2 max.
Mercury	3 max.
Other non-noble metals	0.1 max.

**Table 3.** Permitted limits of alloy composition to BS EN 21559: 1992.

In the silver-tin binary alloy system, the gamma phase is an intermetallic compound with the chemical formula  $Ag_3Sn$  and the beta phase is a solid solution of tin in silver. Amalgams made from pure  $Ag_3Sn$  contract slightly on setting; the silver rich beta phase reacts quickly with mercury with expansion on setting. The relative proportions of beta and gamma are determined by the chemical composition, rate of cooling and heat treatments during manufacture. The overall tin content is controlled in order to achieve the desired dimensional

changes on setting. Zinc added to the melt acts as a scavenger during manufacture and in the amalgam, protects the more important constituents from oxidation and improves the clinical handling of the amalgam.

A small amount of copper (about 1%) will dissolve in these silver-tin alloys. Excess copper replaces silver and is present mainly in the form of  $\text{Cu}_3\text{Sn}$ , the epsilon phase of the copper-tin system. Historically, copper was added to  $\text{Ag}_3\text{Sn}$  alloys to improve the manipulative qualities of the amalgam, its strength and hardness. However, alloys containing more than 6% copper were thought to give rise to excessive setting expansion which could cause pain or tooth fracture.

Filings of the very hard Ag-Cu eutectic alloy were mixed with  $\text{Ag}_3\text{Sn}$  powder (Innes and Youdelis, 1962). It was anticipated that addition of hard particles might improve the compressive strength of the amalgam by dispersion hardening. The experimental amalgam showed a 650% reduction in creep but its setting expansion exceeded the limits in the A.D.A. specification. An amalgam alloy mixture of 30% atomised Ag-Cu particles and 70% lathe-cut conventional alloy was marketed under the name Dispersalloy. The overall copper content of this HCA alloy was 12% which exceeded the standard limits of the day but this amalgam did not expand excessively on initial setting. The clinical performance during four years in terms of deterioration in amalgam surface/edge quality at the amalgam-tooth junction was better than that of fine or medium-cut conventional amalgams (Mahler *et al*, 1973).

An all-spherical particle alloy was produced with a similar copper content to that of Dispersalloy from a single melt of Ag-Sn-Cu alloy (Asgar, 1974). Later, a lathe-cut alloy containing 25% copper prepared from a single melt was described (Espevic, 1980). High copper amalgam alloy types are now widely used in restorative dentistry. Control of the chemical compositions of these alloys ensures that undesirable dimensional changes do not occur on setting.

## 2.5 Setting reactions of dental amalgam

The setting of dental amalgam is described briefly here; a detailed resumé of research on these reactions was given by Okabe (1992). During trituration, amalgam alloy particles are rubbed together in the presence of mercury. Any surface oxide film is removed and mercury wets the underlying alloy which dissolves into the mercury. Dissolution of the solid alloy into liquid mercury is followed by supersaturation, nucleation and crystal growth of new amalgam phases. Saturation with silver probably occurs before completion of trituration. The solubilities in mercury (by weight) are: silver, 0.035% (at 20°C); tin, 0.6% (at 15-18°C); copper 0.006% (Hansen and Anderko, 1958).

Some degree of supersaturation is necessary for nucleation to occur. Significant evaporation of the solvent (mercury) was unlikely to occur before the start of setting (Okabe, 1992). Absorption of mercury by the residual alloy particles at intergrain and interphase boundaries could deplete the mercury available for solution and cause supersaturation. The temperature of amalgam mixed in a high energy amalgamator was such that the mix was "too hot to touch" (Curtis and Brown, 1992). Supersaturation could therefore also occur on cooling to mouth temperature before or during condensation. New metallic compounds nucleate on existing solids in the mix and grow from the mercury solution. When mercury is in limited supply, the setting reaction does not proceed to completion and probably never reaches equilibrium. All residual silver-tin alloy was consumed when the mercury content of the amalgam was 62% for conventional True Dentalloy or 60% for HCSC Tytin (Jensen, 1977). Set amalgam has a heterogeneous structure of unreacted residual alloy particles in a matrix of new reaction products and porosity, the relative proportions and grain sizes of which have considerable bearing on the final properties of the amalgam. The setting reactions of high copper amalgams differ from those of conventional amalgams which are considered first.

### 2.5.1 Conventional amalgams

Silver and tin dissolve from the amalgam alloy and react with mercury to form silver-mercury and tin-mercury phases. Silver dissolves more rapidly and is less soluble than tin in mercury: silver-mercury grains ( $\text{Ag}_2\text{Hg}_3$ , known as gamma-1) with a body centred cubic structure nucleate and grow first. The concentration of tin in mercury has reached about 1/50th of saturation at the time silver became saturated. Tin-mercury nucleates and grows later: the compressive strength develops slowly, reaching near its maximum after about 24 hours. The tin-mercury phase ( $\text{Sn}_{7.8}\text{Hg}$ , known as gamma-2: hexagonal lattice) is weak and liable to corrosion. Its solidus temperature is  $90^\circ\text{C}$  (Wing, 1979) and it is therefore prone to plastic deformation under load. Amalgams containing a significant proportion of the gamma-2 phase creep under load.

### 2.5.2 High copper admixed amalgams

The tensile strength of HCA amalgam increased from 1 day to 1 week after amalgamation (Fukuba *et al*, 1977). In HCA alloys, approximately two thirds of the powder is of conventional composition; one third by weight is Ag-Cu alloy usually at or close to the eutectic composition (71.9% Ag, 28.1% Cu). After trituration, silver from the alloy particles reacts with mercury to produce the gamma-1 phase. However, tin diffuses in the mercury to the silver-copper eutectic particles where a reaction layer containing copper-tin intermetallic compounds forms (Mahler, 1971; Asgar, 1971).

Growth to impingement of the surface nucleated crystals produced a continuous reaction layer and little or no further dissolution of Cu into Hg occurred (Boswell, 1980). Gamma-1 and gamma-2 then precipitated in the remaining liquid; the X-ray intensity of gamma-2 in Dispersalloy reached a maximum after 20 minutes but this phase disappeared within a week (Asgar,

1974). Subsequent growth in reaction layer thickness occurs as a result of dissociation of gamma-2 and transport of tin along grain and interphase boundary diffusion paths to the copper-rich areas. A small proportion of  $\text{Cu}_6\text{Sn}_5$  (the eta-prime phase of the copper-tin system) in these amalgams at 24 hours was located as sub-micron sized precipitates throughout the gamma-1 matrix (about 1/50th of the volume fraction in the reaction zones).

Larger numbers of smaller  $\text{Cu}_6\text{Sn}_5$  crystals formed adjacent to Ag-Cu alloy particles with finer microstructures:  $0.05\mu\text{m}$  for eutectic composition particles (lamellar spacing  $0.04\mu\text{m}$ ) but  $1\mu\text{m}$  for off-eutectic (49% Ag, 51% Cu by weight) particles containing large ( $1\mu\text{m}$ ) alpha-Cu inclusions (Mitchell *et al*, 1981). In the latter amalgam, gamma-2 phase was detected after 2 years (Jensen and Jørgensen, 1981). High copper content in alloy particles impedes wetting by mercury. In addition, the copper rich particles may be covered by a relatively thick layer of oxide and intensive mixing required to bring about a reaction between alloy and mercury. Low intensity mixing may cause a deficient reaction between copper and tin and the consequent formation of significant amounts of the harmful gamma-2 phase (Jørgensen, 1976).

### 2.5.3 High copper single composition amalgams

Particles for these alloys are an intimate mixture of beta Ag-Sn, gamma Ag-Sn and  $\text{Cu}_3\text{Sn}$  (the epsilon phase of the copper-tin system). Silver, copper and tin enter solution in mercury. Copper reaches saturation first and tin reacts with this to produce  $\text{Cu}_6\text{Sn}_5$ . So long as copper is available the concentration of tin in solution does not exceed 1/10th of saturation and therefore gamma-2 formation is suppressed (Mitchell *et al*, 1978). Silver reacts with mercury to produce gamma-1. Since gamma-2 is not formed, these amalgams rapidly gain strength on setting. However, if the final mercury content is excessive (over 47% for all-spherical HCSC Tytin) or if the copper is unavailable for reaction, gamma-2 may form. Prolonged heat treatment ( $320^\circ\text{C}$  for 2 weeks)

of the Tytin alloy reduced the reactivity of the copper phase such that the manufacturer's recommended mercury content of 43.5% produced gamma-2 in the set amalgam (Jensen, 1977). Larger crystals present a reduced surface area for dissolution and fewer nucleation sites than the same weight of smaller crystals.  $\text{Cu}_6\text{Sn}_5$  crystals  $0.5\mu\text{m}$  long were distributed throughout the matrix in atomised HCSC amalgams, but were 2 to  $3\mu\text{m}$  long on annealed particles (Mitchell *et al*, 1981). Espevic (1980) manufactured two lathe-cut single composition alloys where the  $\text{Cu}_3\text{Sn}$  grains were relatively large compared to those in the atomised and rapidly cooled Tytin. For the 13.6% Cu alloy, gamma-2 was detected in the amalgam which exhibited moderate setting expansion, but these were absent in the amalgam from the 25% Cu lathe cut alloy. Mahler and Adey (1977) reported that in HCSC amalgam above 48% final mercury content there was an inordinately high increase in creep; in the gamma-1 phase, the tin content increased and the grain boundaries were less resistant to etching.

#### 2.5.4 Longer term changes

Amalgam is inherently non-equilibrium in its nature. Changes continue throughout the life of the material, although at a very much reduced rate than those which occur in initial setting. Where gamma-2 is present, this phase may decompose into tin salts and mercury. In a corrosion study, corrosion was greatest in the eta-prime phase of HCSC amalgam and in the reaction zone in HCA amalgam (Moberg and Odén, 1985a). A gradual solid state phase change of gamma-1 (silver-mercury,  $\text{Ag}_2\text{Hg}_3$ ) to beta-1 ( $\text{AgHg}$ ) in the set amalgam was associated with a reduction in susceptibility to creep (Espevic, 1977; Jensen and Jørgensen, 1978). Dimensional changes in HCA amalgams after 2 years at  $37^\circ\text{C}$  reached two (for Dispersalloy) to five times the +0.2% limit for setting expansion prescribed in the A.D.A. specification which did not occur in the conventional or HCSC amalgam (Paffenbarger *et al*, 1979).

### Chapter 3. Review of the literature on the amalgam to amalgam bond

This chapter reviews the literature on the amalgam to amalgam bond or joint. "A technique, little recommended ... and perhaps of minimal application by dentists, is to condense freshly mixed amalgam against an already crystallised portion" (Consani *et al*, 1977). "This procedure is rarely indicated clinically" (Kirk, 1962). "It is obvious that the bond between old and new amalgam is the main source of structural weakness of the repaired restoration" (Vrijhoef *et al*, 1980).

Nevertheless, it is acknowledged that repairs to dental amalgam restorations are commonly carried out in clinical dental practice (Terkla *et al*, 1961; Miyata, 1972; Berge, 1982). Repair of amalgam restorations could be advantageous since maximum remaining tooth substance is conserved (Cook, 1981a; Bapna and Mueller, 1989). Parts of the restoration which have proved satisfactory would otherwise be removed with risk of an inferior replacement (Gainsford and Dunne, 1992). More recently, it has been suggested that greater attention should be paid to repair of restorations rather than complete replacement (Corbin and Kohn, 1994). However, there is comparatively little in the literature to support the proposal that repair of dental amalgam achieving strong joints is possible.

In laboratory tests, many authors\* have found that substantial reductions in strength resulted from attempts to repair fully set dental amalgams. On average, joined samples were not more than about half as strong as the one-piece controls and sometimes much weaker.

---

\* These include: Terkla *et al* (1961); Forsten (1969); Scott and Grisius (1969); Miyata (1972); Consani *et al* (1977); Nettelhorst (1977); Berge (1982); Walker and Reese (1983); Bass (1985); Bass and Wing (1985); Brown *et al* (1986); Hornbeck *et al* (1986); Gordon *et al* (1987); Hibler *et al* (1988); Bapna and Mueller (1989, 1993); Lacy *et al* (1989); Schaller *et al* (1989); Erkes *et al* (1990); Carr-Hosie *et al* (1992); Leelawat *et al* (1992b); Bagheri and Chan (1993); Hadavi *et al* (1993).

### 3.1 Work reporting strong joints

Relatively few papers have reported repair joints stronger than about two thirds of the one-piece sample strength. Mean tensile strengths of joined specimens were up to 73% and 92% of unrepaired strengths (Nakaoka *et al*, 1974; Fukuba *et al*, 1977, respectively) and mean joint strengths of up to 79% of the one-piece controls have also been reported (Hadavi *et al*, 1992). However, the testing of samples which did not break at the joint has been reported (Kirk, 1962; Jørgensen and Saito, 1968). The latter authors reported that the mean force to fracture after mercury treatment to the parent surface prior to joining was 97.6% of that for the one-piece control samples.

Twelve dumbbell-shaped amalgam samples were prepared in a split die and subjected to tensile testing after 48 hours (Kirk, 1962). After fracture, the larger broken section was trimmed using sandpaper discs and reinserted in the die. The remainder of the die was filled with new amalgam under the same conditions. Under test, some of the stronger samples broke in the original part and not at the joint. The tensile strength of the unrepaired samples ranged from 4600 to 5700 pounds per square inch; the repaired specimens, from 900 to 5300 pounds per square inch. A third of the repaired specimens were as strong as the original samples, whereas a further third were very much weaker. A six-fold range in results is noteworthy.

No other reports have been found of a satisfactory joint (in terms of strength) without an investigation of various aspects of the techniques used in the preparation of the joined specimens. Some of these experimental techniques produced stronger joints than others and the variation in strengths obtained by any single method has generally been greater than that of the control samples (Jørgensen and Saito, 1968; Fukuba *et al*, 1977; Hadavi *et al*, 1992).

In an amalgam, the establishment of a union was comparable to soldering (Jørgensen and Saito, 1968). A condition for good bond strength was an effective wetting of the solid alloy (the old amalgam) with the liquid (mercury with dissolved alloy components). A cylindrical steel mould was used to produce specimens 5mm in diameter and 10mm long which were tested under three point loading. Specimens were prepared for joining by dividing the amalgam cylinder by saw to make two cylinders 5mm long. After grinding of the end surface with carborundum paper, the short specimens were replaced in the mould and fresh amalgam condensed against the prepared surface. Five experimental groups were used with differing treatments of the end surface:

- (i) No treatment prior to condensation of fresh amalgam produced a flexural strength in the repair of 45.6% of the controls;
- (ii) After wetting with saliva and drying the strength was reduced to 16.8%;
- (iii) Leaving exposed to air for 48 hours reduced the strength to 20.8%;
- (iv) When the end of the specimen was rubbed in a drop of mercury on carborundum paper before replacement in the mould the strength was 97.6% of the controls;
- (v) The strength was reduced to 90% if the end of the specimen was scraped with a plugger in the presence of a drop of mercury.

Amalgam of conventional composition was used. The effect of time on the development of strength in the join was significant. Whereas the strength of unrepaired amalgam increased as a logarithmic function of the age of the amalgam up to 24 hours (when the setting reaction was supposed to be complete), a graph of the strength of joined specimens against a linear time-scale up to 24 hours produced a straight line. The process leading to the setting of amalgam was said to be fundamentally different from the process

leading to the union of new and old amalgam. The high joint strengths achieved by Jørgensen and Saito (1968) have not been duplicated (Erkes *et al*, 1990) but no reports have been found of repeated preparation procedures.

Different alloy types were studied under repair. Joined samples prepared from fine cut alloy for the parent parts gave weaker bonds with spherical alloy additions than other combinations which were about half as strong as the controls (Nagaoka *et al*, 1974). One-piece spherical particle conventional amalgam reached maximum tensile strength after 24 hours while the joint strength increased by about 50% from one day to one week for both high copper dispersed phase and spherical particle conventional amalgams (Fukuba *et al*, 1977). After one week, a spherical-spherical joined group was about twice as strong as a dispersed-dispersed joined group and 85% as strong as its one-piece control which exceeded the strength of the dispersed-phase control. However, at 15 minutes and 1 hour, a dispersed-phase control was very much stronger than both a spherical control and all joined groups. When either alloy was added, joined samples were weaker with parents from dispersed-phase than all-spherical particle amalgams; the magnitude of the differences was dependent on the parent surface abrasion technique.

The results of earlier collaborations with Nagaoka and Fukuba and colleagues were reiterated with identical graphs (Inoue, 1978). Bar charts for strength of bond with different surface treatments prior to joining showed that for a spherical particle conventional amalgam sandpaper grades 100, 150, 240 produced the best joins at about 73%. Abrasive point, grade 320 sandpaper, cross-cut fissure bur, plain-cut fissure bur and diamond point gave strengths progressively reducing in the range 60% to 50%. Joints to a polished surface were about 11% as strong as the one-piece samples (Nagaoka *et al*, 1974). End treatment of a spherical particle amalgam with a plain-cut tungsten carbide fissure bur produced a repair strength of about 92% (Fukuba *et al*,

1977). Grade 320 abrasive paper was less effective than the coarser grades, with additional variations between alloy brands (Miyata, 1972).

### 3.2 Age of repaired parent amalgam

The repair of fully set amalgam is a different type of bonding condition compared to that carried out soon after condensation (Terkla *et al*, 1961). There are inconsistencies in reports on the effect of age of the parent part on joint strength. No difference in tensile strength of dumbbell-shaped specimens made from a spherical particle alloy was found when the second half condensation was carried out 45 seconds after completion of the parent (Scott and Grisius, 1969). All other reports of joining to amalgam which is less than one day old have shown weakness under tensile or flexural test.

There was a reduction in 24 hour flexural strength which was not statistically significant for repairs made to a carved surface after seven minutes with Dispersalloy (Brown *et al*, 1986). The reduction was significant for repairs at 12 minutes and other alloys (Tytin and Contour) but not significant for Sybralloy at either time interval. Repairs to a fractured surface at 12 minutes were 65% to 31% of the one-piece control strengths for all alloys tested and samples repaired after 24 hours were too weak to handle.

A trend of decreasing bond strength occurred with increasing parent age: 70% of the one-piece strength after 15 minutes, 45% after 24 hours and 39% after 7 days (Scott and Grisius, 1969). In results showing a similar trend, the five minute repair using Tytin was 84% of the one-piece tensile strength (Bagheri and Chan, 1993). Earlier results (36% of the one-piece flexural strength for the same alloy and timing) did not agree (Walker and Reese, 1983).

Repairs to seven day (Terkla *et al*, 1961; Miyata, 1972) and 14 day (Schaller

*et al*, 1989) old amalgam produced weaker bonds than 15 minute old parents but no difference has also been found (Walker and Reese, 1983). These inconsistencies may be related to the experimental preparation techniques used as none of these workers reported strong joints.

After 15 minutes, HCA amalgam was considered incompletely hardened and less than normal condensation pressures used; a slight increase in strength was reported for 15 minute (74%) to 10 day (79%) repairs (Hadavi *et al*, 1992). A similar slight increase in bond strength occurred with increasing age of parent amalgam from 15 minutes to 7 days; there were additional variations between spherical and dispersed phase amalgams one hour and one day old (Fukuba *et al*, 1977). Differences were also found between alloys repaired after 1 hour (Schaller *et al*, 1989). There were no differences between 2, 3 and 30 day old parents (Jørgensen and Saito, 1968) and the age of the original (standard or preamalgamated) amalgam when completely set (24 hours) had no influence on the bond strength (Forsten, 1969).

This conclusion does not agree with a finding for high copper admixed amalgam tested 21 days after joining (Carr-Hosie *et al*, 1992). Repairs to seven day old parents were only 25% of the 28 day one-piece strength but with 21 day old parents were 68% of the 42 day one-piece or 50% of the 22 day control sample strengths. One-piece control samples reduced in strength by 25% from 22 to 42 days. Repairs to 24 hour parents were very variable in strength (COV: 66%) which may suggest non-uniformity in preparation procedures or excessive technique sensitivity for the amalgam alloy used.

A high copper dispersed phase alloy produced a weaker bond at seven days than at 10 minutes or 120 days, whereas a spherical HCSC alloy was weakest when repaired at 10 minutes (without Hg treatment) and conventional alloy samples were weakest when tested at 120 days (Hibler *et al*, 1988). On

average, the joined samples were about half as strong as the controls. In view of the considerable scatter (COV over 50% in two thirds of cases, up to 95%) these findings are considered somewhat unreliable.

Repairs using the same mix of amalgam were made in which a spacer was placed in one half of the mould, half of the sample condensed, the spacer removed and the second half of the sample condensed in the same total time taken to prepare a control (Terkla *et al*, 1961). The flexural strength of the repaired samples was 57% of the strength of the controls, which was considered to be a value no repair process was likely to exceed.

A number of authors (Berge, 1982; Gordon *et al*, 1987; Hadavi *et al*, 1992) have attributed results of repairs made after 15 minutes (or immediately after condensation: Walker and Reese, 1983) to Jørgensen and Saito (1968) but no repair of parents less than 48 hours old is reported in that work.

### **3.3 Mercury treatments**

The value of mercury treatment in clinical repairs has been questioned on theoretical grounds because excess mercury might remain in the restoration and adversely affect its properties (Walker and Reese, 1983; MacInnes *et al*, 1992). "Care must be exercised to remove all excess mercury if a strong bond is to be obtained" (Phillips, 1973). Some workers have taken deliberate steps to achieve this objective. A modified syringe was used to carry a drop of mercury which was lightly rubbed on the parent joint surface with a trapezoid condenser for 30s. Excess Hg was removed using a dry mix and discarded prior to condensation of the added amalgam mix. Mercury treatment improved bond strength for most but not all alloys repaired after 28 days but not 10 minutes. Sample strength was in the range 20% to 59.6% of that of the one-piece controls (Nettelhorst, 1977). A similar procedure was

used in the laboratory to absorb and discard excess Hg: weak joints were reported and it was concluded that mercury treatment was not warranted (Erkes *et al*, 1990). Conversely, mercury treatment was the significant factor in making a clinically acceptable repair bond (Cowan, 1983).

The set amalgam structure was unchanged by coverage with mercury expressed during condensation. Joined samples not significantly weaker than those in one-piece were produced by grinding the parent amalgam surface on carborundum paper in the presence of a drop of mercury (Jørgensen and Saito, 1968). A clinical equivalent of this procedure is inappropriate (Schaller *et al*, 1989) and would be contraindicated in clinical practice by reason of mercury hygiene considerations alone (Gainsford and Dunne, 1992). Moreover, liquid mercury is very difficult to manipulate and practical considerations of its handling properties might ensure its rejection by dentists.

Various alternative mercury treatments have been used with conflicting results. An increase in strength resulted compared to no treatment but the joints were relatively weak (Terkla *et al*, 1961; Miyata, 1972; Hornbeck *et al*, 1986). A 2:1 mercury enriched amalgam mix was swabbed against the repair surface and a slight increase in fracture toughness and diametral tensile strength reported (Bapna and Mueller, 1993). In contrast, no marked differences were found between "Jørgensen" and "dry" techniques (Forsten, 1969). No statistically significant differences were found in the observed variations in joint strength after the use of a portion with a mercury:alloy ratio of 3:1 in the added part (Hibler *et al*, 1988) and the mercury content of the repair amalgam did not influence strength (Schaller *et al*, 1989).

No reports have been found where mercury treatment led to a reduction in joint strength compared to the condensation of a normal amalgam mix only.

### 3.4 Amalgam alloy type

Conventional dental amalgam alloys have been used to produce joined samples not significantly weaker than specimens condensed in one piece (Kirk, 1962; Jørgensen and Saito, 1968). Spherical alloys and, in general, alloys exhibiting high compressive strength produced better bonds (Miyata, 1972). In contrast, there was no correlation between strength of bond and compressive or flexural strengths of the different amalgams but a correlation between plastic strain, fracture toughness and strength of bond was found (Berge, 1982).

For repairs using the parent alloy type, high copper admixed alloys produced repairs from 39% to 64% of the joined spherical particle conventional amalgam strength (Fukuba *et al*, 1977). Joined high copper admixed Dispersalloy was only 11.5% as strong as one-piece samples; conventional New True Dentalloy was 19.5% and a preamalgamated alloy ANA 68 produced the best bond which was only 51.4% of the strength of intact specimens of that brand (Berge, 1982). A slight strength improvement occurred with a preamalgamated alloy and a mercury-rich technique but the best bond was only one third of the strength of the controls (Forsten, 1969).

Strength variations resulted from joining different amalgams. Of the 23 combinations tested, the strongest were additions of conventional amalgam to spherical particle parents (78%) while second strongest (64% as strong as the controls) were high copper admixed parents (Bass, 1985). However, none of the amalgams was particularly suitable for use as a repair (Schaller *et al*, 1989) and the same alloy type should be used for repair (Hadavi *et al*, 1992). High copper amalgam should be used in the repair to optimise the chemical bonding of the two amalgams since gamma-2 phase formed at the interface when conventional amalgam was packed against fully set high copper amalgam (Wing, 1983).

### 3.5 Location of fracture in joined samples

The site of fracture for some of the strongest joined specimens has been away from the interface between new and old amalgam, showing that the joint was not the weakest part of the specimen, whereas the weaker specimens fractured at the bond (Kirk, 1962; Jørgensen and Saito, 1968). In other work, the fracture was mostly near the joint on the side of the new amalgam (Miyata, 1972) or specimens always fractured at the bond (for example, Terkla *et al*, 1961; Forsten, 1969; Berge, 1982; Hadavi *et al*, 1992). The fracture path started at the joint but later deviated from the joint even though joined samples were only 25% to 50% as strong as the controls (Bass and Wing, 1985). Samples were excluded where fracture did not occur at the joint (Brown *et al*, 1986) but those samples were abnormally weak, possibly due to bad condensation (Brown, 1994).

### 3.6 Structure of the joint

It is "probable that mercury in the fresh mix dissolves into the set amalgam and the union is achieved by the formation of intermetallic compounds as the amalgam hardens" (Kirk, 1962). Mercury diffuses into the old amalgam from the fresh mix and new crystals were produced on the old amalgam surface (Miyata, 1972). The bond between new and old amalgam probably arises as a result of a reaction between the mercury in the fresh mix and unconsumed gamma particles in the older amalgam (Walker and Reese, 1983).

The fractured surfaces of weak joined specimens were examined and areas found where little or no reaction had taken place (Kirk, 1962). In microstructural examination, areas of continuity of structure were noted across the join interface (Kirk, 1962; Wing, 1966; Jørgensen and Saito, 1968). In specimens which would have been weak, the boundary was well

defined with some areas of porosity and relatively weak gamma-2 phase apparent in the new amalgam adjacent to the join (Wing, 1966; Jørgensen and Saito, 1968) but in strong specimens it would have been impossible to identify the bond interface without prior knowledge of its location (Kirk, 1962).

The interface was revealed by using amalgams with different microstructures (a conventional alloy with distinctive Widmanstätten structures and a spherical alloy) for the two parts (Wing, 1966). The joint in Dispersalloy samples was identified only in regions of poor condensation (Peacocke *et al*, 1989).

The possibility that contamination of the surface to be bonded with saliva or oil from an air-turbine handpiece might prevent amalgamation across the bond interface was also recognised by Wing (1966). Prolonged exposure to air and salivary contamination reduced the bond strength for set amalgam (Jørgensen and Saito, 1968; Consani *et al*, 1977) and for saliva contaminated repairs at 15 minutes (Hadavi *et al*, 1992). A plane of weakness occurs across the junction: "Despite the use of techniques and amalgams which produce excellent amalgamation and eliminate voids and the gamma-2 phase at the joint interface, transverse strength of repaired amalgams is never greater than half of that of an amalgam packed in one operation" (Bass and Wing, 1985).

Autoradiographs were produced after immersion of joined specimens in radioactive solutions (Consani *et al*, 1977). There was some infiltration of solution in some zones, whereas others showed no penetration which were concluded to have produced satisfactory bonding. Scatter was not a feature in the results: the most variation between samples was in the controls (COV: 5.67%). The best bond (produced after roughening with a bur) was only about one third of the strength of the controls. This agrees with the finding of Bass and Wing (1985) that elimination of demonstrable porosity at the bond interface may not necessarily mean that the join will be strong.

Scatter in the results (and those of Kirk, 1962) was attributed to the presence of crevices at the joint surface (Berge, 1982). No evidence of penetration of dye into joined specimens after immersion in methylene blue was found but no mention of crevices was made (Kirk, 1962). Dye penetration was variable from zero to extreme (Leelawat *et al*, 1992a) at the amalgam to amalgam joints which were weak (Leelawat *et al*, 1992b).

### **3.7 Clinical repair of dental amalgam**

Amalgam repair was defined as the removal of part of an existing amalgam and preparing a "cavity" within that restoration (Barbakow *et al*, 1988). A clinical amalgam repair technique (which did not conform to this definition) was reported where an extreme condition was illustrated (Cook, 1981a; Appendix 6). After tooth cusp fracture and loss, a method of bonding a replacement cusp to an existing satisfactory amalgam filling was described. The use of dovetails or undercuts in the original amalgam was "specifically not required". The bond rarely failed so long as the described technique using conventional lathe-cut alloy and vibrated amalgam condensation was followed. Photographs of examples were shown but no long-term survival or other scientific data were presented.

With this exception, references to the clinical repair of amalgam suggest that mechanical methods of retention in the form of dovetails or undercuts should be provided in the original amalgam (for example: Kirk, 1962; Forsten, 1969; Miyata, 1972; Walker and Reese, 1983; Kidd *et al*, 1990; Gainsford and Dunne, 1992). A marginal defect may be cut out and treated as a single surface cavity, where the requirements of extension to sound margins and a caries-free amalgam-cavity interface applied but only slight undercuts were needed for retention. "Repairs of this type will last as long as the restoration, and in their economy of tissue and operative time must clearly be in the

patient's best interests" (Pickard, 1983). The repair should be made in areas of low stress (Terkla *et al*, 1961) if carried out after more than 15 minutes (Scott and Grisius, 1969) when precise mechanical retention was also required (Bagheri and Chan, 1993). Placement in low stress areas would ensure a successful restoration (MacInnes *et al*, 1992) and precise mechanical retention in the remaining amalgam is critical to the longevity of the restoration (Hadavi *et al*, 1992). However, no clinical trials of repaired amalgams have been reported (Erkes *et al*, 1990). Replacement, rather than repair, of an amalgam restoration is indicated whenever flexure forces are expected (Gordon *et al*, 1987).

An existing amalgam restoration may already be retained to the tooth by pins the placement of which can present serious risks to the pulp chamber and periodontium. Removal of such a restoration — either attempting to reuse the existing pins or replacement after drilling new pinholes — carries both risk and potential difficulty (Cook, 1981a). In such cases, the repair technique can be "particularly useful" (Kidd *et al*, 1990).

A clinical technique for the repair of amalgam was described where the repair site was prepared using a plain fissure bur in a slow speed handpiece with air spray only (Cowan, 1983). Undercuts were placed in the amalgam to provide mechanical retention. The prepared amalgam wall was vigorously rubbed with a serrated instrument and a 3:1 mercury:alloy enriched first amalgam increment. "Any undesirable excess mercury" was removed using a fresh mix of standard alloy:mercury ratio with normal condensation pressures for the completion of the restoration. As this was a clinical treatment procedure there was no assessment of the strength of joint obtained. In a single case report, a 7:5 mercury:alloy enriched first increment was used in a cusp restoration repair (Baratieri, 1992).

### 3.8 Corrosion

Apart from considerations of joint strength, the possibility of adverse effects of corrosion on the amalgam have been noted (Terkla *et al*, 1961) particularly if amalgams of differing compositions have been joined (Berge, 1982).

The electrochemical potential (with respect to saturated calomel electrode) of amalgam made from conventional alloy is -969mV whereas Dispersalloy is -549mV and 18ct Class III dental gold is +500mV (Chen and Greener, 1977). The corrosion potentials varied with time, amalgam type and electrolyte solution and all of the elements present in the amalgam were detected in solution (Moberg, 1987). The gamma-2 (tin-mercury) phase is the least noble and subject to earlier dissociation in conventional amalgam than the more noble phases. Tin ions are released (to form oxides or oxychlorides) but mercury may be absorbed by the remaining gamma phase in the amalgam with continuation of the setting reaction of amalgam and further precipitation of gamma-1 and gamma-2, which could be accompanied by expansion (termed mercuroscopic expansion by Jørgensen, 1965b). In high copper amalgams, copper is released from the surface and expansion was observed in HCA Dispersalloy in contact with conventional amalgam (Moberg and Odén, 1985b). Higher initial currents flowed in make and break than steady state conditions (Chen and Greener, 1977). Clinical symptoms ("galvanic shocks") from restorations of dissimilar metals in opposing teeth usually subside within a short time, probably due to passivation of the amalgam surface.

The maximum current density for Dispersalloy joined to conventional amalgam was five times and to itself seven times that of the next nearest group (Ravnholt and Holland, 1988). In contrast, the maximum current for Tytin joined to conventional amalgam was less than a tenth and charge transferred one seventh of the values for Dispersalloy. Maximum current values for conventional or 24% Cu HCSC amalgams were about twice those for Tytin.

From a clinical standpoint, however, no evidence of corrosion or adverse effects was noted after 16 months when bonding a high copper non-gamma-2 to conventional amalgam (Cowan, 1983). Conventional and high copper amalgams in contact in adjacent teeth were not significantly different when assessed by marginal deterioration (Osborne *et al*, 1976) although surface tarnish or pitting assessment might provide a better indicator.

Cast gold crowns repaired by amalgam showed no microleakage at the gold-amalgam interface which could result in an acceptable clinical restoration (Fitch *et al*, 1982). There was apparently little evidence of electrolytic corrosion after the repair of cast gold restorations with amalgam (Cook, 1981a). The author's unreported clinical observations of repairs to amalgam indicate that this could be an area for further investigation. The intense early corrosion current reduced with time and polished amalgam exhibited lower current (von Fraunhofer and Staheli, 1972). Destruction of microstructure was more pronounced, penetration deeper and more metals released from amalgams in contact with cast gold alloy than not (Moberg and Odén, 1985a).

The application of varnish to the prepared old amalgam cavity before repair was recommended due to the risk of corrosion (Rowe *et al*, 1989). Such a procedure is likely to produce a joint of minimal strength: samples were too weak to test after application of varnish to the parent surface prior to condensation of the added amalgam (Hadavi *et al*, 1992). Bonds with varnished parents were 6% to 10% of the one-piece strength (Leelawat *et al*, 1992b). However, after degradation of the varnish, corrosion of both amalgams might be accelerated in the oxygen-depleted gap in the same manner as occurs in the tooth-amalgam interface (Jørgensen, 1965b). Varnish should not be applied to the old amalgam as the bond between new and old amalgam was better than that from amalgam to tooth and might make a useful contribution to retention of the repair (Gainsford and Dunne, 1992).

### 3.9 Unusual preparation or test procedures

A number of authors have reported unusual preparation or test procedures. The test methods used most frequently have been three point loaded flexural tests or tensile tests with dumbbell-shaped samples. Four point loading for 12mm x 4mm x 2mm rectangular samples was reported without specification of the test rig dimensions (Brown *et al*, 1986).

Two reports have been found including a three point bend test where the joint was not placed at the central load. Stepped joints were about half as strong as butt joints when the vertical joint interface was offset in the test rig (Bass, 1985). There were two joint interfaces in each three-part sample when a central one-third part was added to set amalgam at the ends (Forsten, 1969).

Serrated and smooth mould inserts with unspecified "mechanical condensation" of the high copper admixed amalgam produced parent sample parts for joined samples in shear and flexural test modes (Gordon *et al*, 1987). The flexural test used a shaped piston in the apparatus used with a flat ended piston for the shear test so that loading was not at three or four points. Less force was required to fracture joined samples than the controls in flexural mode but in the shear test joined samples manufactured using either mould insert were not significantly weaker than the controls. Use of a serrated mould insert increased joint surface area compared to the smooth insert but improved joint strength only in flexural test mode.

Differences in shear and flexural test results were also found but the Dispersalloy amalgam to amalgam joined samples were only 21% and 13% as strong as the respective controls (Leelawat *et al*, 1992b).

Microscopic crack propagation at the junction was found after thermocycling

(Reitz and Mateer, 1966). However, thermocycling had no effect on the flexural repair strength (Erkes *et al*, 1990) but an adverse effect was found in shear test for admixed amalgam to amalgam joints but not the HCSC spherical alloy type (Hadavi *et al*, 1991).

The Knoop hardness of amalgam at the surface was less than at the centre, but there was no significant difference in hardness adjacent to the joint between the two parts of joined samples (Finkel *et al*, 1962). The influence of a set amalgam on the dimensional changes of setting was not great enough to cause the specimen to exceed A. D. A. specification limits but its effect was not reported.

Mercury penetrated into the old amalgam to a depth of 0.05mm after 1 to 4 days in joined specimens using mercury with radioactive  $Hg^{203}$  as a tracer in the second part (Ayers and Cagan, 1964).

A condition where an access cavity is repaired in an amalgam restoration ("Amalcore") such as might occur after root canal therapy was simulated (MacInnes *et al*, 1992). Repaired cylinders were tested in compression and diametral tensile modes. Mercury enrichment in the repair gave no reduction compared to the controls under compression but were reduced to 79% under diametral test where non-enriched repairs were 69% as strong as the controls. Fracture path included the repair material in significantly more mercury enriched than non-enriched samples.

Fractography after the diametral tensile test and fracture toughness test of chevron notched high copper samples containing 0.3% palladium or 1% zinc was carried out (Bapna and Mueller, 1992). The joined samples were weak in the diametral test but the crack path often deviated from the joint in the zone where the sample contacted the compression plattens.

## **Chapter 4. Experimental Equipment and Method**

This chapter considers the use of equipment and methods employed to produce and test the specimens used in this work.

The specimens were prepared for test either as “one piece” or as “two piece” where an earlier produced sample was joined to a later sample by condensing new amalgam to old.

The amalgam alloys used in this study are described in Chapter 5.

### **4.1 Amalgamators**

The amalgamators used in this study are shown in Plate 1 and the manufacturers' addresses are given in Section 5.2.1. The time for mixing (trituration time) is preset on the machine.

#### **4.1.1 The Dentomat 2 amalgamator**

This machine was generously donated for this work by Degussa Ltd. It dispenses measured volumes of alloy powder and mercury from storage hoppers into a mixing chamber. A motor causes oscillation of the mixing capsule to provide an amplitude of about 19mm. The ratio of alloy to mercury dispensed by the machine can be varied by changing the volume of powder in the measuring chamber.

The amalgamator will produce one dose (or spill) of mix by making two half turns of the dispensing control. The dispensing knob was turned quickly at a frequency of 1s for each half turn. The digital timer was set at 34s and 36s for two and three dose mixes respectively which allowed 30s for mixing after

the completion of dosing.

In operation, the first half turn of the dispensing knob releases a measure of alloy powder into the mixing chamber; simultaneously, mercury fills its measure under gravity. The return half turn of the knob releases this mercury into the mixing chamber. Alloy powder then refills its measuring chamber. It was found during the initial experiments that a larger amalgam dose was dispensed for the first dose after the Dentomat has been moved or left standing for some days. The first dose of the day was therefore discarded before preparation of batches of specimens.

A safety device prevents operation unless the mixing chamber is screwed tightly in place and it is not possible to turn the dispensing control until the motor has started.

The timer controlled the electric motor which on switching off permitted the mixing chamber to oscillate for about 10s but light finger pressure after about 4s curtailed oscillation. The mixing chamber could now be removed from the amalgamator and the amalgam mix was ready for use.

#### **4.1.2 The Silamat amalgamator**

This machine was manufactured by Vivadent and was made available for this study by courtesy of Dr J.D.R. Walker (City University). It will mix precapsulated formulations of alloy and mercury. The Silamat is regarded as a high energy machine. Shorter trituration times are required using this amalgamator than with the Dentomat which is a low-speed mixer (Jones *et al* 1986). The amalgam manufacturers give wide latitude in their recommendations for mixing times due to variations in amalgamators; however, Dr J.D.R. Walker (personal communication) provided reasonable

times for trituration under the laboratory conditions used. These times are tabled in Chapter 5. The Dentomat and Silamat amalgamators are shown in Plate 1.



**Plate 1.** The Dentomat 2 and Silamat amalgamators with the dental amalgam alloys and precapsulated materials used in this study.

#### 4.2 The test specimens

The test specimens used were either (a) one piece or (b) two piece, with approximate overall dimensions given in Figure 1. The moulds used in the preparation of samples are described in the following sections.

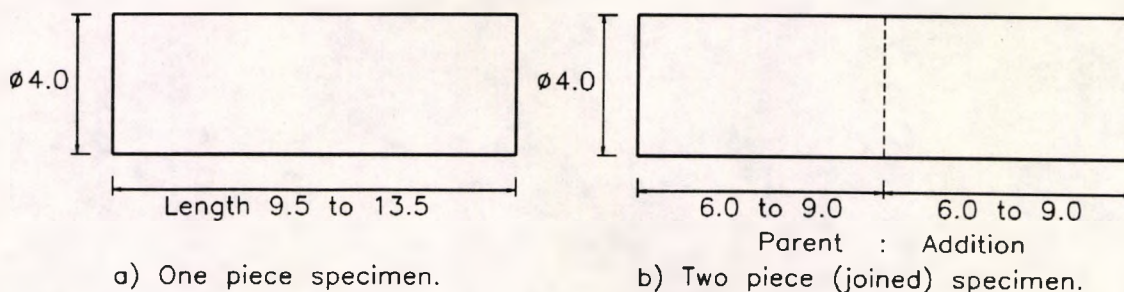


**Figure 1.** The dimensions in mm of the cylindrical test specimens.

#### **4.2.1 The moulds for test specimens**

Two moulds were manufactured for use in this study: (1) a cylindrical ejector-type mould and (2) a split mould for multiple samples.

##### **4.2.1.1 The British Standard mould**

Figure 2 and Plate 2 show the form of this mould together with the holder, pistons and spacers prescribed by BS 2938: 1985 (superseded by BS EN 21559 in 1992). BS Plunger No 1 is not shown as it is prescribed for the preparation of samples for determination of dimensional change by the use of an interferometer. After initial experimental joined samples had been attempted, the use of this mould was abandoned. The preparation of joined samples using this mould is not included.

##### **4.2.1.2 The split mould**

The split mould was manufactured from two plates of ground flat stock steel of dimensions 0.5 inch thick x 1.25 inch wide x 4.8 inch long (12.7 x 30.5 x 122.0 mm). Figure 3 shows the manufacturing details of this mould and Plate 3 shows the assembled mould with pistons and spacers. The disassembled mould is shown in Plate 19.

The two halves were bolted together using three M6 x 25mm long hexagonal headed bolts. Two 4.8 mm diameter steel pins were located at diagonally opposite corners to ensure easy reassembly of the mould. One pin was press fitted in position to one half of the mould while the other was removable to facilitate disassembly of the mould. Ten sample holes (lumens), 4.0mm in diameter and equally spaced at 9.0mm centres in groups of five, were drilled and reamed on the interface between the two steel plates.

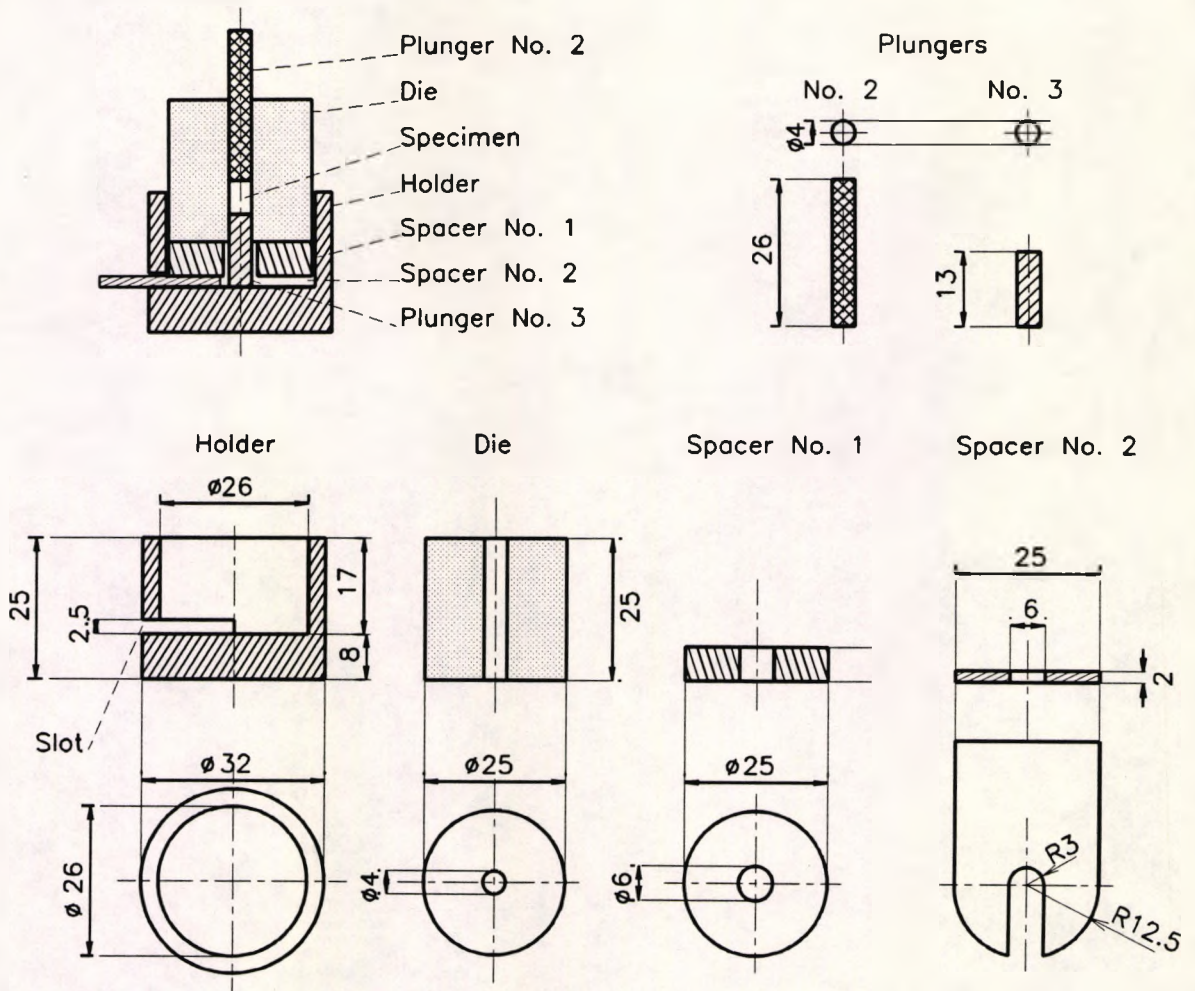


Figure 2. British Standard mould for dental amalgam specimens.

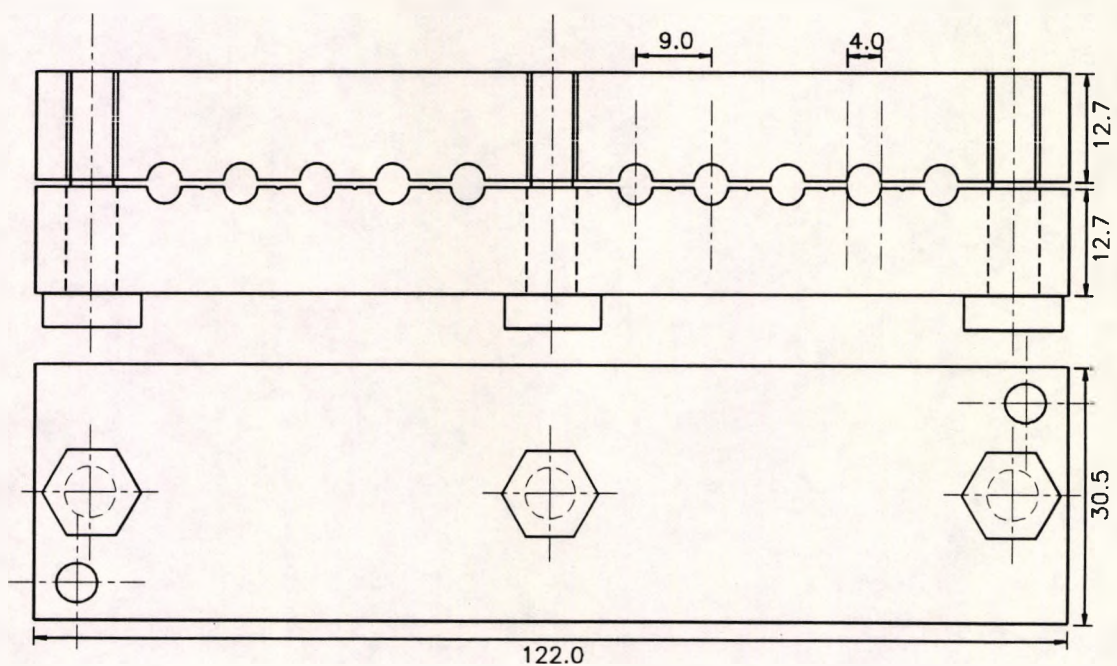


Figure 3. The Split Mould. The dimensions are in mm.

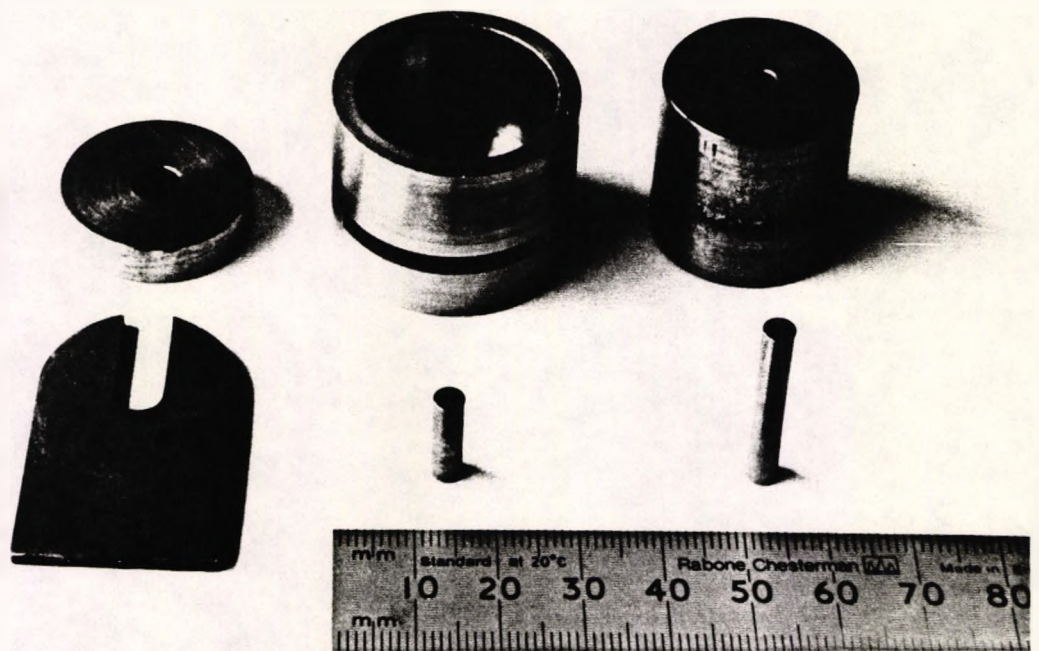


Plate 2. The British Standard mould, holder, pistons and spacers.

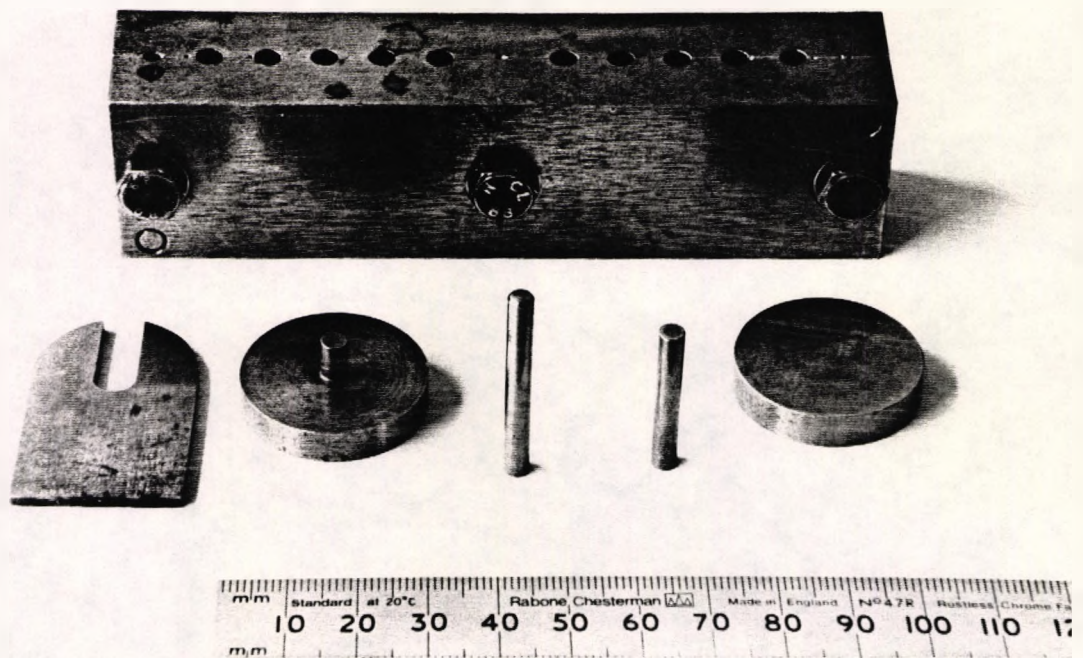


Plate 3. The split mould, pistons, support blocks and spacer.

An identification mark close to one end of the mould was used to define the "upper surface" from which amalgam was introduced into the mould. The lumen nearest that mark was identified as number 1; that furthest as number 10. Prepared amalgam samples were assigned an identification number consisting of a batch number and a decimal suffix to denote the lumen of the mould used.

Pressure relief channels (about 1mm wide x 0.5mm deep) were prepared in the full width of the mating surface of one half of the mould by grinding parallel to and between the lumens. This modification controlled mercury penetration to the adjacent lumens and was used from Batch 32 onwards.

**4.2.1.2.1 Plugs.** Soft plastic tapered plugs (adapted from golf tee pegs) were used (from Batch 32 onwards) to prevent the ingress of foreign material and contamination of adjacent samples in the mould by the mercury expressed at the upper surface of the mould. Each plug was approximately 12mm long and was inserted into the mould to a depth of about 5mm.

### **4.3 The equipment for condensation**

This section describes the equipment used to condense the amalgam mix in the mould. Two modes of condensation were employed with the application of either weights or vibration. Condensation forces were applied to pistons which compressed the amalgam mix in the mould. Special pistons were used in the manufacture of joined amalgam specimens.

### 4.3.1 Weights

Plate 4 shows the ball bearing assembly (Desoutter Die and Mould Sets, Aintree Road, Perivale, Middx.) which supported the weights; its use in this study was by courtesy of Dr J.D.R. Walker (City University). The weights were raised and lowered manually to provide a load of 39.5 pounds to the piston. When applied to a 4.0mm diameter piston, this load produced a condensation pressure of 14.0MPa.

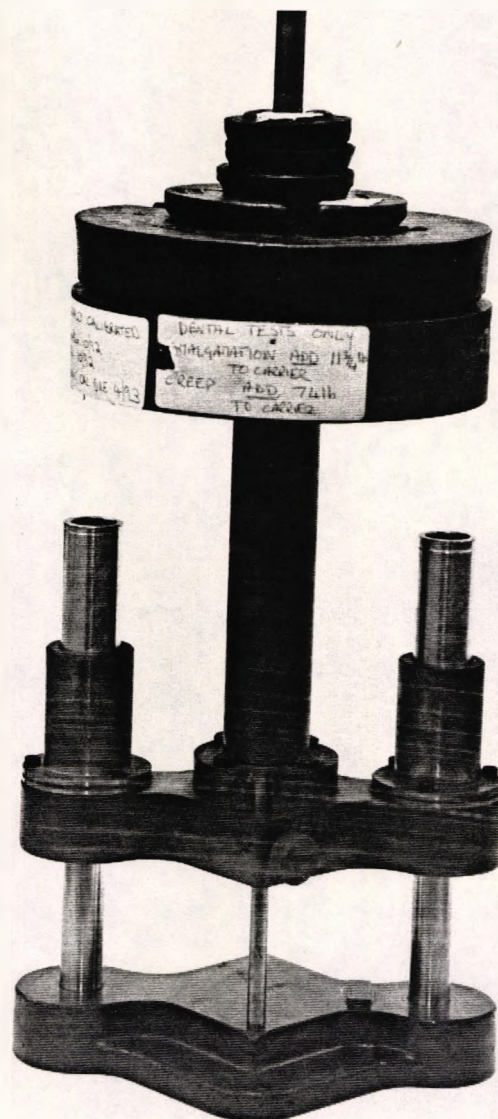
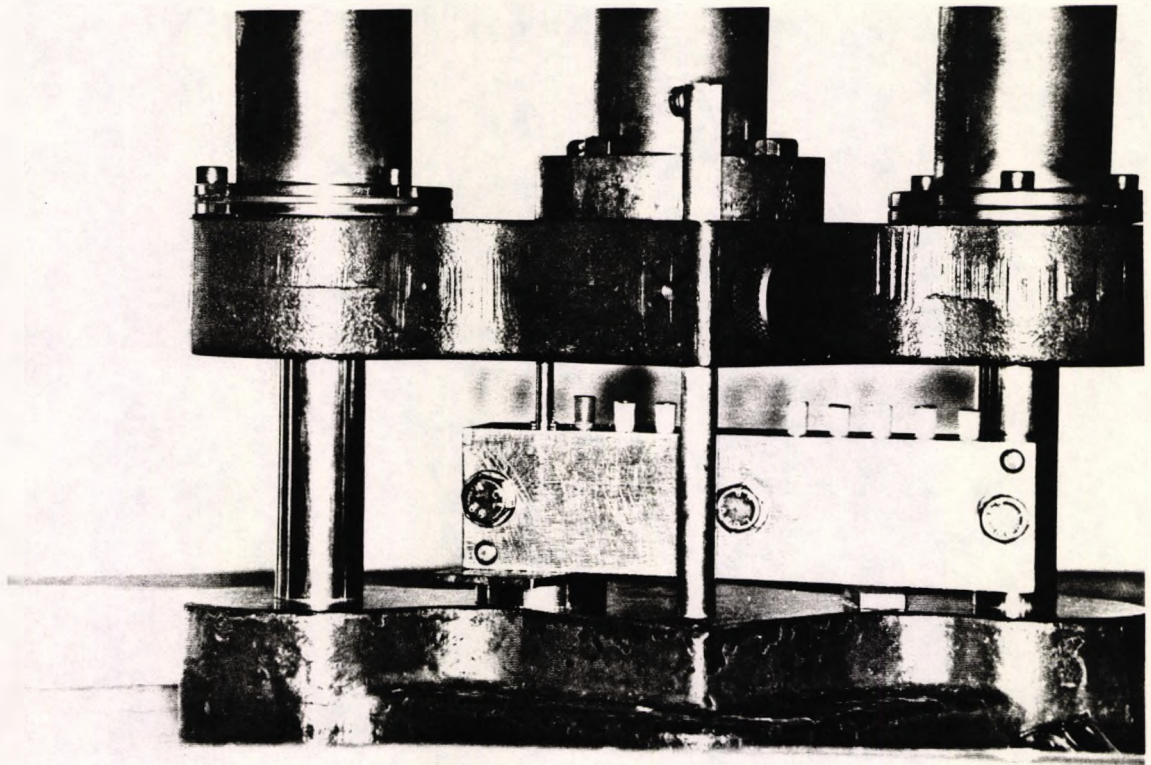
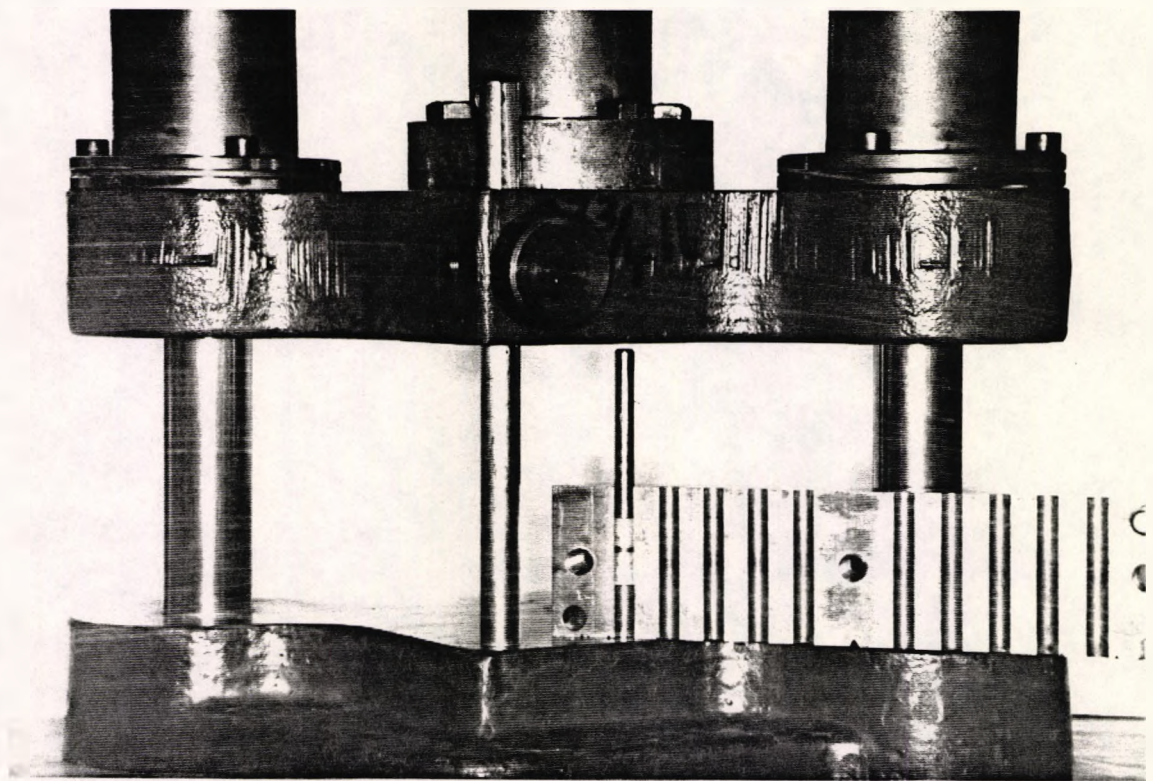


Plate 4. The Desoutter weight bearing assembly.



**Plate 5.** Condensation of amalgam in the split mould (first thrust of the two thrust deadweight method).



**Plate 6.** Pressing a joined sample from the inverted split mould.

The minimum height of the weights above the platform of the weight bearing assembly was controlled by a thumb wheel adjustment screw acting on the machined tapered channel in the 8mm diameter support rod. For the condensation procedure, the support rod was adjusted to a clearance of about 3mm from the base - see Plate 5. The manual work and time required to lift the weights during the condensation procedure was thereby minimised. One anticlockwise turn of the adjustment screw allowed the weights to fall by about 6mm. This feature was used in pressing amalgam samples out of the inverted mould by the application of force to the lower end of the parent amalgam as shown in Plate 6.

#### **4.3.2 Vibration**

Vibration assisted condensation was done with an adapted engraving tool manufactured by Burgess (Model 72, Burgess Power Tools Ltd, Capcote, Leicester). The tool chuck vibrates axially *i.e.* in and out from the body of the machine. Plate 7 shows the tool in its working position with the split mould.

In normal use, a simple split ring under a screw-fitting retaining ring in the chuck holds the chosen engraving tool. Engraving tools are fitted to a shank of 5.5mm diameter - see Plate 8.

The chuck was modified for holding a piston of 4.0mm diameter by using polyolefine heat-shrinkable electrical sleeving to replace the split ring. The modification permitted rapid change of pistons which could also then be rotated in the chuck. Friction created by the sleeve held the piston in place during operation, but only light finger pressure on the piston's cross bar was required to enable rotation along the long axis. A firm finger pull combined with rotation removed the piston from the chuck leaving the polyolefine sleeving in place. Changing of pistons could be completed in 3 to 4 seconds

without unscrewing the retaining ring. The modified chuck is shown in Plate 9.

The vibration amplitude was 0.8mm under no-load conditions at the minimum amplitude setting used for all specimen preparations. The on-off speed switch was used in position 1 for this work. The frequency of vibration was 50Hz and a foot switch controlled the on-off operation as shown in Plate 7.

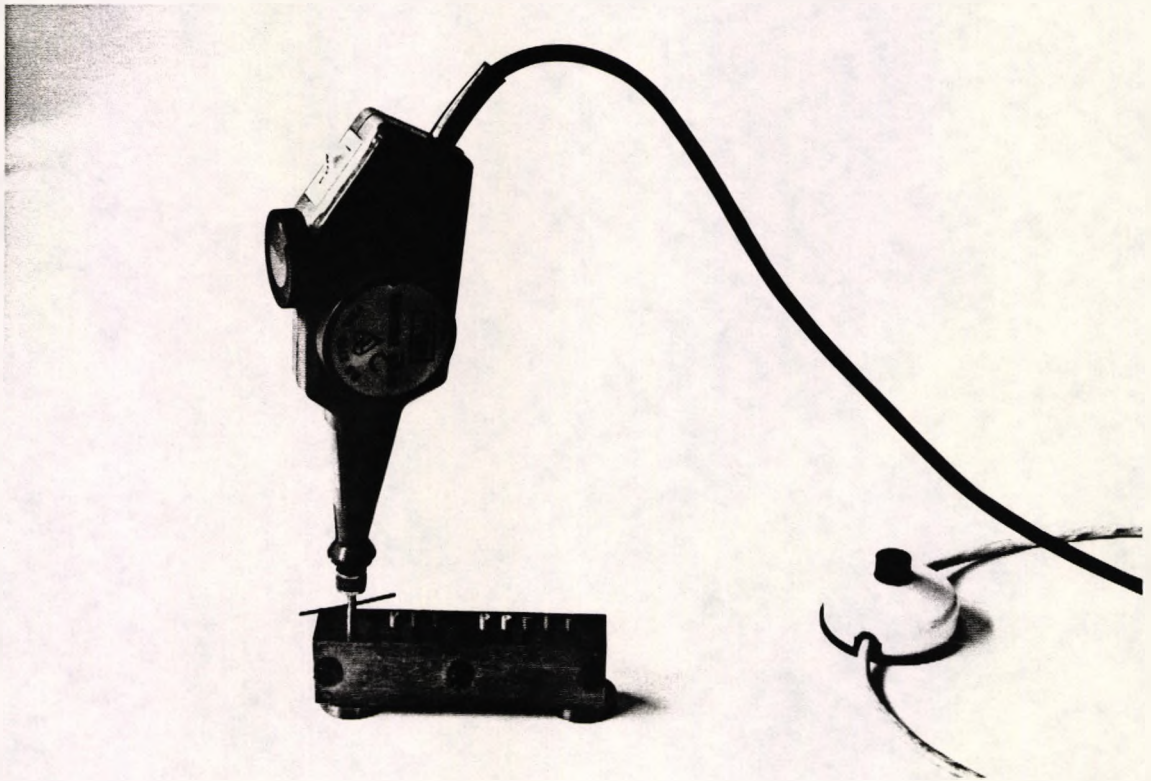


**Plate 7.** The Burgess vibration tool in place in the split mould.

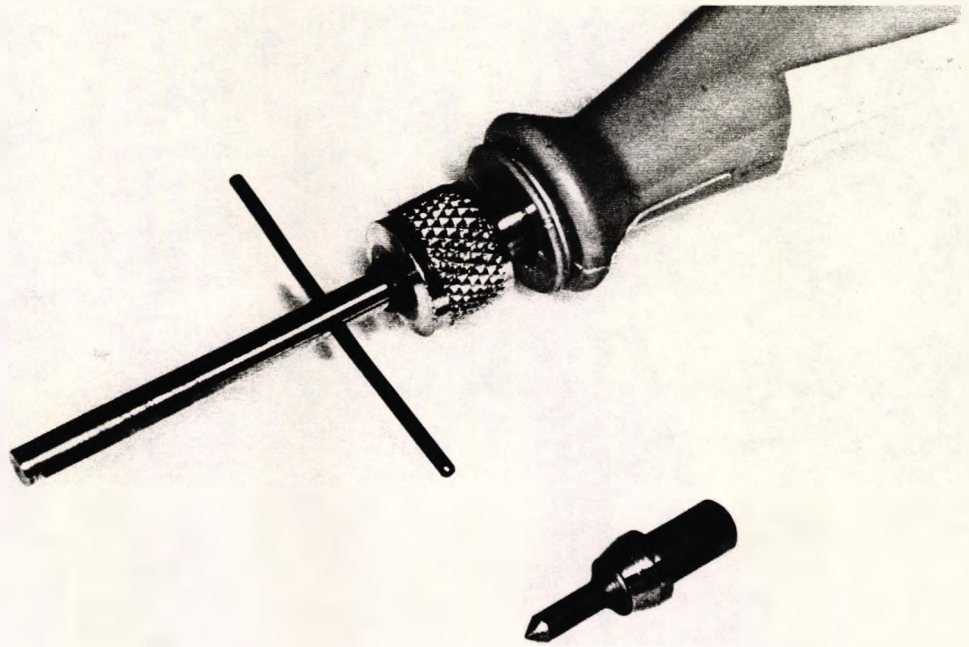


**Plate 8.** The Burgess engraving tool fitted with a flat ended piston. A standard engraving point with the split retaining ring is inset.

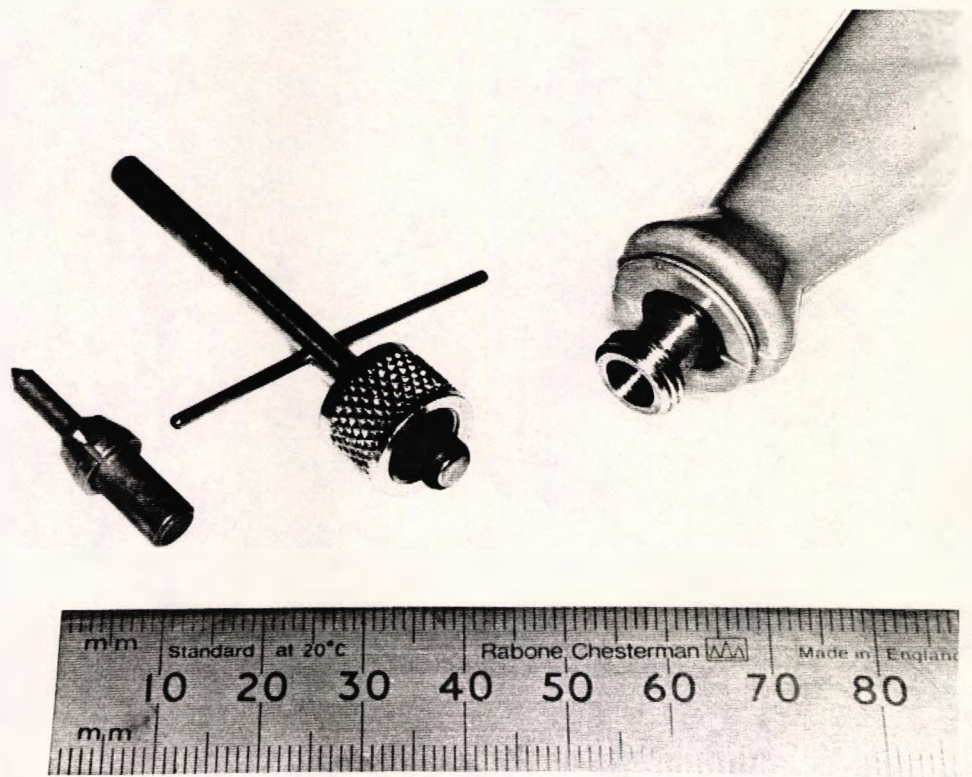


**Plate 9.** The disassembled modified chuck of the Burgess engraving tool.

### **4.3.3 Pistons**

Load was applied to the amalgam via close fitting silver steel pistons which confined the amalgam mix within the mould. Pistons were applied to both the upper and lower ends of the mould lumen.

#### **4.3.3.1 Lower piston**

A combined short piston 6.25mm long x 4.00mm diameter and support block 5.85mm thick x 28.5mm diameter was used as the bottom piston in the mould. An additional support block 5.85mm thick x 28.5mm diameter balanced the split mould except when using lumens 5 and 6. A spacer of thickness 2.0mm conforming to BS spacer No. 2 was used during condensation of amalgam by the deadweight method. These are shown in Figure 4 and Plate 3.

#### **4.3.3.2 Upper pistons for use with the weights**

These pistons are shown in Plate 3 together with the lower piston, split mould, support block and BS Spacer No 2.

**4.3.3.2.1 B.S. piston.** One piston similar to BS plunger No 2 25.5mm long x 4.00mm diameter was used for the preparation of samples where the deadweight method was used up to Batch 108.

**4.3.3.2.2 Bevelled piston.** From Batch 109 onwards, a longer piston (33.7mm) was used. One end of the long piston was machined flat, normal to the long axis of the piston. The opposite end was bevelled. This piston is identified as the bevelled piston. The load was applied from the weight bearing assembly to the bevelled end of this piston. Only the prepared flat

end of the piston made contact with amalgam. The bevelled piston is shown in place in the split mould in Figure 4.

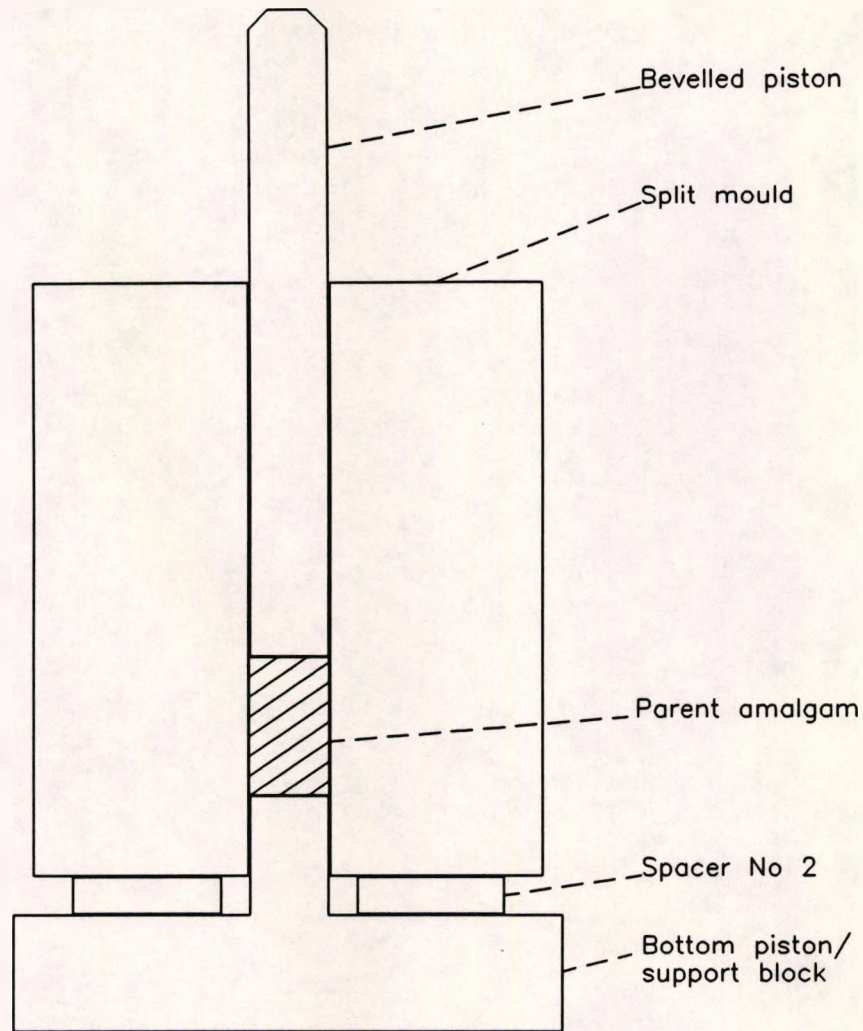


**Figure 4.** The split mould, bevelled piston and BS spacer No 2.

#### **4.3.3.3 Pistons used for vibrational condensation of amalgam**

Pistons using condensation tips with several experimental shapes were manufactured from 4.00mm diameter silver steel for use with the engraving tool. The tips of these pistons are shown in Plate 10. Each piston was drilled to take a 1/16th inch cross bar at approximately 22mm from the chuck end. The overall length of the old flat, RI and SRI pistons was about 48mm. However, in the later stages of the study, longer pistons were found to be more convenient in use. The lengths of the new flat, cut cone, dome and

paddle pistons ranged from 57 to 66mm. The force from the engraving tool was applied from the top of the mould through the piston to the amalgam being condensed.

**4.3.3.3.1 Flat ended pistons.** A flat ended piston was manufactured and after about 120 minutes of operation wear was noted around the tip of the piston. This piston was therefore termed "old flat". A new piston was manufactured and was termed "new flat". In the course of time at the end of this study, the "new flat" piston had also become worn. These pistons are shown in Plate 10; for comparison, a "brand new" flat ended piston is included in the plate.

**4.3.3.3.2 Shaped ended pistons.** These pistons were shaped as modified truncated cones identified as (1) cut cone and (2) dome. These are also shown in Plate 10.

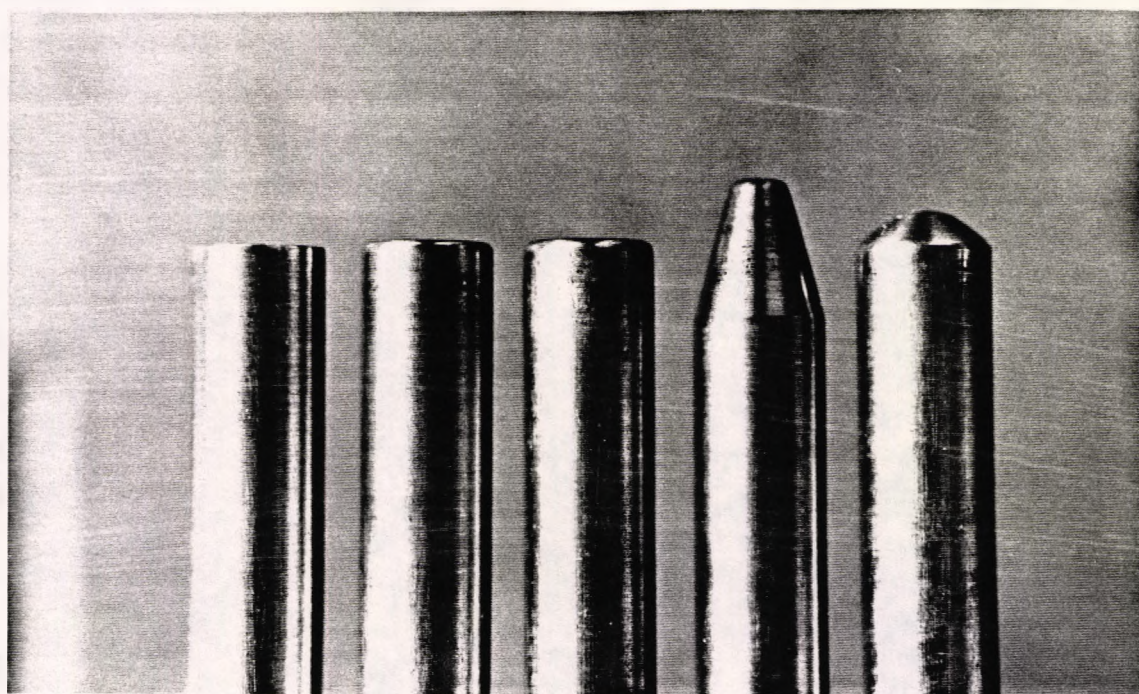


**Plate 10.** The pistons used for vibrational condensation of amalgam. From left to right: "brand new" flat; new flat; old flat; cut cone; dome.

#### **4.3.3.4 Pistons used for condensation of amalgam at the joint**

Special pistons having shaped tips were used for the condensation of the first increment of the addition part of joined specimens. These pistons are described below and are shown in Plates 11 and 12. The second and subsequent increments of the joined specimens were condensed using the pistons described in Section 4.3.3.3 above.

**4.3.3.4.1 RI piston.** The end of this piston is tent or wedge shaped having two flat surfaces at 60° to the long axis; it is identified as the RI (“rubbing-in”) piston.

**4.3.3.4.2 SRI piston.** This piston has a “comma” shaped curved blade at the end; it is identified as the SRI (“spiral rubbing-in”) piston.

**4.3.3.4.3 Paddle piston.** This important device was intended to cause close adaptation of the addition amalgam mix to the prepared surface of “parent” without causing removal of mercury from the mix. This piston, termed the “paddle”, is shown in Plate 13. The construction details are shown in Figure 5. The weight of the engraving tool was supported via four rubber O-rings which formed a resilient mounting between the shaft of the piston and the upper surface of the split mould. The working end of the condensing piston was machined to form a blade, where the volume of space adjacent to the blade exceeded the likely volume of a one quarter division of a mix. The blade of the device is offset from the rod centre.

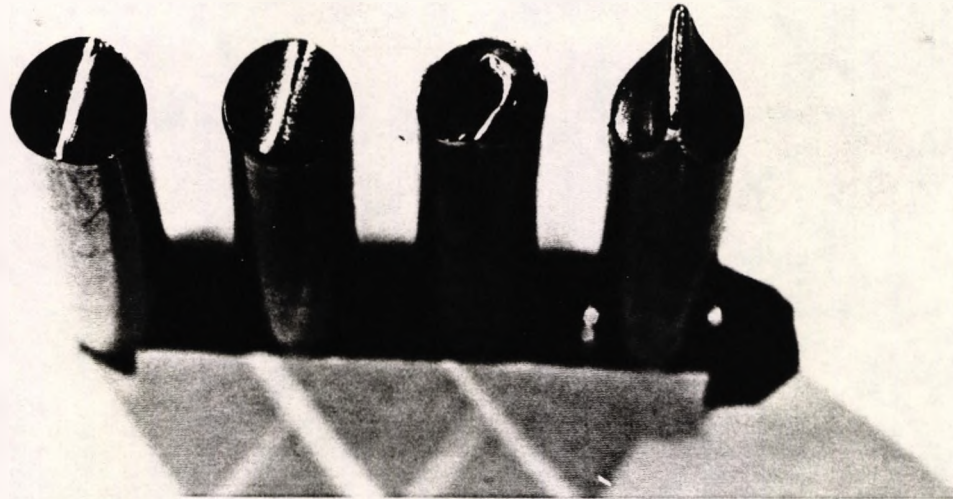


**Plate 11.** End views of the pistons used for condensation of amalgam at the joint. From left to right: "brand new" RI; used RI; SRI; Paddle piston.



**Plate 12.** Side views of the shaped condensation pistons.

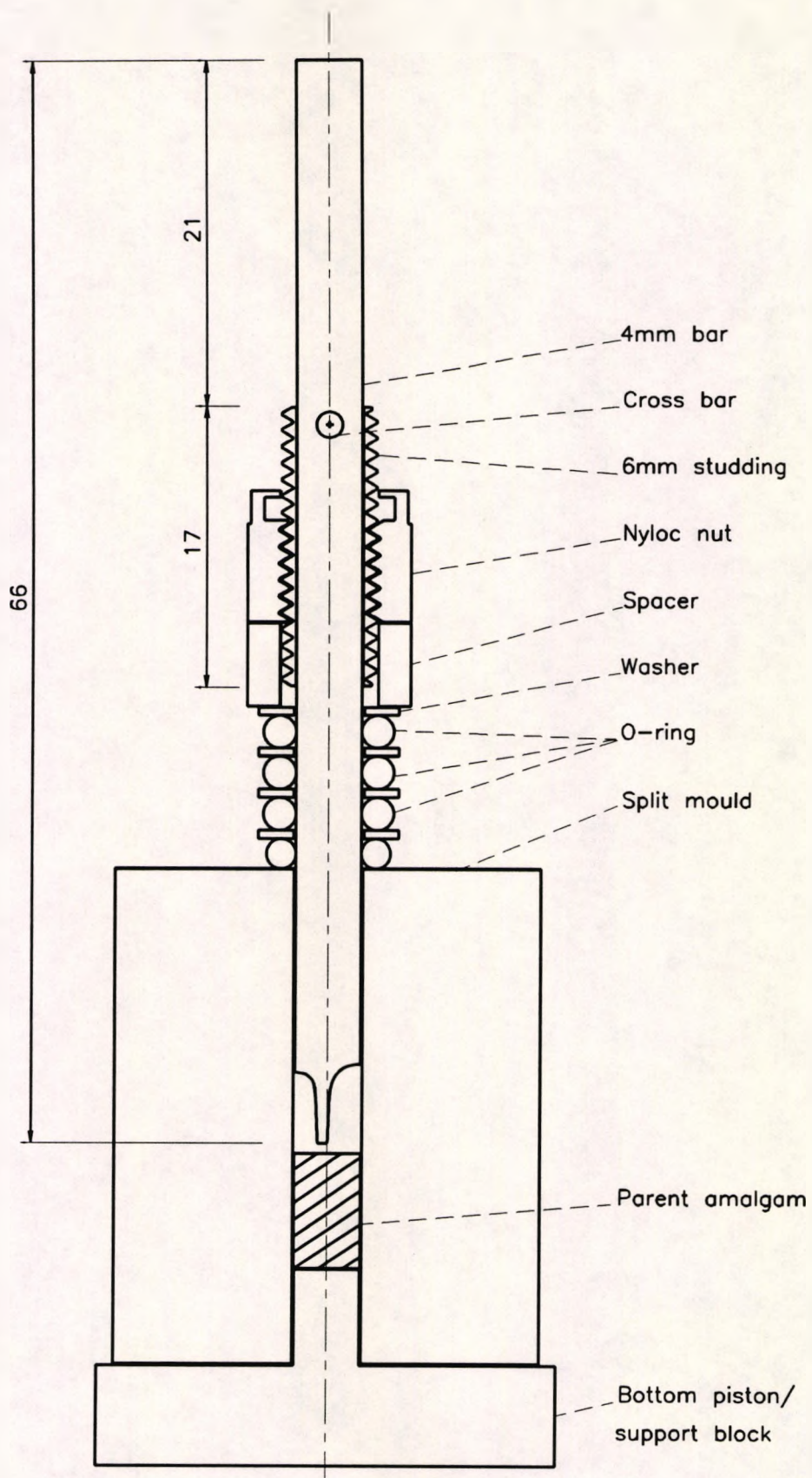


**Figure 5.** Diagram of the paddle condensation piston with the split mould ready for condensation of the addition amalgam to the parent amalgam which is in place in the mould. The dimensions are in mm.

An adjustment mechanism controls the depth of the blade within the mould. A 17mm length of M6 threaded studding was drilled longitudinally to a diameter of 4.0mm. This was fixed in position by the cross bar acting through a single drilled hole in the studding. A Nyloc self locking nut allowed adjustment by hand without tools; a M6 hex nut was drilled to make a spacer and steel washers separated the rubber O-rings. Three O-rings were of 4mm internal diameter; the fourth O-ring was 3mm internal diameter which ensured that the components of the support mechanism were kept in position on the shaft of the piston.

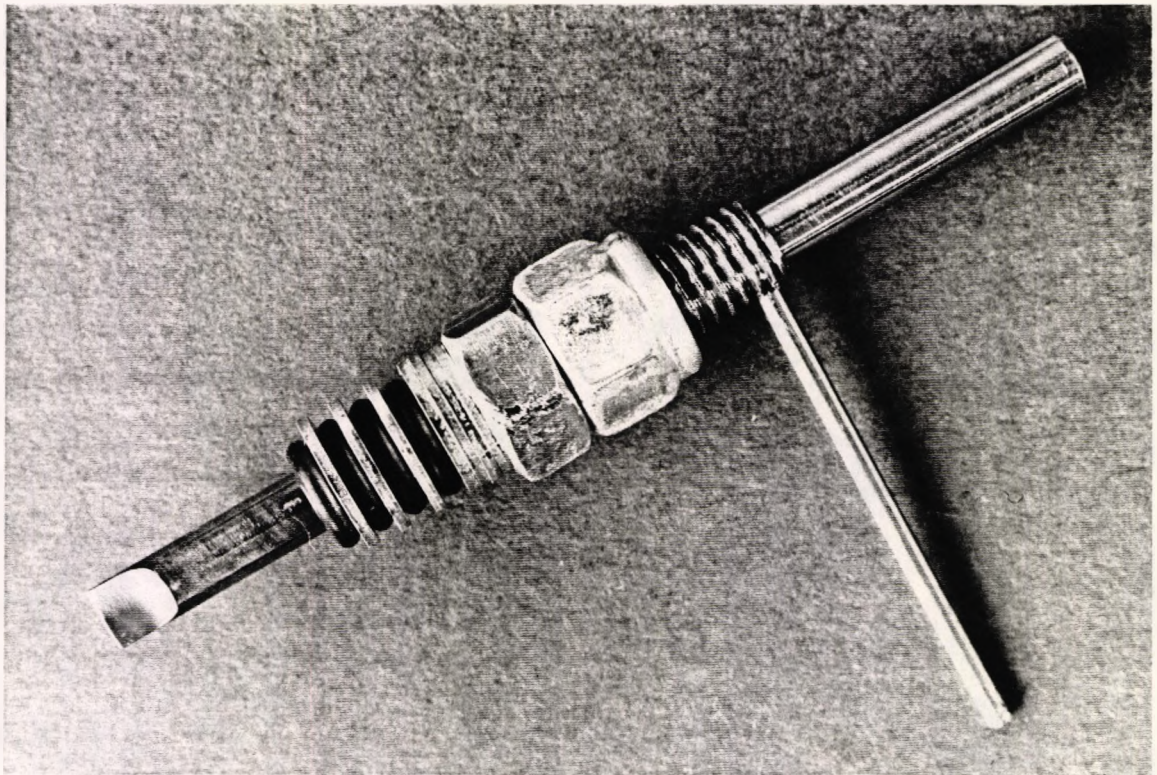


**Plate 13.** The "paddle" piston with depth adjustment mechanism.

#### **4.4 Procedures for the Preparation of Test Samples**

The preparation of one-piece and two-piece (joined) samples is considered in the following sections.

British, European and American standards for dental amalgam (BS 2938: 1985, EN 21559: 1991 and ADA Specification No 1: 1977) prescribe the use of all-mechanical methods for the preparation of test specimens for determination of creep, dimensional change and compressive strength.

Two amalgam condensation procedures were adopted in this study: one based on BS 2938: 1985 and an experimental method using vibration. BS EN 21559: 1992 became available after most of the work had been completed.

The amalgam mix was confined in the mould by pistons. The condensation procedure removed excess mercury from the mix so that mercury emerged from the lumen ends and from the pressure relief channels while some liquid mercury exuded into the space between the two halves of the mould or remained as droplets adhering to the surface of the lumen.

The variables tested included use of flat ended and specially shaped pistons for vibrated condensation, its duration and the size of amalgam increment or mix. The height setting and number of turns applied to the paddle piston were also considered. Inverted or non-inverted parent orientations were used.

##### **4.4.0.1 The quantity of mix used**

One-piece test specimens were condensed from mixes of 3 doses from the Dentomat which were divided into 6 portions when vibrational condensation was used. "Parent" and "addition" parts of joined specimens were condensed from mixes of 2 Dentomat doses or 2-spill sized capsules which were divided into 4 portions for vibrational condensation.

#### 4.4.1 Condensation procedure: deadweight method

The method used the time schedule prescribed in BS 2938: 1985 for the preparation of laboratory test specimens (Table 4).

The mould was prepared with the lower piston support block and BS spacer No 2 in place. A mix of amalgam was fed into the mould and the upper piston was inserted. A load of 39.5 pounds was applied to the piston for the duration of 15s starting 30s after completion of trituration. The spacer was removed after the first thrust and the lower piston/support block repositioned. The load was reapplied for 40s. No mercury was expressed from the amalgamated mass before application of the load.

Procedure	Time s
End of amalgamation	00
Place amalgamated mass in mould and apply 14MPa pressure	30
Release load; remove spacer; reposition lower piston/amalgam	45
Replace load	50
Release load	90

**Table 4.** Schedule for condensation of amalgam by the two thrust deadweight method.

On completion of condensation of a sample, excess mercury was brushed away from the exterior of the mould. A tapered plastic plug was placed in the lumen to prevent the ingress of mercury expressed during the preparation of subsequent specimens.

The split mould was opened at least 30 minutes after completion of the condensation of sample No 10, *i.e.* up to 90 minutes after the preparation of sample No 1. Each specimen was identified on the selected end surface according to the batch number and lumen of the mould. Samples were then removed from the split mould.

#### **4.4.2 Condensation procedure: vibration assisted methods**

This section considers condensation of “one-piece” (3-dose) test specimens and the “parent” parts (2-dose) of joined samples. The condensation method used experimental vibrational techniques developed during the study which were applied to the amalgam mix divided into portions.

##### **4.4.2.1 Manipulation and division of amalgam mix**

When vibration was used for condensation, as yet unused portions of the amalgam mix tended to move from the upper surface of the mould to the preparation tray. A stainless steel indoor gardening tool, known as the *Widger*, (manufacturer’s address not known) was adapted for use in this study and is shown in Plate 14. The modification reduced the radius of curvature of the smaller end and formed a lip at the end which assisted in the control of movement of increments of amalgam mix. The *Widger* was gripped in the jaws of a floor mounted laboratory stand and its smaller end was positioned directly above the lumen of the split mould.

The fresh amalgam mix was placed on the *Widger* near the broad end. It was divided into approximately equal portions using a Swann Morton No. 21 scalpel blade held in a No. 4 handle. As required, each increment of amalgam mix was moved using a condensation piston along the *Widger* towards the modified end and from there into the mould. The mix was therefore isolated from vibration and waste mercury at the upper surface of the mould.

##### **4.4.2.2 Condensation of one-piece specimens using vibration**

The schedule for the condensation of a divided amalgam mix in the manufacture of one-piece or the parent parts of samples is shown in Table 5.

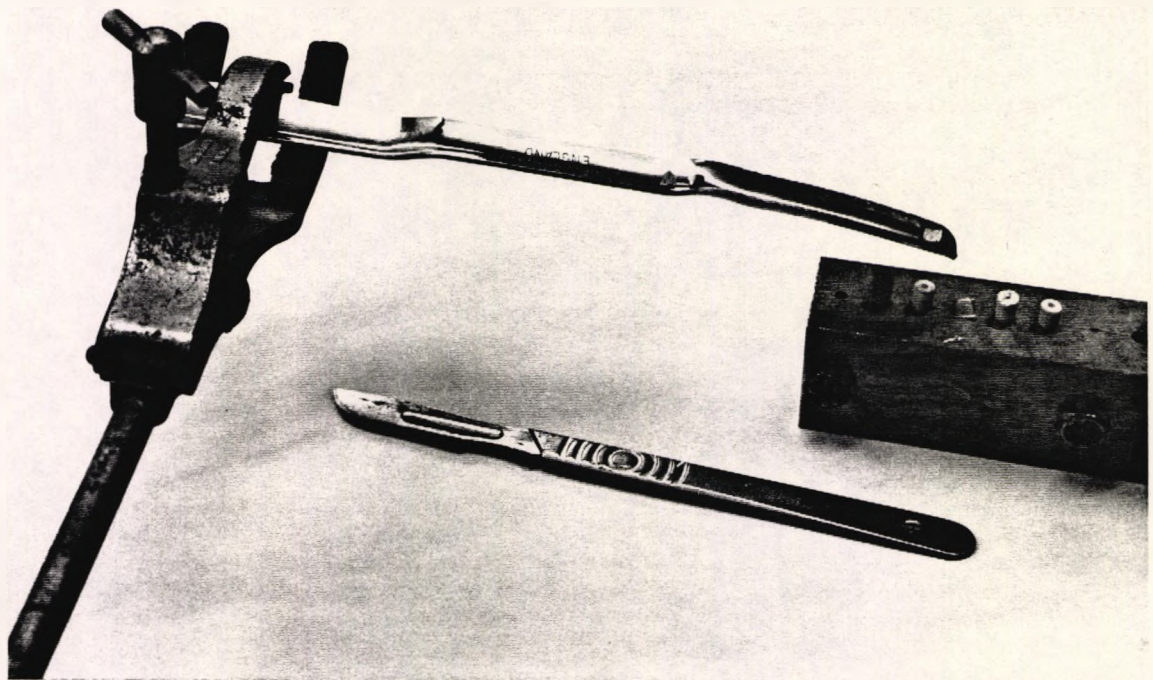


Plate 14. The mix was divided on the Widger and fed into the split mould.

Procedure	Time s
End of amalgamation	00
Place amalgamated mass on Widger and divide into portions. Introduce one portion into mould; insert piston into mould.	
Apply vibration for specified experimental time period	37
Withdraw piston; insert second increment of amalgam mix	
Apply vibration for specified time	+10
Repeat for third and subsequent increments of amalgam mix	

Table 5. Schedule for vibrational condensation of one piece samples and the parent parts of samples to be joined.

#### 4.4.2.3 Condensation when using "cut-cone" or "dome" pistons

All increments of the divided mix were condensed using the shaped piston. The upper end surface of the condensed amalgam was therefore indented by the piston. In order to give the amalgam specimen a flat end, the condensed material was fragmented using the "spoon" end of a Le Cron dental carving instrument (Catalogue no: 62004012, Ash Instrument Division, Dentsply Ltd,

9 Madleaze Estate, Bristol Road, Gloucester GL1 5SG). The loosened amalgam was recondensed using vibration with a flat ended piston for 2s.

#### **4.4.3 Manufacture of two-piece specimens**

Joined samples were prepared by the condensation of new amalgam to the end of a cylinder of 7 day old set amalgam. The selected end of the "parent" amalgam specimen was marked to identify the joint interface and the end surface was prepared using a sandpaper disc. The specimen was replaced in the split mould. The "addition" part of the specimen was condensed by application of vibration to the divided mix. Special and/or flat end pistons were used for the condensation of the first increment of the mix.

##### **4.4.3.1 Marking of the joint interface**

The location of the joint interface was defined on the parent amalgam by marking the amalgam cylinder surface in a band about 2mm wide using Staedtler Lumocolor 317 Medium Blue permanent overhead projection pens prior to the end preparation.

##### **4.4.3.2 End preparation of parent amalgam for joining**

The preparation of the end surface of the parent amalgam for joining is shown in Plate 15. The selected amalgam cylinder was gripped in the chuck of a hand held low voltage electric drill run at its slowest speed (Buffalo Model No: 0526 with variable speed transformer Model MB 0730; Minicraft, Black and Decker, Cannon Lane, Maidenhead, Berks SL6 3PD). According to the manufacturer's specification the speed was 1,000 r.p.m.

The end surface amalgam was trimmed using a new 7/8 inch medium grit sandpaper disc (Kemdent, Associated Dental Products Ltd, Kemdent Works, Purton, Swindon, SN5 9HT) mounted on a screw mandrel in a dental laboratory handpiece at about 6,000 r.p.m. The disc was applied to the amalgam for 1 to 2 seconds over a laboratory dust extraction unit. The pattern of scratches formed depended on the direction of movement of the edge of the sandpaper disc relative to the amalgam cylinder. The typical pattern of radial score marks is shown in Plate 16. In a limited number of experiments, an end preparation procedure producing circular or "gramophone groove" scratch marks was used.

The depth of the drill chuck was controlled by an adjustment screw device such that the length of amalgam sample gripped by the jaws was 4mm. The disassembled chuck is shown in Plate 17.

Generally, the "upper" end surface of parent amalgam samples (*i.e.* the surface condensed in the mould adjacent to the moving piston) was prepared for joining so that samples were replaced in the mould in the longitudinal orientation used for condensation. However, inversion of the parent amalgam was considered as a variable in some experiments: the "lower" end surface was prepared in these cases.

#### **4.4.3.3 Measurement for location in 3 point bend**

Any flash formed at the end of the specimen between the piston and mould was removed. Sample length was recorded using a screw micrometer before and after end preparation. The micrometer ball attachment was applied to the centre of the prepared surface as shown in Plate 18. The ball attachment was generously supplied free of charge by Draper Tools Ltd, Hursley Road, Chandlers Ford, Eastleigh, Hampshire, SO5 5YF.

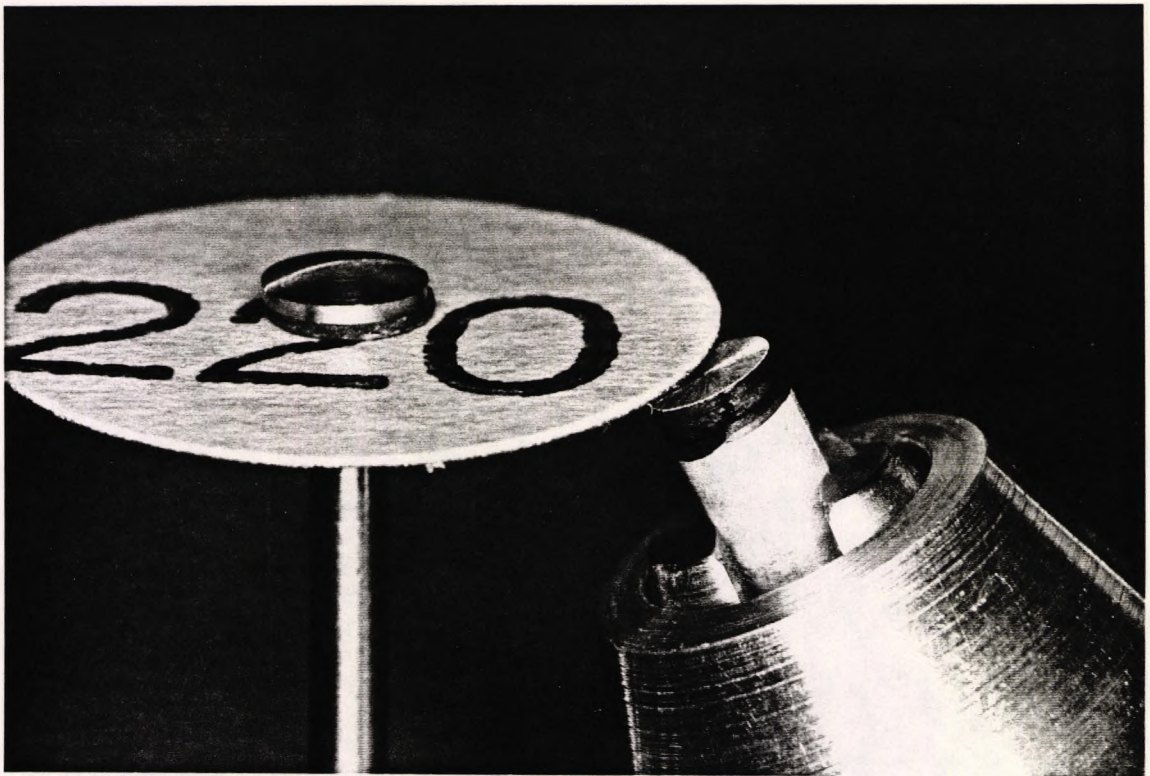


Plate 15. End preparation of the parent amalgam sample.

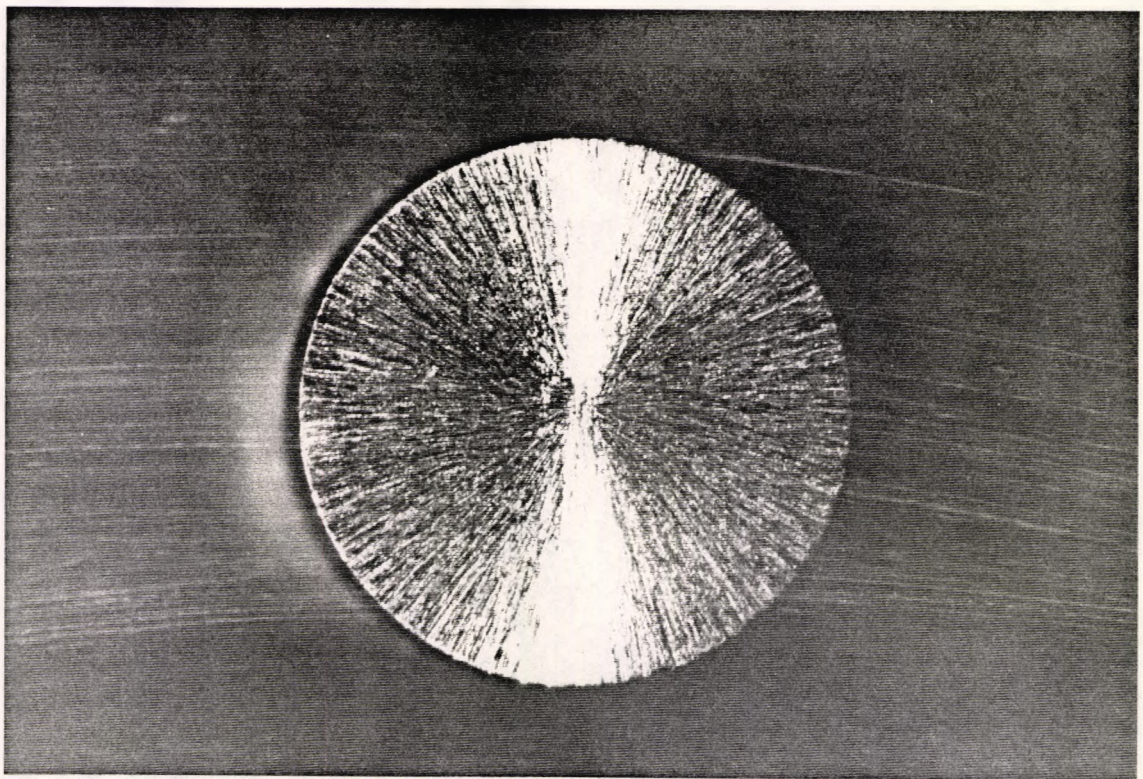
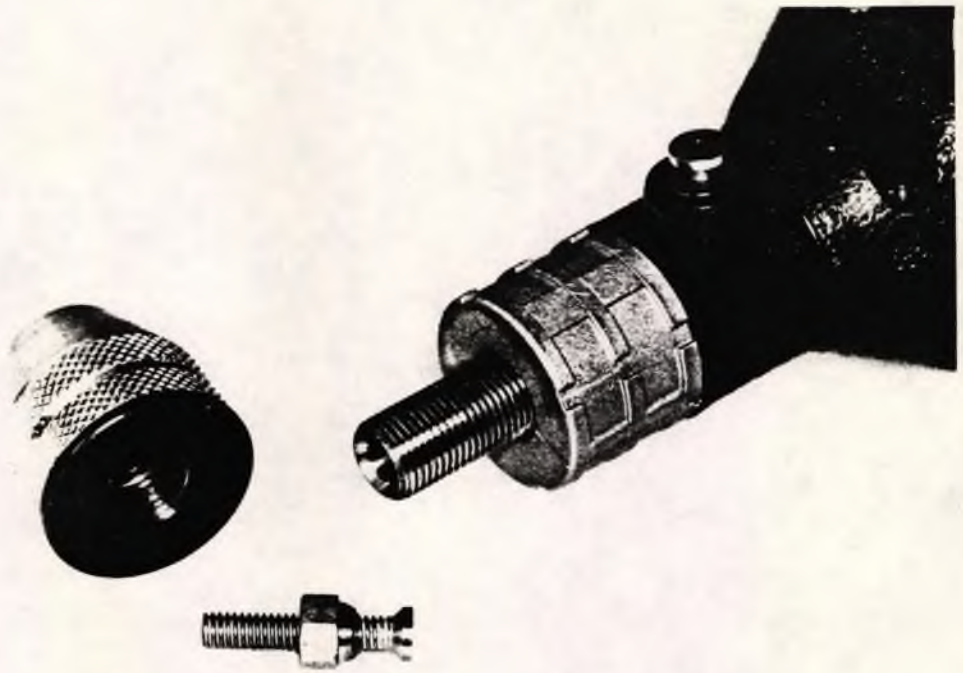
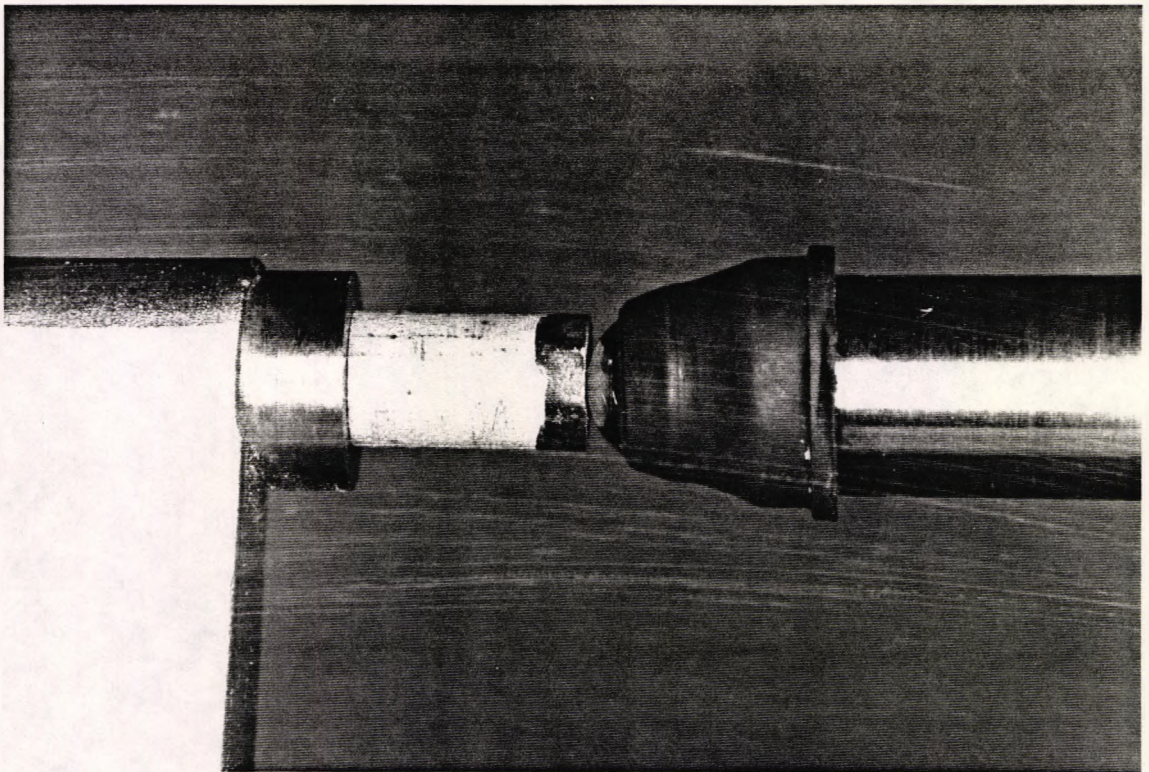


Plate 16. Radial score marks in the end-prepared parent amalgam.



**Plate 17.** The disassembled drill chuck used in end preparation.



**Plate 18.** Measurement of the sample using ball attachment micrometer.

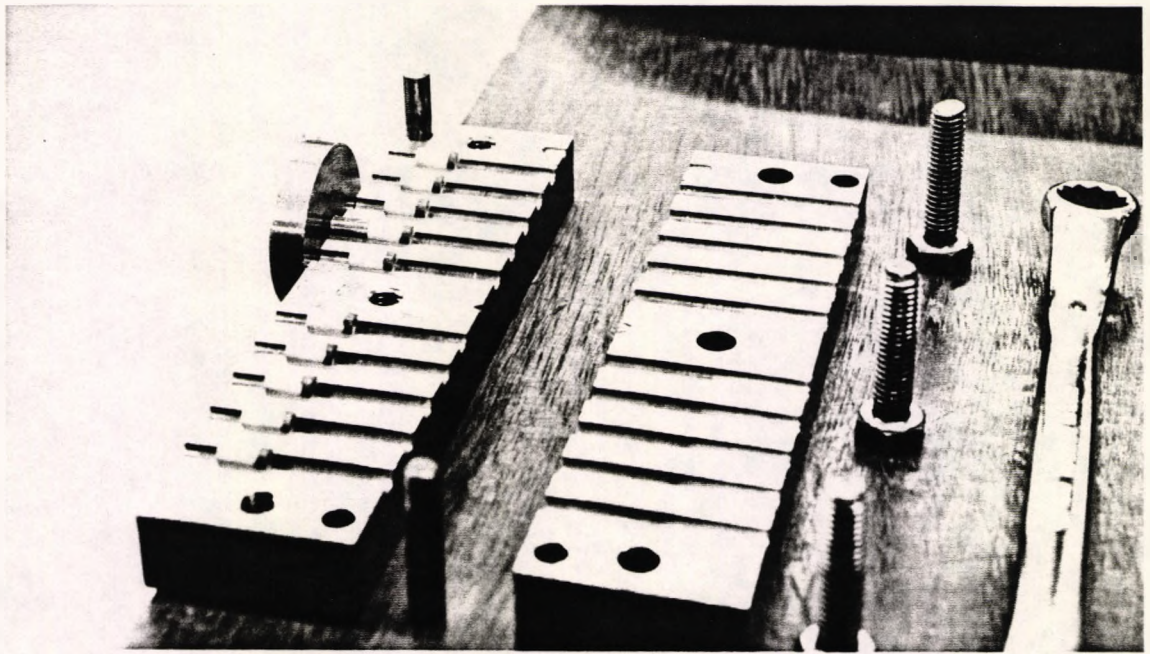


Plate 19. Placement of parent amalgam samples in the split mould.

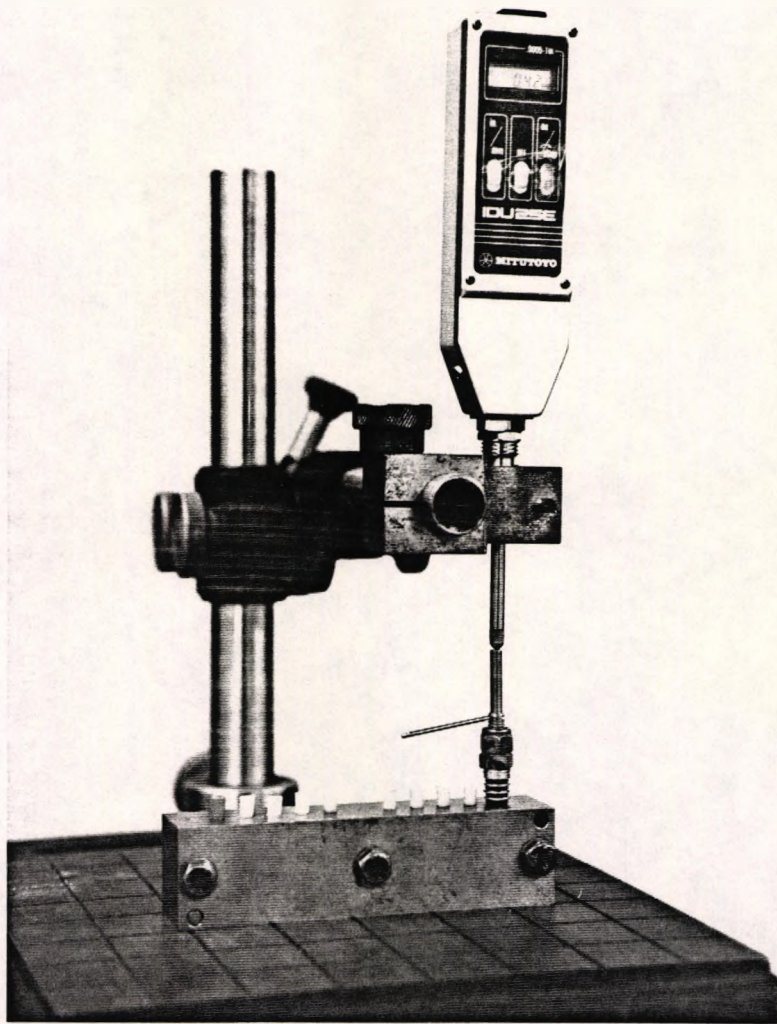


Plate 20. Adjustment of the depth of the "paddle".

#### **4.4.3.4 Placement of parent amalgam samples in mould for joining**

End-prepared parent samples were replaced in the same lumens in the split mould as used for condensation. Plate 19 shows the bottom piston/support block in use to locate each sample before reassembly of the mould. Tapered plastic plugs were placed in the upper aperture of each lumen to protect the prepared amalgam surfaces from contamination by foreign material.

#### **4.4.3.5 Condensation of the addition part of joined amalgam**

The addition part of joined specimens was condensed from a 2-spill amalgam mix divided into four portions. Vibration assisted condensation was carried out using the condensation pistons described in Section 4.3.3. The condensation time for each increment was the subject of experimental variation. The RI, SRI or "paddle" pistons were rotated by hand during application of vibration.

When the RI piston was used for condensation of the first increment of an addition, the second increment was condensed directly onto the indented surface of the first increment using a flat ended piston.

When the SRI piston or paddle was used in the condensation of additions, vibration was applied to the first increment of the mix for the specified time. The special piston was then exchanged for a flat ended piston and the application of vibration was repeated for 2s. The second and subsequent increments were then introduced into the mould and condensed.

Procedure	Time s
End of amalgamation	00
Place amalgamated mass on Widger and divide into portions. Introduce one portion into mould; insert paddle into mould.	
Apply 6 rotations of paddle under vibration in less than 10s	37
Remove paddle; replace with flat ended piston	47
Apply vibration for 2s	57
Insert second increment of amalgam mix	+2
Condense second increment of amalgam mix for 2s	+10
Repeat for third and fourth increments of amalgam mix	
Condensation completed	95

**Table 6.** The Standard Paddle Procedure: schedule for vibrational condensation of the addition part of joined samples using the “paddle”.

#### 4.4.3.6 Adjustment of the depth of the “paddle”

Adjustment of the depth of the “paddle” was carried out before condensation of the addition part of each joined sample. The paddle ended piston was inserted into the mould, placed on a measuring table and a digital dial gauge applied to the chuck end of the piston, as shown in Plate 20. Hand pressure was applied to the piston causing compression of the rubber O-rings. When the blade made contact with the prepared surface of the parent amalgam the dial gauge was zeroed. The piston was released and light lateral finger pressure was applied to the cross bar to ensure free movement of the piston within the mould. Movement of the piston continued for about 10s. The Nyloc nut was adjusted to allow movement of 0.60mm between the steady state released position and that of contact with the parent amalgam.

#### 4.4.4 Notes on specimen preparation

##### 4.4.4.1 Temperature of preparation, storage and test

All test specimens were prepared and tested at a laboratory temperature of  $23^{\circ}\text{C} \pm 2^{\circ}\text{C}$ . Between condensation and testing, specimens were stored in

an oven at  $37^{\circ}\text{C} \pm 1^{\circ}\text{C}$ . At least 30 minutes was allowed for equilibration of the samples to room temperature before the test.

#### **4.4.4.2 Timing**

Trituration time was controlled by the timer on the amalgamator. Subsequent times relevant to sample condensation were taken from the end of mechanical amalgamation using a stop watch recording at 1s intervals.

#### **4.4.4.3 Storage of specimens prior to test**

After removal from the mould, samples were placed on foam plastic channels (adapted from pipe insulation sleeving) in a polythene box for storage pending further preparation or test.

#### **4.4.4.4 Photography after fracture**

After fracture, samples were placed on grooves cut into mounting board for photographic records of batches. Samples from lumens 1 to 5 occupied the left column and 6 to 10 the right column in numerical order with samples 1 and 6 at the top. Where applicable, the force to fracture values in Newtons are presented adjacent to each sample in the Plate.

#### **4.4.4.5 Long term storage of specimens**

After test, each amalgam sample was stored in a resealable polythene bag about 40 x 65 mm (Catalogue No: PA 020, supplied by G.W. Heath & Co. Ltd, Trinity Works, Lockfield Ave, Enfield, EN3 7PY). The sample bags for each batch were kept together in a similar bag. The batch and sample numbers and other relevant information were recorded on write-on panels.

#### **4.4.4.6 Mercury hygiene**

Care was taken to avoid skin contact with mercury and contamination of the working environment with mercury and its vapour. Disposable surgical gloves were worn at all times when contact with mercury might occur. Condensation of amalgam was carried out in the central part of a metal tray and waste mercury was collected and stored in a sealed container under water pending disposal. The workbench was dusted with Flowers of Sulphur.

### **4.5 Testing procedures**

#### **4.5.1 The compression testing machines**

Two testing machines were used in this study. An Instron TTC tensile testing machine fitted with a compression cage was used at a cross head speed of 2.5 mm/min. A pen and moving paper chart recorded the applied load and crosshead movement data. A typical chart is shown on page 113. The chart was calibrated in pounds force; these values were converted to Newtons for inclusion in this work. During the work, a new Lloyd M30 test machine became available and testing continued using this machine fitted (from Batch 46) with compression plattens and a 5kN load cell at the same crosshead speed. Force to fracture and deflection data were again recorded. The two machines were not considered to produce significantly different results.

#### **4.5.2 The 3-point bend testing apparatus**

Specimens were fractured using a three point loading apparatus.

Figure 6 shows the schematic diagram and the disassembled apparatus is shown in Plate 21. The major components are the main steel body, the

plunger and the retaining plate and the minor components the location pins, the partially threaded location push-rods and the assembly screws.

Contact was made with the specimen by means of parallel hardened steel roller bars, each bar being 2.5mm in diameter. Two lower support roller bars were fitted to the main body of the apparatus at a spacing of 8.0mm.

The central plunger was of rectangular section steel bar 10mm x 12mm x 84mm long. The lower end of the bar was machined to carry a single loading roller bar as an interference fit. The plunger was located within the milled slot in the main body of the apparatus where it was able to slide freely. The maximum free play of the plunger, measured with a dial gauge was 0.03mm.

The retaining plate was fitted to the main body by countersunk screws. The aperture in the plate facilitated the placement of specimens for test.

#### **4.5.3 Location of samples in the 3 point loading apparatus**

Amalgam samples were located at the centre of the loading piston in the "front to back" direction by removable pins 1.5mm in diameter fitted parallel to the lower support bars. Location of the specimen in the "side to side" direction was done using push rods fitted through drilled holes in the body concentric with the long axis of the amalgam sample. The setting of the M3 adjustment nut on the partially threaded bar was by reference to the recorded length of the specimen. Figure 7 is a diagram of the placement of the joined amalgam sample for test. Plate 22 shows the location pins and push rods in the test area of the 3 point loading apparatus. Plate 23 shows a joined amalgam sample in position for the flexural strength test.

#### 4.5.4 The test to fracture

Specimens were located in the 3 point rig with the centre loading piston over the joint in 2 piece samples. Both the Instron and the Lloyd machines were calibration checked prior to use. The load reading was then zeroed, the crosshead motor started and the load to fracture recorded.

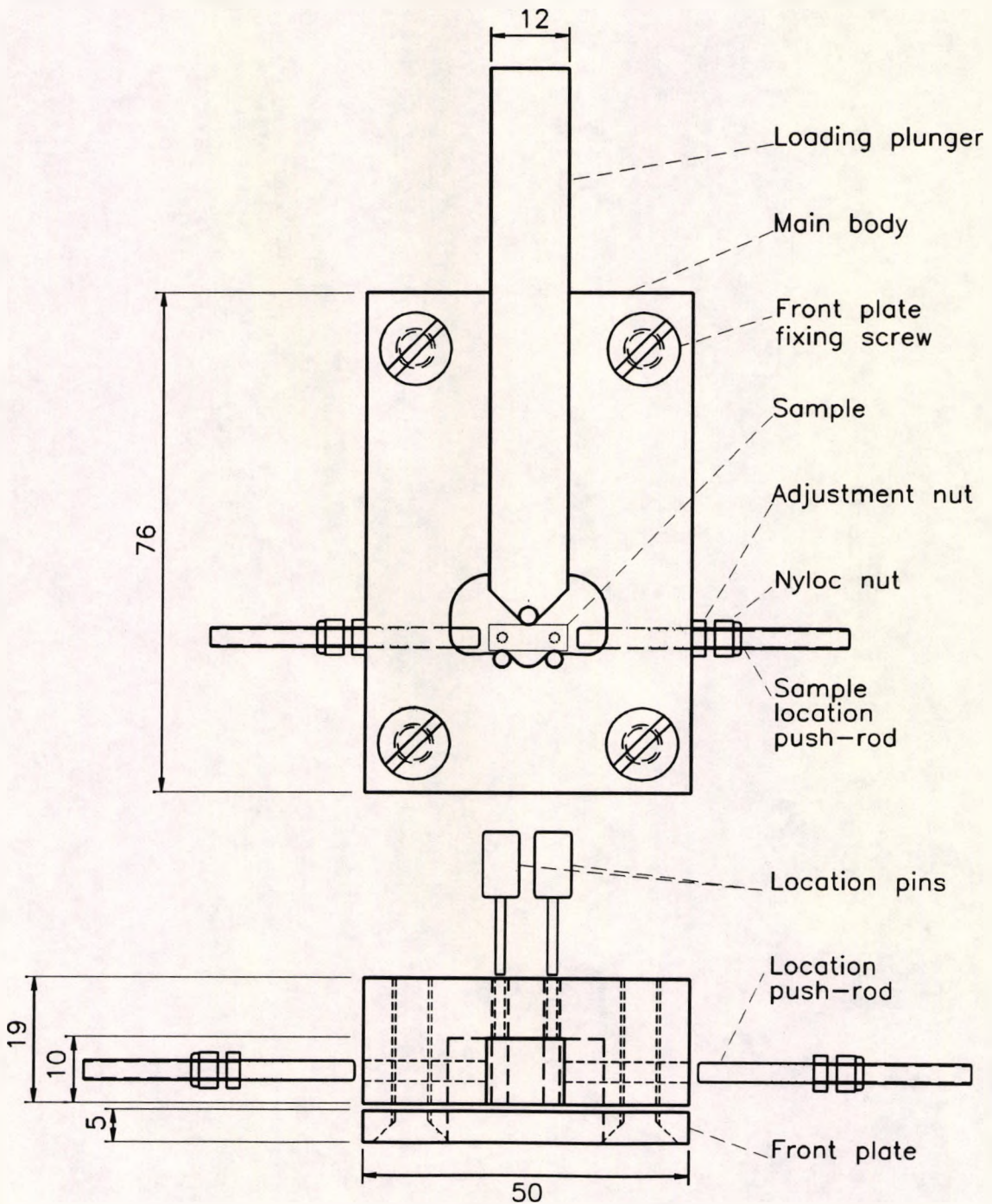


Figure 6. Diagram of the 3 point loading apparatus.

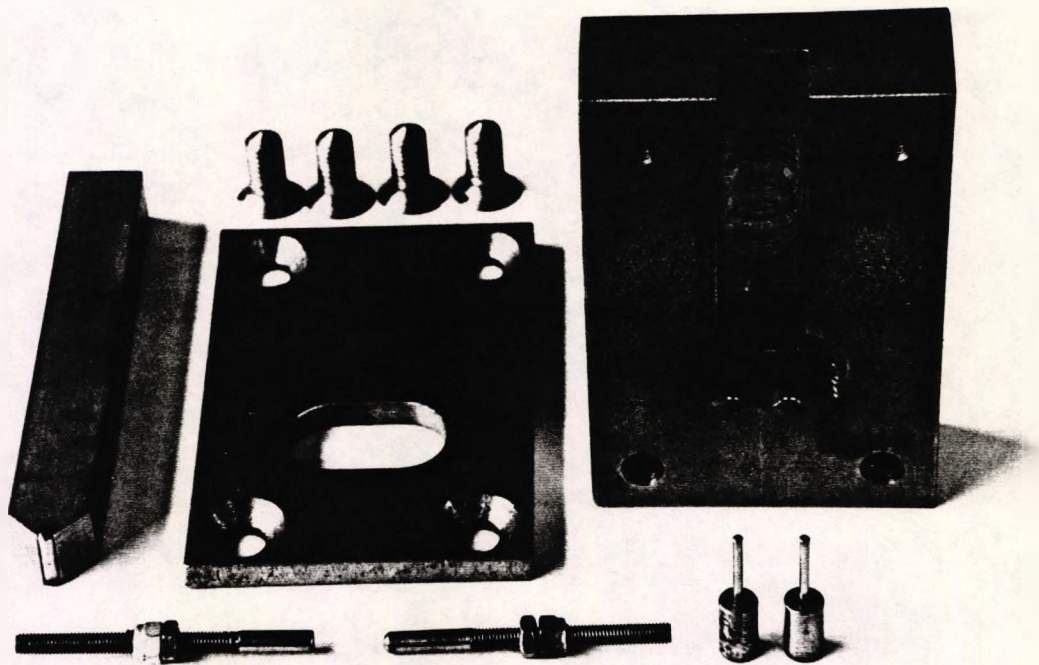


Plate 21. The disassembled 3 point loading apparatus.

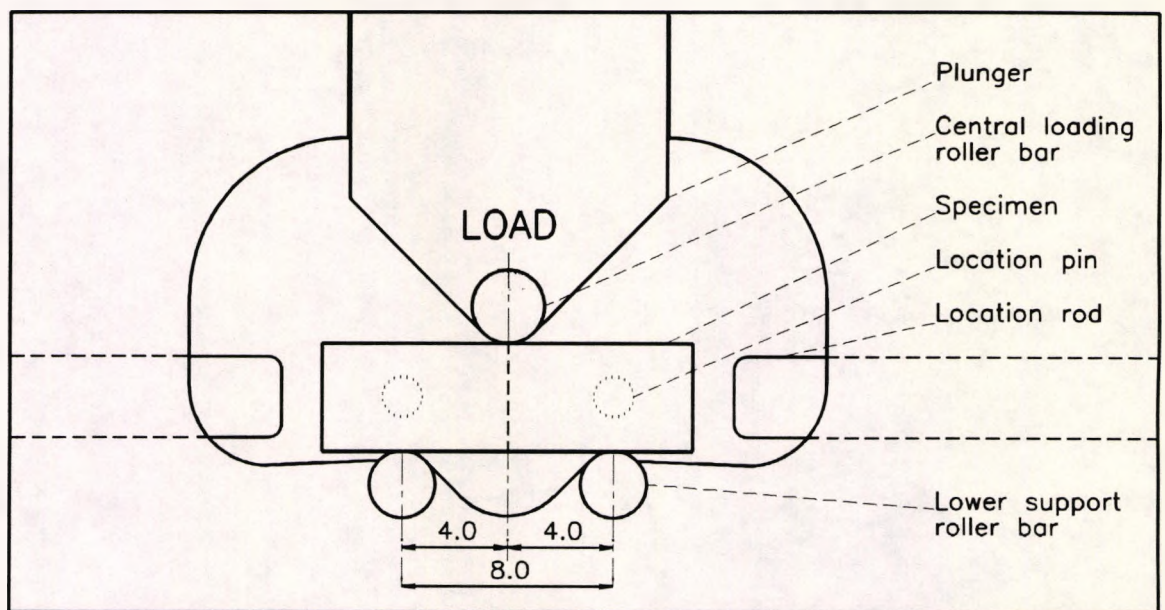
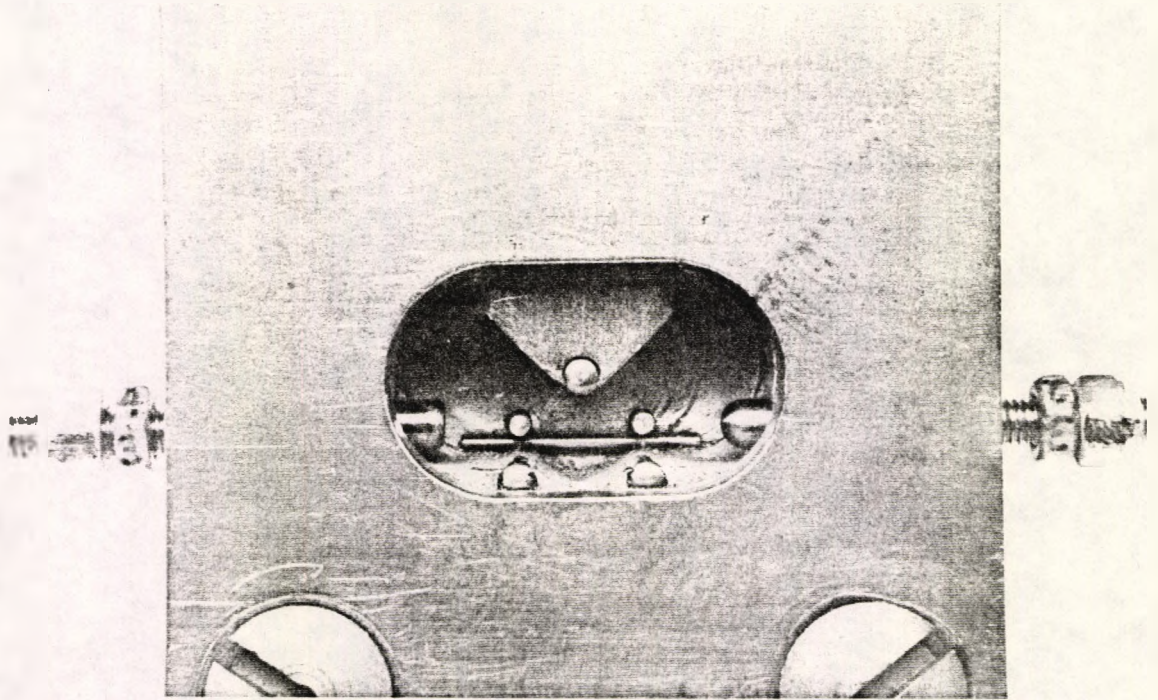
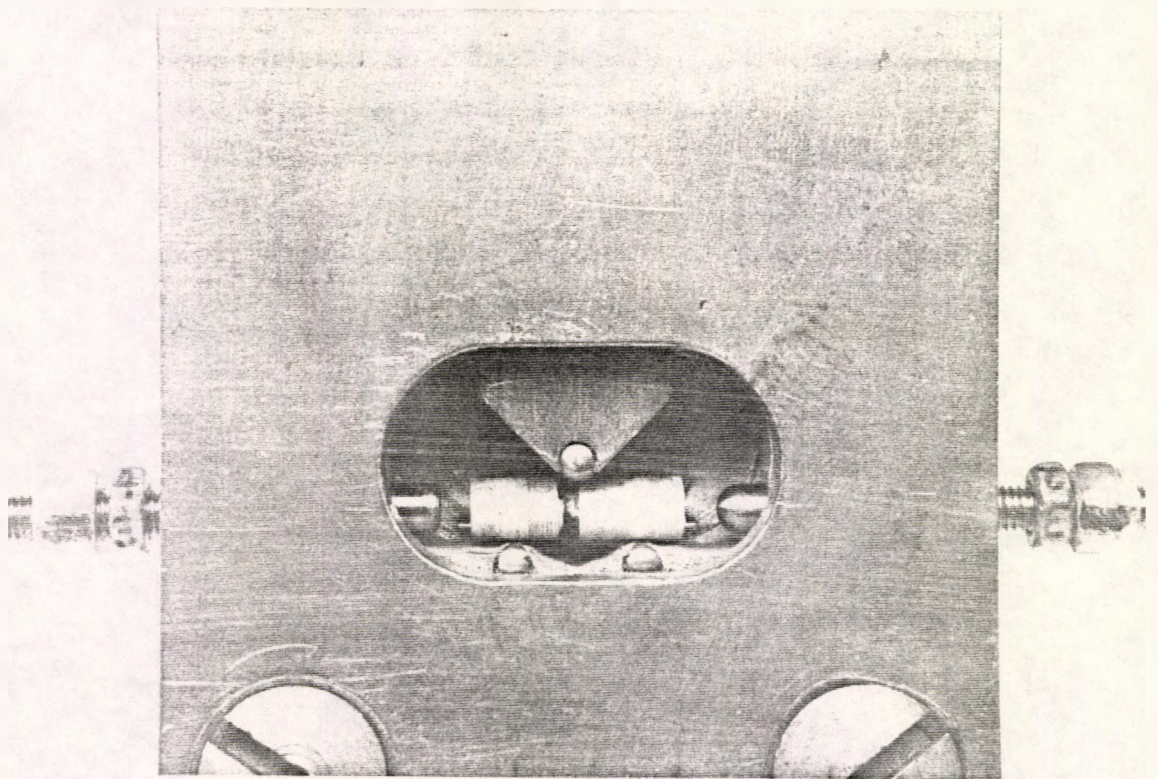


Figure 7. Diagram of the joined amalgam specimen in place in the 3 point bending apparatus.



**Plate 22.** The test area of the 3 point loading apparatus.



**Plate 23.** A joined amalgam sample positioned for 3 point loading test.

#### **4.5.5 Notched samples**

Later in the experimental programme it was desired to control the point where specimen failure initiated. This was achieved by notching the joined samples at or adjacent to the joints.

##### **4.5.5.1 The notching procedure**

A Hounsfield notching machine (normally used for producing notched steel test pieces for Hounsfield Balanced Impact testing) was adapted to receive amalgam samples by provision of a split reducing ring in the sample holder to reduce the required sample diameter from 8.0mm to 4.0mm. Additionally, the split ring enabled the holding of the sample without crushing. The machine is shown in Plates 24 and 25. The hand operated machine produced a notch about 0.3mm deep with a tip radius of 0.2mm.

The location of notch on the amalgam sample was determined by control of the length of amalgam protruding from the split reducing ring.

##### **4.5.5.2 The location of the notch**

Joined amalgam samples were notched (1) in the parent material adjacent to the joint; (2) in the addition material adjacent to the joint; or (3) at the joint.

The notched amalgam specimens were placed off-centre in the testing apparatus, the joint being located 0.2mm from the central loading contact as shown in Figure 8. The central loading roller made contact with either the parent amalgam or the addition amalgam. A typical example of the indentation due to the central loading roller (in sample Amalcap SAS P4) is shown in Figure 81 (page 218).

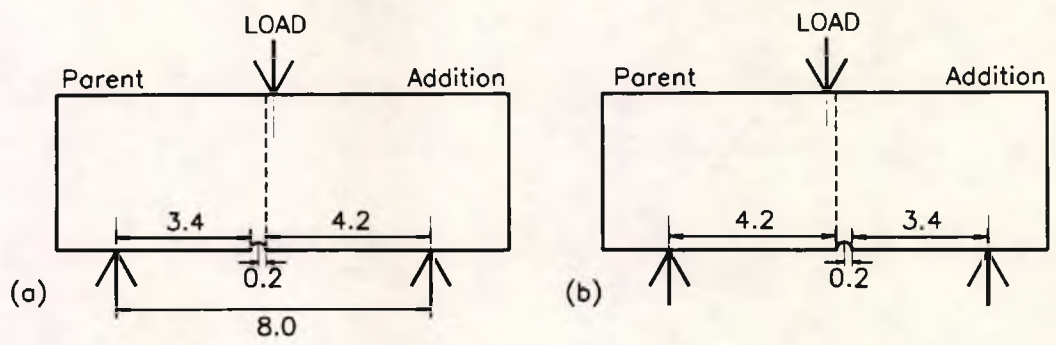


**Figure 8.** The position of the notched specimens in the test apparatus.  
 (a) Notch to Parent; (b) Notch to addition.

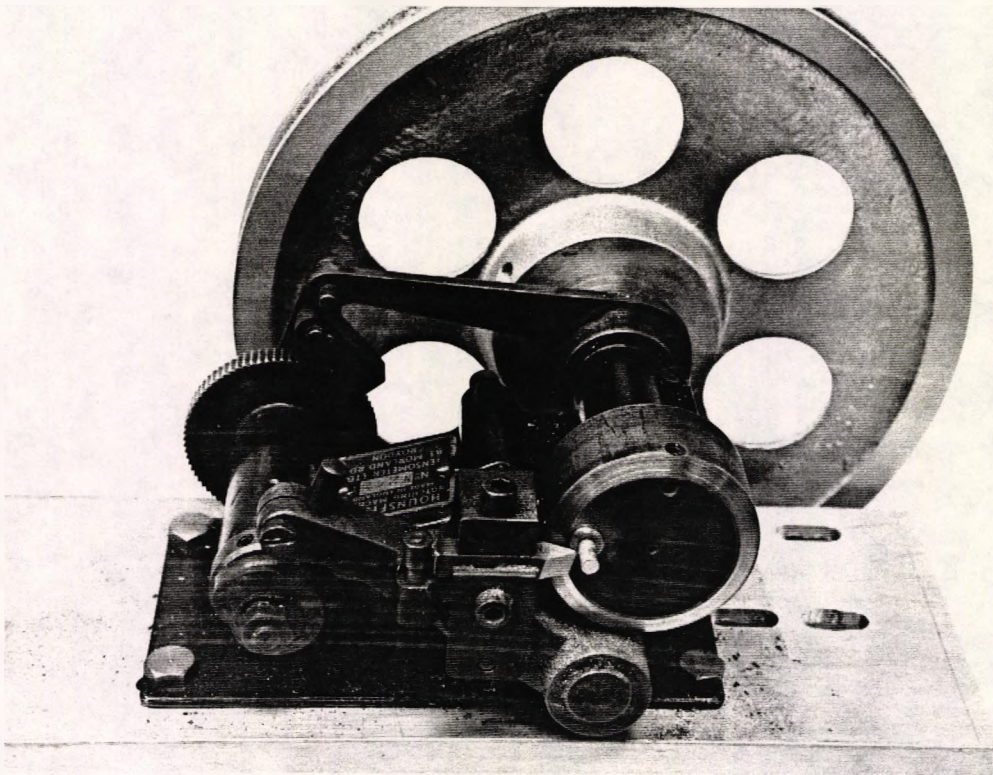


**Plate 24.** The Hounsfield notching machine.

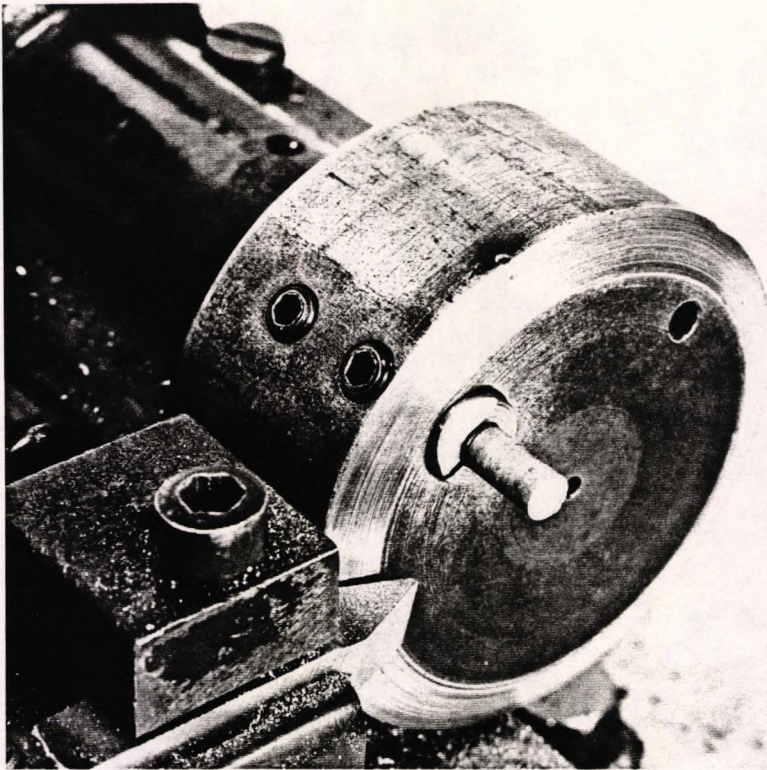


**Plate 25.** The notching procedure on a joined amalgam sample.

## **4.6 Metallography**

### **4.6.1 Preparation of Samples for Microstructure Examination**

The procedure used was generally that for metallographic examination of low melting point and soft alloys and involved mounting, grinding, polishing and etching procedures.

#### **4.6.1.1 Mounting Materials**

These were supplied by Buehler U.K. Ltd, Science Park, University of Warwick, Coventry CV4 7HS.

30mm diameter nylon mounting ring and base.

Buehler Sampl-Kwick powder and liquid.

Disposable plastic cup and plastic disposable stirrer.

In addition, small identification paper squares were embedded in the mounts.

#### **4.6.1.2 Pre-mounting procedure**

**4.6.1.2.1 Intact samples.** To ensure samples could be easily located a flat was ground on the cylindrical surface using water washed 150 grit abrasive paper.

**4.6.1.2.2 Fractured samples.** The two parts were held together lightly using a bent paper clip and since it was not practical to grind a flat on the reassembled samples a piece of adhesive paper was used to stop rolling.

#### **4.6.1.3 Mounting**

The recommended proportions of three parts by volume of Buehler Sampl-Kwick powder to two parts of liquid were mixed and poured without delay around the sample placed on the base of the mounting ring.

#### **4.6.1.4 Grinding**

This was done by hand on silicon carbide papers under running water using grades of paper from 150, 240, 320, 600. Light pressure was used with generally 20 to 30 strokes on each paper. For final grinding, the best results were obtained by using very light pressure on the well worn 600 grade paper. With at least 200 strokes to eliminate the previous cross scratches, the easier and quicker was the subsequent polishing. Relief polishing effects could be minimised.

#### **4.6.1.5 Polishing**

**4.6.1.5.1 First polish.** This was done on a 150mm diameter wheel rotating at 300 r.p.m. covered with a polishing cloth impregnated with 6 $\mu$ m diamond

paste for 4 to 8 minutes.

**4.6.1.5.2 Second polish.** This was accomplished by about 500 hand strokes against Selvyt cloth (supplied by Process Supplies Ltd, 13-25 Mount Pleasant, London WC1X 0AA) well wetted with Silvo metal polish (Reckitt Household Products, Hull). The optimum speed of hand polishing was less than 100 strokes per minute. Faster speeds and/or other than light pressure resulted in the smearing of the structure.

#### **4.6.1.6 Etching**

A two stage etch procedure was used as described by Allan, Asgar and Peyton (1965). A potassium chromate pre-etch solution was applied for about 20s, then rinsed with water. Iodine in ethanol was then applied for about 20s followed by a Hypo rinse. This procedure was successful in this work when swabbing with loosely wound cotton buds.

Pre-etch	4g $K_2Cr_2O_7$ , 1g KI in 100ml water
Etch	4g Iodine in 100ml 70% Ethanol
Hypo rinse	10g sodium thiosulphate in 100ml water

**Table 7.** The etchants used.

#### **4.6.2 Optical microscopy**

The microstructure was examined using a Nikon Optiphot metallurgical microscope Model AFX - II with attachment for 35mm camera. Both bright and dark field illumination modes were used. Three lens systems were used which gave magnifications of about 110, 225 and 900 when printed on 150mm x 100mm photographic paper. In this work, markers adjacent to the micrograph borders indicate the estimated location of the joint interface.

## **4.7 Statistical analysis of the results**

The methods used in the statistical analysis of the results are described in this section. The results from batches of samples which had been prepared and tested in the same or a similar manner were pooled into sets. Each set was identified by a number. Sets were divided into subsets according to the location of the fracture origin: whether this had occurred in the parent amalgam, at the joint or in the addition. Each subset was identified by its set number and a suffix letter to denote the fracture origin. The recorded force to fracture data for the test together with the mould sample hole number, location of fracture origin, batch and set numbers are tabulated in Appendix 1.

Force to fracture data were loaded into a personal computer statistical analysis program (Minitab Release 7.1, Clecom Ltd, The Research Park, Vincent Drive, Edgbaston, Birmingham B15 2SQ). The computers and software in the Department of Statistics and Actuarial Science, City University, were used by kind permission of Professor H.P. Wynn. The tests used and their Minitab program commands are described below.

### **4.7.1 Descriptive statistics**

Descriptive statistics of force to fracture for Batches 1 to 125 are given in Appendix 2 and for sets and subsets in Appendix 3. These were prepared by the DESCRIBE command which calculates the arithmetic mean, minimum, maximum, median, standard deviation and standard error of the mean for the data in the column of the Minitab worksheet. The standard deviation was the "n-1" weighted estimate of the population standard deviation. The TINTERVAL 95 command provides the 95% confidence limits for the estimate of the mean of the statistical population. Similarly, the WINTERVAL 95 command provides the 95% confidence limits for the median.

#### **4.7.2 The tests for normality**

The distribution of the force to fracture data for each data set was tested for normality by use of the HISTOGRAM and DOTPLOT commands on the relevant data column and by the PLOT command on the results of the NSCORES command against the data in that column.

The representation of the results produced by the HISTOGRAM command is bell shaped if the distribution is normal. The graph plotted from the results of the NSCORES command against those data is a straight line if the distribution is normal.

#### **4.7.3 The tests for differences between data sets**

This section describes the statistical tests used in analysis of the results of this study. In addition to force to fracture data, for a limited number of samples weight and dimensions were also considered.

A hypothesis can be made (the "null hypothesis") that the statistical samples were drawn from the same statistical population. Acceptance of this hypothesis is not proof that the tested samples have been drawn from the same statistical population; if there is insufficient evidence for its rejection, any observed differences between data sets could be due to chance variation (known as sampling error). If the hypothesis is rejected, it is concluded that the samples came from different statistical populations. The value for  $p$  from these tests is the probability of rejecting the null hypothesis when in fact the observed differences were due to sampling error. Probability is given by a number between zero and one.

#### 4.7.3.1 Student's t-test

The Student's t-test was considered to be sufficiently robust to give valid results for the difference between arithmetic means of data for Batches or Sets where there might have been departures from true normality in the results analysed (Wynn, 1994). In addition, non-parametric tests were carried out when the normality of distribution was in doubt. The TWOSAMPLE 95 command was used for the unpaired two tail t-test on data columns. This command provides a value for "t" which is the difference between sample means divided by its standard error. The probability (p) of the observed difference in means having occurred by chance for the applicable degrees of freedom and the 95% confidence interval for the difference between means are also given.

#### 4.7.3.2 Analysis of variance

The AOVONEWAY Minitab command performs one way analysis of variance (ANOVA) to compare the means of several data columns. The test computes the ratio of between group to within group variances with an associated probability for the degrees of freedom applicable. In this work, the results of ANOVA are presented thus: (F = \_ [\_,\_ df] p = \_) where F is the ratio of the between-samples variances to the within-samples variances; df are the degrees of freedom in the test; p is the probability of wrongly rejecting the null hypothesis and underscores represent these values.

Easistat, a statistical analysis program for personal computers (ARC Scientific Ltd., 257 Woodstock Road, Oxford OX2 7AE) performs an analysis of variance test. In addition to the calculation of the F ratio and its probability, the ANOVA command produces a table of t-test results where the mean of each selected data set is tested against the others using the pooled variance.

### **4.7.3.3 Non-parametric tests**

The MANN-WHITNEY (Minitab) or WILCOXON (Easistat) commands were used to perform the U-test or Rank Sum non-parametric tests respectively which are independent of distribution normality in the statistical samples. The result is presented as the probability (p) of wrongly rejecting the null hypothesis.

### **4.7.4 Graphical presentation of the results**

#### **4.7.4.1 Scatter plots**

Vertical scatter plots of the force to fracture results for Batches were prepared. The marker used for each data point in joined samples depended on the location of fracture origin. Failure in the parent was marked by an open box, failure at the joint by a cross and failure in the addition part of the sample by a downwards pointing triangle. The data points for the results of one-piece sample testing were represented by the hatch symbol (#).

For a limited number of results, the length and weight of sample or added (for joined samples) were plotted in x-y graphs.

#### **4.7.4.2 Cumulative frequency of force to fracture**

Graphs of the cumulative frequency of force to fracture for selected data sets were prepared. The force to fracture values were arranged in ascending order of magnitude. The total number of test results in the data set determined the percentage increment for each data point in the cumulative frequency distribution where the maximum value at failure corresponded to 100% failed. The graph lines were drawn by joining the data points for each set. Where graphs were prepared from subsets, data points for fractures originating in the

parent, joint or addition were marked using the convention described in the section above.

#### 4.7.5 Examination of the numbers failing in the parent, joint or addition

From already published literature (excluding work of Kirk, 1962 and Jørgensen and Saito, 1968: see Section 3.1), it can be considered that 100% of joined samples fail in the joint interface. This appears not to apply in this work. A hypothesis could be made that if no part of the joined specimen was exceptionally weak or strong, the expected outcome of the 3 point bending test would be for 50% of samples to fail at the joint. Specimens which did not fail at the joint would be expected to fail in the parent or addition parts with equal frequency. Therefore, under this hypothesis, 25% of specimens were expected to fail in the parent, 50% at the joint and 25% in the addition. This is identified as the  $\frac{1}{4}:\frac{1}{2}:\frac{1}{4}$  hypothesis.

The number of test samples in a set exhibiting a particular characteristic (*i.e.* having failed in the parent, at the joint or in the addition) compared to the remainder were tested against this hypothesis. The Easistat CHISQ F N 2 2 command performs Fisher's Exact Test (Armitage and Berry, 1987) in a two-by-two table on data entered from the keyboard. The results for selected data sets were compared against each other or the  $\frac{1}{4}:\frac{1}{2}:\frac{1}{4}$  hypothesis.

The CHISQ N 3 2 command similarly performs the Chi-squared test on a three-by-two table and was used with Yates's correction for testing of the overall location of sample failure results for Sets against the  $\frac{1}{4}:\frac{1}{2}:\frac{1}{4}$  hypothesis. The null hypothesis in the Fisher and Chi-squared tests is that there is no association between columns and rows in the table. The results of these tests are tabulated in Appendix 5. A high value for probability does not prove that the hypothesis is true; there is merely insufficient evidence for its rejection.

## **Chapter 5. The materials used**

This chapter identifies the dental materials which have been examined in this research.

### **5.1 Mercury**

The mercury used in all dental amalgams must conform to recognised standards which relate to permitted levels of impurity. Mercury used in this work was stated by the manufacturers to conform to BS 4227: 1967 or BS 4227: 1986 for Dental Mercury, except Degussa mercury which was manufactured in Germany and stated (at least 99.99% pure) to exceed the requirements of the American Dental Association, ISO and DIN standards but did not refer to the British Standard.

### **5.2 Amalgam Alloys**

The amalgam alloys used in this study were obtained either as loose powder or precapsulated with mercury. Powdered alloys and Duralloy capsules were generously supplied by the manufacturers. Other precapsulated materials were generously supplied for this study by Dr J.D.R. Walker, City Consultancy Services, City University.

The amalgam alloys used in this study were of the lathe-cut or spherical type or mixtures of both particle types. The particle morphologies are listed in Table 8. The alloy powders are shown in Plates 26 to 34 (Pages 99 to 103).

### 5.2.1 Chemical composition of amalgam alloys used in this study

The chemical compositions of the amalgam alloys used in this study are reported in Table 8. Where available, the manufacturer's specification has been listed. Values shown in parentheses represent the chemical composition as determined by chemical analysis; none of the alloys used contained more than 0.02% Indium (personal communication, Dr J.D.R. Walker).

Brand of alloy and code used to identify manufacturer	Alloy type	Particle morphology	Manufacturer's composition specification, where available				
			Ag%	Sn%	Cu%	Zn%	Hg%
Amalgam M <sup>E</sup>	Conventional I	lathe cut <sup>1</sup>	67.7 (67.6)	26.8 (27.0)	5.0 (5.1)	0.5 (0.44)	(<0.1)
Duralloy <sup>D</sup>	"Hybrid" III	Overall: <sup>2</sup> 80% spherical <sup>2</sup> 20% lathe cut <sup>2</sup>	50 (49.3) 45 71	30 (30.5) 31 25.7	20 (20.6) 24 3.3	0 (<0.22)	(<0.1)
Aristalloy 21 <sup>E</sup>	"Blend" HCSC III	35% spherical <sup>1</sup> 65% lathe cut <sup>1</sup>	45 (46.9)	31 (29.8)	24 (23.5)	(<0.01)	(<0.05)
Veraloy <sup>E</sup>	HCSC III	lathe cut <sup>1</sup>	45 (44.8)	31 (31.1)	24 (23.9)	(<0.01)	(<0.05)
Amalcap SAS Non gamma 2 <sup>I</sup>	HCA II	Overall: <sup>3</sup> 30% spherical <sup>3</sup> 70% lathe cut <sup>3</sup>	70.1 (70.9) 68 71	18 (18.5) 25.7	11.9 (11.6) 32 3.3	(<0.02)	(<0.1)
Dispersalloy <sup>J</sup>	HCA II	Overall: <sup>4</sup> 30% spherical <sup>5</sup> 70% lathe cut <sup>5</sup>	69.6 (69.7) 70 69	17.7 (18.9) 26	11.8 (11) 30 4	0.67 (0.75) 1	(<0.1)
Tytin <sup>K</sup>	HCSC III	spherical	60 (59.2)	28 (28.5)	12 (13)	(0.01)	(<0.05)
Matticap Fine 68 <sup>M</sup>	Conventional I	lathe cut	(68.9)	(26.3)	(5)	(0.39)	(<0.1)
ANA2000 <sup>N</sup>	HCSC III	lathe cut	43 (44.5)	29.6 (29.8)	25.4 (23.5)	(<0.01)	<sup>2</sup> (1.99)

**Table 8.** The chemical composition (by weight) of the amalgam alloys used.

The superscripted numbers in Table 8 denote references on the composition of the alloys. These are:

- <sup>1</sup> personal communication, Engelhard Sales Ltd.
- <sup>2</sup> personal communication, Degussa AG, Germany.
- <sup>3</sup> personal communication, Vivadent, Liechtenstein.
- <sup>4</sup> values reported by de Freitas (1979).
- <sup>5</sup> values reported by Wing (1979)

The superscripted letters in Tables 8, 9 and 10 under the brand of alloy or capsule refer to the manufacturers or distributors whose names and addresses are listed below:

- <sup>D</sup> Degussa Ltd, Dental Department, 134-136 Lane End Road, Sands, High Wycombe, Bucks HP12 4HX.  
<sup>E</sup> Engelhard Sales Ltd, Engineered Materials Division, Davis Road, Chessington, Surrey KT9 1TD.  
<sup>I</sup> Ivoclar-Vivadent Ltd, 44 Boston Road, Beaumont Leys Business Centre, Leicester LT4 1AA.  
<sup>J</sup> Johnson & Johnson Consumer Products Inc, New Brunswick, NJ 08903-2400, USA.  
<sup>K</sup> Kerr Manufacturing Company, 28200 Wick Road, PO Box 455, Romulus, MI 48174, USA.  
<sup>M</sup> Johnson Matthey Dental Products, Vittoria Street, Birmingham B1 3NZ.  
<sup>N</sup> Nordiska Dental AB, Helsingborg, Sweden.

Micrographs of the alloy powders used are shown in Plates 26 to 34.

### 5.2.2 Amalgam alloys supplied as loose powder

These alloys were triturated using the Dentomat amalgamator and are listed in Table 9.

Brand of alloy	Abbreviation used in this study	Manufacturer's batch number	Batches prepared in this study	Mass of 1 dose mix from Dentomat, grams	wt % Hg in Mix
Amalgam M <sup>E</sup>	AmM	290885/AM/1	Start to B30	0.579	53.5
		230287/AM/6	B31 to B45	0.563	55
		231189/AM/1	B118 to B125	0.565	55
Duralloy <sup>D</sup>	DUR	40360	B46 to B55	0.658	47
Aristaloy 21 <sup>E</sup>	A21	040690/A21/2	B62 to B87	0.597	52
Veraloy <sup>E</sup>	VER	180190/VER/1	B88 to B108	0.555	56

**Table 9.** Amalgam alloys supplied as loose powder.

### 5.2.3 Amalgam alloys supplied precapsulated with mercury

These alloys are listed in Table 10. They were triturated using a Silamat.

In this study, one conventional alloy (Amalgam M) and one HCSC (Veraloy) lathe cut alloy were chosen in loose powder form. Similar alloy types

(Matticap Fine 68 and ANA 2000 respectively) were chosen in precapsulated form where a 1:1 ratio of mercury to alloy was supplied by the manufacturer.

Brand of Capsule	Abbreviation used in this study	Manufacturer's batch number	Batches prepared in this study	Silamat time setting	Stated alloy content, grams	wt % Hg in mix
Duralloy <sup>D</sup>	DUR	40185	B6	7s	0.640	50
Aristaloy 21 <sup>E</sup>	A21	300490	B109	8.5s	0.600	50
Amalcap SAS <sup>I</sup>	ACAP	457702	B113, B116	7s	0.600	52.5
Dispersalloy regular set <sup>J</sup>	DISP	None stated*	B110	7s	0.600	50
Tytin <sup>K</sup>	TYT	082190	B112, B115	5s	0.600	43
Matticap <sup>M</sup>	MCAP	003018	B114	7s	0.600	50
ANA2000 <sup>N</sup>	ANA	002 7-1775	B111; B117	5s	0.600	50

\* City Consultancy Services batch number AMA9091/04 (personal communication, Dr J.D.R. Walker).

**Table 10.** Amalgam alloys supplied precapsulated with mercury.

Aristaloy 21 (Plate 28) was also used in this study. It is composed of a mixture of both atomised and lathe cut particles having the same HCSC (24% Cu) composition (personal communication, Engelhard Sales Ltd). This type of mixture is described here as a "blend". The alloy was available both as loose powder and as predosed capsules. The chemical composition of Aristaloy 21 is identical to that of Veraloy which is produced by the same manufacturer. However, a proportion of atomised particles are combined with lathe cut particles which resulted in denser packing of the powder into the measuring chamber of the Dentomat. The alloy:mercury ratio is adjustable on the Dentomat by changing the internal volume of the powder chamber. The setting was unchanged between Batch 62 (Aristaloy 21) and 108 (Veraloy). It may be seen from Table 9 that a reduced weight of Veraloy alloy was dispensed by the Dentomat compared to Aristaloy 21 due to the differing powder-packing qualities of the two alloy particle types. The amalgam mixes used were considered to be of the consistency dentists might normally use. Perhaps Veraloy was verging towards "wet" and Duralloy was a little "dry".

Tytin was an all-spherical single melt encapsulated alloy of 12% Cu content. Spherical particle alloys are known to require less mercury than lathe cut alloys for a coherent mix. The mercury content of these capsules was 43%.

Certain amalgam alloys were manufactured by mixing particles of differing compositions or modes of manufacture. Amalcap SAS (Plate 30) and Dispersalloy (Plate 31) are examples of Type II high copper admixed (or dispersed phase) alloys where conventional  $\text{Ag}_3\text{Sn}$  lathe cut alloy is mixed with spherical Ag-Cu alloy particles. Duralloy (Plate 27), is a mixture of 80% HCSC (24% Cu) spherical particles with 20% conventional lathe cut particles. This alloy fails to meet the compositional requirement for Type II dispersed phase alloys, having 30% Sn and only 50% Ag content overall. Wing (1979) termed mixtures of this type as "reverse dispersed phase" but the term "hybrid" is applied to them here. Duralloy was used both as loose powder in the Dentomat and in precapsulated form.

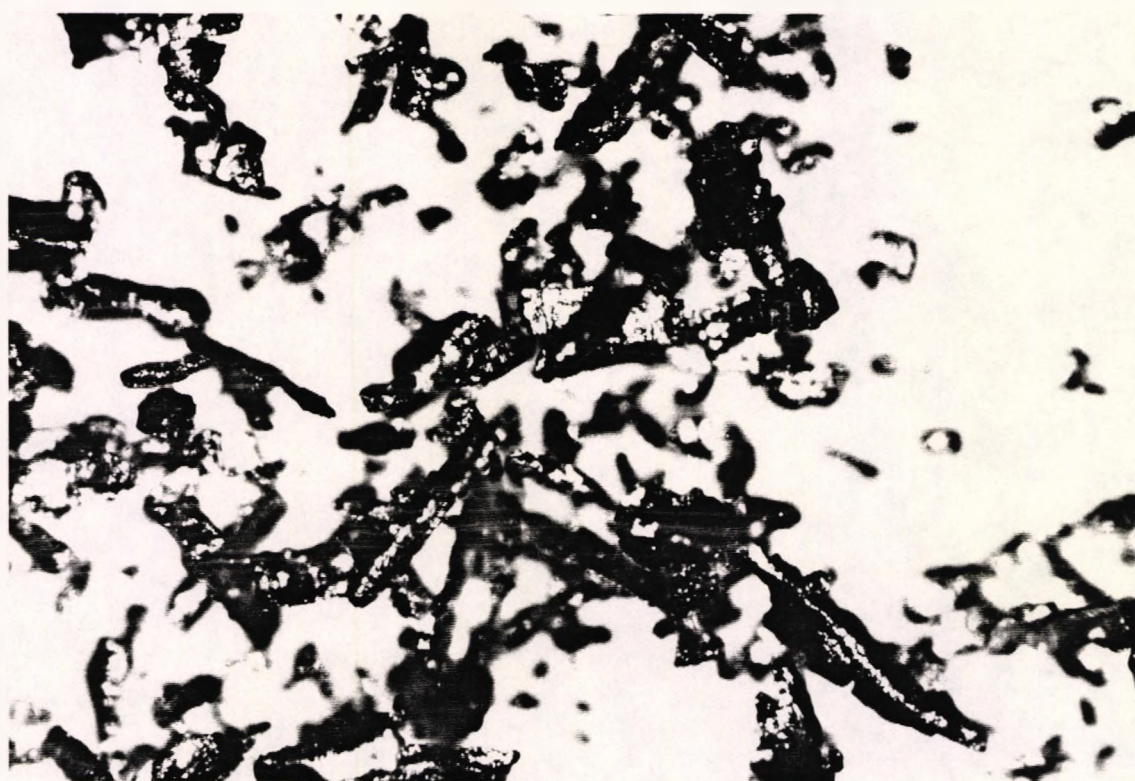


Plate 26. Amalgam M conventional alloy powder.

x900

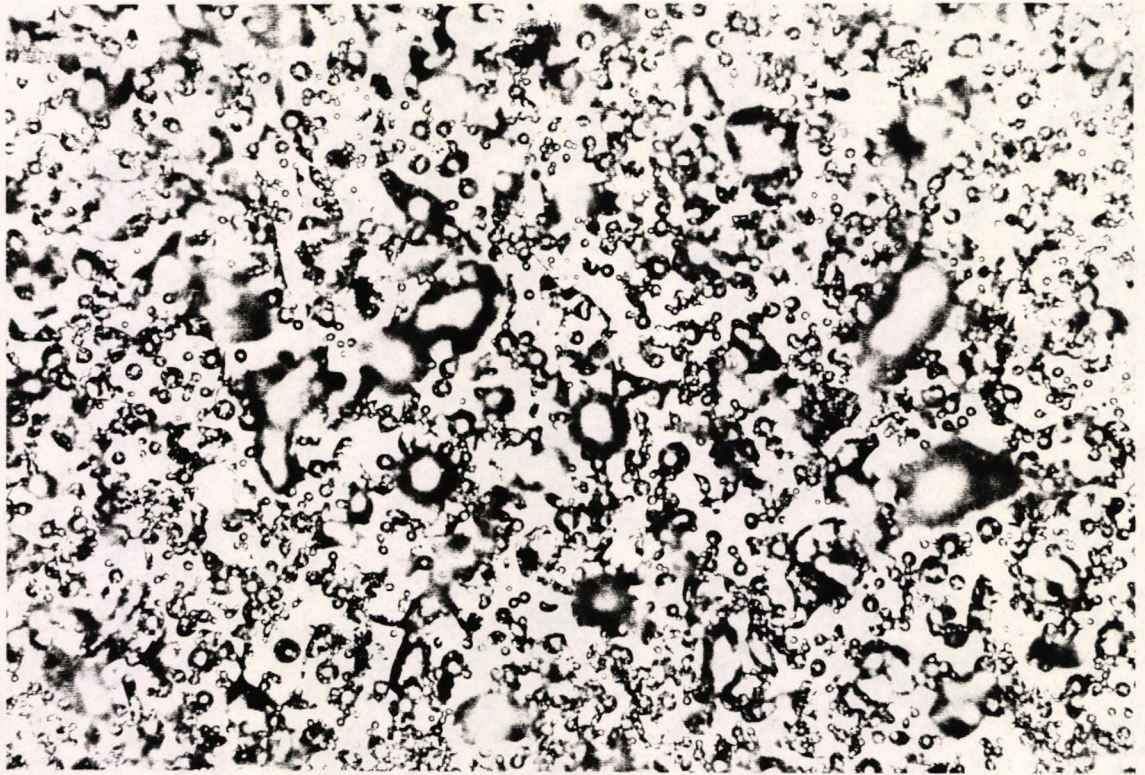


Plate 27. Duralloy powder.

x225

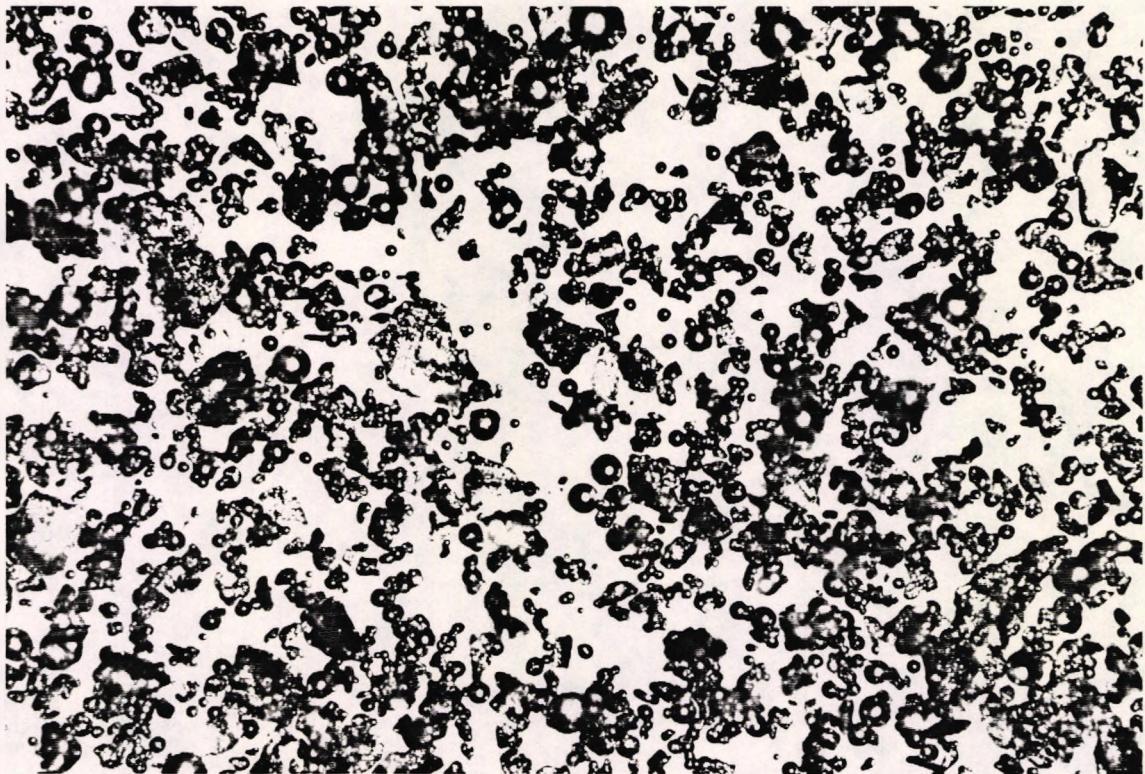


Plate 28. Aristaloy 21 powder.

x225

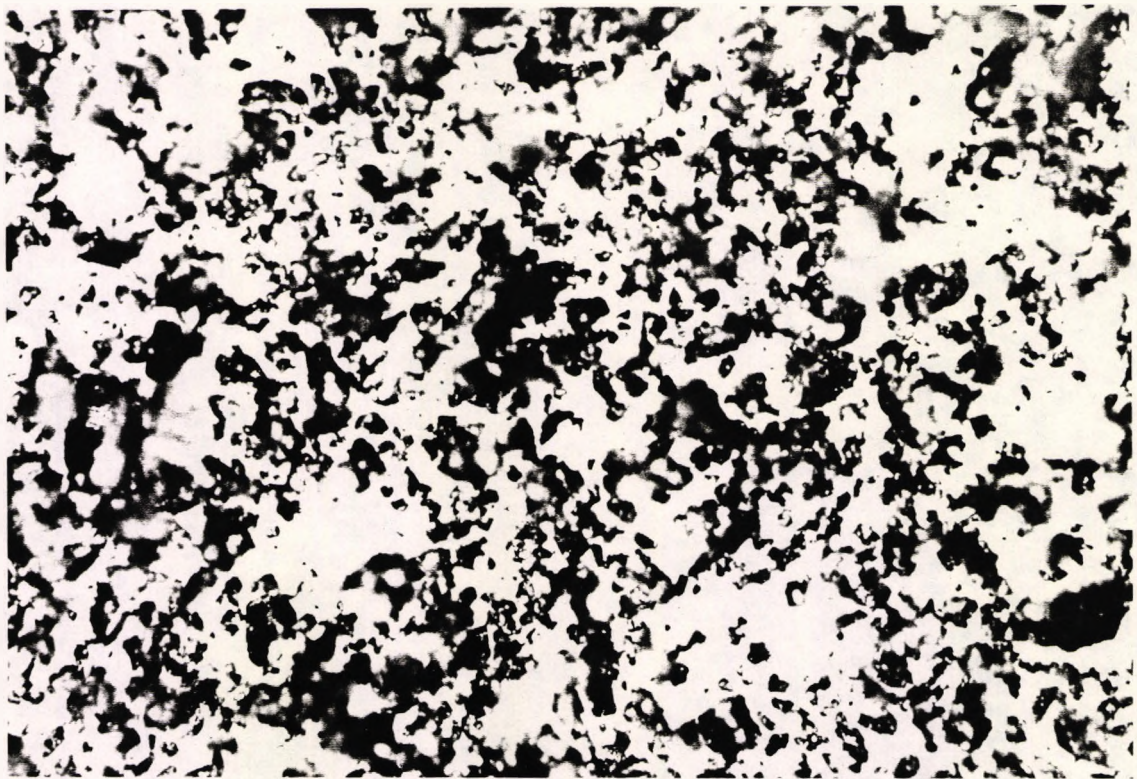


Plate 29. Veraloy powder.

x225

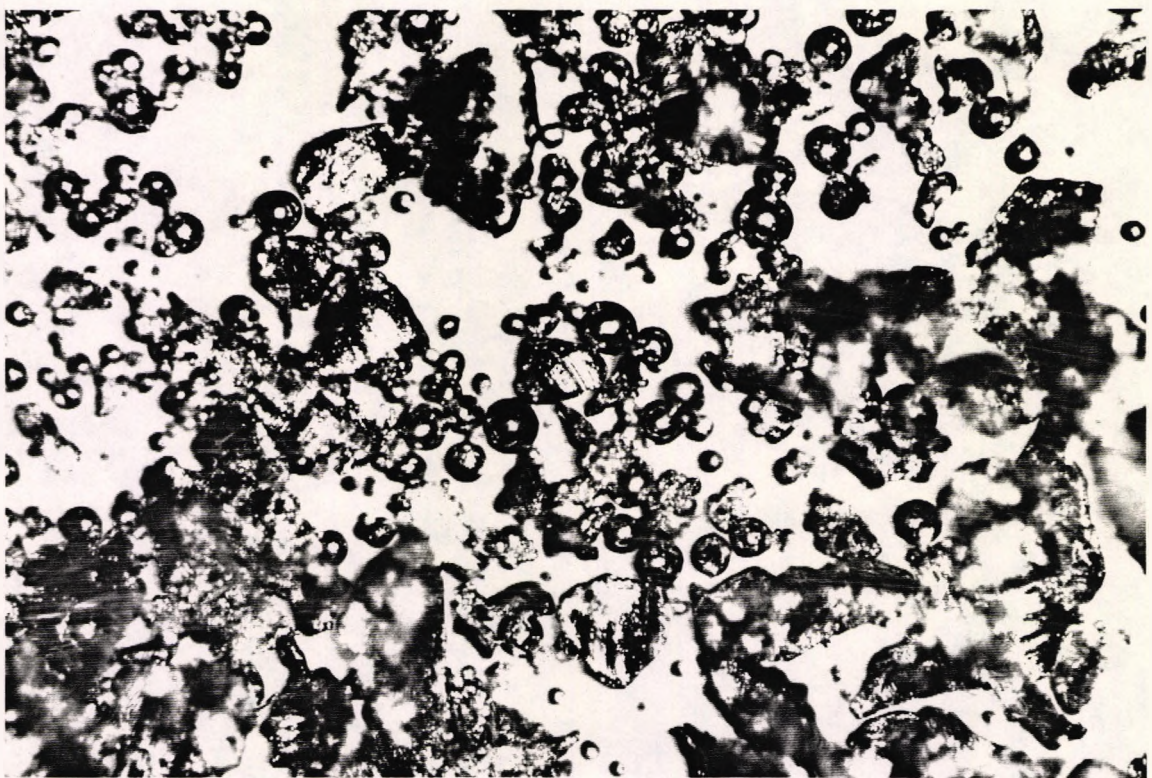


Plate 30. Amalcap SAS Non gamma 2 powder.

x225

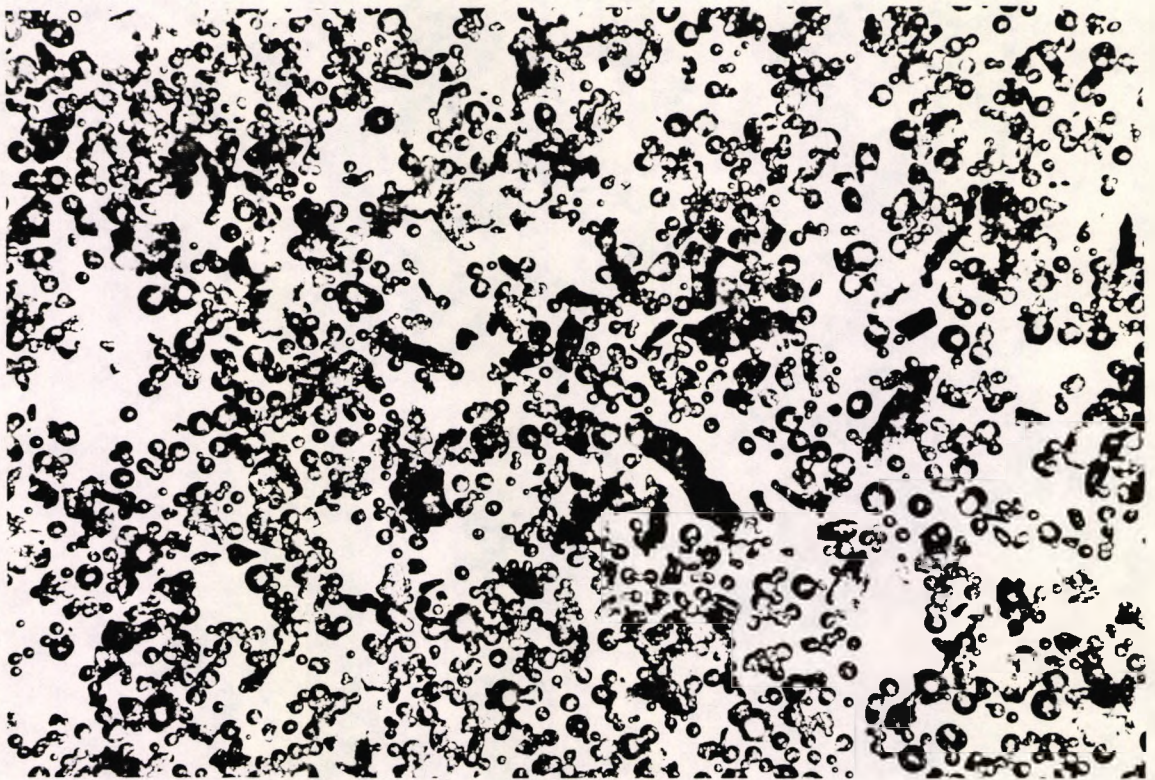


Plate 31. Dispersalloy powder.

x225

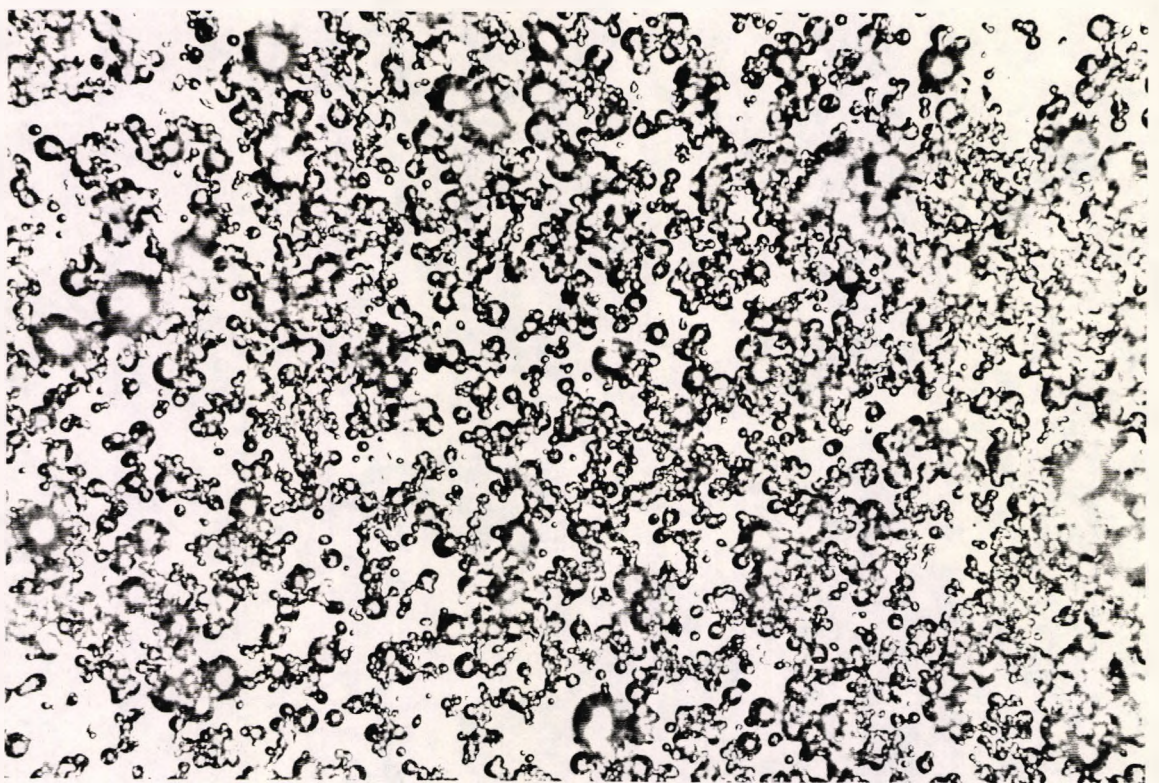


Plate 32. Tytin powder.

x225

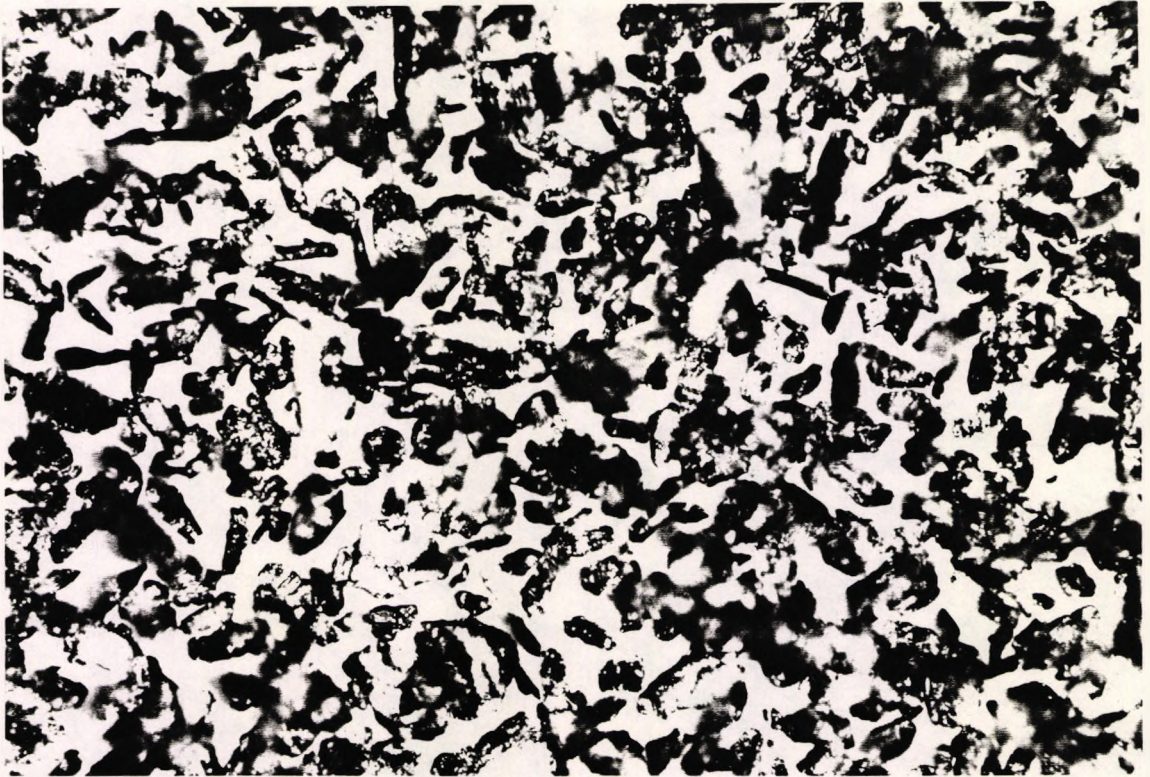


Plate 33. Matticap Fine 68 powder.

x225

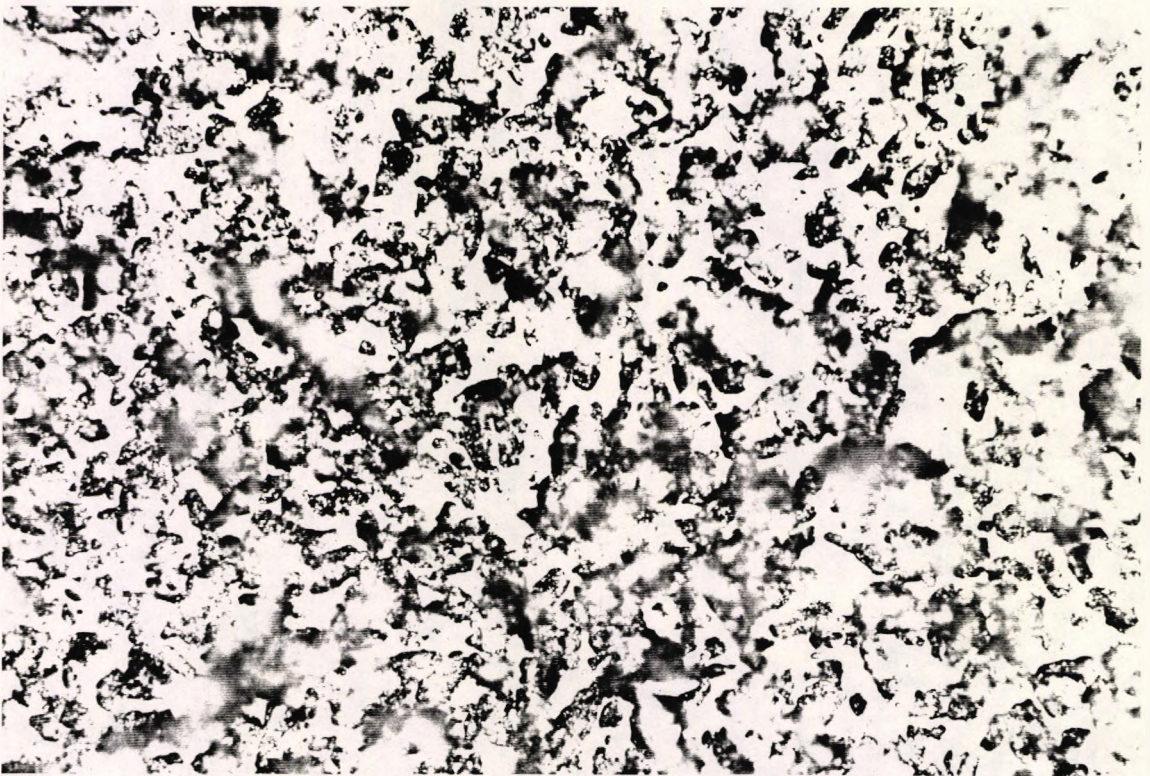


Plate 34. ANA 2000 alloy powder.

x225

## Chapter 6. Results and analysis

This chapter reports the results and statistical analysis which supported the development of the experimental programme. Part of the study was spent in the refinement of sample preparation methods using vibration with shaped pistons for amalgam condensation. At an early stage, joined amalgam samples were prepared where the majority did not fail at the joint when tested under 3-point bending. Overall, about 40% of the vibration condensed joined samples did not fail at the joint. The force required to fracture joined samples was generally greater than that for one-piece samples condensed by the DW method (possible reasons for this are considered on pages 127 to 129).

Joined samples were examined after test to determine the location of the fracture origin. In samples which had apparently failed at the joint, the fracture surfaces were examined for visual evidence of the characteristic pattern of scratch marks which occurred during the end preparation procedure to the parent part. This gave an indication of the extent to which failure at the joint had occurred. In areas where there was partial union, material originating in one part adhered to the opposite part.

Later in the study, samples were prepared with notches adjacent to the joint. These samples were tested in the 3 point bending rig with the joint off-centre so that the fracture path started at the notch, traversed the joint interface and terminated at the loaded area. Selected samples were reassembled and prepared for microstructural examination. When amalgam alloys with spherical particles were used, the location of the joint interface was evident where flat cut surfaces on the spherical particles resulted from the end preparation procedure. In admixed high copper amalgams, there was a reaction zone in the added material adjacent to silver-copper particles in the parent at the joint interface. This reaction zone reduced in thickness or disappeared towards the

centre of the flat cut surface. In samples made from exclusively lathe cut amalgam alloys, it was often not possible to identify the exact location of the joint interface from the microstructure.

## **6.1 Statistical analysis of results**

This section considers the analysis of the results from this study using statistics. The results of the tests for normality of distribution are considered first. In this work, the results of strength testing for sample batches are presented graphically in vertical scatter plots. The cumulative frequency of force to fracture for selected Batches, Sets and subsets (refer to Section 4.7) are also presented. Each cumulative frequency graph is accompanied by a table of descriptive statistics including the mean and median force to fracture, the estimate of population standard deviation and 95% confidence interval for the mean. The results of two sample t-testing and 95% confidence intervals for the differences in mean force to fracture for the data sets are included.

### **6.1.1 The tests for normality**

Tests for normality (see Section 4.7.2) were carried out on the force to fracture data. In the opinion of Professor H.P. Wynn (City University) the distributions were considered to be near normal. These tests were repeated using the natural logarithm of the force to fracture. The distribution of the transformed data was judged to be "skewed to the right" and the normality of its distribution was considered to be less good than that of untransformed data. Log transformation of the data was not necessary for the statistical analysis of these results (Wynn, 1994).

The coefficient of variation for Sets was in the range 16 to 27%. For a small number of batches (11 joined and 5 one-piece) this coefficient exceeded 30%.

The Student's t-test was considered to be sufficiently robust to give valid results for the test of differences between arithmetic means of the data sets where there might have been departures from true normality in the results analysed (Wynn, 1994). Where the normality of distribution was in doubt, non-parametric tests were also carried out.

## **6.2 Preliminary work**

This section describes the preliminary work during which the first experimental techniques were developed. The equipment and methods which produced unsatisfactory results were omitted from Chapter 4.

### **6.2.1 Use of a rectangular mould**

Samples about 4.8mm wide x 4mm thick x 10mm long were prepared in a rectangular mould using conventional Amalgam M condensed by the author's normal clinical technique using a Condensaire mechanical condenser fitted with a flat ended cylindrical condensation tool. The mould was open on its largest surface. After one week, each sample was cut to produce two cubes using a hacksaw. The sawn surface was ground flat using a cylindrical diamond bur in a hand held dental air turbine handpiece. The prepared half-sample was replaced in the mould. The remaining half of the mould formed a "cavity", one wall of which was formed by the prepared surface. A fresh mix of amalgam was condensed into this cavity to produce a joined sample.

Examination of the surfaces formed against the mould showed that the amalgam mix had failed properly to adapt to the line and point angles of the "cavity". There were crevices at the joint. These were generally larger in the side surfaces of the sample than at the base. This corresponded to areas where the curved cylindrical surface of the condensing instrument had

provided poorer adaptation to the mould than the sharp angle at the end.

It was considered that the point angles at the confluence of the parent amalgam with the walls and floor of any rectangular mould might impair condensation of the addition amalgam forming the joint. A further potential problem might occur due to undesirable torsional stresses (with flat-sided test samples) if the loading rollers of the three point bending rig were non-parallel or the sample was twisted and thus unevenly loaded. Samples of rectangular cross section were used by for example, Terkla, Mahler and Mitchem (1961), Forsten (1969), Miyata (1972), Nagaoka *et al* (1974), Fukuba *et al* (1977), Bass and Wing (1985) and Schaller *et al* (1989) but the use of cylindrical samples was preferred for this study.

Surface voids were seen on these samples and were considered to have occurred between portions during incremental build-up with a relatively small condenser in a large mould. A laboratory condensation method which used a mould with close fitting pistons was therefore preferred. It was considered that there was little point in undertaking strength testing of joined samples until they could be produced without obvious porosity or crevices at the joint.

### **6.2.2 Use of a cylindrical steel mould**

A cylindrical steel mould was manufactured to the design of BS 2938: 1985. Although Jørgensen and Saito (1968) and Berge (1982) had replaced the "parent" parts of their samples into their ejector-type moulds for condensation of the "addition" part, considerable difficulty was encountered in this study when replacement of amalgam samples into the BS mould was attempted. When replacement was achieved, the use of a vibration tool for condensation was necessary to avoid the occurrence of porosity at the joint. Some joined samples were found to be cracked. Damage might have occurred during or

after ejection from the mould. On close examination, the bore of the BS mould was found to be slightly out of true. The attempt to use the BS mould for the manufacture of joined samples was discontinued. A split mould with ten cylindrical sample holes was manufactured as an alternative.

### **6.3 Preliminary experiments using the split mould**

Experiments were carried out using the split mould for preparation of both one-piece and joined samples. The end preparation procedure for joined samples described in Section 4.4.3.2 was used throughout the study.

In initial work, experimental condensation procedures were carried out on joined samples. These were assessed on a qualitative basis regarding surface porosity. As a result, a condensation procedure was developed where the occurrence of surface voids at the joint was eliminated.

#### **6.3.1 Condensation of joined samples by weights**

The two thrust deadweight condensation procedure with repositioning of the sample between thrusts was used for the preparation of one piece samples and for the parent parts of joined samples. However, it was not feasible to use the repositioning procedure for condensation of the addition part of joined samples because the parent part of the sample was firmly held in position by closure of the split mould. The addition part of those joined samples was condensed by the application of the BS load to BS plunger No. 2 for 60s in a single thrust.

Plate 35 compares the pronounced surface porosity in the addition adjacent to the joint and relatively little porosity in the parent part which identified the location of the joint. Crevices were evident at the joint: these became more

conspicuous when condensation was delayed. Berge (1982) commented on the occurrence of crevices at the joint in his joined amalgam samples using a similar condensation method.

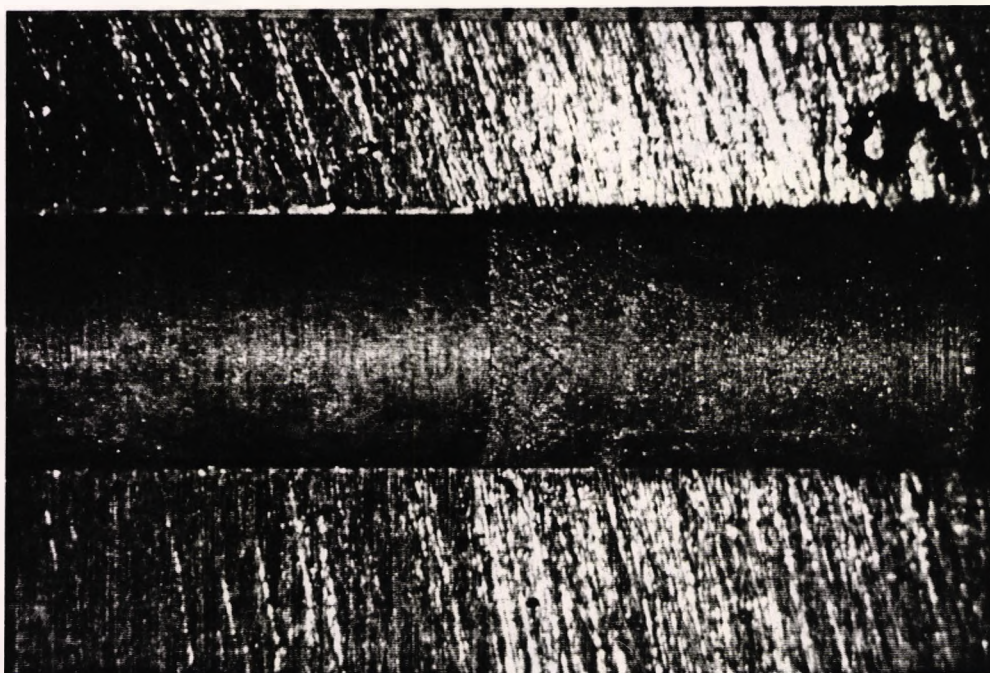


**Plate 35.** Surface porosity in the addition after condensation by weights.

### **6.3.2 Condensation of joined samples by vibration**

A procedure was considered using vibration for the condensation of joined samples. The amalgam mix for the addition part was divided into two unequally sized portions: the smaller portion was approximately one quarter of the mix. The smaller division of the mix was introduced into the mould and condensed against the old amalgam for 10s with the Burgess vibrating tool by the application of the rubbing-in piston which was rotated through  $180^\circ$  at a frequency of 1 Hertz. The remaining portion of the mix was then condensed in the mould by application of vibration for 10s using (a) the rubbing-in piston; (b) a flat ended piston; or (c) by application of the BS load in a single thrust for 60s.

It was difficult to identify the junction between the new and old amalgam: no

porosity was seen at the joint interface. However, voids were evident at the junction between the smaller and larger portions of the addition in samples condensed by each method. The larger portion appeared to be imperfectly condensed in its deeper layers. It was considered that reduction of the volume of each increment by division of the amalgam mix into smaller portions might eliminate this porosity. The use of four approximately equally sized portions was considered to give a reasonable balance between the volume of each increment and time required to complete condensation of the mix.

### **6.3.3 Marking of the joint interface**

Joined samples were prepared by division of the mix for the addition part into four portions which were condensed using vibration. This group of samples is identified as Batch 1 and is shown after fracture under 3 point loading in Plate 36. The parent parts of the samples were marked with four longitudinal pencil lines prior to end preparation. This method of marking the joint interface was considered to be both insufficiently visible and limiting in that only four small areas on the circumference of the interface were defined.

During the subsequent preparation of samples, a more effective method was devised and refined to reveal the location of the joint interface over the entire circumference. Prior to end preparation (see Section 4.4.3.2), the amalgam cylinder surface was marked using an indelible felt tip marker. Marking of the cylindrical surface after trimming in a preliminary trial had led to contamination by spread of the ink on to the freshly cut surface. Various marking inks were tried: the most reliable was found to be a Staedtler Lumocolor 317 Medium Blue permanent overhead projection pen. Some colours (red or green) were insufficiently dense to reveal the interface unequivocally. The dry ink from other markers tended to flake off or transfer to the mould.

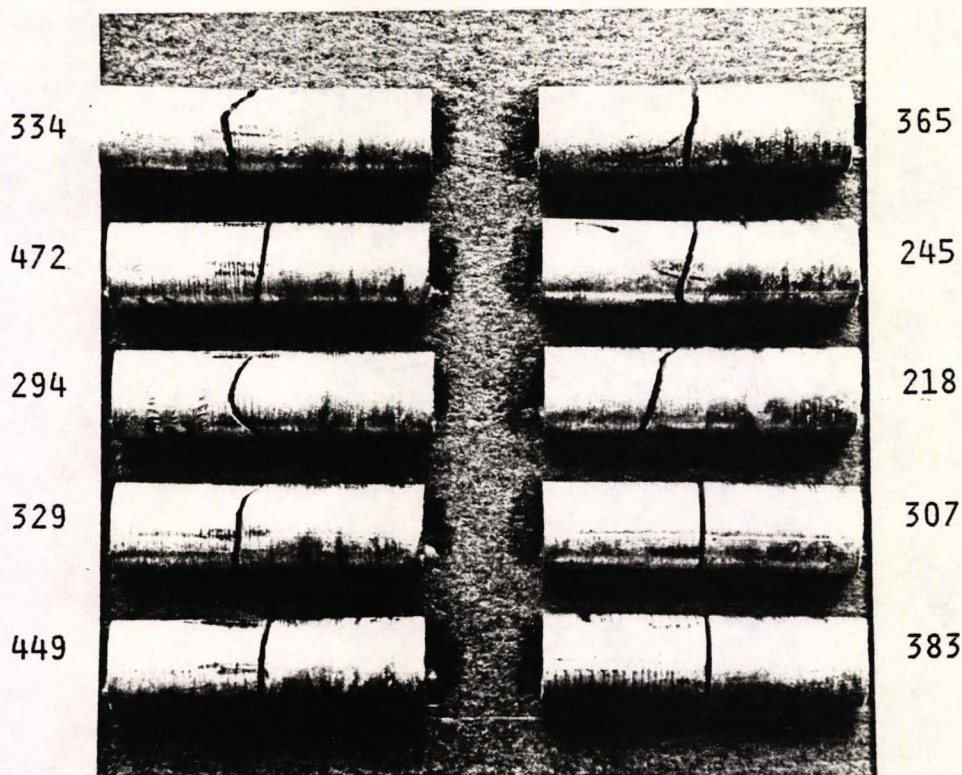


**Plate 36.** Batch 1 after fracture.  
Mean force to fracture: 339N.

x3

#### 6.4 Preparation of joined samples: deadweighted parents

Flexural strength tests were carried out on samples prepared by various methods. The force to fracture data for all samples in Batches 1 to 55 and 62 to 125 are recorded in Appendix 1. Descriptive statistics for these Batches are listed in Appendix 2. In the tests reported in this section, joined samples were condensed in the same manner but the timing of preparation was varied. The effect of early opening of the mould was considered and the conventional Amalgam M and non-gamma-2 Duralloy amalgams were compared. One-piece "control" samples were prepared by the DW method or by application of vibration to the divided mix.

The parent parts of Batches 1, 4, 5 and 7 were prepared from a 2 dose amalgam mix by the DW method. The amalgam mix for the "addition" was divided into four portions. The first increment of the mix was condensed for

10s with the Burgess vibrating tool by the application of the rubbing-in piston which was rotated through 180° at a frequency of 1 Hertz. The remaining three increments of mix were condensed for 10s each using a flat ended piston. Figure 9 shows the force to fracture data with reference to fracture location for these Batches.

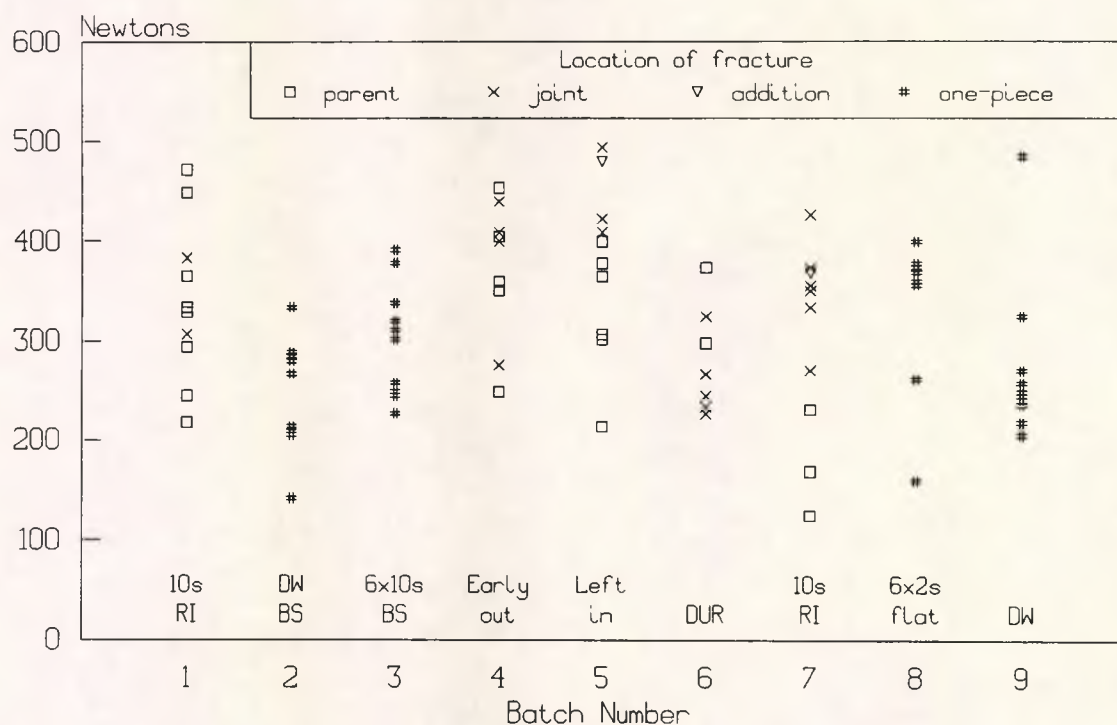
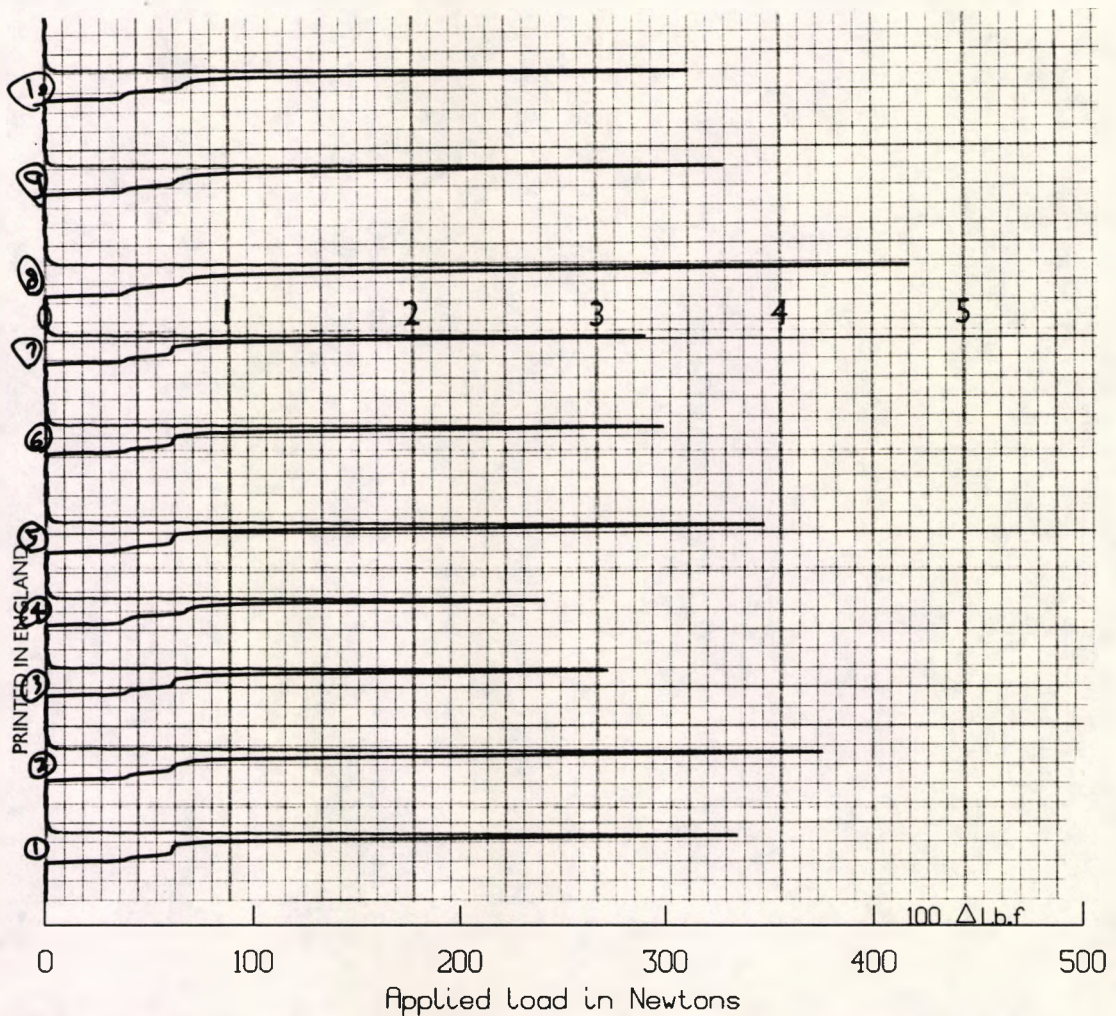


Figure 9. Force to fracture for Batches 1 to 9.

The parent parts for Batch 1 were end-prepared after 3 days and replaced in the split mould for joining. The joined samples were removed from the mould after 4 days and tested under 3 point loading. It may be seen in Plate 36 that it was difficult to determine the exact location of the joint interface. Only two of the ten samples in the batch had obviously fractured at the joint. Sample 1.6 (top of the right column; see Section 4.4.4.4) showed mixed fracture: examination of the fracture surface immediately adjacent to the central contact of the three point bend apparatus revealed the radial pattern of score marks made during end preparation with the sandpaper disk; diametrically opposite this point, the amalgam had fractured within the bulk of the material of the parent part. The force to fracture for these three samples was close to the mean of the batch. Seven samples had not fractured at the joint.



**Figure 10.** Instron test machine moving paper pen chart.

Figure 10 shows a typical example of the moving paper pen chart recorded (in the testing of Batch 15) by the Instron TTC tensile test machine. The paper moved downwards at a speed of 25mm per minute. Two “dips” may be seen where the strain increased without proportional increase in applied load. These are probably due to indentation at the points of contact by the loading and support rollers where the surface amalgam material yielded under compressive stress. The applied load was shared equally between the two support roller bars. The first dip corresponds to yielding at the central loading roller and the second dip to simultaneous yielding at the points of support.

The load then increased rapidly until catastrophic sample failure occurred.

#### 6.4.1 Comparison of Batch 1 with one-piece Batches 2 and 3

Because each part of the joined amalgam samples in Batch 1 had been condensed by different methods, *i.e.* deadweighted or by vibration, two “control” groups using 3-spill mixes of amalgam condensed in these differing ways were prepared. One-piece samples were prepared in the BS mould using the DW method (Batch 2) or by application of vibration with a flat-ended piston for 10s to each of six increments of a divided mix (Batch 3). These one-piece samples were tested after 28 days whereas Batch 1 was removed from the mould and tested 4 days after condensation of the addition parts. The disparity in age of these samples was considered unlikely to be significant, as Jørgensen and Saito (1968) reported that conventional amalgam reached maximum strength after 24 hours with very little variation after that time.

In Figure 9 the deadweighted one-piece Batch 2 appears to be weak. The mean force to fracture was 243N compared to 301N for Batch 3 (one-piece vibrated). Student's t-test result was  $t = 2.29$ ,  $p = 0.034$ . The mean force to fracture (339N) for the joined samples in Batch 1 exceeded that for one-piece Batch 2 ( $t = 3.067$ ,  $p = 0.007$ ). Batch 3 was slightly but not significantly weaker ( $t = 1.2$ ,  $p = 0.24$ ) than the joined batch. It was considered that the one-piece samples might have been weakened by the process of ejection from the BS mould and its use was abandoned.

#### 6.4.2 Opening the mould after 30 minutes or 7 days

In initial work, many joined samples broke on ejection from the BS cylindrical mould after condensation of the addition. It was considered that a factor which could influence the consumption of time in this study might be the minimum time required before joined samples could safely be removed from

the split mould. The mould was opened after a given time had elapsed after completion of the tenth sample. These samples were pressed by application of the loaded piston to the recently condensed part of the joined sample. At other times (unless stated differently) sample removal used the method described in Section 4.3.1 where load was applied to the parent part of the sample in the inverted mould.

Two time intervals were selected: 30 minutes was considered as a possible safe minimum (Batch 4: Plate 37); another group of joined samples were removed from the mould after 7 days (Batch 5: Plate 38). About 5 minutes elapsed between opening the mould and starting removal of the samples. The results indicated no significant difference ( $t = 0.2$ ,  $p = 0.84$ ) between the mean force to fracture for the two groups: 371N and 377N where the time elapsed between completion of the tenth sample and opening the split mould had been 30 minutes and 7 days respectively. In particular, the most recently prepared samples (and possibly therefore the most vulnerable to damage) were not obviously weaker than the others in the batch. It was concluded that opening the mould after 30 minutes had not adversely influenced the strength of the joined samples.

In Batch 5 (Plate 38), it is evident that fracture could occur in three possible locations: at the joint; in the parent (older) part or in the added (newer) part of the sample. Fracture across the joint line was also possible. Marking of the parent surface prior to end preparation, as described above, distinguishes the addition from the parent. The six weakest samples fractured in the parent. Of the four strongest samples, three failed at the joint. There was evidently some degree of structural discontinuity or easy crack path at the joint even though these samples were strong compared to others.

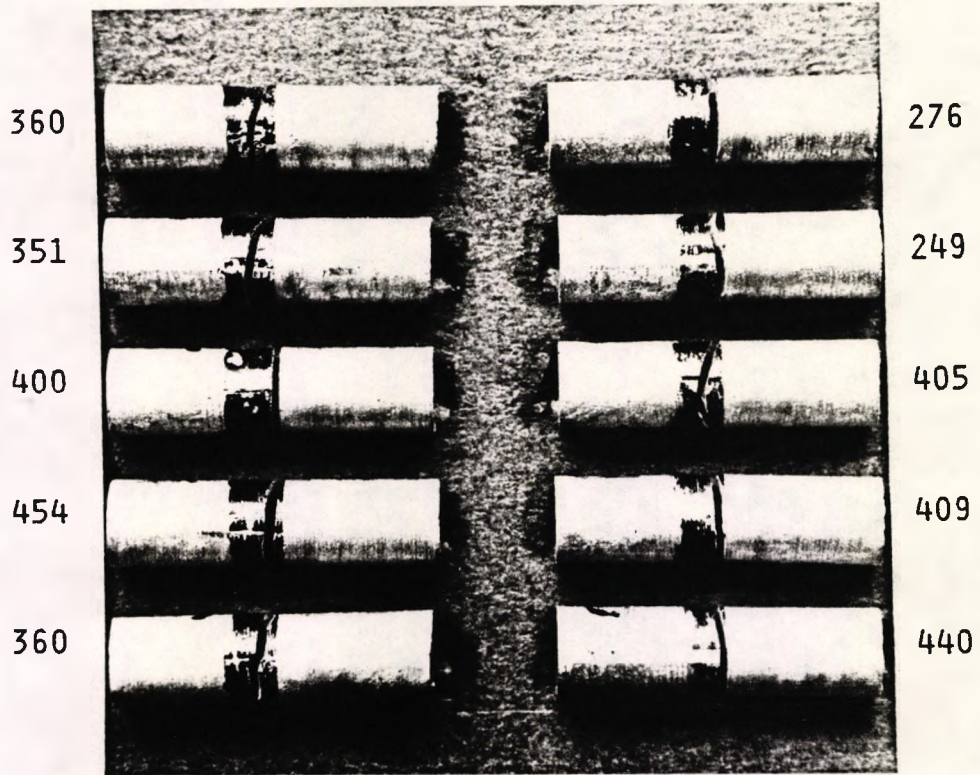


**Plate 37.** Batch 4: removed from the mould 30 mins after tenth sample. x3  
 Mean force to fracture: 371N.

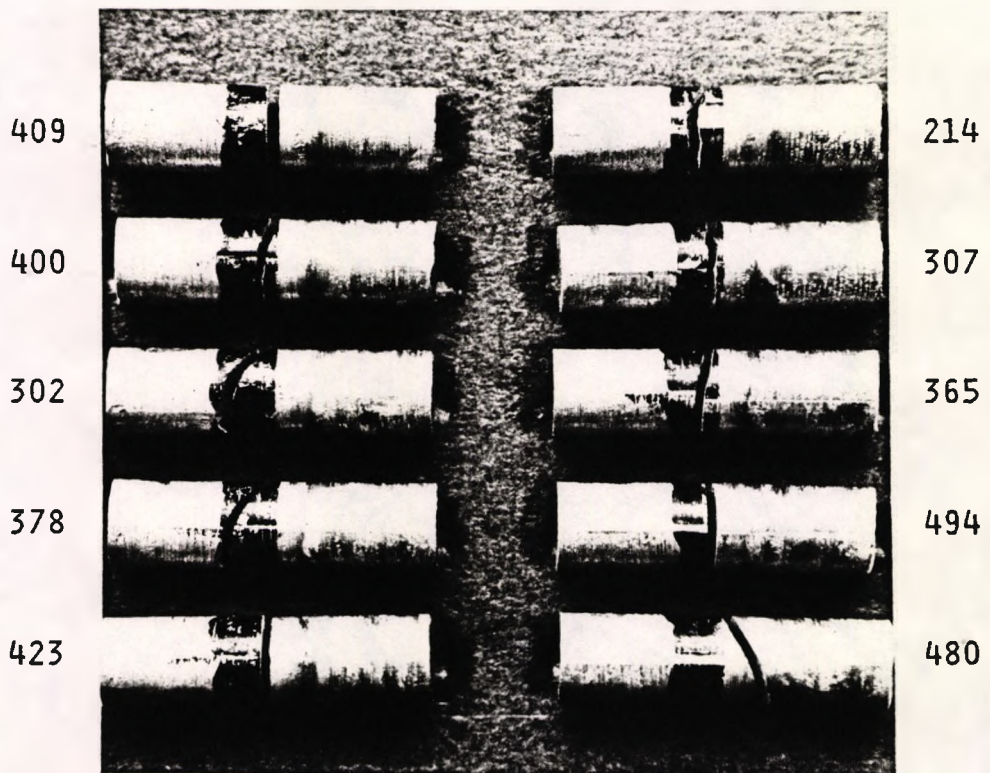


**Plate 38.** Batch 5: left in the mould for 7 days.  
 Mean force to fracture: 377N.

x3



Plate 39. Fractured surfaces of specimen 4.3.

x18



Plate 40. Fractured end surfaces of specimen 4.6.

x18

The fracture surfaces of these specimens were examined. Selected examples are shown in Plates 39 and 40. Sample 4.3 (Plate 39) was somewhat stronger than average: a force of 400N was recorded at fracture. Evidence of the radial pattern of end preparation scratches is visible over the majority of the end surfaces. In small areas amalgam had adhered to the joint.

In contrast, Sample 4.6 (Plate 40) was relatively weak: 276N to fracture. The end prepared surface of the joint is visible in about a quarter to one third of the fracture. In each case, each part of the fractured sample shows a mirror image of the opposite part. It appeared that failure had occurred due to a relative weakness in the parent material.

#### **6.4.3 Duralloy capsules and conventional Amalgam M**

According to several authors, for example, Miyata (1972); Fukuba *et al* (1977); Berge (1982); Hibler *et al* (1988); Schaller *et al* (1989) and Bass and Wing (1985), the bonding behaviour of amalgams of different compositions varies. High copper amalgams have produced weaker joints than amalgams of conventional composition. Degussa Ltd supplied a limited number of capsules of Duralloy when they generously donated the Dentomat 2 amalgamator for use in this project. These capsules were used for a preliminary trial of joining with this high copper "hybrid" amalgam. For comparison, conventional Amalgam M was used for joined samples condensed using the same condensing procedure. The parent parts were condensed by the deadweighted method. The first increment of the addition was condensed by vibration of the rubbing-in piston for 10s and the remaining three increments for 10s each using a flat ended piston.

The two groups differed in several respects. The mix of each amalgam was not identical in mass, volume or mercury/alloy ratio: the Dentomat dispensed

about 538mg Amalgam M alloy and 620mg mercury for each 2-dose mix, compared to 640mg alloy + 640mg Hg (manufacturer's specification) in the 2-spill Duralloy capsules. A fork attachment was available on the Dentomat to enable capsules to be mixed, but no recommended mixing time could be found in the manufacturer's product literature when using it. Therefore, an additional difference was that a Silamat amalgamator machine was used for 7s as recommended by Degussa for amalgamation of the capsules. In personal correspondence (1990) with Degussa, the company would not make a recommendation on use of the Dentomat fork attachment for amalgamation of Duralloy capsules. Jones *et al* (1986) found that two alloys (Solila Nova and Starburst) showed reduced compressive strength after both 1 hour (70%) and 24 hours (57%) when mixed for 30s in a slow speed Dentomat than 8s in a high speed Silamat, but these were both high copper alloys; there was no comparison with conventional amalgam alloy.

The mean force to fracture for Duralloy (282.2N, Batch 6, Plate 41) was not significantly less ( $t=0.5$ ,  $p=0.6$ ) than that for the conventional amalgam (300.7N, Batch 7, Plate 42). The three weakest Amalgam M samples fractured in the parent part. In contrast, 7 out of 9 Duralloy samples fractured at the joint and only two (including the strongest) fractured in the parent. The strength of the joint is determined when a sample fractures at the joint. When a joint survived the test, the strength of joint was not less than that represented by the recorded force to fracture. Generally, therefore, the joints of Duralloy samples appeared to be weaker than those of Amalgam M. One Duralloy sample was found in two pieces on opening the mould.

Examination of the fracture surface of those Duralloy samples which had broken at the joint showed a clear negative impression in the amalgam of the second part of the score pattern from end preparation. There appeared to be excellent adaptation of the new amalgam to the old amalgam surface, but

there was little evidence of union having occurred. This was in contrast to the Amalgam M conventional amalgam where there was usually evidence of some degree of union in those samples which had apparently fractured at the joint.

In Duralloy specimen 6.10, approximately 80% of the fracture surface included the joint interface but in the area close to the central loading roller, the fracture deviated away from the joint. It appeared that the joint had not been located exactly centrally in the 3 point loading rig. This had also happened in testing samples 4.9 and 4.10.

Compared to Batches 4 and 5 which were prepared and tested earlier in the study, Duralloy was significantly weaker. The 95% confidence intervals for these differences in mean force to fracture were from more than 30N to over 140N. Batch 1 was somewhat stronger: the 95% confidence interval for the difference between the mean force to fracture for this and Duralloy was from -2.8N to 117.6N ( $p=0.09$ ). [Note: the resolution of the test machine used for this work, the Instron TTC, is approximately 2N; hence 2.8N is possibly insignificant].

At this early stage in the study, in view of the apparent difference in behaviour of this high copper amalgam for joining compared to conventional amalgam, it was decided to pursue refinements to the methods of sample preparation using only the conventional amalgam alloy with which the author was very familiar. After further development of experimental techniques, high copper amalgam alloys were used for joined samples.

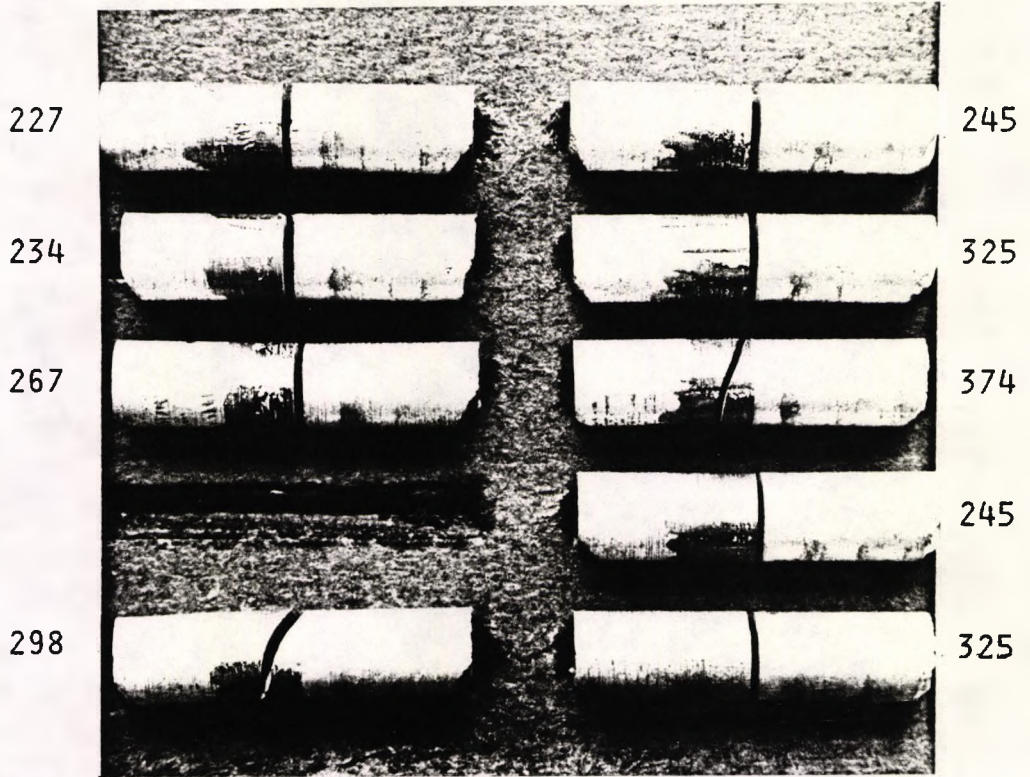


**Plate 41.** Batch 6. Duralloy (capsules).  
 Mean force to fracture: 282N.

x3

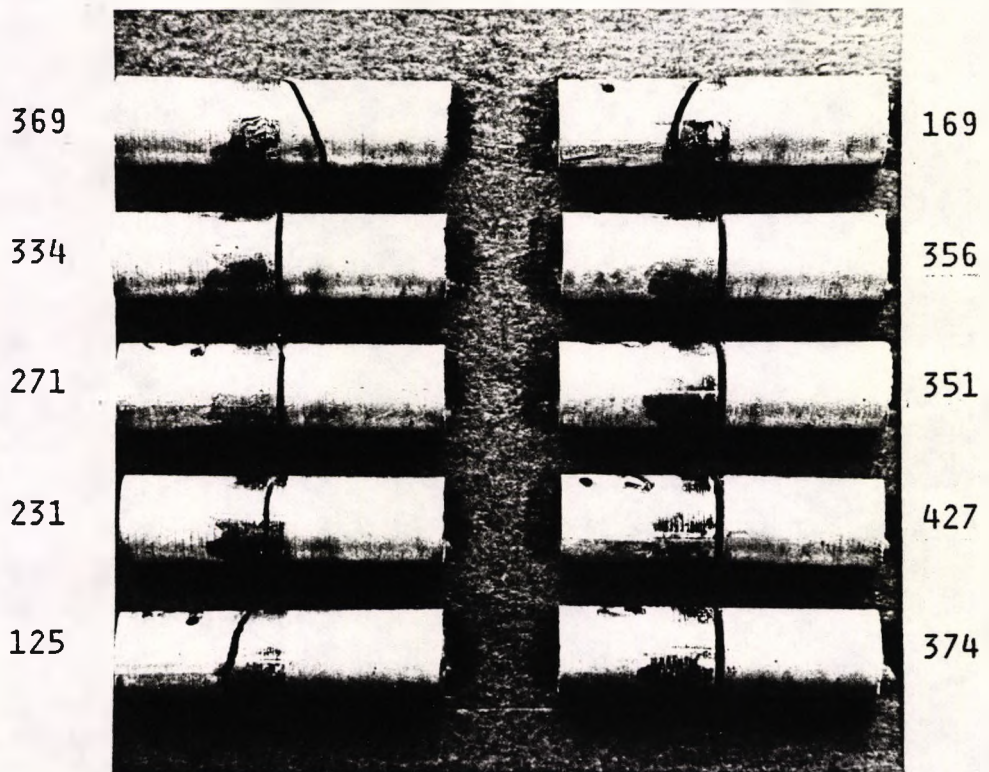


**Plate 42.** Batch 7. Amalgam M.  
 Mean force to fracture: 301N.

x3

#### 6.4.4 One-piece Batches 8 and 9

In view of the fact that only two joined samples in Batches 1, 4, 5 and 7 had fractured in the addition, it was considered that vibration applied to each increment for the duration of 10s might be excessive. The condensation time for one-piece Batch 8 was reduced to 2s per increment. Although the mean force to fracture was similar to that for Batch 3 ( $p=0.38$ ), Figure 9 shows that two samples were notably weak. When the DW condensation procedure was repeated for Batch 9, the mean force to fracture was not significantly greater than that of Batch 2 ( $p=0.24$ ). One sample was very much stronger than the others in the batch. Batches 8 and 9 were prepared in the split mould and were tested after 14 days.

#### 6.4.5 Sample diameter

The flexural strength of a cylindrical sample varies with the square of the radius (Jones and Berard, 1972). The diameters of samples from different lumens of the split mould were tested for uniformity. Measurements were made with a screw micrometer using the ratchet thimble to avoid overtightening. Care was taken to avoid parallax errors in reading the vernier scale which gave millimetre measurements to three decimal places. The instrument calibration was checked against standards and the estimated accuracy was better than 0.01mm. Eight readings were recorded after rotation of each sample through about  $20^\circ$ . Where there was visible evidence of the interface between split mould parts (either "flash" or surface abrasion), apposition of these areas with the micrometer contact faces was avoided.

Analysis of variance (ANOVA) of the results for Amalgam M samples in Batches 4 to 9 ( $F=5.02$  [9,390df]  $p=0.0000$ ) indicated statistically significant differences in sample diameter measurements with respect to

mould lumen. For sample 8.1, the range of readings obtained was 0.076mm. Excluding this result, the range for measurements of samples from different mould lumens was from 0.025mm to 0.050mm. The difference between the smallest mean diameter, 4.0255mm (for lumens 2 and 5) and the largest, 4.0369mm (for lumen 10) was 0.0114mm *i.e.* about one quarter of one per cent of the mean. Assuming that the mean value for sample diameter (rather than for example the minimum recorded value) is related to sample strength, the range in flexural strength due to sample diameter variation was therefore about one half of one per cent. This is small compared to the range in force to fracture results obtained and thus for practical purposes was considered insignificant.

A possible error in the measurements was due to surface roughness to which mould irregularities could have contributed. Subjectively, pronounced machining marks were noted in lumen 10 where the maximum mean diameter was recorded. Such marks produced elevations on the sample surface which might have prevented contact of the micrometer faces with the underlying material. Measurement of sample surface roughness or porosity and their relation to flexural strength were considered beyond the scope of this study.

#### **6.4.6 Review of the initial experiments: Sets 1 (joined), 2 and 3 (one-piece)**

The parent parts of Batches 1, 4, 5 and 7 were condensed by the DW method and the first increments of the addition parts were condensed by application of the RI piston for 10s. Although there were differences in the timing of preparation and test for these batches, the results suggested that the variables investigated may have had little effect on the strength. The result of ANOVA on the force to fracture results from these batches was not significant ( $F = 1.752 [3,36 \text{ df}] p = 0.17$ ). The largest difference in mean force to fracture was between Batches 5 and 7 where Student's *t*-test did not achieve

significance at the 5% level of confidence. The results were pooled to make Set 1.

Batches 2 and 9 were one-piece samples condensed by the DW method but using different moulds and tested after 28 and 14 days respectively. The means of force to fracture for these batches were not significantly different ( $p = 0.24$ ). Set 2 was formed by pooling the results.

Similarly, the samples in Batches 3 and 8 were condensed using different moulds and test intervals for each batch. Vibration was applied for differing durations (10s or 2s respectively) on each portion of a 3-spill mix divided into six parts. However, the mean force to fracture results were not significantly different ( $p = 0.38$ ) and they were pooled to form Set 3.

The cumulative frequencies of force to fracture for Sets 1, 2 and 3 shown in Figure 11 demonstrate that Set 2 (DW one-piece) was weaker than Sets 1 and 3. Tables 11 and 12 show the force to fracture statistics and the differences between means for these Sets.

A quarter of samples in Set 1 exceeded the maximum recorded for Set 3 but the difference between the means of Sets 1 and 3 was not statistically significant.

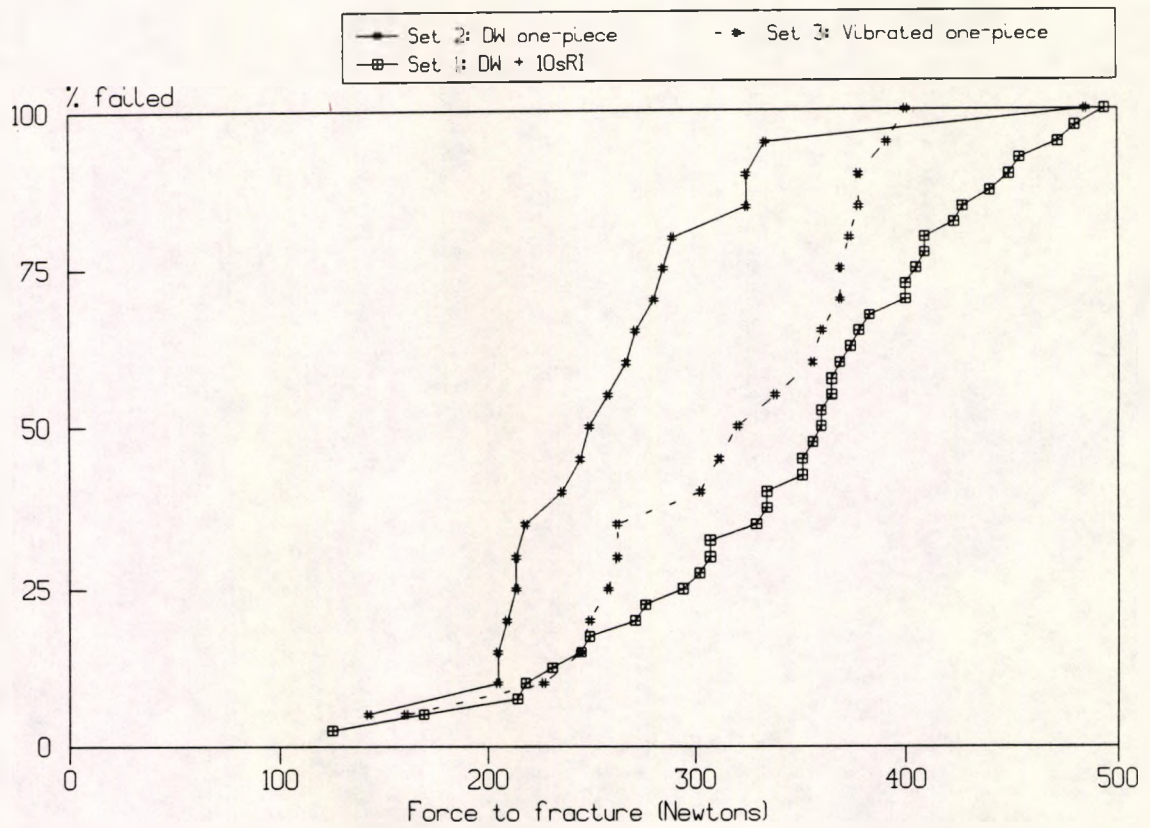


Figure 11. Cumulative frequencies of force to fracture for Sets 1, 2 and 3.

Set	Batches	No.	Mean Load	S.D.(n-1)	95% C.I. for Mean		Median Load
					From	To	
1	1,4,5,7	40	347.0	85.8	319.5	374.4	360.0
2	2,9	20	262.8	71.0	229.5	296.0	253.5
3	3,8	20	315.5	66.7	284.2	346.7	329.0

Table 11. Force to fracture statistics of Sets 1, 2 and 3 (Newtons).

Sets	95% C.I. for the difference in means		Student's t-test	
	From (Newtons)	To (Newtons)	t =	P =
1 & 2	42	126	4.03	0.0002
1 & 3	-9	72	1.56	0.12
2 & 3	8	97	2.42	0.021

Table 12. Confidence intervals for differences in mean force to fracture between Sets 1, 2 and 3 and results of two sample t-testing.

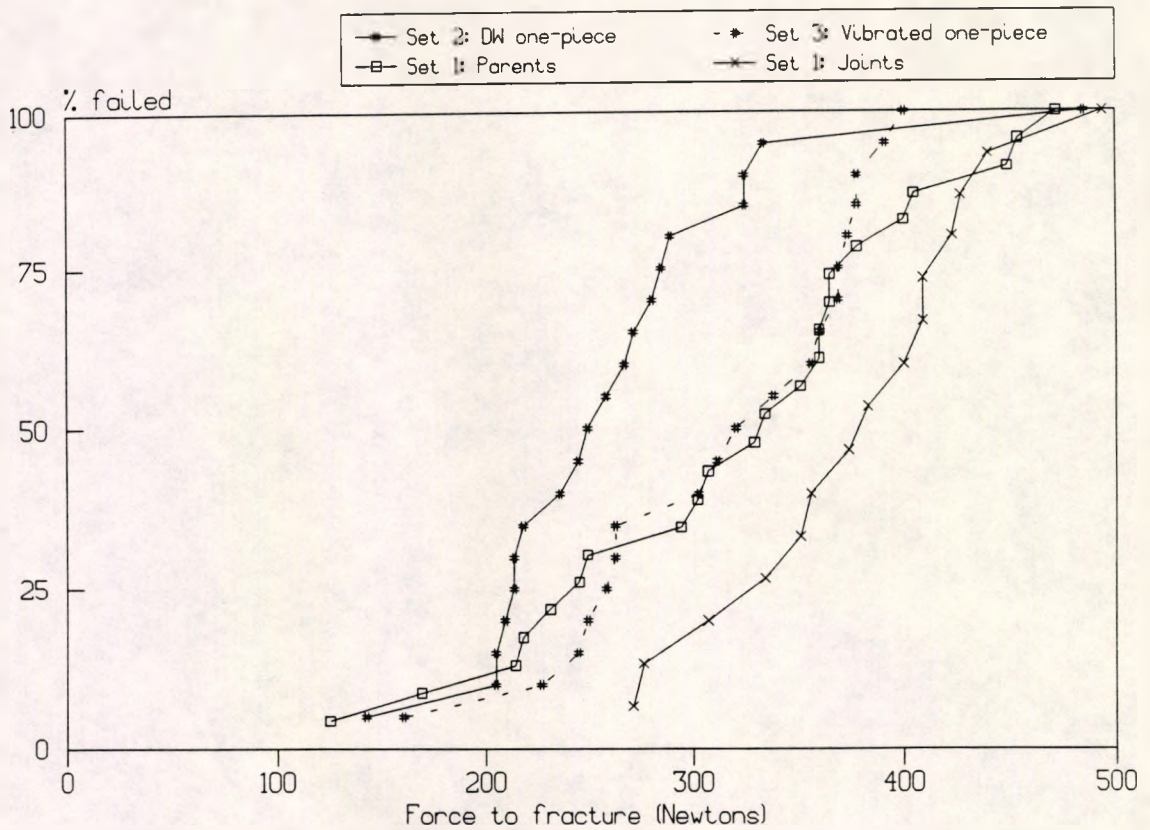


**Figure 12.** Cumulative frequencies of force to fracture for Sets 1, 2 and 3 where Set 1 has been divided into subgroups according to the location of fracture origin.

Set	Batches	No.	Mean Load	S.D.(n-1)	95% C.I for mean		Median Load
					From	To	
2	2,9	20	262.8	71.0	229.5	296.0	253.5
3	3,8	20	315.5	66.7	284.2	346.7	329.0
1 P	1,4,5,7	23	320.7	91.8	281.0	360.4	326.7
1 J	1,4,5,7	15	376.9	62.2	342.5	411.4	380.0

**Table 13.** Force to fracture statistics (Newtons) of Sets 2, 3 and Set 1 which was divided into groups where the fracture originated in the Parent or Joint.

Sets	95% C.I for the difference in means		Student's t-test	
	From (Newtons)	To (Newtons)	t =	p =
1P & 1J	5	107	2.25	0.031
1P & 2	8	108	2.33	0.025
1P & 3	-54	44	0.22	0.83
1J & 2	68	160	5.05	0.0000
1J & 3	17	106	2.80	0.0086

**Table 14.** Confidence intervals for difference in mean force to fracture between Sets 2, 3, and Set 1 Parents and Joints and results of two sample t-testing.

In Set 1, 23 out of 40 joined samples failed in the parent part, 15 failed at the joint and only 2 failed in the addition part. There were significantly more parent failures than expected under the  $\frac{1}{4}:\frac{1}{2}:\frac{1}{4}$  hypothesis (see Section 4.7.5; Fisher's test  $p=0.003$ ) and fewer addition failures ( $p=0.013$ ). The force to fracture results for Set 1 were divided into subgroups where the fracture occurred in the parent or joint (Sets 1P and 1J). These are shown in Figure 12 and Table 13 with Sets 2 and 3 for comparison. The mean force to fracture for Set 1J (which failed at the joint) was significantly higher than Set 1P where failure occurred in the parent ( $p=0.03$ ). One third of samples which failed in the parent were weaker than the weakest joint.

The mean forces to fracture of these subsets were compared to the one-piece "controls". These are shown in Table 14. Set 1P, where failure occurred in the parents, was stronger than DW condensed one-piece Set 2 ( $p=0.025$ ) but not significantly different to the vibration condensed Set 3 ( $p=0.83$ ). In contrast, Set 1J failed at a significantly higher mean load than either one-piece set.

These findings are at variance with the view that the joint interface between new and old amalgam is weaker than a one-piece condensed sample. If there had been a significant reduction in strength at the joint compared to the adjacent material all of the failures would have occurred at the joint which was at the centre of the span under 3 point bending. The fact that only two samples in Set 1 failed in the addition suggested that these parts were generally not the weak link in the joined samples. No reports have been found in the literature where the mean force to fracture for failed joints exceeded that for the one-piece controls.

The following possible explanations were considered for these findings. Jørgensen and Saito (1968) found that doubling of the volume of mix was

without influence on various physical properties of the amalgam. It was therefore considered that an increase in size of mix of only 50% *i.e.* three doses of amalgam for one piece samples condensed at one time compared to two doses in each half of the joined samples would be unlikely to influence the flexural strength of the amalgam.

It is known that the final mercury content and compressive strength of amalgam is dependant on the pressure applied during condensation and that pressure in a powder varies with distance from the plunger and walls of the containing vessel (Gray, 1968). A fresh mix of amalgam is composed of liquid mercury, alloy powder and recently precipitated new phases which are growing from the mercury solution. Although the analogy with dry powder technology might not be exact, similar pressure variations in amalgam during condensation by the deadweighted method could be expected to occur. Granath *et al* (1967) found that the mercury content of amalgam cylinders condensed in one piece was increased at the middle one third compared to the ends and also in the "core" compared to the "mantle". These variations in residual mercury content could be expected to influence the tensile and flexural strength of the amalgam in a similar manner to such variations in compressive strength.

During condensation, movement of the loaded piston occurs as a result of compression of the fresh amalgam mix within the mould. Under pressure, solid particles in the mix might engage in any surface irregularities in the imperfectly smooth mould and tend to resist further movement of the piston. This was borne out by the experience that moderate force may be required to reposition the amalgam sample in the mould after removal of the load and BS spacer No 2 prior to the second thrust of the BS condensation procedure. Due to reason of possible contamination of the amalgam mix the use of a mould lubricant to reduce friction was rejected.

The amalgam cylinders which formed the parent parts of these joined samples had been replaced in the split mould in the same longitudinal orientation as when condensed. The material adjacent to the joint surface had been immediately under the condensing piston where the pressure would have been greatest. Any fractures located close to the joint in the parent part of joined samples would have occurred in this layer of amalgam. In contrast, in samples condensed in one piece, the fracture would occur in the middle part of the sample, *i.e.* approximately 5 to 6mm from either end, where the condensation pressure would have been reduced.

Jørgensen and Saito's joined samples were not stronger than their one piece controls. In their preparation method, one piece samples 10mm in length were cut into two sections each 5mm long. After polishing, cleaning and treatment of the cut end surface, the addition part of the joined samples was condensed against it. The amalgam adjacent to the joint in the parent part had therefore originated from the central part of the long cylinder where it must have experienced a reduced condensation pressure compared to the ends. This might explain the similarity between the strengths of their one piece and strongest joined samples. Their condensation procedure applied a higher pressure (about 20 MPa for 3 minutes) than the BS requirement of 14 MPa pressure for a total time of 55s which was used in this study. It may be possible that the BS condensation procedure allowed weaknesses to remain in the middle of a sample which could have been eliminated by prolonged or increased condensation pressures.

Jørgensen and Saito reported that fractures were most frequent outside the joint in the experimental groups receiving mercury (Hg) treatment. They did not specify whether the failures occurred in the parent or addition parts. They showed fractured examples where the curved fracture plane had originated at a substantial distance away from the joint and ended at the central area

loaded by their 3 point bending apparatus. However, all samples not receiving Hg treatment fractured at the joint.

In this study, the parent parts in Set 1 failed most frequently. Only two of the joined samples fractured in the addition part. The incremental and vibrational method of preparation clearly produced stronger amalgam than condensation by the deadweighted method. However, the maximum force recorded to fracture incrementally condensed one-piece samples was less than the maxima for other types of sample. It was considered possible that the incremental method might have introduced a potential reduction of tensile strength between adjacent incremental layers. Any such weakness might become more prominent with increased duration of vibration in condensation, so there might be an optimum duration of condensation for maximum strength. Too short a time might result in excess mercury remaining in the sample but too long a time leading to effective removal of mercury and high strength in each layer but introducing a weakness between layers.

Attention was given to the development of vibrational procedures for the condensation of both the parent and addition parts of joined samples. The preparation of one piece samples was also investigated further.

#### **6.5 Preparation of joined samples: parents condensed by vibration**

The weakest Amalgam M joined samples in Batches 1 to 7 fractured in the parent and one-piece samples were stronger when condensed by vibration than by the DW method. In light of these findings, the use of vibration for condensation of both parts of joined amalgams was considered with a view to increasing the parent strength. The parents of the joined samples in Batches 10 to 15 were condensed by vibration using a flat ended piston for 2s on each of four increments. Either a flat ended piston or the RI piston was

used for condensation of the first addition increment of the joined samples. For one-piece samples a 3-spill mix was divided into six increments each condensed using a flat ended piston for 2s. The force to fracture data for these batches are shown in Figure 13 and Appendices 1 and 2.

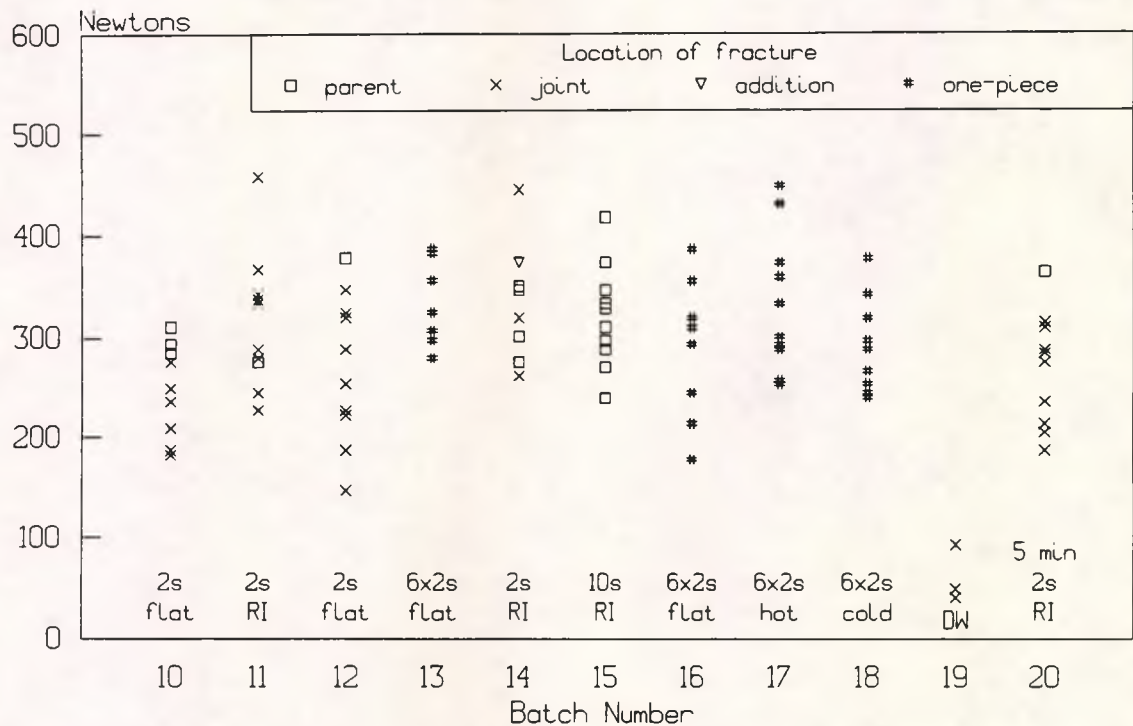


**Figure 13. Force to fracture for Batches 10 to 20.**

The parent parts were condensed using a flat piston under vibration for 2s on each of four portions.

#### 6.5.1 Addition condensed using the flat ended piston for 2s: Set 4

All four increments of the addition part of joined samples in Batches 10 and 12 were condensed for 2s using a flat ended piston. These batches were not significantly different in mean force to fracture ( $p=0.46$ ). It may be seen in Figure 13 that failure occurred at the joint in all except the strongest samples in each batch. The results were pooled to make Set 4.

### 6.5.2 Addition condensed using the RI piston for 2s: Set 5

When the first increment of the addition was condensed using the RI piston for 2s (Batch 11), 9 out of 10 fractured at the joint. The preparation procedure was repeated for Batch 14 but only 4 samples broke at the joint. Since the difference in mean force to fracture was not significant ( $p = 0.56$ ), Batches 11 and 14 were pooled to form Set 5. ANOVA for the one-piece condensed Batches 13, 16 and 18 ( $F = 1.778$  [3,27df]  $p = 0.19$ ) revealed no differences and these were pooled to make Set 6.

In Figure 14 and Tables 15 and 16, it may be seen that Set 4 was significantly weaker than both Set 5 and one-piece Set 6. The use of the RI piston (Set 5) for condensation of the first increment of the addition produced stronger joined samples than the flat ended piston (Set 4). However, the distribution of location of failure origin for Set 4 was similar to that for Set 5. In contrast to the result for testing Set 1, about three quarters of the samples failed at the joint. Fisher's test of these distributions (Set 1 vs Set 4 or 5) was significant at  $p < 0.03$ . Only one sample (in Batch 14, Set 5) failed in the addition (see Plate 43).

Five samples in each set failed in the parent. It was considered that these numbers were too few to produce meaningful statistical analyses of the force to fracture data for these subsets. The mean force to fracture for Set 5 exceeded that for Set 6 but the difference was not significant ( $p = 0.13$ ).

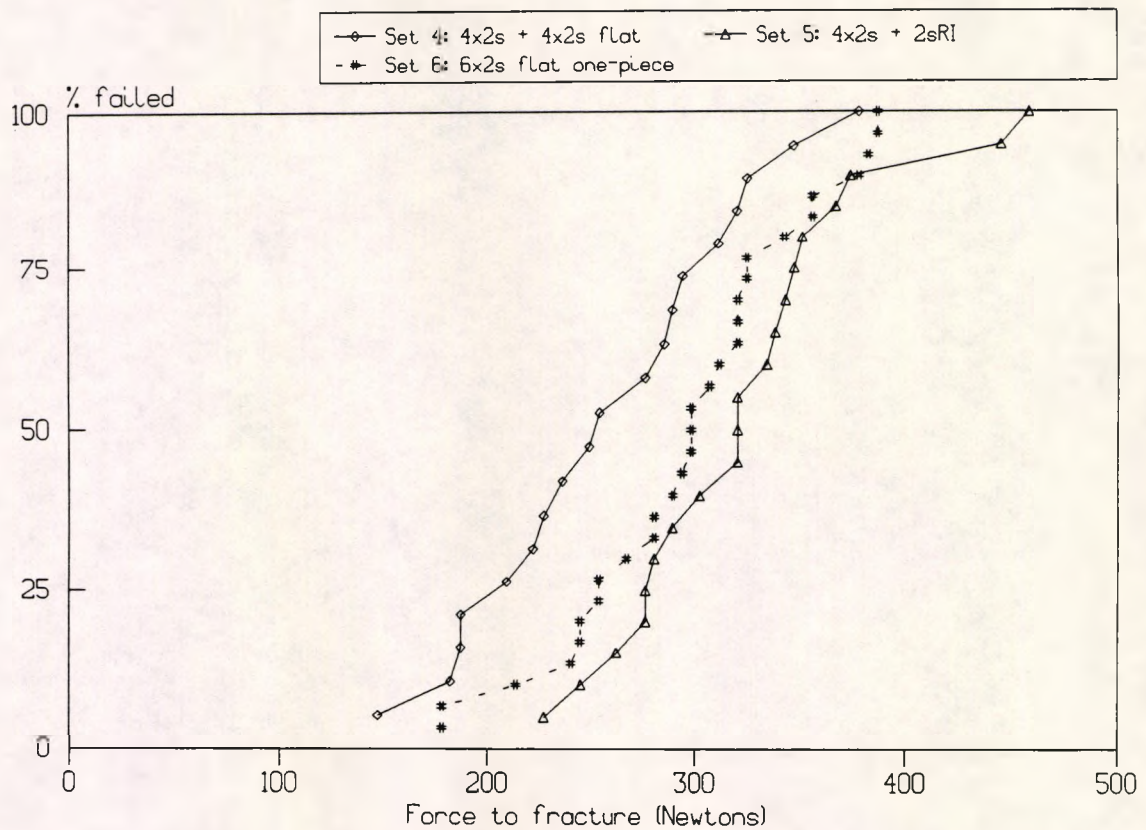


Figure 14. Cumulative frequencies of force to fracture for Sets 4, 5 and 6.

Set	Batches	No.	Mean Load	S.D.(n-1)	95% C.I. for Mean		Median Load
					From	To	
4	10,12	19	259.2	62.4	229.1	289.3	254.0
5	11,14	20	323.7	59.2	296.0	351.4	320.0
6	13,16,18	30	297.7	56.3	276.7	318.7	298.0

Table 15. Force to fracture statistics for Sets 4, 5 and 6 (Newtons).

Sets	95% C.I. for the difference in means		Student's t-test	
	From (Newtons)	To (Newtons)	t =	P =
4 & 5	25	104	3.31	0.0022
4 & 6	3	74	2.18	0.036
5 & 6	-8	60	1.55	0.13

Table 16. Confidence interval for difference in mean force to fracture between Sets 4, 5 and 6 and results of two sample t-testing.

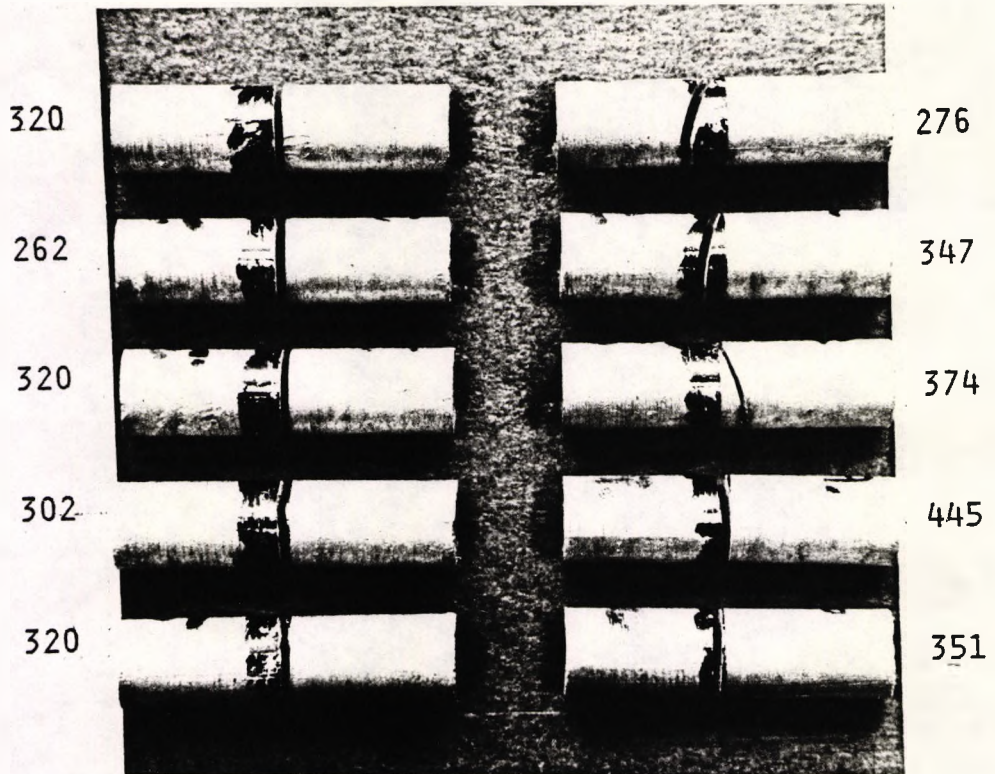


Plate 43. Batch 14: 2s RI piston. Mean force to fracture: 332N x3

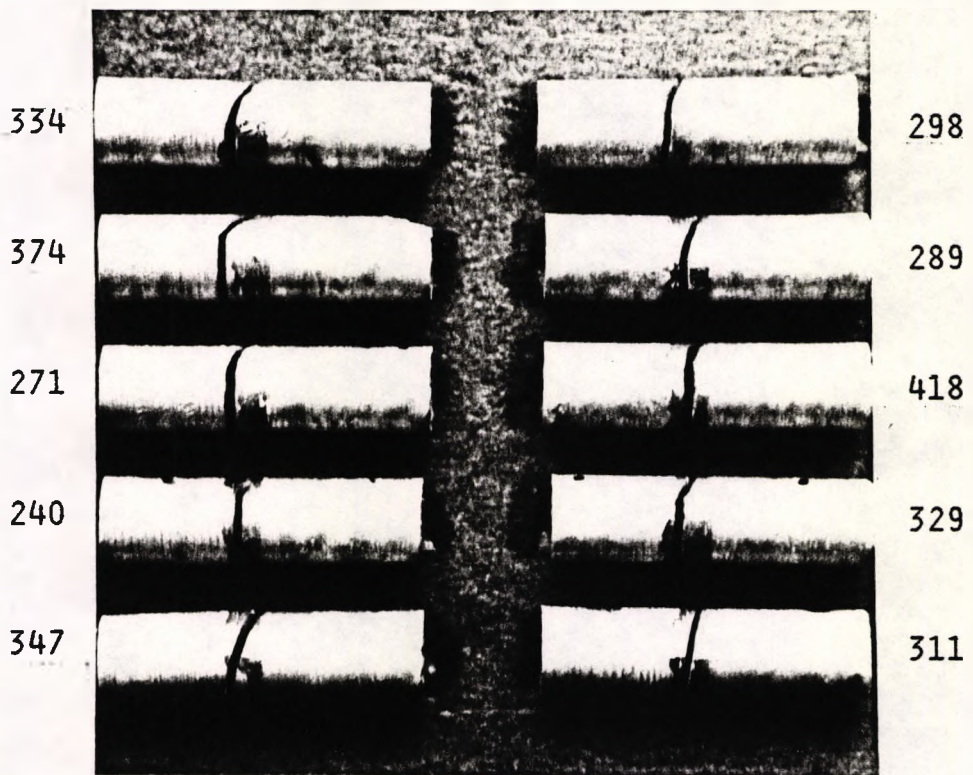


Plate 44. Batch 15: 10s RI piston. Mean force to fracture: 321N x3

The mean force to fracture for Set 5 was not significantly different to that of Set 1 but it was somewhat less than Batches 4 and 5 ( $0.05 < p < 0.07$ ). When the force to fracture data for Batches 4 and 5 were pooled to produce statistical samples of equal numbers, the 95% confidence interval for this difference in means was from 7N to 93N ( $t = 2.36$ ,  $p = 0.024$ ). This, together with the relatively high frequency of joint failures in Set 5, suggested that the reduced vibration time of 2s with the RI piston for the first addition increment may have produced slightly weak joints.

### **6.5.3 Addition condensed using the RI piston for 10s: Batch 15**

It was considered that increasing the duration of condensation of the first increment of the addition part of joined Amalgam M might increase the strength of joint sufficiently for the fracture to occur in the parent. Failure in the addition had occurred rarely and was not expected. It was anticipated that the strength of these joined samples might be similar to those where the RI piston was used for 2s. The first addition increment of Batch 15 was condensed using the RI piston for 10s and the remaining three increments for 2s each with the flat ended piston. All samples failed in the parent as shown in Plate 44. The mean force for fracture was not significantly different ( $p = 0.9$ ) to those for joined Set 5 and one-piece Set 6 ( $p = 0.25$ ).

### **6.5.4 Opening the mould 5 minutes after completion of batch condensation**

The effect of opening the mould 30 minutes after completion of condensation of the tenth sample in the batch was considered in Section 6.4.2. A more severe test of possible vulnerability of recently condensed samples was considered.

The split mould was opened five minutes after completion of condensation of

the tenth sample. Samples were pressed out of the mould by application of load to the added amalgam. If a reduction in strength of the most recently condensed samples compared to the others occurred it might indicate a problem; if no reduction in strength were observed, then there would almost certainly be no cause for concern. These strength tests were carried out two months after preparation due to unavailability of the Instron TTC testing machine but this delay was considered unlikely to be of material influence on the test result.

Two groups of joined samples (Batches 19 and 20, Figure 13) were prepared where the parents were condensed by vibration using a flat ended piston for 2s on each quarter. For Batch 19, the additions were condensed in one part by the deadweighted method: similar methods had been used by Jørgensen and Saito (1968) and Berge (1982) using a cylindrical mould. The condensation procedure for Batch 20 repeated that used for Set 5.

#### **6.5.4.1 Deadweighted addition: Batch 19**

In Batch 19, four out of ten samples fractured on removal from the mould. The remaining six samples were very weak: the mean force to fracture was 51.6 N. All samples failed at the joint. It cannot be ascertained from this result whether the condensation procedure for the addition or the early removal from the mould was primarily responsible.

Plate 45 shows specimen 19.3 where the deadweighted condensation method was used for the addition part. In contrast to Plates 39 and 40 (page 117), no obvious common features are evident between the two fracture surfaces. The end preparation pattern is clear in the parent part (on the left) but there was no evidence of union having occurred. No further work was carried out using this method with conventional amalgam alloy.

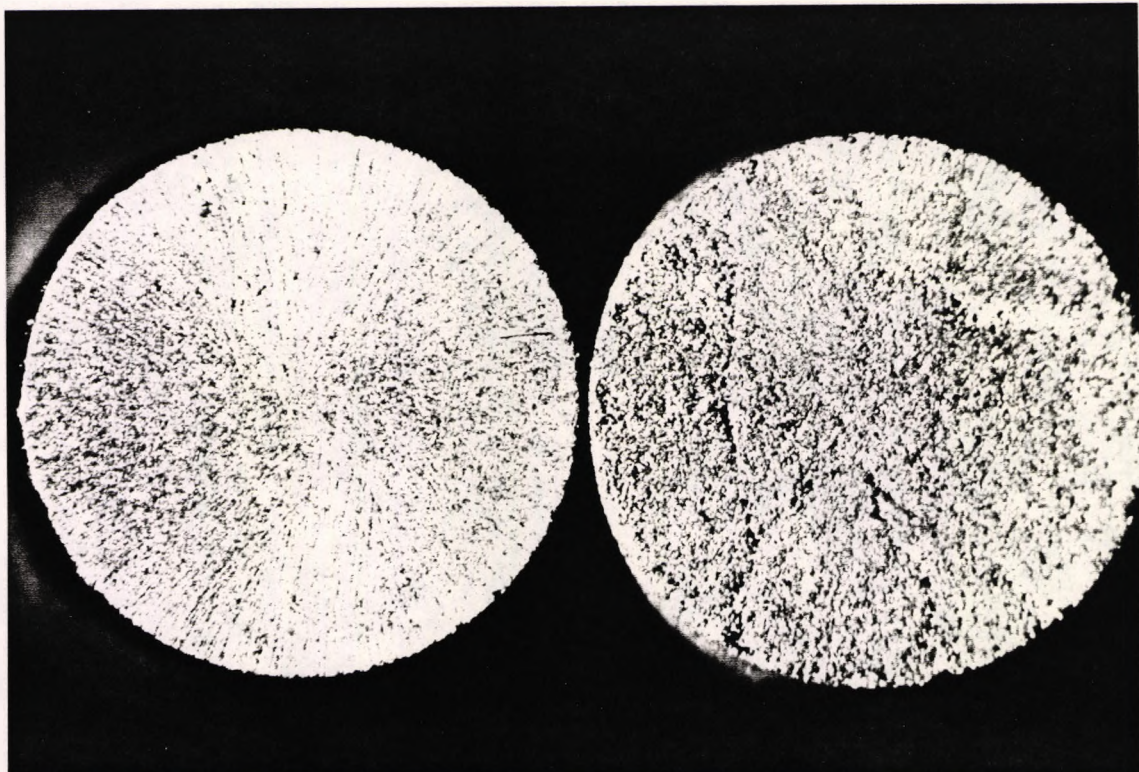


**Plate 45.** Fractured end surfaces of specimen 19.3

x18

#### **6.5.4.2 Addition condensed for 2s by RI piston: Batch 20**

None of the vibration condensed samples in Batch 20 broke on removal from the mould. The mean force to fracture was 268.2 N, but the seventh, ninth and tenth samples to be condensed were among the four weakest in the batch. Conversely, the three strongest samples were condensed second, third and fourth in the batch. All except the strongest sample failed at the joint. The time elapsed between condensation and removal from the mould of the tenth and first samples in the batch was eight and fifty three minutes respectively.

The cumulative failure curves in Figure 15 compare Batch 20 with Set 5. The numerals below the data points for Batch 20 refer to the sample hole number of the mould and the order in which the samples were prepared. The most recently condensed samples were weaker than those prepared earlier. The mean force to fracture for Batch 20 was significantly less than that for Set 5

( $t = 2.48$ ,  $p = 0.023$ ). The 95% confidence interval for the difference in mean force to fracture between Set 5 and Batch 20 was from 9N to 102N.

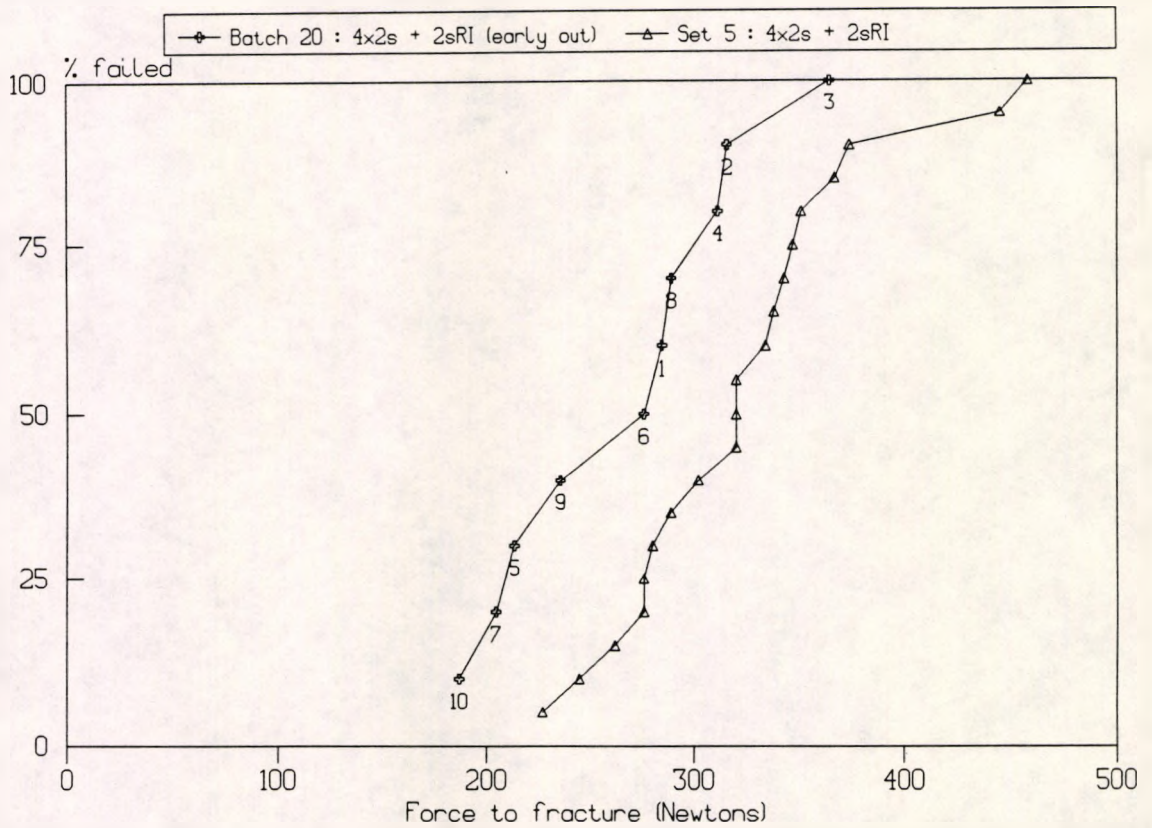


**Figure 15.** Cumulative frequencies of force to fracture for Set 5 and Batch 20. The numbers below the data points for Batch 20 refer to the sample hole in the split mould used for specimen preparation.

Set	Batches	No.	Mean Load	S.D. (n-1)	95% C.I. for Mean		Median Load
					From	To	
5	11, 14	20	323.7	59.2	296.0	351.4	320.0
	20	10	268.4	56.6	227.9	308.9	265.0

**Table 17.** Force to fracture statistics for Set 5 and Batch 20 (Newtons).

It was considered that the stresses early applied to samples unavoidably during their removal from the mould might have weakened the later condensed samples. 30 minutes was considered to be a safe time interval between completion of condensation of the tenth specimen and opening of the mould and its use, adopted after testing of Batch 5, continued for the remainder of the study.

## 6.6 Preparation of joined samples: increased vibration time

The vibration time of 2s for each increment of mix was used for condensation of both parent and addition parts of Batches 10 to 14. As reported in Sections 6.5.1 and 6.5.2, this reduced duration produced weak joints when the flat ended piston was used for condensation of the first increment of the addition. Joints were stronger when the RI piston was used for 2s and all samples failed in the parent when the first increment was condensed for 10s using the RI piston (Batch 15). The use of different durations of vibration for each increment was considered for Batches 21 to 30.

Mercury in a fresh mix is consumed rapidly by precipitation of the silver-mercury phase ( $\text{Ag}_2\text{Hg}_3$ ; known as gamma-1) which causes the amalgam to set. Delayed condensation leads to increased mercury content and reduced compressive strength (Forsten, 1972; Jørgensen *et al*, 1964). Methods of time saving were considered with a view to reduction of the time elapsed between mixing and condensation of the final parent increment. This might reduce the mercury content of the increments and therefore increase strength.

It was not possible reliably to take less time than 10s to introduce each portion of the divided mix into the mould. If 2s vibration on the first and second increments of parents were used, followed by 4s and 10s for the third and fourth portions respectively, completion of condensation would occur 22s earlier than when 10s vibration was applied for each increment. It was considered that extended application prior to the final increment might cause weakness between layers. Prolonged condensation of the final increment was not necessarily disadvantageous since the end surface was to be abraded for joining.

The proposed time schedule (2,2,4,10s) for condensation of parents was

considered to be a reasonable balance between vibration time for each increment and early completion of condensation. The duration of vibration for the addition parts of these joined samples (except Batch 23) was the converse: 10s was applied to the first increment, 4s for the second and 2s for the third and fourth portions. The segment of the sample at the centre of the span i.e. the fourth increment of the parent and first increment of the addition were therefore each condensed by vibration for 10s. The first increment of the addition was condensed using either the RI piston or the flat ended piston. For Batch 23, the flat ended piston was applied to the first increment for the reduced duration of 2s and the remaining three increments for 10s, 4s and 2s respectively. The results for Batches 21 to 30 are shown in Figure 16.

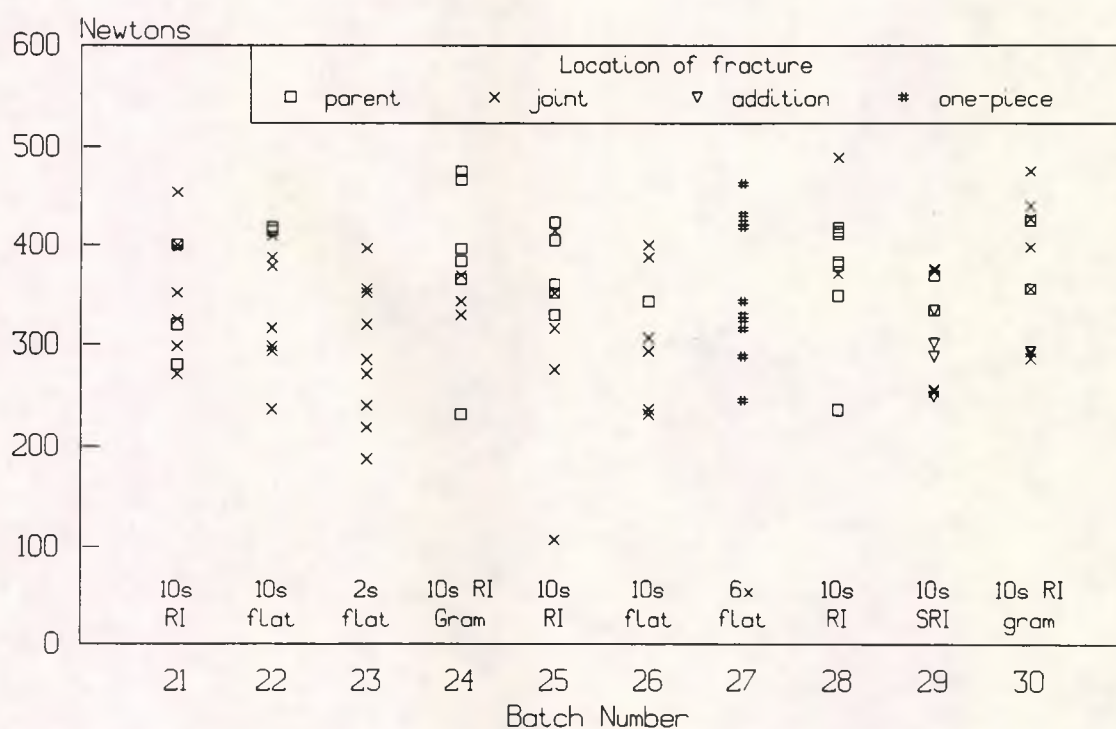


**Figure 16.** Force to fracture for Batches 21 to 30. The four parent increments were condensed for 2,2,4,10s respectively.

### 6.6.1 Addition condensed using the RI piston for 10s: Set 7

The RI piston was applied to the first increment of joined samples for 10s. The force to fracture values for these batches (21, 25 and 28) were tested by

ANOVA. Since the differences in the mean force to fracture results were not significant ( $F = 1.369$  [2,27df]  $p = 0.27$ ) they were pooled to make Set 7.

#### **6.6.2 Addition condensed using the flat ended piston for 10s: Set 8**

The first increment of the addition of Batches 22 and 26 was condensed by application of a flat ended piston for 10s. The means of force to fracture for these batches were not significantly different ( $t = 0.74$ ,  $p = 0.47$ ) and were pooled to make Set 8.

Figure 17 and Tables 18 and 19 show the results for Sets 7 and 8 with Set 6 for comparison purposes. The means of force to fracture for these experimental joined groups were not significantly different. However, compared to the one-piece Set 6, Set 7 was highly significantly stronger but Set 8 was only stronger at the 5% level of statistical significance.

The distribution of the location of the fracture origin was different (Fisher's Exact test  $p = 0.0087$ ) for the two experimental joined groups. In Set 8, 16 out of 19 samples failed at the joint, whereas 14 failed at the joint and 16 failed in the parent (out of 30) in Set 7. No failures occurred in the additions. When the RI piston was used for condensation of the first increment of the addition the strength of joint was increased so that more samples failed in the parent than at the joint.

#### **6.6.3 Addition condensed using the flat ended piston for 2s: Batch 23**

When the flat piston was applied for 2s for the first increment of the addition (Batch 23), all failed at the joint. The mean force to fracture (see Appendix 3) was significantly less than Set 7 (RI piston for 10s;  $p = 0.026$ ) but only somewhat reduced when compared to Set 8 (flat piston for 10s;  $p = 0.12$ ).

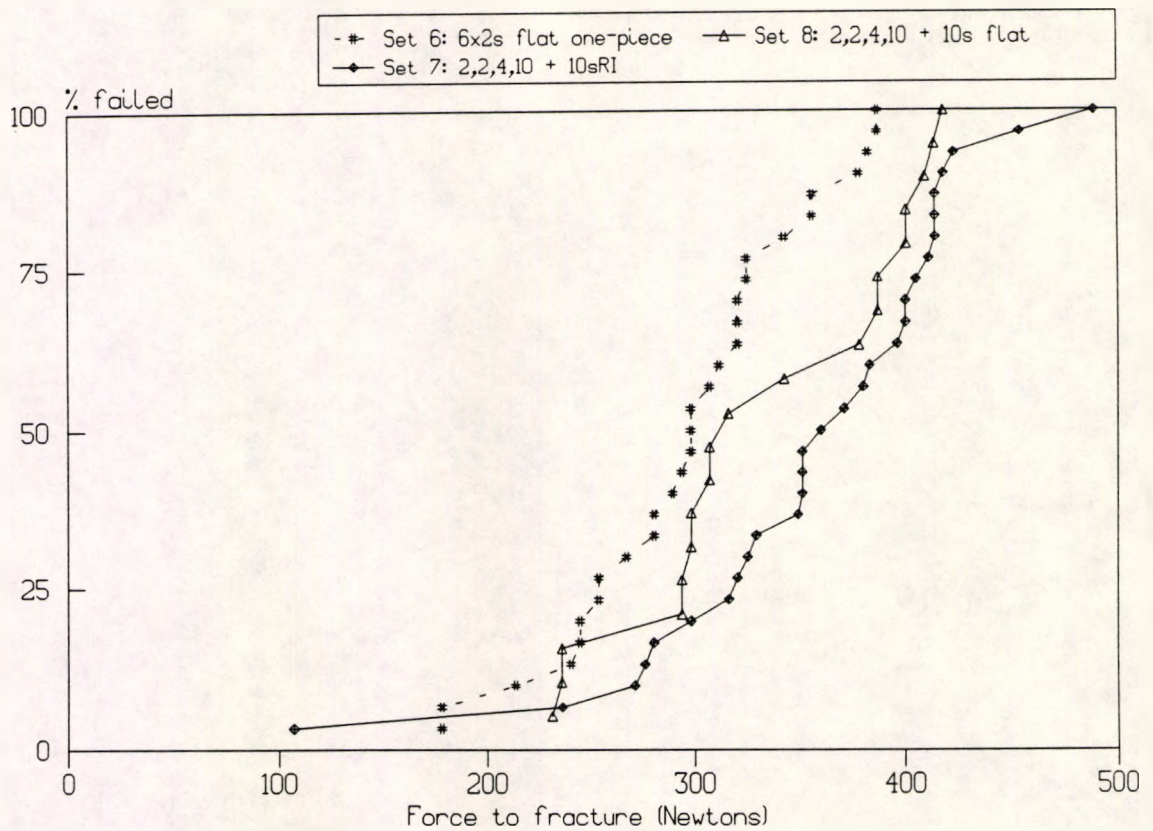


Figure 17. Cumulative frequencies of force to fracture for Sets 6, 7 and 8.

Set	Batches	No.	Mean Load	S.D.(n-1)	95% C.I. for Mean		Median Load
					From	To	
6	13,16,18	30	297.7	56.3	276.7	318.7	298.0
7	21,25,28	30	356.4	74.7	328.5	384.3	365.5
8	22,26	20	334.4	63.6	303.7	365.0	316.0

Table 18. Force to fracture statistics for Sets 6, 7 and 8 (Newtons).

Sets	95% C.I. for the difference in means		Student's t-test	
	From (Newtons)	To (Newtons)	t =	P =
6 & 7	24	93	3.44	0.0011
6 & 8	0	73	2.06	0.047
7 & 8	-18	62	1.10	0.28

Table 19. Confidence intervals for differences in mean force to fracture between Sets 6, 7 and 8 and results of two sample t-testing.

There were no significant differences in the mean force to fracture between Batch 23 and one-piece Set 6 ( $t=0.27$ ,  $p=0.79$ ), joined Set 4 ( $t=1.234$ ,  $p=0.23$ ) and Set 5 ( $t=1.28$ ,  $p=0.2$ ) tested earlier in the study.

#### 6.6.4 "Gramophone groove" end preparation: Set 9

The sample condensation procedure for Set 7 was repeated for Batches 24 and 30. Only the mode of end preparation was varied to produce circular scratches, described as "gramophone grooves" (Plate 46). These batches were not significantly different in mean force to fracture ( $t=0.17$ ,  $p=0.87$ ) and the results were pooled to make Set 9.

The force to fracture data for Set 9 were compared with those from Set 7 and Set 1 recorded earlier in the study. These are shown in Figure 18 and Tables 20 and 21. The cumulative force to fracture curves for these sets were nearly coincident. A number of the weaker samples were from Set 1, possibly due to relative weaknesses in the parent. However, the differences in mean force to fracture and distribution of fracture origin were not statistically significant.

The results for Sets 7 and 9 were pooled and divided into subsets. Table 22 gives the descriptive statistics and the cumulative failure curves are shown in Figure 19 with one-piece Batch 27. Only one sample failed in the addition. Failures occurred in the parent or joint with almost equal frequencies. Although the mean force to fracture for the samples which failed at the joint was somewhat less than that for parent failures, the difference was not statistically significant ( $p=0.37$ ). Unlike Set 1, however, where the parent failures were weaker than the joint failures, the difference was reversed. When t-tested Set 1P was weaker than Set 7&9P ( $t=2.337$ ,  $p=0.024$ ). The results suggested that incremental condensation using increasing vibration times had produced stronger parents than the DW method used for Set 1.

These parts were stronger than Set 5 (2s on each portion;  $t = 2.7$ ,  $p = 0.01$ ) but the fracture distributions were not significantly different ( $p = 0.06$ ).

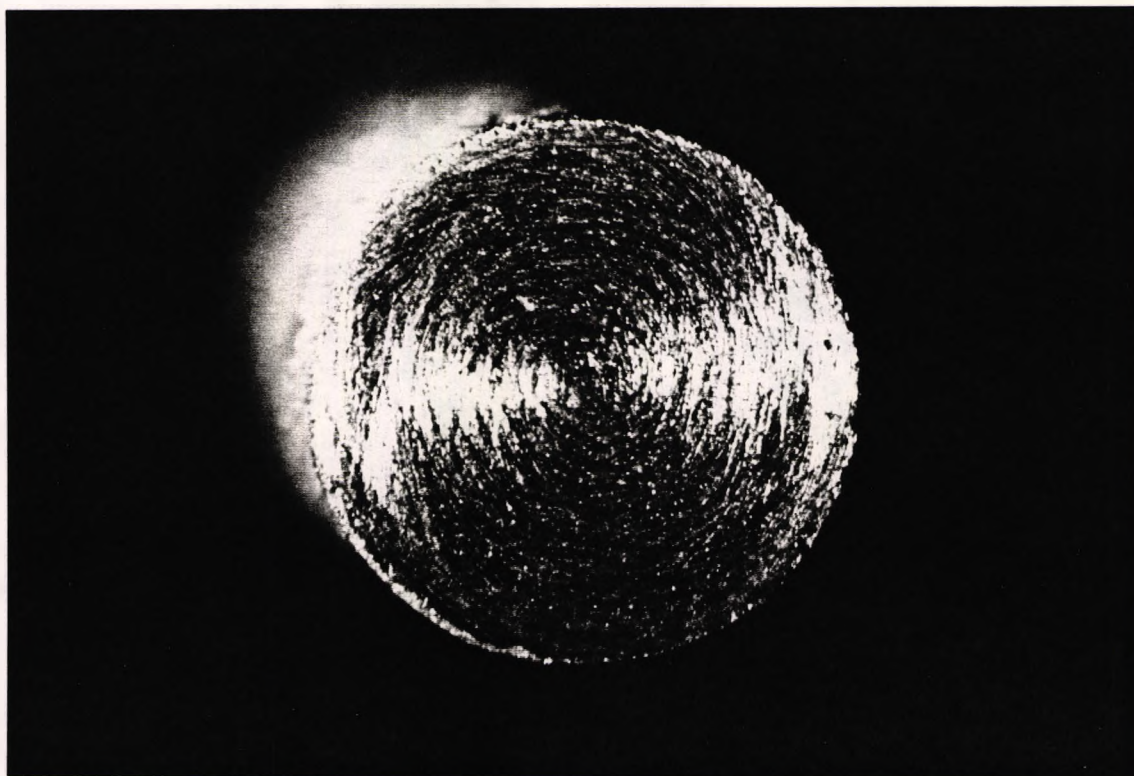


Plate 46. "Gramophone groove" end preparation.

x18

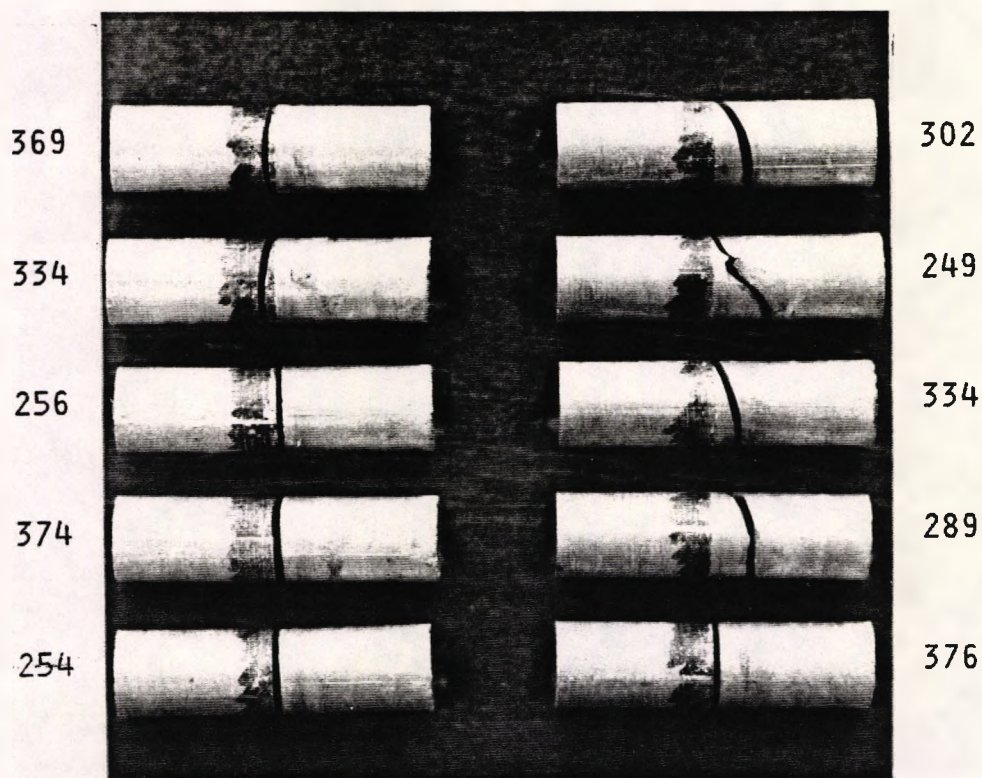


Plate 47. Batch 29. Prepared using the SRI piston.

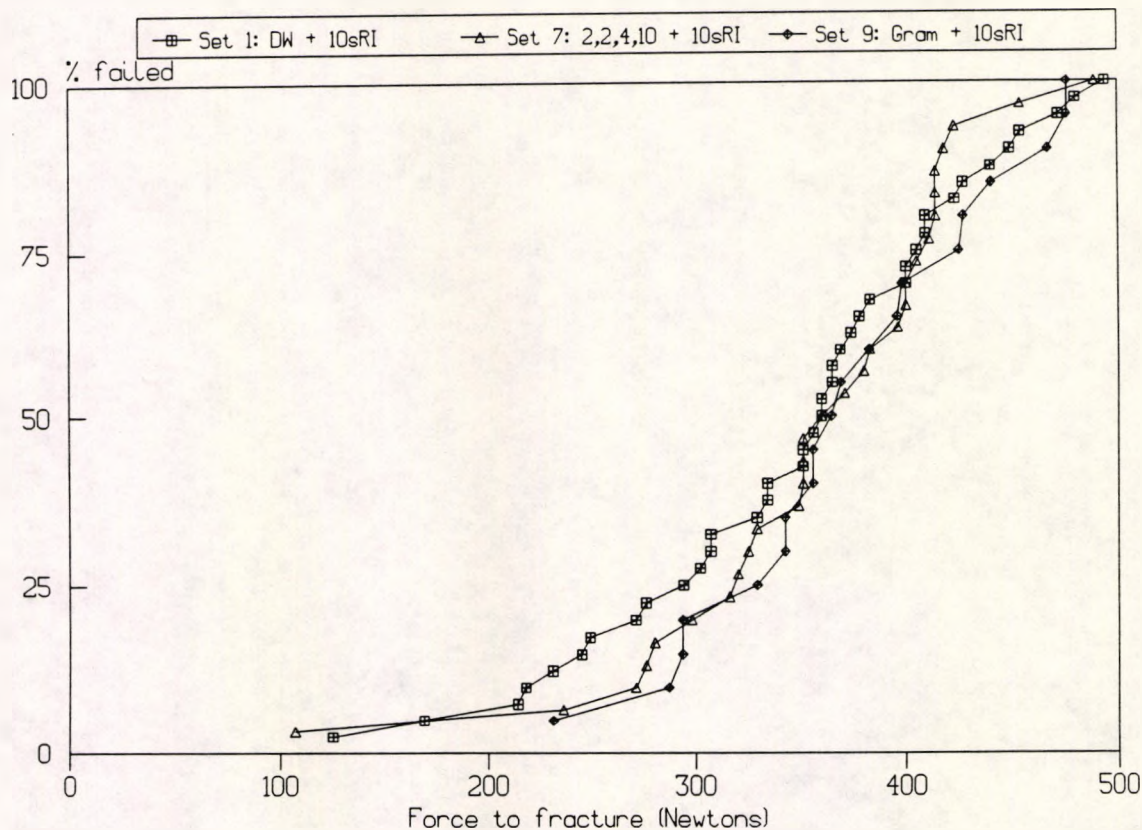


Figure 18. Cumulative frequencies of force to fracture for Sets 1, 7 and 9.

Set	Batches	No.	Mean Load	S.D.(n-1)	95% C.I. for Mean		Median Load
					From	To	
1	1,4,5,7	40	347.0	85.8	319.5	374.4	360.0
7	21,25,28	30	356.4	74.7	328.5	384.3	365.5
9	24,30	20	372.8	67.2	341.3	404.2	367.0

Table 20. Force to fracture statistics for Sets 1, 7 and 9 (Newtons).

Sets	95% C.I. for the difference in means		Student's t-test	
	From (Newtons)	To (Newtons)	t =	P =
1 & 7	-48	29	0.49	0.63
1 & 9	-67	15	1.27	0.21
7 & 9	-57	25	0.81	0.43

Table 21. Confidence intervals for differences in mean force to fracture between Sets 1, 7 and 9 and results of two sample t-testing.

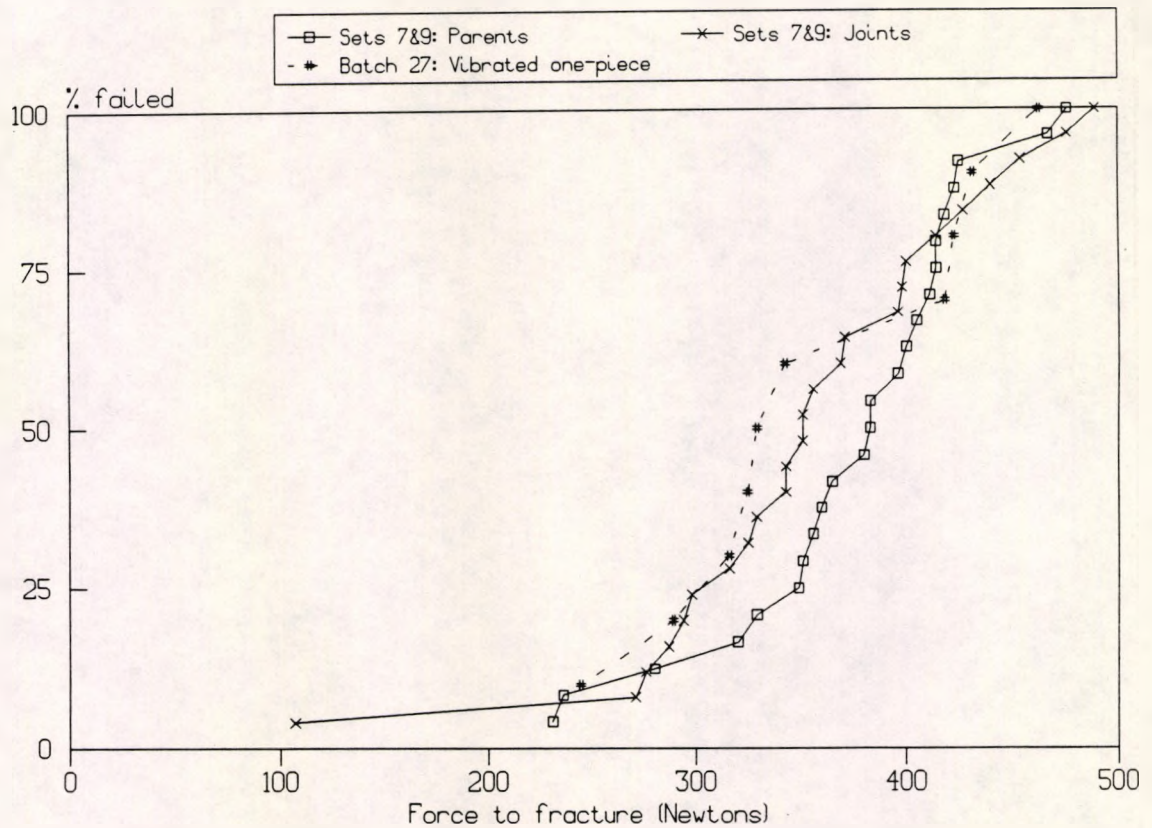


**Figure 19.** Cumulative frequencies of force to fracture of Batch 27 (One-piece) and Sets 7 and 9 which were pooled and divided into Parent and Joint subgroups according to location of fracture origin.

Set	Batches	No.	Mean Load	S.D.(n-1)	95% C.I. for Mean		Median Load
					From	To	
7&9 P	21,24 &	24	373.8	61.8	347.7	399.9	380.7
7&9 J	25,28,30	25	355.2	80.1	322.2	388.3	358.0
	27	10	358.2	71.2	307.3	409.1	336

**Table 22.** Force to fracture statistics in Newtons for Batch 27 (one-piece) and Sets 7 and 9 which were pooled and divided into Parent and Joint subgroups according to location of fracture origin.

When failure was not at the joint, the ultimate strength of the joint was somewhere to the right of the cumulative failure curve for the part which failed. Therefore, the difference between the strength of joints in Sets 7&9P and 7&9J was greater than that represented by Figure 19. The joints were positioned to align as closely as possible with the centre of the test rig. When the location of fracture origin was off-centre, failure occurred at a lower

bending stress than that in the joint. Measurement of the fracture origin location relative to the test rig centre loading position was considered but due to difficulties which would have necessitated development of a special technique, collection of these data and computation of the stress at the fracture origin was not carried out.

Only two out of 110 joined samples in Sets 4 to 9 failed in the addition. This supported the conclusion reached after consideration of Set 1 that the addition parts were not the weak link.

In practice the "gramophone groove" preparation procedure was difficult to achieve without producing steps. Ends prepared with radial scratches were almost flat and this was achieved with ease and speed. It was found to be relatively difficult to make end surfaces which were conical or concave by more than 0.05mm when measured with the ball attachment micrometer at the centre and periphery of the prepared surface. No further investigation of end preparation was made.

#### **6.6.5 Use of the Spiral rubbing-in (SRI) piston: Batch 29**

Due to the difficulty experienced in producing concentric scratch patterns an attempt was made to cause movement of the amalgam mix radially. A piston (identified as the SRI piston) was manufactured with a spiral cutting edge. This piston was applied to the first addition increment under vibration for 10s during which the piston was rotated five times in the anticlockwise direction followed by five turns in the clockwise direction at one turn per second. The flat ended piston was then applied for 2s. The second, third and fourth increments were condensed using the flat ended piston for 4s, 2s and 2s respectively. There was a visible interface between the first and second increments of the addition and four samples fractured in this region (Plate 47).

The volume of the first increment influenced the spacing of the curved edge of the SRI piston from the parent amalgam. If that portion of amalgam were thick, movement of amalgam might not occur along the score marks at the interface. Due to this and the fact that failures had occurred in the addition, condensation by the SRI piston was considered to be unsatisfactory. The "Paddle" piston was developed as a result.

Regarding sample strength, the mean force to fracture for Batch 29 was not significantly different to that for Sets 1, 5, 7 and 8. Set 4 (2s flat piston) was weaker ( $t=2.37$ ,  $p=0.025$ ) and Set 9 (10s RI piston and gramophone grooves) was stronger ( $t=2.44$ ,  $p=0.02$ ).

#### **6.6.6 Increased duration of vibration for one-piece samples: Batch 27**

The one-piece samples in Set 6 were condensed using vibration for 2s on each of six increments. The mean force to fracture was less than those for Set 7 ( $t=3.4$ ,  $p=0.001$ ), Set 8 ( $t=2.115$ ,  $p=0.04$ ) and Set 9 ( $t=4.3$ ,  $p=0.0001$ ) where longer vibration times were used for selected increments. For the one-piece samples in Batch 27 the duration of vibration was increased to 4s for the second and fifth increments and to 10s for the third and fourth increments. Condensation of the central segment of the sample was therefore completed about 14s earlier than was possible by using vibration for 10s on every increment.

The cumulative force to fracture results for Batch 27 are included in Figure 19. The mean force to fracture for Batch 27 was not significantly different to Sets 7, 8 and 9 and subsets 7&9P and 7&9J ( $p>0.5$ ). When compared with the results obtained for Set 6, Batch 27 was stronger ( $t=2.757$ ,  $p=0.009$ ). This was unlike the results for Batches 3 and 8 (see Section 6.4.4) where different durations of vibration (2s or 10s per increment) produced no significant

difference in means of force to fracture. Comparing the results from Batch 27 and Batch 3 earlier in the study, the 95% confidence interval for the difference in means was from -4.2 to 116.8 Newtons ( $p = 0.06$ ). The difference was not significant at the 5% level of confidence but there were only 10 samples in each batch. Batch 31 was prepared in a similar manner to Batch 27. Misplacement in the 3 point bending rig caused some samples to fail at the end. In early consideration of these results, Batches 27 and 31 were pooled to make Set 10. In view of the end failures, these pooled results are not analysed.

## **6.7 Preparation and test of one-piece samples**

No reports have been found where the mean force to fracture for joined samples exceeded that for the one-piece controls. In this study, many joined samples were stronger than the one-piece "control" samples. It was therefore considered appropriate to review and refine preparation procedures for one-piece amalgam samples. It was considered that vibration duration and the interval between amalgamation and condensation may have influenced strength. It was also possible that wear in the flat ended piston had affected sample strength. The work reported in this section includes the use of a new flat ended piston for vibrated condensation; three separate 1-spill divided amalgam mixes with application of vibration for 2s, 4s, 7s and 10s and separate undivided mixes for 20s. The results of sample testing immediately after removal from the 37°C oven are considered first.

### **6.7.1 Testing immediately after removal from 37°C storage oven**

Reisbick and Caputo (1977) found that the bending strength of some amalgams varied with temperature and cross-head speed of testing machine. At 70°F the strength of both conventional and dispersed phase amalgams

reduced with increasing strain rate. However, at 140°F, conventional amalgams increased in strength at high speeds (0.25 to 2.5 inch per minute) compared to low speeds (0.005 or 0.05 inch per minute). The strength of Dispersalloy was not dependent on strain rate at the elevated temperature.

One-piece samples were vibration condensed using the flat piston for 2s on each of six increments. The testing of samples in Batch 17 was completed within 40s of removal from the storage oven. For Batch 18, at least 30 minutes was allowed for cooling to room temperature before test. The results are shown in Figure 13, page 131. The result of ANOVA on Batches 8, 13, 16, 17 and 18 indicated no significant differences in the mean force to fracture ( $F = 1.595 [4,45df] p = 0.19$ ). However, the fracture force for two of the samples in Batch 17 exceeded the maxima for all previous incrementally condensed one-piece samples. From this simplistic comparison it was therefore considered appropriate to allow time for samples to cool from oven to room temperature before test.

### **6.7.2 Use of a new flat ended condensing piston**

Early in the study, for example up to Batch 18, samples condensed by vibration tended to fail at the interface between increments (see Plate 44, page 134). Low power microscopic examination of the fracture surface of later produced samples revealed a "rim" of less granular appearance (Plate 48) on the tension side of the test sample. The fracture path then followed the interface between increments before deviating to the central loaded area.

Examination of the flat ended condensing piston showed that it had become worn and no longer had a sharp edge. The curved interface produced between increments by the old flat piston is shown in a polished metallographic sample in Plate 49.

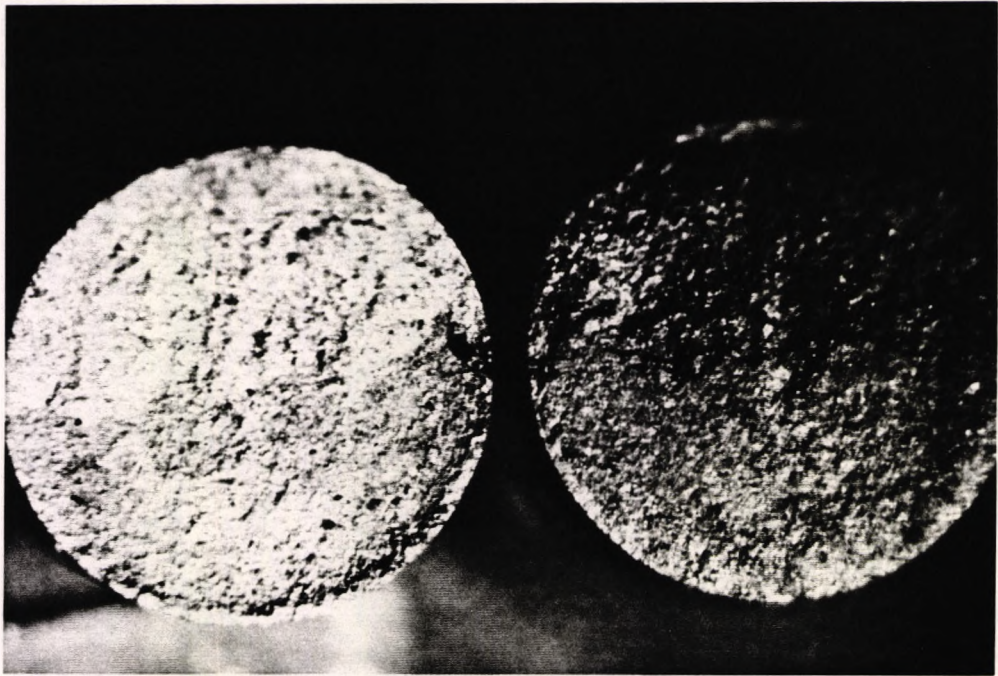


**Plate 48.** A rim of less granular material was visible on the fracture surface when failure occurred between increments condensed using the old flat piston.

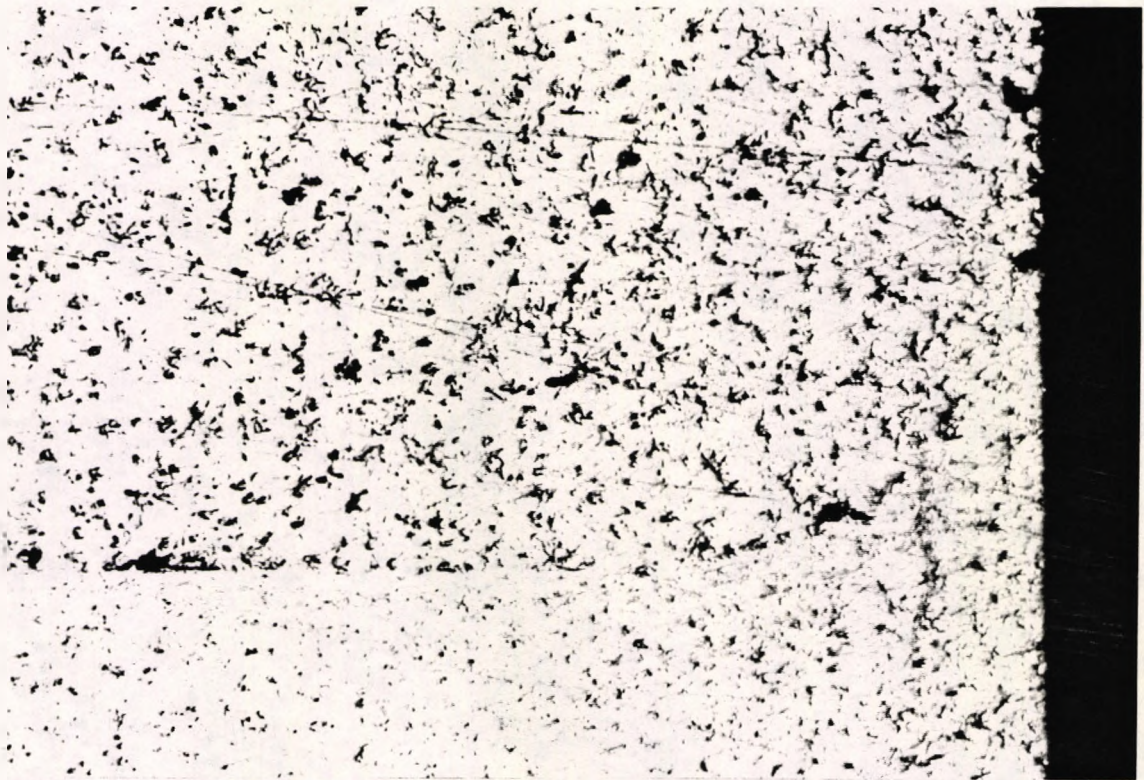


**Plate 49.** Specimen A1.7. The curved interface between increments condensed by vibration using the old flat piston for 10s. x110

A new flat ended condensing piston was manufactured. Amalgam samples were condensed using vibration applied for 10s to each of six increments using the new piston (Batch 34) or the old worn piston (Batch 33). A third experimental group was condensed by the DW method (Batch 32) for comparison with these samples.

The force to fracture results are shown in Figure 20 and Table 23. Scatter in the DW batch was wider than in the incremental groups (the coefficient of variation was more than 40%). The fracture path was somewhat irregular (Plate 50). In contrast, samples condensed using the new piston appeared to show flat fracture faces which finally deviated towards the central load (Plate 51). Samples condensed using the old worn piston (Batch 33) did not tend to fracture at the interface between increments (Plate 52). The difference in mean force to fracture was significant for Batches 32 and 33 ( $t=3.1$ ,  $p=0.006$ ). Batch 34 was intermediate in mean force to fracture between Batches 32 and 33 but the differences were not significant when t-tested ( $0.05 < p < 0.09$ ). The results differed in significance from the t-test result for Batch 3 (condensed when the flat piston was new) and DW condensed Batch 2 ( $p=0.03$ ) which were discussed in Section 6.4.1.

### **6.7.3 Use of three separate amalgam mixes**

The mercury content of amalgam is known to increase, and strength reduce, if condensation is delayed after amalgamation. Consideration was given to minimising the time elapsed after mixing before completion of condensation. One-piece samples were prepared from three separate one-spill mixes from the Dentomat. The second and third doses were mixed during condensation of the current dose. The results are shown in Figure 20 and Table 23.

### 6.7.3.1 Divided or undivided mix: new or old flat piston

Four experimental groups were tested. The "old flat" or "new flat" pistons were used with vibration for 20s on 3 undivided mixes or for 10s on each of 6 increments from 3 halved mixes.

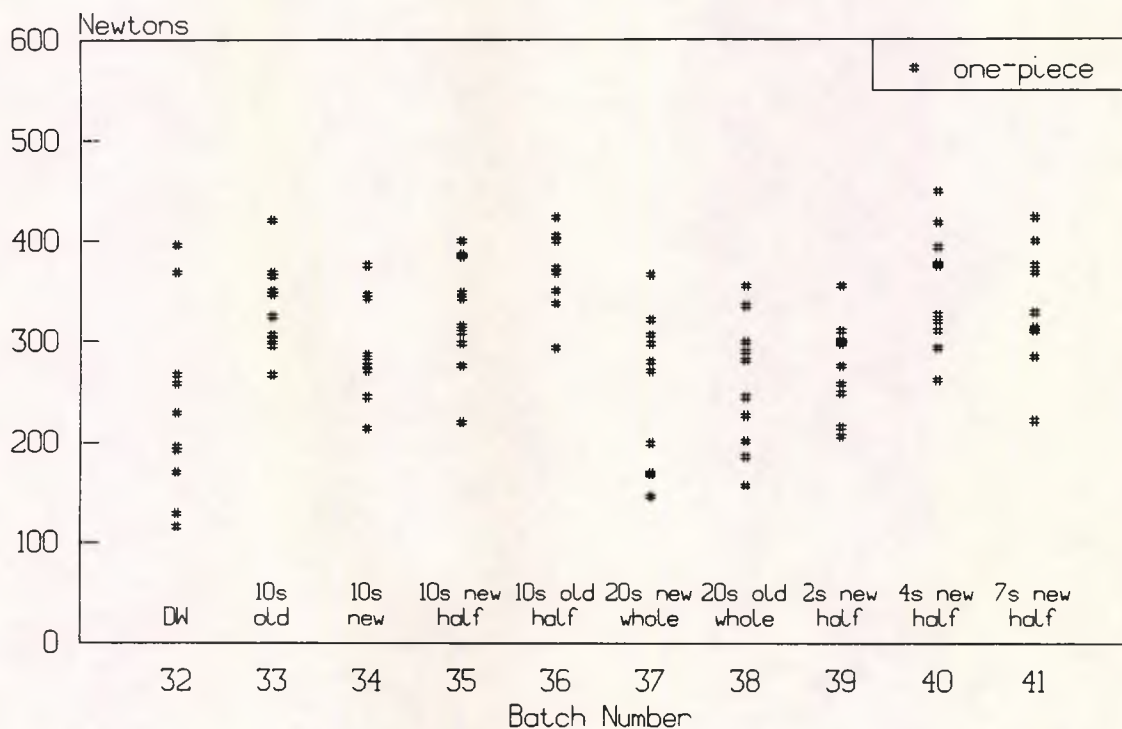
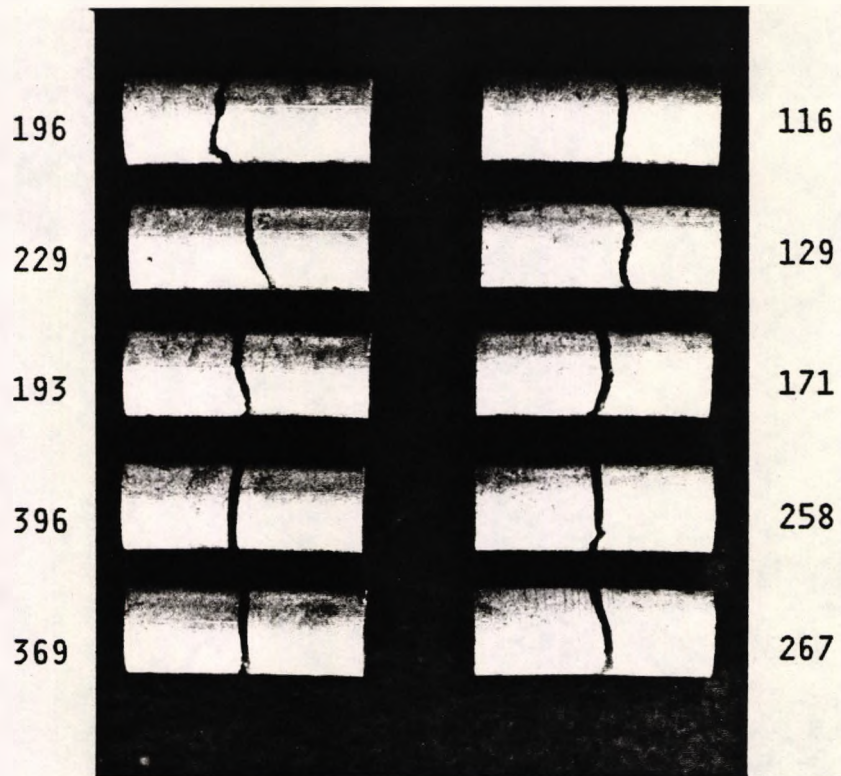


Figure 20. Force to fracture for Batches 32 to 41. Amalgam M.

Batch	Method	No.	Mean Load	S.D. (n-1)	95% C.I. for Mean		Median Load
					From	To	
32	<sup>1</sup> DW	10	232.4	93.2	165.7	299.1	227
33	<sup>23</sup> 6x10s old	10	334.9	44.5	303.1	366.7	333
34	<sup>2456</sup> 6x10s new	10	292.6	49.3	257.3	327.9	287
35	<sup>236</sup> 3x2x10s new	10	328.3	56.1	288.1	368.5	330
36	<sup>3</sup> 3x2x10s old	10	370.2	36.7	343.9	396.5	374
37	<sup>14</sup> 3x20s new	10	253.2	75.7	199.0	307.4	249
38	<sup>145</sup> 3x20s old	10	258.4	65.3	211.7	305.1	259
39	<sup>1456</sup> 3x2x2s new	10	277.3	45.7	244.6	310.0	279
40	<sup>3</sup> 3x2x4s new	10	352.9	59.2	310.6	395.3	352.5
41	<sup>23</sup> 3x2x7s new	10	335.8	58.8	293.7	377.9	340

The superscripted numerals link batches which were not significantly different ( $p > 0.05$ ) when tested by ANOVA with pooled variance.

Table 23. Force to fracture statistics in Newtons of Batches 32 to 41.



**Plate 50.** Batch 32 after fracture: deadweighted condensation.

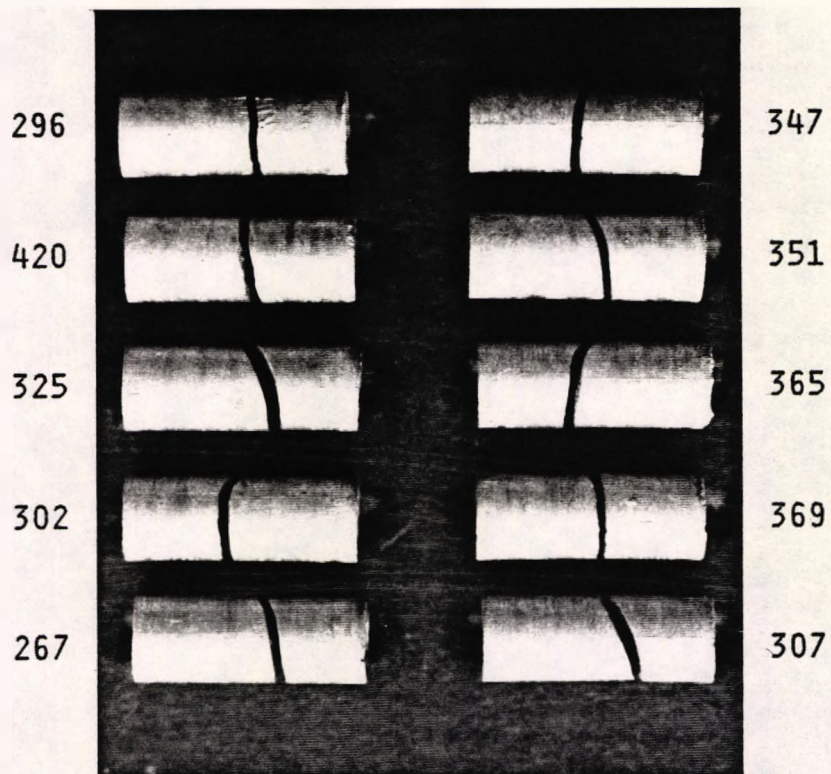


**Plate 51.** Batch 33 after fracture: condensed using the "old flat" piston.

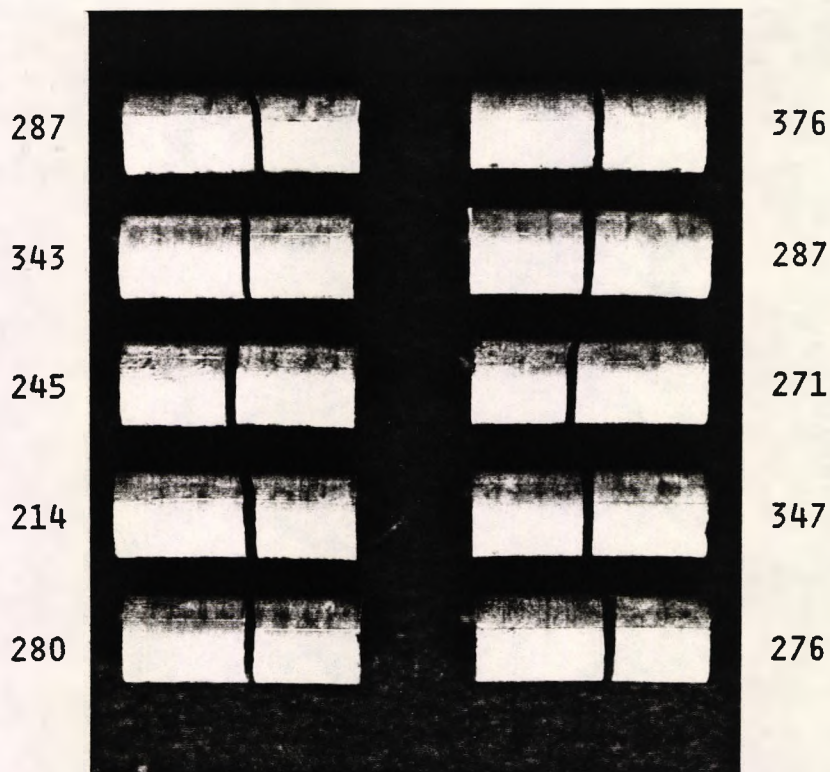


**Plate 52.** Batch 34 after fracture: condensed using the “new flat” piston.

The total time taken for specimen preparation was limited by the amalgamation process itself rather than the division or introduction of portions into the mould.

Samples prepared from **separate** undivided mixes failed at the interface between increments even though this was substantially off-centre in the 3 point bending rig (Plate 53). There was no difference in mean force to fracture for samples condensed using the new or old flat pistons for 20s ( $p=0.87$ ). These samples were weaker than those condensed from divided mixes for 10s on each increment: the difference between the means of force to fracture was highly significant for the old flat piston ( $p<0.0003$ ) and significant ( $p<0.02$ ) for the new flat piston.

The difference between the “old flat” (Batch 36) and “new flat” (Batch 35) pistons was not significant ( $p=0.064$ ) for divided mixes condensed for 10s. The result was similar to that for the 3-spill divided mix (Batches 33 and 34).

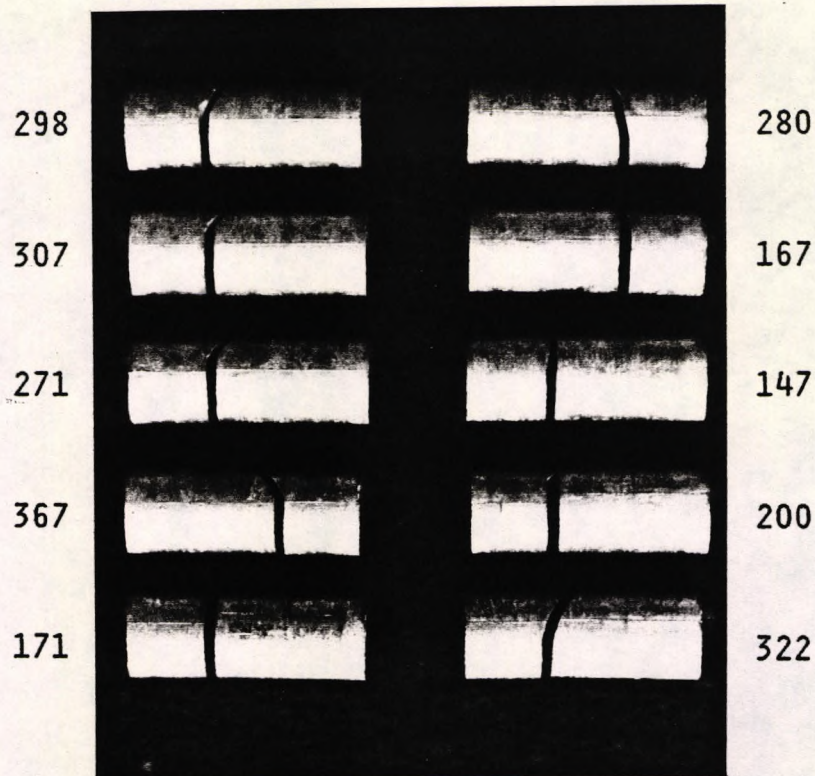


**Plate 53.** Batch 37 after fracture: 3 separate undivided doses.

#### 6.7.3.2 Duration of vibration using divided mixes

It was considered that durations of condensation of 2s or 10s on each portion of a mix might not necessarily produce maximum flexural strength. In order to determine a possible optimum vibration time, Batches 39 to 41 were condensed by vibration for periods of 2s, 4s, and 7s respectively to each half of three separate doses from the Dentomat using the new flat piston. The results are included in Figure 20 and Table 23. Batch 39 (2s) was weaker than Batch 40 (4s:  $t=3.2$ ,  $p=0.005$ ); Batch 41 (7s:  $t=2.48$ ,  $p=0.02$ ) and Batch 35 (10s:  $t=2.23$ ,  $p=0.04$ ) tested earlier. The latter three batches were not significantly different from each other ( $p>0.35$ ). Flexural strength was not increased by the use of vibration for longer than 4s on each half of three separate amalgam mixes.

Ninety separate mixes were amalgamated in the Dentomat for Batches 39 to 41. These were carried out sequentially over a 3 hour period and having noted that the motor became "hot" such practice was discontinued in favour

of 10 mix per hour working.

Inversion of the parent parts of joined samples was attempted in Batches 42 to 45. In the test, a Lloyd tensile test machine was fitted with a compression cage which produced unreliable force to fracture results. The results are listed in Appendix 1 with summary statistics in Appendix 2 but are not included for analysis. New compression plattens were manufactured to fit the test machine.

#### **6.7.4 Use of Duralloy high copper alloy**

As supplies of the Amalgam M conventional alloy became exhausted, work was continued using the Duralloy powder which had been generously supplied by Degussa Ltd with the Dentomat.

##### **6.7.4.1 Condensation using the cut cone piston**

It seemed that the vibrated "old flat" piston had condensed a thin surface layer of dense material at the worn edge. Immediately below the sample surface the fracture proceeded between increments. It was considered that a weakness between layers might be reduced by the use of a piston in the shape of a truncated ("cut") cone. The plane of the interface between increments might not then coincide with the probable fracture path and the surface area of the incremental interface was increased. Condensation pressure might be increased by the angle of taper producing a wedging action to force amalgam against the mould. The cut cone was used for one-piece Batches 48 and 49. For comparison, one-piece samples were condensed by the DW method (Batch 46) or by vibration with the new flat piston (Batch 47). Batches 46 and 47 were tested after 7 days, whereas Batch 48 was 4 days old. Batch 49 repeated the cut cone condensation method but was tested

after 6 weeks. This disparity in ages was considered unlikely to have influenced sample strength.

The results are shown in Figure 21. The cut cone (Batches 48 and 49) produced samples about twice the mean strength ( $t > 8.0$ ,  $p = 0.0000$ ) of either alternative condensation procedure. The fracture surfaces show the reproduced outline of the tip of the cut cone in the central one third of the cylinder in four samples in Plate 54. This area was located in the neutral zone of the beam under bending and therefore did not contribute to weakness before the fracture crack had formed. The flat ended piston produced samples which failed between incremental layers and unlike conventional amalgam were weaker than the DW method ( $t = 2.445$ ,  $p = 0.025$ ).

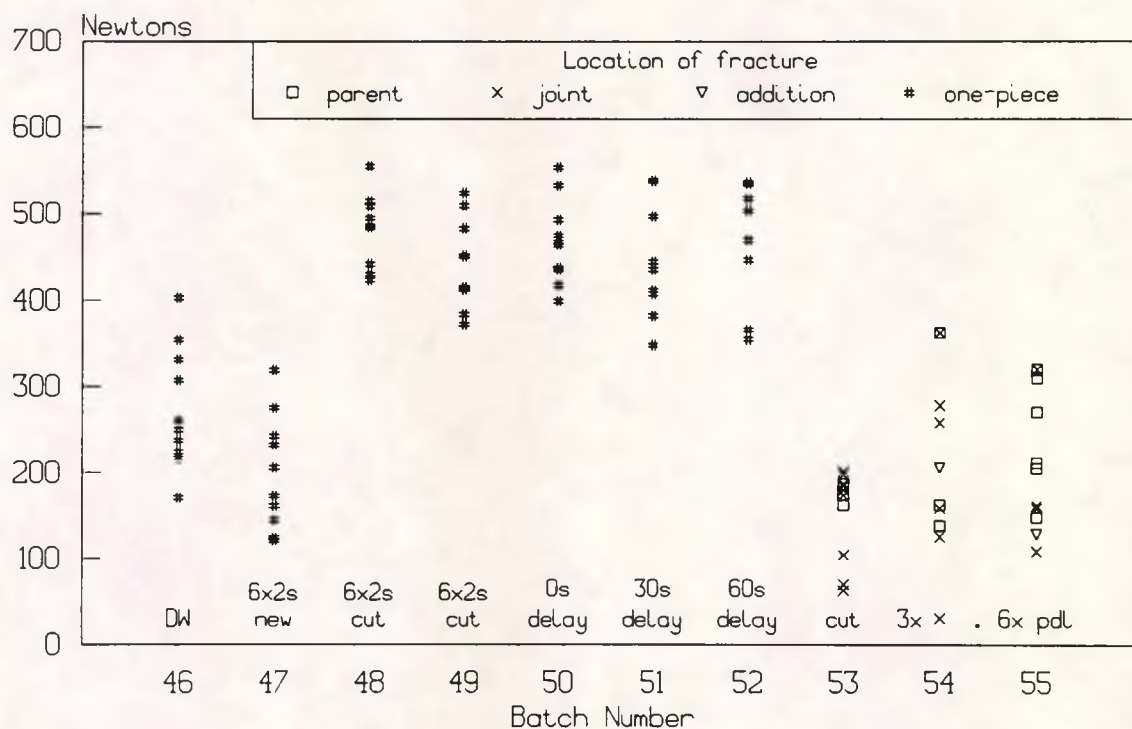


**Figure 21. Force to fracture Batch 46 to 55. Duralloy. Batches 48 to 53 were condensed using the cut cone piston.**

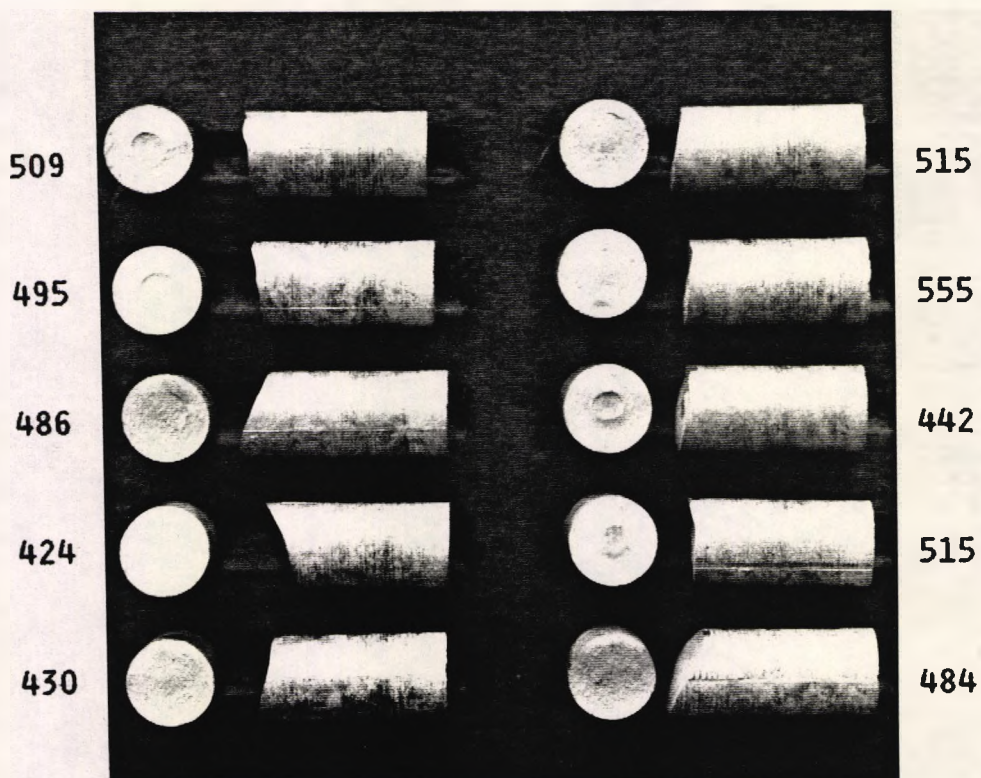


Plate 54. Fracture surfaces of Duralloy Batch 48.

#### 6.7.4.2 Effect of delayed condensation

In the preparation of joined samples, condensation of the first portion of the addition was completed within a few seconds of the freshly mixed amalgam making contact with the prepared parent end surface. It was considered that weakness in a new to old amalgam joint might occur due to porosity resulting from absorption of mercury from the new mix after completion of condensation of the first addition increment. Mercury might be absorbed by the parent amalgam or consumed by the setting reaction in the addition.

It was hypothesised that contact of the new amalgam mix with the parent might be required before completion of its condensation. If this were true, condensation could be delayed for a period of time to allow any absorption of mercury by the parent amalgam to occur.

A preliminary investigation of the effect of delayed condensation on the 7 day flexural strength of one-piece samples was undertaken. The condensation method used the cut cone piston. Batch 50 repeated the preparation method of Batches 48 and 49: condensation commenced 37s after mixing. Batches 51 and 52 were condensed after additional delays of 30s and 60s respectively. ANOVA on the force to fracture results for Batches 48 to 52 ( $F = 1.125$  [4,44df]  $p = 0.36$ ) indicated no significant differences.

### **6.8 Microstructure of joined and repaired amalgams**

Laboratory manufactured samples and failed clinical examples were prepared for metallographic examination (see Section 4.6) and the results are reported in this section.

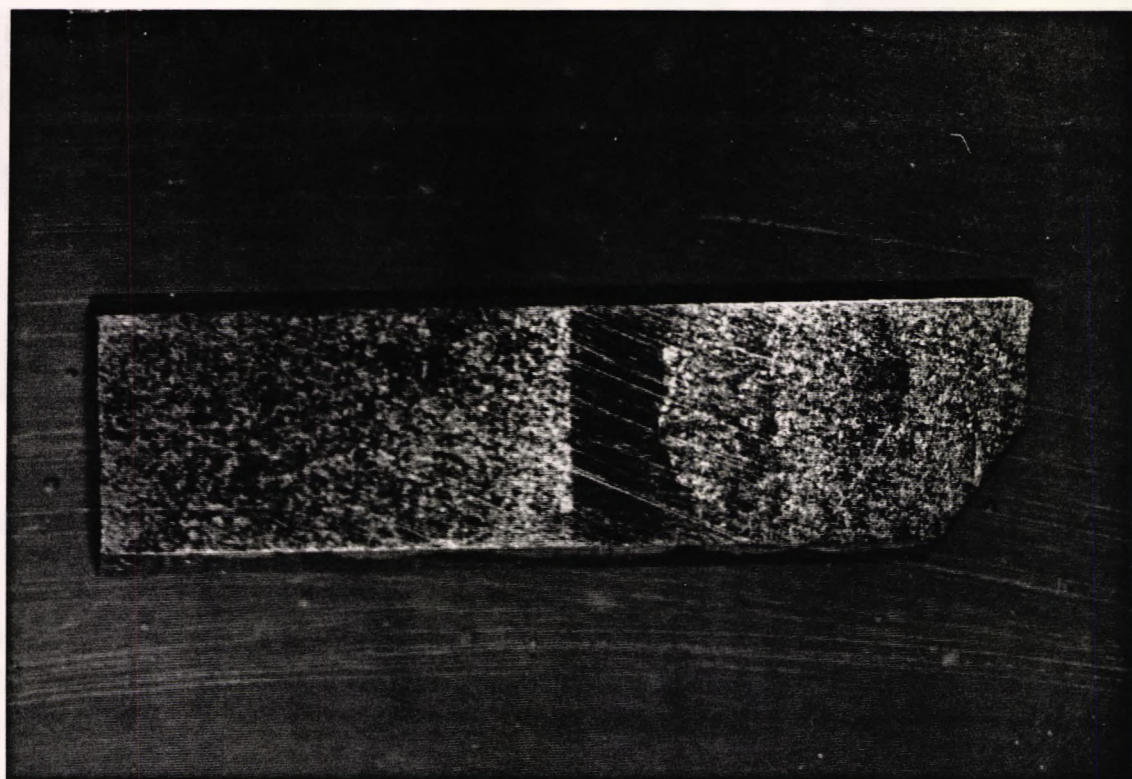


**Plate 55.** Macroscopic appearance of polished specimen A1.9.



Plate 56. Microstructure sample A1.9. Bright field. x80

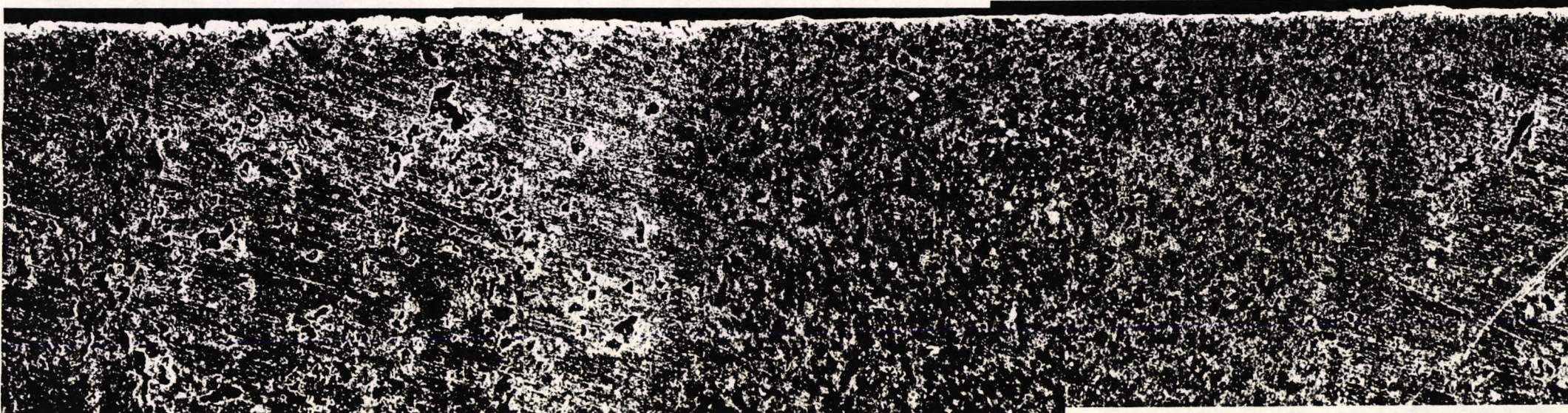


Plate 57. Microstructure sample A1.9. Dark field. x80

### **6.8.1 Laboratory prepared joined sample A1.9**

Plate 55 shows the macroscopic appearance of microstructure sample A1.9, condensed by the method used for Set 1. The DW parent is on the left. The first increment of the addition polished rapidly and since the light was not scattered it shows as a dark band. The profile of the RI piston and layering in the remaining increments are visible. The composite micrographs were illuminated in bright field (Plate 56) and dark field (Plate 57) modes.

Residual alloy particles ( $\gamma$ ) are distributed throughout the parent matrix where "caverns" of porosity may be seen under dark field illumination. These areas may have contained the weak  $\gamma$ -2 (Sn-Hg) phase. The location of the joint interface is indistinct. To the right of the joint is a band of densely packed alloy particles. Further to the right is a zone smaller  $\gamma$  particles with more matrix corresponding to the material which had been "churned up" by rotation of the RI piston. The material on the far right was vibrated for 10s with a flat ended piston: the structure is similar to the parent part.

### **6.8.2 Retrieved clinical amalgam addition restoration**

Much experience was gained from a failed clinical sample. The patient knew of the author's interest in the repair of dental amalgam restorations and kindly retained the sample shown in Plates 58 to 61. The history of this case was as follows. The patient had attended the dental practice for seventeen years. The palatal cusp of the upper left first premolar tooth fractured and a clinically satisfactory mesio-occluso-distal amalgam filling was in place. There was no record of the tooth having received treatment, so the restoration was probably at least seventeen years old. The palatal cusp was restored by amalgam addition (Cook, 1981). Retention of the restoration failed after fifteen months but the tooth was free of decay.

In the micrographs, the original amalgam (on the left of Plates 58 and 59) is porous for some thickness beneath the occlusal surface and at the base of the restoration. There are relatively few gamma particles in the area of matrix. The restored cusp is obviously dense, although large voids are present in scattered locations. Plate 59 shows the original and added amalgam at the occlusal surface including the interface. Residual alloy particles in the addition appear to be orientated parallel to the joint. The small dark areas are porosity.

Although there are differences in structure between the two parts, one can not ascertain the exact location of the interface in Plate 58 or 59. Careful examination of the sample revealed a small area where porosity was visible in a horizontal line on the right of Plate 60 and at higher magnification in Plate 61. This porosity appears to be related to gamma particles in the new amalgam and is taken to be the location of the interface. There appears to be continuity of microstructure between the pores.

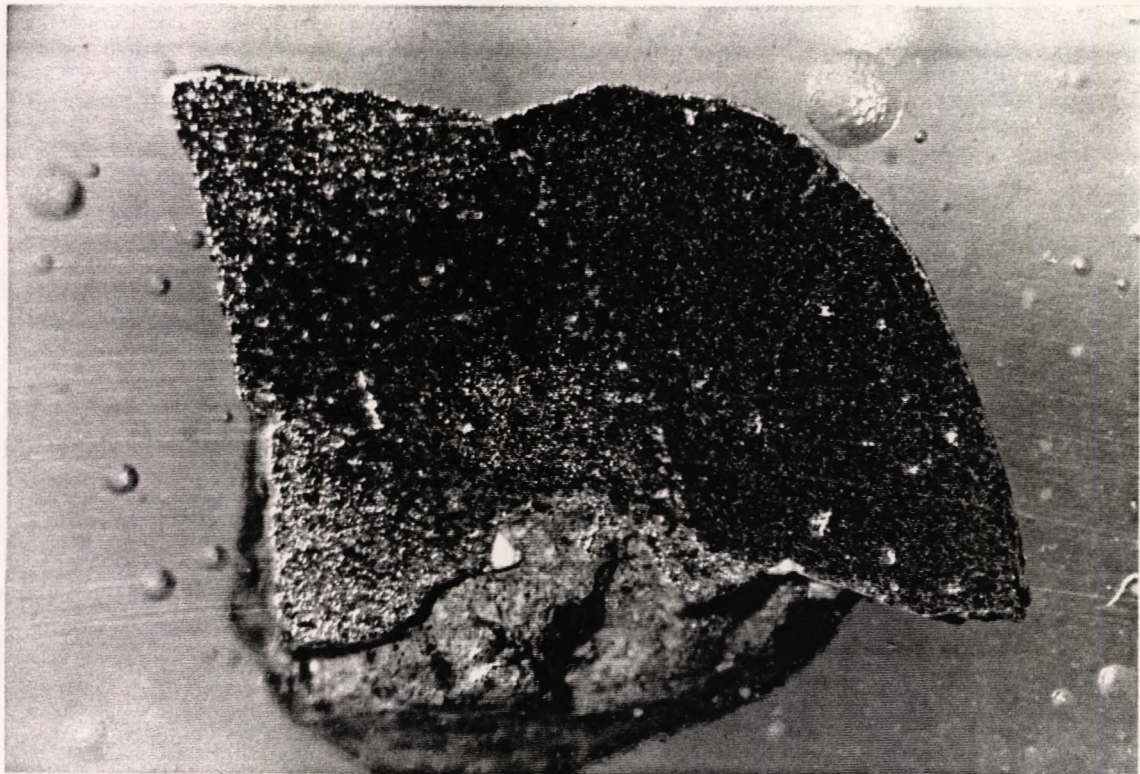


**Plate 58.** Macrostructure of a retrieved clinical sample.

x18

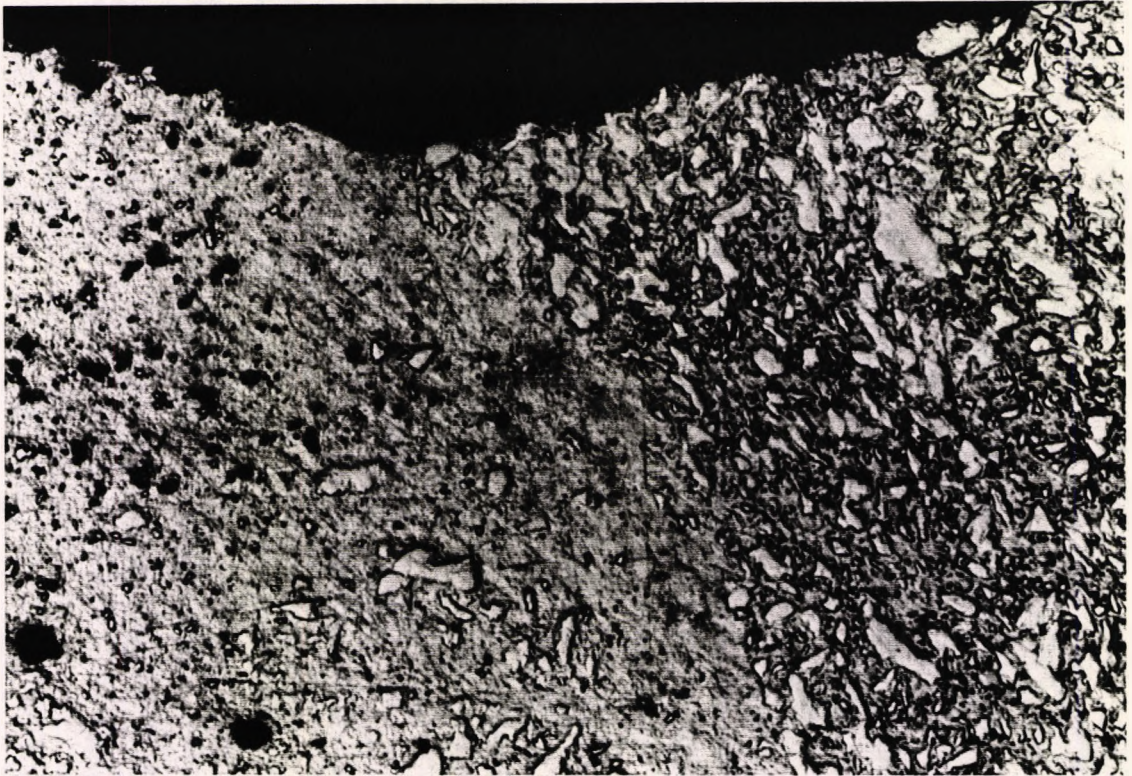


**Plate 59.** Microstructure at the occlusal surface of the clinical sample. Unetched. x110

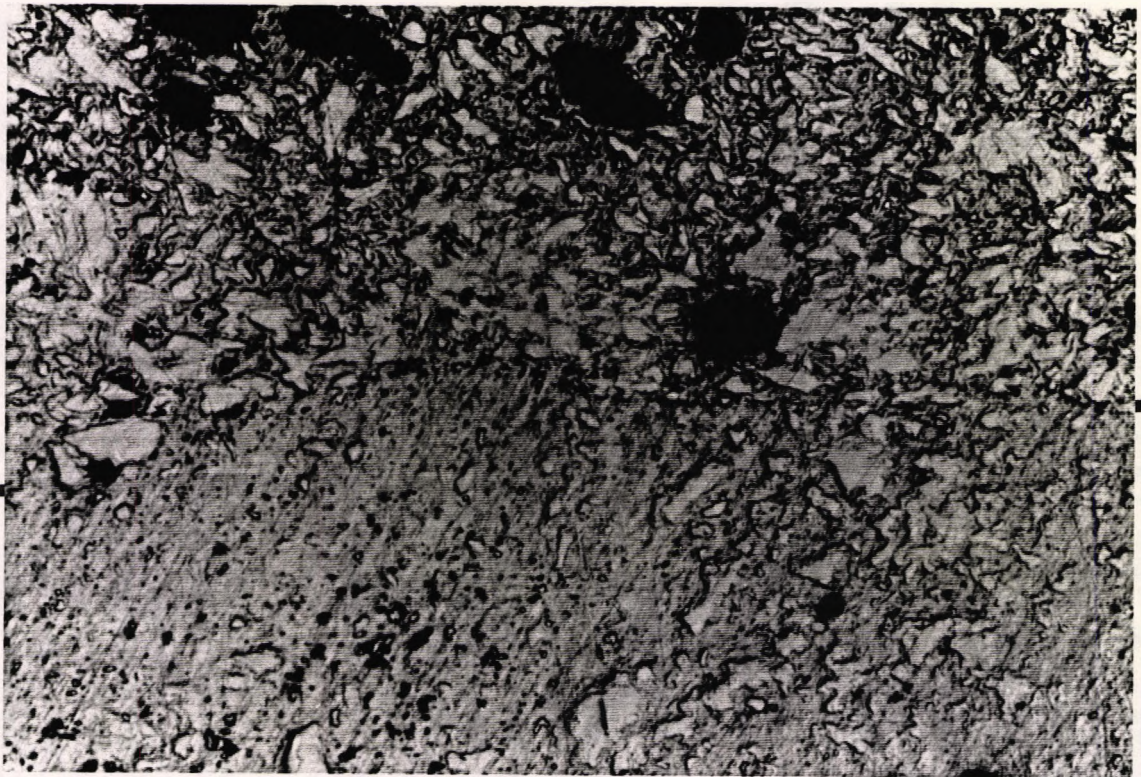


**Plate 60.** Microstructure of clinical sample. The parent material is at the bottom of the frame. x110

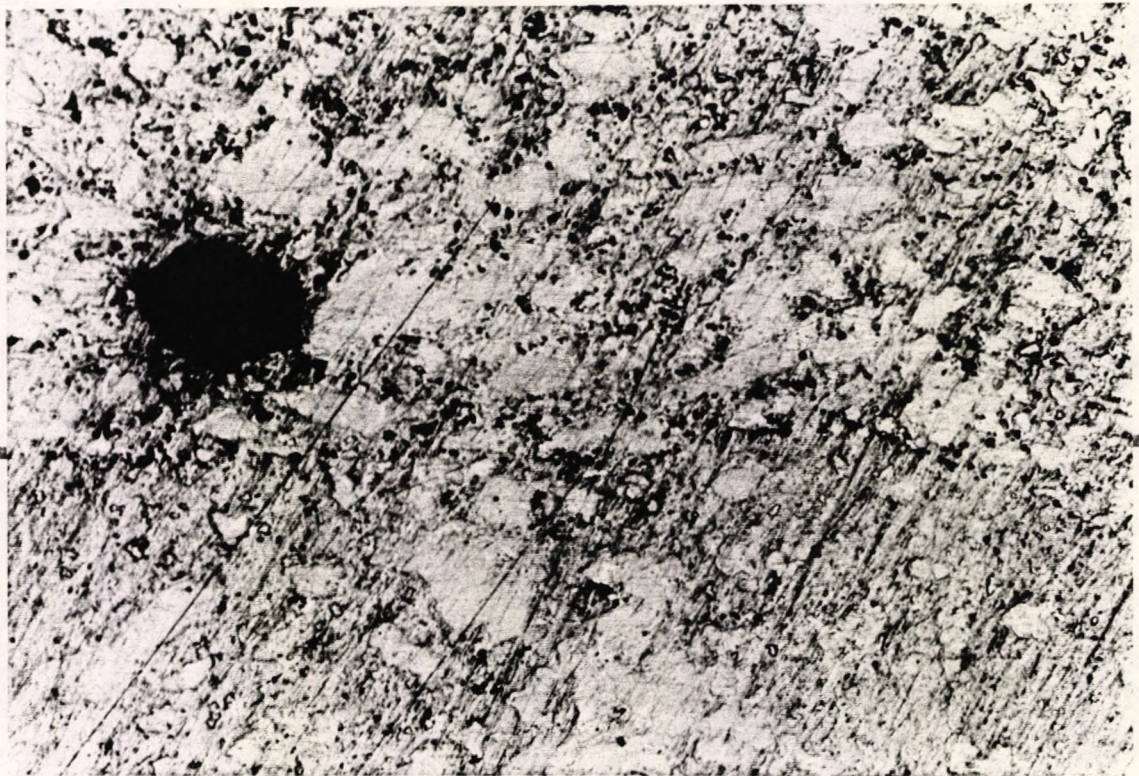


**Plate 61.** Microstructure of clinical sample.

x225

## **6.9 Development of joined sample preparation procedures using the Paddle**

Duralloy was used for preliminary work with the Paddle. Further development was carried out using Aristaloy 21 and later, Veraloy. As a result, a standardised procedure using the Paddle was adopted. The design and adjustment of the Paddle were described in Sections 4.3.3.4.3 and 4.4.3.6.

### **6.9.1 Preliminary work using Duralloy: Batches 53, 54 and 55**

Parents were condensed by the deadweight method using two-spill mixes of Duralloy from the Dentomat. Samples were end-prepared and replaced in the mould but marking of the parent surface was omitted. For Batches 54 and 55, the Paddle was utilised for the first increment. Vibration was applied for the duration of each revolution of the paddle (1.5s to 2s) and repeated at a frequency of 10s three and six times respectively. The four addition

increments were condensed using the cut cone piston for 2s. After fragmentation of the indented surface with a Le Cron carving instrument, condensation of the final increment was completed using a flat ended piston. Batch 55 was left in the mould for 7 days after condensation of the addition, whereas Batches 53 and 54 were removed from the mould 30 minutes after completion of the tenth sample. Figure 21 shows the results.

#### **6.9.1.1 Flexural strength tests**

Where 3 Paddle turns were applied 7 samples failed at the joint (Plate 62) but only 3 joints failed where 6 turns were used (Plate 63). These small numbers were not significantly different (Fisher's test  $p = 0.09$ ). The difference in mean force to fracture was not significant ( $p = 0.9$ ). Figure 21 (page 158) shows that use of the paddle increased strength (mean force to fracture about 200N) but this was not significant ( $p > 0.1$ ) compared to the cut cone alone (Batch 53: 153N) where all samples failed at the joint. The coefficient of variation for force to fracture for these batches was high (between 34.6% and 47.6%): Wilcoxon's Rank Sum test revealed no significant differences.

These joined samples were weaker (by Wilcoxon's test) than DW condensed one-piece samples (Batch 46) but not significantly weaker than Batch 47 condensed using vibration and the new flat piston. One-piece samples condensed using the cut cone piston were much stronger than one-piece Batches 46 and 47 and the joined samples ( $t > 6.7$ ,  $p = 0.0000$ ).

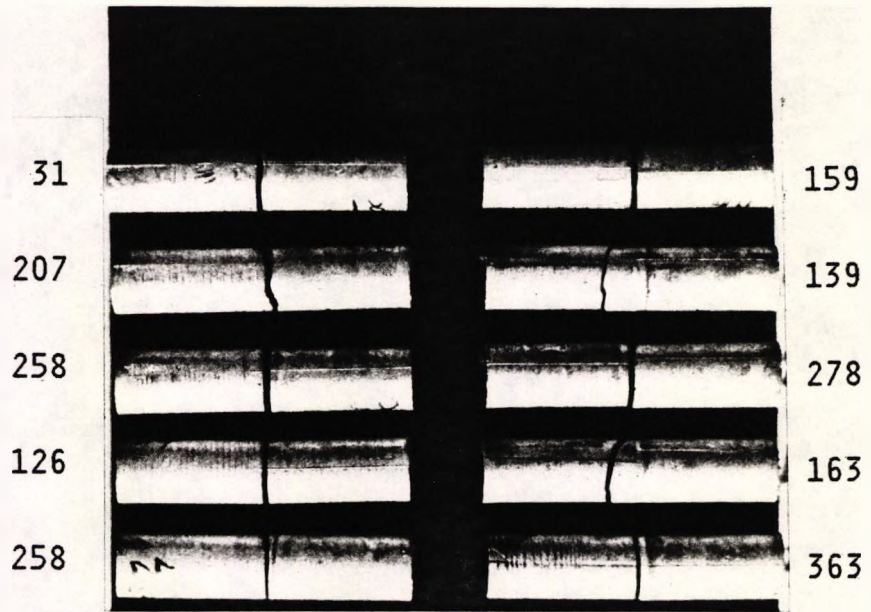


**Plate 62.** Duralloy Batch 54 after fracture.  
 Mean force to fracture: 198N.

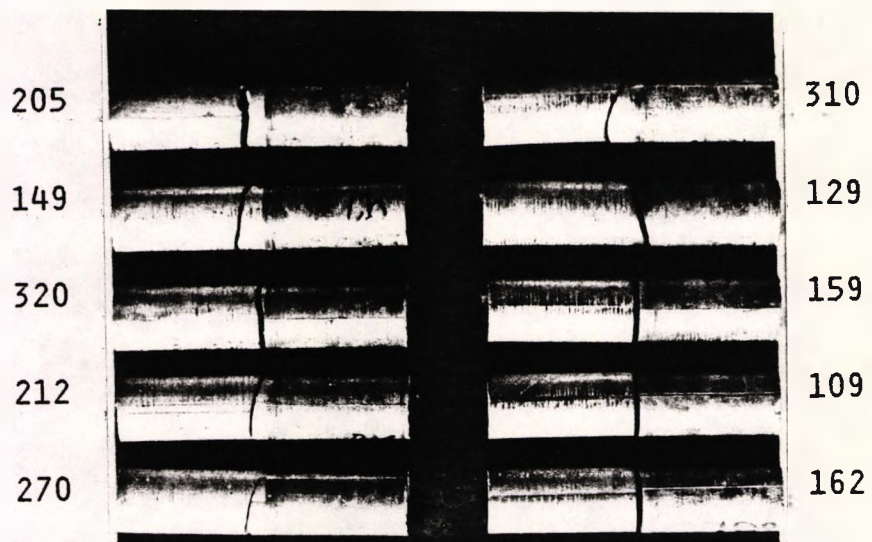


**Plate 63.** Duralloy Batch 55 after fracture.  
 Mean force to fracture: 202N.

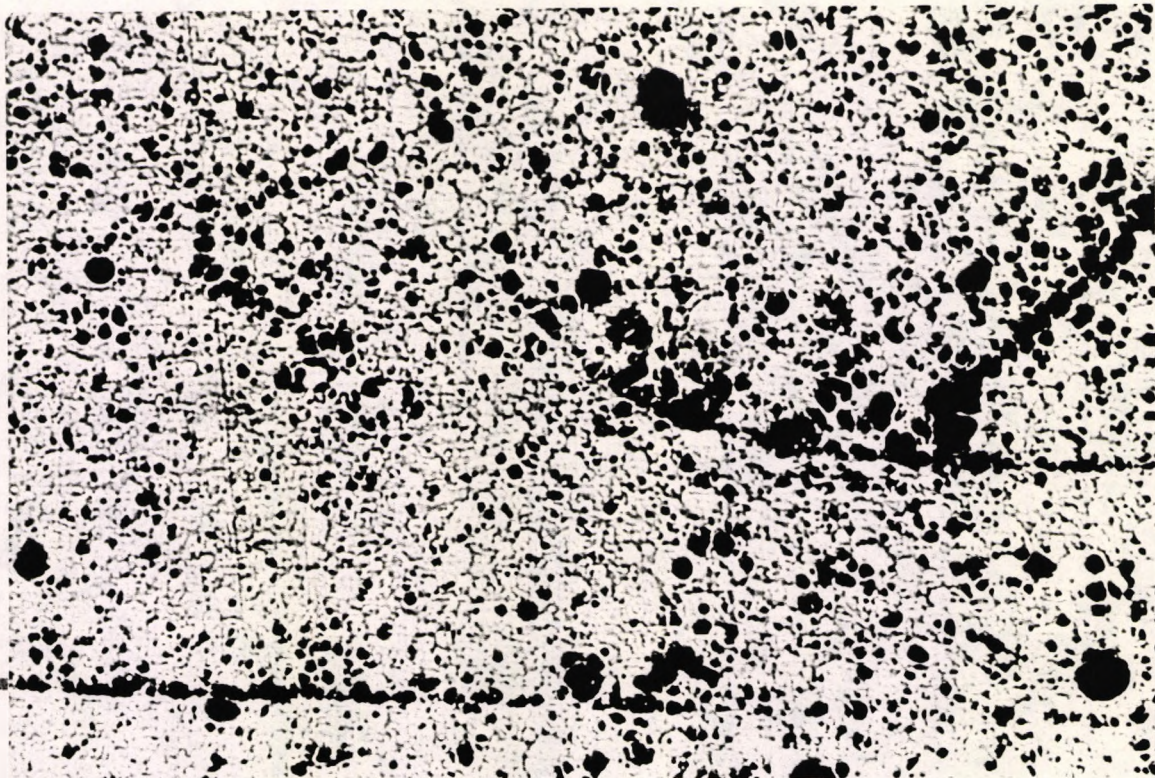


Plate 64. Microstructure of Duralloy specimen A5.2. (Cut cone). x110

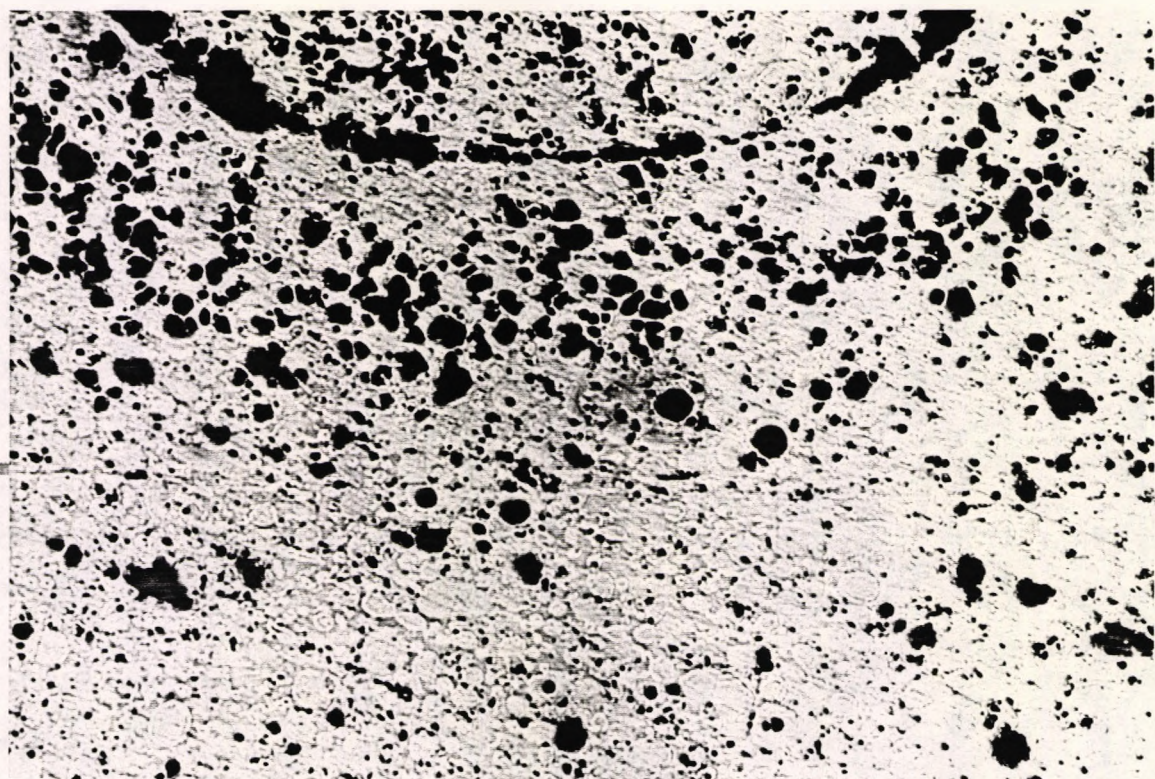


Plate 65. Duralloy specimen A5.4. Three turns given to the paddle. x110

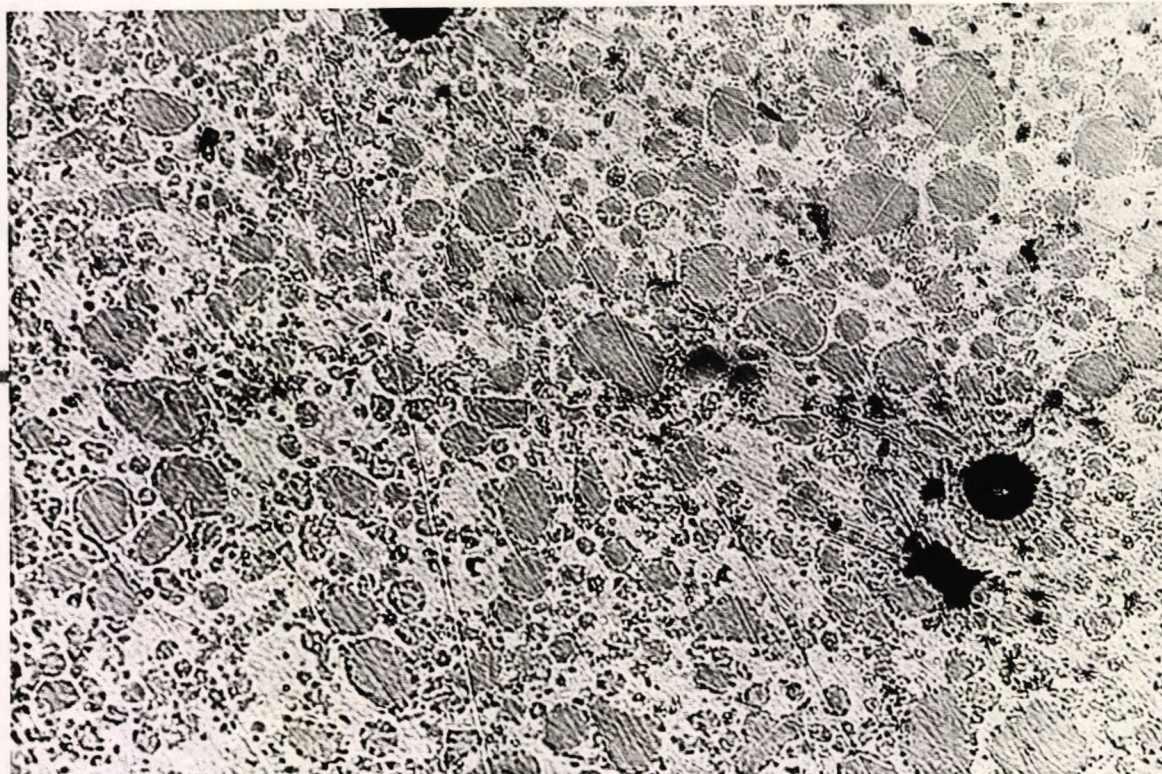


Plate 66. Duralloy specimen A5.5. Six turns given to the paddle. x225

#### 6.9.1.2 Microstructure

Joined samples were manufactured in the manner used for Batches 53 to 55. The polished microstructure revealed porosity at the apex of the interface between increments formed by the cut cone piston. There was obvious porosity at the joint when the cut cone was used alone (Sample A5.2, Plate 64). Sample A5.4 (Plate 65, 3 turns of the paddle) shows relatively little porosity at the joint but this was marked in the bulk of the adjacent added material. There is no porosity visible at the joint in Sample A5.5 (Plate 66) where 6 turns were applied to the paddle.

It was considered that the delay between each revolution of the paddle might have been unnecessary. Although a delay of 60s was without influence on the strength of one-piece samples condensed using the cut cone this might not be the case for joints. Possibly the number of turns applied to the paddle might affect joint strength. Additionally, if the volume of the first amalgam

increment were too small, the cut cone piston might impact on the parent part impairing condensation. If a weakness existed between flat piston condensed addition increments, sample failure might occur at that location (if the joint and parent parts were stronger) whereas failure might not initiate at the incremental interface in cut cone piston condensed samples. Use of the cut cone piston for condensation of the addition was discontinued. Supplies of Duralloy powder became exhausted and further development was carried out using Aristaloy 21.

### **6.9.2 Further work using Aristaloy 21**

The force to fracture data for Aristaloy 21 Batches 62 to 87 are presented in Figure 22, Appendices 1 and 2 and Table 24 which includes brief descriptions of the preparation procedures used for these one-piece and joined samples.

The parents of Batches 65 to 79 were condensed by the deadweight method. 7 day intervals were used before joining and test, except in Batches 72 to 75 as discussed below. Experimental variables were used in the condensation of the first increment of the addition; condensation was completed using the new flat piston for 2s on each increment. The parent preparation of Batches 81 to 84 was varied.

#### **6.9.2.1 One-piece samples**

One piece samples were condensed in the manner used for Duralloy Batches 46 to 48 and tested after 7 days. Unlike Duralloy, mean force to fracture for samples produced using the new flat piston (Batch 63) was similar to that for the DW method (Batch 62;  $p = 0.86$ ). Samples condensed using the cut cone (Batch 64, mean: 547.0N) were again much stronger than either batch ( $t > 9.0$ ,  $p = 0.0000$ ). The mean force to fracture for DW one-piece Batch 80

was less than that for Batch 62 ( $t = 3.7$ ,  $p = 0.002$ ) suggesting that the sample preparation had not been identical as intended. Since these one-piece sample test results were not reproduced they were unsuitable as “controls” for the joined sample tests.

#### **6.9.2.2 Extended application**

ANOVA for the force to fracture results for one-piece Batches 62 and 63 and joined samples prepared using the RI piston for 4s (Batch 65) or 6 turns of the paddle completed in less than 10s (Batch 66) revealed no significant differences ( $F = 0.24$  [3,36df]  $p = 0.87$ ). When the condensation procedure was extended by repeating each revolution of the vibrating paddle 6 times at a frequency of 10s (Batch 67) the mean force to fracture was less than that for one-piece Batches 62 ( $p = 0.02$ ) and 63 ( $p = 0.046$ ) and all samples failed at the joint.

The mean force to fracture for Batch 67 was less than for Batch 65 ( $t = 2.125$ ,  $p = 0.048$ ). Batch 67 was significantly weaker than Batch 66 when compared using Wilcoxon's test ( $p = 0.04$ ) but the t-test of means was not significant ( $t = 0.9$ ,  $p = 0.35$ ). One sample in Batch 66 was very weak (force to fracture: 50N) and the coefficient of variation for the batch was 33.2%. This case illustrates the effect of a single outlying result on the mean. These results suggested that delay between revolutions of the paddle during condensation of the first addition increment may have contributed to reduced strength in the joints.

Batch Number	Preparation procedure		Force to fracture (Newtons)		
	Parent	Addition part	Mean	95% C.I. for mean	
				From	To
62	One-piece DW		324.3	288.2	360.4
63	One-piece 6x 2s flat		319.9	276.7	363.1
64	One-piece 6x 2s cut cone		547.0	509.7	584.3
65	DW	4s RI, 3x2s flat	323.2	274.9	371.5
66	DW	6x pdl < 10s	300.4	229.0	371.8
67	DW	6x pdl @ 10s	266.3	229.7	302.9
68	DW	6x pdl @ 0.70	356.1	276.4	435.9
69	DW	6x pdl @ 0.60	359.7	293.6	425.8
70	DW	6x pdl @ 0.50	395.9	361.0	430.8
71	DW	12x pdl @ 0.70	373.8	335.3	412.3
72	DW	6x pdl @ 0.50 tested at 10 days	338.4	276.1	400.7
73	DW	6x pdl @ 0.60 see text	375.3	315.9	434.7
74	DW 10 day	6x pdl @ 0.60	339.1	295.6	382.6
75	DW 10 day	6x pdl @ 0.70	291.5	223.7	359.4
76	DW	4x pdl @ 0.60	370.5	324.3	416.7
77	DW	8x pdl @ 0.60	388.2	337.5	438.9
78	DW	12x pdl @ 0.60	387.8	320.5	455.1
79	DW	16x pdl @ 0.60	327.1	292.3	361.9
80	One-piece DW		238.5	200.1	276.9
81	4x2s cone	SPP	357.3	302.6	412.0
82	DW	SPP	357.9	284.9	430.9
83	4x2s flat	SPP	320.5	286.6	354.4
84	DW inv	SPP	281.8	258.4	305.2
85	DW	SPP	343.2	289.2	397.2
86	DW	6x pdl 10s delay then 4x2s flat	311.9	285.2	338.6
87	DW	6x pdl 20s delay then 4x2s flat	388.0	312.1	463.9

Table 24. Preparation procedures and force to fracture results for Batches 62 to 87. Aristaloy 21.



### **6.9.2.3 Number of turns**

The number of turns of the paddle was varied from 4 to 16 for Batches 69, 74 and 76 to 79 at a height setting of 0.60mm. ANOVA on the force to fracture values revealed no significant differences ( $F = 1.66$  [5,54 df]  $p = 0.34$ ). Batch 79 (where 16 turns were applied to the paddle) was weakest and Batch 77 (where 8 turns were applied) was strongest: the difference in mean force to fracture was significant ( $t = 2.25$ ,  $p = 0.037$ ). Batch 76 (4 turns) was not weak: 3 samples failed at the joint and 4 additions failed. Batch 66 (the first Aristaloy 21 batch to be prepared using the paddle; 6 turns) was weaker than Batch 77 ( $t = 2.27$ ,  $p = 0.036$ ) and all samples failed at the joint. This did not recur when the 6-turns procedure was repeated: Batches 69, 74 and 85 were not significantly weaker than Batches 76 and 77 and 13 (out of 30) joints failed.

The results were equivocal for the variables considered. There appeared to be no strength advantage by application of the paddle for more than 12 turns. As few as 4 turns produced strong joins but the 4 and 16 turn results were from only one unrepeated batch test in each case.

### **6.9.2.4 Height setting**

The condensation schedule in Table 6, page 78 was used and the unloaded paddle height was adjusted as described in Section 4.4.3.6. Settings of 0.50mm and 0.70mm were selected. It was estimated that impact of the vibrating paddle blade on the parent amalgam would have occurred at the 0.50mm setting but that there was clearance at 0.60mm. However, the possible influence of the amalgam mix in restricting movement of the paddle is not known.

The mean force to fracture for Batch 68 (0.70mm) was less than that for Batch 70 (0.50mm) but the difference was not significant ( $t = 1.2$ ,  $p = 0.24$ ). When the preparation settings were repeated (Batch 72: 0.50mm and Batch 75: 0.70mm) there was no significant difference in mean force to fracture ( $t = 1.2$ ,  $p = 0.26$ ). However, on reviewing the results, Batch 75 was weaker than Batch 70 ( $t = 2.9$ ,  $p = 0.005$ ) but these samples were prepared on different occasions. It is therefore possible that an uncontrolled factor was responsible. The results showed no clear effect on sample strength for the height variables considered: possibly, the elevated setting of 0.70mm was slightly disadvantageous for 6 paddle turns.

Batch 71 combined 12 turns of the paddle at a height setting of 0.70mm which was not significantly different to the strongest Aristaloy 21 joined batches.

Illness interrupted the preparation of the addition parts of Batches 72 to 75. Batch 73 was abandoned after completion of 6 samples. The remaining four parents were exposed to the air for three days before resumption of condensation of the additions which were tested after 7 days. Three of these four samples fractured at the joint and were the weakest in the batch. Jørgensen and Saito (1968) found that exposure to the air caused oxidation of the prepared surface and reduced the strength of bond obtained. The findings of Consani, Ruhnke and Stolfe (1977) were similar. The forces to fracture were considered unlikely to have been influenced by the small variations in age of the parents and intervals before test (7 or 10 days) but this factor could have affected the strength of Batch 75 reported above.

#### **6.9.2.5 Delayed condensation of the first increment**

After using the paddle, the flat piston was fitted to the Burgess tool for final

condensation of the first increment of the addition. It was not possible to exchange the pistons in less than about 3s. It was considered that the strength of joint might be influenced by delayed condensation of this portion. A modification of the schedule shown in Table 6, page 78 was used. In Batches 85, 86 and 87 the flat ended piston was first applied at 57s, 67s and 77s after the end of amalgamation respectively. Figure 22 shows the force to fracture results. The mean force to fracture for Batch 87 (longest delay) exceeded that for Batch 86 (intermediate delay:  $t = 2.14$ ,  $p = 0.046$ ) but was not different to Batch 85 (shortest delay:  $p = 0.3$ ). The possible effect of these delays was therefore unclear.

#### **6.9.2.6 Pooled results: Sets 11 and 22**

Batches 69, 74 and 85 were prepared by application of 6 turns of the Paddle within 10s at a height setting of 0.60mm followed by application of the flat piston for 2s on each of the four addition increments. The results were pooled to make Set 11. The results for joined samples condensed using the Paddle with non-inverted DW parents between Batches 68 and 87 inclusive but excluding Set 11 and Batch 73 were pooled to make Set 22. The means of force to fracture for these Sets ( $t = 0.65$ ,  $p = 0.5$ ) and the six related parent, joint or addition subsets (ANOVA  $F = 0.565$  [5,140 df]  $p = 0.73$ ) were not significantly different.

The graph points in Figure 22 for Batch 67 (10s delay between turns of the paddle) and DW condensed one-piece Batch 80 are conspicuous representing reduced strengths in these batches. Batch 67 was weaker than both Set 11 ( $t = 3.1$ ,  $p = 0.003$ ) and Set 22 ( $t = 4.2$ ,  $p = 0.0001$ ). Similarly, the mean force to fracture for DW one-piece Batch 80 was less than Set 11 ( $t = 3.55$ ,  $p = 0.0005$ ) and Set 22 ( $t = 4.6$ ,  $p = 0.0000$ ) which did not agree with the result for DW one-piece Batch 62 which was not significantly weaker than

either joined set. The cut cone condensed one-piece Batch 64 is also conspicuous: the mean force to fracture exceeded that for Sets 11 and 22 ( $t > 7.3$ ,  $p = 0.0000$ ).

The results from Sets 11 and 22 were pooled and divided into subsets identified as A21 P, J or A (Parent, Joint or Addition) according to the location of fracture origin. Cumulative failure graphs for these subgroups are shown in Figure 23 and descriptive statistics are presented in Table 25.

The results of t-testing reported in Table 26 revealed no significant differences in mean force to fracture for these subgroups. The numbers of samples in each subgroup were tested against the  $\frac{1}{4}:\frac{1}{2}:\frac{1}{4}$  hypothesis. There were significantly fewer addition failures (24 out of 146,  $p = 0.01$ ) but the numbers of parent and joint failures were not different to those expected.

#### **6.9.2.7 Review of development**

It appeared that the elevated paddle setting of 0.70mm might possibly reduce sample strength. There was no strength advantage in using more than 12 turns to the paddle. Delayed final condensation did not unduly influence strength if paddle application was continuous but intervals between turns of the paddle on the first addition increment produced weaker joints.

Condensation of the first addition increment by 6 turns of the vibrating paddle in less than 10s at a height setting of 0.60mm seemed to be reasonable. These values were adopted for the remainder of the study when the paddle was used and are the basis of the standard paddle procedure (SPP) specified in Table 6, page 78.

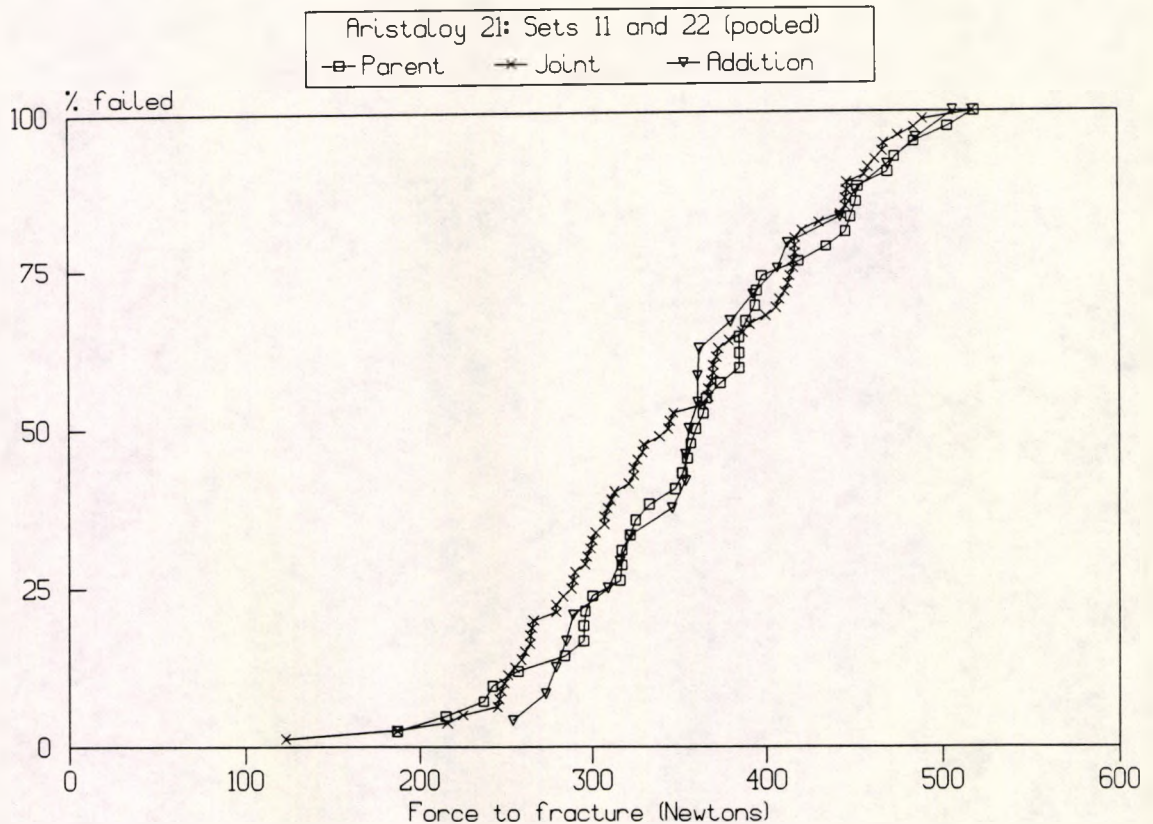


**Figure 23.** Cumulative frequencies of force to fracture for Sets 11 and 22 which were pooled and subdivided according to location of fracture origin.

Group	Sets	No.	Mean Load	S.D. (n-1)	95% C.I. of Mean		Median Load
					From	To	
A21 P	11 & 22	42	363.1	79.1	338.5	387.8	363.5
A21 J	11 & 22	80	348.9	81.3	330.8	367.0	350.0
A21 A	11 & 22	24	365.5	70.1	335.9	395.1	361.5

**Table 25.** Force to fracture statistics in Newtons of Sets 11 and 22 (Aristaloy 21), which were pooled and subdivided according to the location of fracture origin (Parent, Joint or Addition).

Groups	95% C.I. for the difference in means		Student's t-test	
	From (Newtons)	To (Newtons)	t =	P =
A21 P & J	-16	44.5	0.94	0.35
A21 P & A	-40	35	0.13	0.90
A21 J & A	-18	50.8	0.98	0.33

**Table 26.** Confidence intervals for differences in mean force to fracture between the Parent, Joint and Addition subgroups of pooled Sets 11 and 22 (Aristaloy 21) and results of two sample t-testing.

### 6.9.2.8 Mode of condensation and inversion of the parent

Earlier in the study, all parents in Batch 15 failed where 2s condensation time was applied to each increment using a flat piston (Section 6.5.3). Further consideration was given to variation of the condensation mode for the parent.

Two batches were condensed by application of the BS weights in a single thrust for 60s: the spacer was not used. Batch 82 was prepared for joining as described in Section 4.4.3.2 but Batch 84 was inverted: the surface which had been condensed against the lower piston was end-prepared for joining. The cut cone (Batch 81) and flat (Batch 83) pistons were used in parent condensation for two further batches. The SPP was used for all additions.

DW inverted Batch 84 (Figure 22 and Table 24) was weaker than the non-inverted groups against which the results were t-tested. Compared to flat piston vibrated parents ( $t = 2.1$ ,  $p = 0.047$ ) the difference was less significant (even though the coefficient of variation was less than 15%) than for standard DW parents ( $t = 2.25$ ,  $p = 0.037$ ) and cut cone vibrated parents ( $t = 2.87$ ,  $p = 0.01$ ) where the COV was greater (28% and 21% respectively). Samples from cut cone parents gave nearly the same mean force to fracture as those from DW parents. The mean force to fracture for flat piston condensed samples was not significantly less than for the other non-inverted parents ( $p > 0.2$ ).

Three or four parents failed in each alternative batch but no fractures initiated in cut cone parents (Batch 81). Eight joints failed in this batch: the two strongest samples failed in the addition suggesting that the parent material was strong. The fracture surfaces showed small areas where material had pulled from the parents. The final portion of the parent had been recondensed with a flat ended piston: parts of this layer appeared to be less coherent.

## **6.10 Preparation of joined samples: further work using Veraloy**

As supplies of Aristaloy 21 powder became exhausted, Veraloy was used for the tests reported in this section. Joined sample preparation included variation of addition condensation with DW parents and DW or dome piston condensed parents in inverted and non-inverted orientations with SPP additions. One-piece samples were condensed by the DW method or by vibration using flat or dome ended pistons for 2s on each increment (Section 4.4). The batch test results are shown in Figure 24 and Table 27. There was sometimes considerable scatter in the force to fracture values recorded for samples prepared using this alloy. Analysis of the length and weight of the sample parts is considered briefly.

### **6.10.1 Addition condensed using the RI piston, flat piston or weights**

Joined samples were prepared using DW parents. The addition amalgam mix was divided and the first increment condensed by vibration using the RI piston for 4s (Batch 88) or the flat piston for 2s (Batch 89), or condensed undivided by deadweighting (Batch 90). As can be seen in Figure 24, all samples failed at the joint except two parents in the RI group. The coefficients of variation were high (Batch 88: 34.8%; Batch 89: 25.9%): although the means of force to fracture for these batches were not significantly different ( $t=1.79$ ,  $p=0.09$ ), by Wilcoxon's test Batch 88 was stronger ( $p=0.038$ ). Joined Batch 90 (DW addition) was much weaker than either vibration condensed batch ( $p=0.0000$ ). The difference between the flat and RI piston condensed Veraloy batches was less significant than for Amalgam M Sets 4 and 5.

### **6.10.2 Delayed condensation of the first increment after paddle use**

The condensation procedures reported in Section 6.9.2.5 were repeated in

Batches 91, 92 and 93 (Figure 24) but the first application of the flat piston was 50s, 70s and 90s after completion of amalgamation respectively. In all other respects, the SPP schedule was followed. The force to fracture values in these batches were similar (ANOVA  $F = 1.16$  [2,26 df]  $p = 0.33$ ). Only one out of thirty samples fractured in the addition: the joint failed in 23 cases.

### **6.10.3 Mode of condensation and inversion of the parent**

Section 6.9.2.8 considered use of inverted DW, cut cone or flat piston condensed parents. Further attention was given to variation in parent preparation. This included use of DW and a new dome shaped vibration piston for parents in both non-inverted and inverted orientations and additions were by the standard paddle procedure. A limitation of the results presented in this section is that the force to fracture results for samples prepared in the same manner on different occasions were sometimes not reproduced. Pooled force to fracture results are given in Figure 25 and Table 28.

#### **6.10.3.1 Deadweight: non-inverted Set 12; inverted Set 13**

The two thrust procedure was used with repositioning for condensation of DW parents in Veraloy. Unlike the finding for Aristaloy (Section 6.9.2.8), Batch 97 (inverted) was not significantly weaker than Batch 96 (non-inverted:  $t = 1.8$ ,  $p = 0.09$ ). On repeating the non-inverted DW preparation there was no difference in the results for Batches 96, 99 and 103 (ANOVA  $F = 0.125$  [2,27 df]  $p = 0.88$ ) and these were pooled to make Set 12.

For the inverted DW parents (Batches 97, 100 and 104), the result of ANOVA was significant ( $F = 5.09$  [2,27 df]  $p = 0.01$ ): Batch 97 was weakest. No reason for the difference was identified and the results for the three batches were pooled to make Set 13.

### 6.10.3.2 Dome piston: non-inverted Set 14; inverted Set 15

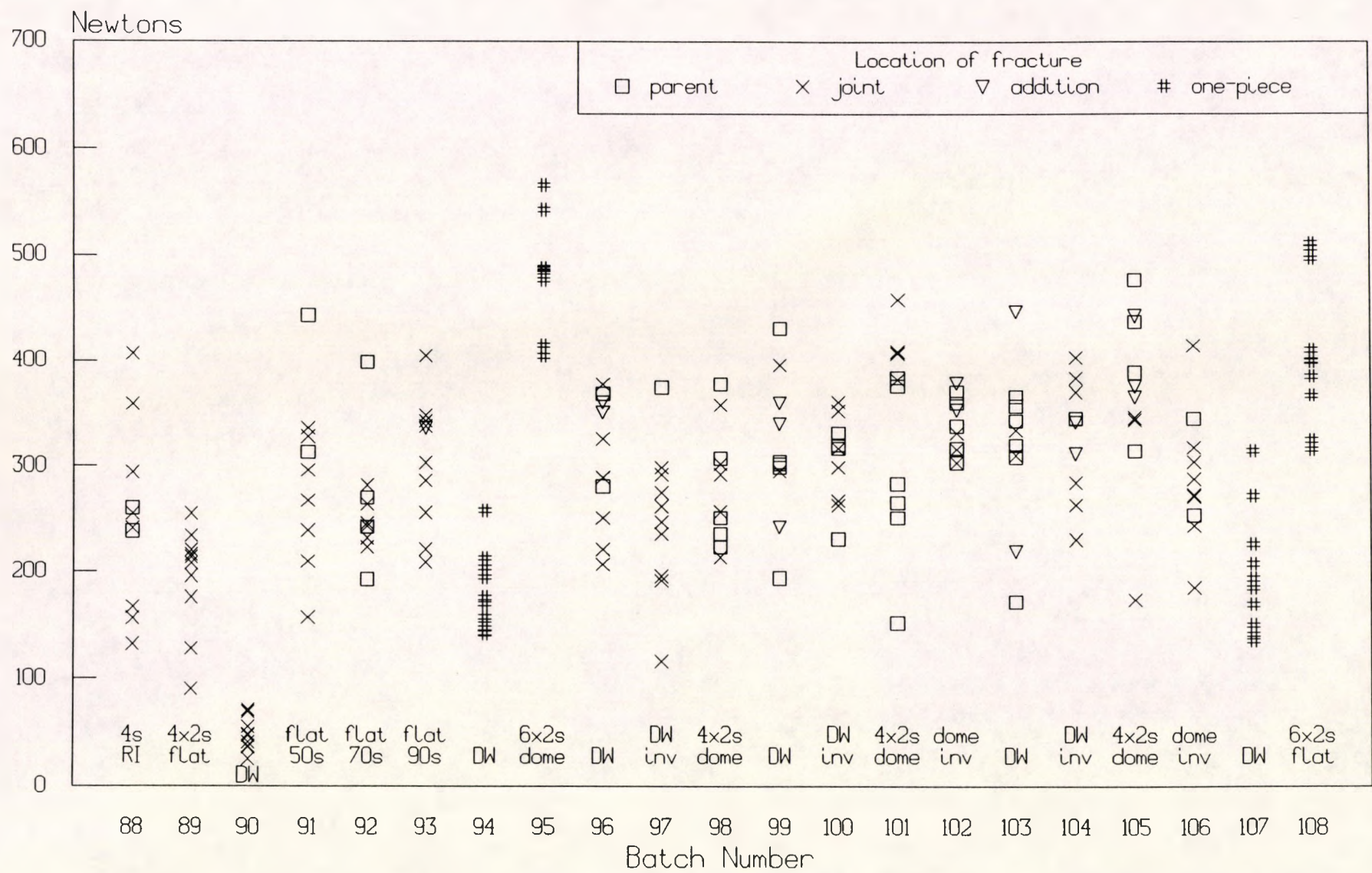
The earlier finding that very much stronger samples had been produced by the cut cone piston than other methods (Batches 48 to 52, Section 6.7.4.1; Batch 64, Section 6.9.2.1) was reconsidered. The tapered end of this piston might have given a mechanical advantage to the applied condensation forces resulting in higher condensation pressures. The "wedging" action could have forced the amalgam mix against the wall of the mould. Porosity (shown in Plate 65) occurred in the central part, perhaps due to trapped air.

A new blunt ended piston design, identified as the "dome", was considered and manufactured. Joined samples were prepared from parents condensed using the dome piston for 2s on each increment and as described in Section 4.4.2. These were end-prepared in both non-inverted (Batches 98, 101 and 105) and inverted orientations (Batches 102 and 106).

The result of ANOVA for the non-inverted group was not significant ( $F = 2.89$  [2,27 df]  $p = 0.07$ ) but on t-testing Batch 105 was stronger than Batch 98 ( $t = 2.64$ ,  $p = 0.017$ ). No reason for the difference was identified and the results were pooled to make Set 14. Similarly, the means of force to fracture for the two inverted dome condensed batches were different ( $t = 2.23$ ,  $p = 0.039$ ) and were pooled to make Set 15.

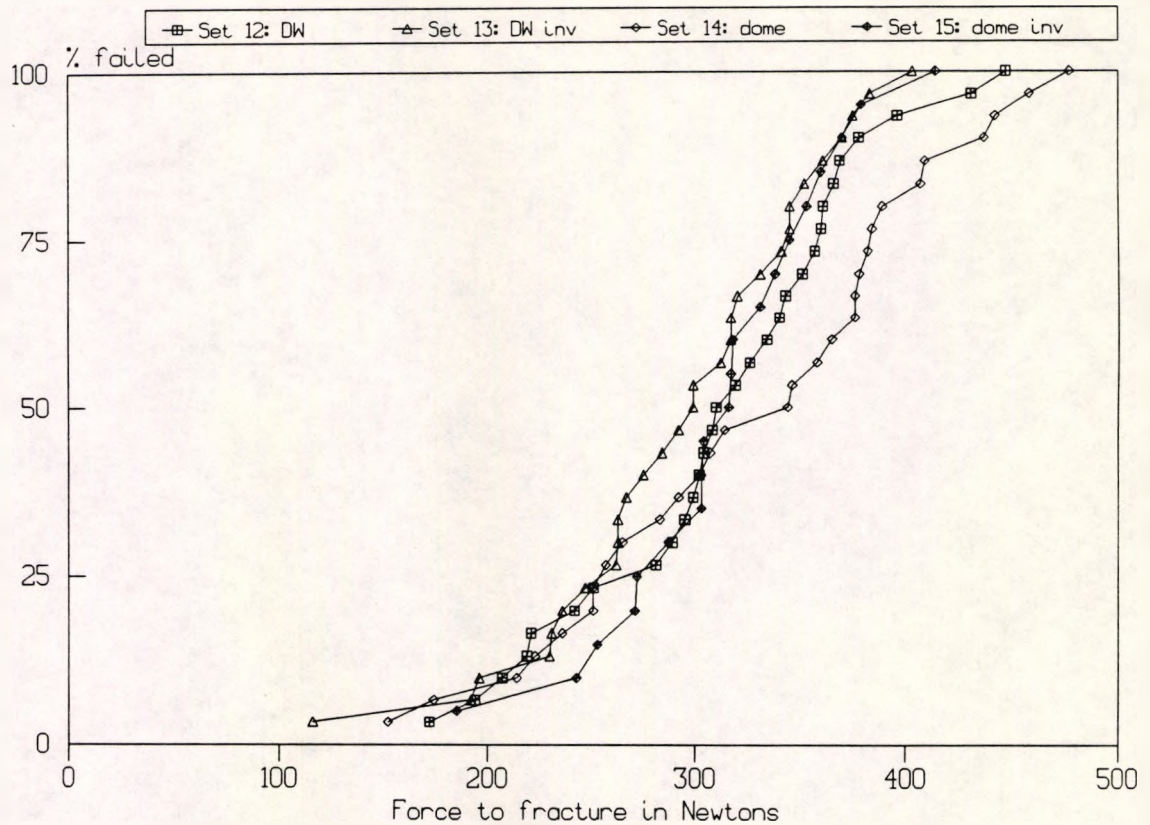
Cumulative failure graphs in Figure 25 reveal close similarities in the force to fracture results for Sets 12 to 15. Set 14 was strongest but Table 29 shows that the result of t-testing for this Set against the others was not significant. More parent failures occurred in Set 14 than expected under the  $\frac{1}{4}:\frac{1}{2}:\frac{1}{4}$  hypothesis (15 out of 30:  $p = 0.04$ ) but for the numbers of samples in Sets 12 to 15, no other test outcomes were significantly different from those expected.

Figure 24. Force to fracture for Batch 88 to 108. Veraloy.



Batch Number	Preparation procedure		Force to fracture (Newtons)		
	Parent	Addition part	Mean	95% C.I. for mean	
				From	To
88	DW	4s RI, 3x2s flat	251	188.6	313.3
89	DW	4x 2s flat only	194	157.9	229.6
90	DW	DW	48	36.0	59.4
91	DW	6x pdl >10s 2s flat @ 50s	287	224.1	351.2
92	DW	6x pdl >10s 2s flat @ 70s	259	220.0	298.9
93	DW	6x pdl >10s 2s flat @ 90s	304	260.3	348.7
94	One-piece DW		181	154.6	207.4
95	One-piece 6x 2s dome		477	438.8	515.0
96	DW	SPP	303	258.5	348.3
97	DW inverted	SPP	249	198.4	299.6
98	4x 2s dome	SPP	282	242.0	321.6
99	DW	SPP	316	266.5	366.1
100	DW inverted	SPP	306	276.4	335.2
101	4x 2s dome	SPP	337	269.2	404.2
102	4x 2s dome inverted	SPP	337	317.3	356.7
103	DW	SPP	318	262.8	372.2
104	DW inverted	SPP	328	288.3	366.9
105	4x 2s dome	SPP	366	306.0	426.8
106	4x 2s dome inverted	SPP	289	244.8	333.6
107	One-piece DW		199	157.8	240.8
108	One-piece 6x 2s flat		411	360.2	462.8

**Table 27.** Preparation procedures and force to fracture results for Batches 88 to 108. Veraloy.



**Figure 25.** Cumulative frequencies of force to fracture for Sets 12, 13, 14 and 15 (Veraloy) where the preparation of the parent parts was varied.

Set	Batches	No.	Mean Load	S.D.(n-1)	95% C.I. of Mean		Median Load
					From	To	
12	96,99,103	30	312.4	67.7	287.1	337.7	316.0
13	97,100,104	30	294.1	64.4	270.1	318.2	297.5
14	98,101,105	30	328.3	84.9	296.6	360.0	330.0
15	102,106	20	313.1	52.8	288.4	337.8	316.0

**Table 28.** Force to fracture statistics of Veraloy Sets 12 to 15 (Newtons).

Sets	95% C.I. for the difference in means		Student's t-test	
	From (Newtons)	To (Newtons)	t =	P =
14 & 12	-24	56	0.80	0.43
14 & 13	-5	73	1.76	0.085
14 & 15	-24	54	0.78	0.44

**Table 29.** Confidence intervals for differences in mean force to fracture between Set 14 and Sets 12, 13 and 15 and results of two sample t-testing.

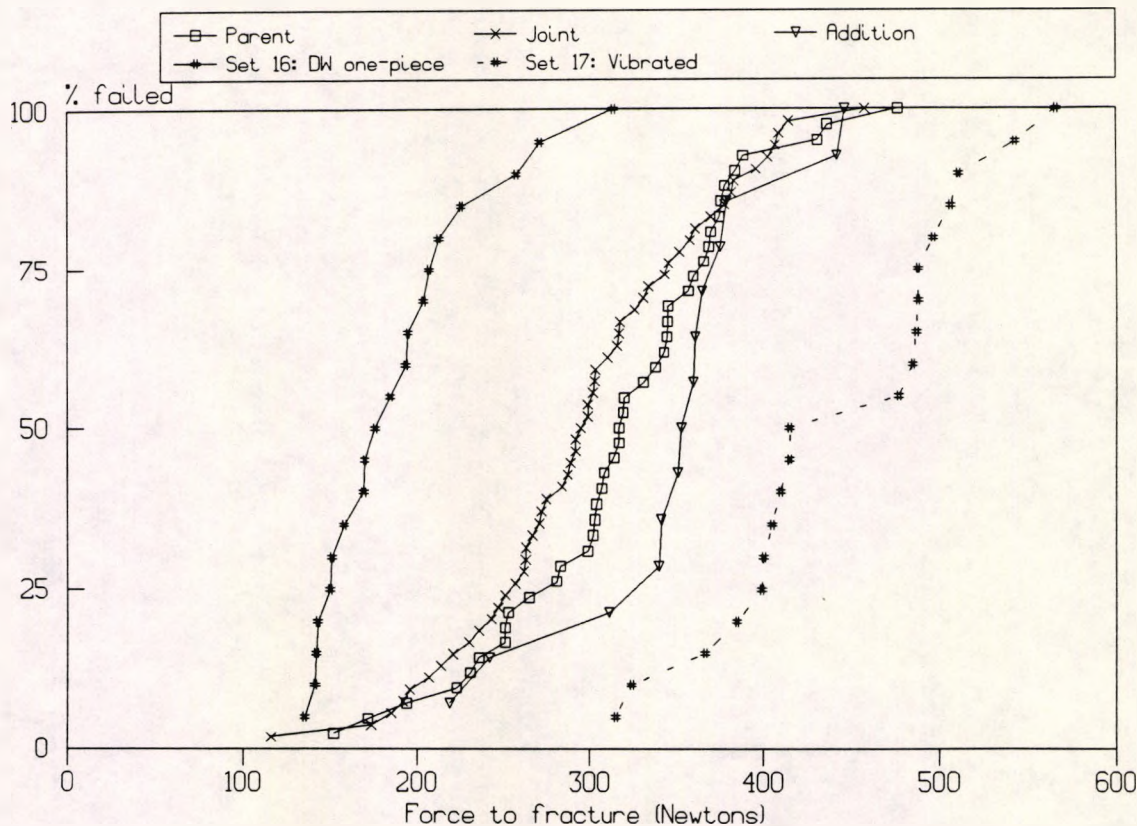


**Figure 26.** Cumulative frequencies of force to fracture for Veraloy Sets 16 and 17 (one-piece) and joined samples in Sets 12 to 15 which were pooled and grouped according to the location of fracture origin.

Set	Batches	No.	Mean Load	S.D.(n-1)	95% C.I. of Mean		Median Load
					From	To	
Ver P	96 to 106	42	317.1	68.7	295.7	338.5	319.0
Ver J	96 to 106	54	298.2	69.8	279.1	317.2	298.0
Ver A	96 to 106	14	349.1	62.2	313.2	385.1	353.0
16	94, 107	20	190.1	48.2	167.6	212.7	183.8
17	95, 108	20	444.2	70.0	411.4	477.0	446.0

**Table 30.** Force to fracture statistics in Newtons of one-piece Sets 16 and 17 and Veraloy joined samples grouped according to location of fracture origin.

Sets	95% C.I. for the difference in means		Student's t-test	
	From (Newtons)	To (Newtons)	t =	P =
Ver P & J	-9	47.2	1.33	0.19
Ver P & A	-9	73	1.63	0.12
Ver J & A	11	90.7	2.66	0.014

**Table 31.** Confidence intervals for differences in mean force to fracture and results of t-testing for the pooled results from Sets 12 to 15 (Veraloy), which were grouped according to the location of the fracture origin.

### 6.10.3.3 Pooled and subdivided results from Sets 12 to 15

The results for Sets 12 to 15 were pooled and divided into subsets identified as Ver P, J or A according to the location of fracture origin (Parent, Joint or Addition). These, together with one-piece test results are shown in Figure 26 with descriptive statistics in Table 30. The mean force to fracture for parent failures was intermediate between those for failed joints and additions. Table 31 shows that these differences were not significant and that the mean force to fracture for addition failures exceeded that for failed joints. Almost half (54 out of 110) of the samples failed at the joint which was expected under the  $\frac{1}{4} : \frac{1}{2} : \frac{1}{4}$  hypothesis but more parents ( $p = 0.02$ ) and fewer additions ( $p = 0.02$ ) than expected failed.

### 6.10.4 One-piece samples

One-piece samples condensed in six increments for 2s each using the dome (Batch 95) were approximately  $2\frac{1}{2}$  times stronger than deadweighted Batch 94 ( $t = 14.4$ ,  $p = 0.0000$ ). The effect was similar to use of the cut cone piston with Aristaloy 21 or Duralloy. In view of the difference, use of a flat ended piston for one-piece sample preparation was reconsidered.

One piece samples were prepared by the DW method (Batch 107) and using the new flat (but now somewhat worn) piston (Batch 108). The vibrated batch was about twice as strong as the DW batch ( $t = 7.3$ ,  $p = 0.0000$ ), in contrast to the similar procedures using Aristaloy 21 (Batches 62 and 63) which showed no difference in mean force to fracture (Section 6.9.2.1). The results for DW Batches 94 and 107 were not significantly different ( $t = 0.8$ ,  $p = 0.4$ ) and were pooled to make Set 16. Although the mean force to fracture for vibration condensed batches using the dome piston exceeded that for the flat ended piston ( $t = 2.3$ ,  $p = 0.03$ ): the pooled results make Set 17.

Cumulative failure curves for these Sets are included in Figure 26 which shows that the one-piece Sets were different from the Veraloy joined samples. The smallest difference in means was between the addition failures and Set 17 ( $t=4.1$ ,  $p=0.0003$ ) where there is a step in the distribution. It was considered that the force to fracture data for these one-piece samples did not compare well with those for the joined samples. The mean force to fracture for pooled Sets 12 to 15 was 64% greater than the value for the DW condensed one-piece Set 16. On the other hand, the joined Sets could be considered only 70% as strong as Set 17. The discrepancies were considered to be unsatisfactory but no further detailed work on one-piece sample preparation was carried out since this was beyond the scope of this study.

#### **6.10.5 Further considerations: sample length and weight**

The strength of fully set amalgam reduces when its mercury content exceeds an optimum proportion. In amalgam mixes containing a given quantity of alloy, it was hypothesised that sample length and weight might provide an indication of the effectiveness of the condensation procedure. BS EN 21559: 1992 requires that the coefficient of variation of mass for alloy and mercury in pre-dosed capsules shall not exceed 1.5%. Allowance for possible variation in the quantity of mix dispensed by the Dentomat (or capsules) and sample cross sectional dimensions were considered to be beyond the scope of this study. Scatter diagrams and statistical analysis of the length and weight of Veraloy samples in Sets 12 to 17 are presented in the following sections.

##### **6.10.5.1 One-piece samples**

The sample length and weight for one-piece Sets 16 and 17 are shown in Figure 27 and the descriptive statistics are presented in Table 32. There is no overlap between the maxima for vibrated condensation and the minima for DW

condensation: the probability of these differences arising by chance is  $p = 0.0000$ . On average, vibration condensed samples were 92% of the length and 90.6% of the weight of the DW samples and the COV for length or weight was less than 1.5% except for DW samples where the COV for weight was 1.8%. These variations, to which all errors in dosing, mould dimensions, sample preparation and measurement contribute, are low compared to those for force to fracture which exceeded 25% for DW one-piece Set 16 and 15% for vibrated Set 17.

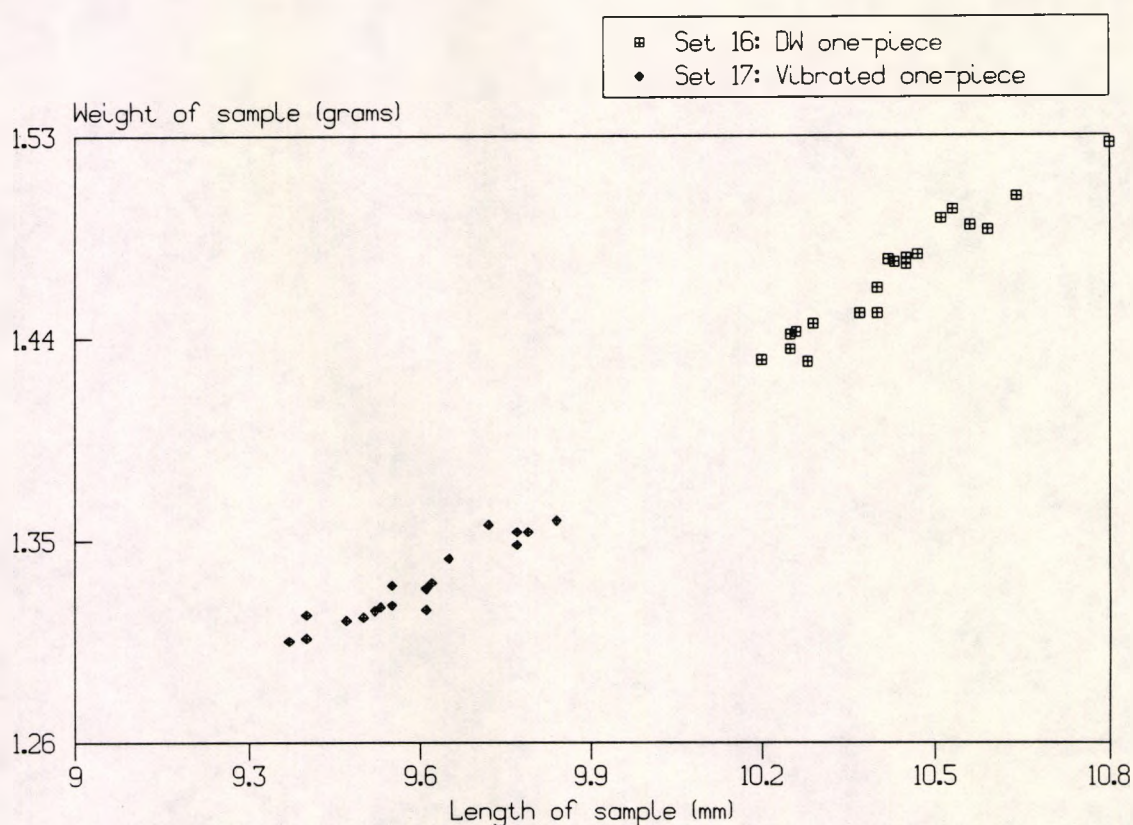


**Figure 27.** Graph of length vs weight of Veraloy one-piece samples: Set 16: DW condensation; Set 17: Vibrated condensation.

Set	Length of sample (mm)				Weight of sample (grams)			
	Mean	S.D.	95% C.I. for mean From                  To		Mean	S.D.	95% C.I. for mean From                  To	
16	10.428	0.151	10.357	10.498	1.4685	0.02680	1.4560	1.4811
17	9.594	0.138	9.527	9.660	1.330	0.0173	1.322	1.339

**Table 32.** Descriptive statistics of the lengths and weights of Veraloy one-piece samples: Set 16: DW condensation; Set 17: Vibrated condensation.

Linear regression analysis was carried out to determine any relationship between length and weight for these results. There was good correlation for both Set 16 and Set 17. The lowest limit of the 95% confidence interval for the regression coefficients was  $r=0.869$  and the attached probability was  $p=0.0000$  for these one-piece samples.

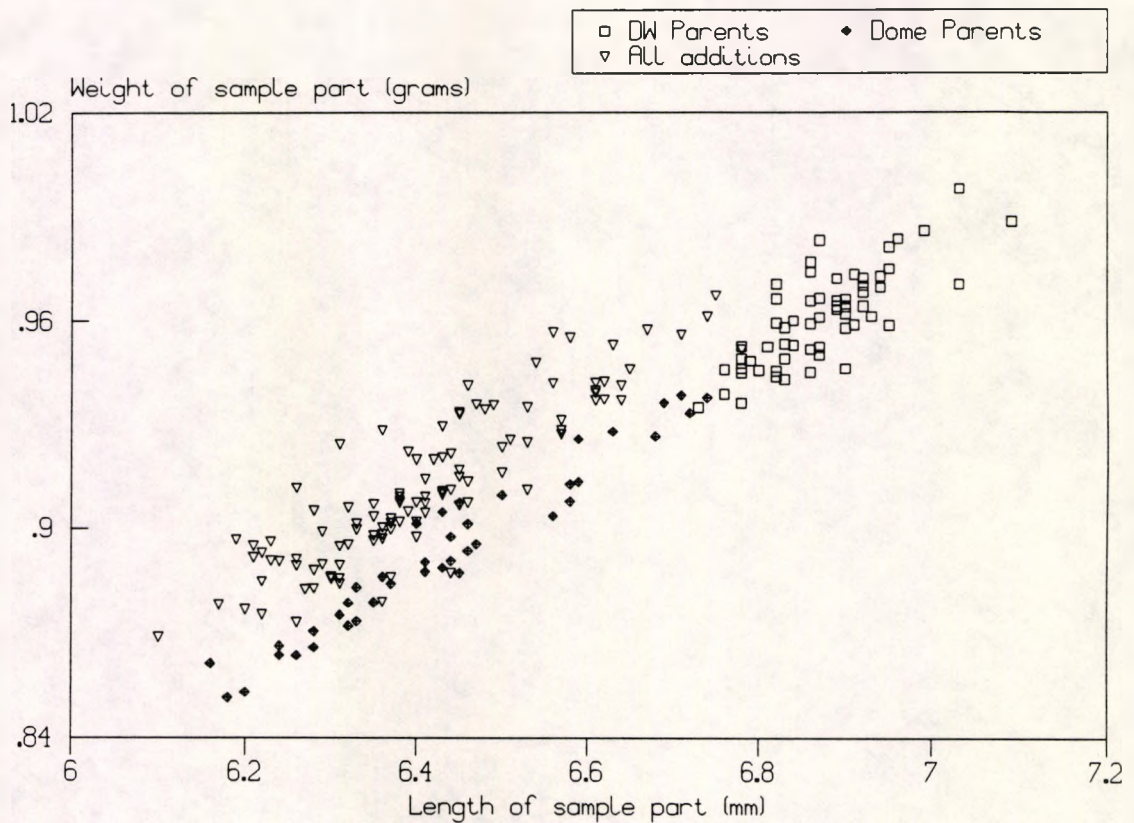


**Figure 28.** Graph of length vs weight of parts of Veraloy samples: DW parents; Dome vibrated parents and all additions.

Set	Length of sample part (mm)				Weight of sample part (grams)			
	Mean	S.D.	95% C.I. for mean From To		Mean	S.D.	95% C.I. for mean From To	
12&13 P	6.873	0.07069	6.855	6.891	0.96146	0.01356	0.95797	0.96498
14&15 P	6.434	0.15690	6.384	6.484	0.89380	0.02435	0.88601	0.90159
All Add	6.414	0.13914	6.387	6.440	0.91257	0.02271	0.90828	0.91686

**Table 33.** Descriptive statistics of the lengths and weights of the parts of the Veraloy samples in Sets 12 and 13 (DW parents), Sets 14 and 15 (Dome vibrated parents) and the pooled data from all addition parts of Sets 12 to 15.

#### 6.10.5.2 Joined samples

Addition lengths were calculated by subtraction of the trimmed parent length from the joined sample length. The value for weight added was obtained by subtraction of the trimmed parent weight from the joined sample weight. This calculation does not determine the weight of the addition part exclusively since some mercury expressed from the mix during addition condensation might have been absorbed and retained by the parent.

The results are shown in Figure 28 and Table 33. Variations in length and weight were greater for the parts of joined samples condensed by vibration ( $COV > 2.2\%$ ) than those condensed by DW ( $COV < 1.4\%$ ) or in one piece. DW parents were significantly longer and heavier than dome condensed parents. Since all additions were condensed by SPP, these results were pooled. Compared to vibration condensed parents, the additions were not different in mean length but significantly more weight was added to the joined samples.

One-piece samples were prepared from 3-dose mixes; each part of joined samples from 2 Dentomat doses. If this difference in quantity of mix was without influence on the samples, it was expected that the length and weight of one-piece samples would be 50% greater than parents condensed in the same manner. The means of these measurements for Set 17 were compared to the dome condensed parents of Sets 14 and 15 (length: 149.1%; weight 148.8%). In contrast, compared to Sets 12 and 13 parents, the values for DW condensed Set 16 were increased: 151.7% (length) and 152.7% (weight). It appeared therefore that the 3-dose mix may have been condensed less well by the DW method than the smaller mix. Mercury is denser than amalgam: these differences could indicate increased mercury content in the one-piece DW samples compared to DW parents. This consideration and the

possibility of reduced condensation pressure in the central part of the sample compared to the ends (considered in Section 6.4.6) might explain the comparative weakness of these DW one-piece samples. Detailed analysis of sample mercury content was beyond the scope of this study.

#### **6.10.5.3 Homogeneity of samples from different lumens of the mould**

The recorded force to fracture values were reexamined and it was seen that the weakest sample had been prepared in lumen 1 of the mould on 9 occasions in the 21 Batches using Veraloy. The DW procedure had been used for condensation of the parents in 8 of these cases. The longest and heaviest samples had been produced in lumen 1 in 9 of the 21 Batches, though not all of these were the weakest. Since the first amalgam dose of the day from the Dentomat was discarded it was not considered likely that the error of a larger mix was responsible. Samples produced from lumen 2 also tended to be long, heavy or weak. Further analysis was required to check for sample homogeneity between mould lumens.

ANOVA was carried out on the force to fracture results and length and weight values for samples prepared in each lumen of the mould. The analysis indicated that differences existed between these groups.

**6.10.5.3.1 Mean force to fracture.** ANOVA for pooled Sets 12 and 13 (DW parents:  $F = 2.365$  [9,50 df]  $p = 0.026$ ) suggested significant weaknesses in samples prepared in Lumens 1, 2 and 3 compared to the strongest samples. No differences between lumens were revealed for pooled Sets 14 and 15 ( $F = 0.49$  [9,40 df]  $p = 0.87$ ) where vibrational parent condensation was used.

**6.10.5.3.2 Parent sample length.** The mean length of DW parents from lumen 2 exceeded all except those from lumens 1 and 3 (Sets 12 and 13:  $F = 2.57$  [9,50 df]  $p = 0.016$ ). For vibrated dome condensed parents (Sets 14 and 15:  $F = 2.5$  [9,30 df]  $p = 0.029$ ) samples from lumens 1 to 4 ranked longest. The results for Batch 105 were excluded from these calculations because recording of the untrimmed parent length was omitted.

**6.10.5.3.3 Parent sample weight.** Differences were less marked for DW parents ( $F = 1.9$  [9,50 df]  $p = 0.07$ ) than for dome condensed parents ( $F = 4.2$  [9,40 df]  $p = 0.0008$ ). In the former case, samples from lumens 1, 2 and 3 were significantly heavy whereas in the latter group, the mean weight for samples from lumens 1 to 4 exceeded those for lumens 7 to 10.

**6.10.5.3.4 Addition parts.** The result of ANOVA was highly significant for both length ( $F = 3.97$  [9,100 df]  $p = 0.0002$ ) and weight ( $F = 4.47$  [9,100 df]  $p = 0.0001$ ). Lumen 2 produced the longest sample parts with most added weight; lumens 1 and 3 ranked second and third. Samples from Lumen 10 were notably light and short.

Both parent and addition parts of samples prepared in lumens 1, 2 or 3 tended to be long and heavy. This could have been explained by dispensation of larger mixes for these samples but random variation from this cause would have been expected. If any lumens (for example: 1, 2 or 3) had been slightly undersize in diameter, movement of condensing pistons might be impaired resulting in bad condensation, retained mercury and weakness. Samples from these lumens were weak but only when prepared by the DW method. Vibration condensed one-piece samples were much stronger and subject to less variation than those by the DW method. The measurements for vibration condensed joined samples were subject to variation but were less than the length and weight values for DW parents. Hence, possibly the final mercury

content of vibration condensed samples did not reach the values occurring in DW condensed samples which may have been more critical for strength.

Earlier in the study (see Section 6.4.5), measurement of sample diameter using a screw micrometer revealed differences between samples condensed in different mould lumens. The range of mean diameter measurements was about one quarter of one per cent of the mean and *per se* was considered to exert insignificant influence on flexural strength. It was noted that the mean diameter measurements for samples from Lumen 10 were largest. Movement of the piston could have been less restricted in a wider lumen enabling better condensation: Veraloy samples from Lumen 10 were light and short. Conversely, bad condensation might occur if piston movement was restricted.

The BS piston was examined and damage was found at the end, possibly having been caused by contact with bolt holes in the Desoutter weight bearing assembly. It was considered possible that the damaged BS piston might sometimes have jammed slightly in the mould causing bad condensation. In use, the piston had been regarded as a 2 ended tool: either end could have been applied to the amalgam mix. It was not possible to link samples with the end of the BS piston used and it was not known when the damage occurred. The weakest samples in Batches 76 and 77 were condensed in lumen 1 but this may have been coincidence: no pattern was identified in a review of the earlier results. ANOVA for force to fracture and lumens for pooled Sets 11 and 22 ( $F = 0.899$  [9,132df]  $p = 0.5$ ), pooled Amalgam M joined Sets ( $F = 0.73$  [9,138df]  $p = 0.68$ ) and one-piece samples in Batches 32 to 41 ( $F = 0.3$  [9,90df]  $p = 0.97$ ) revealed no differences.

This uncontrolled variable might have been responsible for some of the lumen related effects seen in the values recorded. However, these also occurred where vibration was used exclusively: the BS piston was not used in all cases.

A new non-reversible piston was manufactured from 4.00mm diameter silver steel bar. One end was flat for application to the amalgam mix: the opposite end was bevelled for contact with the weight assembly. The bevelled piston was used from Batch 109 to the end of the study.

In cases where the parent had been inverted, characteristically weak samples had been condensed in lumen 3. A small flaw was found about 8mm from the bottom surface of the mould. On reassembly of the mould, excessive pressure on the elevation in the corresponding area of the amalgam led to cracking 1 to 2mm from the end of these samples. In non-inverted samples, the crack was beyond the lower supports of the 3 point bend rig. Occasionally, joined samples had fractured in this location simultaneously with the primary failure during test. When the parent part was inverted, the surface flaw was close to the joint interface. Any cracking on reassembly therefore resulted in a weak test.

The flaw in lumen 3 was identified as a cause of weakness in joined samples where the parent was inverted. Apart from this problem, reassembly of the split mould for joined sample preparation was considered to work well.

An interruption due to the telephone caused a delay of 4 minutes 40s in removal of the load during condensation of the parent part of sample 103.5. In a review of the results, it was seen that this sample was the strongest in the batch and it failed in the addition. It was considered possible that extended application of the load might have improved the strength of the parent sufficiently for failure to occur elsewhere.

#### **6.11 Joined samples from amalgam alloys supplied in capsules**

Joined amalgams were prepared from precapsulated amalgam alloys. The

parent parts were condensed by the deadweight method and the standard paddle procedure was used for preparation of the additions. The alloys used were supplied by Dr J.D.R. Walker, City University and amalgamation was carried out using a Silamat. The force to fracture results and sample lengths and weights are considered briefly in this section.

### 6.11.1 Force to fracture

Figure 29 shows the force to fracture values for Batches 109 to 117. These data and the lengths and weights of all samples in these Batches are given in Appendix 4.

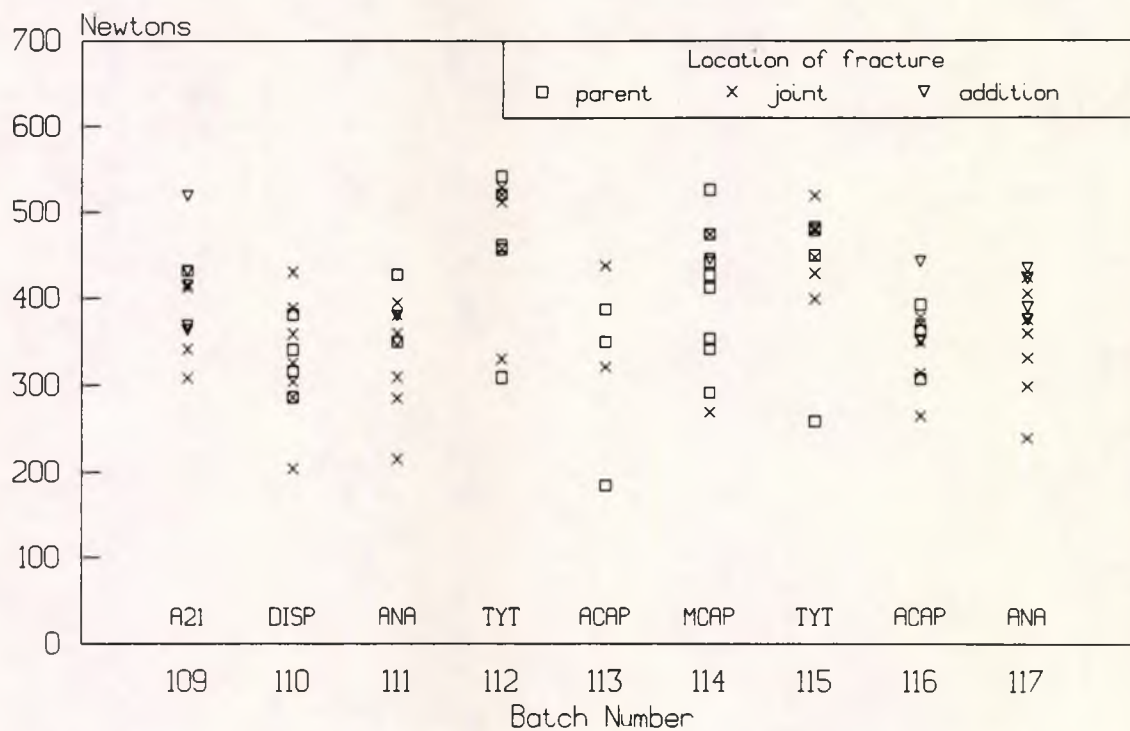


Figure 29. Force to fracture Batch 109 to 117. Pre-capsulated amalgams.

In the plates in this section, samples are ranked in order of strength with the strongest at the top of the left column and the numerals between the sample columns refer to the mould lumens. Plate 67 shows Tytin Batch 112 after fracture. Unfortunately, the trays holding this batch and Amalcap SAS Batch

113 were accidentally dropped before testing. Two Tytin and four Amalcap SAS samples were broken; these are identified by the letters NR indicating "no result" from the test. The fracture involved the joint in only one (specimen 113.9) out of those six broken samples.

Under test, five out of eight Tytin samples failed at the joint including three of the four strongest where a force of over 500N was recorded at fracture. The characteristic pattern of radial scratch marks from end-preparation was clearly visible over the majority of the fracture surfaces. Force to fracture values had exceeded 500N in only four specimens in the 67 batches of joined samples tested prior to Batch 108.

When the preparation using Tytin was repeated (Batch 115) six samples failed at the joint; four failed in the parent. None of the tested Tytin samples failed in the addition.

In contrast, four samples of Aristaloy 21 Batch 109 (Plate 68) failed in the addition: the fractures appeared to start at the interface between the first and second increments some distance from the joint. Of the five samples which apparently failed at the joint, radial scratch marks were assessed as showing in 10%, 35%, 50%, 50% or 65% of the fracture surface area. In the complementary areas the material adjacent to the joint had failed. The test machine failed to record the force to fracture for sample 109.4 where scratch marks were seen in 65% of the surface. However, the four strongest recorded samples did not fail at the joint.

The conventional (5% Cu) lathe cut alloy Matticap Fine 68 (Batch 114, Plate 69) showed radial score marks on only 20% of the fracture surface of the two samples where failure involved the joint. The addition part failed in only one specimen: the parent material failed in nine cases.

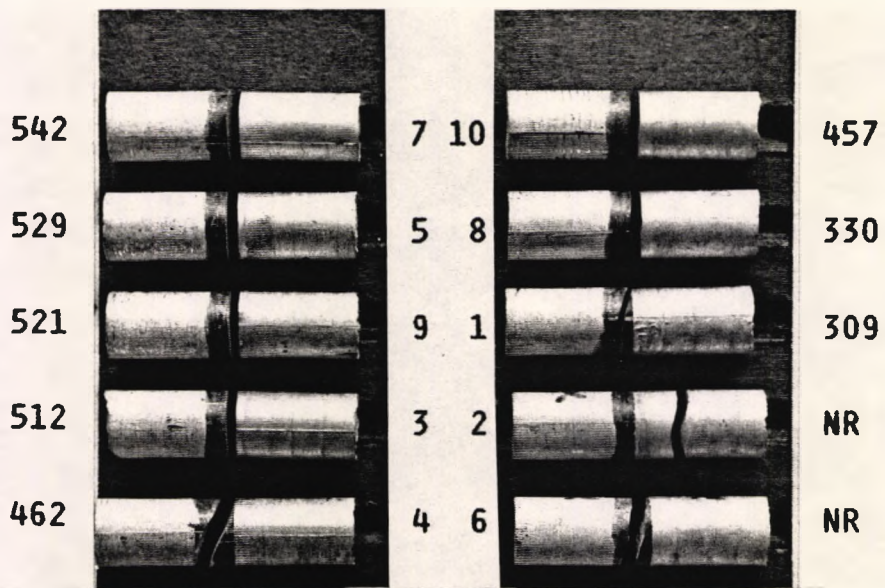


Plate 67. Batch 112: Tytin.

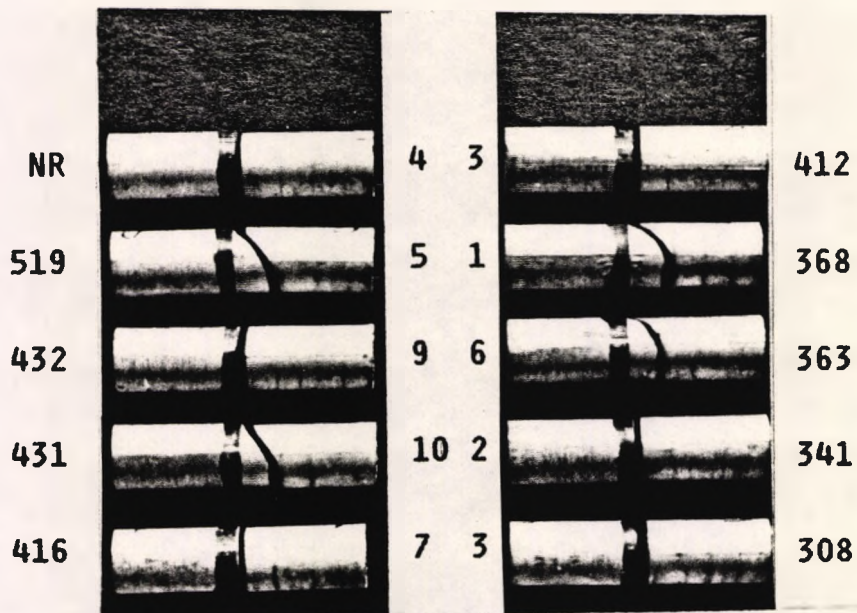


Plate 68. Batch 109: Aristaloy 21.

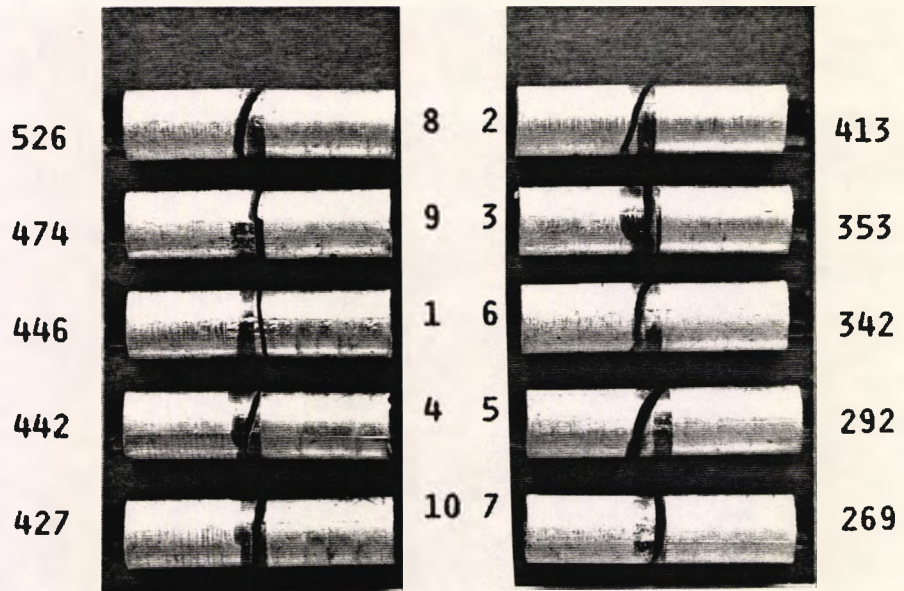


Plate 69. Batch 114: Matticap Fine 68.

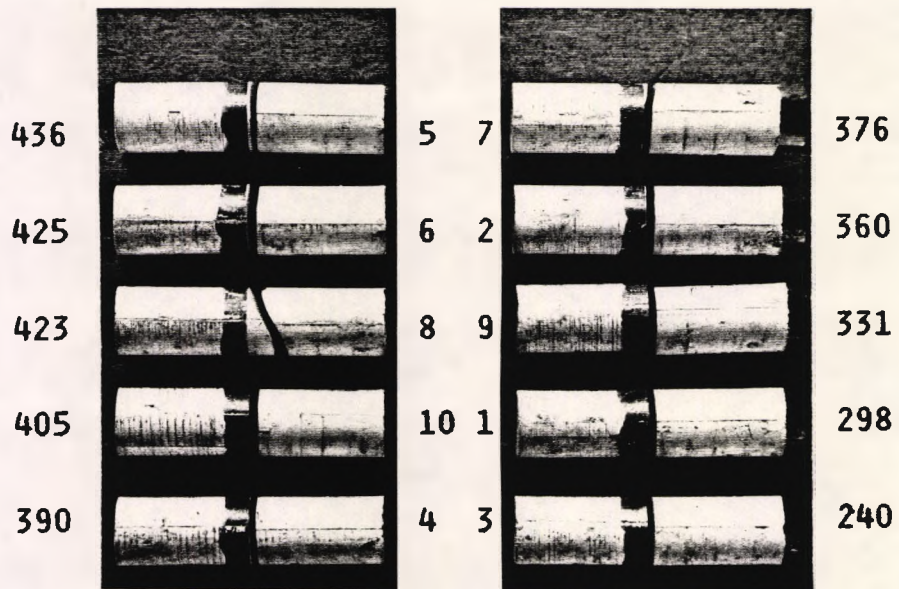


Plate 70. Batch 117: ANA 2000.

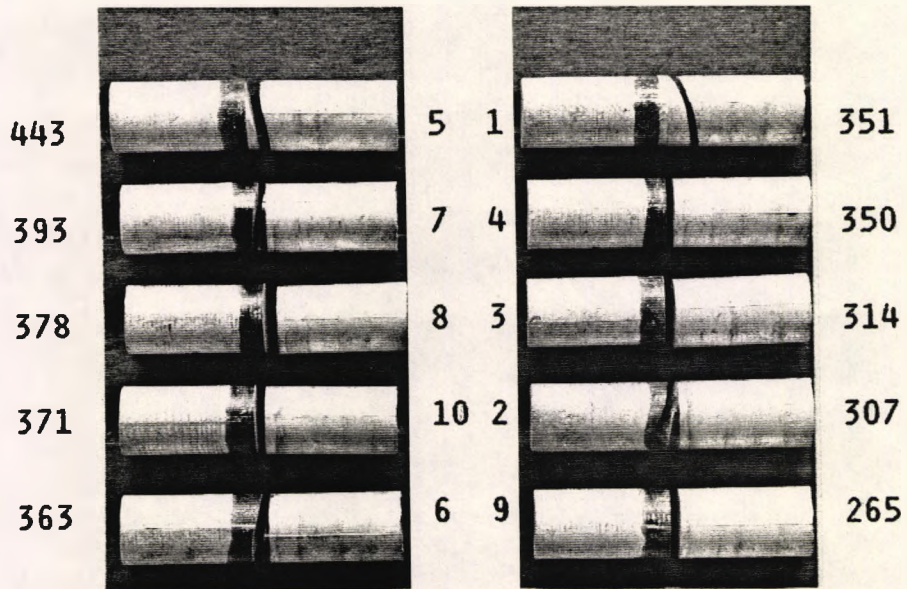


Plate 71. Batch 116: Amalcap SAS.

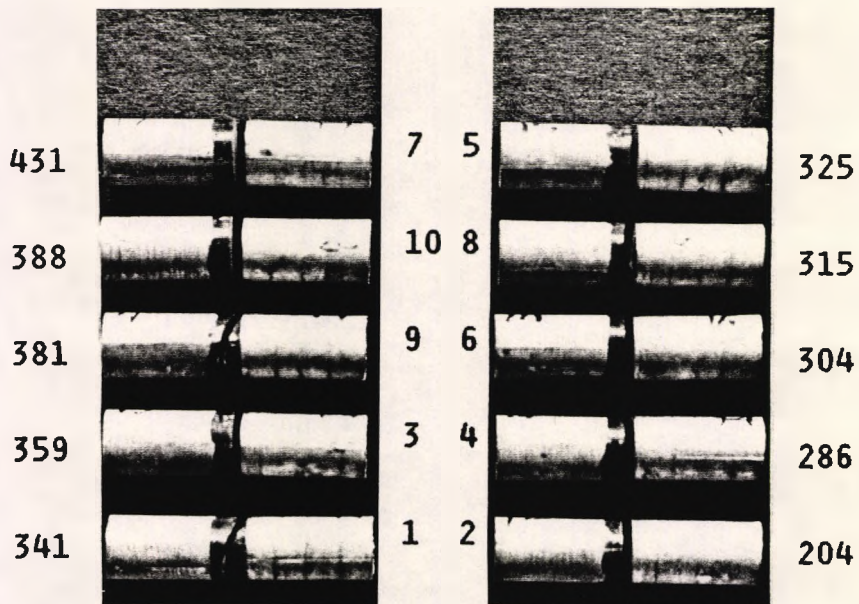


Plate 72. Batch 110: Dispersalloy.

The 24% Cu HCSC lathe cut ANA 2000 (Batch 111 and Batch 117, Plate 70) showed joint failure in 14 out of 20 samples. The parent material failed in only one case which was the strongest sample in Batch 111. Slight off-centre placement of the samples in the test rig had occurred accidentally in specimens 5, 6 and 7 of Batch 117. The central loading roller had been applied to the addition part where the fracture had ended. The edge of the indentation of the loading roller was seen to contact the marked band on the parent surface.

Of the six Amalcap SAS admixed alloy samples in Batch 113 which survived falling on the floor, two failed at the joint showing score pattern over 75% and 90% of the fracture surface. The parent material failed in the four remaining specimens. When the preparation procedure was repeated in Batch 116 (Plate 71), the joint failed in 5 cases; failure was in the addition in two cases including the strongest.

No samples in Dispersalloy Batch 110 (Plate 72) failed in the addition. In six cases, failure was at the joint. In these cases, score pattern was visible over the majority of the fracture surface area. Where the scratch marks were obscured, broken parent material was attached to the addition material at the joint. In sample 110.4, the fracture began at the joint showing score pattern in about 20% of the fracture surface. However, in this case the fracture ended in the parent material due to mis-positioning of the sample in the test rig.

It was noted that a grey-brown tarnish appeared on the surface of the parent part of the Dispersalloy samples after joining. No similar effect was seen during this study with other amalgams.

Even though the mercury content of Amalcap SAS was 52.5%, both admixed

amalgams were subjectively considered to produce rather "dry" mixes which tended to crumble on division into portions. These capsules incorporated pestles: the mix was of irregular shape. Manipulation of the mix was therefore somewhat more difficult than in cases where mix coherence was better.

Although many samples from capsulated alloys fractured at the joint, some of these (particularly Tytin) had been strong compared to the other amalgams. Three out of the four strongest conventional Amalgam M samples in Batch 5 (Plate 38, page 116) early in this study had also fractured at the joint. It seemed that a form of microstructural discontinuity must have existed at the joint in these samples even when the joint was strong.

There appeared to be a difference between Tytin and Aristaloy 21 capsules in that fracture had not involved the joint in the four strongest samples in Batch 109. In other amalgams, for example ANA 2000, Amalcap and Dispersalloy (Plates 70, 71 and 72) the weaker samples generally failed at the joint.

In contrast, the joint was rarely involved in the fracture of the conventional amalgam Matticap Fine 68. Since the samples were generally strong, the joints were not considered to have contributed to weakness in this amalgam.

It is considered that there are too few samples in these data sets for reliable force to fracture analysis by subsets. Cumulative force to fracture curves for these amalgams are shown in Figure 30 and descriptive statistics are given in Table 34. The curve for Tytin is to the right of all others: the difference in mean force to fracture (Table 35) was not significant for Aristaloy 21 or Matticap but was significant for Dispersalloy, ANA 2000 and Amalcap SAS. The force to fracture differences between the amalgams excluding Tytin were not significant.

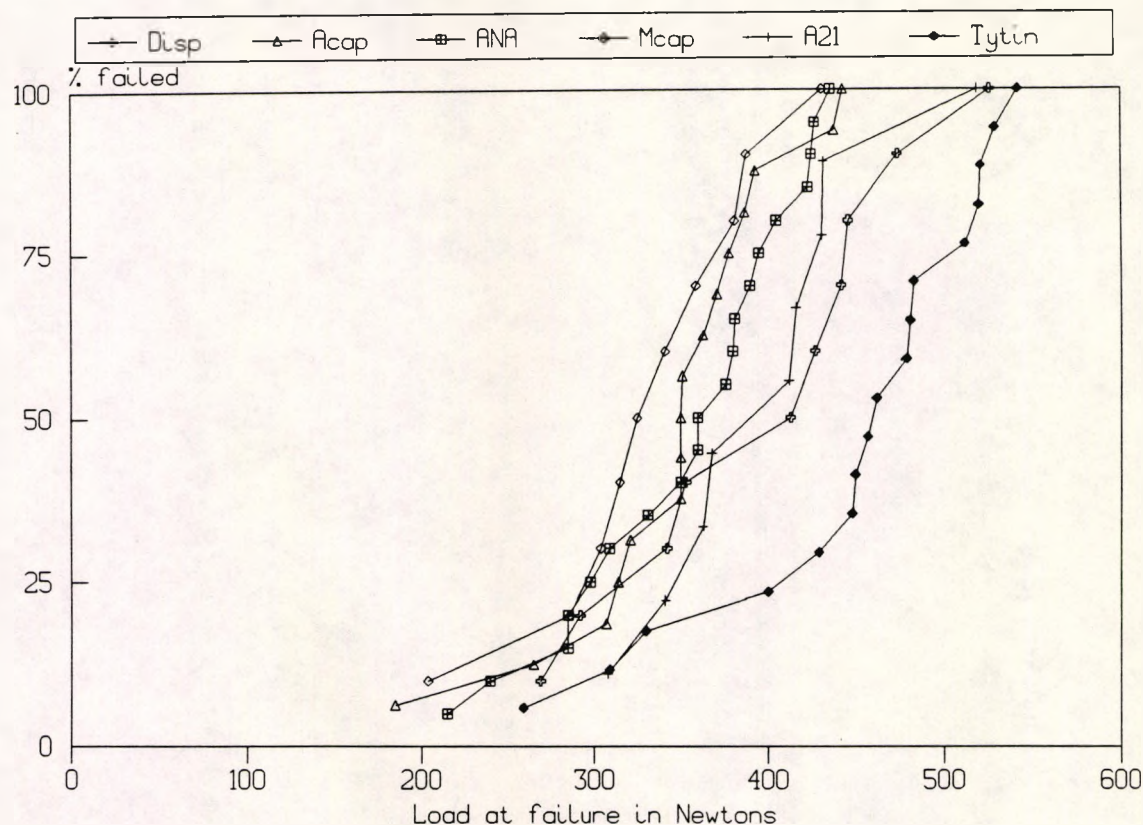


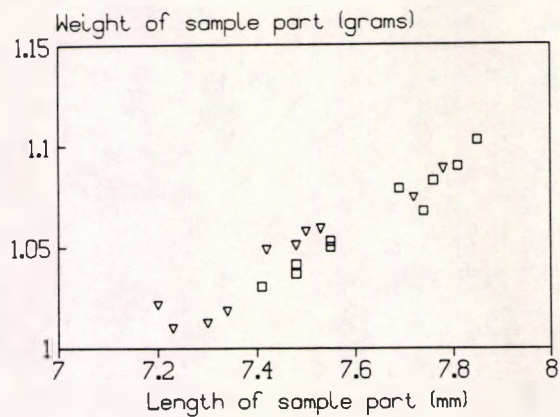
**Figure 30.** Cumulative frequencies of force to fracture for joined samples prepared from pre-capsulated amalgam alloys.

Alloy	Batches	No.	Mean Load	S.D. (n-1)	95% C.I. of Mean		Median Load
					From	To	
DISP	110	10	333.4	63.0	288.3	378.5	337.0
ACAP	113,116	16	347.9	62.9	314.3	381.4	350.8
ANA	111,117	20	353.6	63.6	323.8	383.3	358.5
MCAP	114	10	398.4	82.0	339.7	457.1	398.0
A21	109	9	398.9	62.1	351.1	446.7	397.0
TYT	112,115	17	447.7	81.1	406.0	489.4	460.5

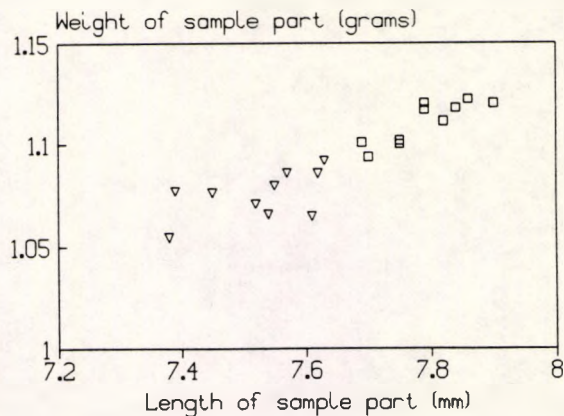
**Table 34.** Force to fracture statistics in Newtons of joined samples prepared from pre-capsulated amalgam alloys.

Sets	95% C.I. for the difference in means		Student's t-test	
	From (Newtons)	To (Newtons)	t =	P =
TYT & A21	-11	108	1.71	0.10
TYT & MCAP	-19	118	1.52	0.15
TYT & ANA	45	144	3.88	0.0005
TYT & ACAP	48	151	3.96	0.0004
TYT & DISP	56	172	4.08	0.0005

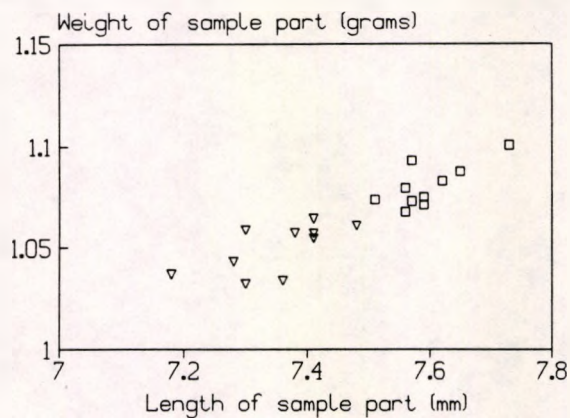
**Table 35.** Confidence intervals for differences in mean force to fracture and results of t-testing for Tytin and joined specimens prepared from different pre-capsulated alloys.



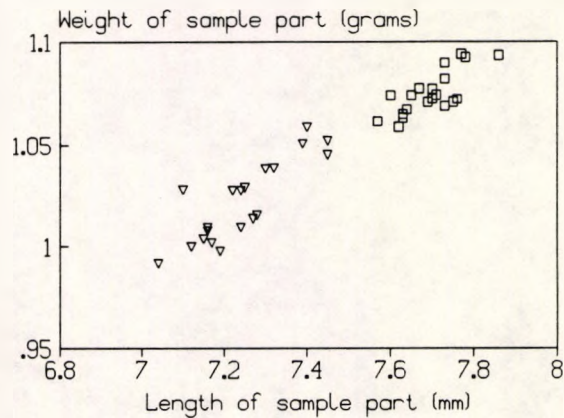
**(A) Aristaloy 21 (Batch 109)**



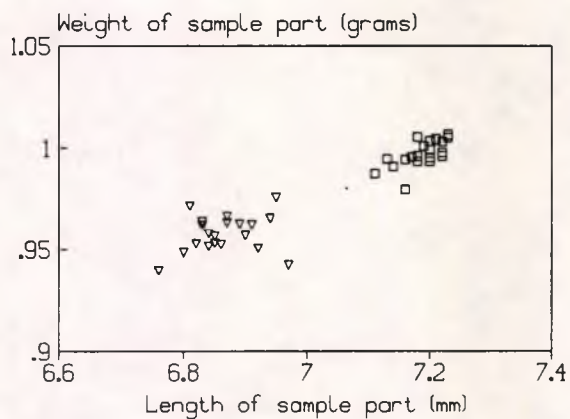
**(B) Dispersalloy (Batch 110)**



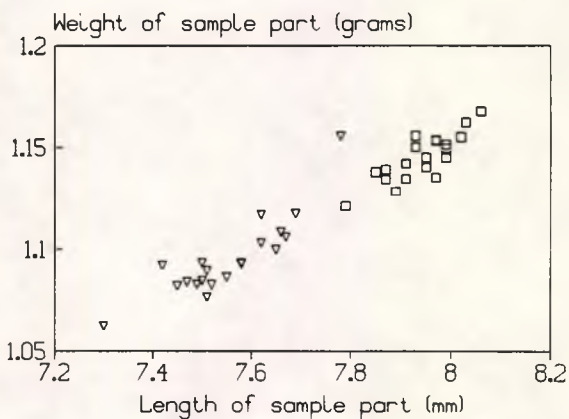
**(C) Matticap (Batch 114)**



**(D) ANA 2000 (Set 18)**



**(E) Tytin (Set 19)**



**(F) Amalcap SAS (Set 20)**

□ DW parents      ▽ SPP additions

**Figure 31. A to F. Graphs of weights and lengths of the parent parts and added to samples from encapsulated amalgams.**

### 6.11.2 Sample length and weight

Scatter plots of sample length against weight for parent and added parts of pre-capsulated amalgams are given in Figure 31 A to F. The graph points for Aristaloy 21 overlap and although the differences in mean length were significant ( $t = 2.3$ ,  $p = 0.03$ ), the differences in mean parent and added weight were not ( $t = 1.68$ ,  $p = 0.11$ ).

Excluding Aristaloy 21 and one outlying point in Figure 31 F (Amalcap SAS), there is no overlap in the parent and added weights and lengths for any pre-capsulated amalgam. The means of parent length and weight were significantly greater than those added for each brand, the smallest value of  $t$  being 6,  $p = 0.0000$ .

According to the manufacturer's specifications, all capsules in this section contained 600mg of alloy but this was not verified for this study. Comparison of Figure 31 E with the five alternatives shows that the all-spherical particle Tytin exhibited the least scatter and greatest differences ( $t > 11.5$ ) in parent and added length and weight values. It is considered that variations in sample length and weight between the brands could be dependent on the packing properties of the mix under the differing conditions for parent and addition condensation. Further consideration of these data and any possible relationship with mercury content and quantitative phase distributions in the sample parts were considered beyond the scope of this study.

No one-piece samples were manufactured from the alloys supplied in capsules. Capsules were available for this study only in the 2-spill size, whereas 3-spill capsules were required to provide the quantity of mix needed for one-piece samples (at least about 9.5mm long) for testing in the 3 point bend rig without undue risk of sample failure occurring at the end. Commonly, a factor of two

covered the highest to lowest values in the range of force to fracture values for a given batch (either one-piece or joined). The results for Veraloy (reported in Section 6.10.4) showed that further refinement of the preparation procedures of one-piece samples was required before strength values could be used for reliable comparison with joined samples. Work on one-piece sample preparation from precapsulated materials was considered beyond the scope of this study into joined amalgams.

## **6.12 Retest of Amalgam M**

This section reports the results of use of the standard paddle procedure and dome piston with Amalgam M alloy which had been used early in the study. The force to fracture and preparation data are shown in Table 36 and Figure 32 shows the scatter plots. Cumulative failure graphs for the pooled results are shown in Figure 33, their descriptive statistics are presented in Table 37 and results of t-testing are given in Table 38.

### **6.12.1 Joined samples: Batches 118 to 121**

The joined samples are shown after fracture in Plates 73 to 76. The parents for Batches 118 and 119 were condensed by the DW method; the dome piston was used for vibrated parent condensation of Batch 120 and the new flat ended piston for Batch 121. The addition parts of Batches 118, 120 and 121 were condensed using the standard paddle procedure. For Batch 119, the RI piston was applied to the first addition increment for 10s, repeating the timing used for the same increment in Set 1.

It may be seen in Plate 73 that 7 of 10 samples in Batch 119 failed in the parent. Three out of the four strongest samples failed at the joint. This repeated the general pattern of the earliest results: the RI piston, when

applied for 10s produced strong joints. Similarly, in Batch 118 (Plate 74) the weakest samples failed in the parents and joints produced by the standard paddle procedure were reasonably strong. Only one dome piston condensed parent failed (Batch 120, Plate 75): these parts were strong. Two samples in Batch 121 were unusually weak. ANOVA of the force to fracture results ( $F=0.46$  [3,36 df]  $p=0.7$ ) revealed no significant differences in means and the four batches were pooled to make Set 23. For the limited numbers of samples prepared by these methods, there was insufficient evidence to conclude that the results differed.

### **6.12.2 One-piece Batches 122 to 125**

The question arose as to whether the marking ink had any adverse effect on amalgam strength. The cylindrical surface of DW condensed Batch 123 which would be subjected to bending under test was covered with marker ink 45 to 56 minutes after completion of condensation. The mean force to fracture ( $t=0.6$ ,  $p=0.56$ ) was similar to Batch 122. It was concluded that marking had no effect on the strength of the amalgam and these batches were pooled to make Set 24.

The mean of force to fracture for Batch 124 condensed by vibration using the new flat ended (but now worn) piston was not significantly less than for dome condensed Batch 125 ( $t=1.6$ ,  $p=0.13$ ). The results were pooled to make Set 25: the force to fracture mean of this Set was considerably greater than that for the one-piece deadweighted Set 24 ( $t=7.7$ ,  $p=0.0000$ ).

In the pooled results, joined Set 23 was stronger than DW condensed one-piece Set 24 ( $t=3.9$ ,  $p=0.0002$ ): a similar result to the difference between Sets 1 and 2 earlier in the study. Unlike the difference for Sets 1 and 3, vibrated Set 25 was stronger than joined Set 23 ( $t=2.5$ ,  $p=0.014$ ).

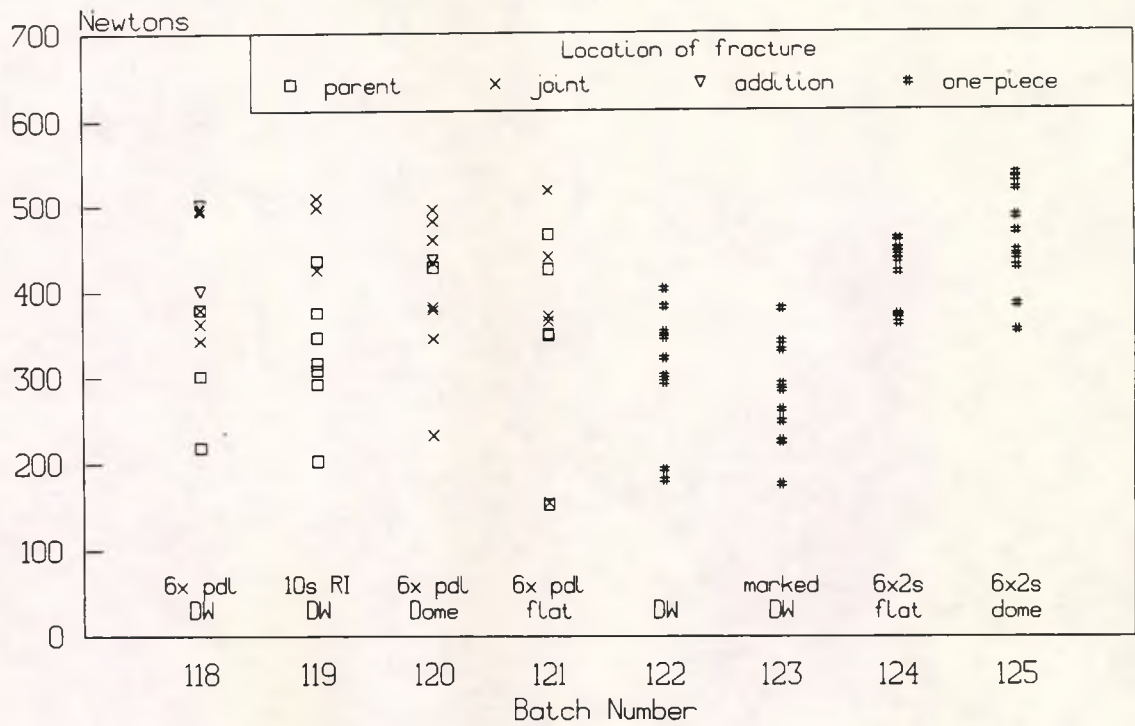
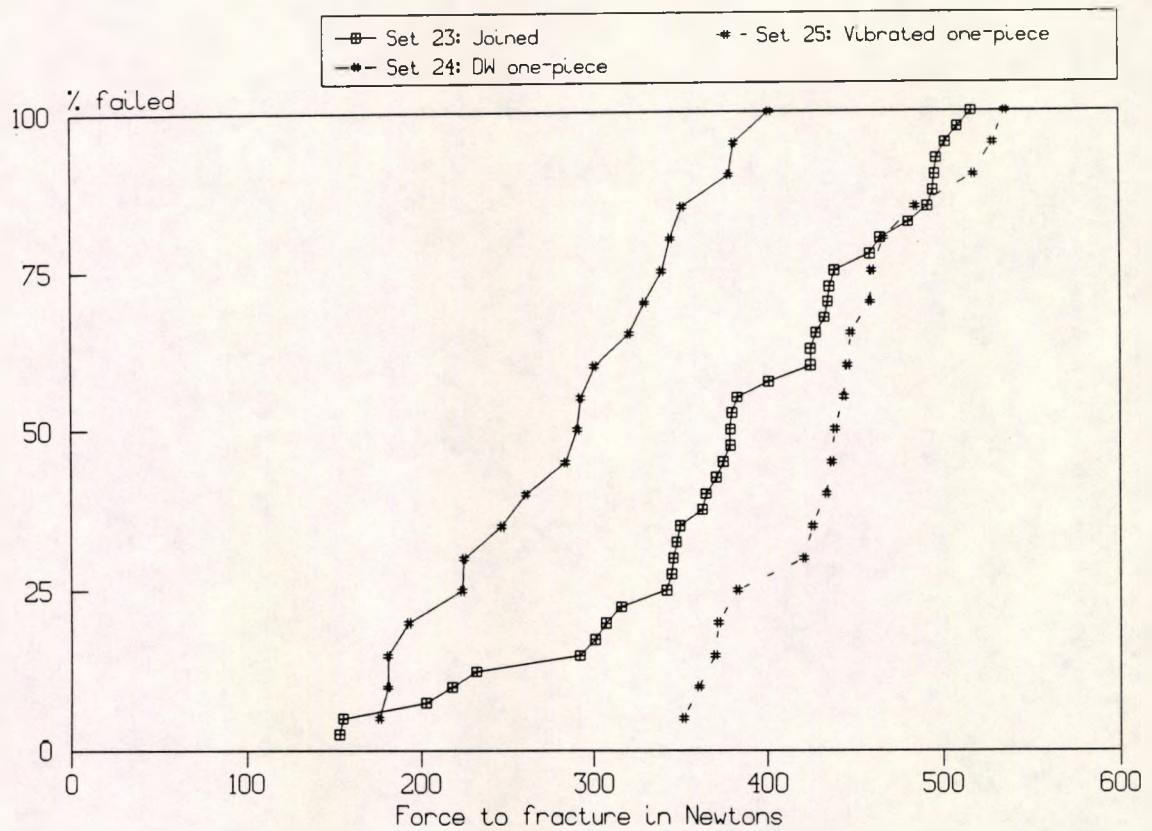


Figure 32. Force to fracture for Batches 118 to 125. Amalgam M.

Batch Number	Preparation procedure		Force to fracture (Newtons)		
	Parent	Addition part	Mean	95% C.I. for mean	
				From	To
118	DW	SPP	387	322	452
119	DW	10s RI, 3x2s flat	371	301	440
120	4x2s dome	SPP	407	352	462
121	4x2s flat	SPP	359	272	445
122	DW		295	236	354
123	DW marked		276	232	320
124	6x2s flat		421	393	449
125	6x2s dome + 2s flat		458	414	502

Table 36. Preparation procedures and force to fracture results for joined Batches 118 to 121 and one-piece Batches 122 to 125. Amalgam M.



**Figure 33.** Cumulative frequencies of force to fracture for Sets 23, 24 and 25.

Set	Batches	No.	Mean Load	S.D.(n-1)	95% C.I. for Mean		Median Load
					From	To	
23	118 to 121	40	381.0	95.7	350.3	411.6	380.0
24	122, 123	20	285.4	71.8	251.8	319.0	292.0
25	124, 125	20	439.4	53.4	414.4	464.3	441.5

**Table 37.** Force to fracture statistics for Sets 23, 24 and 25 (Newtons).

Sets	95% C.I. for the difference in means		Student's t-test	
	From (Newtons)	To (Newtons)	t =	P =
23 & 24	47	144	3.9	0.0002
23 & 25	12	105	2.5	0.014
24 & 25	113	195	7.7	0.0000

**Table 38.** Confidence intervals for differences in mean force to fracture between Sets 23, 24 and 25 and results of two sample t-testing.

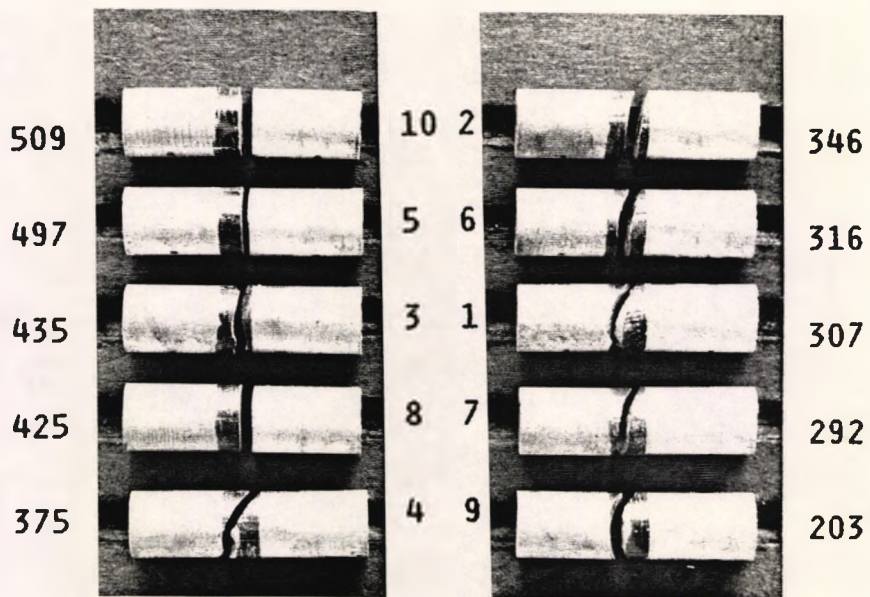


Plate 73. Amalgam M Batch 119 after fracture.

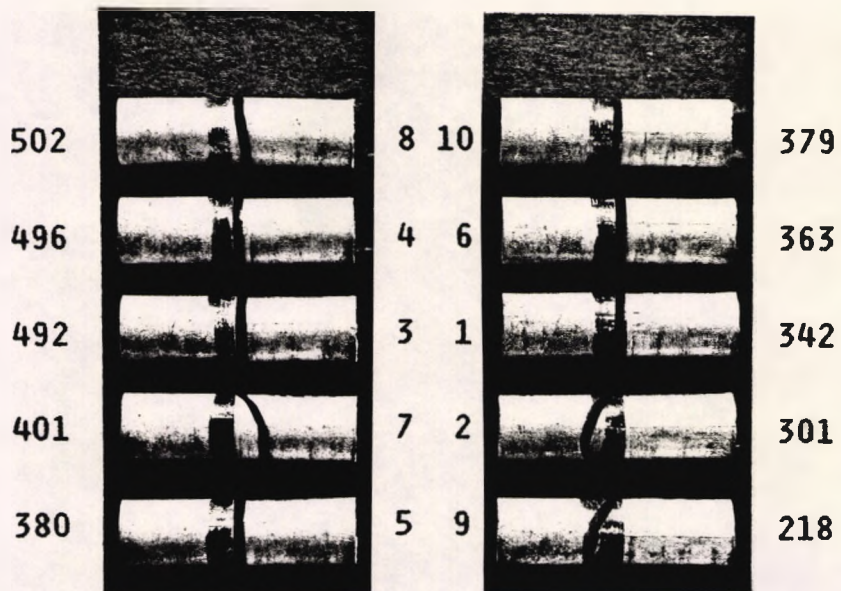


Plate 74. Amalgam M Batch 118 after fracture.

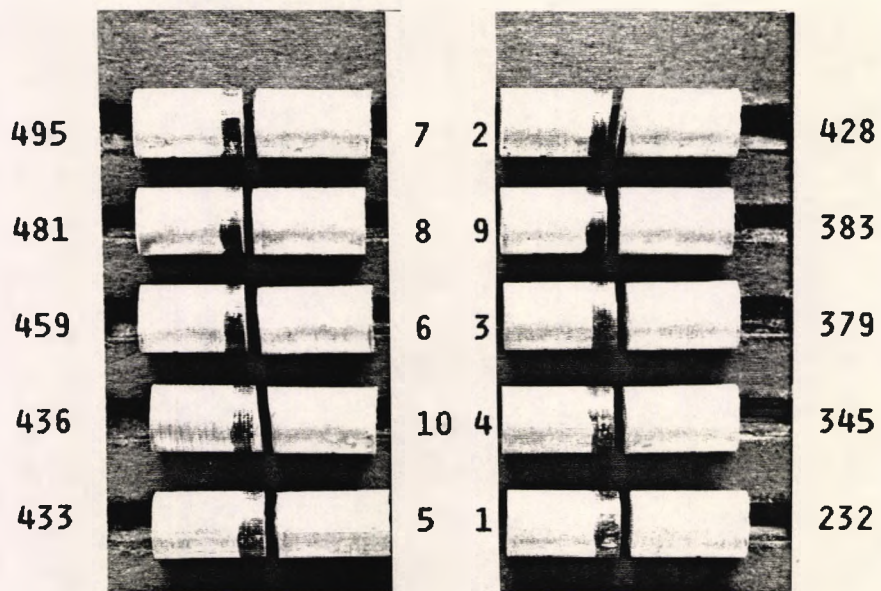


Plate 75. Amalgam M Batch 120 after fracture.

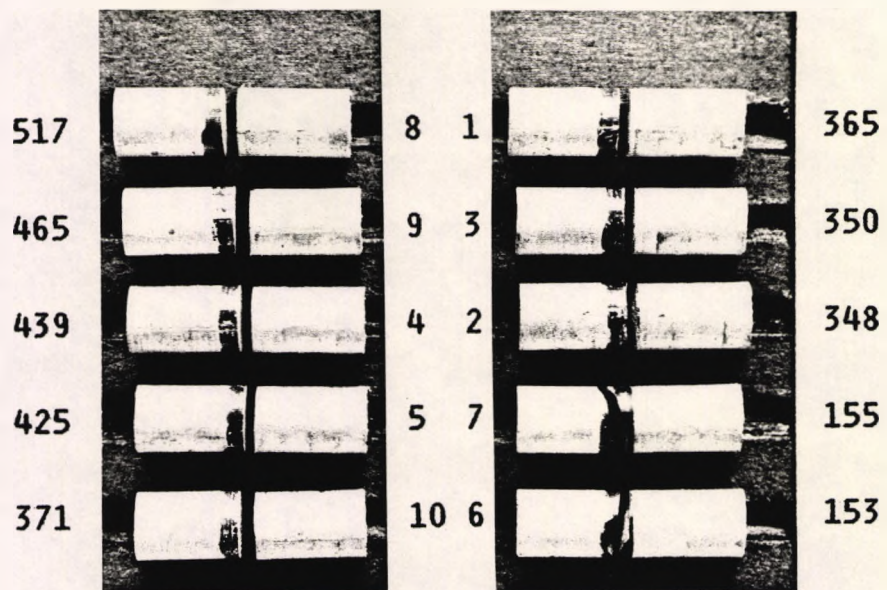


Plate 76. Amalgam M Batch 121 after fracture.

Comparing the results for these joined samples with those tested earlier in the study, the results of t-testing on the force to fracture data for Set 23 and Sets 1, 7 or 9 were not significant ( $t < 1.67$ ,  $p > 0.1$ ). Similarly, there was no significant difference between DW condensed one-piece Sets 2 and 24 ( $t = 1.0$ ,  $p = 0.3$ ). In contrast, the vibration condensed one-piece Sets 3 and 25 were markedly different ( $t = 6.45$ ,  $p = 0.0000$ ).

The mean force to fracture for flat piston condensed one-piece Batch 124 was compared to all previous one-piece Amalgam M samples and was found to exceed the maximum recorded mean value (for Batch 36:  $t = 3.0$ ,  $p = 0.007$ ).

Further investigation of one-piece sample preparation was considered beyond the scope of this study but the analysis is included for information. The author's view that the force to fracture results for one-piece samples could not be compared reliably to those for joined samples in this study was reaffirmed.

It has been noted that samples on occasion were misplaced with the joint in a slightly off-centre position in the 3 point bending rig. If the path of crack propagation involved the joint, the fracture departed from the joint towards the area of contact with the central loading roller.

Previously reported work on joined dental amalgams has compared strength with that of one-piece samples. The results in this study show that certain preparation procedures have been capable of production of strong amalgam joints. It was considered that valuable information could be gained from a study of fractured joined samples without any quantitative comparisons of force to fracture data. Demonstration of the strength of joint compared to the adjacent material on a qualitative basis might be possible using relatively few samples.

## **6.13 Re-assembled fractured samples**

In this study, examination of the amalgam microstructure from spherical particle alloys clearly revealed the location of the joint interface. In contrast, it was often difficult to define the joint in lathe cut amalgams. Examination of the microstructure of fractured samples after reassembly of the parts was considered so that this might reveal the location of the fracture path in relation to the microstructural components of the joined amalgams.

### **6.13.1 Re-examination of Duralloy joined samples**

Duralloy is composed of 80% by weight spherical HCSC particles and 20% conventional lathe cut alloy. Batches 54 and 55 were joined samples prepared from this alloy which was amalgamated in the Dentomat. The first addition increment for Batch 54 was condensed by the application of the paddle for three turns under vibration at intervals of 10s. Three samples out of 10 obviously fractured away from the joint interface. In Batch 55, six turns were applied at intervals of 10s: in six out of 10 samples (including four of the five strongest) fracture was outside the joint (see Plates 62 and 63, page 167). These batches were reassessed with a view to the selection of an example for trial reassembly and microstructural examination. Sample 54.2 appeared to show mixed fracture. The fracture path clearly initiated in the addition part but it appeared that the central loading roller might have been applied to the parent material adjacent to the joint where the fracture terminated. This sample was reassembled and prepared for microstructural examination and is shown in Plates 77, 78 and 79.

The fracture path may be seen to traverse the joint interface where a residual alloy particle in the parent was divided. It was concluded that this trial had been successful in demonstrating the joint and fracture path.

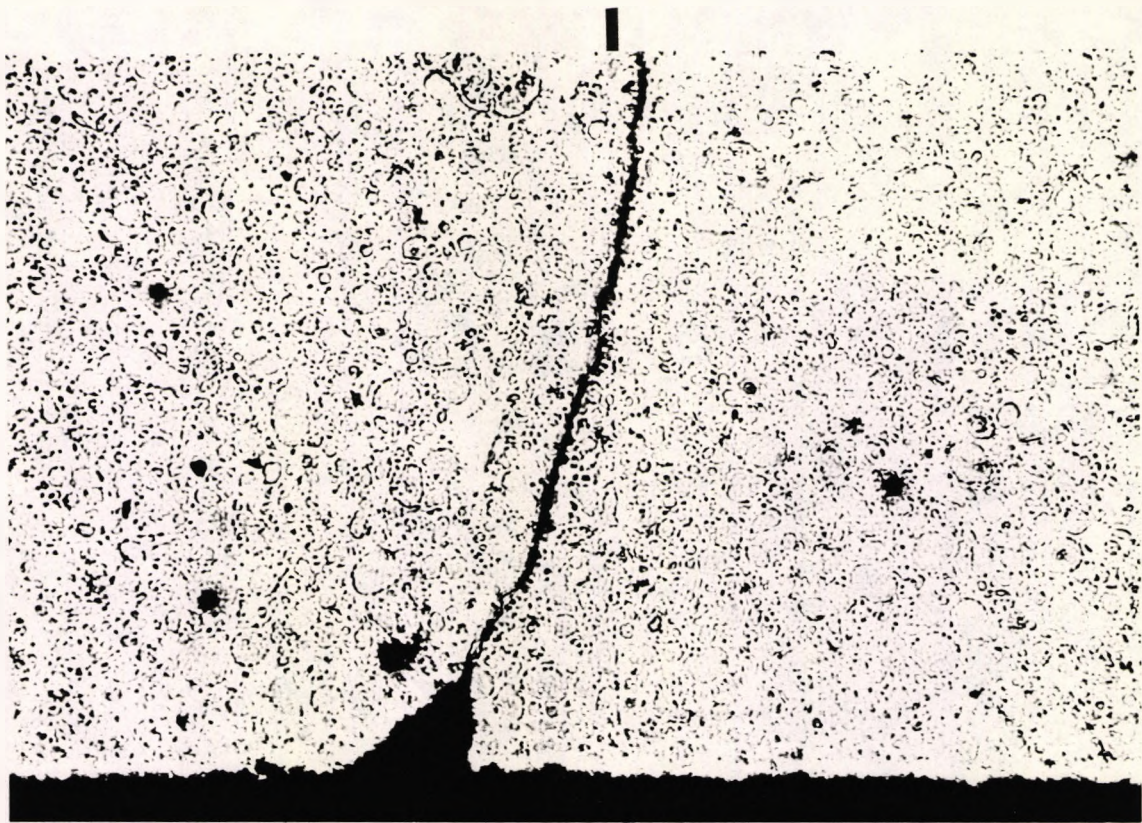


**Plate 77.** Polished section of Duralloy specimen 54.2 after fracture. The fracture terminated at the lower edge of the sample.

x225

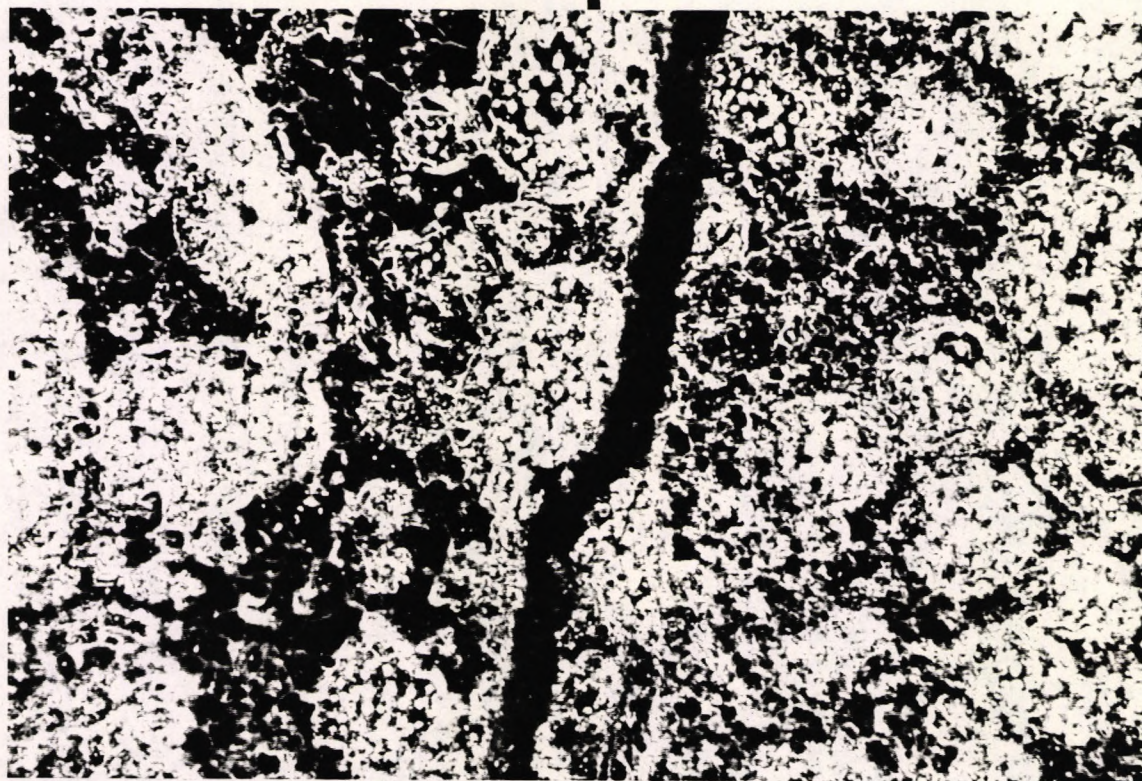


**Plate 78.** Microstructure of Duralloy specimen 54.2. Dark field illumination. The fracture traversed the joint, passing through a spherical residual alloy particle in the parent.

x900

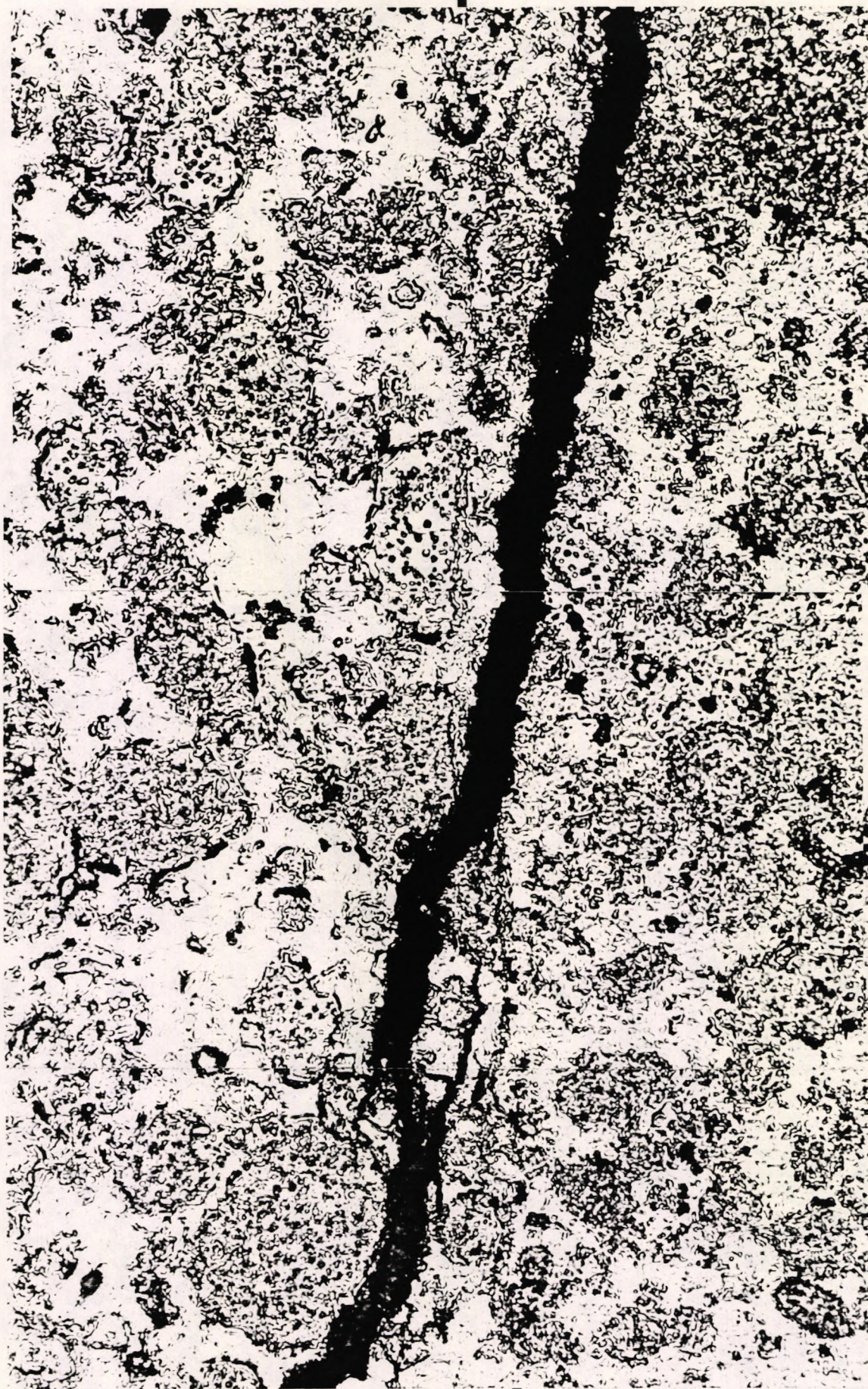


**Plate 79.** Microstructure of Duralloy specimen 54.2. Bright field illumination. The fracture traversed the joint interface. x900

In this thesis, micrographs of reassembled fractured samples are shown with the parent material appearing on the left. For sample 54.2, the direction of fracture was from top to bottom of the photographic frame. Subsequently, the samples shown were mounted so that the parent part is on the left and the direction of crack propagation is from bottom to top. This duplicates the orientation of samples in the three point bending rig.

### **6.13.2 Notched parent: loaded addition**

Many tested joined samples were re-examined for fractures which had traversed or crossed over the joint interface and it was noted that such crack propagation occurred in very few specimens. In order to predispose joined samples to mixed mode fracture, a notch was machined in the parent material adjacent to the joint. Samples were tested by application of the central load to the addition material adjacent to the joint. Unless stated otherwise, notched samples were prepared from DW parents and SPP additions.

The loading and support rollers of the bending rig made indentations in the sample surface. In strong samples, the indentation of the central loading roller on the axis of the sample after fracture was about 0.4mm long and fractures usually terminated at about its centre (Plate 81). The estimated accuracy of sample placement in the test rig was better than 0.1mm and an offset of 0.2mm was selected for the joint from the centre of the loading roller. It was anticipated that the fracture might traverse the joint interface at a small angle. However, in many previous flexural tests, fractures seldom followed a flat plane. When the origin was off-centre, the fracture started in a vertical direction which later curved towards the central loaded area. The angle of the "crossover" might occur at a somewhat less acute angle than that of a flat plane slope of 1 in 10 between the two 0.2mm offsets on the 4.0mm diameter bar, particularly if this occurred close to the upper loaded surface.

Two joined samples were manufactured from each available encapsulated amalgam alloy. In addition, two samples were prepared from the Veraloy HCSC lathe cut alloy which was available in the Dentomat. The samples were identified as M1 to M16 and are shown after notching and fracture in Plates 82 and 83. During the notching procedure, using a motorised Hounsfield Impact notching machine, one ANA 2000 (M5) and both Tytin samples (M7 and M8) fractured. The motor was disconnected for sample M9 onwards and the machine was hand operated for the remainder of the study. The joint was not associated with the fracture in those samples which failed during the notching procedure. These failures occurred within the parent material.

Some difficulty was encountered in locating samples in the notching machine with the result that some notches were misplaced relative to the intended joint position. The preparation procedure was repeated for two specimens each from five alloys (ANA, TYT, MCAP, A21 and DISP): identified as samples N1 to N10 respectively.

These samples are shown in Plates 82, 83 and 84. Examples were selected from each alloy for reassembly and examination of microstructure.

The fractures started at the notch (see Plate 80 where for the sake of clarity a notched addition is shown) and terminated at the indentation of the central loading roller in the addition (Plate 81).

Examination of the fracture surfaces sometimes showed evidence of a transition zone where the fracture passed from the parent to the addition. Generally, the fracture was considered to show a "coarser" grain in the parent and a "finer" grain in the addition.

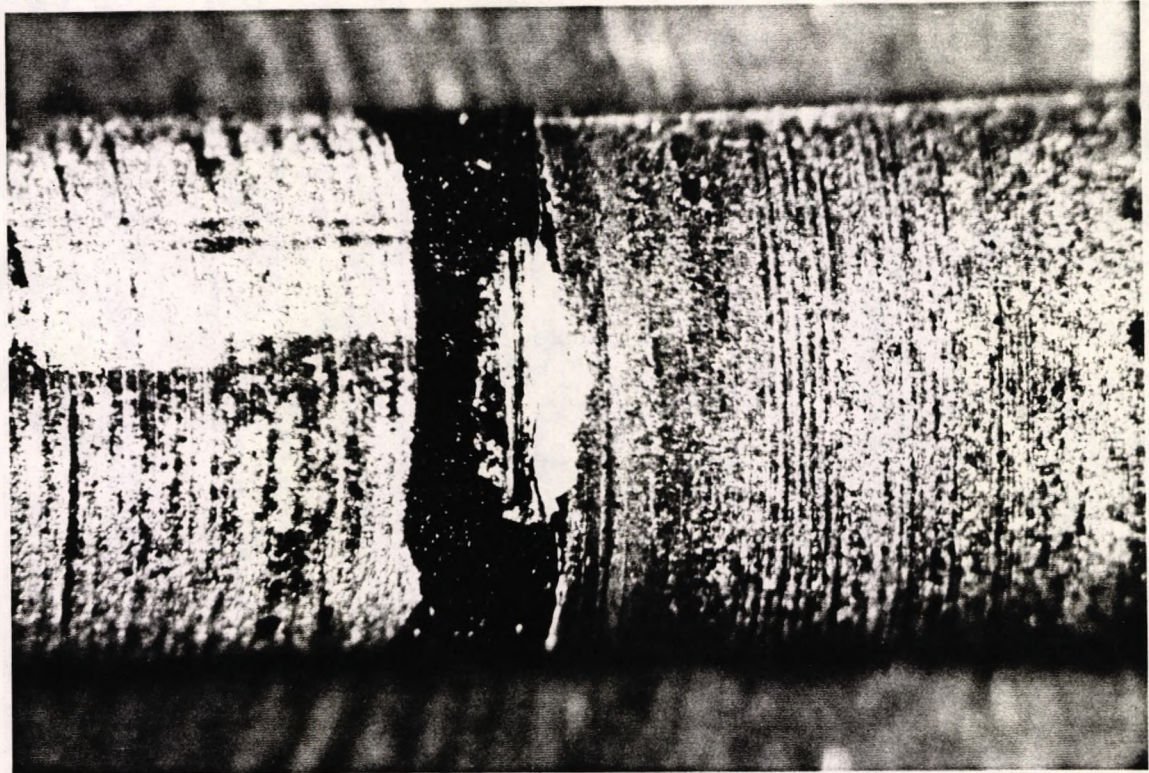


**Plate 80.** Dispersalloy sample R5 after fracture where the parent part was notched. x18

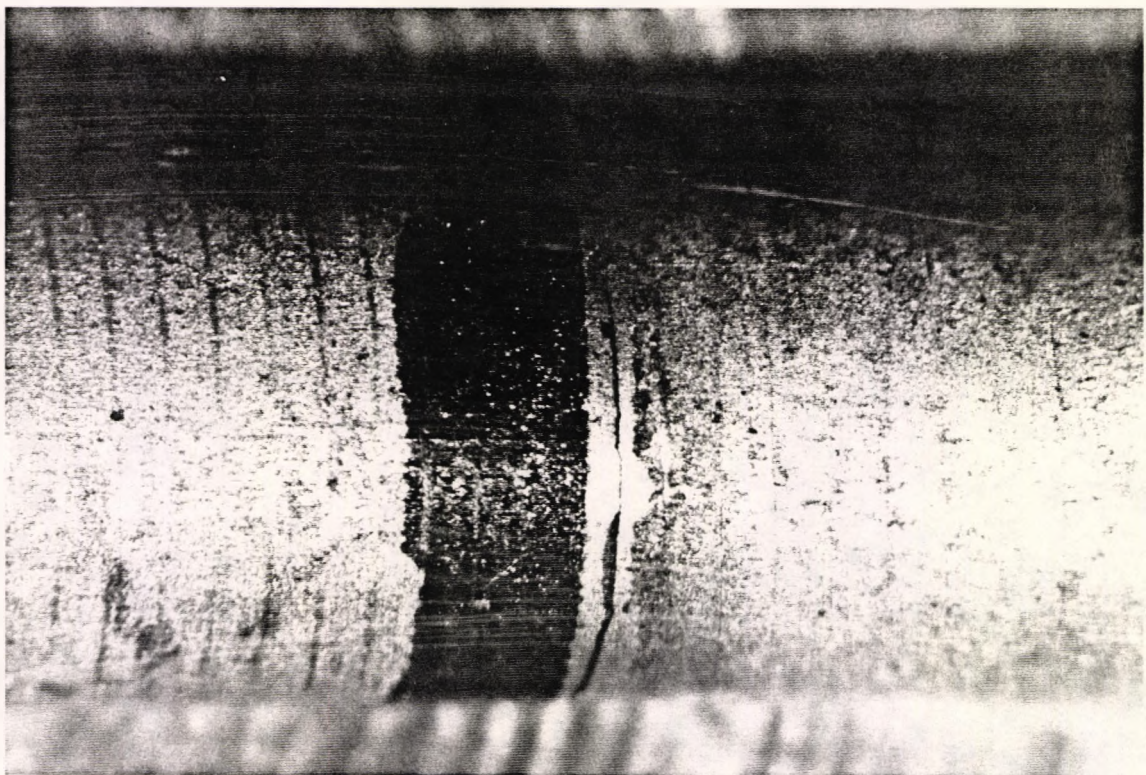


**Plate 81.** The indentation of the central loading roller in Amalcap SAS sample P4. The load was applied to the addition 0.2mm offset from the joint. x18

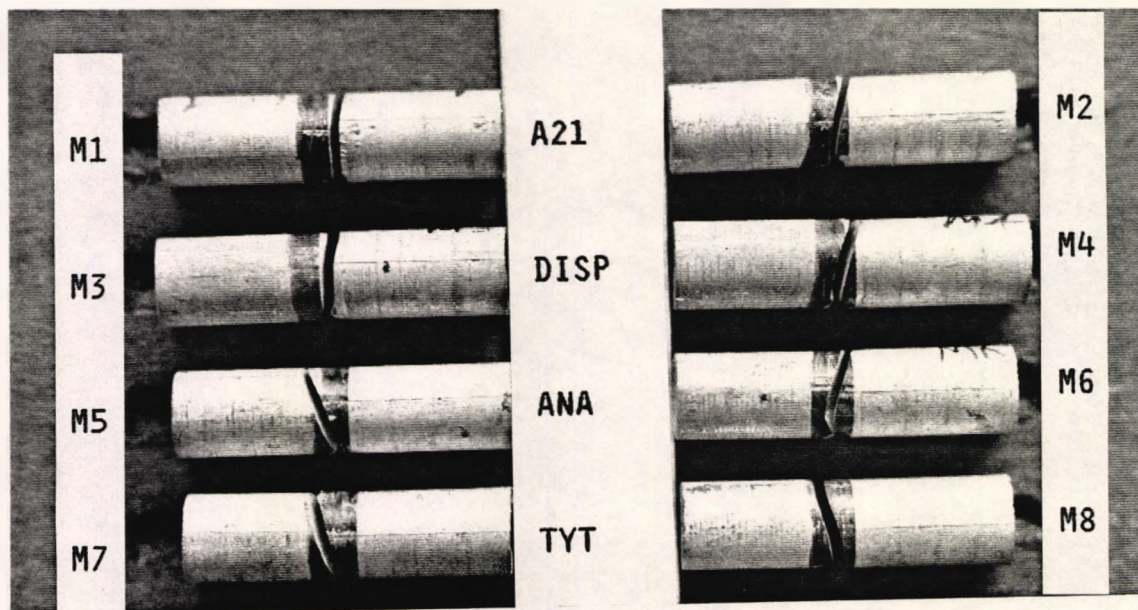


Plate 82. Joined samples M1 to M8 after notching.

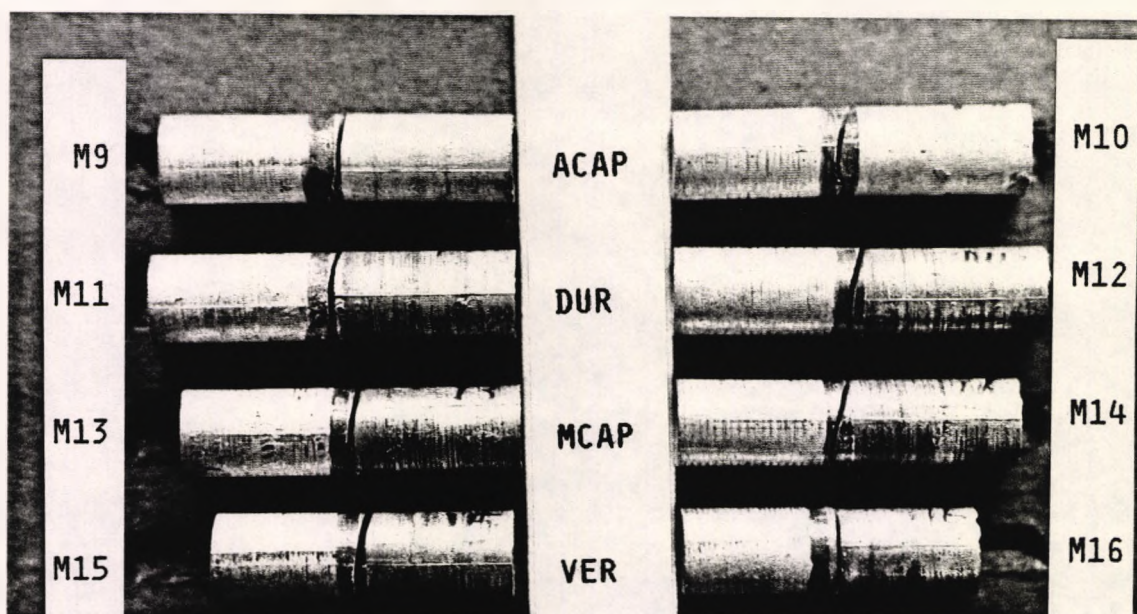
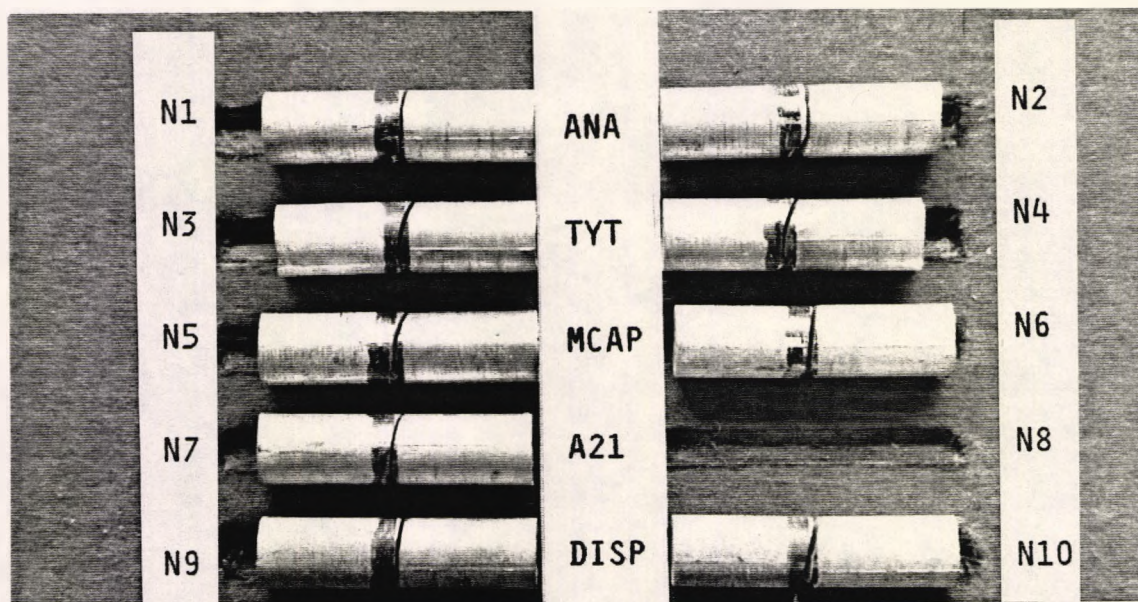


Plate 83. Joined samples M9 to M16 after notching.



**Plate 84.** Joined samples N1 to N10 after notching.

#### 6.13.2.1 Veraloy and Aristaloy

The fractured end surfaces of Veraloy specimen M15 are shown in Plate 85. A broad horizontal band occupying the central area showed a coarse grained fracture surface. Immediately above the notch, the texture was less granular. Similar appearances were seen on many notched high copper amalgam fracture surfaces.

After reassembly and preparation for microstructural examination, the central part of the polished sample revealed the orientation of the fracture (Plate 86). This passed upwards from the notch to the left of the joint. However, the fracture initially deviated to the left, away from the joint and deeper into the body of the parent. Subsequently, the fracture curved to the right and crossed the joint at about one fifth of the diameter from the upper edge.



**Plate 85.** Veraloy specimen M15. Fracture surfaces.

x18

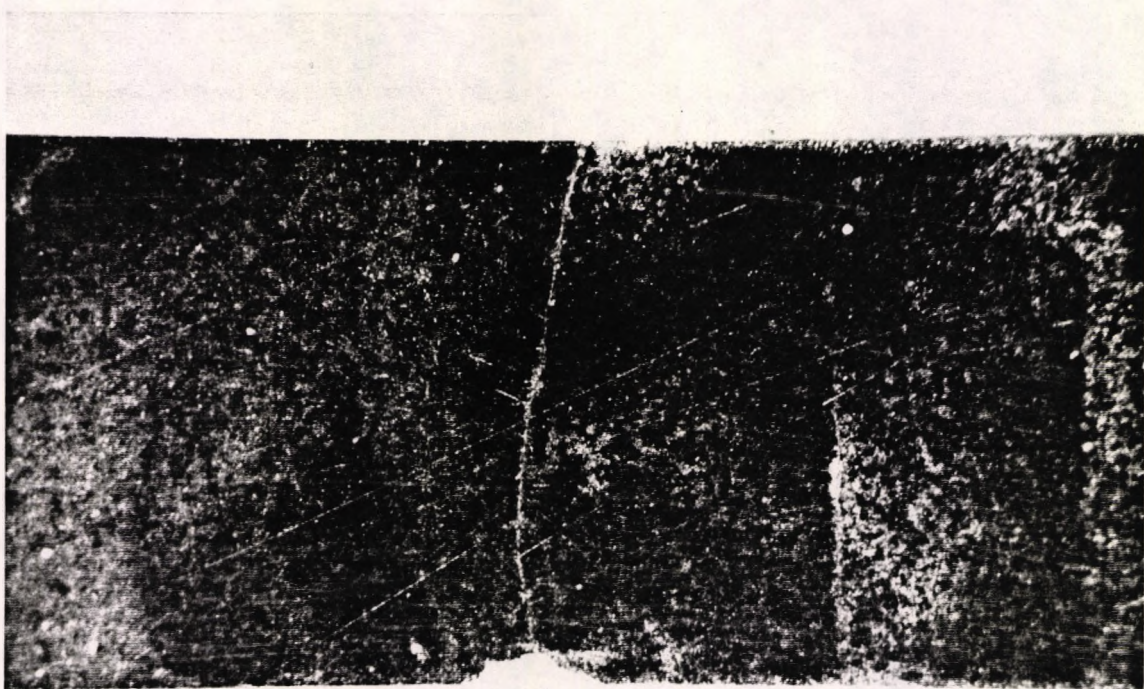


**Plate 86.** Veraloy specimen M15.  
Polished microstructure surface. Unetched.

x18

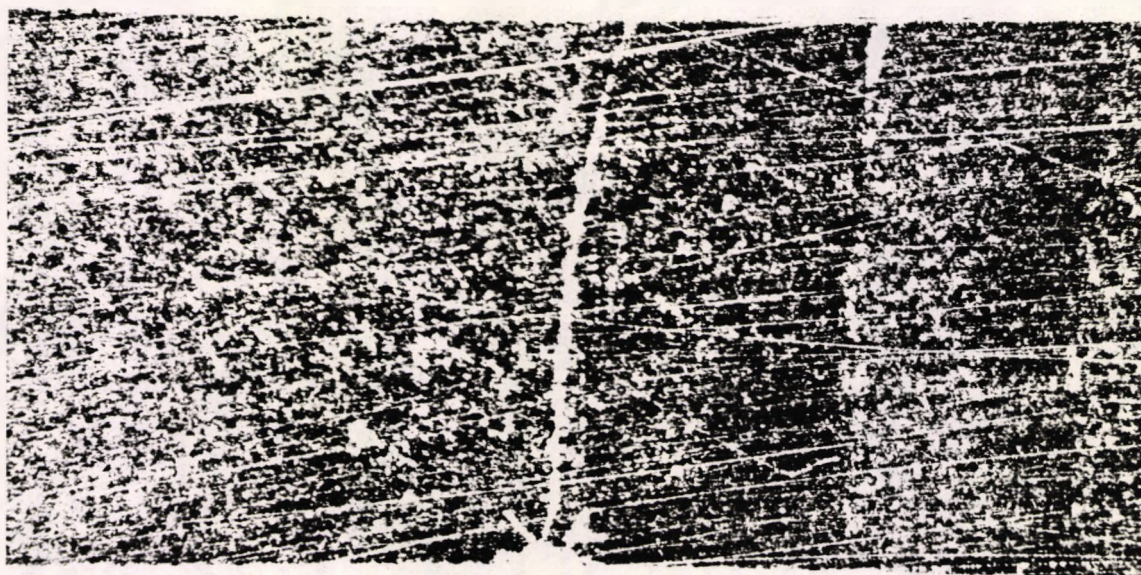


Plate 87. Veraloy specimen M15.  
Microstructure of fracture transition area.

x900

The exact location of the joint interface of sample M15 is indistinct in photomicrograph Plate 87. However, it is believed that the crossover was located at the centre of the field of view. The fracture deviated slightly to the vertical for a distance of about  $90\mu\text{m}$  which may coincide with the joint.

The polished surface and microstructure of Aristaloy 21 specimen N7 are shown in Plates 88 and 89. Residual spherical HCSC particles may be seen but it is similarly difficult to identify the joint precisely in the predominantly lathe cut alloy structure of this HCSC blend amalgam.



**Plate 88.** Aristaloy 21 specimen N7.  
Polished microstructure surface. Unetched.

x18



Plate 89. Aristaloy 21 specimen N7.  
Microstructure of fracture transition area.

x900

### 6.13.2.2 Duralloy specimen M11

The fractured end surfaces of this sample are shown in Plate 90 and the general view of the microstructure is shown in Plates 91 and 92. The transition zone is shown in greater detail under bright field in Plate 93 and under dark field illumination in Plate 94. The joint is identified by cut spherical particles and a narrow vertical band of matrix phase. At the crossover, the fracture deviated to the vertical for about  $60\mu\text{m}$  before resuming its original course.

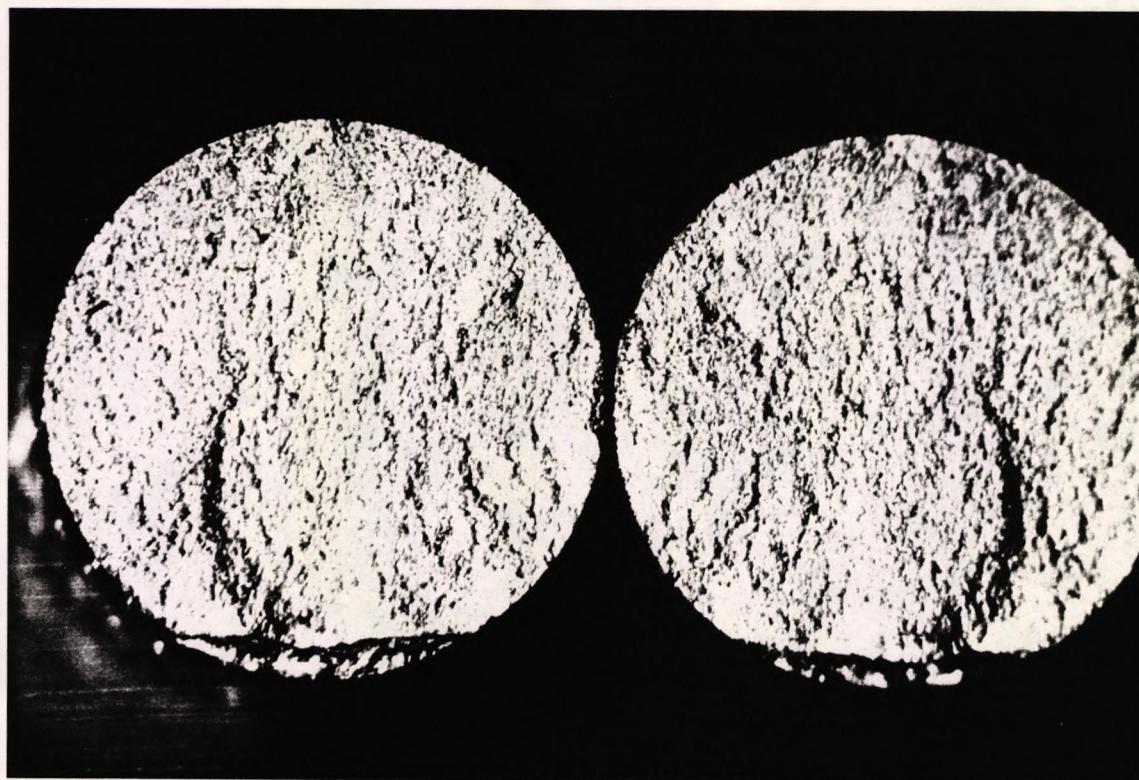


Plate 90. Duralloy specimen M11. Fracture surfaces.

x18

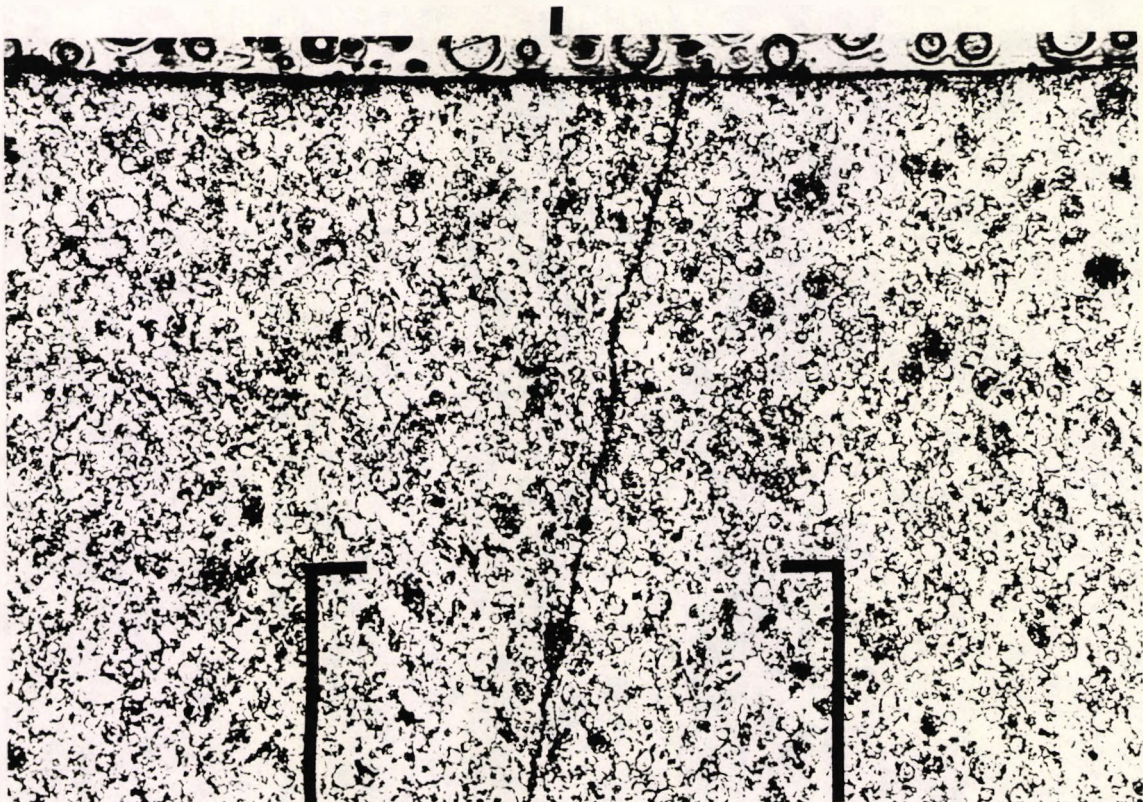


Plate 91. Duralloy specimen M11. Microstructure.

x110

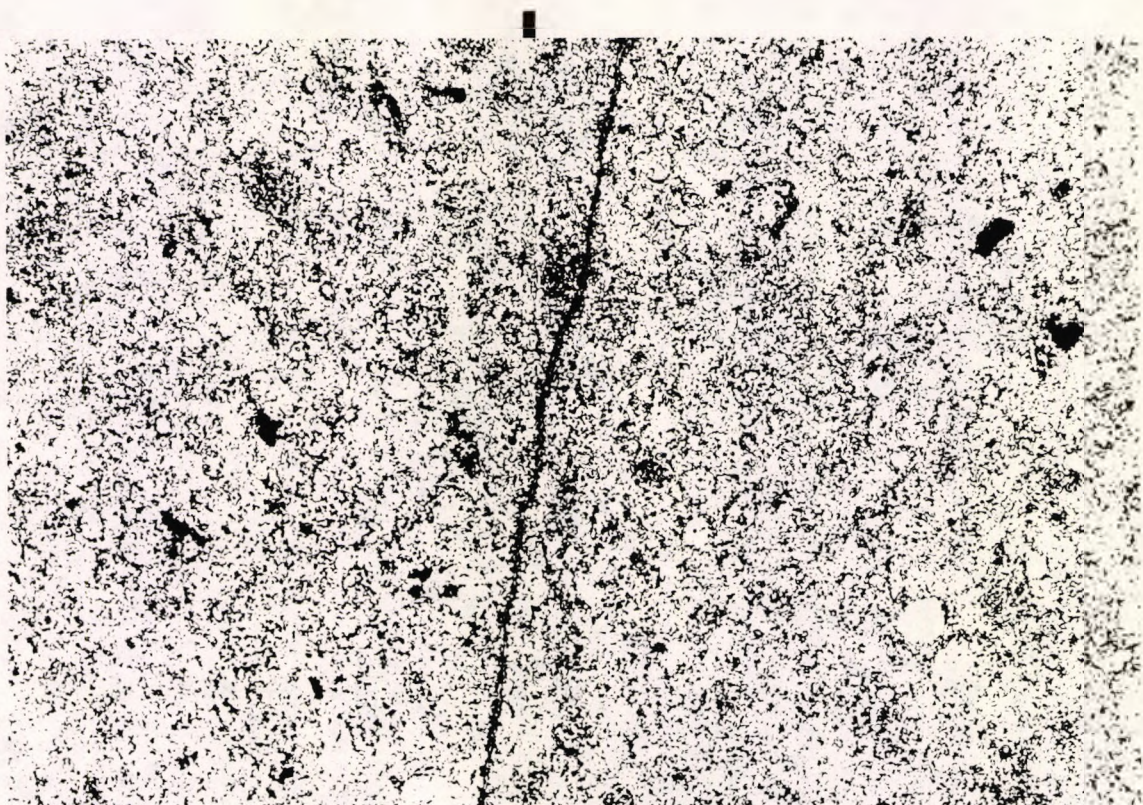


Plate 92. Duralloy specimen M11.  
Lower part of Plate 91 above.

x225

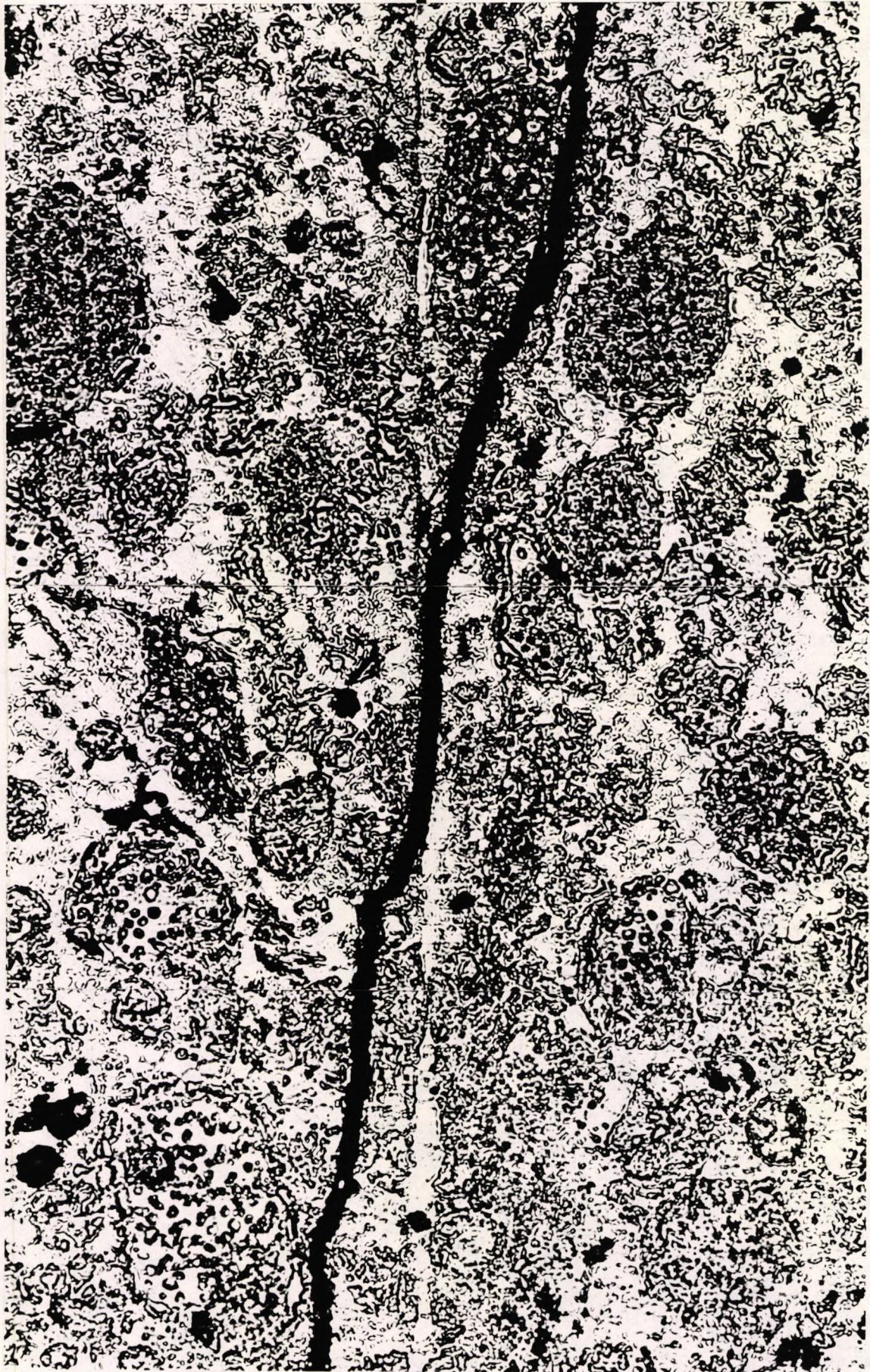


Plate 93. Duralloy specimen M11. Bright field.

x900



Plate 94. Duralloy specimen M11. Dark field.

x900

### 6.13.2.3 Dispersalloy specimen N10

The fractured end surfaces are shown in Plate 95. It was difficult to determine the location of the transition zone where the fracture passed from the parent to the addition, but reference to Plate 84 shows that it occurred at about the centre of the sample.

In the microstructure (Plates 96, 97 and 98), spherical Ag-Cu eutectic particles in the sample are surrounded by the darkly staining so-called Mahler-Asgar reaction ring (Mahler 1971, Asgar 1971). The joint is identified by cut spherical Ag-Cu particles. There is evidence of a narrow, sometimes incomplete band of reaction products between the flat cut surface of these spherical particles and the matrix of the addition.



Plate 95. Dispersalloy specimen N10. Fractured surfaces.

x18

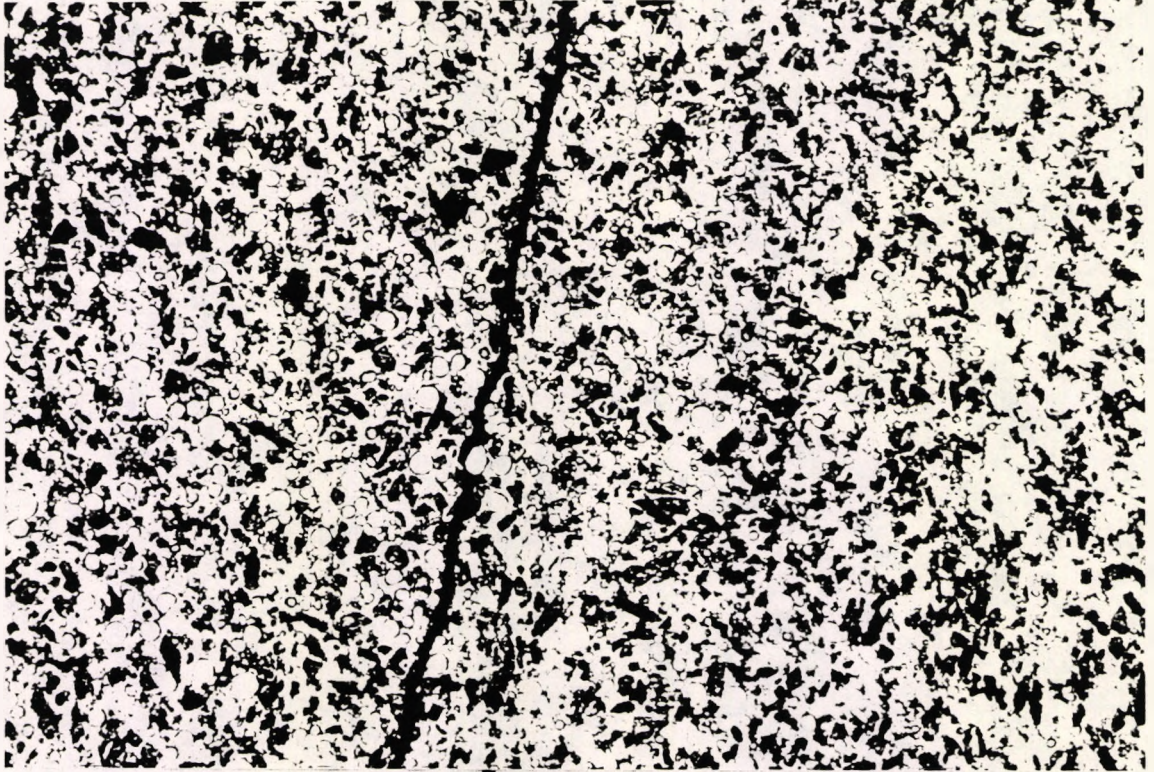


Plate 96. Dispersalloy specimen N10.

x110

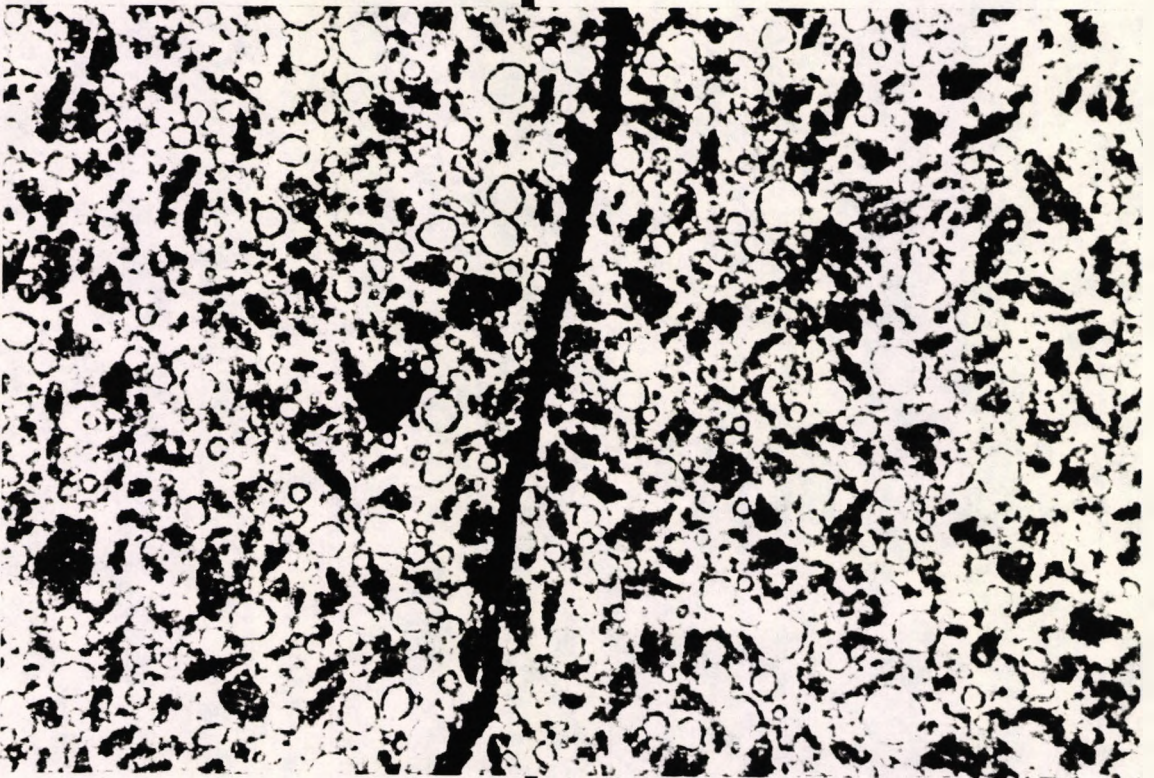


Plate 97. Dispersalloy specimen N10.

x225

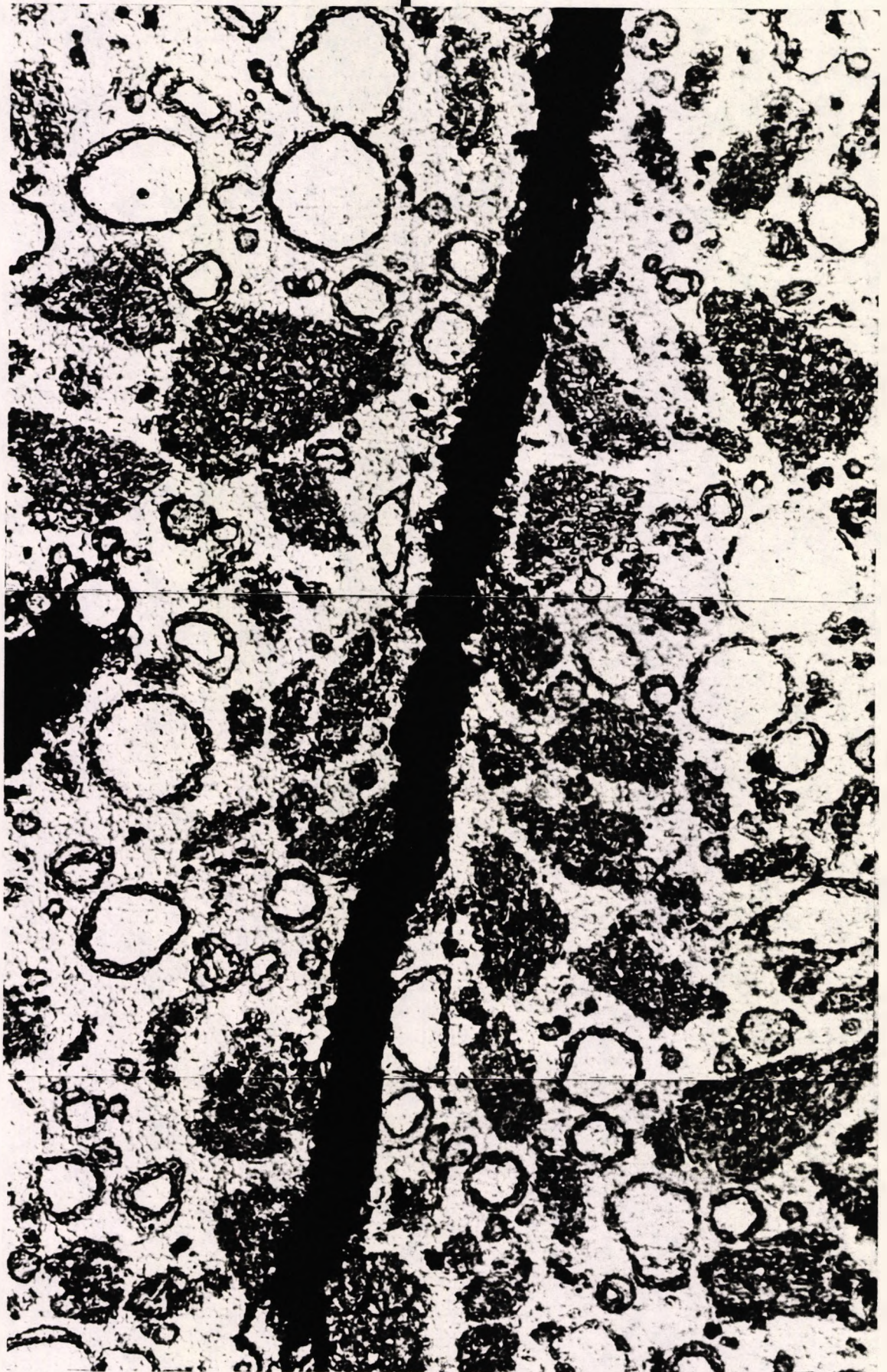


Plate 98. Dispersalloy specimen N10.

x900

The fracture may be seen to pass between two cut spherical particles such that the “upper” particle is retained in the parent part of the sample on the left side of the photomicrograph whilst the “lower” particle is attached to the (largely addition) portion on the right. It is difficult to identify the location of the joint in areas where cut spherical particles are absent. There appears to be continuity of matrix structure between the parent and addition parts of the sample.

#### 6.13.2.4 Dispersalloy specimen M3

In contrast to sample N10 above, the joint interface is visible in a band occupying about 15% of the fracture surface (Plate 99). The characteristic pattern of radial scratch marks resulting from the end preparation procedure may be seen faintly.



Plate 99. Dispersalloy specimen M3. Fractured surfaces.

x18



**Plate 100.** Dispersalloy specimen M3.  
Transition zone: upper part.

x225

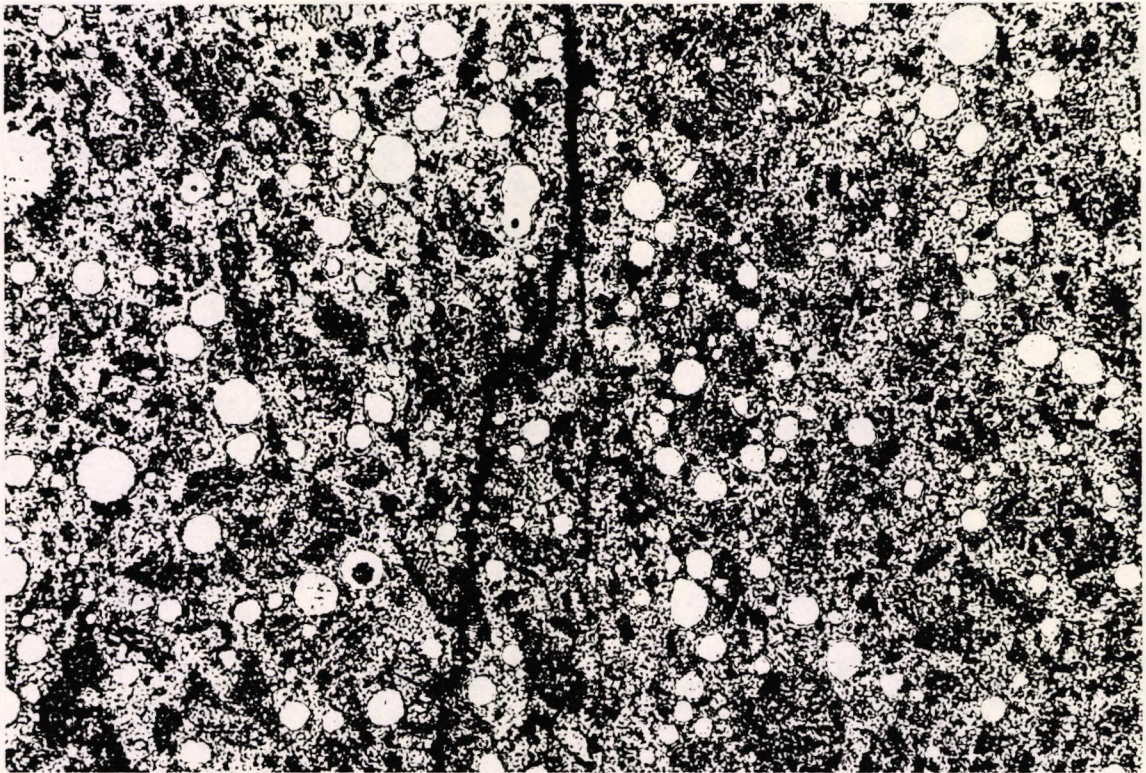


**Plate 101.** Dispersalloy specimen M3.  
Transition zone: lower part.

x225

In Plates 100 and 101, a deviation in the fracture direction to the vertical at the joint interface is visible. This extended over a distance of about 1mm. Areas above and below this zone contain secondary cracks in the matrix adjacent to the fracture and branching from the fracture path.

The direction of the crack propagation was from bottom to top. In the lower transition zone, a supplementary crack formed adjacent to the joint. At a higher level, the crack adopted a course close to or at the joint interface and then joined the main fracture. This may indicate a joint interface easy crack path or a weakness.

In the upper transition zone, a crack formed in the addition material passing generally through the matrix and around the spherical particles. There was no evidence of cracking in the joint above the upper transition zone.

#### **6.13.2.5 Tytin specimen N3**

The fracture surfaces (Plate 102) were generally fine grained and showed a distinct crescent shaped area at the notch. A horizontal line close to the top corresponded to the crossover from parent to addition amalgam.

The presence of HCSC spherical particles in the Tytin alloy (Plates 103, 104 and 105) distinguished the microstructure of this amalgam from the admixed alloys Amalcap SAS and Dispersalloy. The fracture passed through the residual alloy particles, whereas the fracture tended to circumvent spherical Ag-Cu particles in the admixtures. The joint was revealed by many cut spherical particles and a vertical band of matrix to the addition side of the flat cut surfaces.

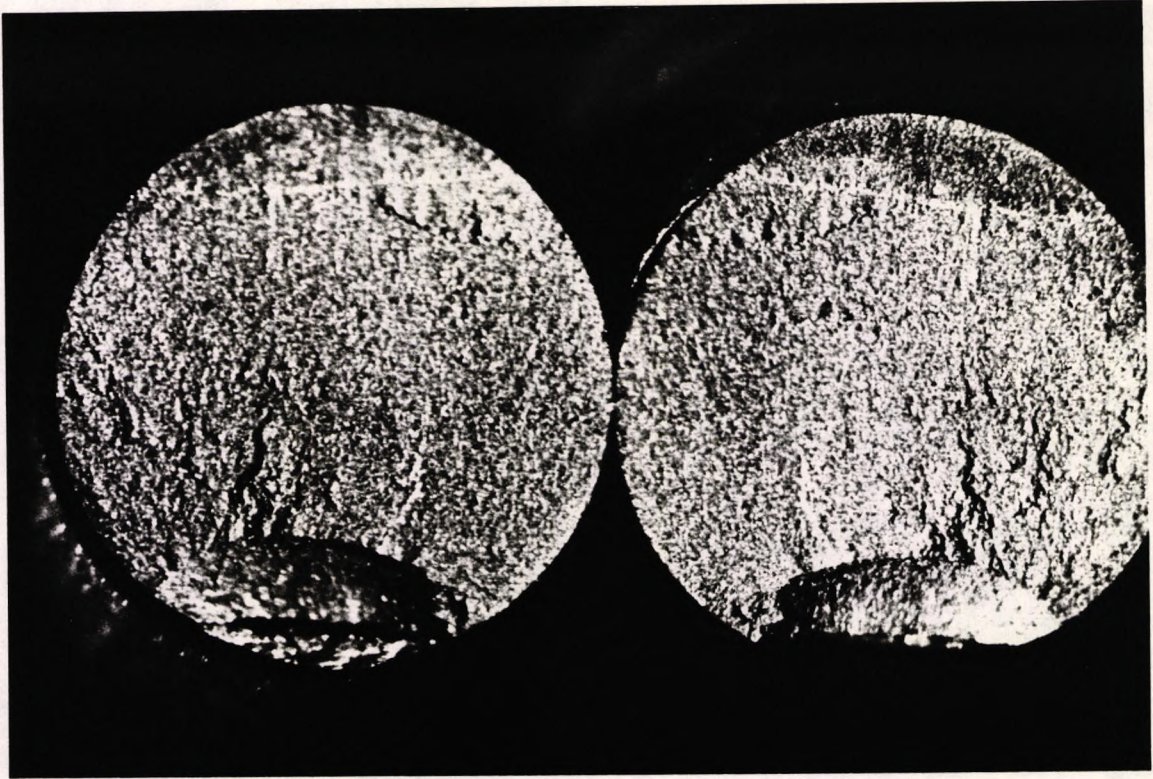


Plate 102. Tytin specimen N3. Fractured end surfaces.

x18

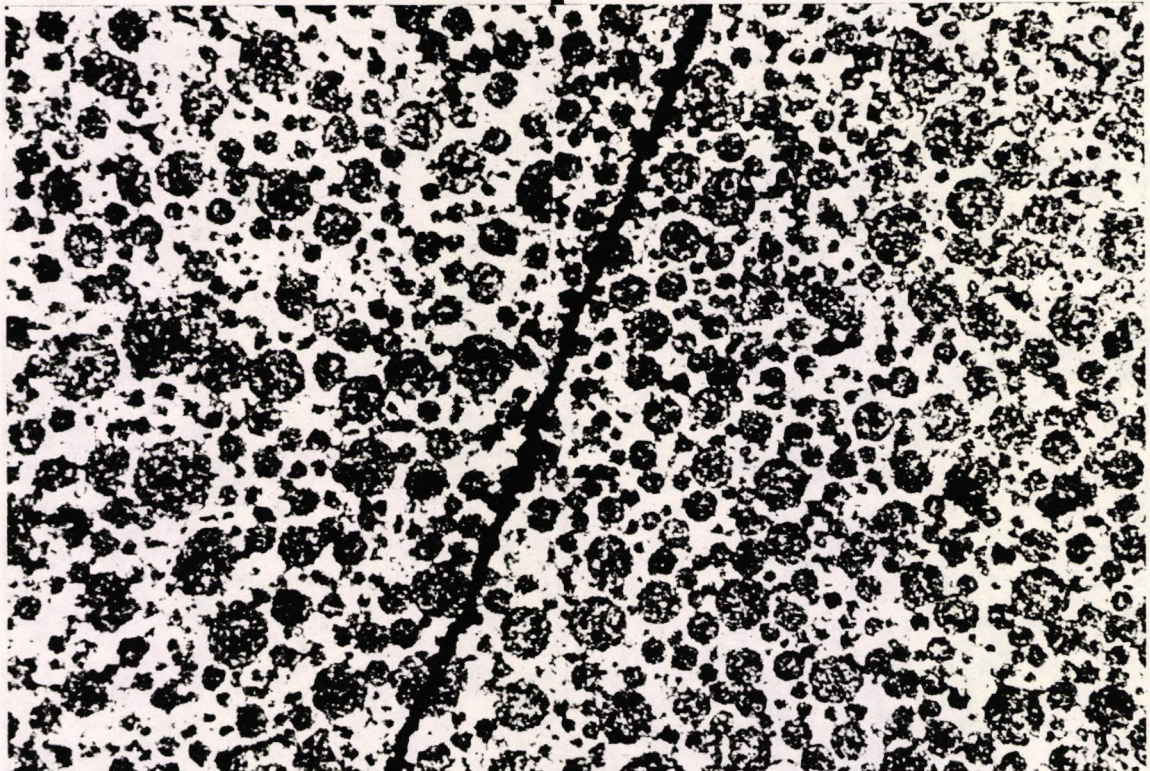
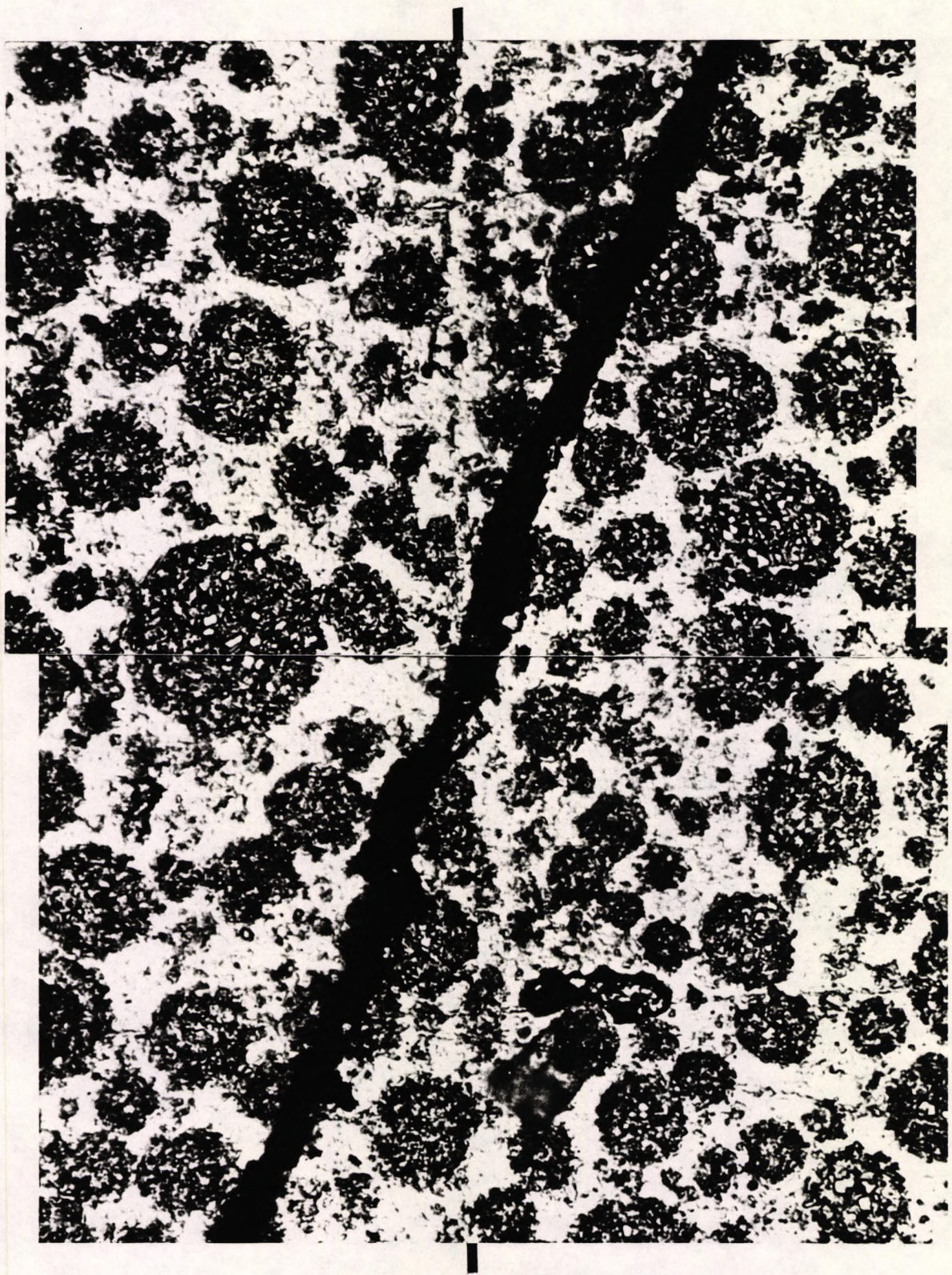


Plate 103. Tytin specimen N3.  
The fracture traversed the joint.

x225



**Plate 104.** Tytin specimen N3.  
Transition area where the fracture traversed the joint.

x900

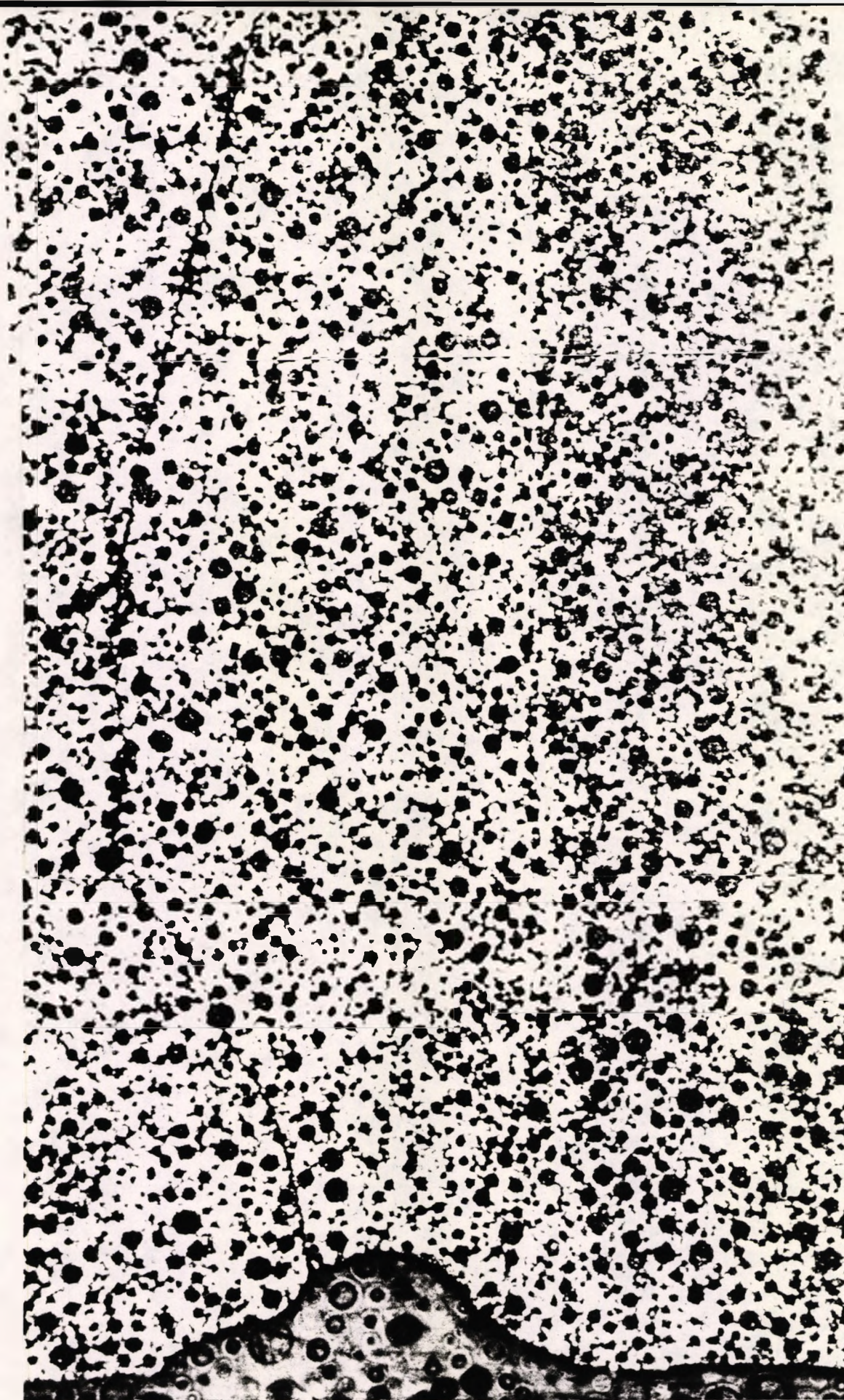
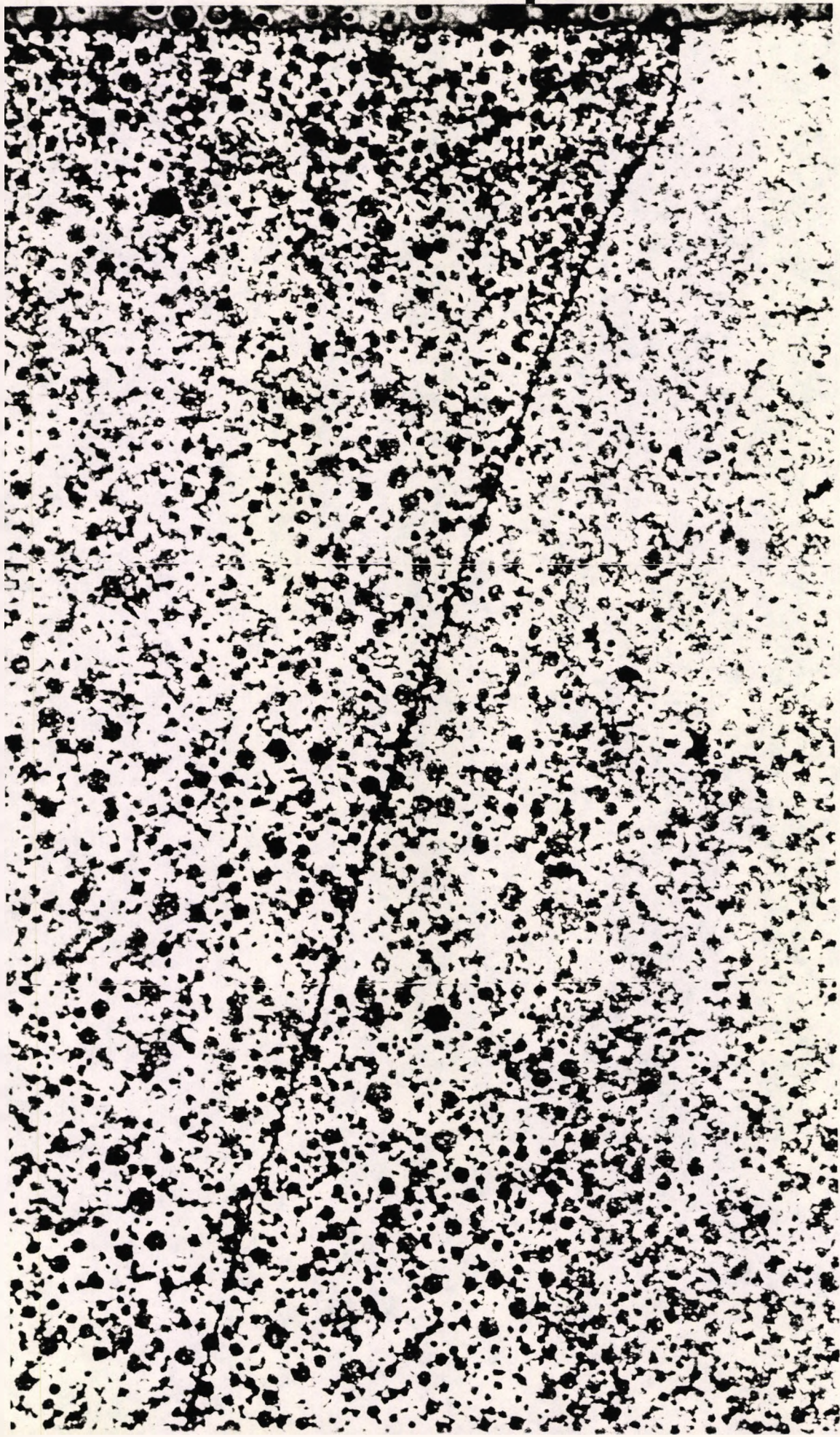


Plate 105. Tytin specimen N3.  
Composite micrograph of the joint and fracture path.  
The fracture traversed the joint about 0.5mm from the top.

x110



Plates 103 and 104 show that the joint was crossed at an angle of about 20°. This occurred at about 0.5mm from the upper surface. The composite photomicrograph (Plate 105) of the fracture and joint show that the fracture started at the left of the notch and progressed within the body of the parent. After about one third of the sample, the direction of the crack changed to the right towards the centrally loaded area.

Samples have been shown where the fracture traversed the joint from parent to addition at a shallow angle. It is considered that the smaller this angle, the more convincing is the hypothesis that the joint presented no easy fracture path and hence no weakness in the sample; *i.e.* if a weakness existed, then when the fracture reached the joint interface its direction would change and tend to follow the interface. The greater this angle, the higher would be the probability that the fracture could cross the joint even if a slight weakness remained in it.

#### **6.13.2.6 Amalcap SAS specimen M9**

The fracture surface of this specimen shows evidence of radial scratch marks over much of the lower half of Plate 106. The fracture started at the notch where a small area of parent material remained attached to the joint. The crack then propagated at the joint interface. At about half way, the fracture had clearly deviated to the right (towards the central loading roller) away from the joint and into the adjacent addition material.

Plate 107 shows the fracture departure from the joint interface. The composite photomicrograph (Plate 108) shows the entire section from notch to end of fracture. The fracture may be seen to extend upwards from the notch (right side) and encounter the joint interface at about 0.5mm from the lower edge of the sample (Plate 109).

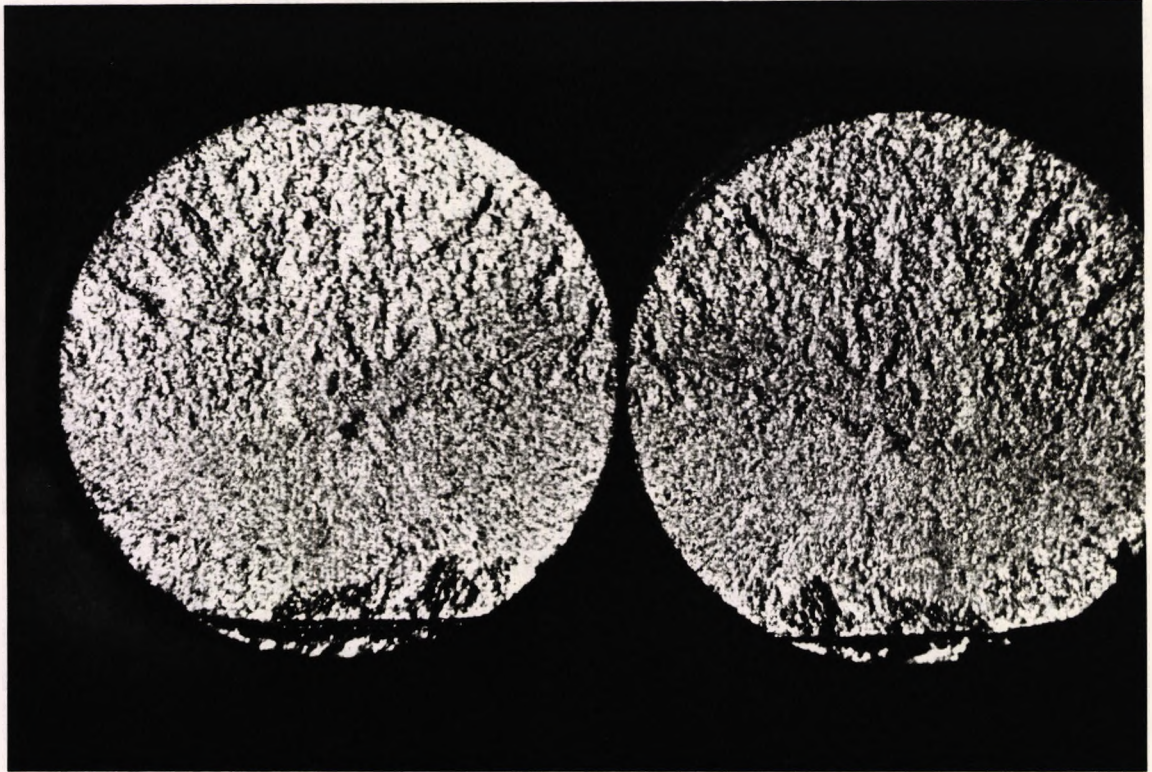


Plate 106. Amalcap SAS specimen M9. Fractured surfaces.

x18

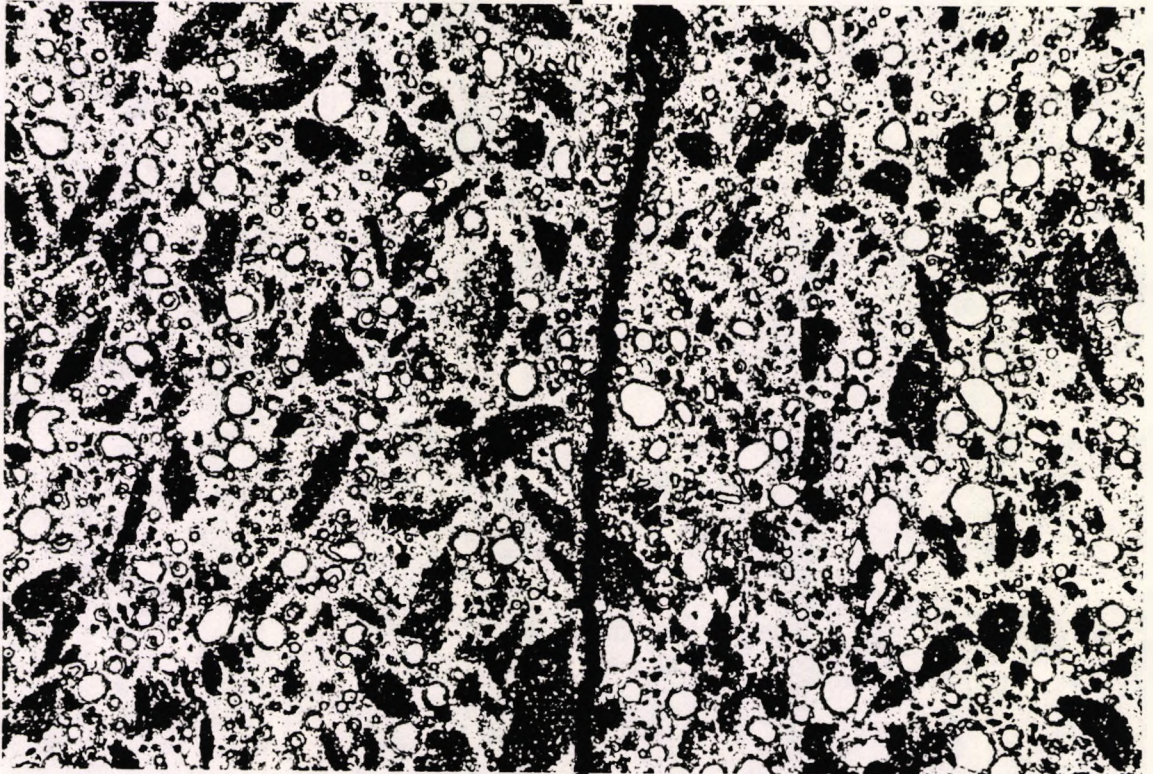


Plate 107. Amalcap SAS specimen M9.

x225

Central part of the specimen where the fracture deviated from the joint.

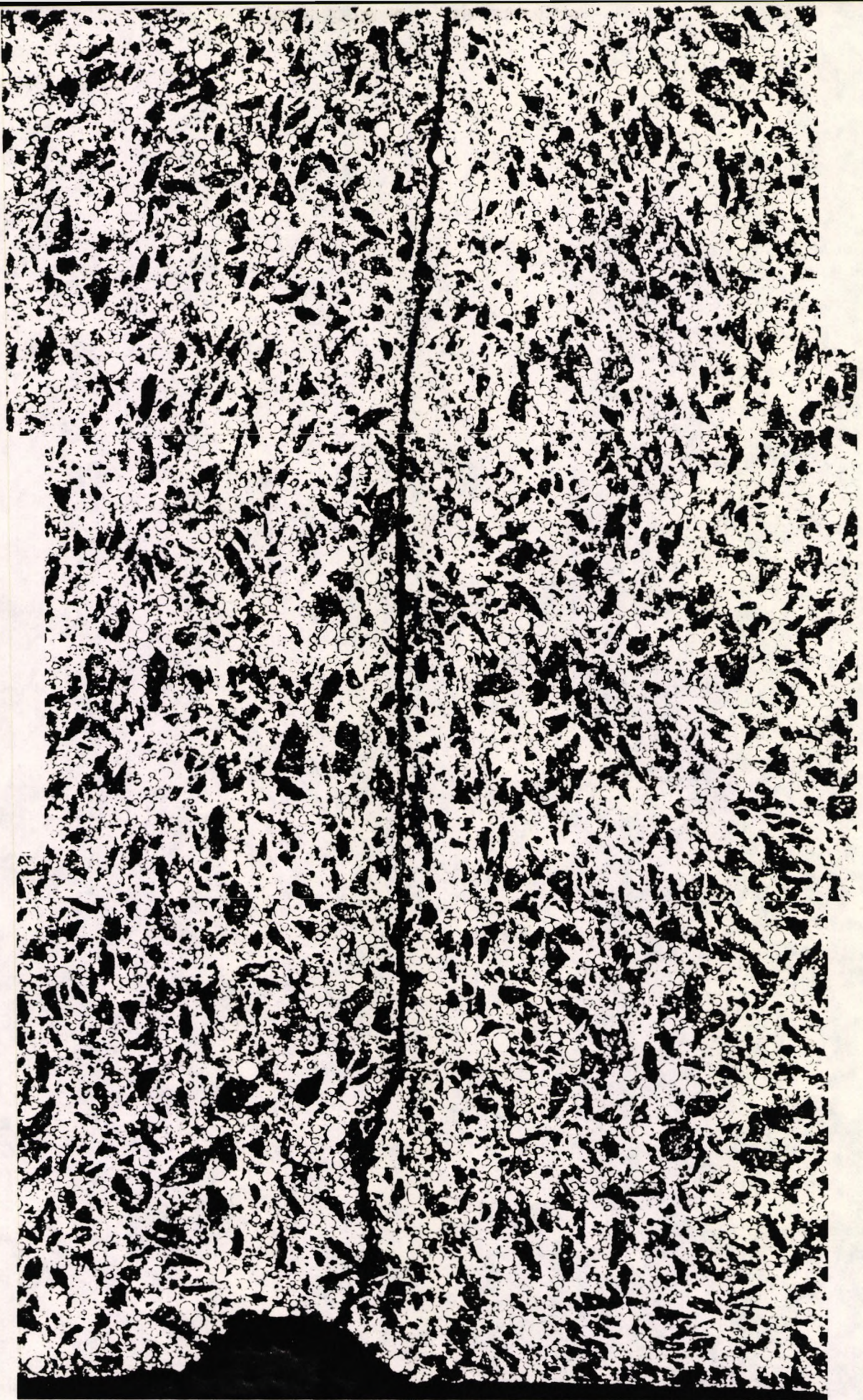
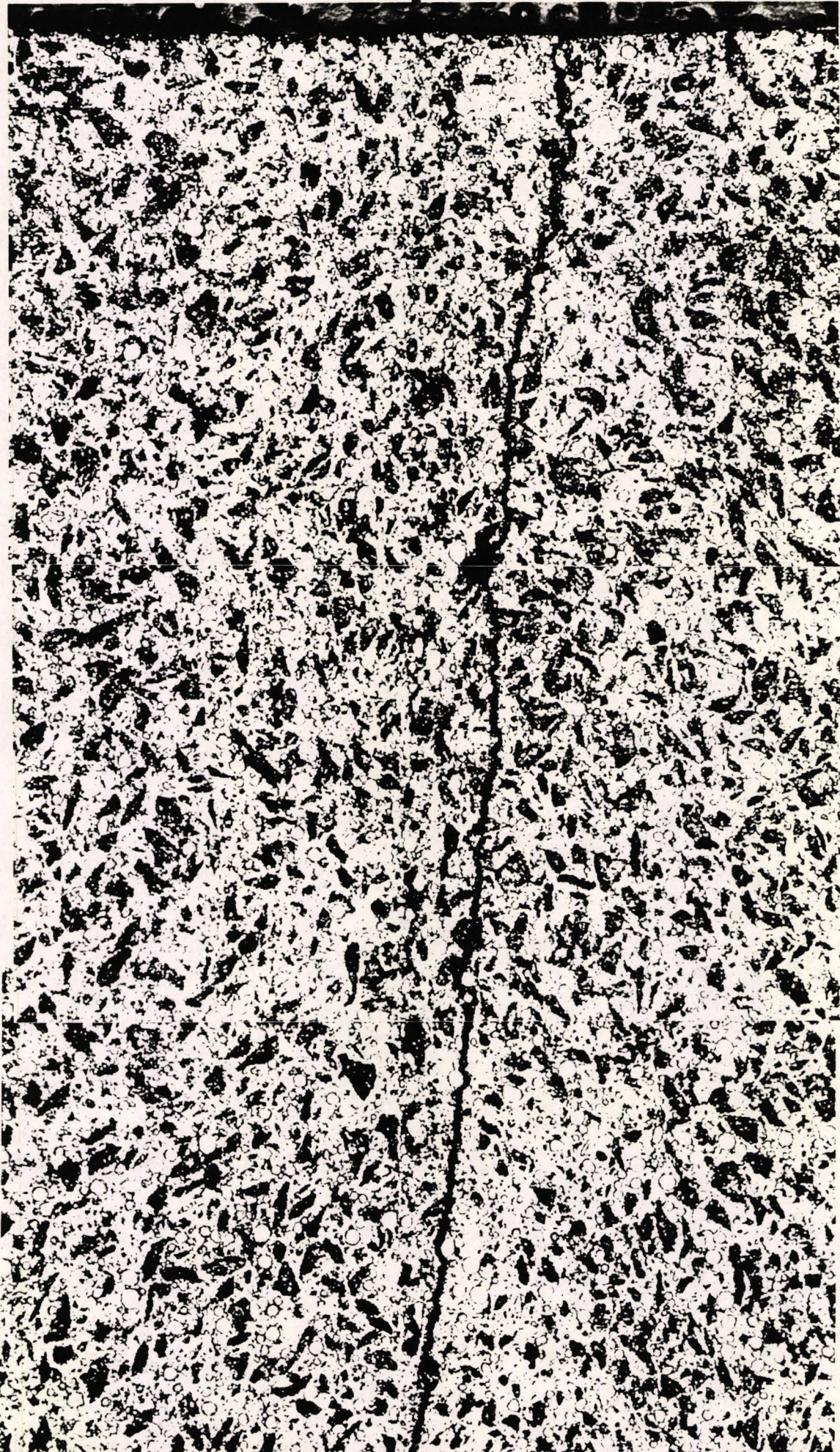


Plate 108. Amalcap specimen M9.  
Composite micrograph of the joint and fracture zone.

x110



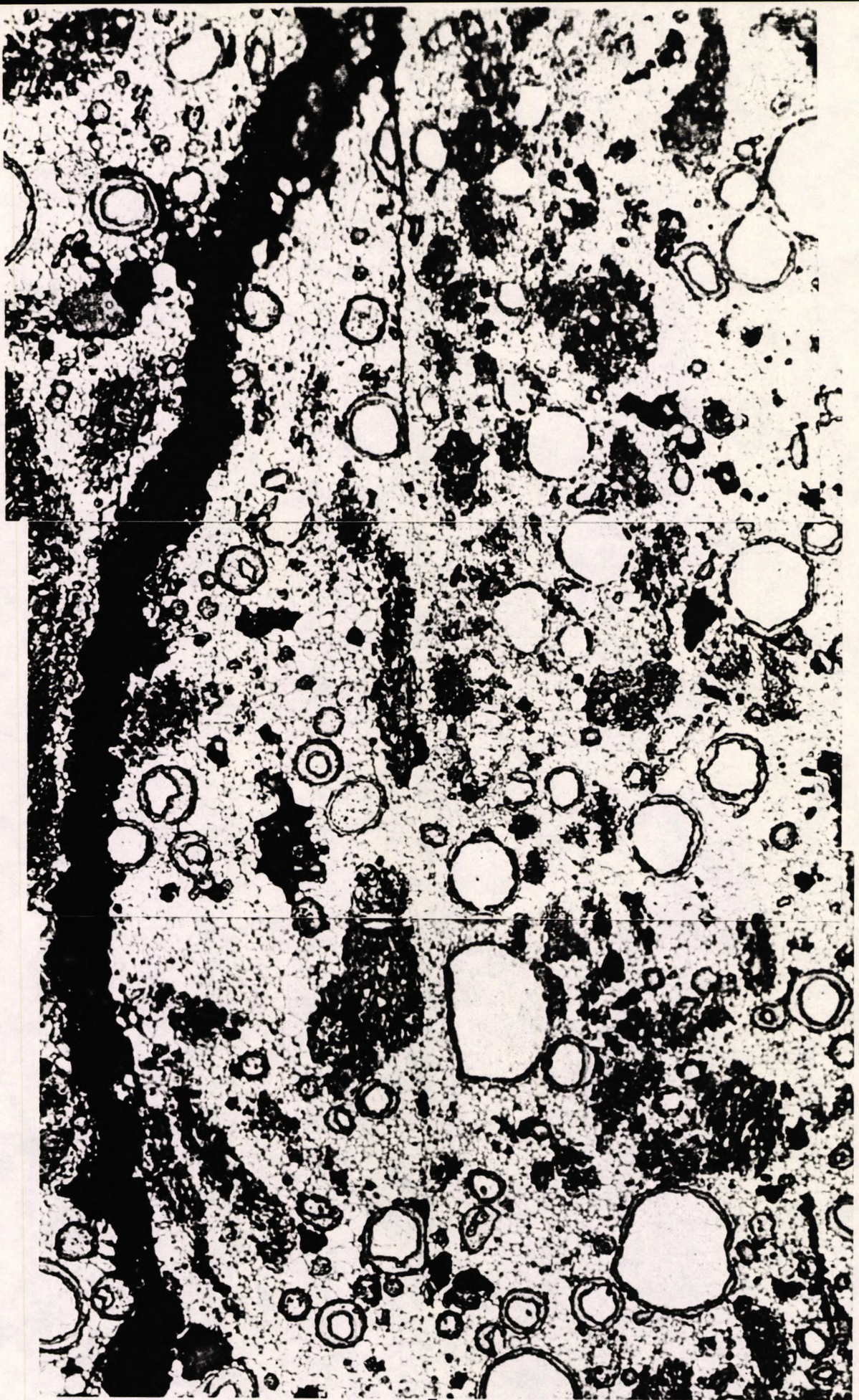


Plate 109. Amalcap specimen M9.  
Lower transition zone.

x900

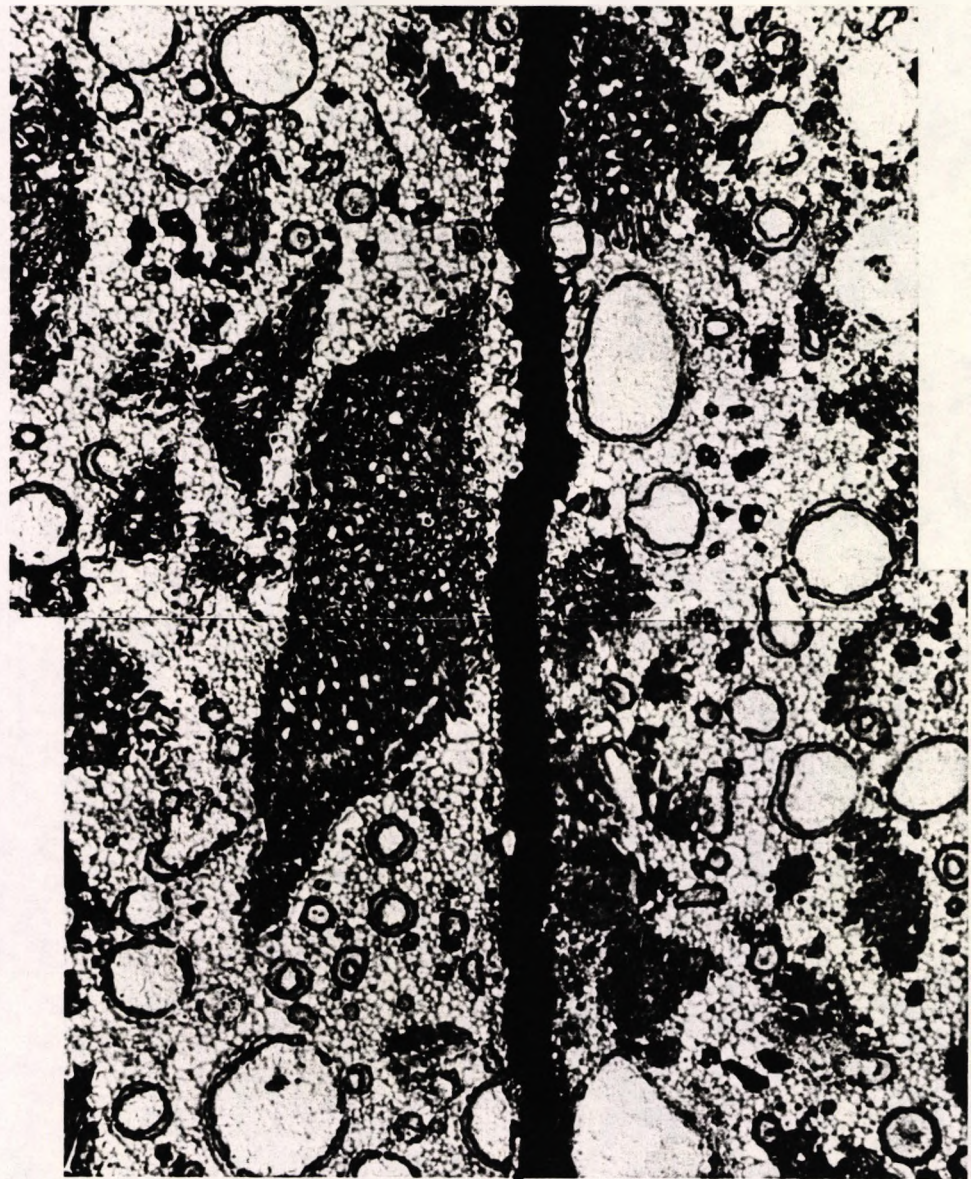
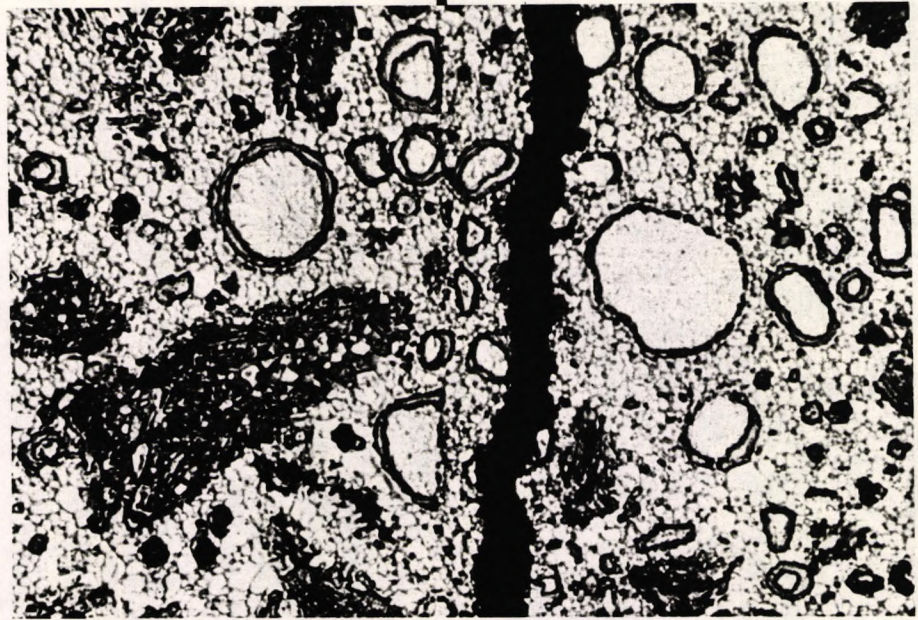
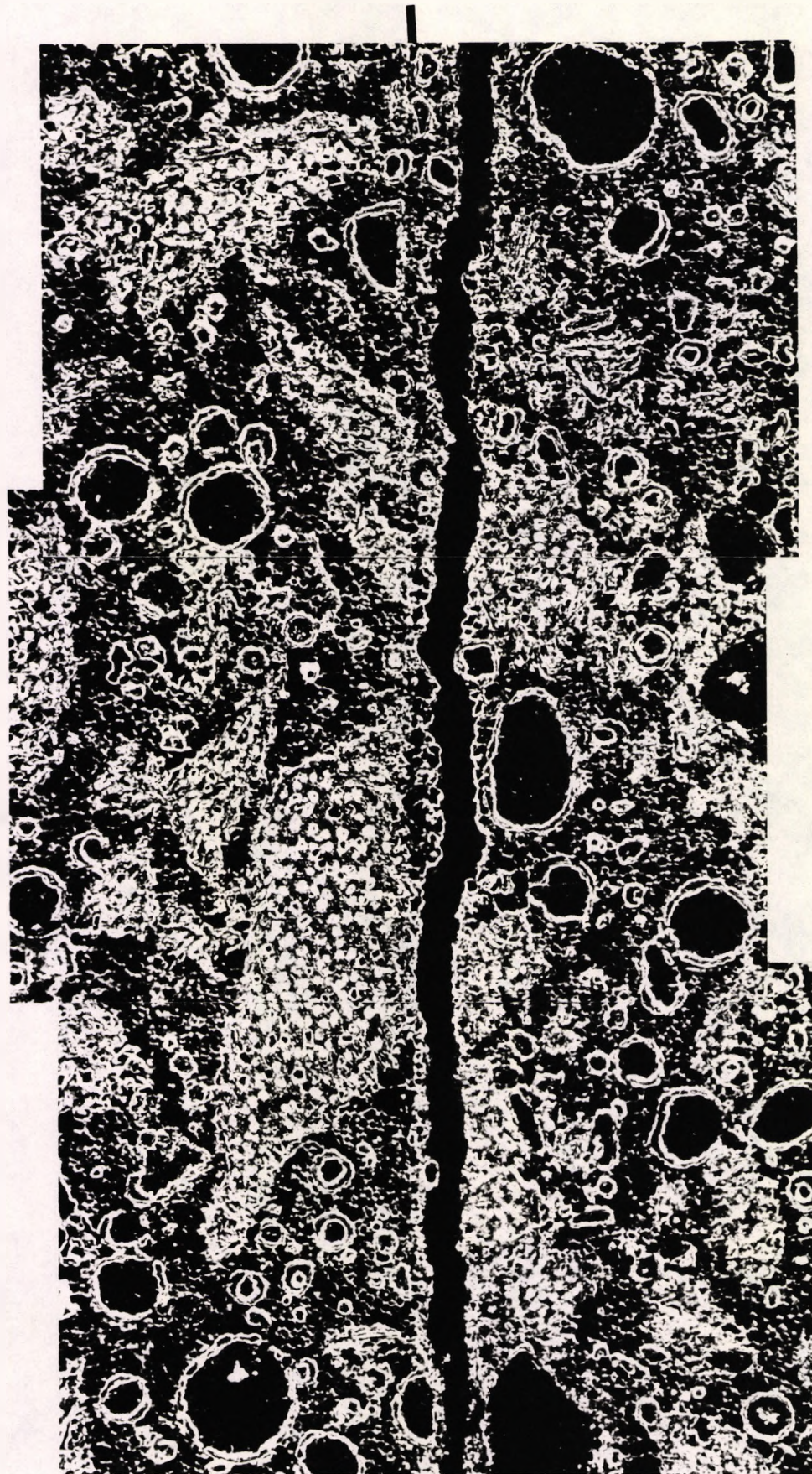


Plate 110. Amalcap specimen M9.  
Upper transition zone. Bright field illumination.

x720



**Plate 111.** Amalcap specimen M9.  
Upper transition zone. Dark field illumination.

x720

In Plate 109, the joint is identified in the lower transition zone by cut spherical particles and a vertical secondary crack which may indicate a slight interface weakness.

The fracture continued along the joint for about 1.0mm then deviated into the addition material. This area is shown at high magnification in Plates 110 and 111 where the fracture appears to be separated from the joint by a narrow band of matrix phase. At the upper part of the specimen the fracture path appears to be entirely within the addition amalgam.

It is considered that since the fracture path departed from the joint in sample M9, this was probably stronger than the adjacent material which failed.

#### **6.13.2.7 Amalcap specimens P4 and P2**

The fracture path of specimen P4 (Plate 112) was similar to M9 (Plate 108). In specimen P2, the fracture started in the parent and traversed the joint (Plates 113 and 114). The fracture then propagated in the addition material close to the interface for a short distance. At a higher distance (upper part of Plates 113 and 115), the fracture departed from the joint.

Notching of the joint was considered: the fracture might initiate in the joint. If the joint was strong, off-centre loading might cause the fracture to deviate from the interface to end at the central loading roller. This would be a "most convincing" demonstration of the integrity of the joint if departure from the joint occurred at a substantial distance from the upper loaded surface. If the joint was not strong, the fracture would surely continue at the joint interface for a substantial proportion of the specimen's diameter.

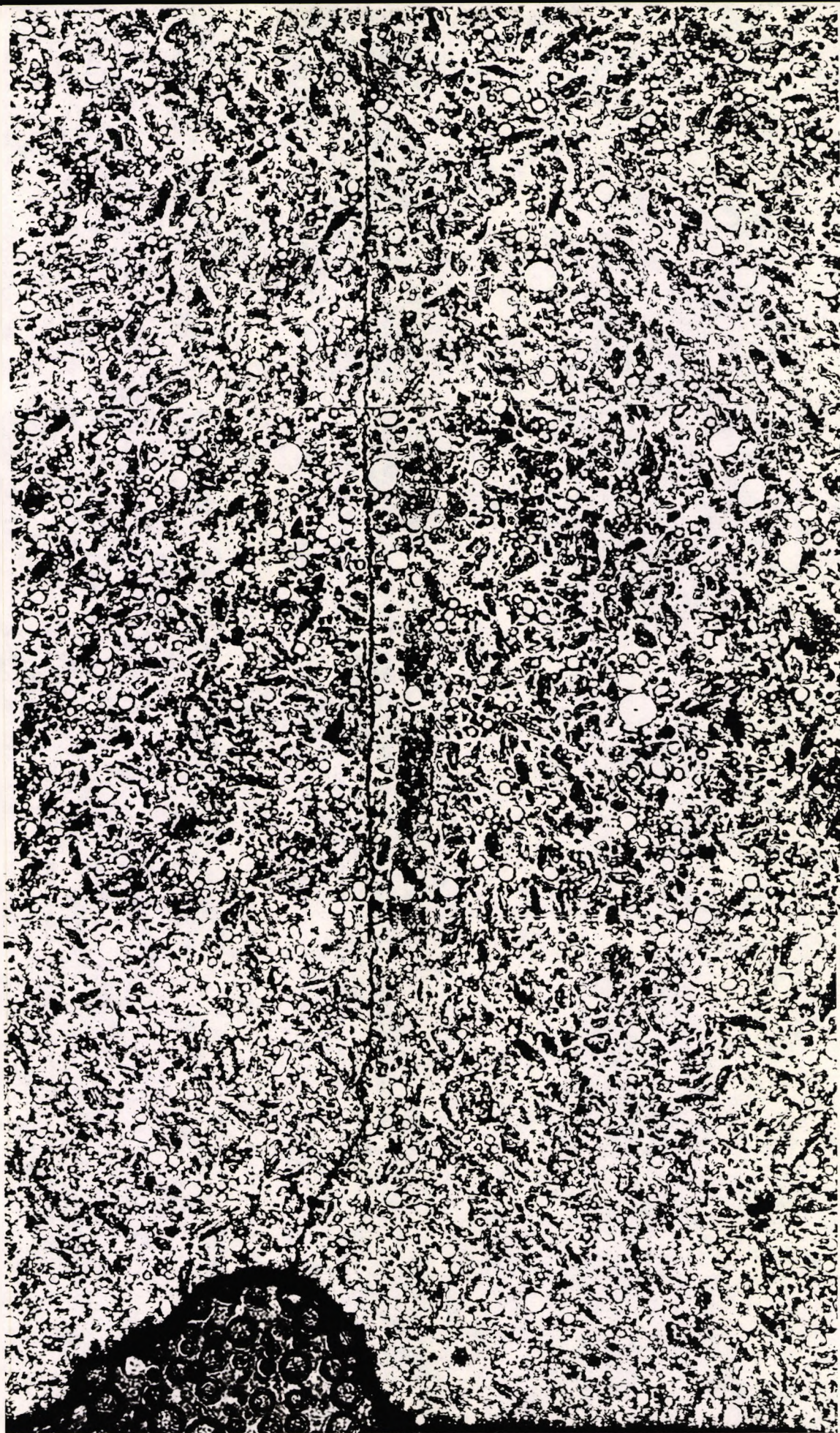


Plate 112. Amalcap SAS specimen P4.  
The fracture path was similar to that of specimen M9 (Plate 108).

x110

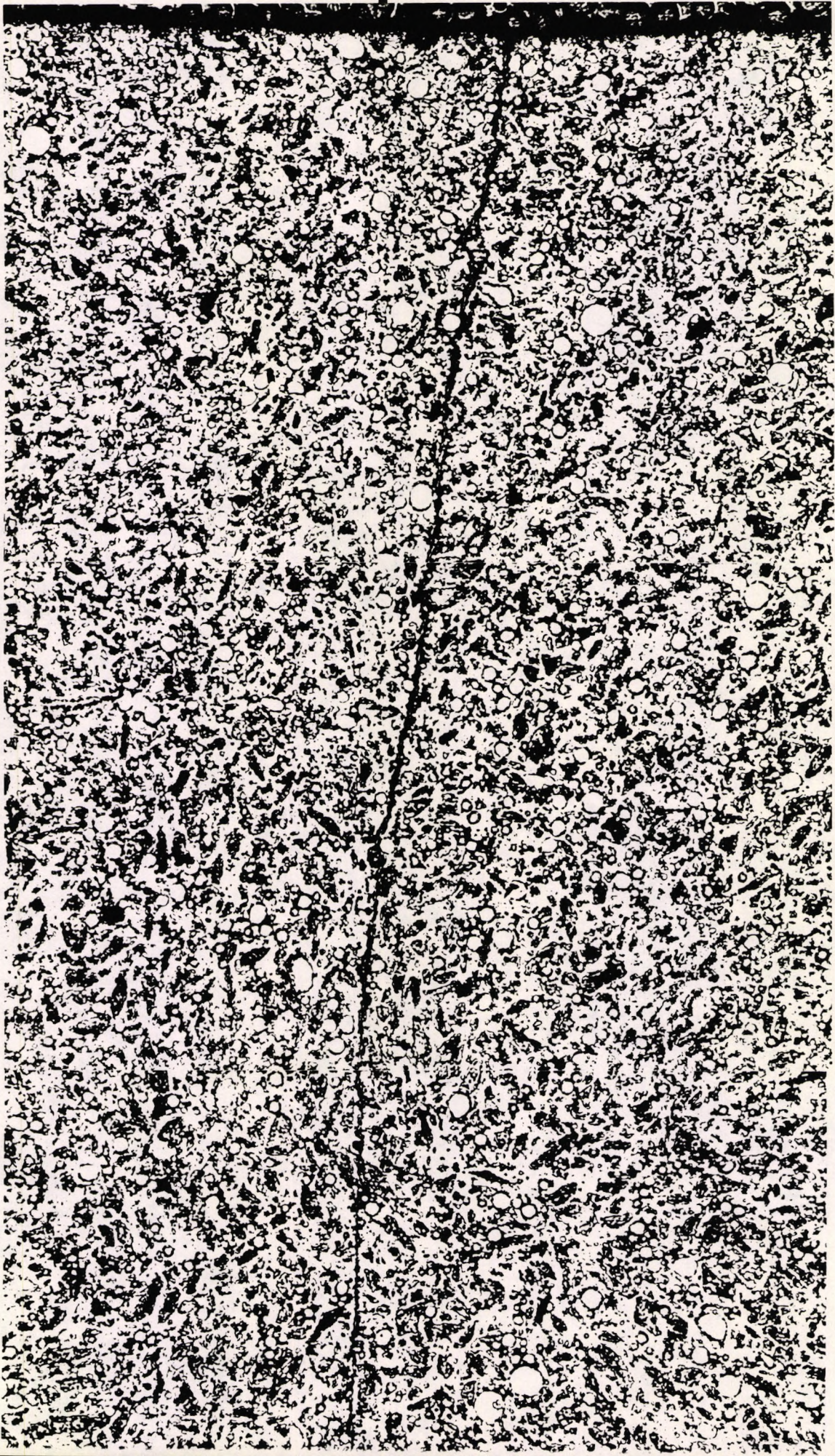




Plate 113. Amalcap SAS specimen P2.

x225

The fracture path traversed the joint from the parent to addition amalgam.



Plate 114. Amalcap SAS specimen P2.  
The fracture path traversed the joint.

x900

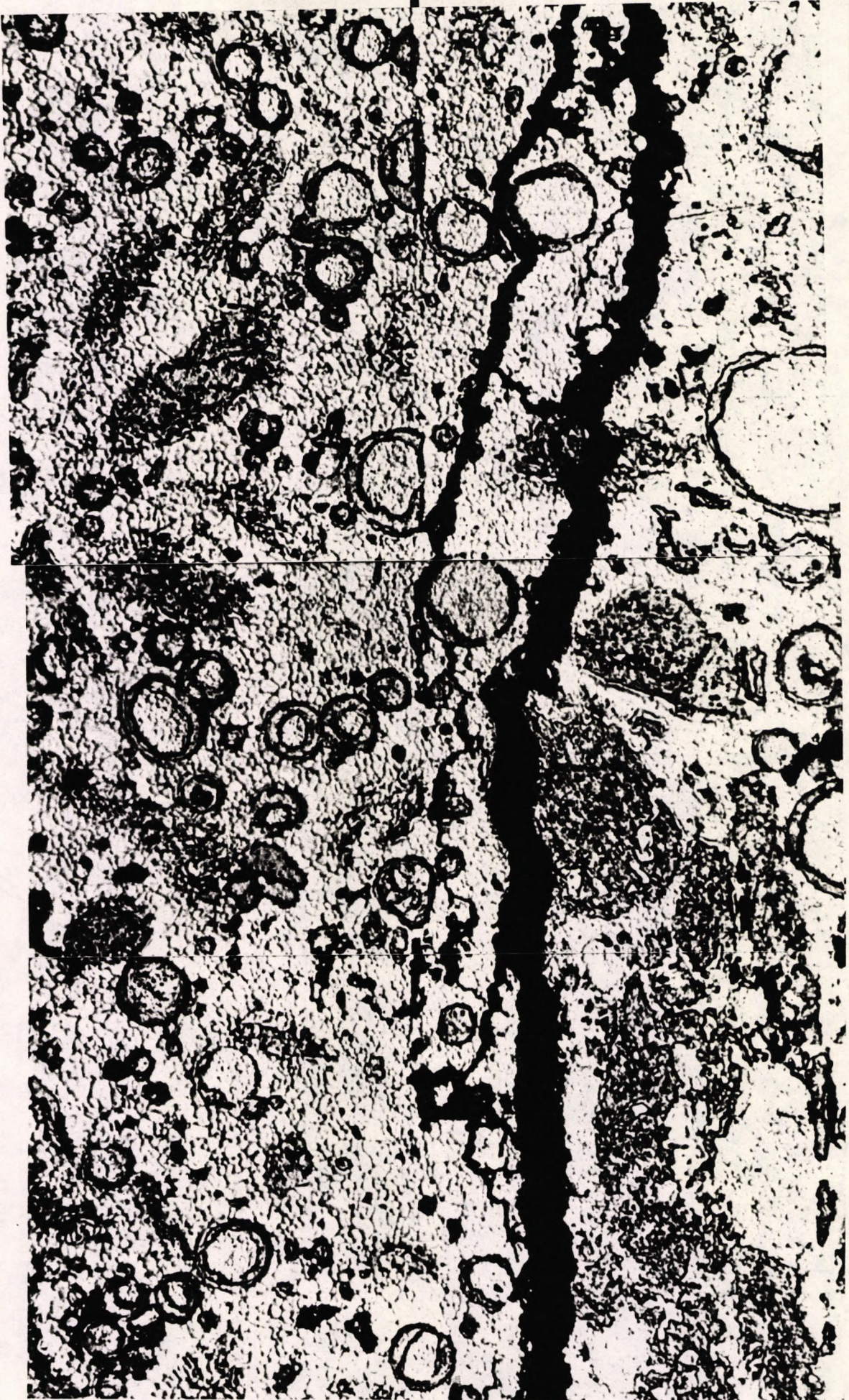


Plate 115. Amalcap SAS specimen P2.  
The fracture path departed from the region of the joint.

x900

### 6.13.3 Notched joint: loaded parent

Amalcap SAS generally polished easily and revealed the microstructure most readily and clearly. The structure of the HCSC all spherical particle alloy Tytin was distinctive. These alloys were selected for further study and subsequently Dispersalloy was also used.

Six samples of each alloy were prepared using the standard paddle procedure. In addition, four samples were condensed without the paddle, using only a flat ended piston vibrating for 2s on each of four quarters of the divided mix. It was anticipated that this condensation procedure might produce weaker joints.

Two of the six paddle-prepared samples for each alloy broke during the notching procedure. Twenty revolutions of the wheel of the Hounsfield notching machine produced the standard notch: those samples which fractured did so after 12 to 14 revolutions. On the fracture surfaces, there were large areas where old to new amalgam union had occurred. However, the characteristic pattern of end preparation score marks confirmed that the joint had failed in other areas. The breakages were considered to result from the notching procedure itself or perhaps with inherent weakness or low fracture toughness of the amalgam. Difficulties in accurate placement of Amalcap SAS samples P2 and P4 in the notching machine led to notching of the parent material rather than the joint as intended. These samples were loaded on the addition and the fracture paths were shown in the section above. Due to limitations of time at the end of this study, it was not possible to develop improved notching procedures.

Following successful notching of the joint, samples were fractured by application of the load adjacent to the joint. Samples where the parent had been loaded are shown in the next two sections.

### 6.13.3.1 Amalcap specimen P6

The fracture surfaces are shown in Plate 116. Radial scratch marks are visible in the lower half of the surface. The fracture possibly originated at the joint but soon deviated into the parent (Plate 117). A secondary crack may be seen at the right of the cut spherical particle in the centre of Plate 118. The departure of the fracture from the joint is shown at high magnification in Plate 119. In the lower part of the field of view, a cut spherical particle may be seen where the fracture has followed a course around the curved side of the particle. The particle clearly originated in the parent material but it was well attached to the addition part of the sample. After departing from the joint, the fracture followed a course approximately parallel to it for about 0.25mm before finally deviating more sharply into the parent.

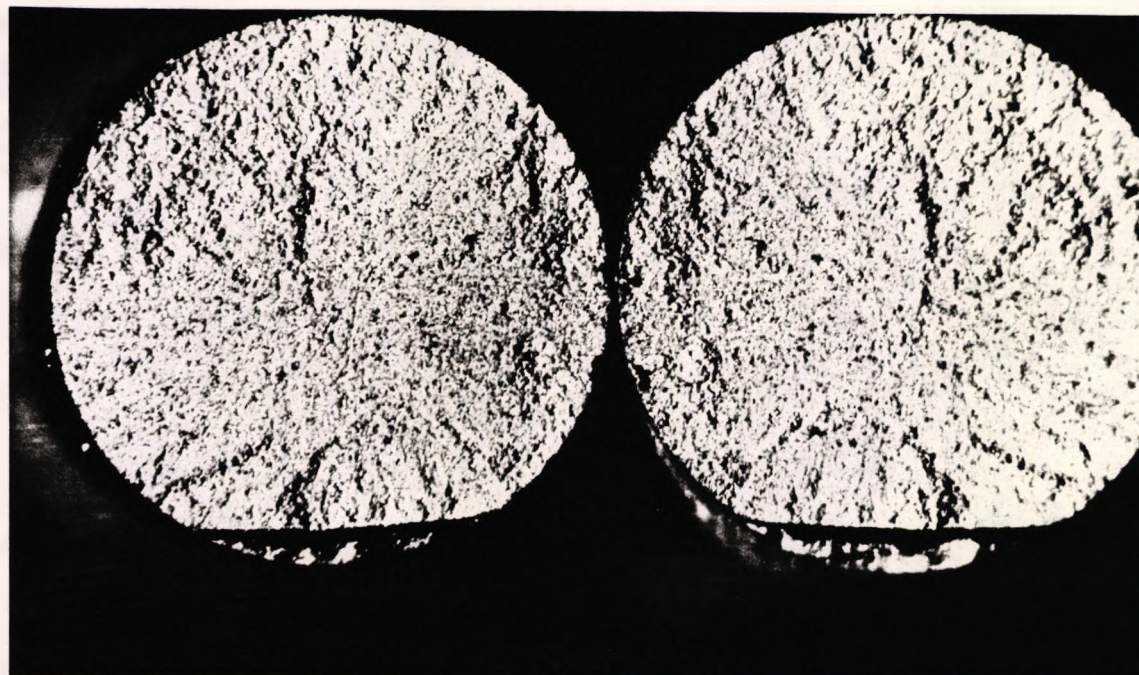


**Plate 116.** Amalcap SAS specimen P6. Fractured surfaces.

x18

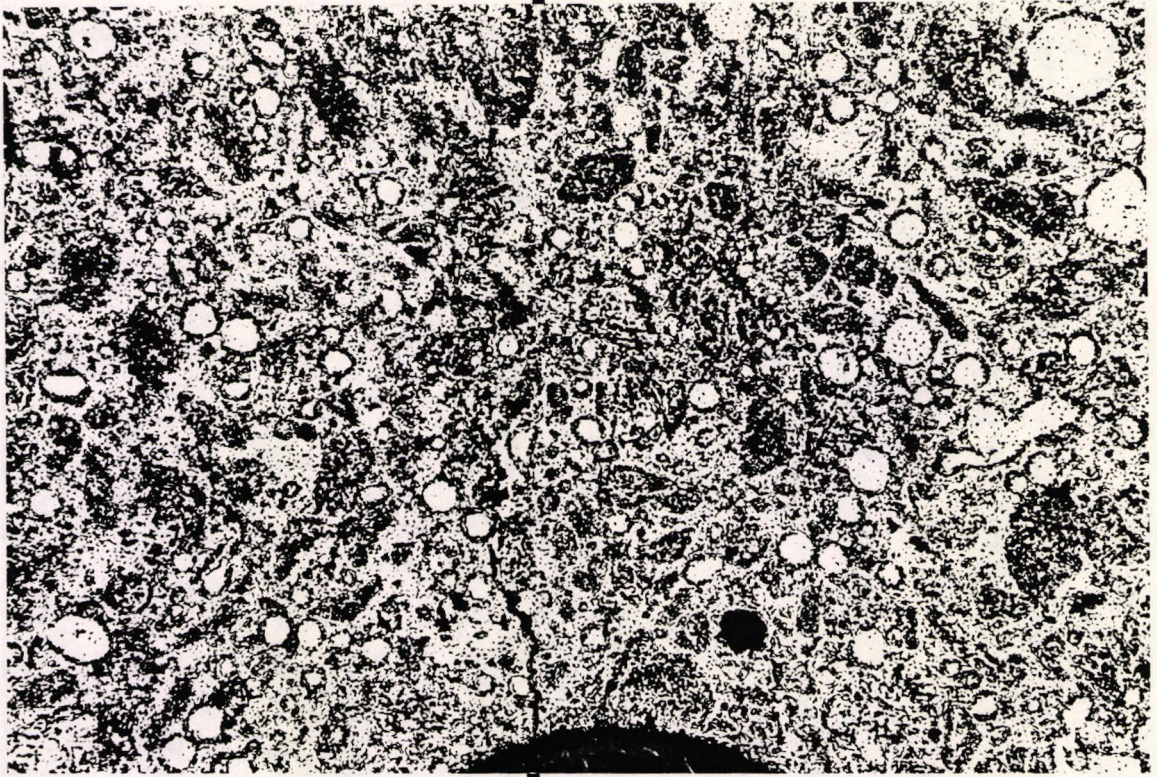


**Plate 117.** Amalcap SAS specimen P6.  
The notched part of the sample.

x225

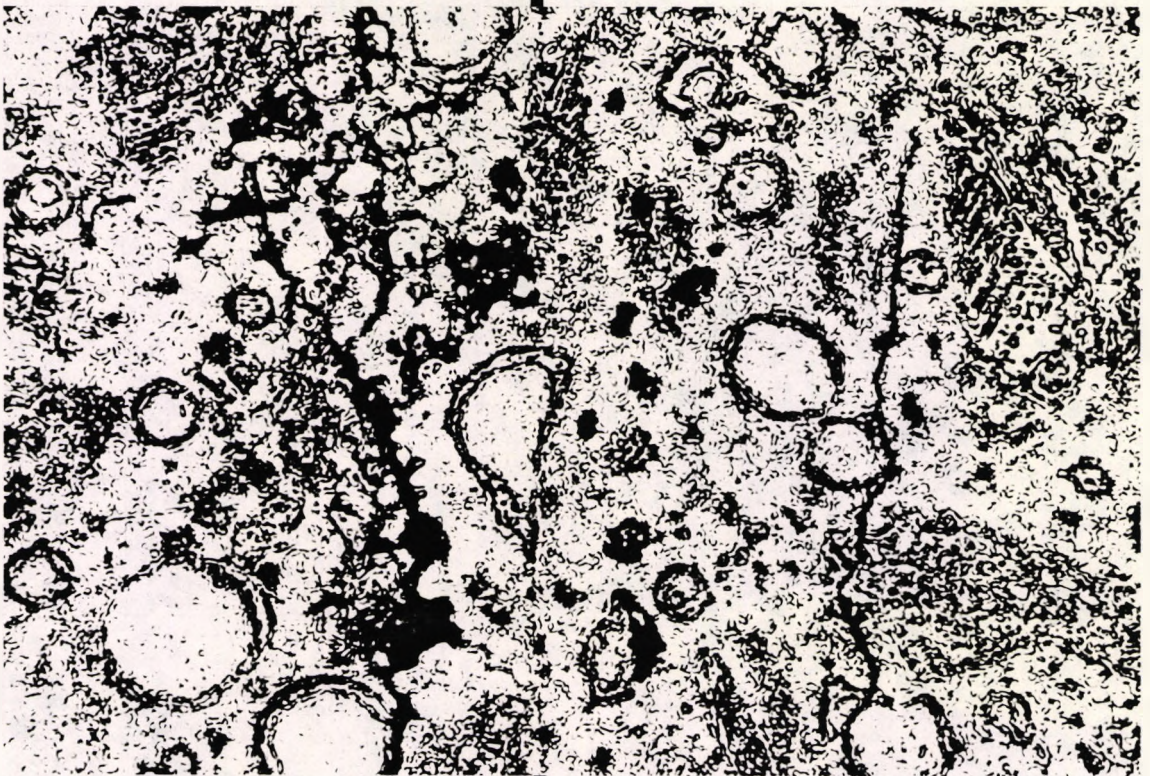


**Plate 118.** Amalcap specimen P6. Centre of Plate 117.  
The fracture path was in the parent to the left of the cut spherical particle  
identifying the joint.

x900

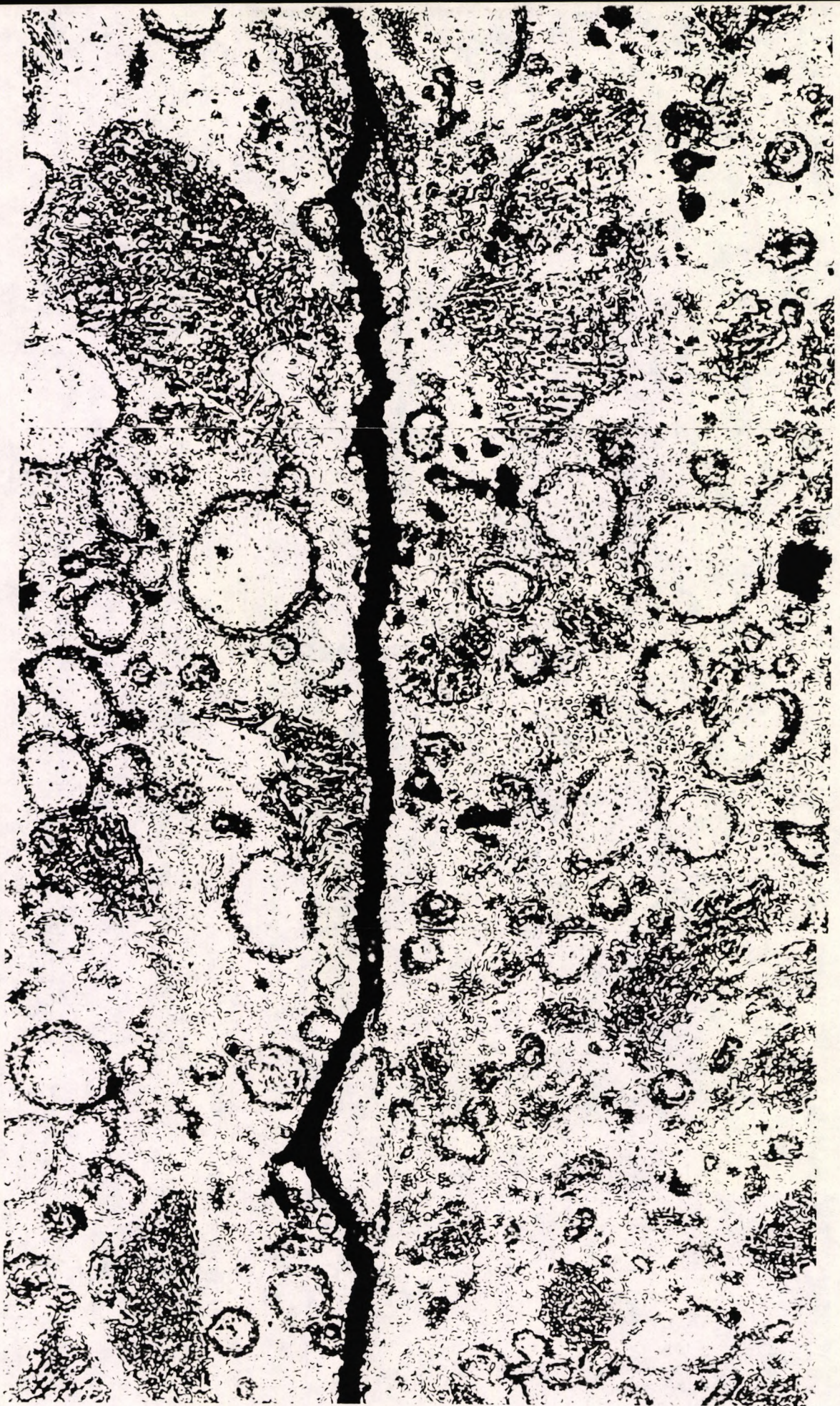
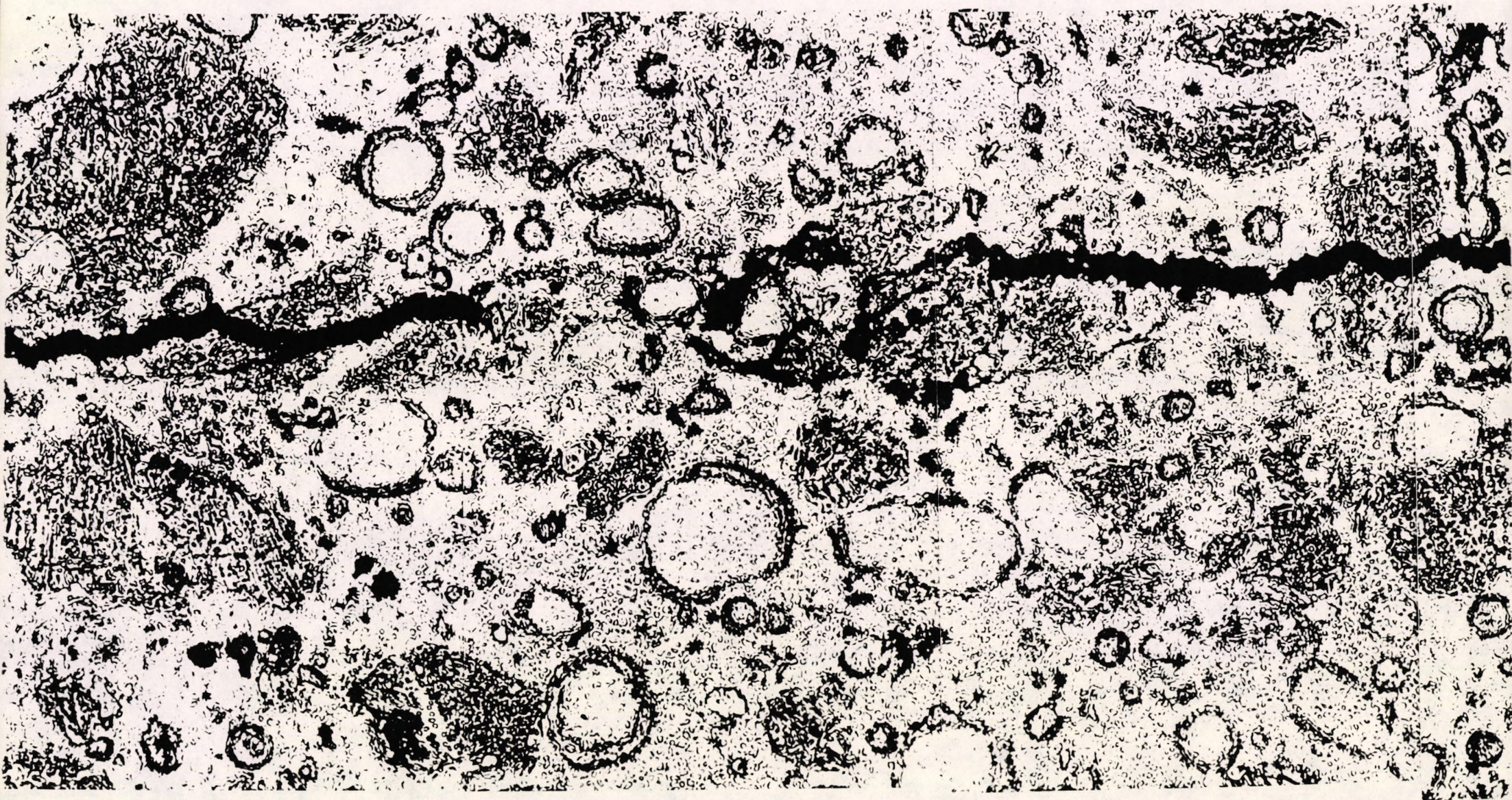
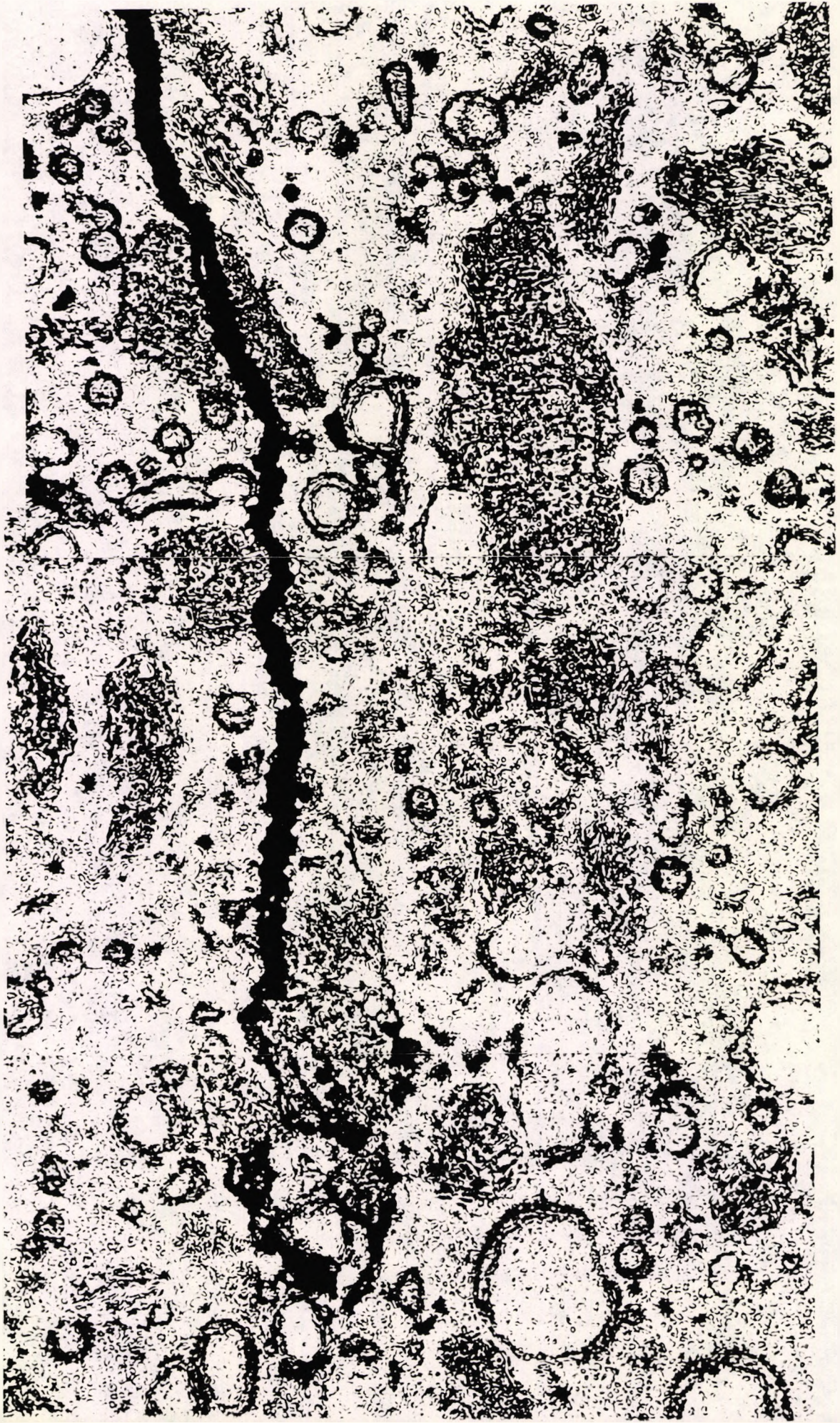


Plate 119. Amalcap specimen P6.  
Departure of the fracture from the joint.

x900



Middle of Plate 119. Page 252.



### **6.13.3.2 Tytin specimen P20**

In contrast to Tytin specimen N3 (Plate 102, page 235), the end preparation score pattern of specimen P20 was visible over about 50% of the fracture area (Plate 120). In Plate 121, the fracture may be seen adjacent to the joint in the region of the notch. Above this area, the fracture propagated in the addition material for about 1mm before reaching the joint. The fracture departed from the joint at about halfway. This is shown in Plate 122.

### **6.13.4 Other notched samples**

It was anticipated that the flat ended piston might produce a weaker joint when applied to the first increment of the addition than use of the paddle. Of the four samples of each alloy condensed using only the flat ended piston, two Tytin and three Amalcap SAS fractured during notching. Score patterns were clearly visible over the entire fracture surface with no large areas of attached material. The one Amalcap SAS sample (P9) which survived the notching procedure was weak under test and showed a similar fracture surface with little evidence of union.

However, the two Tytin samples were tested to fracture, P15 by loading the parent and P17 by loading the addition. In the former case, about 80% of the fracture surface was in the parent; the score pattern was visible in only 20% of the area including a small part immediately above the notch. The fracture deviated into the parent from the joint: it appeared that the joint was strong. In sample P17, the fracture path followed the interface: score pattern was visible over about 85% of the fracture surface. In its final stage when close to the loaded area, the fracture path departed from the joint into the addition part.

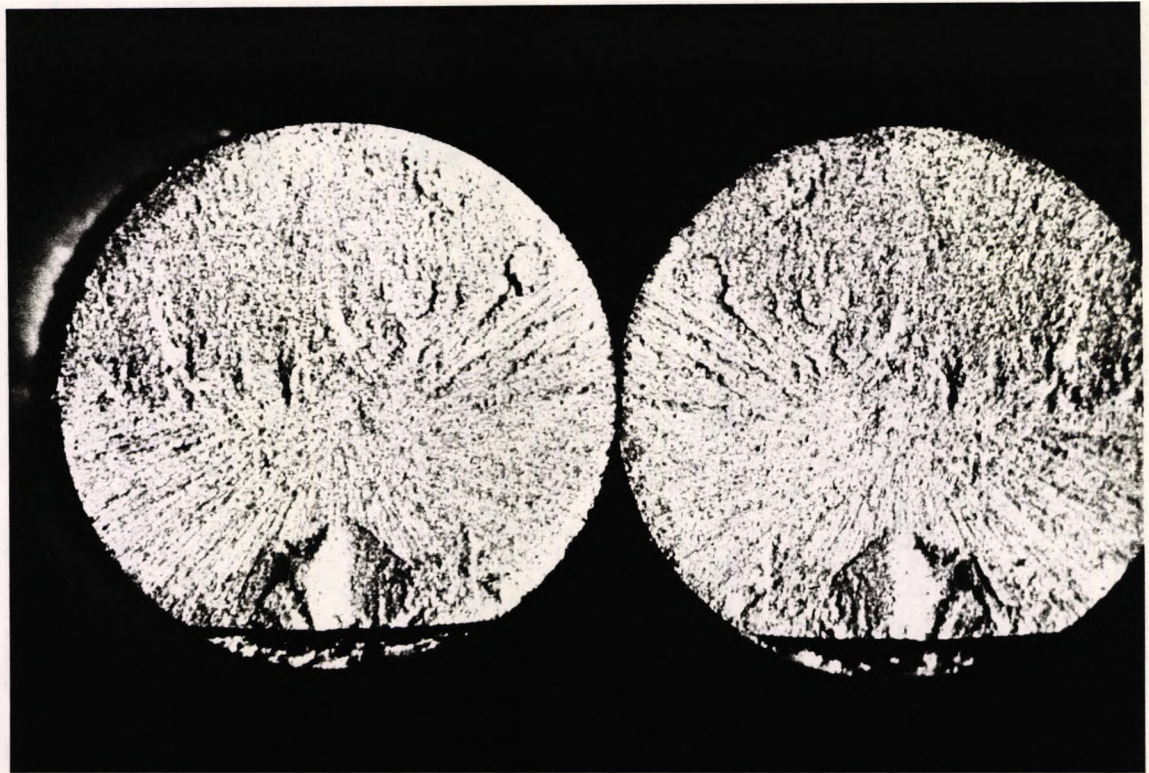


Plate 120. Tytin specimen P20. Fractured end surfaces.

x18

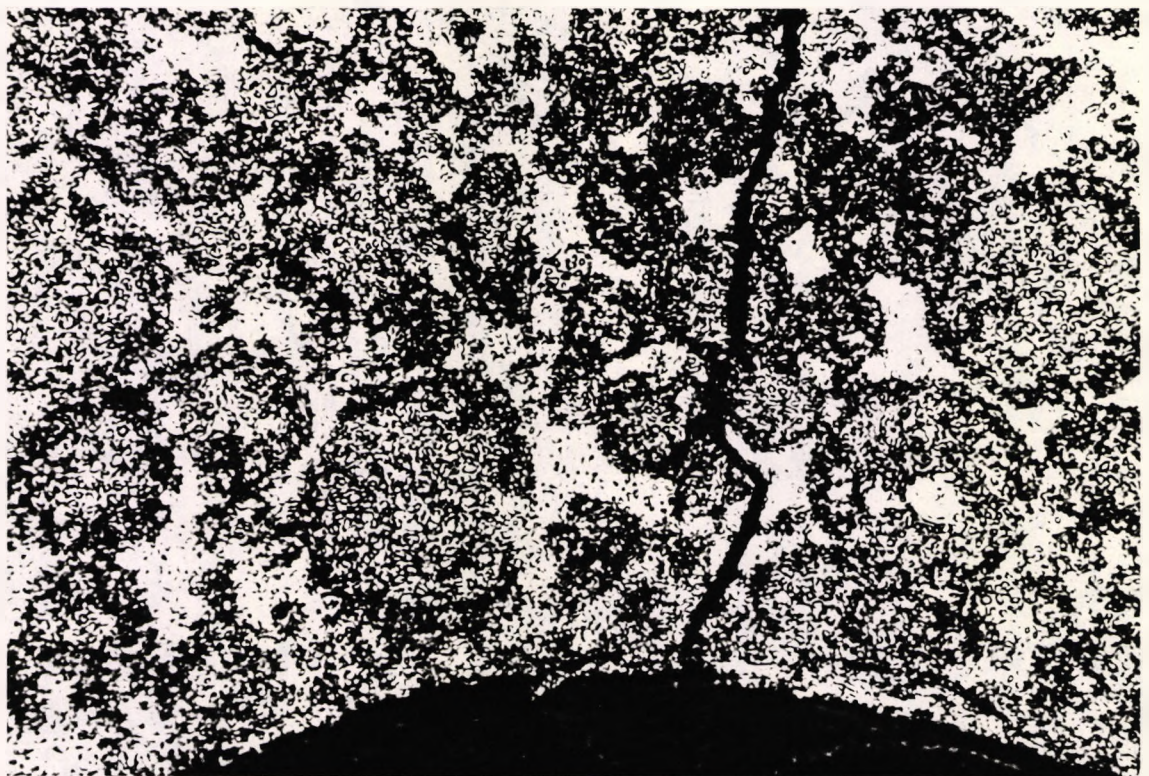


Plate 121. Tytin specimen P20.

The fracture originated at the notch adjacent to the joint.

x900

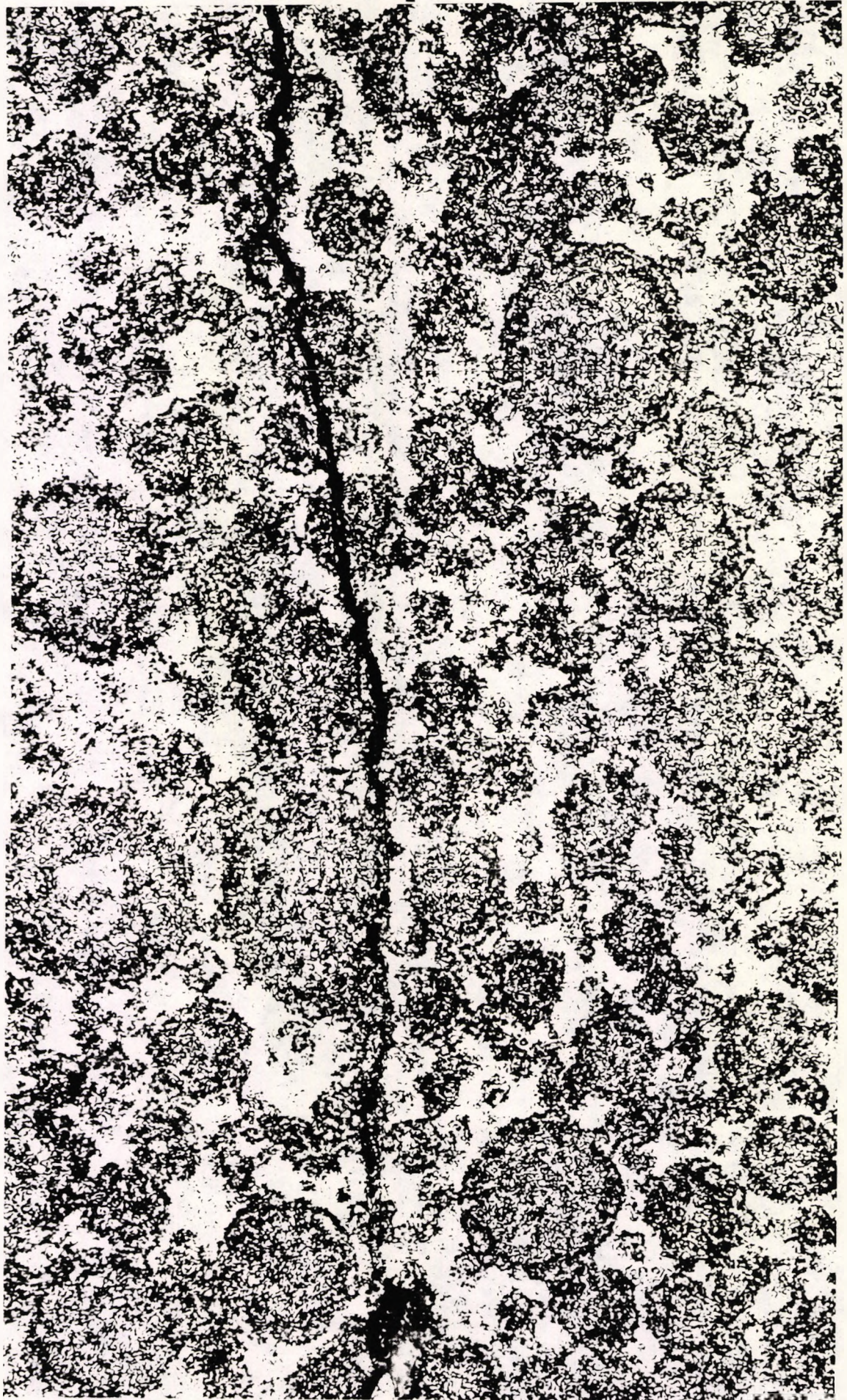


Plate 122. Tytin specimen P20.  
The fracture departed from the joint.

x900

#### 6.13.4.1 Dispersalloy

The preparation procedures used for Amalcap P1 to P10 and Tytin P11 to P20 above were repeated using Dispersalloy. These are identified as samples R1 to R10. However, the first four paddle-prepared samples fractured whilst notching the joint. In view of the possibility that all samples might break before completion of the test, notching at the joint was abandoned. One each of the remaining paddle samples was notched in the parent (R5) or addition (R6) with opposite loading. The samples condensed using only a flat piston were divided into two similar groups.

In sample R5, the fracture reached the joint at about 1mm from the notch and departed from the interface at about the centre. The fracture progressed within the addition parallel to and about  $25\mu\text{m}$  from the interface for about 0.2mm before leaving the area. In sample R6 (Plates 123, 124 and 125), the fracture reached the joint but remained in the addition for about 0.6mm before deviation. The fracture appeared to have been "deflected" by the parent.

Plate 126 shows the macroscopic fracture directions of Batch R, Dispersalloy. It may be seen that the fractures of samples R7 to R10 have traversed the joint. The addition parts of these four samples were condensed using only the flat piston for 2s on each quarter division of the mix. The two samples where notching was in the addition showed evidence of radial scratch marks in the lower half of the fracture surfaces. In contrast, it was difficult to discern the location of the joint interface in samples R8 and R10 which had been notched in the parent. This suggested that the restricted condensation procedure had never-the-less produced strong joints in these Dispersalloy samples. The finding is reported here and is suggested as a subject for possible further investigation.

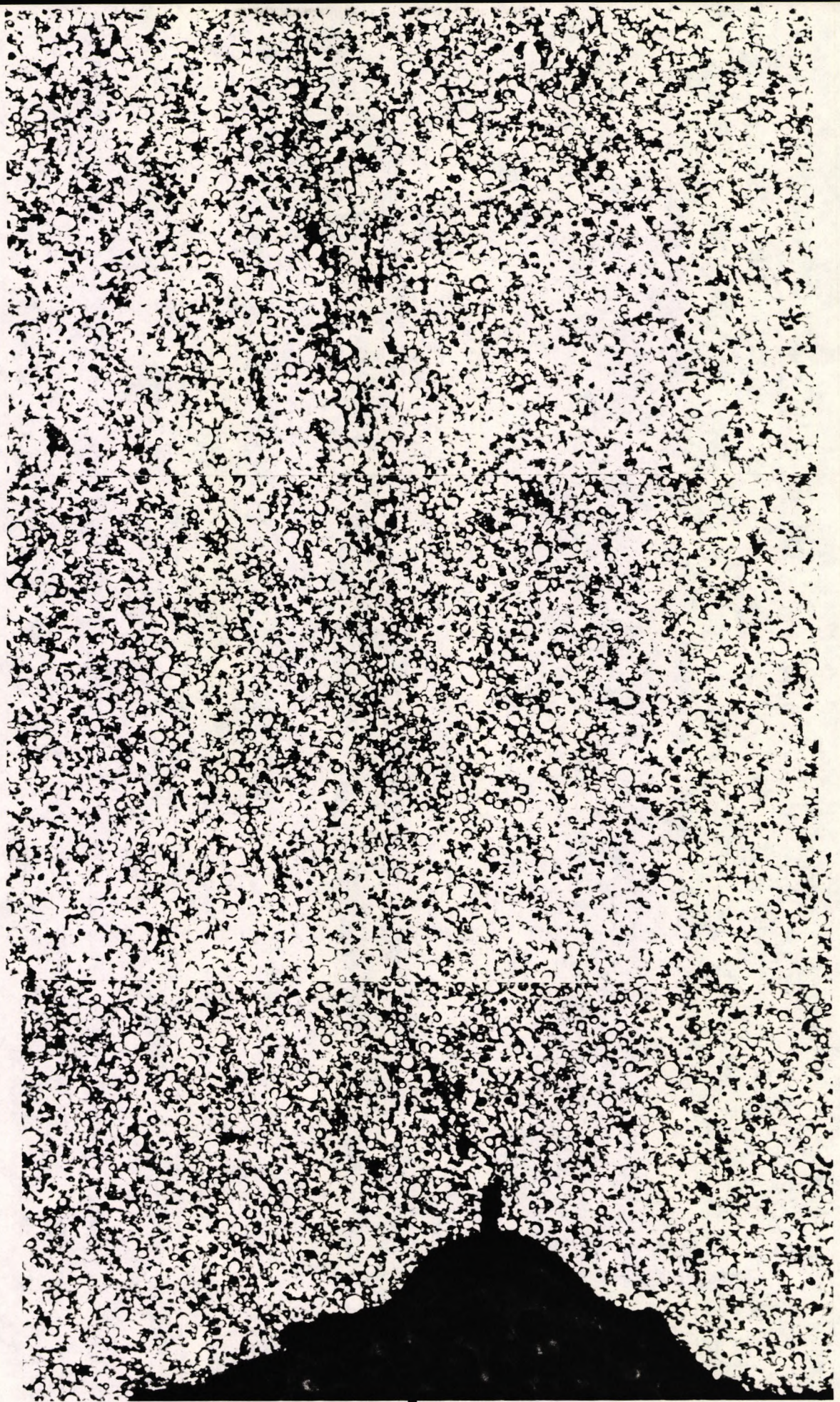


Plate 123. Dispersalloy sample R6. Composite micrograph. x110  
The fracture reached the joint interface about 0.6mm from the lower surface.

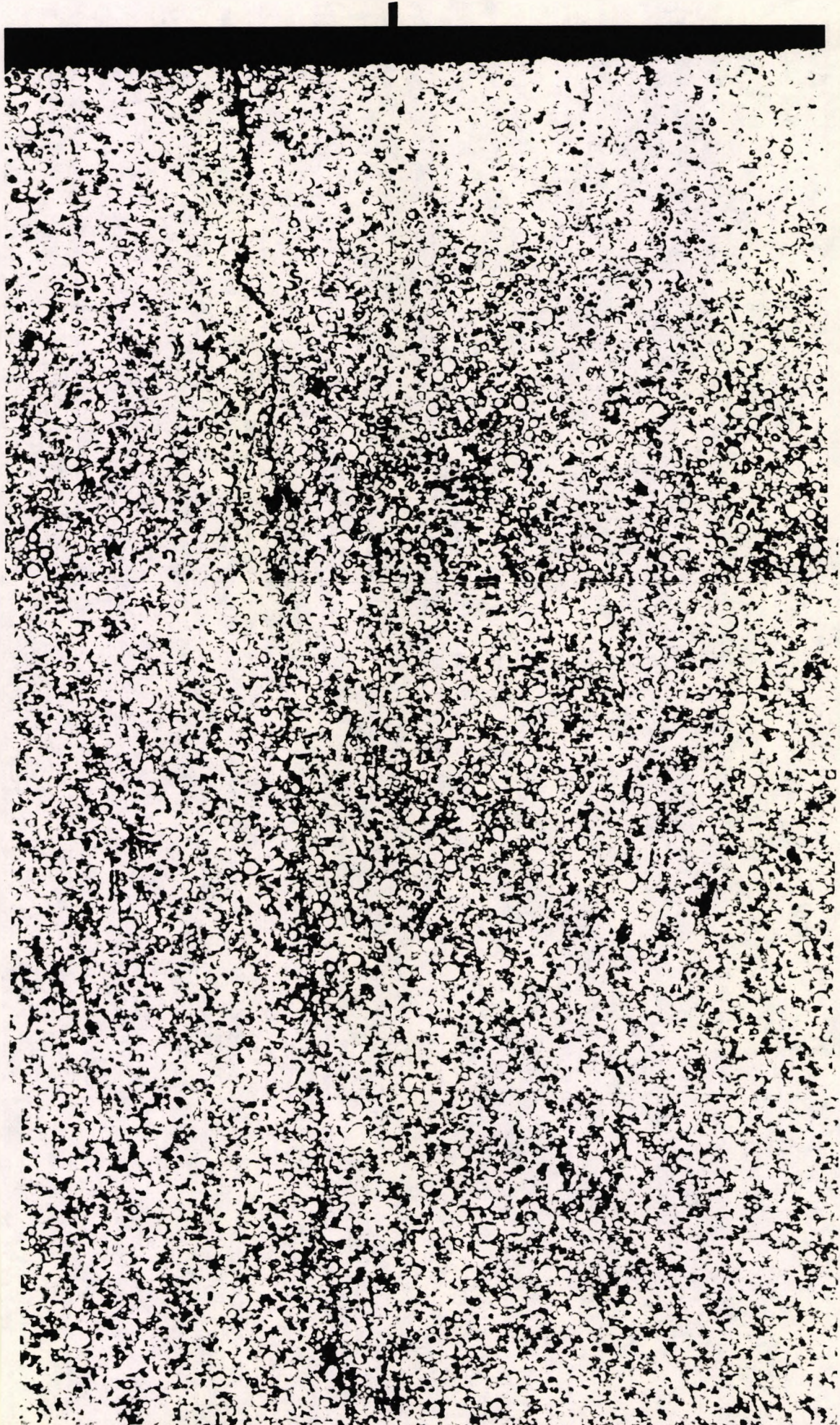




Plate 124. Dispersalloy sample R6.

x225

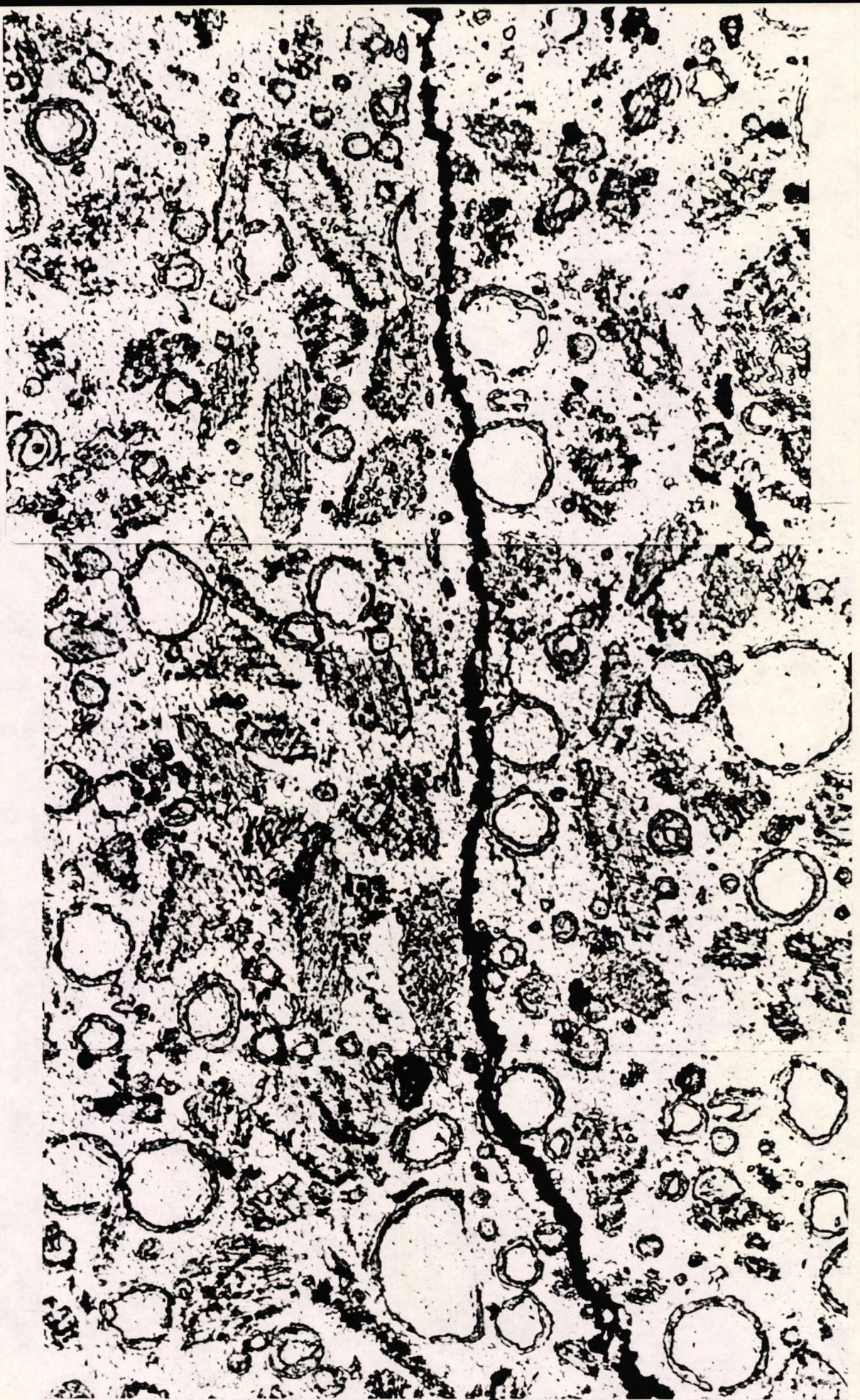
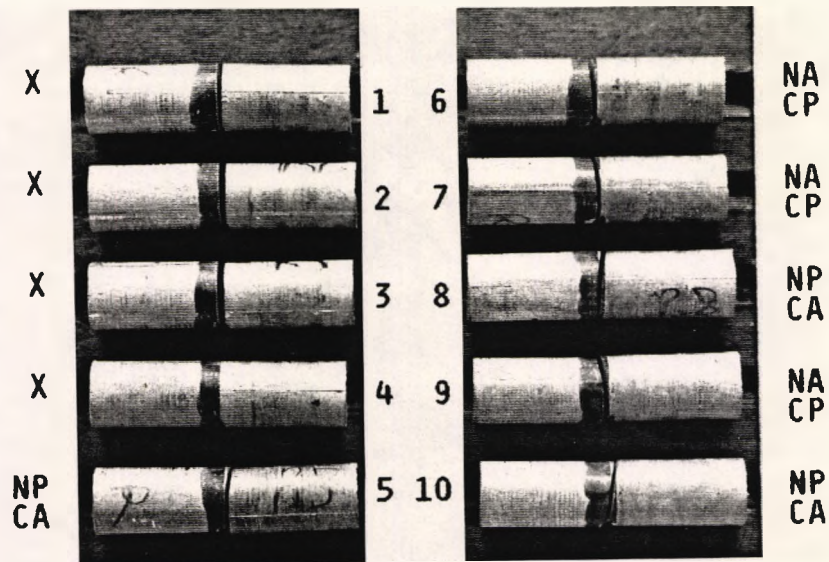


Plate 125. Dispersalloy sample R6.  
The zone where the fracture reached the joint interface.

x900



Samples 1 to 6: SPP additions; 7 to 10: 4x2s flat.  
 Key: X Sample failed during notching the joint  
 NA Notch applied to the addition  
 NP Notch applied to the parent  
 CP Central load applied to the parent  
 CA Central load applied to the addition

**Plate 126.** Dispersalloy Batch R after notching and test.

#### 6.13.4.2 Amalgam M

Samples were prepared using the Amalgam M conventional lathe cut alloy which had been used at the start of the study. Four samples (identified as T1 to T4) were prepared from DW parents and the standard paddle procedure for the additions. Two each were notched in the parent and addition (Plate 127). All fractures traversed the joints with only slight indication of the interface on the fracture surface. Fractures in the parent showed a coarser granular surface while the addition parts showed a finer grained fracture surface.

The microstructure of Specimen S20 (Plate 128) shows a fine grain structure in the addition on the right (condensed by the SPP), compared to the relatively coarse structure in the deadweighted parent.

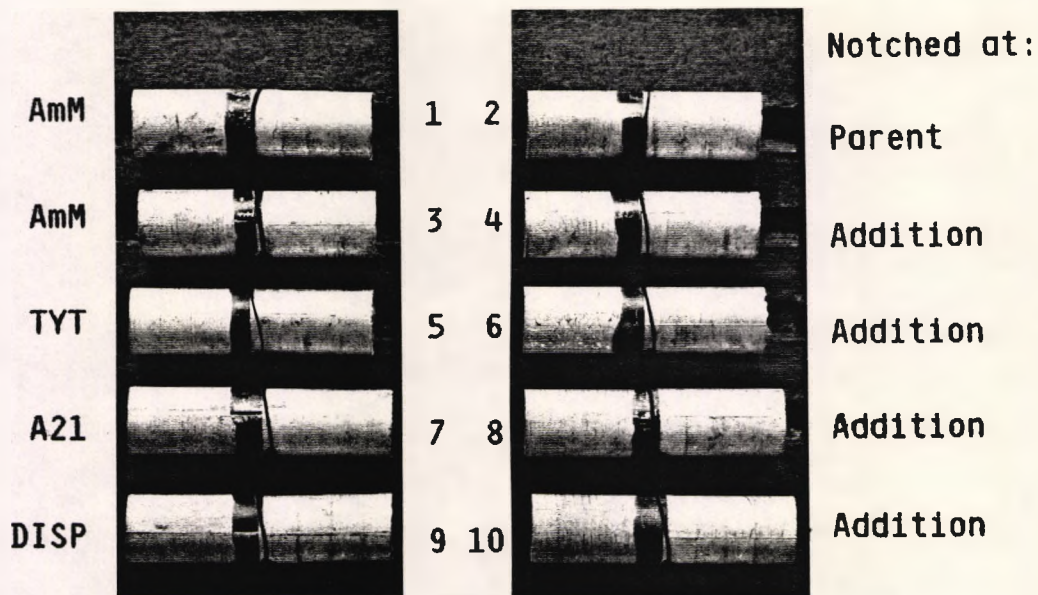


Plate 127. Batch T. Notched samples.  
Amalgam M, Tytin, Aristaloy 21 and Dispersalloy.

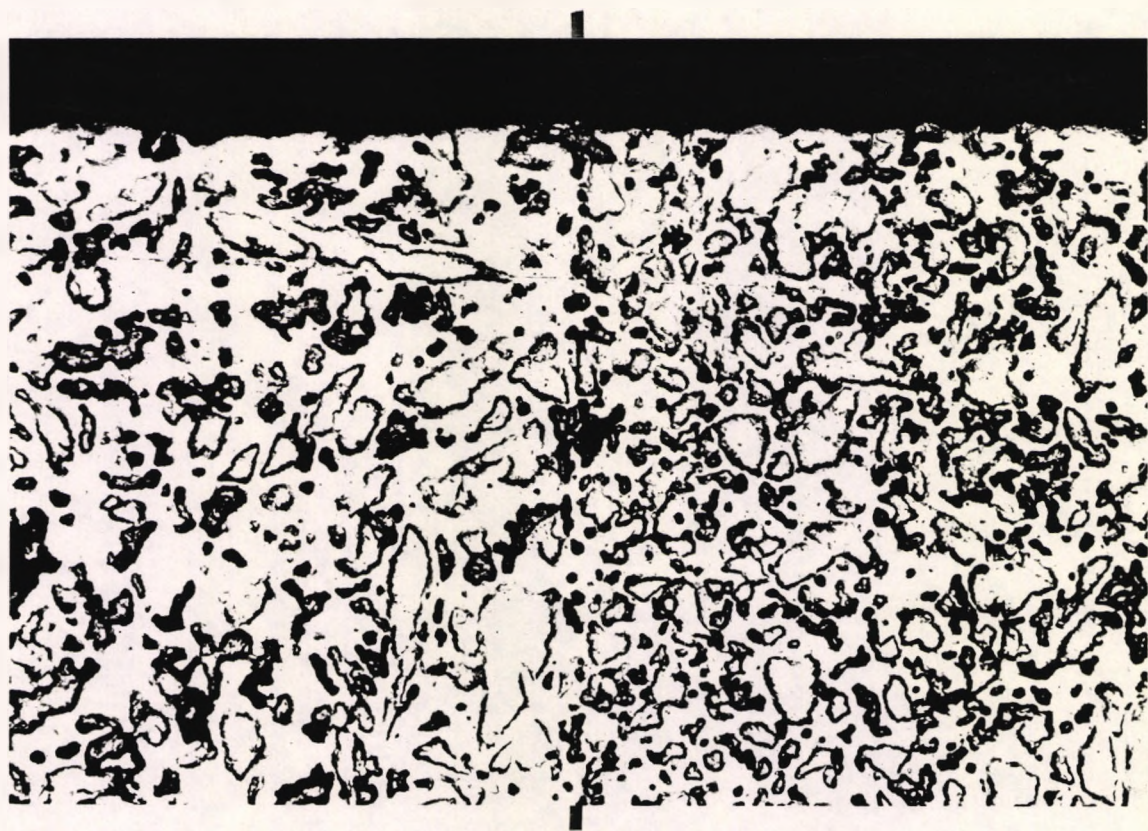


Plate 128. Amalgam M microstructure sample S20.

x225

In addition, two samples each of Tytin, Aristaloy 21 and Dispersalloy (identified as T5 to T10) were prepared for notching in the addition with parent loading. The fractures in Dispersalloy (T9 and T10) traversed the joint at approximately the centre of the specimen. The direction of propagation in both Tytin cases and one A21 initially was vertical: deviation towards the central load occurred near the end of the fracture. An error occurred in notching Aristaloy 21 sample T8 such that the notch was placed at the joint: the fracture was entirely within the parent.

There was variability in the results from these tests but shortage of time precluded further investigation and refinement of the preparation and test of notched amalgams. The results are however considered relevant in indicating an area for possible further study and were therefore included.

## Chapter 7. Discussion

The results of this work do not agree with those workers (see the footnote on page 32) who concluded that there is always a substantial reduction in strength when set dental amalgam is repaired. Very few workers *i.e.* Kirk (1962) and Jørgensen and Saito (1968) have reported the production of amalgam specimens which did not break at the joint during test and conventional amalgam alloys were used. No reports have been found where amalgams from high copper alloys have produced strong joints. Fukuba *et al* (1977) reported moderately strong joined samples (tensile strength about 70% of the controls) using HCA amalgam; the joint strength of their spherical particle conventional amalgam was about 92% of the controls. Hadavi *et al* (1992) reported mean tensile strength of uncontaminated joined HCA amalgams in the range from 62% to 79% of the controls depending on the parent end surface.

In the present study, a total of 769 joined cylindrical amalgam samples were manufactured using vibration procedures and successfully tested under three point loading with the joint at the centre of the span. Although 456 samples failed at the joint, failure originated in 241 parents and 72 additions showing that the joint was not the weak link in about 40% of tests. The amalgam alloys used included conventional, HCSC spherical and lathe cut, blended, hybrid and admixed types and all produced joints which did not fail.

A limited number of samples were notched adjacent to the joint and fractured under three point loading with the joint slightly off centre in the test rig. The fracture path traversed the joint interface and terminated at the location of the applied load. When the notch was located at the joint, the fracture path started at or adjacent to the joint but departed from it about halfway through the sample.

## 7.1 Sample preparation and test

The present study used amalgam mixes from alloys supplied both as powder triturated in a Dentomat and precapsulated varieties: there was no mercury enrichment. Three point loading to fracture of joined samples in this study was carried out (with few exceptions) seven days after joining to seven day old parents. Although long term strength and phase changes may occur, the use of those time intervals is regarded as a reasonable approximation to the mature joint strength with fully set parents. Further work on preparation and test of older samples should be carried out to confirm this supposition for all alloy types. Testing of immature joint strength, manufacture of joints with young parents and use of intermediate bonding resins or adhesives were not undertaken.

The amalgam condensation procedures used shaped vibration tools developed for this purpose and vibration is considered essential to the successful manufacture of strong joined samples. Although hand condensation procedures for the preparation of joined amalgams have been used by many workers, clinical methods are potentially variable and only Kirk (1962) has been successful in the production of samples which did not break at the joint. Clinical amalgam vibration instruments were used with moderate success by Nagaoka *et al* (1974) and Fukuba *et al* (1977) but such tools produced bonds of limited strength when used by Hornbeck *et al* (1986), Schaller *et al* (1989) and Erkes *et al* (1990). Miyata (1972) found little improvement in joint strength when mechanical condensation was used.

Early in this study, crevices were found at the joint in samples prepared by the author's clinical method using vibration with a cylindrical piston (diameter 1.14mm). These were considered to result from incompatibility between the cylindrical condensing tool and rectangular mould and the inability to evenly

distribute the vibration forces or strains since square corners will be "dead" zones. Many authors have used rectangular moulds where amalgam was condensed from the long open face. Erkes *et al* (1990) used the Condensaire vibration tool with a cylindrical piston 2mm in diameter but did not report crevices at the joints (which were weak). Nettelhorst (1977) used a special trapezoid-shaped condensing instrument for hand condensation in the rectangular mould but no attempt was made to rub the new mix against the parent amalgam surface: the joined samples were weak. Terkla, Mahler and Mitchem (1961) considered the direction of hand condensation (parallel or normal to the parent surface) as a variable: no significant difference in transverse strength was found but joints to 7 day old parents were less than one third as strong as the one-piece controls. In these and other reports, excess material forming a mercury rich layer was removed in keeping with clinical methods. The trimmed surface was within the tested part of the sample and its quality was determined by the operator and therefore susceptible to variability.

In this study these possible operator variables were overcome by preparation of cylindrical samples in a split mould incrementally condensed from the end. The mix was confined by close fitting pistons and only liquid mercury (with dissolved metals and possibly small alloy particles in suspension) was removed during condensation. If a mercury rich end surface layer formed this was not located within the tested area for one-piece samples. A surface layer (of variable thickness) was removed during preparation for joining and the first addition increment condensed by vibration acting at right angles to the parent end. Although the timing of sample preparation was potentially variable, these methods were considered to offer improved control of sample manufacture.

Application of a static load in this study for condensation of the added amalgam without mercury treatment produced weak joints which agreed with

the results of Jørgensen and Saito (1968) and Berge (1982). Bass (1985) hand wound a Hounsfield tensometer to produce the considerable pressure of 55 MPa for one minute and the joints were also weak.

In the present work, the mean force to fracture for one-piece samples when prepared in a manner similar to BS 2938: 1985 was less than that for joined samples condensed by vibration with special pistons. However, a considerable increase in strength resulted when one-piece samples were condensed using experimental vibration pistons than when condensed under a static load. A possible criticism of the adapted Burgess engraving tool which was used for condensation was that it was unrefined. Its merits were that it was convenient in use, inexpensive, easily adapted, appeared to condense amalgam effectively and produce strong joints. These features are considered advantages over those of the mechanical devices of Ware and Docking (1954), Nagai *et al* (1966), Basker and Wilson (1969) and the hydraulic machine of Nagai *et al* (1967), none of which were used for joined sample manufacture. A limitation of this study was that it was not possible to record the waveform of the piston movement and condensation forces applied.

Walker and Reese (1983) calculated a Modulus of Rupture for their cylindrical samples after fracture under three point bending using a formula which omitted  $\pi$  from the denominator though this may have been a typographical error. Brown *et al* (1986) were unable to reconcile the modulus obtained for four point loaded Tytin one-piece controls with the results of Walker and Reese which differed by a factor of two. The reliability of these calculated values for Modulus of Rupture are considered to be somewhat doubtful.

Jones and Berard (1972) suggested that corrections were to be applied to results when the ratio of span to sample thickness was less than 10 to 1 or if the fracture occurred away from the centre of the span. However, the corrections were not specified and no reports of their use have been found.

Terkla *et al* (1961) used rectangular samples, 4mm wide x 1mm thick, tested on a 10mm span which therefore met the above dimensional requirements. Mahler and Mitchem (1964) considered that a flexural strength test might become standard as it combined compressive, tensile and shear stresses and was independent of loading rate in the range studied but this has not happened. Samples only 1mm thick were considered to be inconveniently thin for use in this study. Flat samples might also be sensitive to torsion if the loading bars of the test rig were non-parallel and nominally flat sided samples could be twisted or unevenly loaded due to surface roughness. Any possible effect due to these considerations was overcome in this study by the use of cylindrical samples. A further advantage of the flexural over the tensile test is the latter's requirement for specially shaped samples, mould and grips.

This study used the methods of Jørgensen and Saito (1968) and Berge (1982) where the recorded force to fracture was taken to represent sample strength and no further calculations were made. This is a simplification because if a joined sample fails elsewhere, the joint survived the applied stress. One does not know if the joint was close to breaking or was well within its capacity.

Tensile tests give the ultimate strength of the sample part which failed, whether or not this was at the joint. Under three point loading, the stress due to bending reduces with increasing distance from the central load. If a sample failed other than at the centre of the span, failure occurred at a lower bending stress than the recorded force to fracture would suggest. These considerations represent limitations of the work in this study: the force to fracture in three point loading was the value recorded.

Joined specimens were located in the three point bend rig with the joint at the central load so that stresses were concentrated at the interface. The test used was therefore a rigorous test: specimens which failed to fracture at the joint interface had endured "worst case" conditions.

No allowance was made in the analysis for variations in sample diameter on the force to fracture. Surface roughness due to irregularity of the mould might have given a small error in the measured diameter. Roughness due to surface open porosity caused by bad condensation might act as a stress concentration feature and possibly cause a severe reduction in force to fracture.

The author's expectation at the start of the study was that the strength of joined samples could be related to that of one-piece samples as reported in all previous work in this field. The fact that this did not happen may be a limitation of the methods used for one-piece sample preparation. However, scatter in the force to fracture values obtained caused the author to explore methods other than recorded force to fracture in destructive tests to demonstrate the strength or integrity of the joint.

No reports have been found of the testing of notched joined samples by eccentric placement of the joint in a three point bending rig. Bass and Wing (1991) carried out microstructural examination of reassembled fractured amalgam samples but the use of reassembled notched joined samples in this study to demonstrate the fracture path in relation to the joint is original.

The notching procedure was subject to some difficulties. The sample notch was not always placed in the intended location and a number of samples fractured during machining of the notch. Possibly for future work, a spark erosion, grinding or other precision cutting technique might be used to produce suitable notches without causing premature failure.

Although samples showed some interface failure when notched at the joint, the fact that the fracture path departed from the joint under slightly eccentric loading indicates that the joint was probably stronger than the material through which the crack propagated at the point of departure. This might not

be the case where departure from the joint occurred close to the central load or if the joint was substantially off-centre in the three point bending rig (as was the case in Bass and Wing's work above).

Further study is required to elucidate the effect on crack path of variations in strength of the inhomogeneous material on a microstructural scale. It seems that there may sometimes have been a gradient of strength from the central part of the parents to the joint end surface when the crack direction was initially away from the joint. This was notwithstanding the fact that the stress due to bending was concentrated at the centre of the span and the crack path would have tended to "lean" towards the central loaded area.

In samples notched in the addition and loaded on the parent, the end surface of the parent appeared to resist penetration of the advancing crack. The surface appeared to be more fracture resistant or "harder" than the adjacent addition material. When the parent was notched and the addition loaded, the fracture was not deflected because any increase in "hardness" occurred gradually: there was no abrupt change. Microhardness tests might reveal a gradation in hardness, but it is possible that variations in hardness or strength may be too small for detection by such tests. Further work on joined notched samples prepared from different alloys using for example the Paddle, RI or flat ended pistons may reveal differences in the joints.

Stress concentration by notching appeared to change the mode of failure, possibly causing failure in a notch tip zone where the crack will initiate and propagate somewhere within this zone and be dependent on microstructural properties. Crack formation in notched amalgams should be studied further.

This study has shown that mercury treatment (either liquid applied to the parent or use of a mercury rich first addition increment) is not necessary for

the production of strong amalgam joints. Since no special mercury treatment or mix enrichment was carried out in this study, this aspect of preparation procedures regarding any possible sample weakness or improved strength in the joint remains controversial. Future use of the preparation procedures described in this thesis with mercury enriched amalgam mixes could clarify the position regarding its influence on sample and joint strength.

A limitation of this study was that chemical analysis of the sample mercury content was not undertaken. Although determination of average mercury content was carried out by Jørgensen and Saito (1968), layering was observed in samples in this study. Mercury content could therefore vary within samples and average values for entire samples might not relate to the mercury content of the material which failed under test.

## 7.2 The nature of the joint

Published views on the nature of the joint were considered briefly in Section 3.6. Micrographs are included in this thesis showing fractures passing through residual alloy particles at the joint which indicates that they were attached to the new matrix (see for example Figures 79 and 104). Intimate contact on an atomic scale must have occurred between the new and old material for the joint to be strong enough for the fracture to take a path which traversed or departed from it. Set amalgam is composed of unreacted original alloy particles, the products of the setting reaction and porosity. Unreacted alloy particles in the parent, freshly exposed by the end preparation procedure, may dissolve in and absorb mercury from the new mix in the same manner as occurs in the normal setting reaction.

It is considered that reactions with unconsumed gamma particles may contribute to joint strength. However, matrix phases may predominate over

unreacted alloy in a set amalgam and therefore a contribution to strength in strong joints could have been made by atomic attractions between the new and old matrix. The nature of any possible reaction between mercury in the added mix and matrix in the parent is not known.

Jørgensen (1965a) found that amalgam condensed by vibration exhibited good adaptation to the mould. In this study, when vibration condensed samples failed at the joint the addition fracture surface showed evidence of the end preparation pattern of radial scratch marks. Vibrated condensation might therefore produce strong joints by minimisation of voids or trapped air and promotion of close physical contact between the parent and added materials.

Two factors which could affect sample strength after condensation using vibration are its duration and the pressure applied throughout the amalgam increment. The volume of each increment was subject to some variation since division of the mix was estimated "by eye" and the total quantity triturated differed by brand. Such variations could have influenced the condensation pressures applied both within and between samples. It could be considered that the RI piston, rotated during use, applied forces to a smaller area and thereby increased the condensation pressure. Joined samples prepared using only a flat piston on each increment were weaker than those where the RI piston was used for the same periods. Use of the RI piston for 10s (Batch 15) compared to 2s increased the joint strength to the extent that all samples failed in the parent at a similar mean force to fracture.

Only four out of 190 joined samples from Batch 1 to Batch 30 inclusive where the first increment had been condensed using either flat or RI pistons failed in the addition. The design of the Paddle piston was considered with a view to reduction of addition strength (so that the addition part might fail more frequently) whilst maintaining joint strength.

Compared to the RI or flat ended pistons, use of the Paddle could have improved the wetting of the prepared parent surface by mercury in the new mix perhaps aided by abrasion with solids in the paste. Localised heating due to friction during vibrated condensation could increase dissolution of parent phases. The possible contributions of these suggested mechanisms to joint continuity and strength are not known but should be studied further.

Nucleation of new matrix phases may occur on solids in the old amalgam, either unreacted alloy particles or matrix phases, making close contact with them as the crystals grow. In the absence of wetting of the old amalgam surface with mercury, neither dissolution nor nucleation at the interface is likely to occur. A weaker joint could therefore be expected.

Closeness of the contact between old and new solid phases might be influenced by any volumetric changes accompanying setting. A reduction of new phase volume might cause microporosity but a slight increase in phase volume could force closer contact of new phases with the parent matrix.

The relative importance of contributions to strength of joint by the matrix or residual particles might be investigated by examination of amalgams with differing final mercury contents. Spherical particle alloys require less mercury than lathe cut types for amalgamation and differing condensation methods may lead to variations in the residual mercury content of the amalgam. Accordingly, the relative proportions of matrix to residual alloy in the set amalgam microstructure may vary. Variations in the rate of development of strength in the joint may occur between these differing amalgams.

Leelawat *et al* (1992c) made repairs to amalgam restorations in extracted teeth. When no intermediate varnish or resin coating was used on the parent surface, micrographs of the joint interface showed large voids with small

islands of matrix continuity. No similar appearances were seen in this study but in small numbers of samples small areas of porosity with larger zones of apparent matrix continuity at the joint were seen.

It was difficult or impossible to identify the joint in the microstructure in amalgams from lathe cut alloys. However, in amalgams containing spherical particles which were cut during the end preparation procedure, the joint was defined.

In dispersed phase amalgams, the fracture path tends to circumvent the residual spherical Ag-Cu particles in the parent. Poor interphase bonding may be caused by any volume change of reaction products in the ring around those particles. In this study, evidence of a partial reaction layer was seen on the addition side of cut spherical Ag-Cu particles. Dispersalloy sample R6 (lower part of Plate 125, page 259) shows a typical "hole in the reaction layer". Possibly tin was attracted to copper in the cut surface from the surrounding new matrix. This precipitated as Cu-Sn close to the existing exposed reaction ring. However, due to competition with other sources of copper, the supply of tin became exhausted and therefore the reaction layer in the centre of the cut area was incomplete. Any volume changes, with associated microporosity which might have occurred, were reduced. In Amalcap sample P6, a cut residual particle in the parent was sufficiently strongly attached to the new matrix for the fracture to take the path around the curved surface between the particle and the parent where interphase bonding was weakest (Plate 119, page 252).

Medium grade sandpaper discs were used for end preparation throughout this study. Finer grades might have produced a smoother surface but these were considered to produce a greater tendency to smearing rather than clean cutting of the prepared surface.

It is estimated that the dimensions of the sandpaper scratches used for end-preparation were large compared to the size of gamma-1 grains in the addition and small compared to residual alloy particles. Each scratch may be regarded as a trough with associated micro deformation of the amalgam phases. Possibly, movement of growing phases with or without enhanced diffusion resulting from the higher energy state from deformation could lead to improved bonding than might occur if the bonding surface was flat. Nagaoka *et al* (1974) found that a polished surface gave a poor bond strength. It is possible that the presence of an amorphous Beilby layer or surface oxidation or contaminant was responsible because a plain-cut tungsten carbide fissure bur gave a reasonably smooth surface and the joint was about 50% of the strength of the controls. Fukuba *et al* (1977) found that a plain-cut tungsten carbide fissure bur and a spherical particle low copper amalgam alloy produced their best joints which were 92% as strong as the controls.

Watts *et al* (1992) found that a polished or smooth surface gave a poor bond strength when a repair was made using a phosphonated anaerobic resin adhesive (Panavia-Ex) to bond amalgam to brass rods. The joints were weak and no samples failed in the amalgam. There was considerable scatter in their results for strength (COV from 38 to 57%); in some cases factor of more than 10 covered the range from strongest to weakest: the bond was unreliable and was not compared to one-piece sample strength. They used Weibull analysis (Weibull, 1951) which can be used where extreme range in results occurs, for example in fatigue testing. Had the results in this study exhibited such wide variations, attention would have been given to modification of the preparation methods for improved reliability. No work has been found reporting Weibull analysis in work on amalgam to amalgam joints and its use was considered unnecessary for the statistical analysis of these results (Wynn, 1994).

The  $\frac{1}{4} : \frac{1}{2} : \frac{1}{4}$  hypothesis (Section 4.7.5) was tested by Chi-squared on a three

by two table against the location of fracture origin for each Set. There was sufficient evidence for its rejection in only two cases: Set 1 and Set 4, where more than half of failures originated in the parent parts (Appendix 5). In the pooled results for Sets 12 to 15, the test was also significant. In all three cases, Fisher's exact test for the subsets individually was significant for Parent and Addition failures. Fisher's test of the  $\frac{1}{4}:\frac{1}{2}:\frac{1}{4}$  hypothesis gave significant results in 17 out of 69 cases and was therefore considered to provide more useful information on the differences in test outcomes than the Chi-squared test on the three by two table. Taken as a whole, the results of these tests are incompatible with substantially weak joints having been prepared in this study. Frequently, fewer samples failed in the addition than expected under this hypothesis. Possibly for future work, sample preparation procedures could be modified with a view to further increasing the frequency of addition failures. The  $\frac{1}{4}:\frac{1}{2}:\frac{1}{4}$  hypothesis is considered a reasonable reference point for future work.

The setting reaction of amalgam may never reach equilibrium. In the first period after mixing and condensation of an amalgam, the reaction is strongly in favour of dissolution of original alloy and precipitation of matrix. As mercury is consumed, the reaction approaches equilibrium and its speed reduces. It may be possible that the act of cutting the old matrix during the end preparation procedure using sandpaper raises the free energy of those surface deformed layers. In near equilibrium conditions, these higher energy atoms may preferentially enter solution rather than those more recently precipitated on the surface of growing crystals. Eventually, all of those high energy atoms may undergo dissolution and contribute to further crystal growth elsewhere. The matrix microstructure may then appear to be continuous through the joint.

The final structure of set amalgam may be likened to the overlapping of bricks

in a wall where the residual alloy particles represent the bricks and the matrix the mortar. It is generally held that residual gamma ( $Ag_3Sn$ ) alloy particles are stronger than matrix and fractures tend to circumvent them. Setting occurs as a result of development of strength in the matrix. When a partially set amalgam fails, shear strains must occur in the matrix due to movement between adjacent residual alloy particles. The more advanced the setting reaction, the more resistance given by the matrix. At the joint, there can be no overlapping of residual alloy particles: there must be a band exclusively formed from new matrix (see for example Plate 94, page 228). Any increase in shear strength of the matrix during setting does not resist separation of the residual alloy particles on either side of the joint. The joint becomes strong only on development of resistance of the matrix to tensile stresses.

These suggested mechanisms may account for the finding of Jørgensen and Saito (1968) that the development of strength in the joint increased at a slower rate than that occurring in amalgam setting normally. In this study, preparation and test of joined amalgams was carried out on set samples, normally after 7 days. There was no testing of immature joints which should be carried out in future work.

### **7.3 Conclusions and the relation of this work to dental practice**

The author believes that the interdisciplinary approach which has been available in this study has been instrumental in achieving the results obtained. There has been an uncommon combination of circumstances leading up to the work reported in this thesis. Further investigation of the subject might never have been contemplated but for the adverse reception of the clinical repair procedure by some dentists. The view was held that amalgam repair was one of the most useful operative procedures available in the clinical repertoire. An obligation was felt to share the experience with the profession for the greater

good of humanity (Cook, 1981b; Appendix 7).

As a non-engineer in the Mechanical Engineering Department of City University, where dental amalgam had never previously been studied both the author and the academic staff were able to view the subject afresh.

Fruitful discussions have been held with specialists in many fields. The availability of such diverse expertise has improved the author's insight into materials and test procedures, resulting in the development of the techniques used. The tolerance of these experts in explaining their knowledge in terms a dentist could understand was essential and most appreciated. The author hopes that the flow of information and ideas was not always unidirectional.

It is considered strange that more than thirty years have elapsed since Kirk (1962) reported the tensile strength of his joined amalgams and yet the belief has been expressed by dental authorities that the material cannot be repaired or resurfaced (Bayne, 1988).

The author's clinical amalgam repair technique has been modified as a result of study for this work. In the freshening-up treatment of the old amalgam surface, it is no longer considered necessary to roughen the surface: only a fresh diamond-cut surface is required. Conventional Amalgam M has been replaced by the gamma-2-free Aristaloy 21 HCSC blend, mixed in a Dentomat as before. Sufficient mercury should be used in the mix for good coherence of the amalgamated mass: a dry mix should be avoided. For amalgam addition restorations the height of the cusp need not be shortened unduly to reduce occlusal stresses. The importance of repeated use of a burnisher after carving and shaping is emphasised. When possible, light hand application of a burnisher or smooth metal instrument to the entire new amalgam surface repeated at intervals up to 15 minutes after condensation is recommended.

The author used Amalgam M conventional alloy for amalgam restoration repair for more than two decades. At the time of writing, the author's clinical experience of only 2 years duration with Aristaloy 21 suggests satisfactory bonding behaviour. Osborne *et al* (1991) used Ridit analysis (Relative to an Identified Distribution) to assess differences in the marginal quality of clinical restorations in service. At the 14 year follow-up, the extent of marginal deterioration was well correlated with quality assessments made after a 1 year period. If these findings apply to repaired amalgam restorations, the author anticipates that long term experience will confirm his present opinions.

Many reports suggest that the significance of reduced strength in repaired amalgam restorations can be limited by placement in areas away from maximum stress. These texts emphasise the need for independent mechanical retention by dovetails and undercuts. The author believes that such devices may be counter productive. They impede movement of the new amalgam mix on the prepared surface and therefore possibly reduce the wetting of the old amalgam by the mercury in the new mix. Imperfect adaptation of amalgam into the small recesses may occur. For this reason roughening of the prepared surface has been abandoned in the clinical cusp repair procedure.

A possible criticism of many papers on amalgam joints is the implied assumption that conclusions from laboratory experiments could be applied directly to predict the clinical behaviour of repaired dental amalgam. The author has attempted to construct a laboratory simulation of the clinical amalgam repair procedure which has been used for over two decades. Although it is believed that this objective was met, the results of this laboratory work should not be taken as a prediction of the strength of clinical amalgam repairs. Carr-Hosie *et al* (1992) commented that the exact clinical relevance of their *in vitro* study could only be conjectured. Moderate scatter in the results of strength tests has occurred. Under clinical conditions, where

the working environment may be subject to many uncontrollable variables, the reliability of amalgam repairs has yet to be determined scientifically. No controlled clinical trials of amalgam repair procedures have been reported (Erkes *et al*, 1990). The author's experience, stated in Dental Update (Cook, 1981a), that the clinical bond rarely fails remains unchanged.

Silver amalgam has sustained popularity in dentistry over the years because it can provide serviceable dental restorations when used under less than ideal circumstances. Further work may clarify the "user tolerance" of the different amalgam alloy formulations. Alloys which produce acceptable repairs more easily or under adverse clinical conditions must be preferred to those which demand strict attention to detail of technique. Some alloy types may be better suited for use as a "parent" or "addition" which may help in alloy selection for future clinical use.

It is considered possible that excessive dimensional changes during setting in the addition amalgam could prestress the joint. If an amalgam resists creep, then such stresses could remain, whereas modest creep might slowly reduce their effect. Alloys for which the trituration time and handling are critical to development of optimum dimensional changes would fare less well than those which were more tolerant of these variables. In experimental work undertaken at City University (private communication, Dr J.D.R. Walker), admixed alloys were most critical to variations in trituration time when this was assessed as a multiple of the coherence time (Brockhurst and Culnane, 1987). Additional work may be done on the amalgam mix during application of the "Paddle" to the first addition increment, effectively extending the trituration time, which might therefore affect the properties of the added amalgam. In this study, secondary cracks were seen adjacent to the fracture path in admixed amalgams. This may indicate a critical aspect of the behaviour of HCA amalgams in joining.

Ideally, the strength of bond and clinical life expectancy of an amalgam repair should be correlated with simple standard laboratory tests.

#### **7.4 Further work**

The work reported here should be re-examined and repeated by workers in other centres. An assessment should be made of results of the laboratory procedures for comparability with clinical repairs. Any critical aspects of the restorative procedure should be identified.

Further refinement of the laboratory procedures could improve the reproducibility of the methods. BS EN 21559: 1992 prescribes the use of an amalgam condenser slightly less than 4mm in diameter to pack the amalgam mix into the mould before application of the 14MPa condensation pressure which was not required under BS 2938: 1985. Use of longer experimental condensation times (for example, 2, 3 or 5 minutes) than those prescribed is suggested to determine the optimum condensation time for any particular amalgam alloy mix.

Vibrational condensation methods have led to the production of strong amalgam samples, both one-piece and joined. These methods are considered to be essential for the production of strong joints and should be reassessed with a view to measurement and control of the vibration waveform and applied forces with the special pistons used.

Relatively few notched joined samples have been prepared and tested. This work may be regarded as a pilot study in this regard. Sufficient numbers of these should be used to enable conclusions to be made with the added confidence of repeatability.

The nature of the metallurgical bond should be investigated. The rate of development of early strength in joined samples should be studied using a range of test machine crosshead speeds. Similarly, study of the fracture path relative to the immature joint in notched and offset loaded samples may help in the determination of the mechanism by which the bond is formed.

Use of finite element analysis methods may clarify reasons for deviations in fracture path within the amalgam cylinder, particularly in the region of the joint. However, the limitations of such analyses are appreciated because of the microscopic inhomogeneous nature of dental amalgams which are multiphased and the possible net sizes which would be needed.

Corrosion of repaired amalgams should be studied. Hibler *et al* (1988) recommended the use of the same brand of alloy in the repair as used in the original amalgam. For practical purposes this would restrict amalgam repair to the dentist who placed the original restoration and assumes that he had recorded the alloy brand and that it was still available. Skinner and Phillips (1967) considered that bond weakness and corrosion processes at the joint interface presented "formidable barriers" to the integrity of the repaired restoration. However, whether or not significant corrosion in the original and repair amalgams occurs in service and its effect on strength of the joint has yet to be determined.

All previous reports have assessed the strength of the joint in a short time destructive test. It is not known whether joints found to be strong in this way would necessarily have survived well in long term use. Rotary fatigue testing of the cylindrical bar joined samples or prolonged subfracture loading might be used to detect differences between alloy types or preparation procedures.

This study has been restricted to amalgam alloys composed of silver, tin and

up to 24% copper which may also contain zinc. Alternative alloys are available containing palladium, indium, or up to 30% copper. Cruickshanks-Boyd (1983) found that although in 12% copper HCSC amalgams the fracture path passed through residual alloy particles (which was found in this study), in 30% copper all-spherical HCSC amalgam (Sybralloy) the fracture path tended to circumvent these particles. Inclusion of a wider range of alloy types in further studies would be advantageous.

Elderton and Mjör (1992) commented that marginal deterioration of amalgam restorations was not in itself sufficient reason for replacement. Although it was suggested that repair rather than replacement should be undertaken, the subject was not considered for future research; *e.g.* methods by which strong repair joints might be achieved or assessment of their clinical success. The use of effective clinical amalgam repair procedures for the resurfacing of restorations with marginal deteriorations in the absence of dental caries could prolong service life and delay progress down the "restorative spiral".

The author's belief is that many dental patients experience pain and discomfort and are exposed to the risks which accompany restorative dental treatment unnecessarily. Dentists should repair rather than replace dental amalgam restorations where appropriate. It is hoped that dental teachers may read or review the author's clinical procedure and thesis. After clinical trials to validate their merits, the teaching of amalgam repair techniques and their use in suitable cases, possibly in combination with adhesive resins for bonding amalgam to tooth substance, may benefit many people.

## **7.5 Originality of this work**

Successful results in this study could not have been obtained had the sample preparation methods been ineffective. Parts of the experimental equipment

and procedures used were adapted from published work while other parts have been developed independently by the author. Two reports have been found including small numbers of joined samples which did not fail at the joint: conventional low copper amalgam alloys were used. No reports have been found where amalgams from high copper alloys have produced joints as strong as the one-piece controls or where the joints did not fail.

The proportion and total number of samples where the joint survived the rigorous test represent a substantial original contribution. No reports have been found where failures occurred in the parent, joint or addition parts in sufficient numbers for comparison of their respective cumulative failure curves and force to fracture data.

Penetration of mercury from one lumen to the next in the multiple sample split mould was controlled by pressure relief channels and ingress of foreign matter and mercury at the top of the mould was prevented by use of tapered plastic plugs which have not previously been reported.

No reports have been found where the amalgam condensation procedures used close fitting pistons for application of axial vibration to the divided mix. Use of the adapted engraving tool and modified chuck with shaped and flat ended pistons (with or without a worn edge) for one-piece sample preparation are original. Use of shaped pistons *i.e.* the "Rubbing-in" piston and the "Paddle" with its adjustable resilient support mechanism for condensation of the first addition increment are original.

The end preparation procedure where the marked parent sample was gripped in the adapted drill chuck for spinning during abrasion is original. Examination of fracture surfaces for evidence of the characteristic pattern of radial scratch marks so produced revealed the extent to which the joint interface was

involved in the fracture path.

The three point bend test rig used threaded rods to control test sample location. This original feature enabled placement of the joint interface in the desired location with respect to the loaded roller bar and centre of the span.

No reports have been found where notched and offset loaded joined samples have been tested and reassembled after fracture for microstructural examination of the fracture path in relation to the joint.

The fact that the force to fracture values for one-piece samples generally could not compare with those for joined samples is considered to be a limitation of this work. However, no reports have been found where the force to fracture for joined samples exceeded that for samples condensed in one piece by the British Standard method.

## **7.6 The contribution to knowledge**

This work has shown that it is possible to manufacture joined dental amalgams where the joint is not weak. The experimental preparation and test procedures developed in this study could be used as described for further study of the joining of new to old dental amalgam.

Previous workers have found that high copper alloys produced weaker joints than alloys of conventional composition but all alloys tested produced strong amalgam joints when prepared by the vibration methods used in this study.

The strength of joint relative to that of the parent or addition material has been demonstrated by the use of cumulative failure graphs for the subsets and by the crack path in notched, offset loaded and reassembled samples.

Study of the microstructure after fracture has demonstrated continuity of matrix across the joint interface and residual alloy particles from the parent were attached to the added material. An incomplete reaction layer against the cut surface of silver-copper eutectic spherical particles at the joint in the parent part of high copper admixed amalgams has been shown.

## 7.7 Conclusions

1. The results of this study disagree with the conclusions of earlier workers that there is always a substantial reduction in strength when new dental amalgam is condensed against old.
2. Use of abrasion to the repair surface and vibrational condensation of the addition amalgam using special condensing pistons produced strong joints when tested after 7 days.
3. The force to fracture for joined samples under 3 point loading generally exceeded that required to fracture one-piece samples which had been condensed using a static load.
4. Each amalgam alloy type used, *i.e.* conventional, HCSC and HCA produced strong joins.
5. Mercury enrichment of the amalgam mix for the addition was not necessary for the production of strong joins.
6. The fracture path traversed or followed and then departed from the joint when notched samples were loaded adjacent to the joint.
7. In the microstructure of amalgam prepared from lathe-cut alloy, it was difficult to identify the exact location of the joint, but in amalgam prepared from alloys with spherical particles, the joint was identified by flat cut surfaces in the residual alloy.
8. An incomplete copper-tin reaction layer was formed in the addition matrix adjacent to the flat cut surface of residual silver-copper alloy particles in the parent material at the joint interface.
9. There were areas of matrix continuity across the joint interface.

## References and Bibliography

- American Dental Association, (1977)  
Revised American Dental Association Specification No.1 for Alloy for Dental Amalgam.  
*Journal of the American Dental Association* **95**: 614-617.
- Allan, F.C., Asgar, K., Peyton, F.A., (1965)  
Microstructure of Dental Amalgam.  
*Journal of Dental Research* **44** (5): 1002-1012.
- Armitage P., Berry G., (1987)  
*Statistical methods in medical research*. 2nd edition: 115-132.  
(Oxford: Blackwell Scientific Publications).
- Asgar, K., (1971)  
Behaviour of Copper in a Dispersed Phase Amalgam Alloy.  
*Journal of Dental Research* **50**: IADR/AADR Program and abstracts of papers, No. 15.
- Asgar, K., (1974)  
Amalgam Alloy with a Single Composition Behaviour Similar to Dispersalloy.  
*Journal of Dental Research* **53**: 60. IADR/AADR Program and abstracts of papers, No. 23.
- Ayers, H.D., Cagan, R.S., (1964)  
Mercury at Amalgam Interfaces.  
*Journal of Dental Research* **43** Supplement to No. 5: 922, IADR Abstract M30.
- Bagheri, J., Chan, K.C., (1993)  
Repair of newly condensed amalgam restorations.  
*Iowa Dental Journal* **79** (3): 13-14.
- Bapna, M.S., Mueller, H.J., (1989)  
Diametral stress and fracture toughness of repaired amalgams.  
*Journal of Dental Research* **68**: 188 Abstract No. 55.
- Bapna, M.S., Mueller, H.J., (1993)  
Fracture toughness, diametral strength and fractography of amalgam and of amalgam to amalgam bonds.  
*Dental Materials* **9**: 51-56.
- Baratieri, L.N., Monteiro, S. Jr., de Andrada, M.A.C., (1992)  
Amalgam repair: a case report.  
*Quintessence International* **23** (8): 527-531.
- Barbakow, F., Gaberthuel, T., Lutz, F., Schuepbach, P., (1988)  
Maintenance of amalgam restorations.  
*Quintessence International* **19**: 861-870.
- Basker, R.M., Wilson, H.J., (1969)  
A machine for packing amalgam specimens under simulated clinical conditions.  
*British Dental Journal* **126**: 209-215.
- Bass, E.V., (1985)  
Amalgam Repair. MDS thesis: University of Sydney, Australia.
- Bass, E.V., Wing, G., (1985)  
The strength and microstructure of joined amalgams of different copper contents.  
*Journal of Dental Research* **64**: 652 Abstract No. 19.
- Bass, E.V., Wing, G., (1991). Personal communication.

- Bayne, (1988)  
*Advances in Dental Research* 2 (1): 90.  
 In discussion following Amalgam: Reactor Response by Marek, M.I.
- Berge, M., (1982)  
 Flexural Strength of Joined and Intact Amalgam.  
*Acta Odontologica Scandinavica* 40 (5): 313-317.
- Berry, T.G., Laswell, H.R., Osborne, J.W., Gale, E.N., (1981)  
 Width of isthmus and marginal failure of restorations of amalgam.  
*Operative Dentistry* 6: 55-58.
- Boswell, P.G. (1980)  
 The suppression of gamma-2 precipitation and the kinetics of gettering on Sn in dispersed phase dental amalgam.  
*Journal of Materials Science* 15: 1311-1315.
- BS 2938: (1961)  
 British Standard Specification for Dental amalgam alloy.  
 British Standards Institution.
- BS 2938: (1985)  
 British Standard Specification for Dental amalgam alloy.  
 British Standards Institution.
- BS EN 21559: (1992)  
 Specification for alloys for dental amalgam.  
 British Standards Institution.
- Brockhurst, P.J., Culnane, J.T., (1987)  
 Optimization of the mixing time of dental amalgam using coherence time.  
*Australian Dental Journal* 32 (1): 28-33.
- Brown, K.B., Molvar, M.P., Demarest, V.A., Hasegawa, T.K.Jr., Heinecke, P.N., (1986)  
 Flexural strength of repaired high-copper amalgam.  
*Operative Dentistry* 11: 131-135.
- Brown, K.B., (1994). Personal communication.
- Carr-Hosie, M.A., Miranda, F.J., Collard, E.W., Duncanson, M.G.Jr., (1992)  
 The effect of Amalgambond on the flexural bond strength of dental amalgam.  
*Journal - Oklahoma Dental Association* 82 (3): 20-24.
- Chen, C.P.W., Greener, E.H., (1977)  
 A galvanic study of different amalgams.  
*Journal of Oral Rehabilitation* 4: 23-27.
- Consani, S., Ruhnke, L.A., Stolf W.L., (1977)  
 Infiltration of a radioactive solution into joined silver-amalgam.  
*Journal of Prosthetic Dentistry* 37 (2): 158-163.
- Cook, A.H., (1981a)  
 Amalgam Addition Restorations.  
*Dental Update* 8 (6): 457-463.
- Cook, A.H., (1981b)  
 Response to a letter to the editor.  
*Dental Update* 8 (8): 601.

- Corbin, S.B., Kohn, W.G., (1994)  
The benefits and risks of dental amalgam: current findings reviewed.  
*Journal of the American Dental Association* 125: 381-388.
- Cowan, R.D., (1983)  
Amalgam Repair - A Clinical Technique.  
*Journal of Prosthetic Dentistry* 49 (1): 49-51.
- Cruickshanks-Boyd, D.W., (1983)  
Physical metallurgy of dental amalgams.  
3. Transverse strength and fracture behaviour during setting.  
*Journal of Dentistry* 11 (3): 214-223.
- Curtis, R.V., Brown, D., (1992)  
The Use of Dental Amalgam - An Art or a Science?.  
*Dental Update* 19 (6): 239-245.
- de Freitas, J.F., (1979)  
A survey of the elemental composition of alloy for dental amalgam.  
*Australian Dental Journal* 24 (1): 17-25.
- Degussa Ag, (1990). Personal communication.
- Dwyer, S.L., (1981)  
Letter to the editor.  
*Dental Update* 8 (8): 601.
- Eames, W.B., (1959)  
Preparation and condensation of amalgam with a low mercury-alloy ratio.  
*Journal of the American Dental Association* 58: 78-83.
- Eames, W.B., (1967)  
Factors influencing the marginal adaptation of amalgam.  
*Journal of the American Dental Association* 75: 629-637.
- Elderton, R.J., (1977)  
The quality of amalgam restorations. *In: A series of monographs on the assessment of the quality of dental care.* (Ed: H. Aldred)  
London: London Hospital Medical College: 45-81.
- Elderton, R.J., Mjör, I.A., (1992)  
Changing scene in cariology and operative dentistry.  
*International Dental Journal* 42: 165-169.
- Engelhard Ltd., (1992). Personal communication.
- Erkes, E.O., Burgess, J.O., Hornbeck, D.D., (1990)  
Amalgam repair: an in vitro evaluation of bond integrity. .  
*General Dentistry* 38 (3): 203-205.
- Espevik, S., (1977)  
Creep and phase transformation in dental amalgam.  
*Journal of Dental Research* 56: 36-38.
- Espevik, S., (1980)  
Properties of amalgams made from lathe cut, high Cu amalgam alloys.  
*Acta Odontologica Scandinavica* 38: 145-150.

- Finkel, A.N., Ayers, H.D., Cacioppi, J.T., Guggenheimer, J., (1962)  
Physical Properties of Amalgam Joints.  
International Association for Dental Research 40th General Meeting,  
*Journal of Dental Research Supplement*, 41 (5): 96 I.A.D.R. Abstract M41.
- Fitch, D.R., Boyd, W.J., McCoy, R.B., Pelleu, G.B., (1982)  
Amalgam repair of cast gold crown margins: a microleakage assessment.  
*General Dentistry* 30 (4) Jul-Aug: 328-330.
- Forsten, L., (1969)  
Styrkan av fordbindelsen mella - nyft och gammalt amalgam mott med bojfasthetsprov.  
*Odontologiska Samfundets i Finland Årsbok* 70: 52-58.
- Forsten, L., (1972)  
The influence of precondensation mercury content and mulling on the transverse strength of amalgams condensed after a delay.  
*Acta Odontologica Scandinavica* 30: 453-461.
- von Fraunhofer, J.A., Staheli, P.J., (1972)  
Gold-Amalgam Galvanic Cells.  
*British Dental Journal* 132: 357-362.
- Fukuba, S., Hiraoka, K., Shimasue, K., Shintani, H., Inoue, T., (1977)  
Studies on the Repaired Filling - Using Dispersed Phase Amalgam.  
*Journal of Hiroshima University Dental Society* 9: 25-32. [in Japanese].
- Gainsford, I.D., Dunne, S.M., (1992)  
*Silver amalgam in clinical practice*. 3rd ed. (Oxford: Wright). pp 131-132.
- Gordon, M., Ben-Amar, A., Librus, S., (1987)  
Bond strength of mechanically condensed repaired high-copper amalgam.  
*Quintessence International* 18 (7): 471-474.
- Granath, L-E., (1964)  
A Technique for the Preparation of Comparable Amalgam Specimens Standardised by Mercury Content.  
*Acta Odontologica Scandinavica* 22: 185-191.
- Granath, L-E., Bladh, E., Edlund, J., (1967)  
Amalgam Specimen Technique. I. Studies on Comparable Specimens Controlled by Complexometric Titration on Mercury Content.  
*Journal of Dental Research* 46: 417-423.
- Gray, W.A., (1968) .  
*The Packing of Solid Particles*. pp 89-107.  
(London: Chapman and Hall)
- Hadavi, F., Hey, J.H., Ambrose, E.R., elBadrawy, H.E., (1991)  
The influence of an adhesive system on shear bond strength of repaired high-copper amalgams.  
*Operative Dentistry* 16 (5): 175-180.
- Hadavi, F., Hey, J.H., Czech, D., Ambrose, E.R., (1992)  
Tensile bond strength of repaired amalgam.  
*Journal of Prosthetic Dentistry* 67 (3): 313-317.
- Hadavi, F., Hey, J.H., Ambrose, E.R., elBadrawy, H.E., (1993)  
Repair of High-Copper Amalgam with and without an Adhesive System: in vitro Assessment of Microleakage and Shear Bond Strength.  
*Academy of General Dentistry* 41: 49-53.

- Hansen, M., Anderko, K., (1958)  
*Constitution of binary alloys*. (New York: McGraw-Hill Book Company)
- Hibler, J.A., Foor, J.L., Miranda, F.J., Duncanson, M.G., (1988)  
 Bond strength comparisons of repaired dental amalgams.  
*Quintessence International* 19 (6): 411-415.
- Hornbeck, D.D., Duke, E.S., Norling, B.K., (1986)  
 Strength of amalgam following a clinical repair technique.  
*Journal of Dental Research* 65: 218 Abstract No. 442.
- Innes, D.B.K., Youdelis, W.V., (1963)  
 Dispersion strengthened amalgams.  
*Journal of the Canadian Dental Association* 29: 587-593.
- Inoue, T., (1978)  
 (Repair of restoration materials: repair of amalgam and composite resin used in restorations)  
*Dental Outlook* 52 (1): 87-96. ISSN: 0418-694X. [in Japanese].
- Iwalisa, M., Kurosaki, N., Higashi, C., Takemoto, S., Takami, H., (1978)  
 (Newly developed technics in amalgam repair).  
*Dental Outlook* 51 (5): 1045-1061. ISSN: 0418-694X. [in Japanese].
- Jensen, S.J., (1977)  
 Phase content of a high copper dental silver amalgam.  
*Scandinavian Journal of Dental Research* 85: 297-301.
- Jensen, S.J., Jørgensen, K.D., (1978)  
 Creep and Beta-1 formation in dental amalgam.  
*Scandinavian Journal of Dental Research* 86: 408-411.
- Jensen, S.J., Jørgensen, K.D., (1985)  
 Dimensional and phase changes of dental amalgams.  
*Scandinavian Journal of Dental Research* 93: 351-356.
- Jones, J.T., Berard, M.F., (1972)  
*Ceramics Industrial Processing and Testing* (Ames, Iowa: The Iowa State University Press).  
 Chapter 11: 147-154.
- Jones, P.A., Harrington, E., Fisher, S.E., Wilson, H.J., (1986)  
 Standards for dental amalgam.  
*Journal of Dentistry* 14: 251-257.
- Jørgensen, K.D., Holst, K., Palbol, O.P., (1964)  
 Mercury content of silver amalgam. Influence of time between completion of the mix and start of condensation.  
*Acta Odontologica Scandinavica* 22: 207-214.
- Jørgensen, K.D., (1965a)  
 Adaptability of Dental Amalgams.  
*Acta Odontologica Scandinavica* 23: 257-270.
- Jørgensen, K.D., (1965b)  
 The mechanism of marginal fracture of amalgam fillings.  
*Acta Odontologica Scandinavica* 23: 347-389.
- Jørgensen, K.D., Saito, T., (1968)  
 Bond Strength of Repaired Amalgam.  
*Acta Odontologica Scandinavica* 26: 605-615.

Jørgensen, K.D., (1976)

Recent developments in alloys for dental amalgams: their properties and proper use.  
*International Dental Journal* **26**: 369-377.

Jørgensen, K.D., (1983)

Working time of dental amalgams.

*Scandinavian Journal of Dental Research* **91**: 329-333.

Kidd, E.A.M., Smith, B.G.N., Pickard, H.M., (1990)

*Pickard's manual of operative dentistry*. 6th edition: p183.  
(Oxford: Oxford University Press).

Kirk, E.E.J., (1962)

Amalgam to Amalgam Bond: A Preliminary Report.

*Dental Practitioner* **12**: 371-372.

Lacy, A.M., Rupprecht, R., Watanabe, L., Hiramatsu, D., (1989)

Amalgam-amalgam and amalgam-composite resin bond strength.

*Journal of Dental Research* **68**: 189 Abstract No. 59.

Leelawat, C., Scherer, W., Chang, J., Schulman, A., Vijayaraghavan, T., (1992a)

Addition of fresh amalgam to existing amalgam: microleakage study.

*Journal of Esthetic Dentistry* **4** (2): 41-45.

Leelawat, C., Scherer, W., Chang, J., Vijayaraghavan, T., LeGeros, J., (1992b)

Bonding fresh amalgam to existing amalgam: a shear and flexural strength study.

*Journal of Esthetic Dentistry* **4** (2): 46-49.

Leelawat, C., Scherer, W., Chang, J., David, S., Schulman, A. (1992c)

Addition of amalgam to existing amalgam using various adhesive liners: A SEM study.

*Journal of Esthetic Dentistry* **4** (2): 50-53.

MacInnis, W.A., Peacocke, L.E., Zakariasen, K.L., MacDonald, R.M., (1992)

Amalcore strength recovery following refilling of access preparations with amalgam.

*Journal of Prosthetic Dentistry* **68** (1): 59-62.

Mahler, D.B., Adey, J.D., (1977)

Characteristics of a High Copper Amalgam.

*Journal of Dental Research* Supplement to No. 56: B145, Abstract No. 372.

Mahler, D.B., (1971)

Microprobe Analysis of a Dispersant-Amalgam.

*Journal of Dental Research* **50**: IADR/AADR Program and abstracts of papers, No. 14.

Mahler, D.B., Mitchem, J.C., (1964)

Transverse Strength of Amalgam.

*Journal of Dental Research* **43** (1): 121-130.

Mitchell, R., Okabe, T., Fairhurst, C.W., (1978)

Dissolution of Ag-Sn-Cu alloys in Hg.

*Journal of Dental Research* Special Issue A: 125, Abstract No. 202.

Mitchell, R., Okabe, T., Butts, M.B., (1981)

The size of eta crystals in high copper amalgams.

*Journal of Dental Research* **60**: 480 Abstract No. 683.

Miyata, T., (1972)

Bonding of Repaired Amalgam evaluated by Tensile Strength and Scanning Electron Microscope Observation.

*Journal of the Japan Research Society of Dental Materials and Appliances* **28**: 92-108.

- Messing, J.J., Ray, G.E., (1972)  
*Operative Dental Surgery*. p124.  
 (London: Henry Kimpton).
- Moberg, L-E., Odén, A., (1985a)  
 The microstructure of corroded amalgams.  
*Acta Odontologica Scandinavica* **43**: 179-190.
- Moberg, L-E., Odén, A., (1985b)  
 Long-term corrosion studies in vitro of amalgams in contact.  
*Acta Odontologica Scandinavica* **43**: 205-213.
- Moberg, L.E., (1987)  
 Electrochemical properties of corroded amalgams.  
*Scandinavian Journal of Dental Research* **95**: 441-448.
- Nagai, K., Ohashi, M., Miyazu, H. (1966)  
 Studies on Spherical Amalgam Alloy in the Light of Dental Technology.  
*Journal of Nihon University School of Dentistry* **8**: 149-185.
- Nagai, K., Ohashi, M., Nihei, M. (1967)  
 The Pilot Manufacture and Evaluation of Oil Pressure Automatic Condensing Apparatus for the Preparation of Amalgam Test Specimen.  
*Journal of Nihon University School of Dentistry* **9** (4): 188-201.
- Nagaoka, F., Shimasue, K., Awaya, H., Shintani, H., Inoue, T., (1974)  
 Studies on the repaired filling - Amalgam to Amalgam.  
*Journal of Hiroshima University Dental Society* **6**: 100-108. [in Japanese].
- Nettelhorst, R.E., (1977)  
 Bond strength of repaired amalgam using different types of alloys.  
 Thesis: Master of Science in Dentistry, Indiana University.
- Okabe, T., (1992)  
 Setting reaction of dental amalgam: a research review.  
*In: Satellite Symposium, Setting Mechanisms of Dental Amalgams, 1992.*  
 The Dental Materials Group, International Association for Dental Research.
- Osborne, J.W., Norman, R.D., Gale, E.N., (1991)  
 A 14-year clinical assessment of 12 amalgam alloys.  
*Quintessence International* **22**: 857-864.
- Osborne, J.W., Phillips, R.W., Gale, E.N., Binon, P.P., (1976)  
 Three-year clinical comparison of three amalgam alloy types emphasizing an appraisal of the evaluation methods used.  
*Journal of the American Dental Association* **93**: 784-789.
- Paffenbarger, G.C., Rupp, N.W., Patel, P.R., (1979)  
 Linear dimensional change of copper-rich dental amalgams.  
*Journal of the American Dental Association* **99**: 468-471.
- Peacocke, L.E., Macinnis, W.A., Zakariasen, K.L., Macdonald, R.M., (1989)  
 Metallurgical interface between new and old amalgam in amalcore restorations.  
*Journal of Dental Research* **68**: 871 Abstract No. 28.
- Petzow, G., Effenberg, G., (1988)  
 Ternary Alloys: a comprehensive compendium of evaluated constitutional data and phase diagrams.  
 Volume 1: Ag-Al-Au to Ag-Cu-P and Volume 2: Ag-Cu-Pb to Ag-Zn-Zr.  
 (Weinheim, Germany: VCH Verlagsgesellschaft)

Phillips, R.W., (1953)

Amalgam: its properties and manipulation.

*New York Dental Journal* 23: 105-109.

Phillips, R.W., (1973)

*Skinner's Science of Dental Materials*, 7th edition: p362 (Repaired amalgam restorations).

(Philadelphia: W.B. Saunders Co.).

Pickard, H.M., (1983)

*A manual of operative dentistry*. 5th edition: p138.

(Oxford: Oxford University Press).

Pickard, H.M., (1993). Personal communication.

Ravnholt, G., Holland, R.I., (1988)

Corrosion current between fresh and old amalgam.

*Dental Materials* 4: 251-254.

Reisbick, M.H., Caputo, A.A., (1977)

Loading Rate and Temperature as Variables in Amalgam Bending.

*Journal of Dental Research* 56 (8): 933-936.

Reitz, C.D., Mateer, R.S., (1966)

International Association for Dental Research. 44th General Meeting.

IADR program and abstracts of papers: 109, Abstract No: 281.

Bonding of new amalgam to existing amalgam restorations.

Rowe, A.H.R., Alexander, A.G., Johns, R.B., (1989)

*A Comprehensive Guide to Clinical Dentistry*. (London: Class Publishing)

Schaller, H.-G., Götze, W., Kirn, B., Oehler, A., (1989)

Prüfung der Biegefestigkeit reparierter Amalgamprüfkörper.

*Deutsche Zahnärztliche Zeitschrift* 44 (7): 542-543. [English translation by H.F. Cook].

Scott, G.L., Grisius, R.J., (1969)

Bond Strength at the Interface of New and Old Spherical Amalgam.

*U.S. Navy Medical News Letter* 54 (5): 34.

Skinner, E.W., Phillips, R.W., (1967).

*The Science of Dental Materials*, 6th edition: p355 (Repaired amalgam restorations).

(Philadelphia: W.B. Saunders Co.)

Swartz, M.L., Phillips, R.W., (1956)

Residual mercury content of amalgam restorations and its influence on compressive strength.

*Journal of Dental Research* 35: 458-466.

Terkla, L.G., Mahler, D.B., Mitchem, J.C., (1961)

Bond Strength of Repaired Amalgam.

*Journal of Prosthetic Dentistry* 11: 942-947.

Vivadent, (1993). Personal communication.

Vrijhoef, M.M.A., Vermeersch, A.G., Spanauf, A.J., (1980)

*Dental Amalgam*: 106 (Chapter 5.6: Repair of Amalgam Restorations).

(Chicago: Quintessence Publishing Co., Inc.)

Walker, A.C. Jr., Reese, S.B., (1983)

Bond Strength of Amalgam to Amalgam in a High Copper Amalgam.

*Operative Dentistry* 8: 99-102.

Walker, J.D.R., (1985-1993). Personal communications.

- Ware, A.L., Docking, A.R., (1954)  
The Effect of Manipulative Variables on Dental Amalgams. Part 1 - Objective Methods of Testing.  
*Australian Dental Journal* **58**: 283-287.
- Watts, D.C., Devlin, H., Fletcher, J.E., (1992)  
Bonding characteristics of a phosphonated anaerobic adhesive to amalgam.  
*Journal of Dentistry* **20** (4): 245-249.
- Weibull, W., (1951)  
A Statistical Distribution Function of Wide Applicability.  
*Journal of Applied Mechanics* **18**: 293-297.
- Wing, G., (1966)  
The Junction Between Set and Added Amalgam.  
*Journal of Dental Research* **45** (2): 408.
- Wing, G., (1979)  
The New Amalgams: Biologically, environmentally, mechanically and clinically sound.  
*Annals of the Royal Australasian College of Dental Surgeons* **6**: 28-35.
- Wing, G., (1983)  
The Optical Microscopy of Junctions between Ag<sub>3</sub>Sn and High Copper Amalgams.  
*Journal of Dental Research* **62**: 403 Abstract No. 1.
- Wynn, H.P., (1994). Personal communications.

### Appendix 1. Raw data for test results

This appendix lists the results of sample testing (Load at fracture in Newtons under three point bending) together with the data set [Set] and batch numbers [Bat] and the lumen of the mould used for sample condensation [Lum]. The designation of the location of fracture origin [Loc] is Parent = 1, Joint = 2, Addition = 3. One-piece samples are listed as 4 in column Loc.

Set	Bat	Lum	Loc	Load	Set	Bat	Lum	Loc	Load	Set	Bat	Lum	Loc	Load
1	1	1	1	334		6	1	2	227	5	11	1	1	276
1	1	2	1	472		6	2	2	234	5	11	2	2	280
1	1	3	1	294		6	3	2	267	5	11	3	2	245
1	1	4	1	329		6	4			5	11	4	2	289
1	1	5	1	449		6	5	1	298	5	11	5	2	338
1	1	6	1	365		6	6	2	245	5	11	6	2	458
1	1	7	1	245		6	7	2	325	5	11	7	2	367
1	1	8	1	218		6	8	1	374	5	11	8	2	334
1	1	9	2	307		6	9	2	245	5	11	9	2	343
1	1	10	2	383		6	10	2	325	5	11	10	2	227
2	2	1	4	280	1	7	1	3	369	4	12	1	2	222
2	2	2	4	289	1	7	2	2	334	4	12	2	2	227
2	2	3	4	285	1	7	3	2	271	4	12	3	2	347
2	2	4	4	205	1	7	4	1	231	4	12	4	2	147
2	2	5	4	214	1	7	5	1	125	4	12	5	2	254
2	2	6	4	142	1	7	6	1	169	4	12	6	2	325
2	2	7	4	214	1	7	7	2	356	4	12	7	2	289
2	2	8	4	267	1	7	8	2	351	4	12	8	2	320
2	2	9	4	334	1	7	9	2	427	4	12	9	2	187
2	2	10	4	209	1	7	10	2	374	4	12	10	1	378
3	3	1	4	391	3	8	1	4	400	6	13	1	4	280
3	3	2	4	249	3	8	2	4	360	6	13	2	4	356
3	3	3	4	320	3	8	3	4	374	6	13	3	4	325
3	3	4	4	302	3	8	4	4	262	6	13	4	4	298
3	3	5	4	245	3	8	5	4	369	6	13	5	4	307
3	3	6	4	311	3	8	6	4	378	6	13	6	4	383
3	3	7	4	258	3	8	7	4	356	6	13	7	4	387
3	3	8	4	378	3	8	8	4	262	6	13	8	4	298
3	3	9	4	227	3	8	9	4	369	6	13	9	4	280
3	3	10	4	338	3	8	10	4	160	6	13	10	4	325
1	4	1	1	360	2	9	1	4	325	5	14	1	2	320
1	4	2	1	351	2	9	2	4	236	5	14	2	2	262
1	4	3	2	400	2	9	3	4	325	5	14	3	2	320
1	4	4	1	454	2	9	4	4	245	5	14	4	1	302
1	4	5	1	360	2	9	5	4	271	5	14	5	2	320
1	4	6	2	276	2	9	6	4	205	5	14	6	1	276
1	4	7	1	249	2	9	7	4	485	5	14	7	1	347
1	4	8	1	405	2	9	8	4	258	5	14	8	3	374
1	4	9	2	409	2	9	9	4	249	5	14	9	2	445
1	4	10	2	440	2	9	10	4	218	5	14	10	1	351
1	5	1	2	409	4	10	1	2	187		15	1	1	334
1	5	2	1	400	4	10	2	2	182		15	2	1	374
1	5	3	1	302	4	10	3	1			15	3	1	271
1	5	4	1	378	4	10	4	1	285		15	4	1	240
1	5	5	2	423	4	10	5	2	249		15	5	1	347
1	5	6	1	214	4	10	6	1	294		15	6	1	298
1	5	7	1	307	4	10	7	2	209		15	7	1	289
1	5	8	1	365	4	10	8	2	276		15	8	1	418
1	5	9	2	494	4	10	9	1	311		15	9	1	329
1	5	10	3	480	4	10	10	2	236		15	10	1	311

Set	Bat	Lum	Loc	Load	Set	Bat	Lum	Loc	Load	Set	Bat	Lum	Loc	Load
6	16	1	4	178	9	24	1	1	467	32	1	4	196	
6	16	2	4	245	9	24	2	2	343	32	2	4	229	
6	16	3	4	214	9	24	3	1	383	32	3	4	193	
6	16	4	4	178	9	24	4	2	329	32	4	4	396	
6	16	5	4	294	9	24	5	1	365	32	5	4	369	
6	16	6	4	320	9	24	6	1	396	32	6	4	116	
6	16	7	4	320	9	24	7	1	231	32	7	4	129	
6	16	8	4	387	9	24	8	2	369	32	8	4	171	
6	16	9	4	311	9	24	9	1	476	32	9	4	258	
6	16	10	4	356	9	24	10	2	343	32	10	4	267	
	17	1	4	431	7	25	1	2	276	33	1	4	296	
	17	2	4	302	7	25	2	2	351	33	2	4	420	
	17	3	4	289	7	25	3	1	423	33	3	4	325	
	17	4	4	374	7	25	4	1	360	33	4	4	302	
	17	5	4	294	7	25	5	2	316	33	5	4	267	
	17	6	4	258	7	25	6	1	329	33	6	4	347	
	17	7	4	360	7	25	7	2	107	33	7	4	351	
	17	8	4	449	7	25	8	2	414	33	8	4	365	
	17	9	4	254	7	25	9	1	351	33	9	4	369	
	17	10	4	334	7	25	10	1	405	33	10	4	307	
6	18	1	4	343	8	26	1	2	231	34	1	4	287	
6	18	2	4	289	8	26	2	2	236	34	2	4	343	
6	18	3	4	267	8	26	3	1	343	34	3	4	245	
6	18	4	4	298	8	26	4	2	400	34	4	4	214	
6	18	5	4	254	8	26	5	2	307	34	5	4	280	
6	18	6	4	245	8	26	6	2	400	34	6	4	376	
6	18	7	4	378	8	26	7			34	7	4	287	
6	18	8	4	320	8	26	8	2	387	34	8	4	271	
6	18	9	4	254	8	26	9	2	307	34	9	4	347	
6	18	10	4	240	8	26	10	2	294	34	10	4	276	
	19	1	2	40	10	27	1	4	418	35	1	4	309	
	19	2	2	40	10	27	2	4	463	35	2	4	220	
	19	3			10	27	3	4	423	35	3	4	387	
	19	4	2	40	10	27	4	4	325	35	4	4	276	
	19	5	2	49	10	27	5	4	289	35	5	4	298	
	19	6			10	27	6	4	343	35	6	4	343	
	19	7	2	93	10	27	7	4	245	35	7	4	316	
	19	8	2	49	10	27	8	4	329	35	8	4	385	
	19	9			10	27	9	4	431	35	9	4	349	
	19	10			10	27	10	4	316	35	10	4	400	
	20	1	2	285	7	28	1	1	383	36	1	4	294	
	20	2	2	316	7	28	2	1	414	36	2	4	374	
	20	3	1	365	7	28	3	1	418	36	3	4	374	
	20	4	2	311	7	28	4	1	411	36	4	4	374	
	20	5	2	214	7	28	5	1	380	36	5	4	400	
	20	6	2	276	7	28	6	2	371	36	6	4	423	
	20	7	2	205	7	28	7	2	489	36	7	4	351	
	20	8	2	289	7	28	8	1	349	36	8	4	369	
	20	9	2	236	7	28	9	1	414	36	9	4	405	
	20	10	2	187	7	28	10	1	236	36	10	4	338	
7	21	1	2	351		29	1	1	369	37	1	4	298	
7	21	2	2	271		29	2	1	334	37	2	4	307	
7	21	3	2	298		29	3	2	256	37	3	4	271	
7	21	4	1	280		29	4	2	374	37	4	4	367	
7	21	5	2	400		29	5	2	254	37	5	4	171	
7	21	6	2	454		29	6	3	302	37	6	4	280	
7	21	7	1	400		29	7	3	249	37	7	4	169	
7	21	8	1	320		29	8	3	334	37	8	4	147	
7	21	9	2	325		29	9	3	289	37	9	4	200	
7	21	10	2	396		29	10	2	376	37	10	4	322	
8	22	1	2	236	9	30	1	3	294	38	1	4	227	
8	22	2	2	294	9	30	2	2	427	38	2	4	202	
8	22	3	2	409	9	30	3	2	398	38	3	4	356	
8	22	4	2	316	9	30	4	2	476	38	4	4	336	
8	22	5	2	298	9	30	5	2	440	38	5	4	282	
8	22	6	2	298	9	30	6	1	356	38	6	4	300	
8	22	7	2	387	9	30	7	2	356	38	7	4	291	
8	22	8	1	418	9	30	8	1	425	38	8	4	158	
8	22	9	2	378	9	30	9	2	287	38	9	4	245	
8	22	10	1	414	9	30	10	2	294	38	10	4	187	
	23	1	2	187		31	1			39	1	4	216	
	23	2	2	396		31	2			39	2	4	302	
	23	3	2	356		31	3			39	3	4	207	
	23	4	2	351	10	31	4	4	276	39	4	4	311	
	23	5	2	320		31	5			39	5	4	258	
	23	6	2	271	10	31	6	4	436	39	6	4	249	
	23	7	2	218	10	31	7	4	343	39	7	4	300	
	23	8	2	240		31	8			39	8	4	356	
	23	9	2	285	10	31	9	4	265	39	9	4	298	
	23	10			10	31	10	4	440	39	10	4	276	

Set	Bat	Lum	Loc	Load
40	1	4		394
40	2	4		449
40	3	4		294
40	4	4		320
40	5	4		327
40	6	4		418
40	7	4		311
40	8	4		376
40	9	4		262
40	10	4		378
41	1	4		400
41	2	4		329
41	3	4		423
41	4	4		376
41	5	4		314
41	6	4		222
41	7	4		329
41	8	4		311
41	9	4		369
41	10	4		285
42	1	2		350
42	2	2		266
42	3	2		293
42	4	2		273
42	5	2		297
42	6	2		334
42	7	1		316
42	8	2		268
42	9	2		359
42	10	2		383
43	1	2		315
43	2	2		282
43	3	2		374
43	4	2		324
43	5	2		258
43	6	1		250
43	7	1		294
43	8	1		229
43	9	2		226
43	10	2		239
44	1	2		215
44	2	1		254
44	3	2		178
44	4	1		300
44	5	1		323
44	6	1		187
44	7	1		219
44	8	2		226
44	9	2		362
44	10	2		433
45	1	2		323
45	2	2		407
45	3	1		376
45	4	1		350
45	5	2		325
45	6	2		330
45	7	1		362
45	8	1		258
45	9	3		327
45	10	1		336
46	1	4		237
46	2	4		224
46	3	4		260
46	4	4		217
46	5	4		403
46	6	4		171
46	7	4		331
46	8	4		249
46	9	4		307
46	10	4		354
47	1	4		319
47	2	4		242
47	3	4		232
47	4	4		275
47	5	4		173
47	6	4		121
47	7	4		145
47	8	4		206
47	9	4		124
47	10	4		161

Set	Bat	Lum	Loc	Load
48	1	4		509
48	2	4		495
48	3	4		486
48	4	4		424
48	5	4		430
48	6	4		515
48	7	4		555
48	8	4		442
48	9	4		515
48	10	4		484
49	1	4		451
49	2	4		524
49	3	4		413
49	4	4		510
49	5	4		483
49	6	4		384
49	7	4		372
49	8	4		451
49	9	4		452
49	10	4		415
50	1	4		418
50	2	4		554
50	3	4		533
50	4	4		399
50	5	4		438
50	6	4		493
50	7	4		436
50	8	4		475
50	9	4		464
50	10	4		467
51	1	4		382
51	2	4		497
51	3	4		348
51	4	4		539
51	5	4		412
51	6	4		408
51	7	4		408
51	8	4		538
51	9	4		445
51	10	4		436
52	1	4		537
52	2	4		537
52	3	4		470
52	4	4		504
52	5			
52	6	4		366
52	7	4		355
52	8	4		535
52	9	4		518
52	10	4		447
53	1	2		105
53	2	2		63
53	3	1		163
53	4	2		174
53	5	2		202
53	6	2		70
53	7	2		198
53	8	2		180
53	9	2		185
53	10	2		187
54	1	2		31
54	2	3		206
54	3	2		258
54	4	2		126
54	5	2		258
54	6	2		159
54	7	1		139
54	8	2		278
54	9	1		163
54	10	2		363
55	1	1		205
55	2	1		149
55	3	1		320
55	4	1		212
55	5	1		270
55	6	1		310
55	7	3		129
55	8	2		159
55	9	2		109
55	10	2		162

Set	Bat	Lum	Loc	Load
21	62	1	4	329
21	62	2	4	281
21	62	3	4	432
21	62	4	4	325
21	62	5	4	292
21	62	6	4	260
21	62	7	4	281
21	62	8	4	327
21	62	9	4	362
21	62	10	4	354
	63	1	4	362
	63	2	4	306
	63	3	4	346
	63	4	4	231
	63	5	4	398
	63	6	4	260
	63	7	4	302
	63	8	4	251
	63	9	4	405
	63	10	4	338
	64	1	4	551
	64	2	4	430
	64	3	4	539
	64	4	4	551
	64	5	4	576
	64	6	4	567
	64	7	4	503
	64	8	4	562
	64	9	4	560
	64	10	4	631
	65	1	2	282
	65	2	2	300
	65	3	2	431
	65	4	2	310
	65	5	1	354
	65	6	2	242
	65	7	2	309
	65	8	2	233
	65	9	1	345
	65	10	2	426
	66	1	2	318
	66	2	2	307
	66	3	2	300
	66	4	2	307
	66	5	2	442
	66	6	2	50
	66	7	2	268
	66	8	2	308
	66	9	2	343
	66	10	2	361
	67	1	2	162
	67	2	2	284
	67	3	2	226
	67	4	2	218
	67	5	2	320
	67	6	2	267
	67	7	2	329
	67	8	2	287
	67	9	2	301
	67	10	2	269
22	68	1	2	
22	68	2	2	
22	68	3	2	
22	68	4	1	385
22	68	5	2	467
22	68	6	2	373
22	68	7	2	347
22	68	8	2	265
22	68	9	2	225
22	68	10	2	431
11	69	1	1	470
11	69	2	2	247
11	69	3	2	313
11	69	4	1	385
11	69	5	1	474
11	69	6	2	259
11	69	7	2	408
11	69	8	1	452
11	69	9	1	237
11	69	10	1	352

Set	Bat	Lum	Loc	Load
22	70	1	2	457
22	70	2	2	369
22	70	3	1	395
22	70	4	2	329
22	70	5	2	417
22	70	6	2	468
22	70	7	2	372
22	70	8	1	322
22	70	9	1	419
22	70	10	2	411
22	71	1	1	348
22	71	2	2	447
22	71	3	1	357
22	71	4	2	447
22	71	5	2	311
22	71	6	2	413
22	71	7	2	416
22	71	8	1	333
22	71	9	1	366
22	71	10	1	300
22	72	1	3	279
22	72	2	1	215
22	72	3	3	289
22	72	4	2	518
22	72	5	2	345
22	72	6	1	316
22	72	7	2	443
22	72	8	2	309
22	72	9	2	370
22	72	10	2	300
	73	1	2	373
	73	2	2	460
	73	3	2	380
	73	4	3	465
	73	5	2	476
	73	6	2	353
	73	7	2	222
	73	8	2	358
	73	9	3	399
	73	10	2	267
11	74	1	3	346
11	74	2	3	393
11	74	3	2	370
11	74	4	1	257
11	74	5	1	295
11	74	6	1	355
11	74	7	2	266
11	74	8	3	452
11	74	9	3	361
11	74	10	2	296
22	75	1	2	406
22	75	2	2	251
22	75	3	2	216
22	75	4	1	187
22	75	5	2	387
22	75	6	2	187
22	75	7	2	
22	75	8	2	264
22	75	9	3	362
22	75	10	1	364
22	76	1	3	254
22	76	2	2	302
22	76	3	1	389
22	76	4	1	374
22	76	5	3	413
22	76	6	2	459
22	76	7	3	354
22	76	8	3	443
22	76	9	2	400
22	76	10	1	317
22	77	1	2	283
22	77	2	3	356
22	77	3	2	463
22	77	4	3	309
22	77	5	2	417
22	77	6	2	476
22	77	7	1	394
22	77	8	1	360
22	77	9	1	485
22	77	10	2	339

Set	Bat	Lum	Loc	Load
22	78	1	1	325
22	78	2	2	307
22	78	3	3	507
22	78	4	1	449
22	78	5	3	486
22	78	6	2	485
22	78	7	1	435
22	78	8	2	344
22	78	9	2	261
22	78	10	2	279
22	79	1	2	290
22	79	2	1	398
22	79	3	2	299
22	79	4	1	296
22	79	5	3	380
22	79	6	2	289
22	79	7	1	317
22	79	8	3	316
22	79	9	3	407
22	79	10	2	279
21	80	1	4	320
21	80	2	4	284
21	80	3	4	185
21	80	4	4	262
21	80	5	4	187
21	80	6	4	311
21	80	7	4	168
21	80	8	4	232
21	80	9	4	219
21	80	10	4	217
	81	1	2	324
	81	2	2	404
	81	3	2	384
	81	4	3	439
	81	5	2	423
	81	6	2	386
	81	7	3	439
	81	8	2	267
	81	9	2	267
	81	10	2	240
22	82	1	2	379
22	82	2	1	284
22	82	3	1	519
22	82	4	2	245
22	82	5	2	446
22	82	6	1	504
22	82	7	1	295
22	82	8	3	285
22	82	9	2	367
22	82	10	2	255
	83	1	2	264
	83	2	2	322
	83	3	2	306
	83	4	1	329
	83	5	3	406
	83	6	2	291
	83	7	2	333
	83	8	1	387
	83	9	2	308
	83	10	1	259
	84	1	2	280
	84	2	2	283
	84	3	2	226
	84	4	1	287
	84	5	3	344
	84	6	1	268
	84	7	2	301
	84	8	1	252
	84	9	1	312
	84	10	2	265
11	85	1	1	242
11	85	2	2	414
11	85	3	2	391
11	85	4	1	453
11	85	5	2	246
11	85	6	2	416
11	85	7	3	322
11	85	8	3	354
11	85	9	2	264
11	85	10	2	330

Set	Bat	Lum	Loc	Load
22	86	1	2	326
22	86	2	2	249
22	86	3	2	288
22	86	4	2	307
22	86	5	3	273
22	86	6	2	324
22	86	7	2	324
22	86	8	2	297
22	86	9	2	367
22	86	10	2	364
22	87	1	2	123
22	87	2	3	361
22	87	3	3	470
22	87	4	2	417
22	87	5	2	490
22	87	6	2	321
22	87	7	1	385
22	87	8	2	421
22	87	9	2	446
22	87	10	1	446
	88	1	2	156
	88	2	1	238
	88	3	2	255
	88	4	2	241
	88	5	2	359
	88	6	2	132
	88	7	1	260
	88	8	2	294
	88	9	2	407
	88	10	2	167
	89	1	2	90
	89	2	2	216
	89	3	2	176
	89	4	2	196
	89	5	2	220
	89	6	2	128
	89	7	2	255
	89	8	2	208
	89	9	2	234
	89	10	2	214
	90	1	2	25
	90	2	2	36
	90	3	2	41
	90	4	2	37
	90	5	2	47
	90	6	2	71
	90	7		
	90	8	2	55
	90	9	2	69
	90	10	2	48
	91	1	2	157
	91	2	1	443
	91	3	2	336
	91	4	1	313
	91	5	2	239
	91	6		
	91	7	2	267
	91	8	2	210
	91	9	2	296
	91	10	2	328
	92	1	1	193
	92	2	1	270
	92	3	2	282
	92	4	2	246
	92	5	1	399
	92	6	1	242
	92	7	2	264
	92	8	2	223
	92	9	2	243
	92	10	2	232
	93	1	2	343
	93	2	2	286
	93	3	2	256
	93	4	2	221
	93	5	2	338
	93	6	2	303
	93	7	2	405
	93	8	3	336
	93	9	2	209
	93	10	2	348

Set	Bat	Lum	Loc	Load
16	94	1	4	176
16	94	2	4	143
16	94	3	4	158
16	94	4	4	213
16	94	5	4	195
16	94	6	4	151
16	94	7	4	142
16	94	8	4	258
16	94	9	4	170
16	94	10	4	204
17	95	1	4	415
17	95	2	4	477
17	95	3	4	488
17	95	4	4	487
17	95	5	4	405
17	95	6	4	543
17	95	7	4	488
17	95	8	4	566
17	95	9	4	485
17	95	10	4	415
12	96	1	2	207
12	96	2	3	351
12	96	3	1	281
12	96	4	2	221
12	96	5	2	289
12	96	6	3	361
12	96	7	2	326
12	96	8	2	378
12	96	9	2	251
12	96	10	1	369
13	97	1	2	247
13	97	2	2	192
13	97	3	2	116
13	97	4	2	275
13	97	5	2	292
13	97	6	2	196
13	97	7	2	236
13	97	8	2	299
13	97	9	2	262
13	97	10	1	375
14	98	1	2	358
14	98	2	1	307
14	98	3	2	214
14	98	4	1	251
14	98	5	2	257
14	98	6	1	223
14	98	7	2	302
14	98	8	2	292
14	98	9	1	378
14	98	10	1	236
12	99	1	3	340
12	99	2	1	194
12	99	3	1	304
12	99	4	2	295
12	99	5	3	242
12	99	6	1	302
12	99	7	3	360
12	99	8	1	431
12	99	9	1	299
12	99	10	2	396
13	100	1	2	352
13	100	2	2	299
13	100	3	2	263
13	100	4	1	320
13	100	5	1	231
13	100	6	2	361
13	100	7	2	317
13	100	8	1	331
13	100	9	2	267
13	100	10	1	317
14	101	1	1	251
14	101	2	2	409
14	101	3	1	283
14	101	4	1	376
14	101	5	1	265
14	101	6	2	407
14	101	7	2	458
14	101	8	1	384
14	101	9	2	382
14	101	10	1	152

Set	Bat	Lum	Loc	Load
15	102	1	3	353
15	102	2	1	317
15	102	3	1	370
15	102	4	3	379
15	102	5	1	360
15	102	6	2	331
15	102	7	2	303
15	102	8	1	303
15	102	9	1	338
15	102	10	2	316
12	103	1	1	172
12	103	2	3	219
12	103	3	1	319
12	103	4	1	308
12	103	5	3	447
12	103	6	1	366
12	103	7	2	334
12	103	8	1	357
12	103	9	1	343
12	103	10	2	310
13	104	1	2	230
13	104	2	2	263
13	104	3	2	284
13	104	4	3	341
13	104	5	2	403
13	104	6	1	345
13	104	7	2	370
13	104	8	3	312
13	104	9	1	345
13	104	10	2	383
14	105	1	2	174
14	105	2	1	314
14	105	3	2	344
14	105	4	3	376
14	105	5	3	442
14	105	6	1	477
14	105	7	2	346
14	105	8	1	389
14	105	9	3	365
14	105	10	1	437
15	106	1	1	345
15	106	2	2	414
15	106	3	2	287
15	106	4	2	185
15	106	5	2	304
15	106	6	1	253
15	106	7	2	243
15	106	8	2	271
15	106	9	2	318
15	106	10	2	272
16	107	1	4	135
16	107	2	4	169
16	107	3	4	207
16	107	4	4	185
16	107	5	4	141
16	107	6	4	150
16	107	7	4	226
16	107	8	4	272
16	107	9	4	194
16	107	10	4	314
17	108	1	4	400
17	108	2	4	399
17	108	3	4	367
17	108	4	4	497
17	108	5	4	385
17	108	6	4	315
17	108	7	4	507
17	108	8	4	410
17	108	9	4	511
17	108	10	4	324
	109	1	3	368
	109	2	2	341
	109	3	2	308
	109	4	2	
	109	5	3	519
	109	6	3	363
	109	7	3	416
	109	8	2	412
	109	9	1	432
	109	10	3	431

Set	Bat	Lum	Loc	Load
	110	1	1	341
	110	2	2	204
	110	3	2	359
	110	4	2	286
	110	5	2	325
	110	6	2	304
	110	7	2	431
	110	8	1	315
	110	9	1	381
	110	10	2	388
18	111	1	2	215
18	111	2	3	380
18	111	3	2	309
18	111	4	3	350
18	111	5	2	395
18	111	6	2	285
18	111	7	2	381
18	111	8	2	360
18	111	9	1	427
18	111	10	2	285
19	112	1	1	309
19	112	2		
19	112	3	2	512
19	112	4	1	462
19	112	5	2	529
19	112	6		
19	112	7	1	542
19	112	8	2	330
19	112	9	2	521
19	112	10	2	457
20	113	1	1	350
20	113	2	1	350
20	113	3	1	185
20	113	4		
20	113	5	2	321
20	113	6		
20	113	7	1	387
20	113	8		
20	113	9		
20	113	10	2	438
	114	1	3	446
	114	2	1	413
	114	3	1	353
	114	4	1	442
	114	5	1	292
	114	6	1	342
	114	7	2	269
	114	8	1	526
	114	9	2	474
	114	10	1	427
19	115	1	2	400
19	115	2	2	448
19	115	3	2	481
19	115	4	1	450
19	115	5	1	483
19	115	6	1	479
19	115	7	2	520
19	115	8	1	259
19	115	9	2	429
19	115	10		
20	116	1	3	351
20	116	2	1	307
20	116	3	2	314
20	116	4	2	350
20	116	5	3	443
20	116	6	1	363
20	116	7	1	393
20	116	8	2	378
20	116	9	2	265
20	116	10	2	371
18	117	1	2	298
18	117	2	2	360
18	117	3	2	240
18	117	4	3	390
18	117	5	3	436
18	117	6	2	425
18	117	7	2	376
18	117	8	3	423
18	117	9	2	331
18	117	10	2	405

Set	Bat	Lum	Loc	Load
23	118	1	2	342
23	118	2	1	301
23	118	3	2	492
23	118	4	2	496
23	118	5	1	380
23	118	6	2	363
23	118	7	3	401
23	118	8	3	502
23	118	9	1	218
23	118	10	2	379
23	119	1	1	307
23	119	2	1	346
23	119	3	1	435
23	119	4	1	375
23	119	5	2	497
23	119	6	1	316
23	119	7	1	292
23	119	8	2	425
23	119	9	1	203
23	119	10	2	509
23	120	1	2	232
23	120	2	1	428
23	120	3	2	379
23	120	4	2	345
23	120	5	2	433
23	120	6	2	459
23	120	7	2	495
23	120	8	2	481
23	120	9	2	383
23	120	10	3	436
23	121	1	2	365
23	121	2	1	348
23	121	3	1	350
23	121	4	2	439
23	121	5	1	425
23	121	6	1	153
23	121	7	2	155
23	121	8	2	517
23	121	9	1	465
23	121	10	2	371
24	122	1	4	352
24	122	2	4	382
24	122	3	4	193
24	122	4	4	321
24	122	5	4	301
24	122	6	4	181
24	122	7	4	181
24	122	8	4	345
24	122	9	4	293
24	122	10	4	402
24	123	1	4	224
24	123	2	4	330
24	123	3	4	225
24	123	4	4	247
24	123	5	4	261
24	123	6	4	176
24	123	7	4	379
24	123	8	4	291
24	123	9	4	284
24	123	10	4	340
25	124	1	4	459
25	124	2	4	439
25	124	3	4	460
25	124	4	4	361
25	124	5	4	421
25	124	6	4	372
25	124	7	4	448
25	124	8	4	434
25	124	9	4	370
25	124	10	4	446
25	125	1	4	467
25	125	2	4	536
25	125	3	4	518
25	125	4	4	352
25	125	5	4	437
25	125	6	4	485
25	125	7	4	383
25	125	8	4	426
25	125	9	4	529
25	125	10	4	444

## Appendix 2. Descriptive statistics of force to fracture for Batches

This appendix tabulates descriptive statistics of force to fracture data (in Newtons) for batches of samples. The confidence level achieved in the confidence interval (C.I.) for the median was 94.7% to 95.6%, except for Batches 19 and 31 where 94.1% was achieved.

Batch	Set	N	Mean	Max	Min	S.D.	SEM	95% C.I. for Mean	Median	C.I. for Median
								From To		From To
1	1	10	339.6	472	218	81.0	25.6	281.7 397.5	331	276.0 400.0
2	2	10	243.9	334	142	56.3	17.8	203.6 284.2	240	209.0 284.5
3	3	10	301.9	391	227	56.8	18.0	261.3 342.5	306	253.5 346.5
4	1	10	370.4	454	249	66.4	21.0	322.9 417.9	380	318.0 420.0
5	1	10	377.2	494	214	85.1	26.9	316.3 438.1	389	307.0 440.0
6		9	282.2	374	227	50.9	17.0	243.1 321.3	279.5	239.5 325.0
7	1	10	300.7	427	125	98.1	31.0	230.5 370.9	302	231.0 369.0
8	3	10	329.0	400	160	75.9	24.0	274.7 383.3	364	265.0 376.0
9	2	10	281.7	485	205	81.8	25.9	223.2 340.2	253	231.0 351.0
10	4	9	247.6	311	182	47.4	15.8	211.2 284.1	249	209.0 289.5
11	5	10	315.7	458	227	67.4	21.3	267.5 363.9	311	267.0 367.0
12	4	10	269.6	378	147	74.5	23.5	216.3 322.9	271	218.0 325.0
13	6	10	323.9	387	280	39.4	12.5	295.7 352.1	316	293.5 354.0
14	5	10	331.7	445	262	52.2	16.5	294.4 369.0	320	298.0 373.5
15		10	321.1	418	240	51.5	16.3	284.3 357.9	320	284.5 358.0
16	6	10	280.3	387	178	73.0	23.1	228.1 332.5	302	229.0 338.0
17		10	334.5	449	254	68.1	21.5	285.8 383.2	332	280.0 383.0
18	6	10	288.8	378	240	46.1	14.6	255.8 321.8	278	254.0 320.5
19		6	51.8	93	40	20.6	8.4	30.2 73.5	44.5	40.0 71.0
20		10	268.4	365	187	56.6	17.9	227.9 308.9	265	225.0 311.0
21	7	10	349.5	454	271	60.8	19.2	306.0 393.0	338	300.0 398.0
22	8	10	344.8	418	236	63.9	20.2	299.1 390.5	347	298.0 398.0
23		9	291.5	396	187	69.7	23.2	238.0 345.1	291	229.0 354.0
24	9	10	370.2	476	231	69.9	22.1	320.2 420.2	367	329.0 420.5
25	7	10	333.2	423	107	91.8	29.0	267.5 398.9	351	261.0 387.5
26	8	9	322.7	400	231	64.9	21.6	272.9 372.7	307	269.0 387.0
27	10	10	358.2	463	245	71.2	22.6	307.3 409.1	336	307.0 420.0
28	7	10	386.5	489	236	64.9	20.5	340.0 433.0	397	327.0 419.0
29		10	313.7	376	249	50.8	16.1	277.4 350.0	312.5	272.5 354.0
30	9	10	375.3	476	287	68.1	21.6	326.6 424.0	377	325.0 427.0
31	10	5	352.0	440	265	84.0	37.6	247.7 456.3	352	265.0 440.0
32		10	232.4	396	116	93.2	29.4	165.7 299.1	227	162.0 299.0
33		10	334.9	420	267	44.5	14.1	303.1 366.7	333	302.0 365.0
34		10	292.6	376	214	49.3	15.6	257.3 327.9	287	258.0 328.0
35		10	328.3	400	220	56.1	17.7	288.1 368.5	330	287.0 368.0
36		10	370.2	423	294	36.7	11.6	343.9 396.5	374	344.5 398.5
37		10	253.2	367	147	75.7	23.9	199.0 307.4	249	186.0 310.0
38		10	258.4	356	158	65.3	20.7	211.7 305.1	259	207.0 309.0
39		10	277.3	356	207	45.7	14.4	244.6 310.0	279	246.0 306.5
40		10	352.9	449	262	59.2	18.7	310.6 395.3	352.5	310.5 397.0
41		10	335.8	423	222	58.8	18.6	293.7 377.9	340	298.0 376.0
42		10	313.9	383	266	41.3	13.0	284.4 343.4	313.5	281.5 346.5
43		10	279.1	374	226	48.0	15.2	244.7 313.5	276	242.0 315.0
44		10	269.7	433	178	82.9	26.2	210.4 329.0	263	206.0 330.0
45		10	339.4	407	258	39.3	12.4	311.3 367.5	338.5	317.0 367.0
46		10	275.3	403	171	71.4	22.6	224.2 326.4	274	224.0 330.0
47		10	199.8	319	121	66.6	21.1	152.2 247.4	198	147.0 246.0
48		10	485.5	555	424	42.1	13.3	455.4 515.6	489.5	457.0 515.0
49		10	445.5	524	372	50.6	16.0	409.3 481.7	448	411.5 483.0
50		10	467.7	554	399	48.9	15.5	432.7 502.7	465.5	433.0 504.0
51		10	441.3	539	348	64.4	20.4	395.2 487.4	439.5	395.0 487.5
52		9	474.3	537	355	71.6	23.9	419.3 529.4	487	413.0 535.0
53		10	152.7	202	63	52.9	16.7	114.9 190.6	163	118.5 189.0
54		10	198.1	363	31	94.4	29.8	130.6 265.6	199	139.0 263.0
55		10	202.5	320	109	74.9	23.7	148.9 256.1	205	145.0 261.0

Batch	Set	N	Mean	Max	Min	S.D.	SEMean	95% C.I. for Mean		Median	C.I. for Median	
								From	To		From	To
62	21	10	324.3	432	260	50.4	15.9	288.2	360.4	326	286.5	358.0
63		10	319.9	405	231	60.4	19.1	276.7	363.1	322	276.5	368.0
64		10	547.0	631	430	52.1	16.4	509.7	584.3	555.5	503.0	576.0
65		10	323.2	431	233	67.5	21.3	274.9	371.5	322.5	271.5	370.0
66		10	300.4	442	50	99.9	31.6	229.0	371.8	309	205.0	361.0
67		10	266.3	329	162	51.2	16.2	229.7	302.9	273	224.5	302.0
68	22	7	356.1	467	225	86.2	32.6	276.4	435.9	373	265.0	431.0
69	11	10	359.7	474	237	92.4	29.2	293.6	425.8	368	286.0	430.0
70	22	10	395.9	468	322	48.7	15.4	361.0	430.8	403	362.0	434.0
71	22	10	373.8	447	300	53.8	17.0	335.3	412.3	361	333.0	414.5
72	22	10	338.4	518	215	87.1	27.6	276.1	400.7	312	284.0	407.0
73		10	375.3	476	222	83.0	26.2	315.9	434.7	376	310.0	429.0
74	11	10	339.1	452	257	60.8	19.2	295.6	382.6	350	295.5	377.0
75	22	9	291.5	406	187	88.3	29.4	223.7	359.4	264	216.0	375.0
76	22	10	370.5	459	254	64.6	20.4	324.3	416.7	381	321.5	416.5
77	22	10	388.2	485	283	70.8	22.4	337.5	438.9	377	335.0	440.0
78	22	10	387.8	507	261	94.0	29.7	320.5	455.1	389	307.0	468.0
79	22	10	327.1	407	279	48.7	15.4	292.3	361.9	307	292.5	357.5
80	21	10	238.5	320	168	53.6	17.0	200.1	276.9	225	200.0	276.0
81		10	357.3	439	240	76.4	24.2	302.6	412.0	353	296.0	413.0
82	22	10	357.9	519	245	102.0	32.3	284.9	430.9	331	375.0	441.0
83		10	320.5	406	259	47.3	15.0	286.6	354.4	318.5	286.0	357.0
84		10	281.8	344	226	32.8	10.4	258.4	305.2	282	258.5	306.0
85	11	10	343.2	453	242	75.5	23.9	289.2	397.2	342	286.0	404.0
86	22	10	311.9	367	249	37.3	11.8	285.2	338.6	315	286.5	344.0
87	22	10	388.0	490	123	106.1	33.5	312.1	463.9	419	296.0	453.0
88		10	250.9	407	132	87.2	27.6	188.6	313.3	249	193.0	322.0
89		10	193.7	255	90	50.1	15.8	157.9	229.6	205	153.0	225.5
90		9	47.6	71	25	15.3	5.1	36.0	59.4	47	36.0	59.5
91		9	287.6	443	157	82.7	27.6	224.1	351.2	288	225.0	355.0
92		10	259.4	399	193	55.1	17.4	220.0	298.9	251	228.5	311.0
93		10	304.5	405	209	61.8	19.6	260.3	348.7	307	256.0	345.5
94	16	10	181.0	258	142	36.8	11.6	154.6	207.4	173	154.5	208.0
95	17	10	476.9	566	405	53.3	16.9	438.8	515.0	486	446.0	515.5
96	12	10	303.4	378	207	62.8	19.9	258.5	348.3	307	251.0	356.0
97	13	10	249.0	375	116	70.7	22.4	198.4	299.6	254	195.0	296.0
98	14	10	281.8	378	214	55.7	17.6	242.0	321.6	274	237.0	325.0
99	12	10	316.3	431	194	69.6	22.0	266.5	366.1	303	268.5	366.5
100	13	10	305.8	361	231	41.2	13.0	276.4	335.2	317	274.0	336.0
101	14	10	336.7	458	152	94.4	29.9	269.2	404.2	379	267.0	407.0
102	15	10	337.0	379	303	27.5	8.7	317.3	356.7	334	316.5	358.5
103	12	10	317.5	447	172	76.5	24.2	262.8	372.2	326	264.0	366.0
104	13	10	327.6	403	230	55.0	17.3	288.3	366.9	343	287.5	370.0
105	14	10	366.4	477	174	84.5	26.7	306.0	426.8	370	308.0	421.0
106	15	10	289.2	414	185	62.1	19.6	244.8	333.6	279	248.0	333.5
107	16	10	199.3	314	135	58.1	18.4	157.8	240.8	189	159.5	241.5
108	17	10	411.5	511	315	71.7	22.7	360.2	462.8	399	357.5	455.5
109		9	398.8	519	308	62.1	20.7	351.1	446.6	397	352.0	443.5
110		10	333.4	431	204	63.0	19.9	288.3	378.5	337	292.5	378.0
111	18	10	338.7	427	215	64.1	20.3	292.8	384.6	355	288.0	387.0
112	19	8	457.7	542	309	90.7	32.1	381.9	533.6	487	383.0	529.0
113	20	6	338.5	438	185	85.3	34.8	249.0	428.0	350	253.0	413.0
114		10	398.4	526	269	82.0	25.9	339.7	457.1	398	342.0	458.0
115	19	9	438.7	520	259	75.9	25.3	380.4	497.1	450	369.0	484.0
116	20	10	353.5	443	265	49.6	15.7	318.0	389.0	357	314.0	385.5
117	18	10	368.4	436	240	62.8	19.9	323.5	413.3	383	322.5	414.0
118	23	10	387.4	502	218	91.3	28.9	322.1	452.7	382	322.0	447.0
119	23	10	370.5	509	203	96.7	30.6	301.3	439.7	370	304.0	436.0
120	23	10	407.1	495	232	77.3	24.4	351.8	462.4	419	345.0	459.0
121	23	10	358.8	517	153	120.9	38.2	272.4	445.2	368	260.0	441.0
122	24	10	295.1	402	181	82.9	26.2	235.8	354.4	297	241.0	352.0
123	24	10	275.7	379	176	61.7	19.6	231.6	319.8	277	230.0	320.0
124	25	10	421.0	460	361	38.6	12.2	393.4	448.6	421	396.5	449.0
125	25	10	457.7	536	352	61.5	19.5	413.7	501.7	456	410.0	501.5

### Appendix 3. Descriptive statistics of force to fracture for Sets

This appendix tabulates descriptive statistics of force to fracture data (in Newtons) for sets of samples. The Standard Deviation (S.D.) is "n-1" weighted. The confidence level achieved in the confidence interval for the median was from 94.8% to 95.0% except for Set 11a where 94.1% and Set 11p where 95.5% was achieved.

	N	Mean	Max	Min	S.D.	SEMean	95% C.I. for Mean		Median	C.I. for Median	
							From	To		From	To
set1	40	347.0	494	125	85.8	13.6	319.5	374.4	360	322.5	378.5
set2	20	262.8	485	142	71.1	15.9	229.5	296.1	253.5	231.5	285.0
set3	20	315.5	400	160	66.7	14.9	284.2	346.7	329	282.5	355.5
set4	19	259.2	378	147	62.4	14.3	229.1	289.3	254	229.0	289.5
set5	20	323.7	458	227	59.2	13.2	296.0	351.4	320	296.0	347.0
set6	30	297.7	387	178	56.3	10.3	276.7	318.7	298	278.0	320.0
set7	30	356.4	489	107	74.7	13.6	328.5	384.3	365.5	338.0	386.0
set8	19	334.4	418	231	63.6	14.6	303.7	365.0	316	302.5	362.5
set9	20	372.8	476	231	67.2	15.0	341.3	404.2	367	342.5	409.5
set10	15	356.1	463	245	72.7	18.8	315.9	396.4	343	309.0	391.5
set11	30	347.3	474	237	75.2	13.7	319.3	375.4	353	316.0	376.0
set12	30	312.4	447	172	67.7	12.4	287.1	337.7	314.5	288.0	338.5
set13	30	294.1	403	116	64.4	11.8	270.1	318.2	299	273.0	320.0
set14	30	328.3	477	152	84.9	15.5	296.6	360.0	345	297.5	364.5
set15	20	313.1	414	185	52.8	11.8	288.4	337.8	316.5	288.0	338.0
set16	20	190.1	314	135	48.2	10.8	167.6	212.7	180.5	164.5	210.0
set17	20	444.2	566	315	70.0	15.7	411.4	477.0	446	406.0	485.5
set18	20	353.5	436	215	63.6	14.2	323.8	383.3	368	322.5	388.5
set19	17	447.7	542	259	81.1	19.7	406.0	489.4	462	400.5	493.0
set20	16	347.9	443	185	62.9	15.7	314.3	381.4	350.5	318.0	378.5
set21	20	281.4	432	168	67.1	15.0	250.0	312.8	282.5	249.0	312.0
set22	116	357.9	519	123	79.9	7.4	343.2	372.6	360.5	342.5	373.5
set23	40	381.0	517	153	95.7	15.1	350.3	411.6	379.5	356.5	419.5
set24	20	285.4	402	176	71.8	16.1	251.8	319.0	292.0	251.0	321.5
set25	20	439.4	536	352	53.4	11.9	414.3	464.4	441.5	410.0	462.0
set1p	23	320.7	472	125	91.8	19.1	281.0	360.4	334	282.5	362.5
set1j	15	376.9	494	271	62.2	16.1	342.5	411.4	383	342.5	413.5
set7&9p	24	373.8	476	231	61.8	12.6	347.7	399.9	383	351.5	402.5
set7&9j	25	355.2	489	107	80.1	16.0	322.2	388.3	351	328.0	389.0
set11p	11	361.1	474	237	93.2	28.1	298.5	423.7	355	295.0	429.0
set11j	13	324.6	416	246	67.3	18.7	283.9	365.3	313	277.5	369.0
set11a	6	371.3	452	322	45.7	18.7	323.3	419.3	357.5	334.0	422.5
set22p	31	363.8	519	187	75.2	13.5	336.3	391.4	364.0	338.5	391.0
set22j	67	353.6	518	123	83.4	10.2	333.2	373.9	347.0	333.5	375.5
set22a	18	363.6	507	254	77.6	18.3	325.0	402.1	358.5	320.0	402.0
a21p	42	363.1	519	187	79.1	12.2	338.5	387.8	362	338.5	389.0
a21j	80	348.9	518	123	81.3	9.1	330.8	367.0	344.5	331.0	368.5
a21a	24	365.5	507	254	70.1	14.3	335.9	395.1	358.5	332.5	396.5
verp	42	317.1	477	152	68.7	10.6	295.7	338.5	318	298.5	340.5
verj	54	298.2	458	116	69.8	9.5	279.1	317.2	297	279.0	318.0
vera	14	349.1	447	219	62.2	16.6	313.2	385.1	356.5	309.0	379.5

#### Appendix 4. Length and weight of samples (Batches 94 to 125)

This appendix tabulates the raw data for lengths (in millimetres) and weights (in grams) of the parent and addition parts of the specimens in Batches 94 to 125. The load at fracture, the set and batch numbers, the lumen of the mould used for condensation and failure origin for each sample are included. The data for joined samples are followed by data for the one-piece samples.

The first five columns use the same headings as those in Appendix 1. For joined samples, the remaining column headings are identified as follows:

Plen= Length of parent; Pwt= Weight of parent;  
 Tlen= Length of prepared parent; Twt= Weight of prepared parent;  
 Jlen= Length of joined sample; Jwt= Weight of joined sample;  
 Alen= Length of added part; Awt= Weight increase after addition.

Set	Bat	Lum	Loc	Load	Plen	Pwt	Tlen	Twt	Jlen	Jwt	Alen	Awt
12	96	1	2	206.8	6.83	0.9436	6.76	0.9327	13.32	1.8751	6.56	0.9424
12	96	2	3	350.8	6.95	0.9591	6.85	0.9489	13.59	1.9104	6.74	0.9615
12	96	3	1	280.7	6.86	0.9773	6.78	0.9698	13.42	1.9115	6.64	0.9417
12	96	4	2	221.3	6.92	0.9646	6.81	0.9552	13.34	1.8804	6.53	0.9252
12	96	5	2	289.2	6.90	0.9467	6.70	0.9284	13.32	1.8661	6.62	0.9377
12	96	6	3	360.9	6.93	0.9616	6.79	0.9469	13.28	1.8830	6.49	0.9361
12	96	7	2	326.1	6.91	0.9592	6.73	0.9375	13.16	1.8474	6.43	0.9099
12	96	8	2	378.2	6.87	0.9529	6.77	0.9417	12.94	1.8197	6.17	0.8780
12	96	9	2	251.3	6.84	0.9535	6.69	0.9370	13.09	1.8389	6.40	0.9019
12	96	10	1	368.7	6.90	0.9645	6.80	0.9511	13.12	1.8465	6.32	0.8954
13	97	1	2	246.8	7.03	0.9983	6.91	0.9884	13.62	1.9448	6.71	0.9564
13	97	2	2	192.3	6.94	0.9700	6.84	0.9620	13.47	1.9155	6.63	0.9535
13	97	3	2	116.4	6.95	0.9816	6.89	0.9728	13.36	1.9090	6.47	0.9362
13	97	4	2	274.9	6.94	0.9732	6.85	0.9677	13.28	1.8884	6.43	0.9207
13	97	5	2	291.9	6.92	0.9705	6.75	0.9554	13.28	1.8909	6.53	0.9355
13	97	6	2	195.5	6.90	0.9666	6.75	0.9520	13.14	1.8744	6.39	0.9224
13	97	7	2	235.9	6.86	0.9744	6.68	0.9534	13.14	1.8952	6.46	0.9418
13	97	8	2	299.4	6.87	0.9669	6.64	0.9422	13.09	1.8593	6.45	0.9171
13	97	9	2	262.4	6.86	0.9596	6.66	0.9407	13.27	1.8833	6.61	0.9426
13	97	10	1	375.1	6.86	0.9661	6.65	0.9490	13.18	1.8602	6.53	0.9112
14	98	1	2	358.3	6.69	0.9368	6.58	0.9250	13.16	1.8805	6.58	0.9555
14	98	2	1	307.0	6.71	0.9390	6.68	0.9287	13.24	1.8858	6.56	0.9571
14	98	3	2	213.5	6.72	0.9338	6.64	0.9247	13.09	1.8586	6.45	0.9339
14	98	4	1	250.9	6.74	0.9382	6.67	0.9308	13.12	1.8642	6.45	0.9334
14	98	5	2	256.7	6.59	0.9137	6.52	0.9086	12.95	1.8384	6.43	0.9298
14	98	6	1	222.6	6.45	0.8873	6.24	0.8702	12.50	1.7819	6.26	0.9117
14	98	7	2	302.3	6.41	0.8877	6.22	0.8665	12.58	1.7951	6.36	0.9286
14	98	8	2	291.8	6.41	0.8905	6.29	0.8754	12.60	1.7999	6.31	0.9245
14	98	9	1	378.3	6.56	0.9038	6.37	0.8828	12.83	1.7966	6.46	0.9138
14	98	10	1	235.5	6.58	0.9129	6.41	0.8960	12.72	1.7817	6.31	0.8857
12	99	1	3	339.7	6.91	0.9737	6.83	0.9644	13.44	1.9047	6.61	0.9403
12	99	2	1	193.8	7.09	0.9888	6.90	0.9680	13.68	1.9202	6.78	0.9522
12	99	3	1	303.5	6.89	0.9646	6.74	0.9485	13.38	1.8860	6.64	0.9375
12	99	4	2	294.6	7.03	0.9710	6.61	0.9113	13.23	1.8541	6.62	0.9428
12	99	5	3	241.9	6.95	0.9754	6.74	0.9530	13.31	1.8817	6.57	0.9287
12	99	6	1	302.3	6.86	0.9523	6.71	0.9391	13.10	1.8441	6.39	0.9050
12	99	7	3	360.4	6.81	0.9530	6.61	0.9283	13.18	1.8601	6.57	0.9318
12	99	8	1	431.2	6.82	0.9667	6.65	0.9501	13.03	1.8520	6.38	0.9019
12	99	9	1	298.6	6.80	0.9462	6.52	0.9115	12.88	1.8087	6.36	0.8972
12	99	10	2	395.7	6.90	0.9624	6.68	0.9293	13.04	1.8278	6.36	0.8985

Set	Bat	Lum	Loc	Load	Plen	Pwt	Tlen	Twt	Jlen	Jwt	Alen	Awt
13	100	1	2	352.0	6.99	0.9863	6.80	0.9599	13.24	1.8818	6.44	0.9219
13	100	2	2	299.0	6.92	0.9727	6.75	0.9519	13.20	1.8670	6.45	0.9151
13	100	3	2	263.3	6.83	0.9539	6.61	0.9259	12.94	1.8273	6.33	0.9014
13	100	4	1	320.2	6.82	0.9444	6.68	0.9286	13.05	1.8302	6.37	0.9016
13	100	5	1	230.8	6.89	0.9637	6.75	0.9489	13.16	1.8582	6.41	0.9093
13	100	6	2	361.0	6.82	0.9599	6.61	0.9335	12.96	1.8370	6.35	0.9035
13	100	7	2	317.4	6.78	0.9531	6.62	0.9359	13.05	1.8464	6.43	0.9105
13	100	8	1	331.1	6.78	0.9467	6.65	0.9330	13.09	1.8443	6.44	0.9113
13	100	9	2	266.7	6.87	0.9614	6.69	0.9395	13.10	1.8469	6.41	0.9074
13	100	10	1	317.3	6.83	0.9586	6.67	0.9396	12.97	1.8252	6.30	0.8856
14	101	1	1	250.6	6.46	0.8937	6.30	0.8758	12.80	1.7995	6.50	0.9237
14	101	2	2	409.2	6.68	0.9271	6.54	0.9112	12.92	1.8205	6.38	0.9093
14	101	3	1	282.5	6.59	0.9262	6.33	0.8968	12.69	1.7972	6.36	0.9004
14	101	4	1	375.9	6.50	0.9097	6.24	0.8827	12.55	1.7722	6.31	0.8895
14	101	5	1	265.3	6.45	0.9076	6.30	0.8926	12.73	1.8036	6.43	0.9110
14	101	6	2	407.1	6.31	0.8751	6.18	0.8631	12.51	1.7629	6.33	0.8998
14	101	7	2	458.2	6.28	0.8704	6.03	0.8447	12.23	1.7214	6.20	0.8767
14	101	8	1	383.7	6.26	0.8635	6.07	0.8451	12.72	1.7916	6.65	0.9465
14	101	9	2	381.7	6.28	0.8658	6.13	0.8484	12.58	1.7551	6.45	0.9067
14	101	10	1	151.8	6.16	0.8612	5.95	0.8404	12.32	1.7264	6.37	0.8860
15	102	1	3	353.2	6.46	0.9014	6.29	0.8830	12.69	1.8031	6.40	0.9201
15	102	2	1	316.9	6.44	0.8909	6.30	0.8761	12.74	1.7634	6.44	0.8873
15	102	3	1	369.7	6.33	0.8831	6.19	0.8694	12.59	1.7671	6.40	0.8977
15	102	4	3	379.3	6.37	0.8842	6.13	0.8572	12.49	1.7360	6.36	0.8788
15	102	5	1	360.4	6.36	0.8862	6.22	0.8718	12.72	1.7881	6.50	0.9163
15	102	6	2	330.6	6.32	0.8786	6.12	0.8568	12.47	1.7534	6.35	0.8966
15	102	7	2	302.8	6.24	0.8636	6.10	0.8490	12.32	1.7242	6.22	0.8752
15	102	8	1	302.8	6.18	0.8514	6.00	0.8322	12.29	1.7219	6.29	0.8897
15	102	9	1	338.3	6.24	0.8662	6.06	0.8459	12.52	1.7535	6.46	0.9076
15	102	10	2	315.9	6.20	0.8530	5.95	0.8227	12.21	1.6956	6.26	0.8729
12	103	1	1	171.7	6.86	0.9456	6.73	0.9296	13.30	1.8572	6.57	0.9276
12	103	2	3	219.1	6.87	0.9508	6.64	0.9220	13.25	1.8594	6.61	0.9374
12	103	3	1	319.4	6.89	0.9726	6.79	0.9588	13.46	1.9166	6.67	0.9578
12	103	4	1	308.4	6.92	0.9686	6.75	0.9462	13.15	1.8539	6.40	0.9077
12	103	5	3	446.5	6.78	0.9368	6.63	0.9196	13.11	1.8544	6.48	0.9348
12	103	6	1	366.0	6.76	0.9394	6.51	0.9090	12.86	1.8160	6.35	0.9070
12	103	7	2	334.0	6.82	0.9460	6.67	0.9286	12.90	1.8194	6.23	0.8908
12	103	8	1	357.1	6.84	0.9605	6.67	0.9384	13.42	1.9060	6.75	0.9676
12	103	9	1	343.0	6.83	0.9496	6.58	0.9184	12.96	1.8260	6.38	0.9076
12	103	10	2	310.3	6.90	0.9584	6.67	0.9257	12.93	1.8150	6.26	0.8893
13	104	1	2	230.2	6.87	0.9834	6.68	0.9601	13.19	1.8860	6.51	0.9259
13	104	2	2	263.1	6.96	0.9840	6.73	0.9617	13.15	1.8818	6.42	0.9201
13	104	3	2	284.0	6.82	0.9710	6.61	0.9460	12.99	1.8563	6.38	0.9103
13	104	4	3	341.3	6.76	0.9464	6.58	0.9240	12.93	1.8221	6.35	0.8981
13	104	5	2	402.8	6.78	0.9455	6.60	0.9275	12.97	1.8274	6.37	0.8999
13	104	6	1	345.1	6.78	0.9497	6.55	0.9243	12.83	1.8294	6.28	0.9051
13	104	7	2	370.0	6.90	0.9646	6.65	0.9434	13.02	1.8463	6.37	0.9029
13	104	8	3	311.5	6.73	0.9355	6.58	0.9188	12.90	1.8249	6.32	0.9061
13	104	9	1	345.3	6.79	0.9489	6.55	0.9202	12.82	1.8026	6.27	0.8824
13	104	10	2	383.3	6.89	0.9662	6.65	0.9387	12.93	1.8214	6.28	0.8827
14	105	1	2	173.7		0.8993	6.32	0.8813	12.55	1.7776	6.23	0.8963
14	105	2	1	314.0		0.9163	6.37	0.8957	12.91	1.8439	6.54	0.9482
14	105	3	2	343.6		0.8949	6.26	0.8804	12.87	1.8200	6.61	0.9396
14	105	4	3	375.6		0.8999	6.31	0.8829	12.69	1.7922	6.38	0.9093
14	105	5	3	442.3		0.8881	6.28	0.8692	12.50	1.7540	6.22	0.8848
14	105	6	1	476.6		0.8803	6.15	0.8594	12.36	1.7511	6.21	0.8917
14	105	7	2	345.6		0.8631	6.14	0.8498	12.36	1.7428	6.22	0.8930
14	105	8	1	388.6		0.9020	6.25	0.8874	12.54	1.7865	6.29	0.8991
14	105	9	3	365.1		0.8875	6.16	0.8629	12.44	1.7509	6.28	0.8880
14	105	10	1	436.6		0.8541	5.94	0.8374	12.25	1.7216	6.31	0.8842
15	106	1	1	344.7	6.58	0.9079	6.45	0.8933	12.69	1.7839	6.24	0.8906
15	106	2	2	414.4	6.40	0.9016	6.30	0.8888	12.68	1.7969	6.38	0.9081
15	106	3	2	287.4	6.47	0.8957	6.35	0.8852	12.76	1.7996	6.41	0.9144
15	106	4	2	185.2	6.63	0.9285	6.48	0.9091	12.74	1.8004	6.26	0.8913
15	106	5	2	303.5	6.43	0.8889	6.29	0.8747	12.70	1.7793	6.41	0.9046
15	106	6	1	252.9	6.44	0.8978	6.31	0.8760	12.50	1.7728	6.19	0.8968
15	106	7	2	243.1	6.35	0.8787	6.25	0.8574	12.46	1.7525	6.21	0.8951
15	106	8	2	270.8	6.43	0.9049	6.27	0.8813	12.37	1.7500	6.10	0.8687
15	106	9	2	317.6	6.32	0.8720	6.13	0.8488	12.43	1.7350	6.30	0.8862
15	106	10	2	272.2	6.33	0.8734	6.18	0.8550	12.49	1.7500	6.31	0.8950

Set	Bat	Lum	Loc	Load	Plen	Pwt	Tlen	Twt	Jlen	Jwt	Alen	Awt
	109	1	3	368.1	7.55	1.0530	7.47	1.0430	14.77	2.0551	7.30	1.0121
	109	2	2	341.4	7.74	1.0676	7.62	1.0520	15.15	2.1108	7.53	1.0588
	109	3	2	308.1	7.85	1.1024	7.68	1.0829	14.91	2.0926	7.23	1.0097
	109	4			7.69	1.0791	7.56	1.0625	15.34	2.1508	7.78	1.0883
	109	5	3	519.2	7.48	1.0372	7.31	1.0142	14.81	2.0717	7.50	1.0575
	109	6	3	363.2	7.41	1.0306	7.23	1.0070	14.95	2.0812	7.72	1.0742
	109	7	3	415.6	7.55	1.0502	7.45	1.0371	14.65	2.0584	7.20	1.0213
	109	8	2	412.4	7.81	1.0897	7.65	1.0708	15.13	2.1217	7.48	1.0509
	109	9	1	431.9	7.48	1.0418	7.41	1.0273	14.83	2.0762	7.42	1.0489
	109	10	3	431.2	7.76	1.0827	7.67	1.0723	15.01	2.0903	7.34	1.0180
	110	1	1	340.6	7.75	1.1018	7.68	1.0940	15.29	2.1586	7.61	1.0646
	110	2	2	203.9	7.75	1.1000	7.72	1.0916	15.34	2.1774	7.62	1.0858
	110	3	2	358.7	7.70	1.0939	7.66	1.0891	15.11	2.1653	7.45	1.0762
	110	4	2	286.0	7.90	1.1202	7.80	1.1082	15.43	2.2001	7.63	1.0919
	110	5	2	325.2	7.82	1.1111	7.73	1.1005	15.30	2.1864	7.57	1.0859
	110	6	2	303.8	7.86	1.1223	7.80	1.1159	15.34	2.1814	7.54	1.0655
	110	7	2	430.8	7.79	1.1169	7.72	1.1090	15.11	2.1862	7.39	1.0772
	110	8	1	315.4	7.69	1.1007	7.63	1.0936	15.15	2.1644	7.52	1.0708
	110	9	1	380.8	7.84	1.1179	7.75	1.1077	15.13	2.1621	7.38	1.0544
	110	10	2	388.4	7.79	1.1203	7.72	1.1105	15.27	2.1904	7.55	1.0799
18	111	1	2	215.3	7.73	1.0820	7.57	1.0615	15.02	2.1067	7.45	1.0452
18	111	2	3	379.7	7.70	1.0725	7.53	1.0520	14.98	2.1042	7.45	1.0522
18	111	3	2	309.3	7.73	1.0691	7.65	1.0595	14.81	2.0691	7.16	1.0096
18	111	4	3	349.6	7.78	1.0923	7.63	1.0741	14.91	2.0896	7.28	1.0155
18	111	5	2	394.6	7.76	1.0724	7.63	1.0584	14.87	2.0678	7.24	1.0094
18	111	6	2	284.7	7.77	1.0940	7.63	1.0784	14.90	2.0922	7.27	1.0138
18	111	7	2	380.8	7.73	1.0897	7.61	1.0740	14.73	2.0739	7.12	0.9999
18	111	8	2	359.8	7.57	1.0617	7.50	1.0510	14.66	2.0589	7.16	1.0079
18	111	9	1	427.3	7.86	1.0933	7.74	1.0791	14.91	2.0809	7.17	1.0018
18	111	10	2	285.1	7.69	1.0709	7.54	1.0527	14.73	2.0505	7.19	0.9978
19	112	1	1	308.9	7.16	0.9941	7.11	0.9875	14.05	1.9524	6.94	0.9649
19	112	2			7.22	0.9959	7.11	0.9827	14.03	1.9331	6.92	0.9504
19	112	3	2	511.7	7.20	0.9951	7.13	0.9865	14.10	1.9286	6.97	0.9865
19	112	4	1	461.5	7.22	0.9977	7.14	0.9898	14.04	1.9465	6.90	0.9567
19	112	5	2	528.5	7.18	0.9931	7.10	0.9839	13.97	1.9467	6.87	0.9628
19	112	6			7.16	0.9793	7.05	0.9793	13.81	1.9187	6.76	0.9394
19	112	7	1	541.8	7.14	0.9907	7.08	0.9825	13.91	1.9458	6.83	0.9633
19	112	8	2	330.1	7.18	0.9959	7.12	0.9881	13.92	1.9365	6.80	0.9484
19	112	9	2	520.8	7.20	0.9989	7.14	0.9919	14.03	1.9540	6.89	0.9621
19	112	10	2	456.7	7.19	1.0007	7.13	0.9926	13.99	1.9449	6.86	0.9523
20	113	1	1	349.6	7.97	1.1349	7.87	1.1239	15.52	2.2236	7.65	1.0997
20	113	2	1	350.3	7.89	1.1282	7.81	1.1183	15.50	2.2355	7.69	1.1172
20	113	3	1	184.6	7.95	1.1401	7.89	1.1329	15.36	2.2167	7.47	1.0838
20	113	4			7.91	1.1344	7.84	1.1252	15.14	2.1874	7.30	1.0622
20	113	5	2	320.9	7.99	1.1447	7.94	1.1408	15.56	2.2438	7.62	1.1030
20	113	6			7.87	1.1341	7.78	1.1241	15.36	2.2172	7.58	1.0931
20	113	7	1	387.3	7.91	1.1420	7.85	1.1353	15.35	2.2197	7.50	1.0844
20	113	8			7.87	1.1389	7.80	1.1312	15.35	2.2174	7.55	1.0862
20	113	9			7.99	1.1515	7.86	1.1363	15.37	2.2123	7.51	1.0760
20	113	10	2	438.1	8.03	1.1622	7.94	1.1511	15.56	2.2677	7.62	1.1166
	114	1	3	445.9	7.51	1.0739	7.40	1.0596	14.88	2.1207	7.48	1.0611
	114	2	1	412.9	7.56	1.0795	7.45	1.0634	14.86	2.1278	7.41	1.0644
	114	3	1	353.4	7.57	1.0730	7.43	1.0551	14.84	2.1099	7.41	1.0548
	114	4	1	442.3	7.65	1.0876	7.63	1.0819	14.99	2.1160	7.36	1.0341
	114	5	1	292.1	7.59	1.0711	7.48	1.0580	14.86	2.1154	7.38	1.0574
	114	6	1	341.7	7.59	1.0750	7.47	1.0604	14.65	2.0975	7.18	1.0371
	114	7	2	269.1	7.56	1.0678	7.47	1.0494	14.77	2.1081	7.30	1.0587
	114	8	1	526.1	7.57	1.0930	7.39	1.0699	14.80	2.1272	7.41	1.0573
	114	9	2	474.3	7.62	1.0830	7.41	1.0552	14.69	2.0984	7.28	1.0432
	114	10	1	427.2	7.73	1.1008	7.58	1.0824	14.88	2.1150	7.30	1.0326
19	115	1	2	399.5	7.11	0.9873	7.06	0.9777	13.97	1.9396	6.91	0.9619
19	115	2	2	447.8	7.22	1.0031	7.12	0.9911	14.07	1.9664	6.95	0.9753
19	115	3	2	481.3	7.17	0.9955	7.11	0.9898	13.96	1.9464	6.85	0.9566
19	115	4	1	450.1	7.23	1.0049	7.14	0.9938	13.98	1.9514	6.84	0.9576
19	115	5	1	482.7	7.20	0.9932	7.15	0.9858	14.02	1.9519	6.87	0.9661
19	115	6	1	479.4	7.21	1.0042	7.17	0.9975	14.00	1.9590	6.83	0.9615
19	115	7	2	519.6	7.18	1.0052	7.19	0.9918	14.00	1.9629	6.81	0.9711
19	115	8	1	258.9	7.13	0.9944	7.04	0.9823	13.88	1.9337	6.84	0.9514
19	115	9	2	429.1	7.20	1.0032	7.13	0.9942	13.98	1.9472	6.85	0.9530
19	115	10			7.23	1.0064	7.15	0.9947	13.97	1.9473	6.82	0.9526

Set	Bat	Lum	Loc	Load	Plen	Pwt	Tlen	Twt	Jlen	Jwt	Alen	Awt
20	116	1	3	351.4	7.95	1.1450	7.88	1.1349	15.40	2.2172	7.52	1.0823
20	116	2	1	307.0	8.02	1.1551	7.93	1.1433	15.51	2.2360	7.58	1.0927
20	116	3	2	314.0	7.97	1.1534	7.86	1.1398	15.53	2.2455	7.67	1.1057
20	116	4	2	349.7	7.99	1.1494	7.91	1.1406	15.57	2.2490	7.66	1.1084
20	116	5	3	443.0	7.79	1.1212	7.72	1.1143	15.50	2.2699	7.78	1.1556
20	116	6	1	363.1	8.06	1.1675	8.00	1.1605	15.49	2.2430	7.49	1.0825
20	116	7	1	392.6	7.93	1.1502	7.83	1.1371	15.25	2.2291	7.42	1.0920
20	116	8	2	378.2	7.97	1.1537	7.91	1.1466	15.36	2.2283	7.45	1.0817
20	116	9	2	265.3	7.85	1.1376	7.79	1.1295	15.29	2.2226	7.50	1.0931
20	116	10	2	371.1	7.93	1.1557	7.74	1.1290	15.25	2.2183	7.51	1.0893
18	117	1	2	298.2	7.63	1.0635	7.57	1.0577	14.96	2.1084	7.39	1.0507
18	117	2	2	359.6	7.64	1.0674	7.56	1.0574	14.80	2.0849	7.24	1.0275
18	117	3	2	239.9	7.67	1.0774	7.59	1.0664	14.91	2.1050	7.32	1.0386
18	117	4	3	389.6	7.75	1.0711	7.67	1.0600	14.89	2.0877	7.22	1.0277
18	117	5	3	435.8	7.70	1.0771	7.59	1.0594	14.84	2.0884	7.25	1.0290
18	117	6	2	424.9	7.62	1.0591	7.54	1.0492	14.84	2.0876	7.30	1.0384
18	117	7	2	375.9	7.63	1.0654	7.55	1.0513	14.65	2.0792	7.10	1.0279
18	117	8	3	423.4	7.60	1.0742	7.52	1.0645	14.56	2.0562	7.04	0.9917
18	117	9	2	331.0	7.65	1.0740	7.56	1.0631	14.96	2.1220	7.40	1.0589
18	117	10	2	405.2	7.71	1.0743	7.59	1.0596	14.74	2.0633	7.15	1.0037
23	118	1	2	342.4	6.87	0.9802	6.80	0.9686	13.29	1.9070	6.49	0.9384
23	118	2	1	301.4	6.89	0.9731	6.81	0.9614	13.22	1.8847	6.41	0.9233
23	118	3	2	492.3	6.87	0.9916	6.74	0.9767	13.14	1.8981	6.40	0.9214
23	118	4	2	495.8	6.80	0.9632	6.70	0.9497	13.09	1.8700	6.39	0.9203
23	118	5	1	379.6	6.80	0.9659	6.66	0.9507	13.14	1.8825	6.48	0.9318
23	118	6	2	362.7	6.83	0.9758	6.73	0.9593	13.03	1.8767	6.30	0.9174
23	118	7	3	401.1	6.79	0.9700	6.67	0.9507	13.07	1.8746	6.40	0.9239
23	118	8	3	501.5	6.78	0.9876	6.65	0.9666	13.05	1.8947	6.40	0.9281
23	118	9	1	218.3	6.82	0.9730	6.73	0.9631	13.13	1.8752	6.40	0.9121
23	118	10	2	379.4	6.73	0.9673	6.57	0.9489	12.94	1.8594	6.37	0.9105
23	119	1	1	307.4	7.11	1.0097	6.97	0.9945	13.38	1.9230	6.41	0.9285
23	119	2	1	346.1	6.98	0.9845	6.90	0.9787	13.19	1.8805	6.29	0.9018
23	119	3	1	434.5	6.95	0.9897	6.80	0.9691	13.10	1.8744	6.30	0.9053
23	119	4	1	375.0	6.95	0.9863	6.83	0.9703	13.05	1.8662	6.22	0.8959
23	119	5	2	496.5	7.00	0.9931	6.91	0.9794	13.48	1.9378	6.57	0.9584
23	119	6	1	315.9	6.88	0.9785	6.75	0.9642	13.10	1.8783	6.35	0.9141
23	119	7	1	292.0	6.93	0.9925	6.79	0.9720	13.09	1.8912	6.30	0.9192
23	119	8	2	424.9	6.91	0.9918	6.80	0.9779	13.10	1.8892	6.30	0.9113
23	119	9	1	203.3	6.91	0.9878	6.79	0.9757	13.01	1.8653	6.22	0.8896
23	119	10	2	509.0	6.94	1.0075	6.75	0.9838	12.98	1.8741	6.23	0.8903
23	120	1	2	231.6	6.71	0.9487	6.62	0.9375	13.25	1.9002	6.63	0.9627
23	120	2	1	428.0	6.73	0.9500	6.61	0.9361	13.14	1.8848	6.53	0.9487
23	120	3	2	379.0	6.69	0.9469	6.58	0.9354	12.96	1.8531	6.38	0.9177
23	120	4	2	345.2	6.79	0.9637	6.53	0.9357	13.01	1.8702	6.48	0.9345
23	120	5	2	433.3	6.67	0.9524	6.51	0.9329	12.99	1.8658	6.48	0.9329
23	120	6	2	458.6	6.38	0.9066	6.20	0.8854	12.78	1.8364	6.58	0.9510
23	120	7	2	495.3	6.40	0.9017	6.30	0.8912	12.92	1.8545	6.62	0.9633
23	120	8	2	480.8	6.37	0.8976	6.17	0.8722	12.64	1.8069	6.47	0.9347
23	120	9	2	382.7	6.43	0.9060	6.22	0.8787	12.76	1.8275	6.54	0.9488
23	120	10	3	435.7		0.9284	6.03	0.8568	12.43	1.7699	6.40	0.9131
23	121	1	2	364.6	6.53	0.9279	6.47	0.9180	13.07	1.8751	6.60	0.9571
23	121	2	1	348.0	6.62	0.9393	6.43	0.9176	12.94	1.8333	6.51	0.9157
23	121	3	1	349.7	6.51	0.9266	6.38	0.9189	12.78	1.8271	6.40	0.9082
23	121	4	2	438.6	6.61	0.9402	6.51	0.9251	13.01	1.8587	6.50	0.9336
23	121	5	1	425.2	6.54	0.9254	6.40	0.9056	12.87	1.8415	6.47	0.9359
23	121	6	1	152.5	6.35	0.8996	6.21	0.8798	12.75	1.8284	6.54	0.9486
23	121	7	2	154.5	6.34	0.8933	6.25	0.8799	12.52	1.7916	6.27	0.9117
23	121	8	2	516.7	6.46	0.9177	6.30	0.8970	12.77	1.8321	6.47	0.9351
23	121	9	1	464.6	6.58	0.9312	6.48	0.9195	12.92	1.8525	6.44	0.9330
23	121	10	2	371.2	6.39	0.9041	6.05	0.8634	12.50	1.7937	6.45	0.9303

This page tabulates the raw data for one-piece samples in Batches 94 to 125.

The new column headings are identified as follows:

Len= sample length; Wt= sample weight.

Set	Bat	Lum	Load	Len	Wt	Set	Bat	Lum	Load	Len	Wt
16	94	1	176.2	10.80	1.5267	24	122	1	352.1	10.62	1.5060
16	94	2	142.8	10.64	1.5033	24	122	2	382.1	10.72	1.5272
16	94	3	158.0	10.51	1.4936	24	122	3	193.0	10.64	1.5178
16	94	4	212.8	10.45	1.4733	24	122	4	320.7	10.72	1.5195
16	94	5	195.2	10.59	1.4886	24	122	5	300.5	10.57	1.4970
16	94	6	151.0	10.53	1.4976	24	122	6	181.3	10.61	1.5124
16	94	7	142.4	10.40	1.4629	24	122	7	181.0	10.77	1.5340
16	94	8	257.9	10.42	1.4754	24	122	8	344.5	10.62	1.5222
16	94	9	170.3	10.56	1.4906	24	122	9	292.5	10.55	1.5064
16	94	10	204.0	10.43	1.4743	24	122	10	401.6	10.35	1.4818
17	95	1	415.1	9.84	1.3592	24	123	1	223.8	10.90	1.5573
17	95	2	477.1	9.79	1.3542	24	123	2	329.5	10.68	1.5258
17	95	3	488.0	9.77	1.3484	24	123	3	224.6	10.66	1.5132
17	95	4	486.7	9.77	1.3542	24	123	4	247.0	10.69	1.5283
17	95	5	404.8	9.55	1.3304	24	123	5	261.0	10.70	1.5202
17	95	6	542.5	9.50	1.3162	24	123	6	176.3	10.56	1.5059
17	95	7	488.4	9.52	1.3191	24	123	7	378.8	10.50	1.4942
17	95	8	566.3		1.3565	24	123	8	291.0	10.56	1.5271
17	95	9	485.4	9.61	1.3290	24	123	9	284.4	10.61	1.5157
17	95	10	414.6	9.62	1.3316	24	123	10	339.6	10.63	1.5206
16	107	1	135.3	10.47	1.4775	25	124	1	459.2	10.02	1.4312
16	107	2	169.3	10.45	1.4761	25	124	2	439.2	9.93	1.4137
16	107	3	207.4	10.40	1.4515	25	124	3	459.9	9.92	1.4065
16	107	4	184.8	10.37	1.4515	25	124	4	360.9	10.05	1.4347
16	107	5	141.3	10.25	1.4354	25	124	5	420.5	9.99	1.4178
16	107	6	150.0	10.26	1.4431	25	124	6	371.9	9.84	1.4037
16	107	7	225.9	10.29	1.4468	25	124	7	448.2	9.91	1.4123
16	107	8	271.5	10.25	1.4420	25	124	8	433.9	9.82	1.3973
16	107	9	193.8	10.28	1.4300	25	124	9	370.3	9.91	1.4014
16	107	10	314.2	10.20	1.4307	25	124	10	445.6	9.76	1.3941
17	108	1	400.1	9.65	1.3424	25	125	1	467.2	10.00	1.4230
17	108	2	399.1	9.61	1.3291	25	125	2	536.4	10.20	1.4650
17	108	3	366.7	9.40	1.3173	25	125	3	518.1	9.88	1.4076
17	108	4	496.6	9.53	1.3208	25	125	4	351.8	9.95	1.4132
17	108	5	384.9	9.72	1.3574	25	125	5	436.8	9.97	1.4091
17	108	6	315.2	9.55	1.3216	25	125	6	484.9	9.77	1.3813
17	108	7	506.5	9.61	1.3197	25	125	7	383.3	9.71	1.3697
17	108	8	409.9	9.37	1.3055	25	125	8	425.9	9.69	1.3663
17	108	9	510.9	9.40	1.3068	25	125	9	529.0	9.72	1.3812
17	108	10	324.3	9.47	1.3147	25	125	10	443.7	9.76	1.3987

### Appendix 5. Statistics for sample failure location

This appendix lists the numbers of joined specimens and the distributions of fracture origin for Sets, pooled sets and subsets. The results of Fisher's Exact Test are displayed on the hypothesis that the expected outcome of the flexural test was that in 25% of samples fracture initiated in the parent part, 50% at the joint and 25% in the addition part.

The results of the Chi-squared test with Yates's continuity correction (Armitage and Berry, 1987) for each data set on a "3x2" table are included.

Set	Number of samples failed at the specified location and outcome of Fisher's test.						Overall Chi <sup>2</sup> p= (2df)	
	Total	Parent	p=	Joint	p=	Addition		p=
1	40	23	0.003	15	0.2	2	0.013	0.012
4	19	4	0.6	15	0.07	0	0.046	0.15
5	20	5	0.6	14	0.17	1	0.09	0.37
7	30	16	0.02	14	0.7	0	0.005	0.018
8	19	3	0.5	16	0.03	0	0.046	0.12
9	20	8	0.25	11	0.5	1	0.09	0.41
11	30	11	0.2	13	0.4	6	0.5	0.82
22	116	31	0.4	67	0.15	18	0.05	0.27
11 & 22	146	42	0.3	80	0.2	24	0.01	0.26
12	30	13	0.1	10	0.15	7	0.6	0.44
13	30	7	0.6	21	0.09	2	0.065	0.24
14	30	15	0.04	12	0.3	3	0.13	0.2
15	20	7	0.4	11	0.5	2	0.2	0.72
12 to 15	110	42	0.02	54	0.5	14	0.02	0.041
18 ANA	20	1	0.09	14	0.16	5	0.6	0.37
19 TYT	17	7	0.3	10	0.4	0	0.04	0.25
20 ACAP	16	7	0.2	7	0.8	2	0.3	0.77
DISP	10	3	0.8	7	0.3	0	0.2	0.60
MCAP	10	7	0.05	2	0.2	1	0.5	0.38
A21	9	1	0.5	3	0.4	5	0.2	0.79
23	40	16	0.12	21	0.67	3	0.03	0.15

## Appendix 6. Published work

This appendix contains a copy of the author's article *Amalgam Addition Restorations*, published in *Dental Update* 1981, 8 (6): 457-463, reproduced from *Dental Update* by permission of George Warman Publications (UK) Ltd.

# Amalgam Addition Restorations

Allan H. Cook

IT may not be commonly known that it is possible to bond new amalgam to an existing amalgam filling with a bond which is strong enough for clinical purposes without using undercuts or dovetails.

A simple method will be described for the addition of amalgam to an existing filling in cases where a cusp has fractured off in a caries-free tooth. Many patients are worse off as a result of conventional treatment for this type of case. Where restorative treatment is difficult or demands strict attention to detail of technique, the greater is the likelihood of deficiencies in the result. Conversely, the use of a simple technique is likely to give improved results.

In the type of case considered here, the patient often attends as an emergency with a history of a piece of tooth having broken off and, although there is no pain, the sharp edges cause irritation to the tongue.

On examination, one finds a mesio-occlusodistal (MOD) amalgam filling firmly in place with a smooth oblique fracture in dentine from occlusal lock down to gingival level. There is no caries (Figures 1 and 2).

## Equipment

A mechanical amalgamator such as a Dentomat is advised to produce a smooth mix with a minimum of mercury. The author always uses Thessco 'M' lathe-cut alloy. A Densco Condensaire mechanical amalgam condenser (Teledyne Dental Equipment Co, Denver, Colorado, USA) is required for producing the bond and cusp build-up. This inexpensive item is regarded as essential equipment. It is an air driven low frequency (70 Hz) vibrator with condensing tips of various sizes and shapes. The smallest cylindrical tip, diameter 1.14 mm is used in this work (see Figure 5).

## Technique

### Preparation

All of the exposed amalgam surface is 'freshened-up' and roughened using a diamond bur in an air turbine

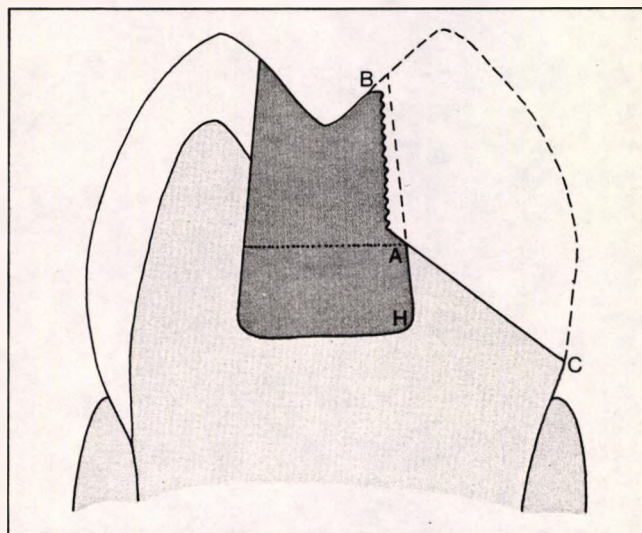
*Allan H. Cook, BDS, LDS RCS (Eng), is a General Dental Practitioner in London. This article is based on a lecture presented to Enfield and District BDA.*

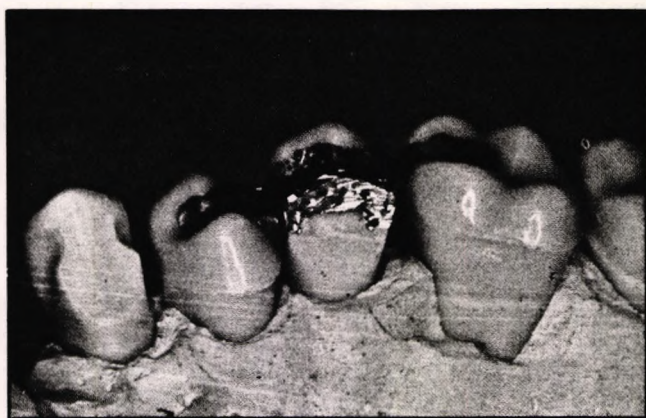


Figure 1. Typical clinical case, preoperatively.

with copious water spray. Dovetails or undercuts in amalgam or tooth substance are specifically not required and should be avoided. The sharp angle at the occlusal surface (B, Figure 2) is bevelled off. This obscures the join at the occlusal giving an improved surface. Roughening of the surface prevents the first

Figure 2. Buccolingual section of a tooth with MOD filling indicating the extent of the preparation in amalgam.





**Figure 3.** Exposed amalgam surface 'freshened up' and roughened.



**Figure 5.** First increment of amalgam is thoroughly 'rubbed in' to all of the freshened-up surface.

increment of new amalgam from slipping off during condensation (Figure 3).

#### Condensation

It is essential that everything is perfectly dry for the next stage. Even the slightest trace of moisture will cause failure of the bond. A small increment of freshly mixed amalgam is 'squidged' from a carrier along the freshened-up surface (Figure 4a and b). Using the Condensaire mechanical condenser, this amalgam is thoroughly 'rubbed in' to all of the freshened-up surface (Figure 5). Small increments are progressively added and condensed into place (Figures 6a and b). With a little practice it is possible to build up a convex cusp which is really solidly condensed. The use of a matrix band is not advised in this type of case. The cusp is very slightly

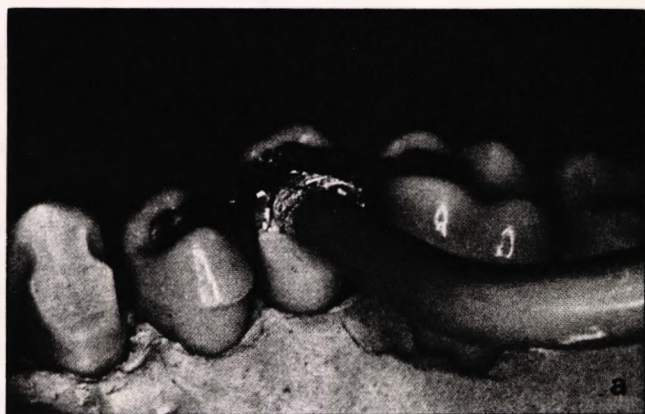
overfilled. Trimming proceeds as soon as condensation is completed. All interproximal and subgingival excess is easily removed with a smooth, straight probe using the tooth surface and amalgam margins as a guide (Figures 7a and b). The amalgam is left with a smoothly bur-nished surface (Figure 8) and all pieces of waste amalgam are washed away with a water jet and aspirated. The patient is told not to eat on that side for the rest of the day to allow maximum strength to develop before stressing the restoration.

#### Possible Criticisms

##### Strength of Bond

My experience of a large number of cases over many years indicates that the bond rarely fails, so long as the technique is followed correctly.

**Figure 4(a) and (b).** A small increment of freshly mixed amalgam is 'squidged' from the amalgam gun along the freshened-up surface.



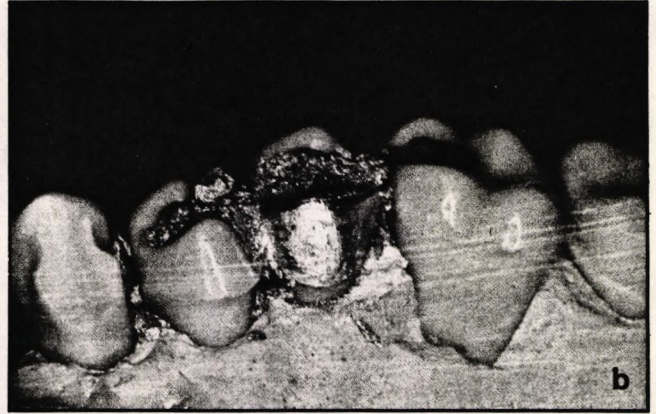
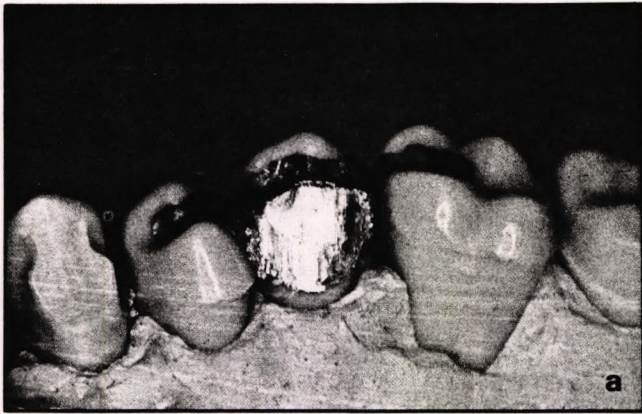


Figure 6(a) and (b). *Progressive increments of amalgam build up a cusp.*

#### Retention of Original Amalgam Fails

This happens infrequently. A conventional pinned amalgam or gold crown is then required. Figure 2 shows a triangular area of dentine, AHC, which is responsible for retention of the original amalgam. It is important to preserve the strength of this dentine: pits or dovetails in this area must be avoided as they might weaken the tooth sufficiently to cause failure of retention.

#### Caries

If caries has caused the cusp fracture it will be seen on the fracture surface. Obviously, all caries must be removed: in most cases involving removal of the entire original amalgam. On the other hand, the operator may have placed the restoration recently himself. He would (of course!) then guarantee the tooth to be caries-free. A

positive diagnosis of caries should be made before destroying an existing satisfactory filling, by making careful visual, mirror and probe, and radiographic examination. An existing restoration should not be removed just because there might be caries underneath it: it may equally well prove to have been caries-free. It does not matter if a proper cement lining is exposed (see Figure 1). A calcium hydroxide type of lining will have disintegrated on exposure to saliva: such fillings should be removed and a lining of strong cement substituted, such as Kalzinol or Poly-F.

#### Advantages of Amalgam Addition

It is quick, easy to do and very effective. It is economical in time and materials used. There is no preparation to dentine so no pain is caused. Maximum remaining tooth substance is conserved. The merits of the original

Figure 7(a). *Removal of interproximal excess.* (b) *Removal of subgingival excess and burnishing with a smooth straight probe.*

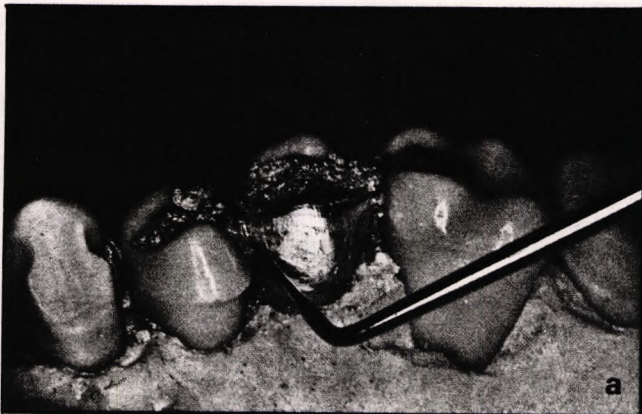




**Figure 8.** The finished restoration showing smoothly burnished surface. Amalgam cusp need not be built so tall as a natural cusp, to reduce occlusal stresses.

restoration are retained: occlusion, contact points, marginal ridges. This is important as these are all aspects which require extreme care if one is forced to make a large MOD + cusp amalgam. It is difficult to make tight contact points when a cusp is missing; the matrix often falls off; or the freshly packed amalgam comes out when removing the band; or the patient crushes the filling when testing the occlusion. These problems all are avoided by retaining the existing amalgam and gratefully accepting its merits: the occlusion is right; it has sound contact points and marginal ridges; and it is retentive.

The use of pins to aid retention is not advised. Retention is normally satisfactory without pins, which can present serious risks to the pulp chamber and periodontium. It is difficult to 'rub-in' the amalgam thoroughly if a pin is nearby and it is difficult to condense amalgam round a pin without a matrix, which has its own disadvantages.

The existing amalgam may already be pin-retained. What is the 'correct' course of action in these circumstances? Should one attempt to reuse the pins by removing the amalgam from around them? Or remove the pins and drill new pinholes with the consequential associated risks? The probability of encountering difficulty is greatly reduced by leaving the original amalgam undisturbed and, in the opinion of the author, this is the best solution in most cases.

### Further Considerations

#### Control of Amalgam Placement

One must exercise a high degree of strength and control to place the correct quantity of amalgam (quarter or



**Figure 9.** Holding amalgam carrier firmly with two fingers and thumb. The plunger is held in the palm of the hand with the ring finger.

half a gun load) in exactly the right place to build up a cusp without a matrix band. It is important to hold the amalgam carrier firmly with two fingers and thumb (Figure 9) and the plunger held in the centre of the palm with the ring finger. A DSA is unlikely to be able to do this correctly, so amalgam placement should be done by the operator as it is a significant factor for success of this technique.

### Amalgam Condensation

The space is not available here to discuss at length the merits of mechanical condensation of amalgam compared with hand packing. Suffice it to say that if anyone chooses to waste his energy on hand packing, he should not be surprised if he experiences unsuccessful or inferior results. The use of the Densco Condensaire is an essential part of this procedure.

### Wider Application of Amalgam Bonding

Minor defects in existing amalgams such as localized caries, defective contact point or marginal ridge can often be repaired easily using amalgam addition. A realistic maxim is: "Treat sound amalgam as sound tooth substance".

The technique has value as a reliable temporary measure in cases where crowning is planned eventually, but where insufficient time is available at that visit to complete the core-preparations for a crown.

It is also useful in patients who are not suitable for crownwork due to poor oral hygiene, high caries activity or for financial reasons.

Amalgam also bonds to gold alloys apparently without much evidence of electrolytic corrosion.

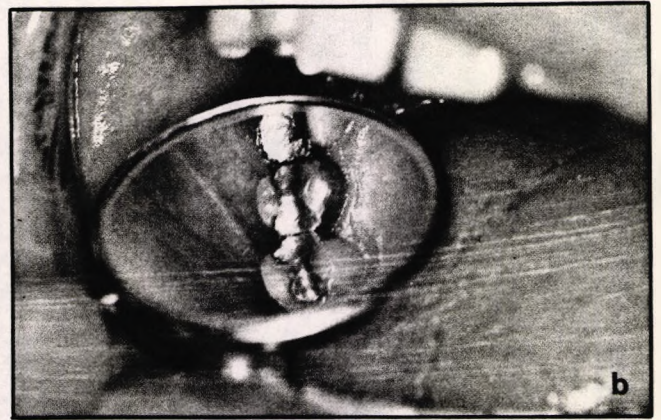
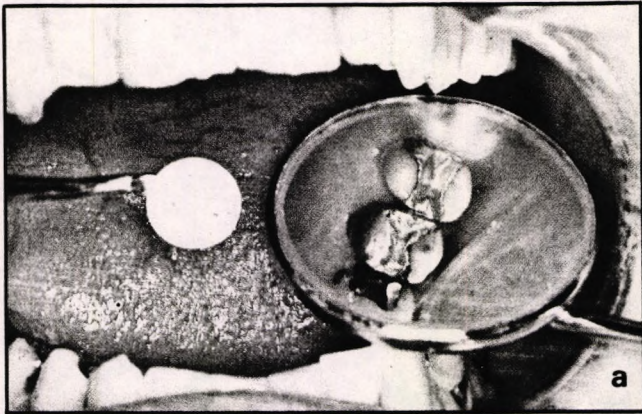
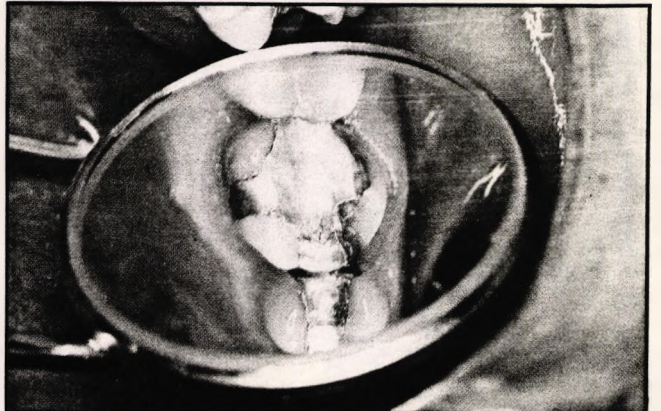
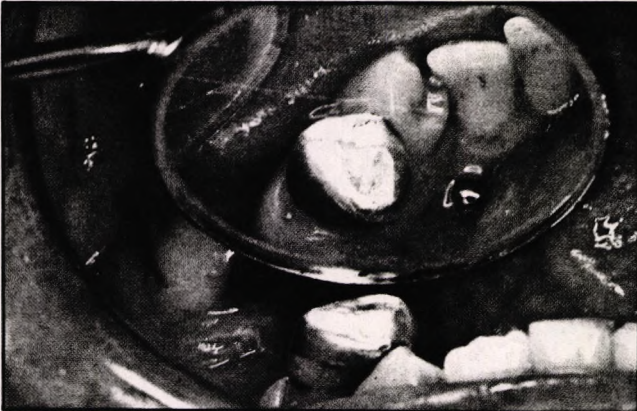


Figure 10(a) Typical clinical case after eight years in the mouth. (b) Another typical case.

Figure 11. Lingual cusp bonded to pin retained MOD + buccal cusp after three years in the mouth.

Figure 12. An amalgam MOD with two cusps and a palatal extension. A difficult case or a simple one?



**Conclusion**

Figures 10 and 11 show typical clinical cases after various periods of time in the mouth. Viewed conventionally, an amalgam MOD with two cusps and a palatal extension (shown in Figure 12) would be an exceedingly difficult restoration. The mesiobuccal cusp was restored by amalgam addition. A simple case or a difficult one?

A technique has been described for bonding new amalgam cusps to existing amalgam restorations. This

offers the prospect of giving satisfactory permanent results with a minimum of trauma, risk and expense to the patient. It is a technique which, once mastered, provides a simple solution for cases which are difficult to treat by conventional means. □

**Acknowledgements**

My thanks to Mr Alan Henstock in whose dental practice this work has been carried out, and to those colleagues whose scepticism has inspired me to write this article.

## Appendix 7. Published correspondence

This appendix contains copies of the correspondence to the editor, published in Dental Update 1981, 8 (8): 601, reproduced from Dental Update by permission of George Warman Publications (UK) Ltd.

Letters

---

### Amalgam Addition Restorations

Sir;

With reference to the article by Mr Alan H. Cook in the September issue, p.457, I presume that this article was originally intended to be published on 1 April! I feel that its content is totally irrelevant to modern dentistry and can only serve as an exceedingly poor example to students and newly qualified dentists.

S. L. Dwyer, BDSU, LDS RCS  
Dental Practitioner  
Farnham, Surrey

*taken seriously. My method of amalgam bonding is one of the most useful techniques I know and I felt a duty to share this experience with my colleagues for the greater good of humanity. One third of all existing restorations may be considered defective (Dental Update 1981); orthodox treatment therefore generally fails to satisfy an expectation of excellence. The time has come for the profession to revise the teaching of conservative dentistry with a view to minimizing the incidence of defective restorations. Mr Dwyer appears to laugh at the concept of amalgam addition yet he offers no specific criticisms. Would he tell us his usual approach to treating broken cusps?*

*I fail to see the justification for put-*

*ting a patient to the trauma, expense and risk of a large pinned amalgam or gold crown unless it is necessary. This simple procedure stands an excellent chance of permanent success with minimal risk. In my opinion, the use of amalgam addition is the treatment of first choice in a case where a cusp has fractured in a caries-free tooth with a sound amalgam filling, where aesthetics are not important. If none of Mr Dwyer's patients meets these simple criteria for case selection then I fear the joke is on him.*

Allan Cook

● *Although my article was written in a light-hearted style, it was intended to be*

### Reference

*Dental Update*, 1981, 8, 5, 285-286.

**PHOTOPOLYMERISATION USING  
ORGANOMETALLIC INITIATORS**

**BY**

**RICHARD BOWSER**

*A thesis submitted for the degree of Doctor of  
Philosophy at The City University for work  
carried out in the Chemistry Department.*

**April 1993**

## CONTENTS

	<u>Page</u>
Chapter 1. Introduction	1
1.1 Introduction to photochemistry	2
1.1.1 Principles of photochemistry	2
1.1.2 Properties of light	2
1.1.3 Molecular energy levels	4
1.1.4 Absorption of light	5
1.1.5 The absorption spectrum	6
1.1.6 Reactions of excited states	9
1.1.7 Electron transfer quenching	12
1.1.8 Heavy atom quenching	13
1.1.9 Quenching by molecular oxygen	14
1.1.10 Electronic energy transfer	14
1.2 Structure, bonding, and excited states of coordination compounds	16
1.2.1 Metal orbitals	17
1.2.2 A complex with $d^3$ configuration	18
1.2.3 A complex with $d^4$ configuration	19
1.2.4 Ligand orbitals	20
1.2.5 Combination of metal and ligand orbitals	21
1.3 Characterisation of excited states	23
1.4 Free radical initiation of polymerisation	23
1.4.1 Photoinitiation	23
1.4.2 Types of photoinitiators	24
1.4.3 Properties of the photoinitiator	26
1.4.4 Kinetics of free radical polymerisation	26
1.4.5 Oxygen inhibition of free radical polymerisation	29
1.5 Cationic initiation of polymerisation	31
1.5.1 Introduction to cationic polymerisation	31
1.5.2 Kinetics of cationic polymerisation	39
1.6 Industrial applications of photopolymerisation	41
1.6.1 Light sources	44
1.7 Experimental test procedures	45
1.7.1 UV curing	46
1.7.2 Real-time infrared (RTIR) spectroscopy	50
1.7.3 Photo-DSC	54
1.7.4 EPR spectroscopy	59
1.8 References	66

	<u>Page</u>
Chapter 2.      Photopolymerisation initiated by allyl, benzyl and associated silanes and stannanes	72
2.1    The synthesis of silanes and stannanes	73
2.1.1      Via Grignard reaction	73
2.1.2      Via Barbier reaction	75
2.1.3      Via reductive silylation	76
2.1.4      Via Wurtz coupling	78
2.2    Physical and chemical properties of silanes and stannanes	79
2.2.1 $p\pi-d\pi$ bonding	79
2.2.2 $\sigma-\pi$ hyperconjugation	80
2.3    Photochemistry of benzylsilanes and stannanes	84
2.3.1      Photochemistry of benzylstannanes	84
2.3.2      Photochemistry of benzylsilanes	85
2.4    Electron paramagnetic resonance (EPR) spectroscopy results	86
2.4.1      EPR results of benzylsilanes	87
2.4.2      EPR results of benzylstannanes	87
2.4.3      EPR results of allyl & cinnamyl stannanes	89
2.4.4      Structure & stability of radical cations	90
2.5    UV curing results	92
2.5.1      UV curing results of benzylsilanes	92
2.5.2      UV curing results of benzylstannanes	102
2.5.2.1    Photo-DSC of benzyltri- <i>n</i> -butylstannane	104
2.5.3      UV curing results of naphthyllic compounds (and higher)	107
2.5.4      UV curing results of allylsilanes	108
2.5.5      UV curing results of allylstannanes	109
2.5.6      UV curing results of cinnamyl and styryl silanes and stannanes	111
2.5.7      Photoinduced electron transfer reactions	113
2.5.8      UV curing: sensitisation using DCA	115
2.5.9      UV curing of benzylsilanes with DCA	117
2.5.10     UV curing of benzylstannanes with DCA	118
2.5.11     UV curing of naphthylsilanes with DCA	119
2.5.12     UV curing of allylsilanes with DCA	120
2.5.13     UV curing of allylstannanes with DCA	121
2.5.14     Sensitisation of polymerisation with aromatic ketones	122

	<u>Page</u>	
2.5.15	UV curing results of benzylsilanes and stannanes with benzanthrone	125
2.5.16	UV curing results of allylsilanes and stannanes with benzanthrone	127
2.5.17	UV curing results of naphthylsilanes and stannanes with benzanthrone	128
2.5.18	UV curing using 4,4'-dimethylbenzil (DMB) as a sensitiser	129
2.5.19	UV curing results using thiopyrylium salts as sensitisers	132
2.6	Real-time infrared spectroscopy (RTIR) results	137
2.6.1	Introduction	137
2.6.2	RTIR results of benzylsilanes	138
2.6.3	RTIR results of benzylic silanes	139
2.6.4	RTIR results of benzylstannanes	140
2.6.5	RTIR results of naphthyl (and higher) silanes and stannanes	142
2.6.6	RTIR results of allylsilanes & stannanes	144
2.6.7	RTIR results of benzylsilanes with DCA	145
2.6.8	RTIR results of benzyl and naphthylstannanes with DCA	148
2.6.9	RTIR results of an allylstannane with DCA	152
2.6.10	RTIR results using 4,4'-dimethylbenzil (DMB) as a sensitiser	152
2.6.11	Introduction	152
2.6.12	RTIR results of benzylsilanes with DMB	155
2.6.13	RTIR results of benzylic silanes with DMB	156
2.6.14	RTIR results of benzylstannanes with DMB	158
2.6.15	RTIR results of naphthylsilanes and stannanes with DMB	159
2.6.16	RTIR results of allylsilanes and stannanes with DMB	160
2.7	Experimental section	163
2.8	References	206
Chapter 3.	Photoinitiation of free radical polymerisation using organometallic amines of silicon and tin	216
3.1	Introduction	217
3.2	Previous synthetic routes	217
3.2.1	Synthetic routes used	218

	<u>Page</u>
3.3 Applications of alkylaminosilanes and stannanes	220
3.4 Electron paramagnetic resonance (EPR) spectroscopy results	222
3.5 UV curing results	225
3.5.1 UV curing results of Et <sub>2</sub> NCH <sub>2</sub> SiMe <sub>3</sub>	225
3.5.2 UV curing results of dimethylaminoalkylsilanes	226
3.5.3 UV curing results of dimethylaminoalkylsilanes and stannanes	228
3.5.4 Sensitisation of polymerisation using benzanthrone	230
3.5.5 UV curing results of dimethylaminoalkylsilanes and stannanes with benzanthrone	232
3.6 Real-time infrared (RTIR) spectroscopy results	233
3.6.1 RTIR results of dimethylaminoalkylsilanes and stannanes	233
3.6.2 RTIR results of dimethylaminoalkylsilanes and stannanes with benzanthrone	236
3.7 Experimental section	241
3.8 References	252
Chapter 4. Photoinitiation of free radical and cationic polymerisation using iron-arene complexes	255
4.1 Introduction	256
4.2 Photochemistry of iron-arene complexes	259
4.3 Photoimaging using iron-arene complexes	262
4.4 UV curing results for iron-arene complexes in cationic polymerisation	264
4.5 UV curing results for iron-arene complexes in free radical polymerisation	269
4.5.1 UV curing results for iron-arene complexes with N-methyldiethanolamine in free radical polymerisation	272

	<u>Page</u>
4.6 Real-time infrared (RTIR) spectroscopy results for iron-arene complexes	275
4.6.1 Introduction	275
4.6.2 RTIR results of iron-arene complexes in free radical polymerisation	275
4.6.3 UV curing results for cationic polymerisation using an iron-arene salt sensitised with a diphenyliodonium salt	277
4.7 Photo-differential scanning calorimetry (Photo-DSC) results of iron-arene complexes	281
4.7.1 Photo-DSC results of iron-arene complexes in cationic polymerisation	281
4.7.2 Photo-DSC results of iron-arene complexes in free radical polymerisation	284
4.8 Experimental section	290
4.9 References	297
 Appendix	 A1
5.1 Introduction	A2
5.2 Cobaloximes	A2
5.3 Porphyrins	A5
5.4 Experimental section	A7
5.5 Table 5.1: The oxidation and ionisation potentials for a number of silanes and stannanes	A12
5.6 Figure 5.1: UV spectra	A14
5.7 References	A17

## LIST OF TABLES

<u>Table 1.1</u>	The timescales of excited state processes
<u>Table 2.1</u>	The Grignard synthesis of silanes and stannanes
<u>Table 2.2</u>	The Barbier synthesis of silanes and stannanes
<u>Table 2.3</u>	Preparation of silanes via reductive silylation
<u>Table 2.4</u>	UV curing results of benzylsilanes incorporated at 5% w/w in TMPTA
<u>Table 2.5</u>	UV curing results of benzylic silanes incorporated at 5% w/w in TMPTA
<u>Table 2.6</u>	Sensitisation of diphenyliodonium hexafluorophosphate for use in cationic photopolymerisation using 'thioxanthone' with all compounds incorporated at 1% w/w in 3,4-epoxycyclohexylmethyl-3',4'-epoxycyclohexane carboxylate
<u>Table 2.7</u>	Evidence for a dual cure system in the photopolymerisation of a 50:50 acrylate:epoxy resin mixture using diphenyliodonium hexafluorophosphate and 9-trimethylsilylthioxanthene
<u>Table 2.8</u>	UV curing results of benzylstannanes incorporated at 5% w/w in TMPTA
<u>Table 2.9</u>	The rate and the degree of conversion values at different light intensities for the photopolymerisation of TMPTA using benzyltri-n-butylstannane as determined by photo-DSC
<u>Table 2.10</u>	UV curing results of naphthyl (and higher) compounds incorporated at 5% w/w in TMPTA
<u>Table 2.11</u>	UV curing results of allylsilanes incorporated at 5% w/w in TMPTA
<u>Table 2.12</u>	UV curing results of allylstannanes incorporated at 5% w/w in TMPTA
<u>Table 2.13</u>	UV curing results of cinnamyl and styryl compounds
<u>Table 2.14</u>	UV curing of TMPTA with benzylsilanes (1% w/w) sensitised using DCA (0.25% w/w)

<u>Table 2.15</u>	UV curing of TMPTA with benzylstannanes (1% w/w) sensitised using DCA (0.25% w/w)
<u>Table 2.16</u>	UV curing of TMPTA with naphthylsilanes (1% w/w) sensitised by DCA (0.25% w/w)
<u>Table 2.17</u>	UV curing of TMPTA with allylsilanes (1% w/w) sensitised by DCA (0.25% w/w)
<u>Table 2.18</u>	UV curing of TMPTA with allylstannanes (1% w/w) sensitised by DCA (0.25% w/w)
<u>Table 2.19</u>	UV curing of TMPTA with benzylsilanes and stannanes (both 5% w/w) sensitised by benzanthrone (1% w/w)
<u>Table 2.20</u>	UV curing of TMPTA with allylsilanes and stannanes (both at 5% w/w) sensitised by benzanthrone (1% w/w)
<u>Table 2.21</u>	UV curing of TMPTA with naphthylsilanes and stannanes (both at 5% w/w) sensitised by benzanthrone (1% w/w)
<u>Table 2.22</u>	UV curing results for the sensitisation of polymerisation of TMPTA using 4,4'-dimethylbenzil (1% w/w) with silanes (1% w/w) and stannanes (5% w/w)
<u>Table 2.23</u>	UV curing results of 2,4,6-triphenylthiopyrylium tetrafluoroborate (0.25%) with benzylic silanes and stannane (all at 1% w/w) in the presence of TMPTA
<u>Table 2.24</u>	UV curing results of 2,4,6-triphenylthiopyrylium tetrafluoroborate (0.25% w/w) with allylic stannanes and silane (all at 1% w/w) in the presence of TMPTA
<u>Table 2.25</u>	UV curing results of 4-n-butoxyphenyl-2,6-bis(4-methoxyphenyl)thiopyrylium tetrafluoroborate (1% w/w) with benzylic and allylic silanes and stannanes (all 5% w/w)
<u>Table 2.26</u>	RTIR results of the photopolymerisation of TMPTA using benzylsilanes
<u>Table 2.27</u>	RTIR results of the photopolymerisation of TMPTA using benzylic silanes
<u>Table 2.28</u>	RTIR results of the photopolymerisation of TMPTA using benzylstannanes
<u>Table 2.29</u>	RTIR results of the photopolymerisation of TMPTA using naphthyl (and higher) silanes and stannanes

<u>Table 2.30</u>	RTIR results of the photopolymerisation of TMPTA using allylic silanes and stannanes
<u>Table 2.31</u>	RTIR spectroscopy results for the photopolymerisation of TMPTA using benzylsilanes sensitised by DCA
<u>Table 2.32</u>	RTIR spectroscopy results for the photopolymerisation of TMPTA using benzylic stannanes sensitised by DCA
<u>Table 2.33</u>	The effect of sensitisation on the $R_p(\text{max})$ value of photopolymerisation of TMPTA using DCA with benzylsilanes and stannanes
<u>Table 2.34</u>	The effect of sensitisation on the degree of conversion value of photopolymerisation of TMPTA using DCA with benzylsilanes and stannanes
<u>Table 2.35</u>	RTIR spectroscopy results for the photopolymerisation of TMPTA using an allylstannane sensitised by DCA
<u>Table 2.36</u>	RTIR spectroscopy results for the photopolymerisation of TMPTA using benzylsilanes sensitised by DMB
<u>Table 2.37</u>	RTIR spectroscopy results for the photopolymerisation of TMPTA using benzylic silanes sensitised by DMB
<u>Table 2.38</u>	RTIR spectroscopy results for the photopolymerisation of TMPTA using benzylstannanes sensitised by DMB
<u>Table 2.39</u>	RTIR spectroscopy results for the photopolymerisation of TMPTA using naphthyllic silanes and stannanes sensitised by DMB
<u>Table 2.40</u>	RTIR spectroscopy results for the photopolymerisation of TMPTA using allylic silanes and stannanes sensitised by DMB
<u>Table 3.1</u>	The reaction times and yields of the synthesis of a number of dimethylaminoalkylsilanes and stannanes using ultrasound
<u>Table 3.2</u>	UV curing results of the polymerisation of TMPTA using $\text{Et}_2\text{NCH}_2\text{SiMe}_3$ in the presence and absence of sensitisers
<u>Table 3.3</u>	UV curing results of dimethylaminoalkylsilanes in the presence and absence of sensitisers

<u>Table 3.4</u>	UV curing results for a number of dimethylaminoalkyl- silanes and stannanes (1% w/w) in TMPTA
<u>Table 3.5</u>	Sensitisation of polymerisation of TMPTA using dimethylaminoalkyl- silanes and stannanes (1% w/w) with benzanthrone (1% w/w)
<u>Table 3.6</u>	RTIR spectroscopy results for the photopolymerisation of TMPTA using organometallic amines
<u>Table 3.7</u>	RTIR spectroscopy results for the photopolymerisation of TMPTA using organometallic amines sensitised using benzanthrone
<u>Table 4.1</u>	UV curing results for the cationic polymerisation of 3,4-epoxycyclohexylmethyl-3',4'-epoxycyclohexane carboxylate using iron-arene photoinitiators
<u>Table 4.2</u>	UV curing results for the free radical polymerisation of TPGDA initiated by iron-arene complexes
<u>Table 4.3</u>	UV curing results for the free radical polymerisation of TMPTA initiated by iron-arene complexes
<u>Table 4.4</u>	UV curing results for the free radical polymerisation of TPGDA initiated by iron-arene complexes (1% w/w) in the presence of N-methyldiethanolamine (5 %w/w)
<u>Table 4.5</u>	RTIR spectroscopy results of the free radical polymerisation of TMPTA initiated by iron-arene complexes
<u>Table 4.6</u>	Cationic polymerisation of an epoxide using diphenyliodonium hexafluorophosphate sensitised with an iron arene salt
<u>Table 5.1</u>	The oxidation and ionisation potentials for a number of silanes and stannanes

#### LIST OF FIGURES

<u>Figure 1.1</u>	The electromagnetic spectrum
<u>Figure 1.2</u>	Photochemically produced excited states
<u>Figure 1.3</u>	Jablonski diagram

- Figure 1.4      The configuration of the d-orbitals in an octahedral complex
- Figure 1.5      The energy levels of the orbitals of pyridine
- Figure 1.6      Electronic transitions in transition metal complexes
- Figure 1.7      The four different irradiation conditions
- Figure 1.8      The UV Colordry apparatus
- Figure 1.9      The RTIR spectroscopy apparatus
- Figure 1.10     The RTIR spectroscopy results
- Figure 1.11     Photo-DSC apparatus
- Figure 1.12     An exothermic polymerisation trace
- Figure 1.13     Schematic diagram of an EPR spectrometer
- Figure 2.1       $p_{\pi}$ - $d_{\pi}$  bonding versus  $\sigma$ - $\pi$  hyperconjugation in allylic and benzylic silanes and stannanes
- Figure 2.2      The limiting conformations of the C=C double bond with respect to the metal-CH<sub>2</sub> in an allylic system
- Figure 2.3      Photo-DSC results of the polymerisation of TMPTA initiated by benzyltri-*n*-butylstannane at two different light intensities
- Figure 3.1      A plot of the degree of conversion versus time obtained from the RTIR spectroscopy results of the curing of TMPTA for an organometallic amine in the presence and absence of a sensitiser (benzanthrone)
- Figure 4.1      The Photo-DSC results for the cationic polymerisation of an epoxide initiated by an iron-arene complex
- Figure 4.2      The Photo-DSC results for the free radical polymerisation of TMPTA, in air and under nitrogen, initiated by an iron-arene complex
- Figure 4.3      The Photo-DSC results for the free radical polymerisation of TMPTA initiated by an iron-arene complex (on it's own in air [b] and nitrogen [d], and in the presence of PhCH<sub>2</sub>SnBu<sub>3</sub> in air [c])

## LIST OF SCHEMES

- Scheme 1.1 The fate of excited states
- Scheme 1.2 Oxygen inhibition of polymerisation
- Scheme 1.3 Cationic polymerisation of an epoxide
- Scheme 1.4 Photolysis of diaryliodonium salts
- Scheme 1.5 Photolysis of triarylsulphonium salts
- Scheme 1.6 The polymerisation of epoxides using iron-arene salts
- Scheme 1.7 The production of a negative-working lithoplate
- Scheme 1.8 The radiolytic processes of  $\text{CFCl}_3$
- Scheme 2.1 Cinnamylation of the polymer chain (PC)
- Scheme 2.2 [2 + 2] cycloaddition of cinnamyl groups
- Scheme 3.1 The proposed fragmentation of  $[\text{Me}_2\text{N}(\text{CH}_2)_3\text{SnBu}_3]^{**}$  at 77K from epr spectroscopic evidence
- Scheme 4.1 Photochemistry of iron-arene complexes
- Scheme 4.2 Mechanism of cationic polymerisation of epoxides using iron-arene salts
- Scheme 4.3 A general mechanism for the polymerisation of epoxides using iron-arene salts
- Scheme 4.4 The nucleophilic character of sulphur in the cationic polymerisation of an epoxide
- Scheme 4.5 The role of oxygen in the sensitisation of diphenyliodonium hexafluorophosphate in cationic polymerisation using  $\eta^6$ -thioxanthene- $\eta^5$ -cyclopentadienyliron hexafluorophosphate
- Scheme 4.6 Proposed reaction scheme for the photopolymerisation of TMPTA in air using  $\eta^6$ -fluorene- $\eta^5$ -cyclopentadienyliron hexafluorophosphate (1% w/w) with benzyltri-*n*-butylstannane (1% w/w)

## KEY TO SYMBOLS & ABBREVIATIONS

CIDNP:	chemically induced dynamic nuclear polarisation
Cp:	cyclopentadienyl
CT:	charge transfer
Conv:	conversion
Decalin:	decahydronaphthalene
DCA:	9,10-dicyanoanthracene
DMB:	4,4'-dimethylbenzil
DSC:	differential scanning calorimetry
EPR:	electron paramagnetic resonance
exciplex:	excited complex
EXPT:	experiment
HOMO:	highest occupied molecular orbital
IPA:	isopropanol
ISC:	intersystem crossing
LUMO:	lowest unoccupied molecular orbital
PE:	photoelectron
RTIR:	real-time infrared
THF:	tetrahydrofuran
TMPTA:	trimethylolpropane triacrylate
TPGDA:	tripropylene glycol diacrylate
% w/w:	percentage weight for weight

## ACKNOWLEDGEMENTS

I would like to thank my supervisor, Professor R S Davidson, for his tuition, advice and encouragement throughout the course of this work. I also wish to thank Dr John Coyle for his assistance and discussions prior to undertaking these studies.

I thank my colleagues and the technical staff who made my time in the laboratories so enjoyable. Thanks to fellow members of Lab 307, Dr Patricia Moran, Dr Stephen Collins, Dr David Chappell, Dr Eleanor Cockburn, & Dr Sandra Lewis, those from 'across the way' in Lab 305, Dr Phil Duncanson, Paul Crick, Nergis Arsu, Niaz Khan, & Audrey O'Donnell, and those Inorganic chaps from the 'other side', Mark Gray, Dr Andy Thomas, & Martin Stimpson. Special thanks to Dr Patricia Moran - for sharing her expertise in organic synthesis, Dr Phil Duncanson - for his general advice and discussions, Jeff Abrahams - for his comments and technical assistance, & Dr Alan Osborne - for useful discussions and suggestions. I would also like to thank Grant Bradley for setting up the RTIR spectroscopy apparatus. I wish to thank Dr Chris Rhodes and his group at Queen Mary & Westfield College for providing several EPR spectra and for the subsequent illuminating discussions. I thank the staff at the CSIC Polymer Institute in Madrid for their technical assistance, particularly on the Photo-DSC.

I am grateful to the SERC and Cookson Group plc and IPC for the provision of funding for the whole of this work. Thanks also to the European Photochemistry Association and to IPC for providing financial assistance for my work in Madrid. I would also like to thank the Royal Society of Chemistry and Cookson Group plc for assistance with expenses towards attending conferences.

I am indebted to my wife, Coz, for her constant source of support and encouragement throughout the course of this work.

## Statement

The experimental work in this thesis has been carried out by the author in the laboratories of the Department of Chemistry at the City University, between November 1988 and October 1991, as well as a short period of this time spent working at the CSIC Polymer Institute in Madrid in June 1991. This work has not been presented for any other degree.

I grant powers of discretion to the University Librarian to allow this thesis to be copied in whole or in part without further reference to me. This permission covers only single copies made for study purposes, subject to normal conditions of acknowledgement.



Richard Bowser

Date 28th April 1993

Some of this work has been previously published, as follows:

Photopolymerisation using Organometallic Initiators, *14th IUPAC Symposium on Photochemistry, Photochemistry Abstracts*, 132-133, 1992

SOME NEW DEVELOPMENTS IN RADIATION CURING, *J.Chem.Soc.*, 1992 (in press)

THE USE OF ULTRASOUND IN ORGANIC SYNTHESIS, '*Current Trends in Sonochemistry*', *Royal Society of Chemistry, Ed. G.J.Price*, 50-58, 1992

STRUCTURES AND FRAGMENTATIONS OF ORGANOSILICON AND ORGANOTIN RADICAL CATIONS, *J.Chem.Soc., Perkin Trans. 2*, 1469-1474, 1992

CLEAVAGE OF ONE ELECTRON BONDS IN ORGANOSILICON AND ORGANOTIN RADICAL CATIONS, *J.Organomet.Chem.* 436, C5-C8, 1992

## ABSTRACT

A number of organometallic compounds have been synthesised and evaluated for use as photoinitiators for polymerisation based on the cleavage of metal-carbon (M-C) bonds.

Numerous allyl, benzyl, and naphthyl silanes and stannanes have been prepared. Both the homolytic M-C cleavage and the cleavage of the radical cations of the organometals (produced via electron transfer to a suitable acceptor such as 9,10-dicyanoanthracene) have been investigated as a means of initiating free radical polymerisation. In certain instances both free radical and cationic polymerisation occurred together, using the same initiating system, giving rise to a dual cure system.

A number of silicon and tin amines were synthesised using a novel 'one-pot' route which reduced the reaction time and the need for several steps. The amines were shown to be effective at initiating free radical polymerisation when used with a suitable aromatic ketone sensitiser.

Electron paramagnetic resonance spectra of the radical cations of the above compounds were recorded in order to gain an insight into the behaviour of the cleavage of the radical cations when used to initiate polymerisation via an electron transfer mechanism. The results indicated that C-Sn cleavage in the radical cations occurred more readily than for C-Si bonds.

A number of iron-arene salts were synthesised and evaluated for use as photoinitiators in both cationic and free radical polymerisation. Thus it was shown that a dual-cure system was possible when using these initiators. Evidence was also presented showing that oxygen had a beneficial effect on both cationic and free radical polymerisation.

Some cobaloximes and some porphyrins were synthesised in an attempt to produce alkyl free radicals via M-C bond homolytic cleavage on irradiation. Initial work with cobaloximes indicated some promise but time did not permit further advances in this area.

The evaluation of photopolymerisation on all the above compounds was carried out using the following techniques:

(i) A commercial UV cure apparatus for thin film polymerisation.

(ii) Real-Time Infrared (RTIR) Spectroscopy which gave the rate of polymerisation and the degree of monomer consumption.

(iii) Photo-Differential Scanning Calorimetry (Photo-DSC) which gave similar parameters as RTIR spectroscopy as well as an assessment of the post-cure which developed after irradiation had ceased (especially important for cationic polymerisation).

*Dedicated to my parents,  
Marjorie and Jack  
and to my wife, Coz,  
for all their help and support.*

**Chapter 1.**  
**INTRODUCTION**

## 1.1 Introduction to Photochemistry

In the following section the basic principles of photochemistry are explained as an introduction to the subject. The behaviour of an electronically excited molecule with a very short lifetime has a number of features that differ from those of ground state chemical species. Firstly, only very fast reactions can take place, and secondly, excited molecules may have sufficient energy to cause bond cleavage.

### 1.1.1 Principles of Photochemistry

It was in the nineteenth century that Grotthus and Draper stated that only light absorbed by the system can cause a chemical change in it which became known as the first law of photochemistry. A later observation by Stark and Einstein was that the rate of chemical change in a given molecular system was proportional to the light intensity. Thus a second law of photochemical equivalence was suggested in which one quantum of light is absorbed for each molecule which reacts.

### 1.1.2 Properties of light

Photochemical action is the result of absorption of light, visible or ultraviolet (UV) for example, by molecular systems.

The duality of light is an important feature in photochemistry. On the one hand the colour of light is determined by its wavelength as a fundamental property, whilst in other cases it is the energy of a particle of light, a photon, that is important. The two are related by the fundamental expression in equation 1.1 below.

$$E = hc/\lambda \qquad 1.1$$

where, E = energy per photon, h = Planck's constant, c = velocity of light, and  $\lambda$  = wavelength of light.

Part of the electromagnetic spectrum is shown below in figure 1.1 to illustrate the relationship between the wavelength and the energy of light.

Figure 1.1 The electromagnetic spectrum

Far UV	Ultraviolet	Visible		Near IR	IR	Far IR
150nm	200	400	800	1000		
			0.8 $\mu$	1	2.5	15
						250

The UV region of the spectrum extends from 200-400 nanometres (nm) and the visible part of the spectrum extends from 400-700 nm. Light can be polychromatic, having a distribution of wavelengths, or monochromatic with its distribution limited to one wavelength or, more realistically, a narrow range of wavelengths.

### 1.1.3 Molecular energy levels

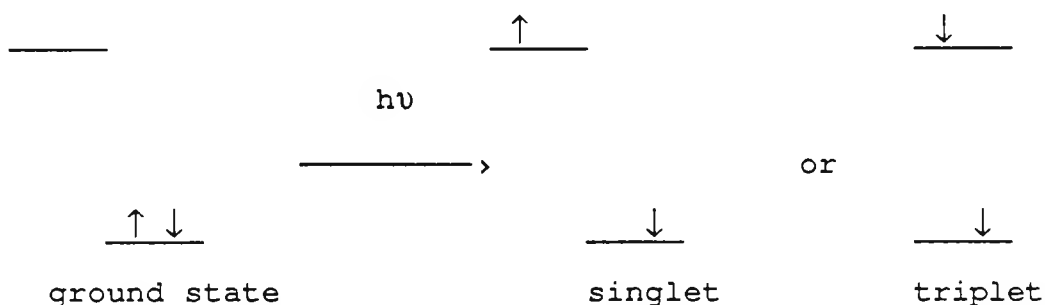
The theoretical model, known as quantum theory, in which a molecule can take up or lose energy was formulated by de Broglie, Schrodinger, and Heisenberg, around 1926. The particular distribution of electrons in a molecule is characterised by a wave function, the square of which, in a given point in space, gives the probability of finding an electron at that point. Each particular electronic distribution has a specific energy and the molecule is only allowed to have these particular electronic energies, and no other energies are allowed.

As well as electronic energy, the molecule can contain translational, rotational, and vibrational energy. It can be shown by quantum theory that the molecule can only contain prescribed amounts of these energies. The particular prescription depends upon the molecular characteristics, such as atomic weight of constituent atoms, bond length, and strength of bonds.

Absorption of light in the photochemically interesting wavelength region of the visible and UV is attributed to changes in the electronic state of the molecule. The change accompanying absorption of a photon redistributes the electrons around the nuclei of the molecule. In molecular orbital terms an electron from an occupied lower energy orbital is promoted to a higher unoccupied orbital.

The redistribution may give rise for example to singlet excited states with no change in spin of the promoted electron, or to triplet excited states which involves an inversion of spin of the promoted electron. Both situations are represented below in figure 1.2.

Figure 1.2 Photochemically produced excited states



#### 1.1.4 Absorption of light

Of fundamental importance is the Lambert-Beer law of absorption in which absorbance,  $A$ , of a material with light path length,  $l$ , is related to the concentration,  $c$ , of absorbent by equation 1.2 below.

$$A = \log(I_0/I_t) = \epsilon cl \quad 1.2$$

where  $I_0$  = incident light intensity,  $I_t$  = transmitted light intensity, and  $\epsilon$  = molar extinction coefficient.

The molar extinction coefficient,  $\epsilon$ , is a fundamental property of the molecule. Its value is characteristic of

the wavelength of absorbance and is normally quoted as such. The Lambert-Beer law cannot be obeyed if the incident light is polychromatic over a range in which  $\epsilon$  is not constant. Further if there are equilibria in the system so that the concentration of the absorbing species is not proportional to the stoichiometric concentration, again the law will not be obeyed. The total absorbance, if there are two absorbing species present, is just the sum of the absorbances of the individual components. The fraction of light,  $f_1$ , absorbed by one of the species is given by equation 1.3 below.

$$f_1 = \epsilon_1 c_1 / (\epsilon_1 c_1 + \epsilon_2 c_2) \quad 1.3$$

Where  $\epsilon_1$  and  $\epsilon_2$  are the molar extinction coefficients for species 1 and 2 respectively, and  $c_1$  and  $c_2$  are the respective concentration of species 1 and 2. This holds providing the above conditions for the validity of the Lambert-Beer law are met.

#### 1.1.5 The absorption spectrum

Absorption of light in the visible and UV regions results in formation of electronically excited states of the absorbing species. Each excited state has a unique energy relative to that of the ground state. Extinction coefficients of bands in the spectra of molecules are related to the nature of transition. The most commonly encountered transitions in organic compounds are  $n \rightarrow \pi^*$ ,  $\pi \rightarrow \pi^*$ ,  $n \rightarrow \sigma^*$ ,

and  $\sigma \rightarrow \sigma^*$  which are listed in order of increasing energy. Thus light of the highest energy (in the far UV) is necessary for  $\sigma \rightarrow \sigma^*$  excitation, while  $n \rightarrow \pi^*$  promotions are caused by ordinary UV light.

For organometallic compounds the situation is often more complicated due to the involvement of d orbitals in bonding which means that other transitions such as  $d \rightarrow d$ , or  $d \rightarrow \pi^*$  can occur (See section 1.2.5).

When a transition is fully allowed by the principles of quantum mechanics, the extinction coefficient at the band centre is large. If the transition is forbidden then the extinction coefficient at the band centre will be relatively small.

The integrated extinction coefficient for one band in the spectrum is directly related to the transitional probability connecting the upper and lower states. The reciprocal of the transitional probability is the lifetime that the upper state would have with respect to spontaneous emission of a photon and reverting to the ground state in the absence of all other possible processes. Although the relationship is not exact an approximation for the radiative constant,  $k$ , can be used to give an estimation of the natural or intrinsic lifetime of the excited state,  $\tau$ , using equation 1.4 below.

$$k = 1/\tau = 3 \times 10^{-9} \epsilon_{\max} \bar{\nu}^2 \Delta\bar{\nu} \quad 1.4$$

where  $\epsilon_{\text{max}}$  = extinction coefficient at centre of band,  $\bar{\nu}$  = wavenumber at centre of band, and  $\Delta\bar{\nu}$  = width of band at half peak height.

This represents a simplified view where the natural lifetime represents only the maximum possible lifetime for an excited state. In reality other processes can contribute to make the lifetime appreciably shorter. This is usually found to be the case.

This effectively means that a range in the lifetime of photophysical processes is observed as illustrated by the documented timescales for a number of different photophysical processes given in table 1.1 (Calvert and Pitts, 1966; Turro, 1978).

Table 1.1 The timescales of excited state processes

STEP	PROCESS	TIMESCALE (s)
1. Excitation	$S_0 + h\nu \rightarrow S_1$	$10^{-15}$
2. Internal conversion	$S_1 \rightarrow S_1 + \Delta$	$10^{-11}$ - $10^{-14}$
3. Fluorescent emission	$S_1 \rightarrow S_0 + h\nu_F$	$10^{-6}$ - $10^{-11}$
4. Intersystem crossing	$S_1 \rightarrow T + \Delta$	$10^{-8}$ - $10^{-11}$
5. Internal conversion	$T_1 \rightarrow T_1 + \Delta$	$10^{-11}$ - $10^{-14}$
6. Phosphorescent emission	$T_1 \rightarrow S_0 + h\nu_P$	$10^2$ - $10^{-3}$

The processes that affect the fate of excited molecules will be discussed in the next section.

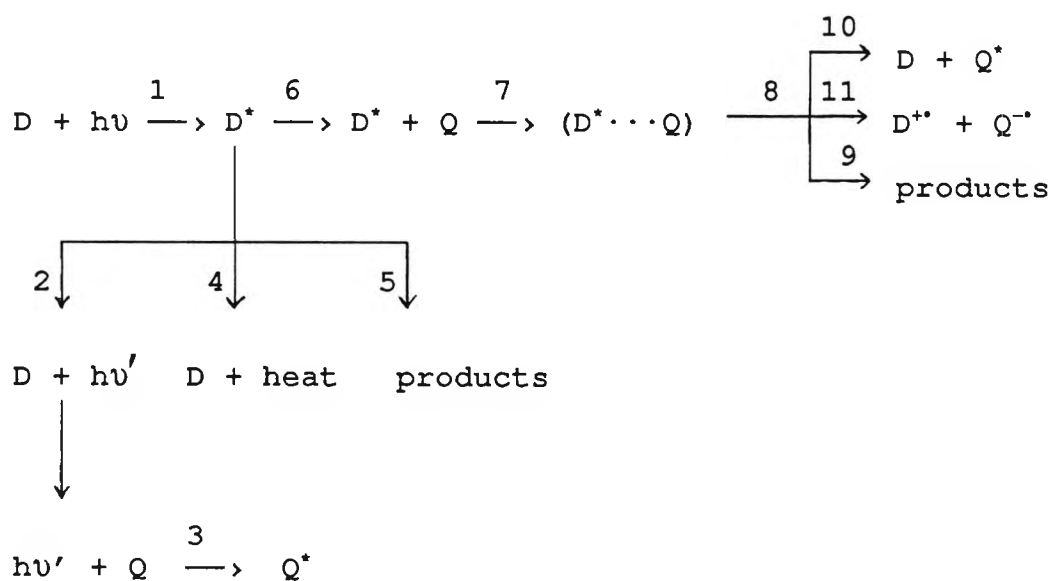
### 1.1.6 Reactions of excited states

There are a number of possible pathways available to an electronically excited state,  $D^*$ , obtained when a molecule,  $D$ , absorbs a photon of suitable energy according to equation 1.5 below.



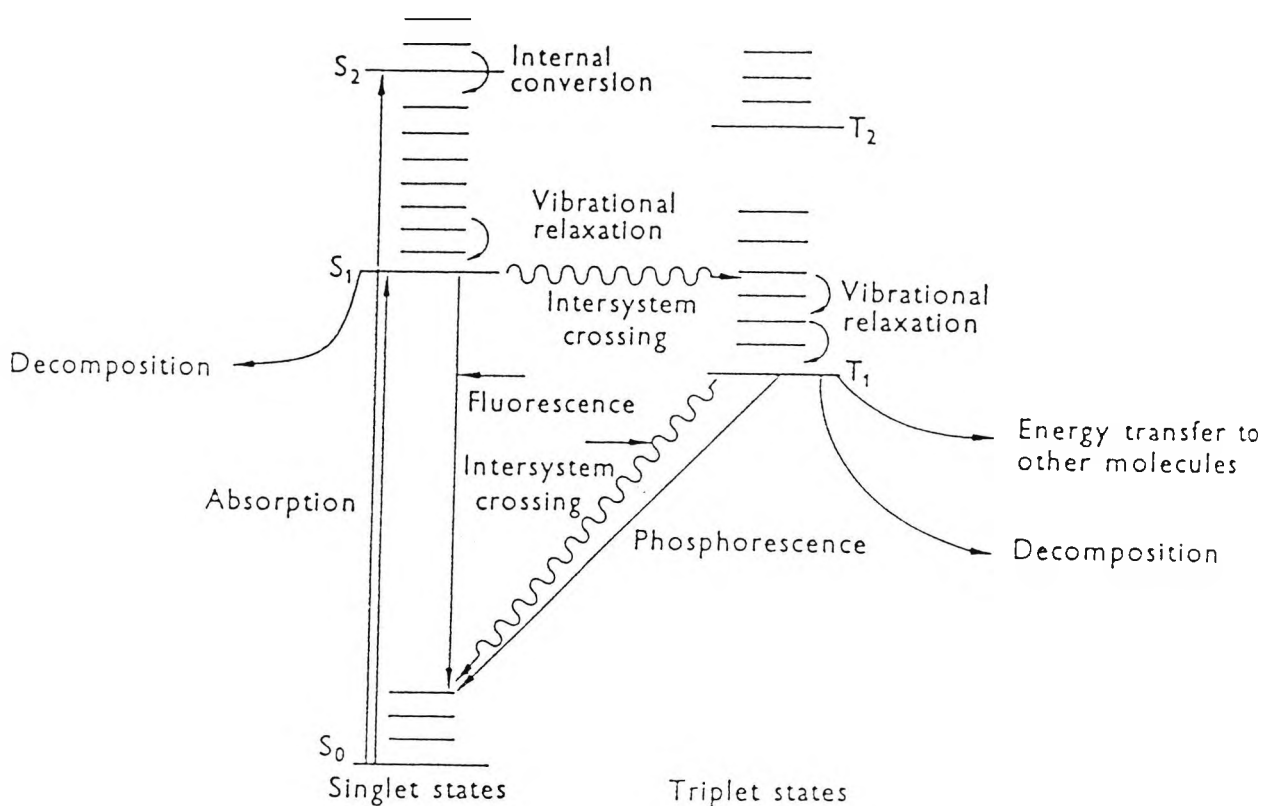
There are a number of possible processes available to the new chemical species,  $D^*$ , which are illustrated in scheme 1.1 below.

Scheme 1.1 The fate of excited states



A brief explanation of the various pathways depicted in scheme 1.1 can be given when used in conjunction with a Jablonski diagram, shown in figure 1.3.

Figure 1.3 Jablonski diagram



The nomenclature used in figure 1.3, whilst normally reserved for organic compounds, may be similar for some organometallic complexes though others have different multiplicity levels. The important feature of all systems is that the excited states have spin multiplicities that can be different or the same as the ground state. Using scheme 1.1 and figure 1.3 the various reaction pathways may be described as follows.

1. A ground state molecule D absorbs a photon of light which promotes it to an excited state  $D^*$ .
2. A radiative, or emissive, transition giving rise to either fluorescence, with no change in spin multiplicity (eg.  $S_1 \rightarrow S_0$ ), or phosphorescence involving a change in multiplicity (eg.  $T_1 \rightarrow S_0$ )
3. Radiative energy transfer
4. A non-radiative relaxation process terminating at the ground state.
5. Excitation may give rise to intramolecular processes leading to reaction including unimolecular cleavage (eg.  $D^* \rightarrow R_1^* + R_2^*$ )
6. The excited molecule,  $D^*$ , may come into contact with a ground state molecule, Q.
7. The interaction of excited molecule,  $D^*$ , and ground state molecule, Q, requires close approach before an encounter can take place. The rate of this diffusion controlled process is found to be dependent on factors such as the viscosity of the medium, the dielectric constant of the medium, and the encounter distance, and may be calculated by means of the Debye equation.

8. Once an encounter complex is formed a number of so called quenching processes are possible for the bimolecular excited state complex.
9. This involves quenching of excited states by "chemical" rather than "physical" processes for example by ligand substitution.
10. Non-radiative energy transfer.
11. Electron transfer quenching.

#### 1.1.7 Electron transfer quenching

Electron transfer involves the complete transfer of an electron from an electron donor (D) to an electron acceptor (A). Commonly a ground state donor molecule donates an electron to a previously excited singlet state of an acceptor molecule. This process occurs in an encounter complex as shown in scheme 1.1 (equation 7). The resultant single electron transfer (SET) in scheme 1.1 (equation 11) is not the only pathway and competes with other deactivation routes. The likelihood of an electron transfer mechanism occurring in a given situation was shown by Rehm and Weller (Rehm and Weller, 1970) to be related to the free energy of the electron transfer process in an expression that they derived shown in equation 1.6 below.

$$\Delta G^0 = E_{ox} - E_{red} - e^2/\epsilon'a - \Delta E_{00}$$

1.6

$\Delta G_0$  = free energy of electron transfer

$E_{ox}$  = oxidation potential of the donor

$E_{red}$  = reduction potential of the acceptor

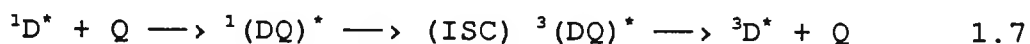
$e^2/\epsilon'a$  = coulombic interaction energy between the two radical ions of charge  $e$  at the encounter distance  $a$  in the solvent of dielectric constant  $\epsilon'$

$\Delta E_{00}$  = the electronic excitation energy of the fluorescer

The rate of quenching,  $k_q$ , can be calculated from spectroscopic and electrochemical data and is shown to be equal to the rate of diffusion,  $k_{diff}$  ( $10^{-10}$  mol/l/s) when  $\Delta G^0$  is more exothermic than 20-40 kJ/mol (or 5-10 kcal/mol).

#### 1.1.8 Heavy atom quenching

Molecular fluorescence is quenched by the presence of species containing heavy atoms and it appears that this is due to the formation of a singlet exciplex, which because of the heavy atom effect, undergoes enhanced intersystem crossing to the triplet exciplex followed by dissociation shown in equation 1.7.



Evidence in support of this mechanism has been provided (Medinger and Wilkinson, 1965) showing the quenching of the fluorescence of several aromatic hydrocarbons by xenon and

various bromine and iodine-containing compounds. It is also known that organometallic compounds can effect the above process (Vander Donckt and Vogels, 1971).

#### 1.1.9 Quenching by Molecular Oxygen

The quenching of the excited states of many organic molecules is known to be diffusion controlled (Birks, 1970). The process may occur via either the singlet or triplet states of the excited molecule. For a singlet state the process depends on enhanced intersystem crossing (ISC) and results in an excited triplet state as shown below in equation 1.8.



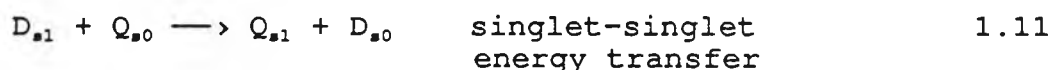
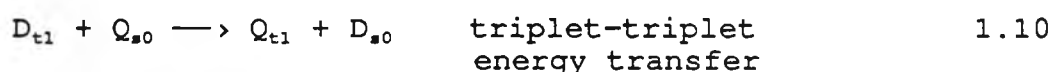
Quenching of the triplet state may occur via ISC or triplet energy transfer with the same end result of loss of energy to reach the ground state as shown below in equation 1.9.



#### 1.1.10 Electronic energy transfer

A molecule in an excited state may transfer its excess energy to another molecule in the environment. The excited molecule (termed D for donor) transfers its energy to a ground state molecule (termed Q for quencher) which itself

becomes excited as shown in scheme 1.1 (equation 10). The likelihood of an energy transfer is related to the relative energies of the donor and the quencher and is most efficient when the excited donor has a higher energy than the excited quencher. The excess energy appears as kinetic energy of D and Q\*. It is also important that the total electron spin does not change after the energy transfer. This is in accordance with the Wigner spin-conservation rule which is actually a special case of the law of conservation of momentum. In the two most important types of energy transfer, both of which obey the Wigner rule, a triplet excited state generates another triplet (Equation 1.10) and a singlet excited state generates another singlet (Equation 1.11) as shown below.



In general singlet-singlet transfer can take place over relatively long distances (40Å) whereas triplet-triplet transfer normally requires a collision between molecules which requires a closer approach (7Å). In most cases quenching processes operate via a collisional mechanism which depends upon both the distance separating D and Q and the rate of diffusion of a given excited state of D\*. Thus during a given lifetime of the excited state a collision with a quencher molecule Q must take place for the process of energy transfer to occur.

From diffusion theory it has been shown that in a non-viscous medium a molecule diffuses  $15\text{\AA}$  in  $10^{-9}\text{s}$  and  $15,000\text{\AA}$  in  $10^{-3}\text{s}$  whereas in a polymer-like viscous medium the same molecule moves  $0.1\text{\AA}$  in  $10^{-9}\text{s}$  and  $50\text{\AA}$  in  $10^{-3}\text{s}$  (Birks, 1973). Energy transfer in polymer-like viscous media may occur under conditions where diffusion is limited. In this case a different model exists which assumes that an effective quenching sphere exists about  $D^*$  and if a quencher molecule,  $Q$ , is within the sphere then  $D^*$  is deactivated with unit efficiency. It is only for concentrated solutions that there is a high probability that  $D^*$  will on average have a molecule of  $Q$  nearby.

## 1.2 Structure, bonding, and excited states of coordination compounds

The existence of coordination compounds in solution opens up a rich field of photochemistry since, after absorption of light, these substances can react or participate in energy transfer or reach excited states where they rapidly equilibrate and become new species with sets of thermodynamic properties entirely different from those characteristics of the ground state.

Since the low-lying electronic states of complexes dominate the photochemistry of inorganic systems, attention is focused on the different types of configuration and energy levels in complexes.

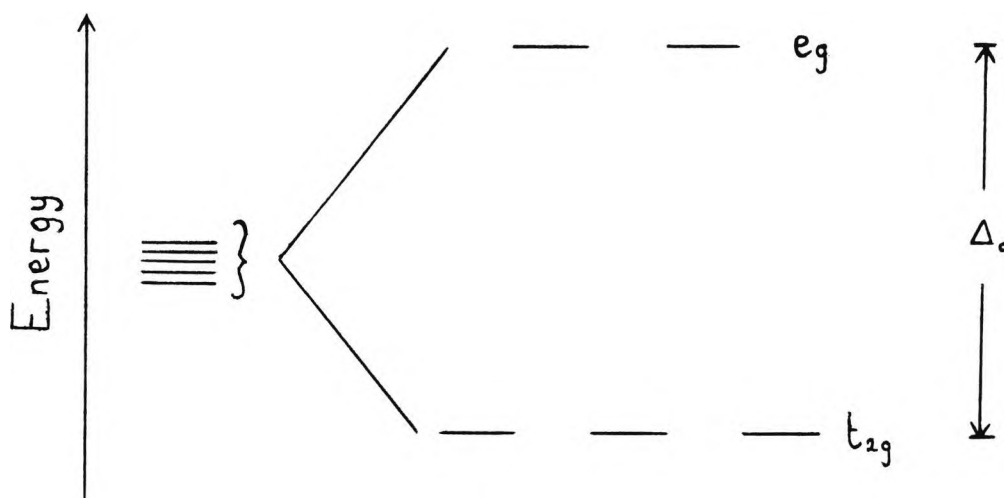
A useful model is to divide the electrons of a complex into two separate sets, one localised on the metal ion and a second set located on the ligand system. After considering the details of each set of electrons separately, one can combine the two to arrive at a electronic model for the complex. New features such as the charge transfer transitions not present in the constituent parts, arise in this composite model. In the following section the metal and ligand orbitals will be looked at separately and the combined picture will be described.

### 1.2.1 Metal orbitals

A large number of coordination complexes can be assumed to possess octahedral symmetry. Consider the metal orbitals of an octahedral complex. The five degenerate d-orbitals are split into two sets ( $t_{2g}$  and  $e_g$ ) as shown below in figure 1.4.

Figure 1.4

The configuration of the d-orbitals in an octahedral complex



$\Delta_o$  = crystal field splitting parameter.

Ligand field theory can be used to explain the electronic distribution of the metal ion and thus predict the most probable excited state transitions. To illustrate some principles of this theory consider the following examples:

### 1.2.2 A complex with $d^3$ configuration

Detailed theory predicts that the ground state configuration will be  $(t_{2g})_3$ . This corresponds to the lowest energy configuration in which each electron occupies a different, but degenerate, orbital and all the spins are parallel. Pairing two of the spins produces states of higher energy. Excitation of a  $(t_{2g})_3$  system can occur in two different ways.

An electron may be promoted to an empty  $e_g$  orbital ( $t_{2g} \rightarrow e_g$ ). This orbital promotion involves the crystal field-splitting parameter and thus energy required for this transition is a sensitive function of the factors involved in determining  $\Delta_o$ . In the second mode of excitation the excited electron remains in the  $t_{2g}$  orbital but its spin is reversed. Pairing energy,  $P$ , must be added but  $\Delta_o$  is not involved in the excitation process and thus the resultant electron redistribution is virtually independent of the excited state.

### 1.2.3 A complex with $d^4$ configuration

For a complex with 4 d-electrons the ground state configuration may exist as  $(t_{2g})_4$  with two electrons paired in one of the  $t_{2g}$  orbitals or as  $(t_{2g})_3(e_g)_1$  with all electrons in single orbitals and of the same spin. The crucial factor in determining which state predominates is the relative energies of  $\Delta_o$  and  $P$ .

If  $\Delta_o > P$   $(t_{2g})_4$  predominates (also known as low spin configuration)

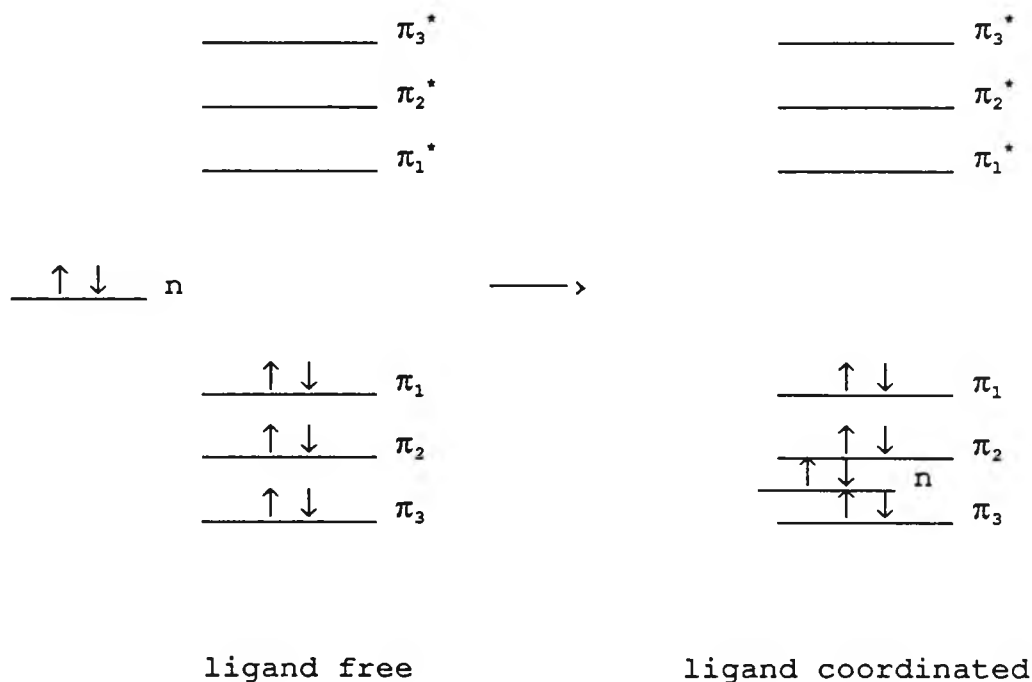
If  $\Delta_o < P$   $(t_{2g})_3(e_g)_1$  predominates (known as high spin configuration)

For complexes where  $\Delta_o \sim P$  an equilibrium between the two different types of ground state may occur.

### 1.2.4 Ligand orbitals

For many ligands the excitation energies of the valence electrons can be comparable to those of the metal electrons described above. Many ligands contain non-bonding electrons, (n), which can be promoted into anti-bonding orbitals, for example ( $\pi^*$ ) orbitals on an aromatic ring. In this case the lowest energy transition of the free ligand is of  $n \rightarrow \pi^*$  character. Complexation often involves the coordination of non-bonding electrons to the metal which lowers the energy of the non-bonding electrons with respect to the ligand electrons and thus the lowest energy transition will be  $\pi \rightarrow \pi^*$ . This situation may be depicted for pyridine, a common ligand, in figure 1.5.

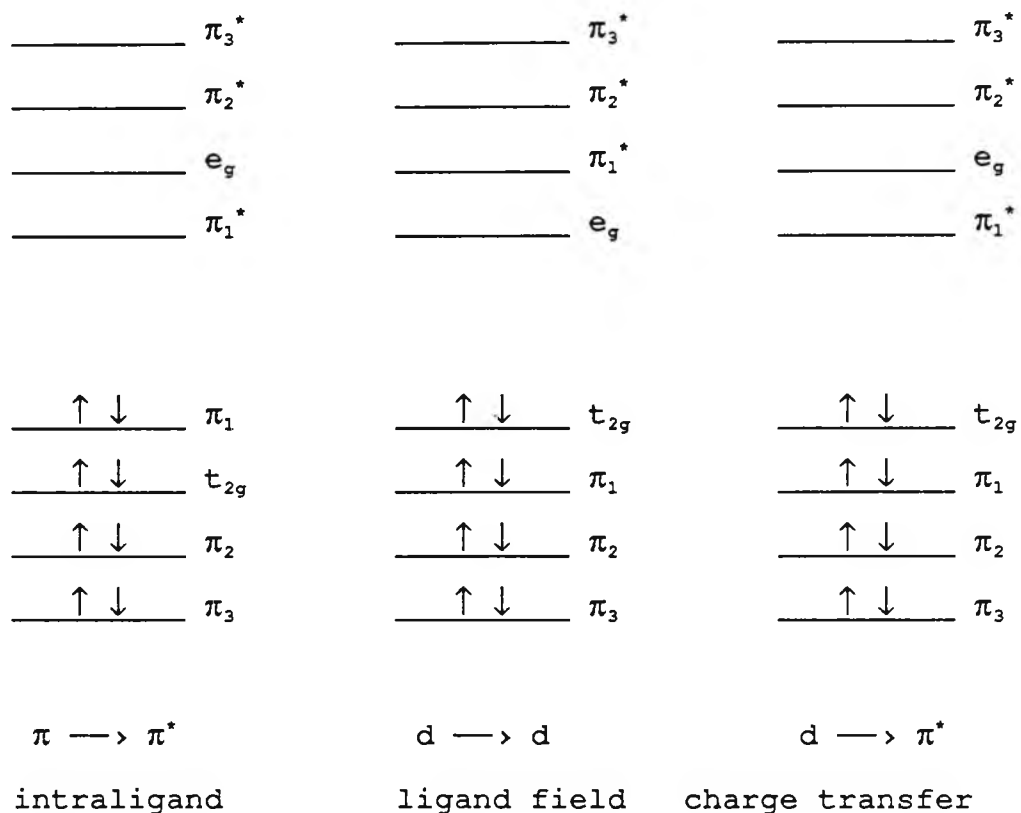
Figure 1.5 The energy levels of the orbitals of pyridine



### 1.2.5 Combination of metal and ligand orbitals

There are a number of different transitions that may occur upon excitation to the lowest (usually) excited state. Some examples of the combination of metal and ligand orbitals for low spin  $d^6$  complexes are given below in figure 1.6 to illustrate the different types of transitions that may occur.

Figure 1.6 Electronic transitions in transition metal complexes



A very elegant study (Crosby et al, 1970) for Iridium III ( $d^6$ ) has shown that it is possible to "tune" the lowest excited state type by altering the ligand. Thus for the same metal ion a  $d \longrightarrow d$ , a  $d \longrightarrow \pi^*$ , or a  $\pi \longrightarrow \pi^*$  emission from complexes with slightly different ligands was obtained. This has obvious implications for designing molecules utilising excited state chemistry.

### 1.3 Characterisation of excited states

The existence of the different types of excited states may be inferred from both absorption and emission spectroscopy. In absorption spectroscopy characteristics of absorption bands give rise to predictions of the transitions involved based on previous results from assigned transitions. Thus from a study of the spectra of a series of closely related complexes of a given metal ion, one can often deduce the configurations and multiplicities of the excited states. The emission spectrum can be a source for deducing the nature of the excited species. Similarly to absorption spectroscopy there are characteristic features of the spectrum which can infer a particular type of excited state.

### 1.4 Free radical initiation of polymerisation

#### 1.4.1 Photoinitiation

The initiation of photopolymerisation requires the presence of a photoinitiating system, PI. The first step involves irradiation of the system to produce an excited state species, PI\*, shown in equation 1.12 below.



The excited state species,  $PI^*$ , as mentioned previously (section 1.1.6) can undergo a number of physical and chemical transformations. The interesting pathway with regard to free radical polymerisation is that pathway that results in a free radical species,  $I^*$ , shown below in equation 1.13.



Presuming that the radical species,  $I^*$ , has suitable reactivity towards a polymerisable substrate such as a monomer,  $M$ , then the radical,  $I^*$ , can go on to initiate polymerisation as depicted in equation 1.14 below.



#### 1.4.2 Types of photoinitiators

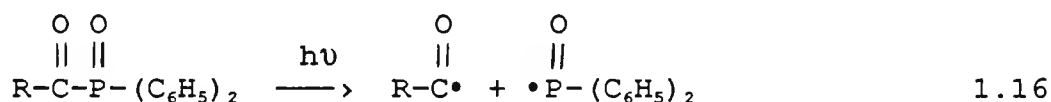
There are numerous reports on the many different types of photoinitiators for free radical polymerisation. In general terms the plethora of initiators may be broadly classified by the mechanism by which they operate. In order to illustrate the principles involved a brief outline of the methods of initiation is presented.

Photoinitiators for free radical polymerisation fall into three main categories, which are:

1. Photoinitiation by homolytic fission from the excited state of the molecule (equation 1.15).



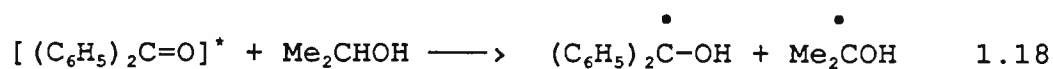
An example of this type of photoinitiator are the acylphosphine oxides (equation 1.16) [Baxter et al, 1987].



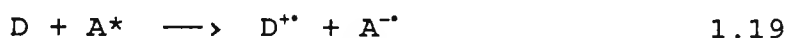
2. Photoinitiation by hydrogen abstraction from a donor molecule (equation 1.17).



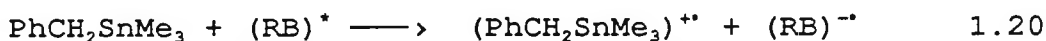
This mechanism is typified by aromatic ketones with various H donors such as alcohols, ethers, and amines. One of the best documented reactions of this type is the photoreduction of benzophenone by isopropanol (equation 1.18).



3. Photoinitiation by electron transfer between a donor, D, and an acceptor, A, as shown below in equation 1.19.



The photoreduction of rose bengal (RB) by benzylstannanes is an example of this type of reaction (equation 1.20) [Eaton, 1979].



#### 1.4.3 Properties of the photoinitiator

The ideal requirements for a good photoinitiator include:

1. High extinction coefficient at the desired absorption wavelength/s.
2. Efficient generation of radicals that are capable of attacking the olefinic double-bond of vinyl monomers.
3. Adequate solubility in the resin system.
4. High storage stability in the dark, and good thermal stability.
5. Do not impart yellowing or unpleasant odours to the cured material.
6. Should be non-toxic itself, as should be any products arising from it.

#### 1.4.4 Kinetics of free radical polymerisation

Free radical polymerisation involves three major processes which are:

1. Initiation (equation 1.21)
2. Propagation (equation 1.22)
3. Termination (equations 1.23, 1.24)

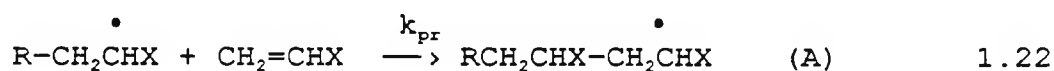
These steps can be represented by following the reaction of a radical,  $R^\bullet$ , with a vinylic monomer  $CH_2=CHX$  ( $X$ =substituent group eg. when  $X=Ph$ , monomer=styrene), by a series of equations.

### 1. Initiation



$k_i$  = rate constant for initiation

### 2. Propagation



$k_{pr}$  = rate constant for propagation

### 3. Termination

(i) by combination



$k_{tc}$  = rate constant for termination by combination

(ii) by disproportionation

eg.



$k_{td}$  = rate constant for termination by disproportionation

It is often difficult to distinguish between  $k_{tc}$  and  $k_{td}$  and an overall rate constant for termination,  $k_t$ , may be determined where;

$$k_t = k_{tc} + k_{td} \quad 1.25$$

Free radical polymerisation is a typical chain reaction in which the polymer chain grows rapidly by successive additions of monomer units during the short interval between initiation and termination of the chain. The actual lifetime of a growing chain radical is of the order of a few seconds, which is sufficient time for successive addition of thousands of monomer units. As is usual for chain reactions the values of the individual rate constants are not readily accessible but the overall characteristics of the reaction can be deduced by using a 'steady-state' assumption that the rate of initiation is equal to the rate of termination. This leads to a number of rate equations for the various stages in polymerisation which can be verified experimentally.

$$\text{Rate of initiation, } R_i = \frac{d[M\bullet]}{dt} = 2k_i[I] \quad 1.26$$

(assuming two radicals produced from one initiator molecule)

$$\text{Rate of propagation, } R_{pr} = \frac{-d[M]}{dt} = k_p[M^\bullet][M] \quad 1.27$$

$$\text{Rate of termination, } R_t = \frac{-d[M^\bullet]}{dt} = 2k_t[M^\bullet]^2 \quad 1.28$$

Under steady state conditions,  $R_i = R_t$  so that

$$[M^\bullet] = (k_i/k_t)^{1/2}[I]^{1/2} \quad 1.29$$

$$\text{Rate of polymerisation, } R_p = k_p(k_i/k_t)^{1/2}[M][I]^{1/2} \quad 1.30$$

where,

[M] = monomer concentration

[M<sup>•</sup>] = concentration of propagating radical

[I] = initiator concentration

#### 1.4.5 Oxygen inhibition of free radical polymerisation

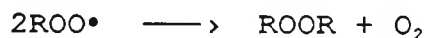
Photoinitiated polymerisation conducted in air is more complicated. The initiator species and the growing polymer chain may be deactivated by reaction with molecular oxygen (a diradical), as shown in scheme 1.2 below.

#### Scheme 1.2 Oxygen inhibition of polymerisation

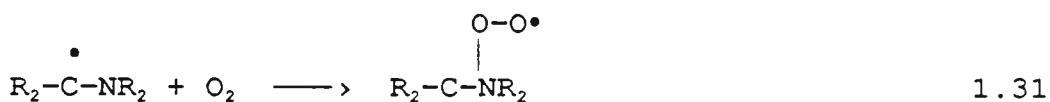
##### Propagation



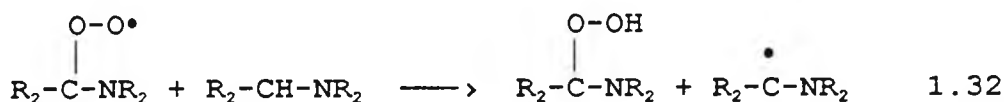
##### Termination



The addition of oxygen to the radical is extremely fast and is probably diffusion controlled in many cases (rate constant =  $10^9 \text{ l mol}^{-1} \text{ s}^{-1}$ , Ingold, 1969). The length of the induction period before polymerisation starts is directly proportional to the number of inhibitor molecules initially present. These undesirable reactions with oxygen occur primarily at the air interface where the concentration of oxygen is the greatest. The result is that an induction period is observed giving a reduction in both the rate of polymerisation and the degree of conversion. A number of different strategies have been used to reduce oxygen inhibition of radical polymerisation. The photopolymerisation can be conducted in vacuo or in an inert atmosphere such as nitrogen. This is difficult to achieve, in practical terms, for the UV coatings industry and so a number of other strategies have been investigated. These include increasing the light intensity (Rubin, 1974), incorporating paraffin waxes in the coating formulation which migrate to the surface on irradiation (Bolon and Webb, 1978), and the use of additives such as *t*-amines in the formulations. It has been shown that the *t*-amines can perform a dual role of both oxygen quenchers and as the initiating species (Bartholomew and Davidson, 1971a; Bartholomew and Davidson, 1971b; Bartholomew *et al*, 1971). The radicals derived from the  $\alpha$ -aminoalkyl groups *t*-amines via hydrogen abstraction can react with oxygen present to form peroxy radicals.



The peroxy radical can then react with another molecule of t-amine.

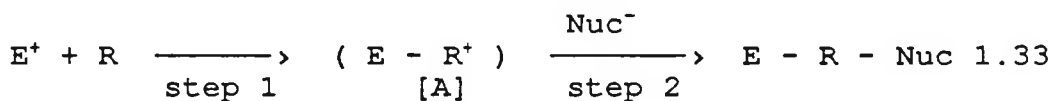


Thus the oxygen inhibition effect is reduced and the added bonus of an initiating  $\alpha$ -aminoalkyl radical is produced in the process.

## 1.5 Cationic initiation of polymerisation

### 1.5.1 Introduction to cationic polymerisation

Cationic polymerisation may be regarded as a special case of electrophilic addition.



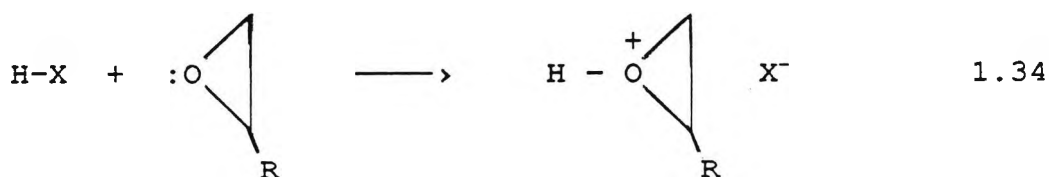
Product [A] shows a positively charged species which must be prevented from collapsing through reaction with a nucleophile [Nuc<sup>-</sup>] (step 2) for long enough to allow a large number of successive monomer additions. It is therefore important that prospective photoinitiators must be designed with non-nucleophilic character of any anions present. In other words there must be propagation of the growing chains giving rise to high reaction rates due to the lack of chain terminating side reactions. Thus low viscosity monomers can

be polymerised as easily as high viscosity monomers. In addition, cations do not react with oxygen, and therefore cationic polymerisation can be carried out effectively in air. This is in marked contrast to free radical polymerisation where oxygen inhibition of polymerisation is an important factor. It has been reported that in certain instances oxygen enhances the rate of cationic polymerisation (Tsuroska and Tanaka, 1988). This is thought to be due to the formation of hydroperoxides which are known to be efficient hydrogen donors and thus will accelerate the production of initiating species. The properties of materials based on photoinitiated cationic polymerisation are generally superior to those obtained from free radical polymerisation. This is particularly so with regard to electrical resistance, stability to heat and chemicals, adhesion, and mechanical strength (Curtis et al, 1986; Green and Stark, 1981; Lohse and Zweifel, 1986). In contrast to free radical systems, only a relatively small number of alkenes and heterocyclic molecules are susceptible to cationic polymerisation. Generally alkenes need adjacent electron-donating groups, such as alkoxy in the case of vinyl ethers, and of the heterocyclic monomers, epoxides are the most common. Epoxides are Lewis bases and their ring opening by cationic species is easy. The polymerisation of an epoxide by a cationic pathway is depicted below in scheme 1.3.

### Scheme 1.3 Cationic polymerisation of an epoxide

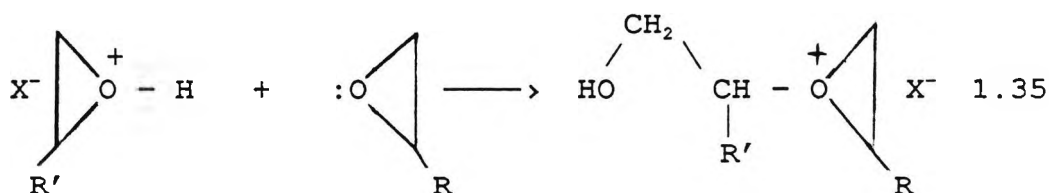
#### 1. Initiation

Initiation involves the nucleophilic attack of the lone pair on the oxygen of the epoxide towards the initiating species.



#### 2. Propagation

Propagation continues via nucleophilic attack by the monomer on the tertiary oxonium ions until either termination or chain transfer of the polymer chain occurs.



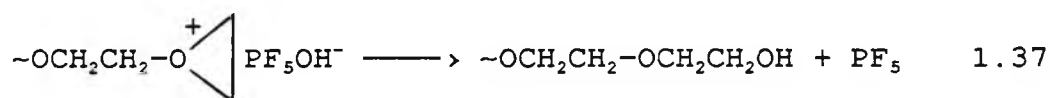
#### 3. Termination

In a very pure system termination reactions are scarce which emphasises the 'living nature' of cationic polymerisation. As this is difficult to achieve there are often trace impurities in the system which can cause termination. Thus

termination of the growing cationic chain end may be via reaction with nucleophilic or basic impurities or corresponding reactive sites of the polymers. One such impurity is water which may have an adverse effect on the polymerisation as follows.



This produces a counterion that is more nucleophilic than the  $\text{PF}_6^-$  counterion and can attack the growing polymer chain.



If as in scheme 1.3 the monomer contains only one epoxide group, photopolymerisation produces a linear polymer. In most commercial systems efficient crosslinking is required to produce mechanically strong and chemically resistant three dimensional macromolecular structures. It is for this reason that bis(epoxides) and poly(epoxides) are commonly used (NB cycloaliphatic epoxies show higher reactivities than glycidyl ethers and glycidyl esters see J.V.Crivello in UV Curing, Science and Technology, (S.P.Pappas, ed) Stamford, Technology Marketing Corp., p23, 1978). Cationic polymerisation, unlike radical polymerisation, involves living polymers, and so polymerisation continues after the light source has been removed. Thus it is possible to observe post-curing in these systems. In one instance 60% of polymerisation was shown to be due to post cure (Decker

and Moussa, 1988). Typical catalysts for cationic polymerisation include aprotic acids (Lewis acids and Friedel-Crafts halides), protonic species (Brönsted acids), and stable carbenium-ion salts. All these are strong electron acceptors. Many of them, particularly the Lewis acids, require a co-catalyst, usually a Lewis base or other proton donor, to initiate polymerisation.

Cationic polymerisation was discovered in 1839 by Deville using tin IV chloride as a catalyst for polymerisation of styrene (Deville, 1839). Since then a number of reports of cationic polymerisation catalysts have been documented. Cationic photoinitiation has received considerable attention over the last 20 years. Prior to this there was a dearth of suitable photoinitiators. The first efficient catalysts for photopolymerisation of epoxides were aromatic diazonium salts with anions of low nucleophilicity (Schlesinger, 1974a; Schlesinger, 1974b). The spectral response of the diazonium salts can be varied throughout the UV-visible region of the spectrum by altering the substituents on the aromatic ring (Schlesinger, 1974a). On irradiation these salts generate Lewis acids which can initiate the polymerisation. The disadvantages of using diazonium salts are the liberation of nitrogen gas on irradiation, which limits the practical usefulness due to formation of bubbles in the polymers, and their limited thermal stability, preventing long term storage of formulated systems.

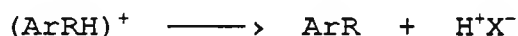
These problems were largely overcome with the discovery of photoactive onium salts and in particular the diaryliodonium salts (Crivello and Lam, 1977; Crivello and Lam, 1979c), and the triarylsulphonium salts (Crivello and Lam, 1979a; Crivello and Lam, 1980a; Crivello and Lam, 1980b), both with anions of low nucleophilicity. On irradiation the onium salts generate Brønsted acids, as shown in schemes 1.4 and 1.5 below, which are very effective catalysts for the polymerisation of epoxides.

Scheme 1.4 Photolysis of diaryliodonium salts

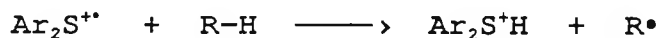
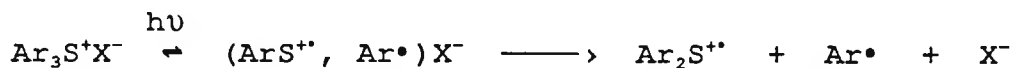
Major



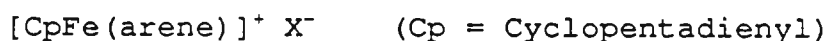
Minor



Scheme 1.5 Photolysis of triarylsulphonium salts

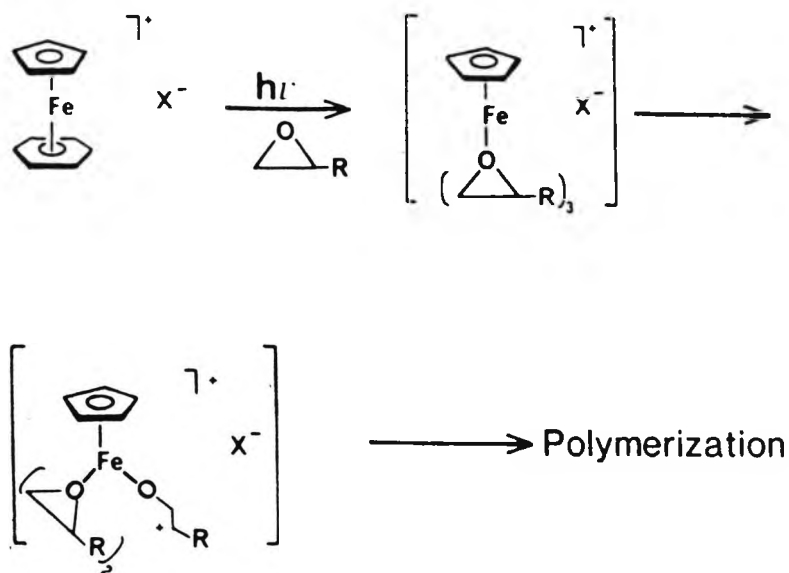


Onium salt photoinitiators have strong absorption bands in the deep UV region, but their sensitivity can be extended to longer wavelengths by use of suitable sensitizers (Crivello and Lam, 1978; Crivello and Lam, 1979b). Also triarylsulphonium salt photoinitiators with extended conjugation systems and thus improved spectral sensitivity have been reported (Crivello and Lam, 1979a; Crivello and Lam, 1980b). Recently Meier and Zweifel have reported that iron arene salts with anions of low nucleophilicity can be used as efficient photoinitiators for the cationic polymerisation of epoxides (Lohse and Zweifel, 1986; Meier and Zweifel, 1985a; Meier and Zweifel, 1986a; Meier and Zweifel, 1986b). Various types of such complexes described by the following general formula are listed in the literature (Schumann, 1984).



Upon irradiation the iron arene complexes lose the uncharged arene ligand and thereby yield a Lewis acid. It is postulated that this Lewis acid reacts with an epoxy monomer to give a complex with three epoxide ligands coordinated to the iron moiety (Klingert et al, 1988). Ring opening polymerisation could then start within the ligand sphere of the iron cation leading to poly(ethers) as shown below in scheme 1.6.

Scheme 1.6 The polymerisation of epoxides using iron-arene salts



Iron arene photoinitiators have good light absorption properties in the UV region of the spectrum. The absorption characteristics can be modified over a wide range by altering the arene ligands. The photolysis has also been sensitised with anthracene derivatives (Meier and Zweifel, 1985b). The oxidation state of the iron in these photoinitiators is +2 before and after exposure to irradiation. Oxidation of the iron complex to the +3 oxidation state leads to a Lewis acid with increased activity for epoxide polymerisation. Thus in the presence of an oxidant, such as cumene hydroperoxide, polymerisation occurs at an enhanced rate compared to the rate obtained in the absence of oxidant (Lohse and Zweifel, 1986). The absorption spectrum of the iron arene complex changes on exposure to irradiation.

As photolysis proceeds the arene fragment is depleted and thus the optical density in the near UV and visible part of the spectrum decreases with time. This effectively means that the system is photobleachable and thus permits light penetration into thick layers as photolysis proceeds. DSC experiments show that the iron arene photoinitiators are generally less reactive than Brönsted acids obtained from sulphonium salts and therefore heat treatment is required after irradiation to effect polymerisation.

### 1.5.2 Kinetics of cationic polymerisation

The steps involved in cationic polymerisation are similar to those in free radical polymerisation and are:

1. Initiation (Equations 1.38, 1.39)
2. Propagation (Equation 1.40)
3. Termination (Equation 1.41)
4. Transfer (Equation 1.42)



where,

A = catalyst, RH = co-catalyst, M = monomer, K = rate constant for formation of initiator,  $k_i$  = rate constant for initiation,  $k_p$  = rate constant for propagation,  $k_t$  = rate constant for termination,  $k_{tr}$  = rate constant for transfer  
This gives rise to a series of rate equations that may be derived from the above expressions.

$$\text{Rate of initiation, } R_i = K k_i [A] [RH] [M] \quad 1.43$$

In strong contrast to free radical polymerisation the termination is first order, thus;

$$\text{Rate of termination, } R_t = k_t [M^+] \quad 1.44$$

Using the steady state assumption that  $R_i = R_t$ ,

$$[M^+] = \frac{K k_i}{k_t} [A] [RH] [M] \quad 1.45$$

and the overall polymerisation rate,

$$R_p = k_p [M] [M^+] \quad 1.46$$

$$= K \frac{k_i k_p}{k_t} [A] [RH] [M]^2 \quad 1.47$$

The degree of polymerisation,  $x_n$ , can be calculated.

If termination predominates over transfer then,

$$x_n = \frac{k_p}{k_t} [M] \quad 1.48$$

Or if transfer predominates then,

$$x_n = \frac{k_p}{k_{tr}} \quad 1.49$$

The ease of polymerisation of a given cyclic monomer depends on the reactivity of the functional group in the ring, the size of the ring, and the catalyst used.

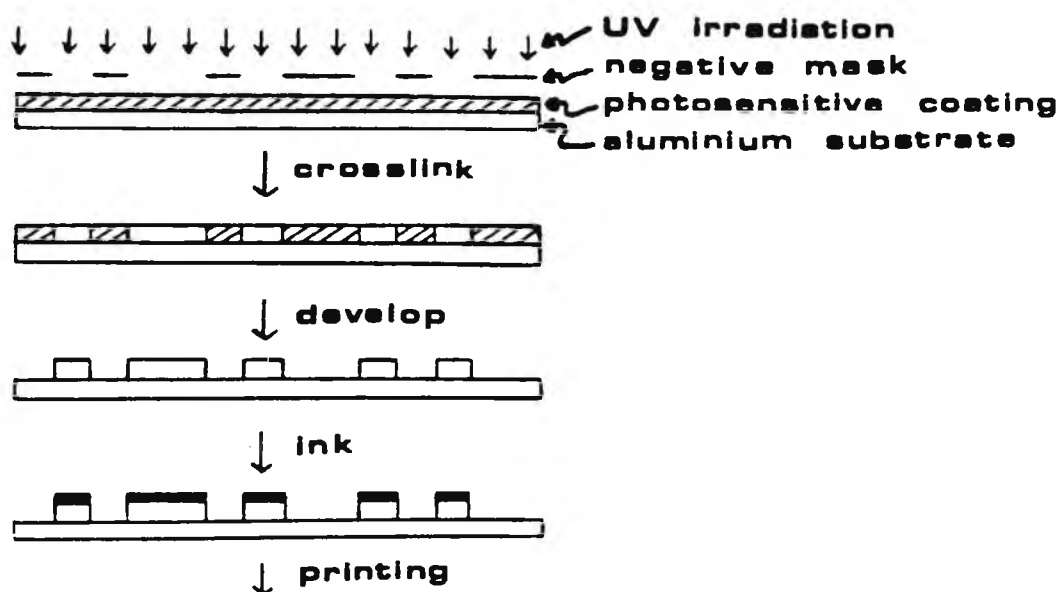
### 1.6 Industrial applications of photopolymerisation

The spirit of enquiry was typified by the ancient Egyptians who wrapped mummies in light-sensitive linen cloths, whose light sensitivity was facilitated by dipping them in a mixture of lavender oil and Syrian asphalt. This procedure was developed thousands of years later in 1822 by Niepce who coated a glass plate with Syrian asphalt and removed the unexposed (and therefore uncrosslinked) part of the coating by washing with turpentine, to yield an early type of lithographic plate for producing prints (Jackel, 1989).

Nowadays photopolymerisation is the basis of an important commercial process with wide ranging applications such as photoimaging (Thompson et al, 1983), and UV curing (Pappas, 1978; Roffey, 1982; Pappas, 1984). Photopolymerisation utilises electromagnetic radiation as the energy source for polymerisation of functional monomers, multifunctional monomers (or oligomers), and pre-polymers used in combination with a photoinitiating system. The polymerisation process effects a modification in the chemical structure of the resin system which in turn alters

the physical properties. This usually results in solvent discrimination between the crosslinked and uncrosslinked areas. There are two main types of photopolymer systems widely employed commercially. Firstly, there are those that crosslink on irradiation forming a three dimensional network which results in a decrease in solubility of the exposed areas, termed negative working systems. Secondly, there are those that are originally macromolecular structures, which on irradiation decrease in molecular weight resulting in an increase in solubility of the exposed areas, termed positive working systems. It is only the former, negative working systems, that will be discussed here. Selective areas can be exposed to UV light through a photographic negative and then these areas alone will become crosslinked and thus insoluble. This is the principle used in the lithographic printing industry to create printing plates. An example of a negative working lithoplate is shown below in scheme 1.7.

Scheme 1.7 The production of a negative-working lithoplate



The main advantages of UV curing over conventional means of effecting polymerisation, such as heating or mixing, are that rapid network formation occurs in a short time period. Generally irradiation times of a few seconds are sufficient and in some cases a few hundredths of a second are adequate. Less energy is required and many systems do not require a solvent to be present.

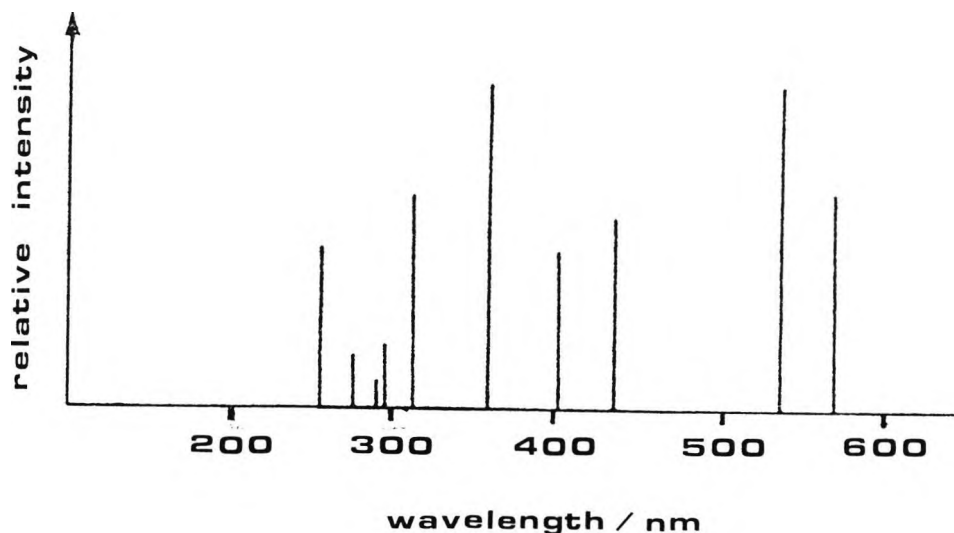
The properties of the coatings such as hardness, flexibility, abrasion resistance, and solvent resistance are determined by the composition of the resin system. The design of the resin system has been the subject of many reports (Roffey, 1982; Pappas, 1984). Commonly free radical photoinitiated polymerisation of acrylate resins has been extensively used commercially. Photoinduced cationic polymerisation can also be used in photoresist and printed circuit technologies (McGinnis, 1979). In general cationic polymerisation has received less attention than radical polymerisation due to the lack of suitable photoinitiators available. The rate of cationic polymerisation is relatively slow when compared to radical polymerisation and it is often the case that the rate of the polymerisation dictates the material used in the commercially orientated marketplace.

Important parameters in photoimaging applications include resolution, sensitivity, and reproducibility.

Resolution may be described as the limit of discrimination between image (crosslinked) and non-imaged (uncrosslinked) areas of the printed typescript. Lithographic sensitivity may be expressed in terms of the dose requirement required to produce a crosslinked network and is generally of the order of tenths to tens of  $\text{mJ}/\text{cm}^2$  for commercial systems.

### 1.6.1 Light sources

Many types of light sources can be used in photopolymerisation (McGinnis, 1978). The light source that is normally used in commercial UV curing is the medium pressure mercury-arc lamp which has its main outputs at 313, 365, 404, and 436nm shown below.



There are also a number of lasers available that can be used in the UV region such as the rare gas halide excimer lasers and in the visible region such as the He-Cd source at 441.6nm and the Ar source at 488nm.

### 1.7 Experimental test procedures

In order to assess the efficiency of photoinitiators in photoinitiated polymerisations, experimental methods are required that enable the rates of polymerisation to be measured under reproducible conditions. A number of different techniques have been developed utilising methods based on differential scanning calorimetry (Tryson and Shultz, 1979; Moore, 1980), dilatometry (Cundall et al, 1987), laser nephelometry (Decker and Fizet, 1980), infrared spectroscopy (Lee and Doorakian, 1977), real-time infrared spectroscopy (Decker and Moussa, 1988), NMR (Barret, 1979), and Fourier Transform infrared spectroscopy (Small et al, 1984).

Of the above methods real-time infrared (RTIR) spectroscopy, and differential scanning calorimetry (DSC), another real-time method, have been used to follow photopolymerisation reactions. UV curing, an important technique in the industrial sector, has also been used to assess the properties of photoinitiators in thin films.

Electron paramagnetic resonance (EPR) spectroscopy has been used to investigate the properties of several radical cations with particular regard to their fragmentation pathways. All four of these experimental techniques are described in the next section.

#### 1.7.1 UV Curing

A number of the prepared compounds have been investigated for use as a component in a photoinitiating system. The photoinitiating systems tested have been comprised of either one component or two components. The photoinitiating system was then mixed with a polymerisable monomer. All of the prepared compounds under test were loaded at various percentage levels (usually at 1-5% weight/weight {w/w} in the monomer), along with the other component of the photoinitiating system if incorporated. This combined mixture was then subjected to light irradiation and the polymerisation was monitored. The monomers under test fall into two categories ; those polymerisable by a radical initiator eg. acrylates, and those polymerisable by a cationic initiator eg. epoxides. The extent of polymerisation both with and without a photoinitiating system present was tested for all formulations. A comparison of the two results then yields useful information on the efficiency of the photoinitiating system present. The choice of monomer is determined by the type of initiating species produced upon irradiation. There are

often proposed mechanisms of initiation given in the literature for given types of compounds which are helpful for choosing monomer type, but occasionally the mechanism is not fully understood and a more investigative approach must prevail.

The formulation of each system was carried out in such a way that as little UV light as possible was able to interact with the initiating/monomer system. The formulation was then coated onto GNT paper substrate using a manually operated R-K Meyer bar coater (No. 3; thickness  $25\mu$ ). A number of operations were then carried out on the coating to give four different test conditions. These are outlined below and represented in figure 1.7 below.

#### 1. Touching quartz

A piece of quartz is placed directly in contact with the film. This allows the full output of the lamp to irradiate the coating, and since the quartz is touching the film the diffusion of oxygen into the film is minimised (especially important in radical polymerisation).

#### 2. Touching glass

A piece of glass is placed in direct contact with the film. This allows the output of the lamp beyond approximately 310nm to irradiate the coating, since the glass is touching the film the oxygen inhibition effect is minimised as above.

### 3. In air

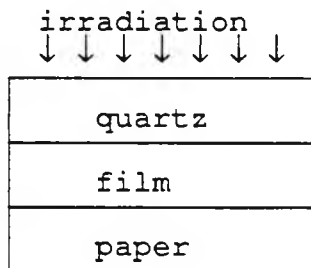
The film is irradiated directly from the light source in the presence of air.

### 4. Glass filter

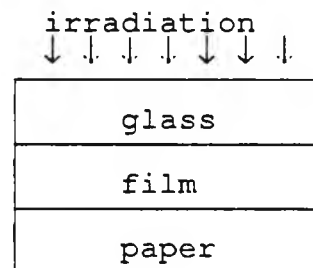
A glass filter is placed above the film, but not touching it, to act as a filter of light with wavelength below 310nm. Thus the film is irradiated in air but without the full spectral output of the lamp.

Figure 1.7 The four different irradiation conditions

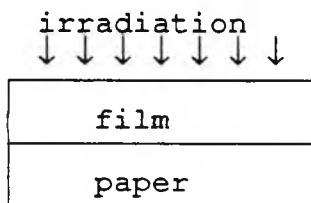
#### 1. Touching quartz



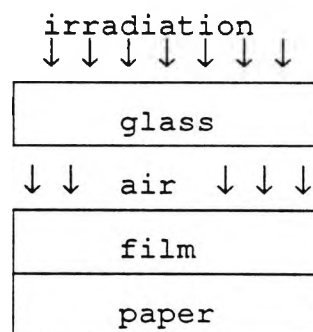
#### 2. Touching glass



#### 3. In air

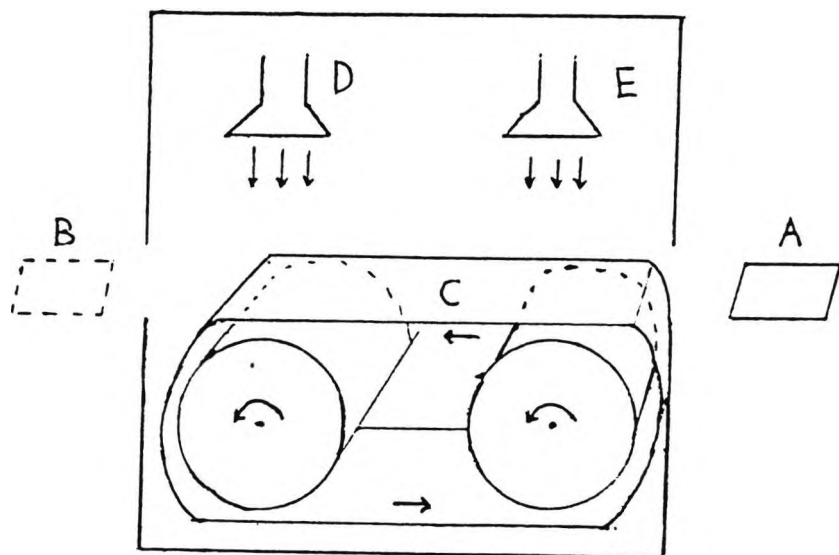


#### 4. Glass filter



The coated substrate is then mounted onto a steel plate and secured . The steel plate is then placed onto a moving belt and irradiated with UV light, using a Colordry twin lamp UV unit (see figure 1.8), operating at various moving belt speeds, and utilising either one lamp or two.

Figure 1.8 The UV Colordry apparatus



The number of passes is recorded for the coated layer to become tack-free. The term tack-free represents the point where the liquid film becomes solid due to the crosslinked network formed during polymerisation. One pass is represented as the movement of the substrate from position A to position B on moving belt C beneath irradiation from lamp(s) D or/and E.

### 1.7.2 Real-time infrared (RTIR) spectroscopy

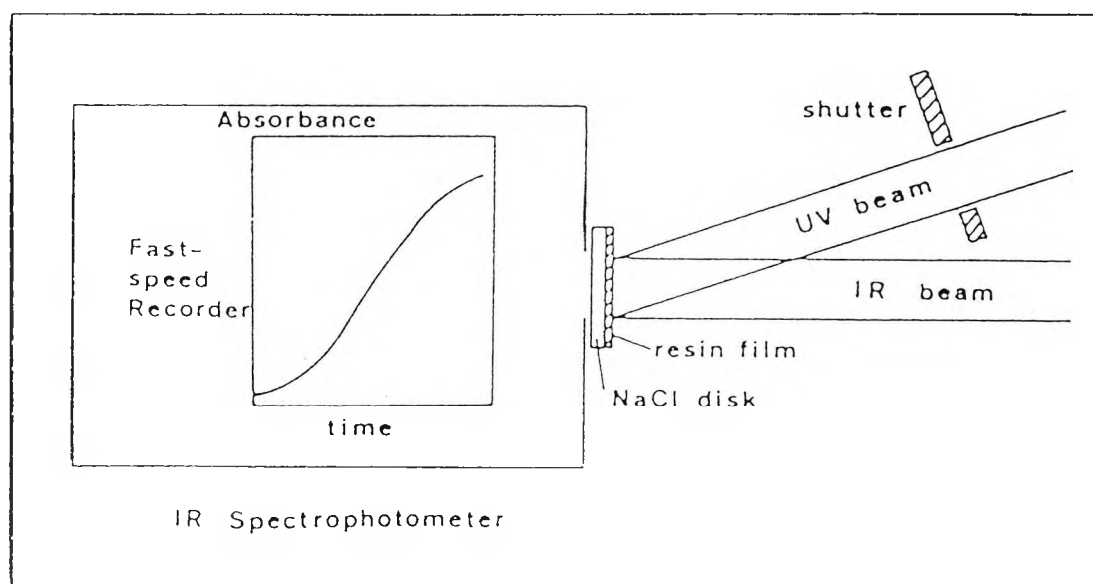
RTIR spectroscopy has been used to monitor polymerisations in real-time, quantitatively and in situ, that take place in less than a second. The technique has been used to study the effect on the polymerisation rate of the photoinitiator efficiency, the monomer reactivity, the light intensity, the film thickness, oxygen inhibition, and the postcure that develops after the end of the irradiation (Decker and Moussa, 1988). The technique has been used to monitor UV and laser induced photopolymerisations of both acrylic (Decker and Moussa, 1990a) and epoxy (Decker and Moussa, 1990b) monomers.

#### Experimental details

RTIR spectroscopy was used to follow quantitatively the photopolymerisation in situ by monitoring the disappearance of the infrared absorption characteristic of the polymerisable monomer under test.

The experimental set-up shown in figure 1.9 was devised so that the sample was exposed to the UV beam and the analysing IR beam at the same time.

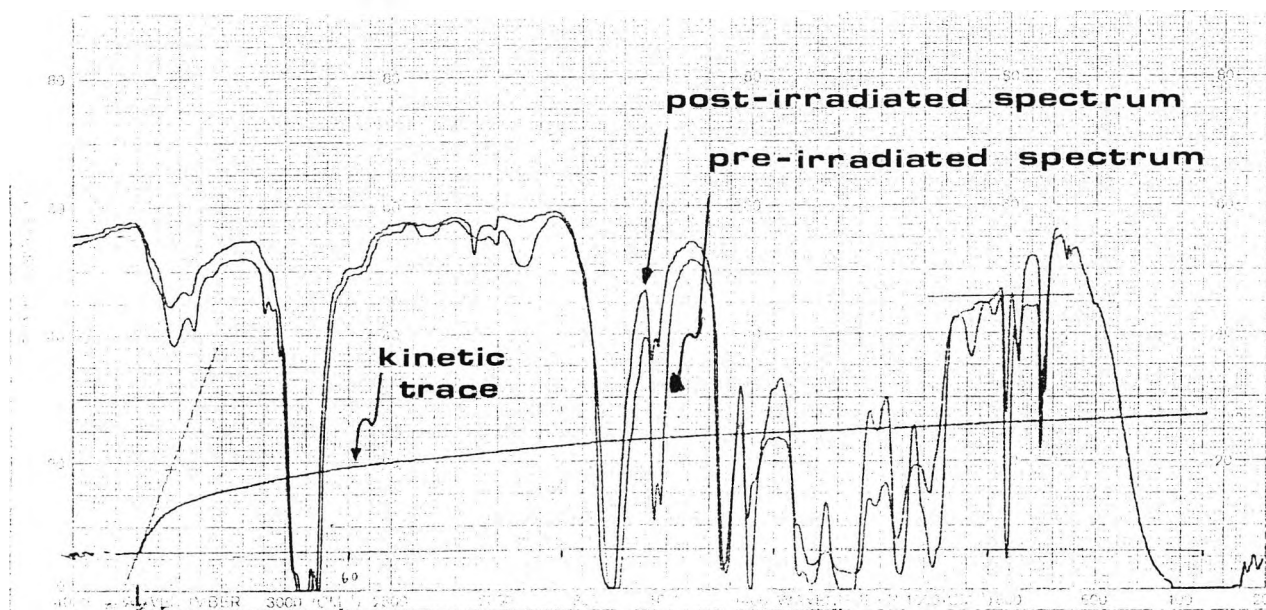
Figure 1.9 The RTIR spectroscopy apparatus



The sample formulation, which consisted of photoinitiating system and monomer, was applied onto a NaCl salt disc using R-K Meyer bar coater No. 3 (thickness 25 microns) and a polyethylene cover slip (for UV see appendix: Figure 5.1) was placed in direct contact with the film. The coated disc was then placed into an infrared spectrometer and a pre-irradiation infrared spectrum was recorded. Then the

spectrometer was programmed to operate in the time-drive mode and thus the infrared wavelength was fixed. For acrylates this corresponds to the strong C=C stretching vibration at  $810\text{cm}^{-1}$ . The detection of the infrared signal was made by operating the spectrometer in the absorbance mode. The sample was then exposed to the radiation of a medium pressure mercury lamp and at the same time the disappearance of the  $810\text{cm}^{-1}$  signal was monitored as a kinetic trace of polymerisation. The irradiation and the kinetic trace were stopped together, unless postcure detection was desired, and the spectrometer was reverted back to the normal working mode. Finally a post-irradiated spectrum was recorded. The pre-irradiated spectrum, kinetic trace, and the post-irradiated spectrum were all recorded on the same axes as shown in figure 1.10.

Figure 1.10 The RTIR spectroscopy results



The degree of conversion is directly related to the decrease of the IR absorbance, and can be calculated (for acrylates) using equation 1.50.

$$\text{Degree of conversion} = \frac{(A_{810})_t}{(A_{810})_0} \times 100\% \quad \text{Equation 1.50}$$

where  $(A_{810})_0$  and  $(A_{810})_t$  are the respective absorbances at  $810\text{cm}^{-1}$  of the sample before and after UV exposure during time  $t$ . Since the degree of conversion can be readily calculated it follows that the degree of residual unsaturation in the photopolymerised coating can be calculated by using the relationship in equation 1.51.

$$\text{Degree of residual unsaturation} = \frac{(A_{810})_0 - (A_{810})_t}{(A_{810})_0} \times 100\% \quad \text{Equation 1.51}$$

From figure 1.10 the rate of polymerisation can be deduced using equation 1.52.

$$R_p = [M]_0 \frac{(A_{810})_{t_1} - (A_{810})_{t_2}}{(A_{810})_0 [t_2 - t_1]} \quad \text{Equation 1.52}$$

where  $[M]_0$  is the original concentration of acrylate double bonds and  $(A_{810})_0$ ,  $(A_{810})_{t_1}$  and  $(A_{810})_{t_2}$  are the respective absorbances at  $810\text{cm}^{-1}$  at times  $t=0$ ,  $t_1$  and  $t_2$  (where  $t_2 > t_1$ ). Thus the rate of polymerisation can be deduced for a particular period of the reaction.

### 1.7.3 Photo-differential scanning calorimetry (Photo-DSC)

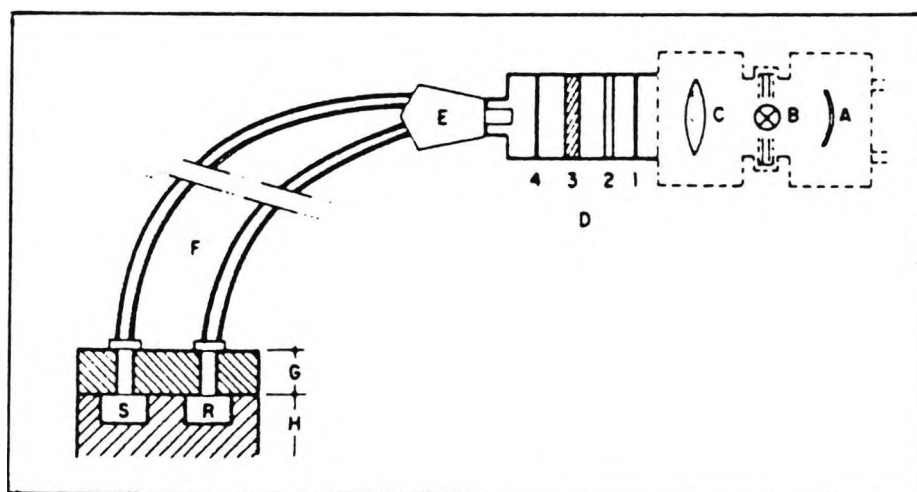
A differential scanning calorimeter can be used to measure the rate of heat produced and the total amount of heat from a chemical reaction. During polymerisation, which is exothermic, this can be related to the rate of conversion of monomer to polymer and to the total amount of monomer polymerised. A conventional commercial differential scanning calorimeter can easily be modified to study photoinitiated polymerisations (Moore et al, 1975). A number of reports appeared in the 1970's that utilised photo-DSC to study acrylate photopolymerisation (Moore et al, 1975; Wight and Hicks, 1978; Tryson and Shultz, 1979), and epoxide photopolymerisation (Crivello & Lam, 1977; Shultz and Stang, 1976). More recently the kinetics of photopolymerisation of epoxides has been studied (Shultz and Stang, 1987) and the technique has been used to study the bulk photopolymerisation of lauryl acrylate (Sastre et al, 1988).

#### Experimental details

The photo-DSC experiments were carried out in the laboratories of the CSIC Polymer Institute in Madrid using a modified Perkin-Elmer DSC-4 calorimeter which has been described previously (Sastre et al, 1989). A schematic representation of the experimental set up is shown below in

figure 1.11.

Figure 1.11 Photo-DSC apparatus



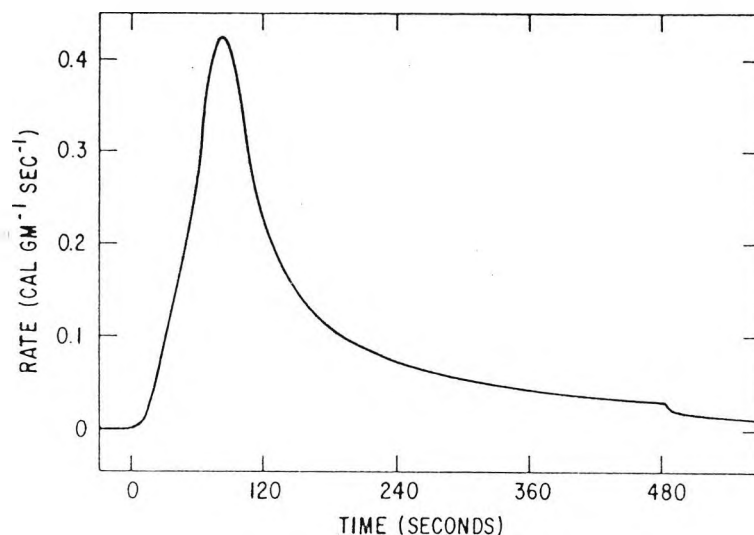
Schematic diagram of modified DSC-4: A, aluminium mirror; B, light source; C, focusing optics; D, aluminium cylinder cavity (1, neutral density filter; 2, solid IR filter; 3, interference filter; 4, shutter); E, fibre optics connector; F, two-branch flexible light-guide fibres; G, DSC swing away cover; H, DSC head; S, sample holder; R, reference holder.

The optics were aligned such that sample and reference cells were irradiated with the same light intensity. All experiments were performed using the calorimeter in the isothermal mode of operation. This means that any temperature difference between sample and reference pans is automatically set to zero by electrical compensation. The energy needed for this compensation corresponds directly to

the absorbed or released heat by the substance tested and is displayed as the measured signal. A purge gas, usually nitrogen, can be introduced into the system. The sample size was kept constant to reduce the possible side effects on the polymerisation rates. Filters could be incorporated in the path of the light source to give irradiation of a fixed wavelength band. A 365nm band pass filter was used in this context for all experiments performed. Prior to irradiation the samples were allowed to equilibrate to the operating temperature of 40°C for 5 minutes. This was also the case when a purge gas was used (eg. nitrogen) to equilibrate the samples to both the temperature and the inert atmosphere. The DSC-4 experimental run was allowed to begin for 1 minute without irradiation. This was to allow the DSC-4 to equilibrate and to check that a suitable flat baseline was recorded for later mathematical calculations. After 1 minute, irradiation from the Hg lamp was started by means of a shutter and the exothermic trace was recorded. After a suitable period of irradiation (generally around 5 minutes) the irradiation was stopped leaving the DSC-4 in the operating mode. This allowed the detection of any polymerisation occurring in the dark and meant that the trace eventually returned to the original baseline position. This was important for later calculations in which the integration of the appropriate area under the polymerisation exotherm was required to give a representative value for the rate of polymerisation. The rate of heat released by the sample ( $dH/dt$  in mcal/sec) was plotted versus the elapsed

time of the reaction. A typical exothermic trace due to polymerisation is shown in figure 1.12.

Figure 1.12 An exothermic polymerisation trace



The data acquired was analysed using the appropriate software programme on the data station. Analysis of the isothermal polymerisation follows the procedure previously documented (Barrett, 1967).

The total area, (A), of the exotherm curve corresponds to the total heat of polymerisation of the sample as shown in equation 1.53.

$$\Delta H_{\text{polym}} = A \qquad 1.53$$

and the degree of conversion can be represented by equation 1.54.

$$\text{Degree of conversion} = \frac{\text{area under exotherm/cal/g}}{\text{heat for 100\% reaction/cal/g}} \times 100\%$$

Equation 1.54

The area under the exotherm can be integrated at different time intervals to give a profile of the polymerisation as it proceeds. This is achieved using cursor lines in the appropriate software. The heat for 100% reaction of TMPTA has been calculated to be 195 cal/g (Tryson and Shultz, 1979).

The rate of polymerisation,  $R_p$ , is given by equation 1.55.

$$R_p = \frac{\text{Degree of conversion} \times [M]}{\text{time}} \quad \text{Equation 1.55}$$

[M] = monomer concentration /  $\text{moll}^{-1}$

Time = time of experimental run / s

Thus the rate of polymerisation can be determined at any point during reaction by integration of the exothermic curves using the necessary software programme. Therefore the efficiencies of different initiating systems can easily be evaluated using this technique.

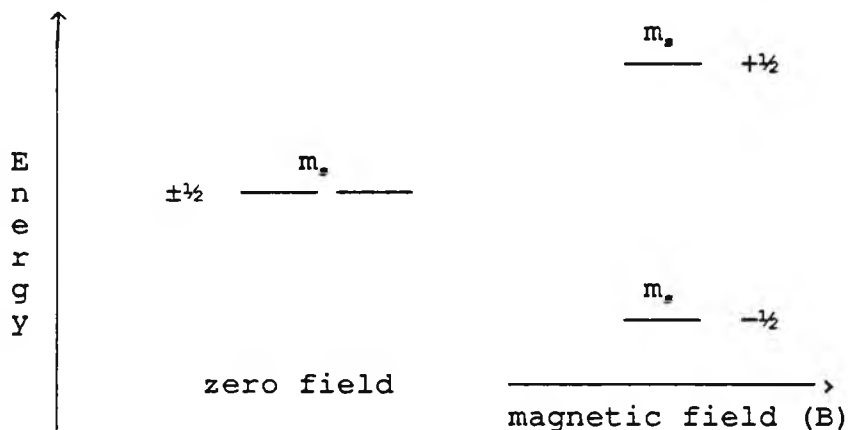
#### 1.7.4 Electron Paramagnetic Resonance (EPR) Spectroscopy

##### Introduction

The first successful EPR experiment was performed by a Russian physicist (Zavoisky, 1945) in the same year that early reports of the related technique nuclear magnetic resonance spectroscopy (NMR) appeared. The EPR method was developed further by chemists when it became apparent that free radicals could be detected and studied using this technique.

##### Principles of EPR

The basic EPR experiment involves the irradiation of a sample containing unpaired electrons with microwave radiation in the presence of an external magnetic field (B). In the absence of a magnetic field there are two possible spin states that may be exhibited by an unpaired electron denoted by spin quantum numbers  $m_s = +\frac{1}{2}$  and  $m_s = -\frac{1}{2}$ . These two spin states have the same energy and are equally populated. On the application of a magnetic field this is no longer the case and there is a net lowering of the energy of the spin state  $m_s = -\frac{1}{2}$  and a corresponding increase for that of the  $m_s = +\frac{1}{2}$  spin state as depicted below.



In practise it is convenient to use a microwave source of fixed frequency and to vary the magnetic field (B) until the condition for resonance is achieved. The energy level splitting ( $\Delta E$ ) between the  $m_s = +\frac{1}{2}$  and  $m_s = -\frac{1}{2}$  states is a function of B and is given by equation 1.56.

$$\Delta E = h\nu = g\mu_B B \quad 1.56$$

where,

$g$  =  $g$  factor (which is dimensionless, compare to chemical shift in NMR)

$\mu_B$  = Bohr magneton

$B$  = magnetic field

Since the  $m_s = -\frac{1}{2}$  state now has a lower energy it is more greatly populated than the  $m_s = +\frac{1}{2}$  state and their relative populations may be expressed using the Maxwell-Boltzmann law.

$$N_{m_s = +\frac{1}{2}} / N_{m_s = -\frac{1}{2}} = \exp(\Delta E/kT)$$

Equation 1.57

where the symbol (N) represents the number of unpaired electrons in each state shown and k is the Boltzmann constant. The EPR spectrometer measures the net absorption of energy created in the 'upward' transition from the  $m_s = -\frac{1}{2}$  state to the  $m_s = +\frac{1}{2}$  state. Thus by sweeping the field (B) at constant frequency ( $\nu$ ) the field ( $B_0$ ) required for resonance may be measured directly at the maximum of the absorption peak with a suitable field probe.

### The g factor

The so called g-factor depends on the orientation of the radical with respect to the magnetic field B. Assuming there are no external factors affecting the spin of the unpaired electron then this 'free electron' would have a g value of 2.0023. This is not the usual case and generally the local field at the electron depends to some extent on its environment (as is the case for nuclei in NMR spectroscopy so that chemical shifts are observed) and its value may be of diagnostic value. Shifts in the g factor value may be positive or negative compared to the free electron value. The source of the variation is due to the differences in spin-orbit coupling, which can create a secondary field, which couples with the magnetic moment of the electron due to its intrinsic spin.

### Hyperfine splitting

This is analogous to nuclear spin-spin coupling in NMR spectroscopy and is an important feature of EPR spectroscopy. It can reveal the nature of the magnetic nuclei that are present in a particular paramagnetic species and is, therefore, of diagnostic value.

For example in the case of the hydrogen atom ( $H^\bullet$ ) the associated proton may take either the  $m_I = +\frac{1}{2}$  or  $-\frac{1}{2}$  state with respect to the electron. Thus the magnetism due to the intrinsic proton spin may either augment ( $+\frac{1}{2}$ ) or detract ( $-\frac{1}{2}$ ) from the applied magnetic field giving rise to four possible spin states of the electron, all of different energies.

In more complex systems quantum mechanical restrictions give rise to the general rule that if a group of (n) equivalent nuclei with spin (I) are coupled to the unpaired electron  $2nI + 1$  spectral lines will be observed arising from the same number of transitions.

### Intensities

As is the case for NMR spectroscopy the net intensities of the lines in any multiplet, arising from the coupling of the odd electron with a set of n equivalent nuclei, are given by the coefficient of the Binomial expansion represented by Pascal's Triangle. Therefore, the four lines in the EPR spectrum of  $CH_3^\bullet$  are in the ratio 1:3:3:1.

## EPR spectra of radical cations

The best method of generating these species is by the use of halocarbon solvents with "freons" being most commonly used (Symons, 1984). The procedure is to prepare a dilute (0.1-1.0 w/w%) solution of the substrate in a solvent such as  $\text{CFCl}_3$ , freeze to 77K and then expose the frozen material to  $\gamma$  radiation. Taking the example of  $\text{CFCl}_3$ , the relevant radiolytic processes may be summarised as follows in scheme 1.8.

### Scheme 1.8 The radiolytic processes of $\text{CFCl}_3$

1.  $\text{CFCl}_3 \longrightarrow \text{CFCl}_3^{+\bullet} + e^-$
2.  $\text{CFCl}_3 + e^- \longrightarrow [\text{CFCl}_3^{\cdot-}] \longrightarrow \text{CFCl}_2\cdot + \text{Cl}^-$
3.  $\text{CFCl}_3^{+\bullet} + \text{CFCl}_3 \longrightarrow \text{CFCl}_3 + \text{CFCl}_3^{+\bullet}$
4.  $\text{CFCl}_3^{+\bullet} + \text{S} \longrightarrow \text{CFCl}_3 + \text{S}^{+\bullet}$

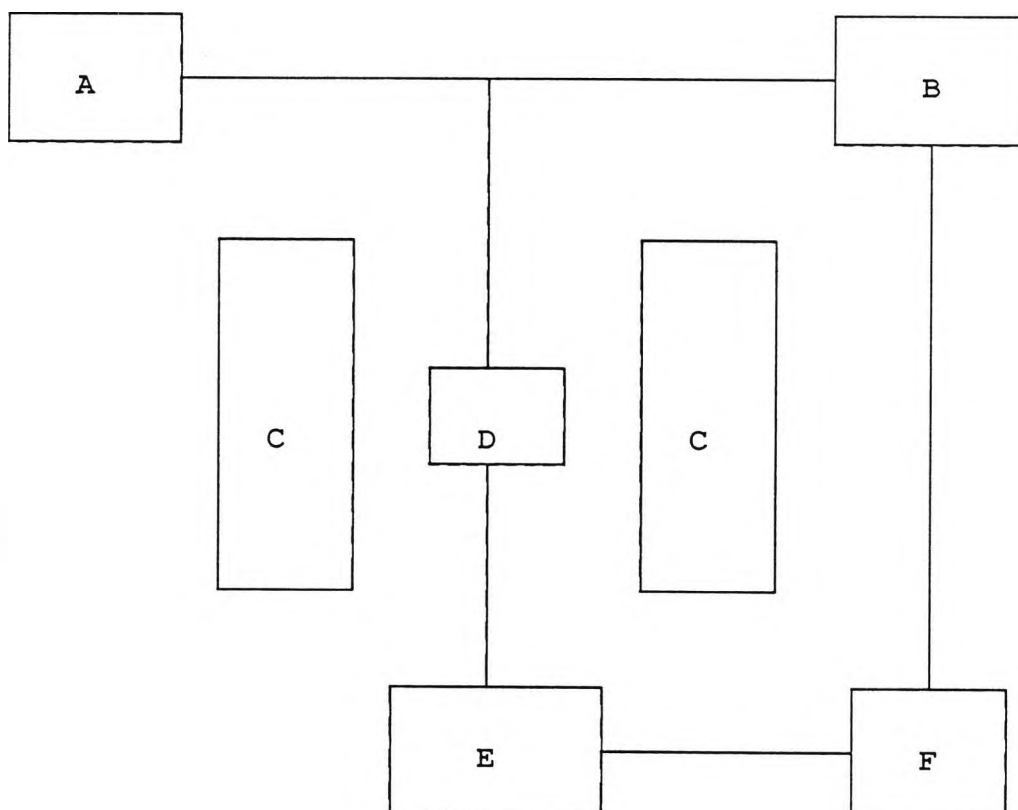
The advantage of this method is that the radiolytically produced electrons are efficiently scavenged (step 2) and are converted to product radicals with very broad EPR signals so that only the sharper features of the substrate (S) radical cations  $\text{S}^{+\bullet}$ , as produced in step 4, are normally

observed. Providing the substrate has a lower ionisation potential than the "freon" solvent (around 12eV) this is an appropriate method to study the behaviour of the radical cation.

### Instrumentation

Full details of the design of EPR spectrometer systems can be found in textbooks on the subject (Poole, 1967; Wilmshurst, 1967). A simplified overview of the essential components used is given in the block diagram in figure 1.13.

Figure 1.13 Schematic diagram of an EPR spectrometer



A = microwave bridge, B = detector crystal, C = electromagnet, D = cavity, E = modulation input, F = phase sensitive detector, G = signal output

Within the microwave bridge is contained the klystron (or Gunn diode) which supplies the microwaves which are transmitted to the resonant cavity and the detector by means of waveguides. A strong magnetic field is applied to the cavity, which contains the paramagnetic sample, by a strong electromagnet. Since the microwave source is of fixed frequency, the magnetic field is 'swept' so as to achieve the condition of resonance.

## 1.8 References

- Barrett, K.E.J., (1967). *J.Appl.Poly.Sci.*, **11**, 1617
- Barret, J.L., (1979). *J.Rad.Curing*, **6** (4), 20
- Bartholomew, R.F., and Davidson, R.S., (1971b). *J.Chem.Soc. (C)*, 2342
- Bartholomew, R.F., and Davidson, R.S., (1971a). *J.Chem.Soc. (C)*, 2347
- Bartholomew, R.F., Davidson, R.S., and Howell, M.J., (1971). *J.Chem.Soc. (C)*, 2804
- Baxter, J.E., Davidson, R.S., and Hageman, H.J., (1987). *Makromol.Chem.,Rapid Commun.*, **8**, 311
- Birks, J.B., (1970). "Photophysics of Aromatic Molecules", Wiley-Interscience, London
- Birks, J.B., (1973). "Organic Molecular Photophysics", Vol. 1, 403 (ed. Birks, J.B.), Wiley, New York
- Bolon, D.A., and Webb, K.K., (1978). *J.Appl.Polymer.Sci.*, **22**, 2543
- Calvert, J.G., and Pitts, J.N., (1966). *Photochemistry*,

Wiley, New York

Crivello, J.V., and Lam, J.H.W., (1977). *Macromolecules*,  
10, 1307

Crivello, J.V., and Lam, J.H.W., (1978). *J.Polym.Sci.,*  
*Polym.Chem.Edn.*, 16, 2441

Crivello, J.V., and Lam, J.H.W., (1979a). *J.Polym.Sci.,*  
*Polym.Chem.Edn.*, 17, 977

Crivello, J.V., and Lam, J.H.W., (1979b). *J.Polym.Sci.,*  
*Polym.Chem.Edn.*, 17, 1059

Crivello, J.V., and Lam, J.H.W., (1979c). *J.Polym.Sci.,*  
*Polym.Chem.Edn.*, 17, 3845

Crivello, J.V., and Lam, J.H.W., (1980a). *J.Polym.Sci.,*  
*Polym.Chem.Edn.*, 18, 2677

Crivello, J.V., and Lam, J.H.W., (1980b). *J.Polym.Sci.,*  
*Polym.Chem.Edn.*, 18, 2697

Crosby, G.A., Watts, R.J., and Carstens, D.H.W., (1970).  
*Science*, 170, 1195

Cundall, R.B., Dandiker, Y.M., Davies, A.K., and Salim,  
M.S., (1987). *Polymers Paint Colour Journal*, 177 (4188),

Curtis, H., Irving, E., and Johnson, B.F.G., (1986).  
*Chem.Brit.*, 327

Decker, C., and Fizet, M., (1980). *Makromol.Chem., Rapid Commun.*, 1, 637

Decker, C., and Moussa, K., (1988). *Makromol.Chem.*, 189, 2381

Decker, C., and Moussa, K., (1990a). *ACS Symp.Ser.*, 417, 438

Decker, C., and Moussa, K., (1990b). *J.Polym.Sci., Polym.Chem.*, 28, 3429

Deville, (1839). *Ann.Chim.*, 75, 66

Eaton, D.F., (1979). *Photogr.Sci.Eng.*, 23, 150

Green, G.E., and Stark, B.P., (1981). *Chem.Brit.*, 17, 228

Ingold, K.U., *Acc.Chem.Res* 2,1

Jackel, K.P., (1989). *Prog.Org.Coatings*, 16, 355

Klingert, B., Riediker, M., and Roloff, A., (1988).  
*Comments Inorg.Chem.*, 7 (3), 109

Lee, G.A., and Doorakian, G.A., (1977). *J.Radiat. Curing*, 4,2

Lohse, F., and Zweifel, H., (1986). *Adv.Polym.Sci.*, 78, 61

McGinnis, V.D., (1978). "Light Sources; in UV Curing Science and Technology" (Pappas, S.P., [ed.]), Technology Marketing Corporation, Stamford, Connecticut 1978 pp96-132

McGinnis, V.D., (1979). *Photogr.Sci.Eng.*, **23**, 124

Medinger, T., and Wilkinson, F., (1965). *Trans.Faraday Soc.*, **61**, 620

Meier, K., and Zweifel, H., (1985a). *Polym.Preprints*, **26**, 347

Meier, K., and Zweifel, H., (1985b). *Eur.Pat.Appl.No.*, 0'152'377 to Ciba-Geigy

Meier, K., and Zweifel, H., (1986a). *J.Rad.Curing*, **26** (October)

Meier, K., and Zweifel, H., (1986b). *J.Imaging Sci.*, **30**, 174

Moore, J.E., Schroeter, S.H., & Shultz, A.R., (1975) *Org.Coat.Plast.Prep.*, **35**, 239

Moore, J.E., (1980). "UV Curing, Science and Technology", Ed. by S.P.Pappas, Technol.Market.Corp., Norwalk, Conn., USA, 133-159

Pappas, S.P., (ed.), (1978). 'UV Curing: Science and Technology', Vol. 1, Stamford Technology Marketing, Norwalk, CT

Pappas, S.P., (ed.), (1984). 'UV Curing: Science and Technology', Vol. 2, Stamford Technology Marketing, Norwalk, CT

Poole, C.P., (1967). "Electron Spin Resonance: A Comprehensive Treatise on Experimental Techniques", Wiley-Interscience, New York

Rehm, D., and Weller, A., (1970). *Isr.J.Chem.*, 8, 259

Roffey, C.G., (1982). 'Polymerisation of Surface Coatings', Wiley-Interscience, New York

Rubin, H., (1974). *J.Paint Technol.*, 46, 74

Sastre, R., Conde, M., and Mateo, J.L., (1988). *J.Photochem.Photobiol.,A:Chem.*, 44, 111

Sastre, R., Conde, M., Catalina, F., and Mateo, J.L., (1989). *Rev.Plast.Mod.*, 393, 375

Schlesinger, S.I., (1974a). *Photograph.Sci.Eng.*, 14, 513

Schlesinger, S.I., (1974b). *Photograph.Sci.Eng.*, 18, 387

Schumann, H., (1984). *Chemiker Zeitung*, 108, 345

Shultz, A.R., and Stang, L.D., (1976). Paper presented at 7th Northeast Regional Meeting ACS, Albany, NY, August 8.

Shultz, A.R., and Stang, L.D., (1987). "Crosslinked Epoxies", Walter de Gruyter & Co., Berlin, 93-115

Small, R.D., Ors, J.A., and Royce, B.S., (1984). ACS Symp.Ser., 242, 325

Symons, M.C.R., (1984). Chem.Soc.Rev., 13, 393

Thompson, L.F., Willson, C.G., and Bowden, M.J., (eds.), (1983). 'Introduction to Microlithography', ACS Symp.Ser., No. 219, ACS Washington, D.C.

Turro, N.J., (1978). "Modern Molecular Photochemistry", Benjamin/Cummings, Menlo Park, California

Tryson, G.R., and Shultz, A.R., (1979). J.Polym.Sci., Polym.Phys.Ed., 17 (12), 2059

Tsuroska, M., and Tanaka, M., (1988). Proceed.Conf.Radiation Curing Tokyo, 403

Vander Donckt, E., and Vogels, C., (1971). Spectrochim.Acta., 27A, 2157

Wight, F.R., & Hicks, G.W., (1978). Polym.Eng.Sci., 18, 378

Wilmshurst, T.H., (1967). "Electron Spin Resonance Spectrometers", Adam Hilger, London

Zavoisky, E., (1945). J.Phys.USSR, 9, 211

## **Chapter 2.**

# **PHOTOPOLYMERISATION INITIATED USING ALLYL, BENZYL AND ASSOCIATED SILANES AND STANNANES**

## 2.1 The synthesis of silanes and stannanes

### Preparation

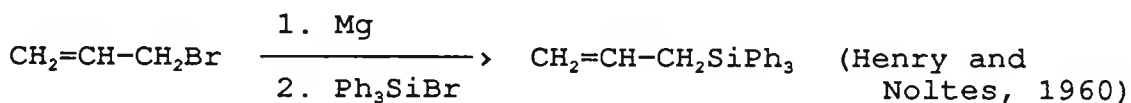
An introduction to synthetic routes that have been used in this work is presented. For a more comprehensive treatise on the many different synthetic methods the reader is referred to a number of excellent articles that have been published (Chan and Fleming, 1979; Colvin, 1981; Wilkinson et al, 1982; Sarkar, 1990a; Sarkar, 1990b).

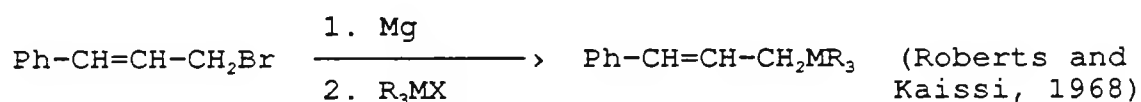
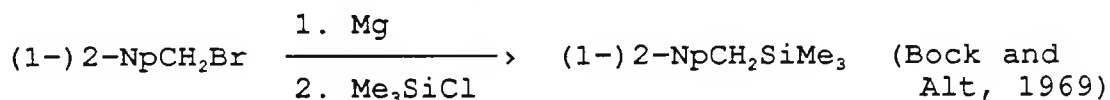
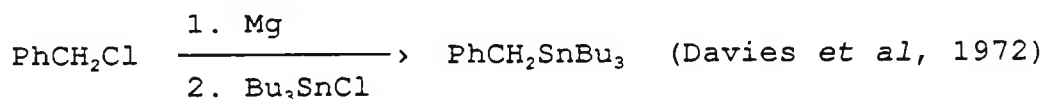
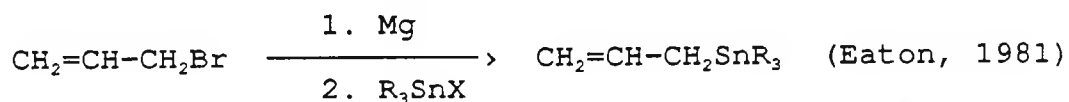
#### 2.1.1 Via Grignard reaction

This is undoubtedly the simplest and most direct route and it is applicable to a variety of substrates. In 1912 an early example of this reaction was the preparation of benzyltrimethylsilane (Bygden, 1912).



A more general reaction of great versatility involves the reaction of the trisubstituted metal halide with the Grignard reagent of the organic halide as demonstrated in the following examples:





A number of compounds have been successfully synthesised in this work using the Grignard route. A summary of the reaction times and yields is given in table 2.1.

Table 2.1 The Grignard synthesis of silanes and stannanes

Compound	Reaction time (h)	Yield (%)	Solvent	Reaction temp/°C
4-Me-C <sub>6</sub> H <sub>4</sub> CH <sub>2</sub> SiMe <sub>3</sub>	5	48	Et <sub>2</sub> O	38
PhCH <sub>2</sub> SnMe <sub>3</sub>	5	63	THF	68
CH <sub>2</sub> =CHCH <sub>2</sub> SiPh <sub>3</sub>	16	74	THF	20
CH <sub>2</sub> =CHCH <sub>2</sub> SnBu <sub>3</sub>	16	56	Et <sub>2</sub> O	38

The main problem of this method is that regioselectivity cannot always be controlled, especially in the case of substituted allylic derivatives, and separation of a required isomer can be tedious.

### 2.1.2 Via Barbier reaction

One possible way to overcome the problem of regioselectivity is to use the related Barbier synthesis using a modified procedure. Using this route the allylic halide is added to a mixture of the trialkylmetal halide and magnesium. This procedure was used to good effect with external irradiation of ultrasound to give an extremely facile and stereoselective preparation of a number of allylstannanes (Naruta *et al*, 1986). This method also has the advantage of converting the allyl halides to the corresponding allylstannanes minimising the formation of Wurtz-type coupling products so often encountered in the course of preparation of allylic Grignard reagents. This procedure was adopted and further extended to synthesise a number of silanes and stannanes in good yield (Bowser and Davidson, 1992). The preparations involved relatively short reaction times and gave great stereoselectivity of products as given in table 2.2.

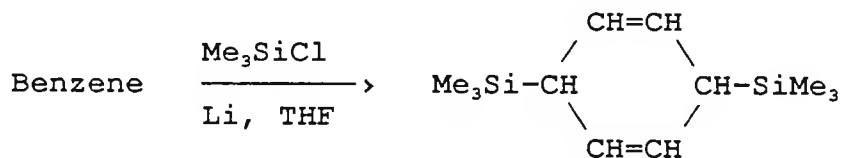
**Table 2.2** The Barbier synthesis of silanes and stannanes

Compound	Reaction time (h)	Yield (%)
4-MeO-C <sub>6</sub> H <sub>4</sub> CH <sub>2</sub> SiMe <sub>3</sub>	3.5	98
PhCH <sub>2</sub> SnBu <sub>3</sub>	1	86
4-Me-C <sub>6</sub> H <sub>4</sub> CH <sub>2</sub> SnBu <sub>3</sub>	1	45
4-MeO-C <sub>6</sub> H <sub>4</sub> CH <sub>2</sub> SnBu <sub>3</sub>	3.5	100
1-NpCH <sub>2</sub> SiMe <sub>3</sub>	10	62
2-NpCH <sub>2</sub> SiMe <sub>3</sub>	10	88
1-NpCH <sub>2</sub> SnBu <sub>3</sub>	5	63
2-NpCH <sub>2</sub> SnBu <sub>3</sub>	5	78
2-NpCH <sub>2</sub> SnMe <sub>3</sub>	2	46
*MeCH=CHCH <sub>2</sub> SnBu <sub>3</sub>	2	69
CH <sub>2</sub> =CMeCH <sub>2</sub> SnBu <sub>3</sub>	2	62
Me <sub>2</sub> C=CHCH <sub>2</sub> SnBu <sub>3</sub>	2	77
*Ph-CH=CHCH <sub>2</sub> SnBu <sub>3</sub>	2	44

\* = trans - isomer

### 2.1.3 Via reductive silylation

Reductive silylations of both dienes and aromatic systems using chlorosilane/metal reagents to yield allylic silanes have been studied (Calas and Dunogués, 1976).

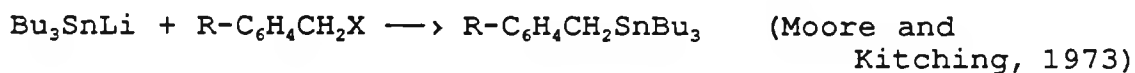


Another useful method was discovered in which the reductive

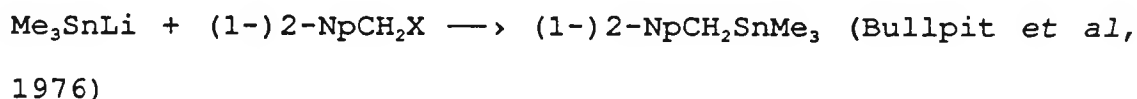


#### 2.1.4 Via Wurtz coupling

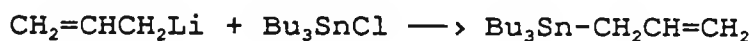
This involves the coupling reaction of a halide with a lithium reagent. Usually a preformed lithiated trisubstituted silane or stannane such as  $\text{Ph}_3\text{SiLi}$  (George et al, 1960),  $\text{Me}_3\text{SnLi}$ ,  $\text{Bu}_3\text{SnLi}$ ,  $\text{Ph}_3\text{SnLi}$  (Tamborski et al, 1963; Still, 1976) or  $\text{Me}_3\text{SiLi}$  (Hudrlik et al, 1984) is reacted with the allylic or benzylic halide as shown below.



R = 4- (H, Me, MeO)



In a similar vein it has also been reported that the lithiated organic moiety will couple with the trisubstituted metal halide (Seyferth and Weiner, 1961).



A Wurtz coupling reaction was used to synthesise hexamethyldisilane in good yield.

## 2.2 Physical and Chemical properties of Silanes and Stannanes

Photoelectron (PE) spectroscopic studies have shown that group 4A organometallics, particularly those containing a metal-carbon bond  $\beta$  to a neighbouring  $\pi$  system, are exceedingly electron rich (Hosomi and Traylor, 1975). Both the ionisation potentials and the oxidation potentials of these compounds are in the range of typical conventional donors effective in charge transfer schemes. The first ionisation potentials and the oxidation potentials for a number of group 4A organometallics are given in table 5.1 (see Appendix). The general trend in the data in table 5.1 is that the ease of ionisation/oxidation is in the order of naphthyl > benzyl > allyl and also Sn > Si. Substituents can also have a marked effect on the ionisation/oxidation potentials. From the data in table 5.1 it appears that the  $R_3M-C$  ( $M=Si, Sn$ ) unit offers a strong stabilising, electron donating effect to an adjacent electron deficient centre. The mechanism of this electron donation has been the subject of contention for a number of years. The two main theories involved in explaining the effects of the  $R_3M-C$  group involve either  $p_\pi-d_\pi$  bonding or  $\sigma-\pi$  hyperconjugation outlined below.

### 2.2.1 $p_\pi-d_\pi$ bonding

$p_\pi-d_\pi$  bonding, also known as neighbouring group participation, is an example of a non-vertical stabilisation

process. This essentially means that the substituent changes its geometry or its distance from the stabilised species as the transition state is approached.

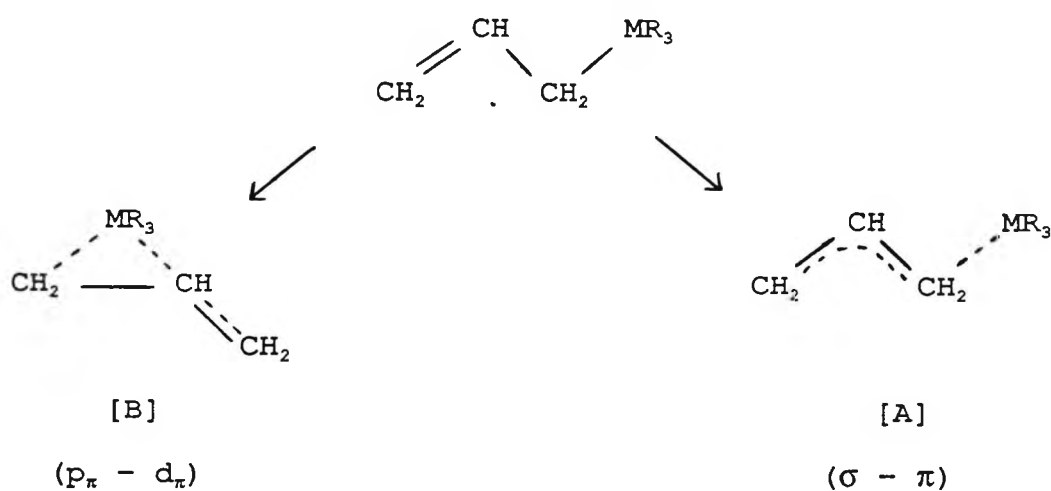
### 2.2.2 $\sigma$ - $\pi$ hyperconjugation

$\sigma$ - $\pi$  hyperconjugation is an example of a vertical stabilisation process. This means that the substituent does not change its geometry or its distance from the stabilised species, as the transition state is approached.

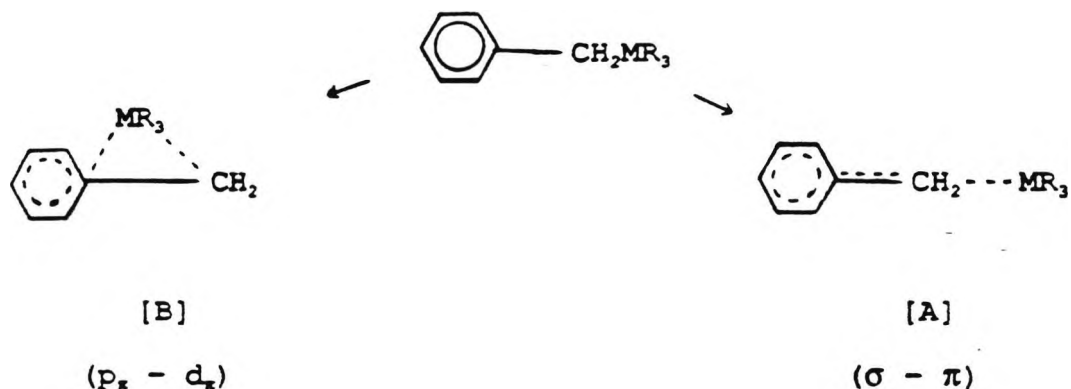
Both these situations may be represented below in figure 2.1.

Figure 2.1  $p_\pi$ - $d_\pi$  bonding versus  $\sigma$ - $\pi$  hyperconjugation in allylic and benzylic silanes and stannanes

Allylic compounds:



Benzylic compounds:



(where M = Si, Sn)

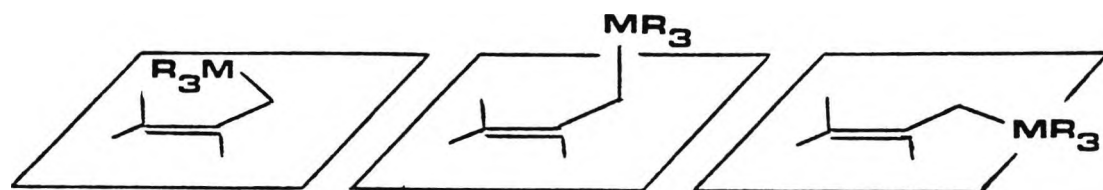
Such vertical  $\sigma$ - $\pi$  hyperconjugation (A) is preferred over the alternative of neighbouring group participation (B) to account for a number of anomalous features in the physical and chemical properties of allylic, benzylic, and related silanes and stannanes. Several Russian authors used this  $\sigma$ - $\pi$  hyperconjugation rationale to interpret the reactivity and spectral behaviour of allyl and benzylsilanes (Petrov et al, 1956; Egorov et al, 1961; Leites, 1963). Around the same time Eaborn suggested the possibility of C-Si  $\sigma$ - $\pi$  hyperconjugation in benzyltrimethylsilane (Eaborn, 1956). It was not until the early 1970s that the  $\sigma$ - $\pi$  hyperconjugation theory was further substantiated. A number of papers from the laboratories of Bock (Pitt and Bock, 1972; Bock et al, 1972;) and Schweig (Weidner and Schweig, 1972a; Weidner and Schweig, 1972b; Schweig et al, 1973a; Schweig et al, 1973b) appeared on the photoelectron spectroscopy of allylic and benzylic organometallic systems.

In these papers the usefulness of  $\sigma$ - $\pi$  hyperconjugation for the interpretation of photoelectron spectra was clearly demonstrated. Other evidence was provided by charge-transfer (CT) spectra (Hanstein et al, 1970a; Hanstein et al, 1970b), particularly with tetracyanoethylene.

In addition to the quantitative interpretation of CT and PE spectra, the hyperconjugation concept has been supported by numerous qualitative arguments based on steric considerations. Thus it has been suggested that  $\sigma$ - $\pi$  hyperconjugation requires coplanarity of the C-M bond and the axis of the electron deficient  $\pi$  orbital (Nesmeyanov and Kritskaya, 1958; Traylor and Ware, 1967). The  $\sigma$ - $\pi$  hyperconjugation effect should be maximised when the  $R_3M$   $\sigma$  bond is parallel to the  $\pi$  orbitals of the C=C double bond (Bach and Scherr, 1973). In other words the extent of the  $\sigma$ - $\pi$  hyperconjugation is dependent on the dihedral angle ( $\theta$ ) between the C-M bond and the  $\pi$  system, being at a maximum when  $\theta$  is at zero (Hanstein et al, 1970b; Pitt, 1970). This conformational requirement has also been invoked from EPR studies of tin-containing radicals (Lyons and Symons, 1971). Trying to assess the relative amounts of  $\sigma$ - $\pi$  hyperconjugation versus  $p_\pi$ - $d_\pi$  bonding in allylic, benzylic, and related organometallics requires an understanding of the relative populations of the ground state conformers. The limiting conformations for an allylic compound, as an example, are shown below in figure 2.2.

Figure 2.2

The limiting conformations of the C=C double bond with respect to the metal-CH<sub>2</sub> in an allylic system.



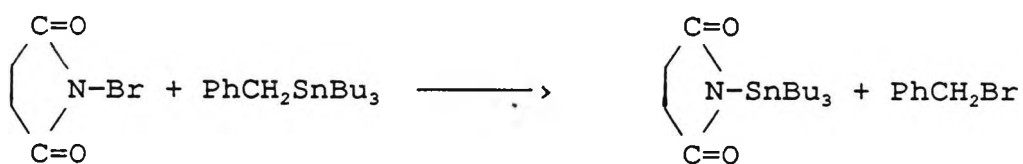
Thus the overall picture may be a combination of several effects, creating the so called  $\beta$ -effect, whilst the most important of these appears to be the  $\sigma$ - $\pi$  hyperconjugation. It is also possible that this  $\sigma$ - $\pi$  hyperconjugation may play a significant role in the weakening of the M-C bond and thus promote the cleavage processes which are often encountered in the reactions of  $\beta$ -functionalised organosilanes and stannanes. In allylic, benzylic and related silanes and stannanes the highest occupied molecular orbital (HOMO) is raised due to the  $\sigma$ - $\pi$  hyperconjugation effect, resulting in a lower ionisation potential of these compounds when compared to the analogous carbon derivative (see table 5.1: Appendix). It is these properties that are thought to be important in the proposed electron transfer reactions of these compounds which are discussed later (see section 2.5.7).

### 2.3 Photochemistry of benzylsilanes and stannanes

It is well known that various benzylic substituted compounds undergo homolytic cleavage upon irradiation (Slocum *et al*, 1981; Hilinski *et al*, 1984; Johnston and Scaiano, 1985). Previous evidence, outlined below, has also been presented that indicates benzylsilanes and benzylstannanes undergo homolytic cleavage reactions to form benzylic and metal centred radicals.

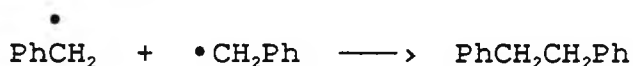
#### 2.3.1 Photochemistry of benzylstannanes

It was proposed in the early 1970's that benzyltri-*n*-butylstannane reacted with N-bromosuccinimide by a free radical chain mechanism involving bimolecular homolytic substitution by the succinimyl radical at the tin centre (Davies *et al*, 1970; Davies *et al*, 1972) shown below.

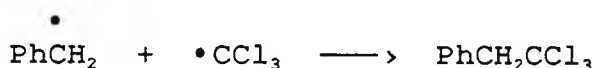
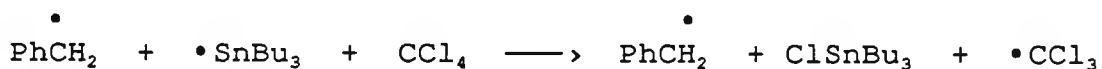


A later study (Soundararajan and Platz, 1987) suggested that photolysis of benzyl and naphthylstannanes leads to homolytic cleavage via the excited singlet state to form the corresponding benzyl (or naphthyl) radical and the tri-*n*-butyltin radical. Evidence was invoked from the photolysis

products of a number of benzylic stannanes in different solvents. The photolysis products in benzene were rationalised by homolytic fission followed by radical recombination shown below for benzyltri-*n*-butylstannane.

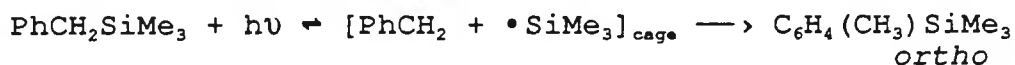


In carbon tetrachloride the developing  $\bullet\text{SnBu}_3$  radical rapidly abstracts Cl from the solvent to form  $\text{Bu}_3\text{SnCl}$  and a new radical pair product which eventually form stable products as depicted below for benzyltri-*n*-butylstannane.



### 2.3.2 Photochemistry of benzylsilanes

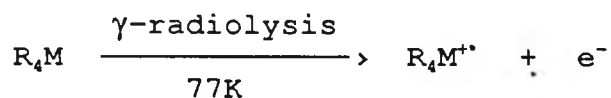
Benzyltrimethylsilane has been described as photochemically inert (Valkovich et al, 1974) but a later study, the first to investigate the intrinsic photochemistry of the benzylsilane chromophore, was reported to give homolysis of the benzylic carbon-silicon bond shown below (Kira et al, 1985).



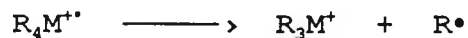
Benzyltrimethylsilane was isomerised to o-tolyltrimethylsilane in 2% yield. It is not clear as to whether the photolysis quantum yield is high and a major process occurs as an in-cage recombination, or that the quantum yield of photolysis is low, explaining the low yield of product.

#### 2.4 Electron Paramagnetic Resonance (EPR) spectroscopy results

EPR spectroscopy has been used to study radical cations derived from organosilicon and organotin compounds, as isolated in solid trichlorofluoromethane matrices at low temperatures. The primary radical cations were formed by  $\gamma$ -radiolysis of the neutral parents in solid  $\text{CFCl}_3$  matrices at 77K as shown below.



In previous photochemical studies of simple silanes and stannanes ( $\text{R}_4\text{M}$ ), in the presence of electron acceptors, the initially formed  $\text{R}_4\text{M}^{\cdot+}$  radical cations were proposed to fragment as follows:



Direct evidence for this reaction has been obtained for tetraalkyltin radical cations (Boschi *et al*, 1973; Evans *et al*, 1979), from which radicals  $R^\bullet$  may be detected by EPR spectroscopy even under cryogenic conditions. In view of the above, it seemed worthwhile to study a range of silanes and stannanes by EPR spectroscopy to determine any relationship between the structure and relative ease of fragmentation of their radical cations.

#### 2.4.1 EPR results of benzylsilanes

EPR spectra of the radical cations of benzyltrimethylsilane and its 4-methyl and 4-methoxy derivatives were recorded at 77K and showed that most of the spin density resided on the aromatic ring and a small amount is located in the silicon to benzylic carbon bond (Butcher *et al*, 1992). On warming the matrix (160K) no direct evidence could be obtained for the formation of benzylic radicals. This observation is in agreement with earlier work claiming that nucleophilic attack at silicon is required to cause fragmentation (Ohga and Mariano, 1982; Dinnocenzo *et al*, 1989; Sirimanne *et al*, 1991).

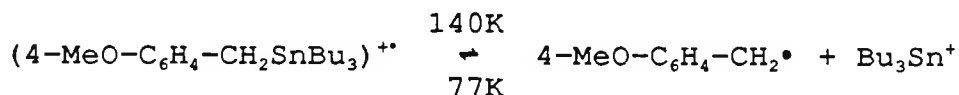
#### 2.4.2 EPR results of benzylstannanes

EPR spectra of the radical cations of benzyltri-*n*-butylstannane and the 4-methoxy analogue were recorded at 77K (Butcher *et al*, 1992). The spectrum of  $[\text{PhCH}_2\text{SnBu}_3]^{+\bullet}$  at

77K shows an intense feature which is associated with the presence of *n*-butyl radicals. This spectrum was compared to that of the radical cation of tetra-*n*-butyltin which was also recorded at 77K. The differences in the spectra reflects some delocalisation of the positive hole from the electron-depleted benzylic C-Sn bond onto the aromatic group. On warming to 155K the spectrum of  $[\text{PhCH}_2\text{SnBu}_3]^{+\bullet}$  showed an overall loss of this signal and new features appeared which can readily be assigned to free benzyl radicals. This is in accordance with the structural view of an electron-depleted C-Sn bond which fragments as shown in equation 2.1.



In the case of the 4-methoxy analogue the radical cation remained intact at 77K. On warming to 140K features assigned to the benzylic radical grew with a similar reduction in the signal associated with the primary intact radical cations. Recooling to 77K resulted in the regeneration of the original radical cation signal with minimal loss in intensity. Thus the fragmentation of the 4-methoxy analogue and its subsequent recombination was shown to be a thermally reversible process as shown below.

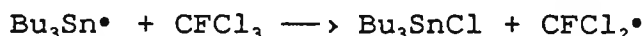
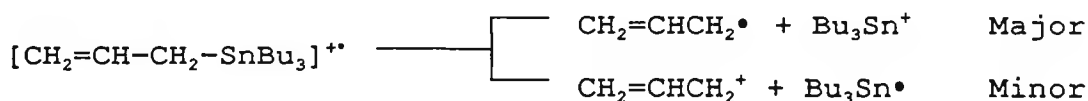


The requirement of a lower temperature for fragmentation for

(4-MeO-C<sub>6</sub>H<sub>4</sub>-CH<sub>2</sub>SnBu<sub>3</sub>)<sup>•+</sup> (140K) compared to [PhCH<sub>2</sub>SnBu<sub>3</sub>]<sup>•+</sup> (155K) shows that the activation energy for benzylic C-Sn bond cleavage of the radical cation is lowered by 4-MeO substitution.

### 2.4.3 EPR results of allyl and cinnamyl stannanes

The EPR spectra of the radical cations of allyl and cinnamyl tri-*n*-butylstannane have been recorded at 77K (Butcher, et al, 1992). On warming the allyltri-*n*-butylstannane radical cation to 120K features were observed belonging to free allyl radicals. This shows that the activation energy for C-Sn bond cleavage for the organotin radical cations is reduced for the allyl derivative (120K) when compared to the benzyl analogues (140K and 155K). A simple explanation for this result is a product development argument based on the greater stability of an allyl radical compared to a benzyl radical (Vedeneyev et al, 1966). There was also evidence (observation of the fluorodichloromethyl radical, CFCl<sub>2</sub>•) that fragmentation of the allyltri-*n*-butylstannane radical cation can occur in two ways.



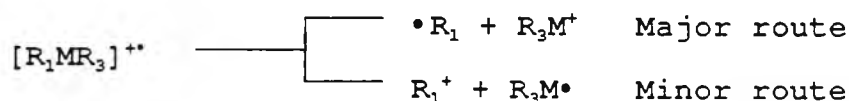
The spectrum of [PhCH=CHCH<sub>2</sub>SnBu<sub>3</sub>]<sup>•+</sup> showed evidence that

fragmentation occurred at 77K to yield the cinnamyl radical and the  $\text{Bu}_3\text{Sn}^+$  species, as observed in the major route for the allylstannane radical cation. Again the fragmentation at the lower temperature is probably due to the greater stability of the carbon-centred radicals produced in the cinnamyl case (77K) when compared to the allyl derivative (120K).

#### 2.4.4 Structure and stability of radical cations

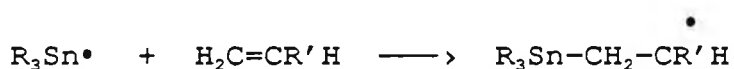
There is a definite depletion of electron density from the C-Sn(Si) bonds on ionisation in all the compounds studied. It was observed that the ease of fragmentation in the radical cations does not follow the order of electron depletion but instead appears to relate to the stabilisation of the developing radical/cation fragments, giving rise to a transition state effect.

An important observation in the context of the UV curing results is the cleavage of the allylstannane via two different pathways. It would seem that radical cations of the type  $[\text{R}_1\text{MR}_3]^{+\bullet}$  have two possible fragmentation routes.



This confirms an earlier report on the fragmentation of radical cations of benzyltrialkylstannanes which suggested that fragmentation occurred by dual modes as above (Eaton, 1980a). Eaton suggested that to increase the favourability

of the minor pathway electron-donating substituents should be incorporated on the aromatic ring. This was to help stabilise the formation of the benzylic cation intermediate and thus increase the ratio of minor route:major route. The major pathway is of no benefit to the curing process whereas the minor pathway is of significance since trialkyltin radicals are known to react with alkenes via a free radical chain mechanism (Neumann *et al*, 1961; Davies, 1977).



From the EPR studies it is not known if the thermal energy which is available to the radical cations at room temperature is able to increase the favourability of the minor pathway to give metal-centred radicals. Fragmentation of benzylsilane radical cations was not observed under the conditions used which suggests that (C-Si)<sup>••</sup> bond cleavage occurs less readily than (C-Sn)<sup>••</sup> bond cleavage. Thus it is the tin compounds that are anticipated to be the more responsive under ionising conditions in developing photoresists.

## 2.5 UV Curing results

### 2.5.1 UV curing results of benzylsilanes

A number of benzylsilanes were tested at 5% w/w in the presence of a free radical polymerisable monomer, (TMPTA), using the UV Colordry apparatus described earlier (see section 1.7.1). This was in order to assess the free radical initiating properties of the compounds under test. The results are presented below in table 2.4.

Table 2.4

UV curing results of benzylsilanes incorporated at 5% w/w in TMPTA

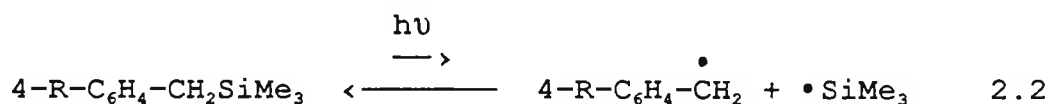
E X P T	INITIATOR	NUMBER OF PASSES			
		Touching Quartz	Touching Glass	In Air	Glass Filter
1	PhCH <sub>2</sub> SiMe <sub>3</sub>	4	28	*	*
2	4-Me-C <sub>6</sub> H <sub>4</sub> CH <sub>2</sub> SiMe <sub>3</sub>	4	*	*	*
3	4-MeO-C <sub>6</sub> H <sub>4</sub> CH <sub>2</sub> SiMe <sub>3</sub>	3	24	*	*
4	4-Ph-C <sub>6</sub> H <sub>4</sub> CH <sub>2</sub> SiMe <sub>3</sub>	2	11	*	*
5	TMPTA	6	40	*	*

Belt speed = 10 ft/min for all experiments

\* = polymerisation not detected after 30 passes

### Touching quartz and touching glass

The results indicate that the benzylsilanes will initiate free radical polymerisation as evidenced by the reduced number of passes required to reach tack free cure when compared to the monomer, TMPTA, on its own (EXPT 5). The mechanism of polymerisation is proposed to be via homolytic cleavage of the C-Si benzylic bond followed by attack by a free radical on the monomer to initiate polymerisation. It appears that the cleavage of the C-Si benzylic bond is not efficient even when using the full spectral output of the lamp and also reducing the effect of oxygen inhibition in the touching quartz experiments. This indicates that either the quantum yield of photolysis is low or the in-cage recombination of photolysis products is high and can be represented by equation 2.2 below.



The improved response of the biphenyl derivative (EXPT 4) in the touching glass experiment can be attributed to the improved absorption properties of this compound in the region beyond the glass filter (>310nm). Consequently further syntheses of substituted benzylic silanes with improved absorption properties were carried out in the hope that better photoinitiating properties would accrue. The results of the UV curing of these compounds are given below

in table 2.5 along with that of benzyltrimethylsilane for comparison.

Table 2.5 UV curing results of benzylic silanes incorporated at 5% w/w in TMPTA

EXPT	INITIATOR	NUMBER OF PASSES			
		Touching Quartz	Touching Glass	In Air	Glass Filter
1	PhCH <sub>2</sub> SiMe <sub>3</sub>	4	28	*	*
2	Ph <sub>2</sub> CHSiMe <sub>3</sub>	3	9	*	*
3	9-trimethylsilyl-fluorene	2	5	30	*
4	9-trimethylsilyl-thioxanthene	2	4	10	16
5	TMPTA	6	40	*	*

Belt speed = 10 ft/min for all experiments

\* = polymerisation not detected after 30 passes

#### Touching glass

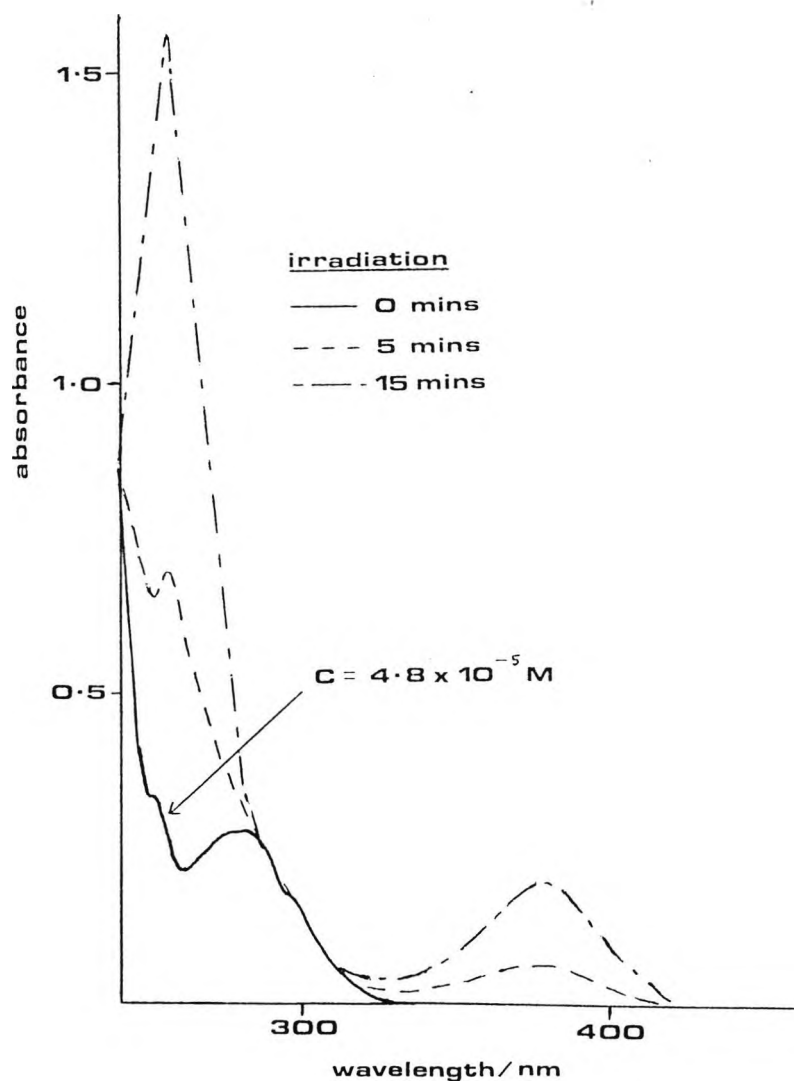
It is noticeable that the more substituted benzylic silanes (EXPT's 2,3, and 4) cure at a greater rate than benzylsilane (EXPT 1) which is linked to their greater absorption in the wavelength region beyond the glass filter range (>310nm).

#### In air

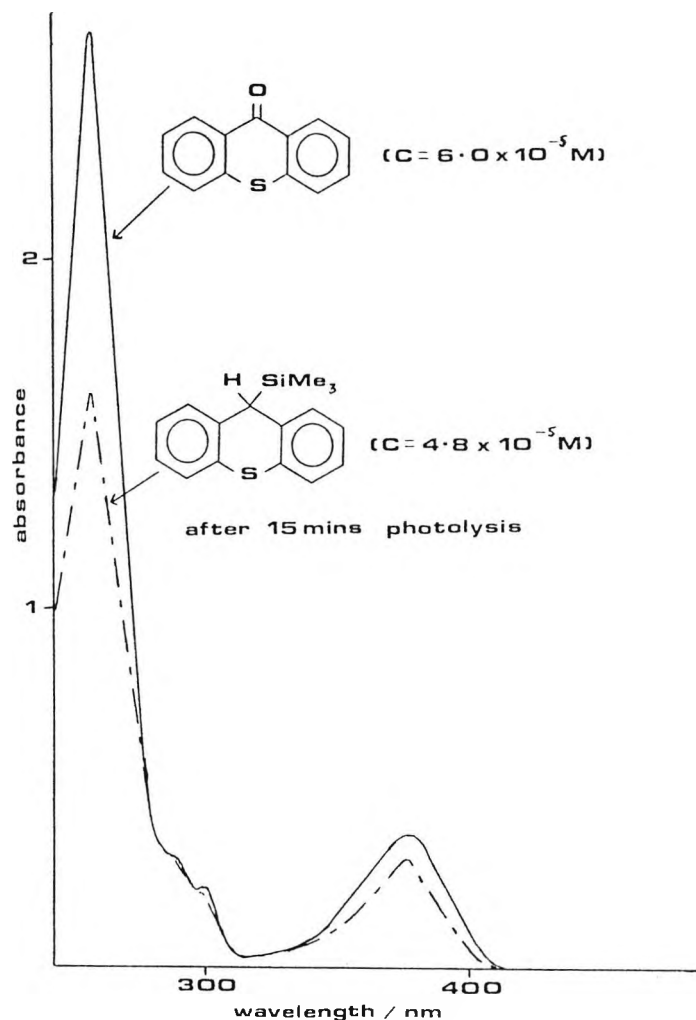
In EXPT's 3 and 4 cure is observed in air. A further

observation made was that with both the fluorene derivative (EXPT 3) and the thioxanthene derivative (EXPT 4) the thin films changed from colourless to yellow on irradiation. This feature was more prominent for the thioxanthene derivative.

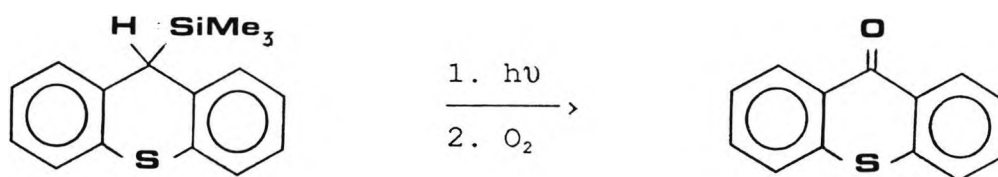
Further insight into this reaction was gained from following the photolysis of the thioxanthene derivative in methanolic solution using UV spectroscopy. The results are presented below.



It is proposed that on photolysis the benzylic C-Si bond is converted to the carbonyl group, C=O, thus giving rise to the yellow coloured compound of thioxanthone. This becomes apparent when the UV spectra of thioxanthone is compared with the corresponding photolysis product of the thioxanthene derivative as shown below.



The above result may be rationalised by the following mechanism:



This reaction reduces the effect of oxygen inhibition of polymerisation and explains why polymerisation is observed in air for the thioxanthene derivative (EXPT 4). A similar effect occurs for the fluorene derivative, albeit to a lesser extent than the thioxanthene derivative, and this explains the polymerisation observed in air for this compound (Table 2.5; EXPT 3).

#### Glass cover

Polymerisation was observed under a glass cover slide for the thioxanthene derivative (EXPT 4) indicating that the conversion of this compound to thioxanthone is a particularly efficient process. In order to verify the proposed mechanism a further UV curing experiment was performed. It is known that thioxanthone sensitises diphenyliodonium salts in cationic polymerisation (Gatechair and Pappas, 1983). It was decided to test the thioxanthene derivative in conjunction with diphenyliodonium hexafluorophosphate in the presence of a cationically polymerisable monomer, 3,4-epoxycyclohexylmethyl-3',4'-epoxycyclohexane carboxylate, to determine whether sensitisation of polymerisation, via thioxanthone, occurred (EXPT 3; Table 2.6). The results presented in table 2.6 can be compared to the experiment where thioxanthone was used as the sensitiser (EXPT 2).

Table 2.6 Sensitisation of diphenyliodonium hexafluorophosphate for use in cationic photopolymerisation using 'thioxanthone' with all compounds incorporated at 1% w/w in 3,4-epoxycyclohexylmethyl-3',4'-epoxycyclohexane carboxylate

EXPT	INITIATING SYSTEM	BELT SPEED/ ft/min	NUMBER OF PASSES	
			In Air	Glass Filter
1	$\text{Ph}_2\text{I}^+\text{PF}_6^-$	10	7	*
2	$\text{Ph}_2\text{I}^+\text{PF}_6^-$ + thioxanthone	10	1	1
3	" + "	230	5	8
4	$\text{Ph}_2\text{I}^+\text{PF}_6^-$ + 9-trimethyl-silylthioxanthene	10	1	6
5	" + "	230	5	17

\* = polymerisation not detected after 30 passes

The first point to make is that sensitisation using thioxanthone with diphenyliodonium hexafluorophosphate occurs (EXPT's 2 and 3) compared to the iodonium salt used on its own (EXPT 1). The second more interesting point is that sensitisation occurs when the thioxanthene derivative is used with the iodonium salt (EXPT's 4 and 5) when compared to the iodonium salt on its own (EXPT 1). The most striking feature of the results is that the number of passes required to reach cure in air in EXPT 3 is identical to that

in EXPT 5. This indicates that the conversion of the thioxanthene derivative to thioxanthone is an efficient process when the full output of the lamp is used (in air). When a glass filter is used (>310nm) with the thioxanthene derivative sensitisation is still achieved (EXPT 5; 17 passes) but to a lesser extent than the corresponding value when thioxanthone was used (EXPT 3; 8 passes).

Another experiment was performed to ascertain if the combination of the thioxanthene derivative and the diphenyliodonium salt could be used to effect both free radical and cationic polymerisation simultaneously to give a dual cure system. A formulation of the thioxanthene derivative and the iodonium salt was incorporated into a 50:50 (w/w) mixture of two monomers, one polymerisable by a free radical pathway (TMPTA), and one polymerisable by a cationic pathway (3,4-epoxycyclohexylmethyl-3',4'-epoxycyclohexane carboxylate). The results are given below in table 2.7.

Table 2.7 Evidence for a dual cure system in the photopolymerisation of a 50:50 acrylate:epoxy resin mixture using diphenyliodonium hexafluorophosphate and 9-trimethylsilylthioxanthene

EX P T	INITIATING SYSTEM	R E S I N	NUMBER OF PASSES			
			Touching Quartz	Touching Glass	In Air	Glass Filter
1	9-Me <sub>3</sub> Si-thioxan thene (TMS-TX)*	<b>A</b>	2	4	10	16
2	Ph <sub>2</sub> I <sup>+</sup> PF <sub>6</sub> <sup>-</sup>	<b>A</b>	4	*	4	*
3	Ph <sub>2</sub> I <sup>+</sup> PF <sub>6</sub> <sup>-</sup>	<b>E</b>	-	-	7	*
4	TMS-TX + Ph <sub>2</sub> I <sup>+</sup> PF <sub>6</sub> <sup>-</sup>	<b>AE</b>	1	1	2	4
5	"	"	2 <sup>a</sup>	5 <sup>a</sup>	8 <sup>a</sup>	18 <sup>a</sup>
6	TMS-TX + Ph <sub>2</sub> I <sup>+</sup> PF <sub>6</sub> <sup>-</sup>	<b>E</b>	-	-	1	6
7	"	"	-	-	5 <sup>a</sup>	17 <sup>a</sup>

a = belt speed 230 ft/min

Belt speed = 10 ft/min for all other experiments

A = acrylate resin = TMPTA

E = epoxy resin = 3,4-epoxycyclohexylmethyl-3',4'-  
epoxycyclohexane carboxylate

AE = 50:50 mixture (w/w) of resins A and E above

- = difficult to evaluate

\* = 5% w/w in TMPTA, for all other instances the initiator/sensitiser is incorporated at 1% w/w in the resin

The curing of an epoxide when touching quartz and glass is difficult to follow since the cured epoxide adheres to the touching quartz and glass slides during the early stages of polymerisation. This makes the detection of tack-free polymerisation difficult and reproducible results are not possible.

When the 50:50 resin system is used in the sensitised polymerisation (EXPT's 4 and 5) the assessment of the touching quartz and touching glass results becomes much easier due to the better film-forming properties of this resin system compared to the epoxide on its own (EXPT's 6 and 7). It is also envisaged that the improvement in the rate of polymerisation of the dual system when touching quartz and touching glass (EXPT's 4 and 5) compared to the epoxide (EXPT's 6 and 7) is due to the incorporation of the acrylate, TMPTA. This dual cure system (EXPT's 4 and 5) does not show an improvement, however, in comparison to the situation where only the epoxy resin is present when in air and with a glass cover (EXPT's 6 and 7). This is probably due to the effect of oxygen inhibition on the free radical polymerisation in the dual cure system. It has been estimated that this oxygen inhibition effect occurs significantly in dual cure systems which incorporate > 40% of the free radical polymerisable monomers (Ketley and Tsao, 1979).

### 2.5.2 UV curing results of benzylstannanes

A number of benzylstannanes were tested (5% w/w) in the presence of a monomer, TMPTA, using the UV Colordry apparatus described earlier (see section 1.7.1). This was in order to assess the free radical initiating properties of the compounds under test. The results are presented below in table 2.8. For comparison the result for benzyltrimethylsilane is also included (EXPT 1).

Table 2.8 UV curing results of benzylstannanes incorporated at 5% w/w in TMPTA

EXPT	INITIATOR	NUMBER OF PASSES			
		Touching Quartz	Touching Glass	In Air	Glass Filter
1	PhCH <sub>2</sub> SiMe <sub>3</sub>	4	28	*	*
2	PhCH <sub>2</sub> SnMe <sub>3</sub>	2	9	*	*
3	PhCH <sub>2</sub> SnBu <sub>3</sub>	1	3	*	*
4	PhCH <sub>2</sub> SnBu <sub>3</sub>	2 <sup>a</sup>	-	-	-
5	4-Me-C <sub>6</sub> H <sub>4</sub> CH <sub>2</sub> SnBu <sub>3</sub>	1	3	25	*
6	4-Me-C <sub>6</sub> H <sub>4</sub> CH <sub>2</sub> SnBu <sub>3</sub>	2 <sup>b</sup>	10 <sup>b</sup>	-	-
7	4-MeO-C <sub>6</sub> H <sub>4</sub> CH <sub>2</sub> SnBu <sub>3</sub>	1	1	*	*
8	4-MeO-C <sub>6</sub> H <sub>4</sub> CH <sub>2</sub> SnBu <sub>3</sub>	1 <sup>b</sup>	4 <sup>b</sup>	-	-
9	TMPTA	6	40	*	*

\* = polymerisation not detected after 30 passes

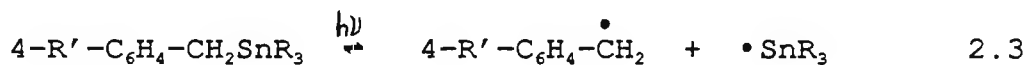
- = experiment not performed

a = belt speed 80 ft/min

b = belt speed 230 ft/min

Belt speed = 10 ft/min for all other experiments

The results show that a much lower number of passes is required to achieve a tack free coating for the benzylstannanes when compared to the benzylsilane (EXPT 1). This indicates that the homolysis of the benzylic C-Sn bond occurs more readily than that of the benzylic C-Si bond and may be represented by equation 2.3.



[R = Me, n-Bu; R' = H, Me, MeO]

A comparison can be made between benzyltrimethylsilane (EXPT 1) and benzyltrimethylstannane (EXPT 2) as to the effect of the different metals on the number of passes required to achieve cure. In both the touching quartz and the touching glass experiments benzyltrimethylstannane requires fewer passes than benzyltrimethylsilane indicating a greater extent of reaction of the tin species. This could be due to a greater degree of homolysis or attributed to an enhanced reactivity of the metal centred radical produced.

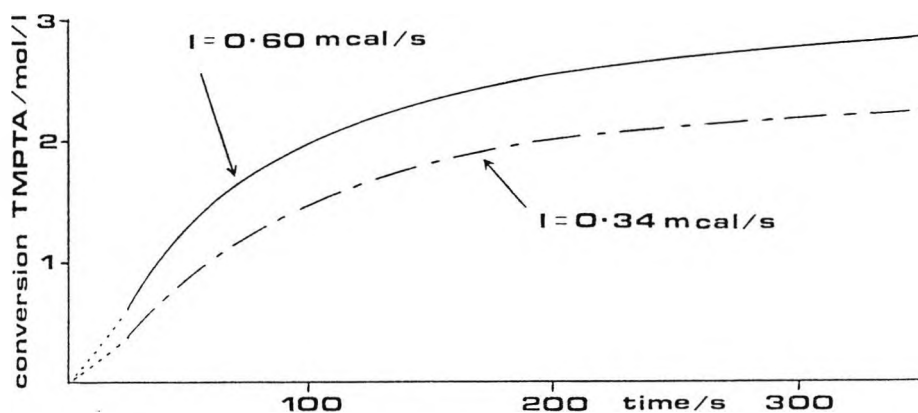
A similar comparison can be made between the results of benzyltri-n-butylstannane (EXPT's 3 and 4) and benzyltrimethylstannane (EXPT 2) to determine the effect of

the R group on changing from SnMe<sub>3</sub> to SnBu<sub>3</sub>. In the touching quartz and touching glass experiments benzyltri-*n*-butylstannane (EXPT's 3 and 4) requires a fewer number of passes to achieve cure than benzyltrimethylstannane (EXPT 2). This probably reflects the relative ease with which the C-Sn bond in the stannanes will undergo homolytic fission, with particular emphasis on the greater degree of stabilisation achieved via hyperconjugation when R = Bu than when R = Me.

#### 2.5.2.1 Photo-DSC of benzyltri-*n*-butylstannane

A photo-DSC experiment was performed on a sample of benzyltri-*n*-butylstannane (7.5% w/w) in TMPTA. The amount of stannane incorporated was calculated to give 'total absorption' of the available light. The intensity of the light was then reduced to determine the effect of this on the polymerisation as followed by photo-DSC. The resultant polymerisation curves are shown in figure 2.3.

Figure 2.3 Photo-DSC results of the polymerisation of TMPTA initiated by benzyltri-*n*-butylstannane at two different light intensities



The effect of reducing the light intensity is to reduce both the maximum rate of polymerisation,  $R_{p(max)}$ , and the degree of polymerisation after one minute illustrated in table 2.9.

Table 2.9 The rate and the degree of conversion values at different light intensities for the photopolymerisation of TMPTA using benzyltri-*n*-butylstannane as determined by photo-DSC

EXPT	Light intensity/ mcal/s	$R_{p(max)}$ / mol/l/s	Degree of conversion after 1 minute/ %
1	0.60	0.040	13.0
2	0.34	0.020	9.1

The values of  $R_{p(max)}$  and the degree of conversion are low because the intensity of the light has been much reduced with the use of a neutral density filter in combination with

a narrow band-width filter centred on 365nm. The reduction in the  $R_p$  value can be predicted from the two curves, using equation 1.30 (see section 1.4.4), assuming total absorption of light by the initiator. For example consider the situation at 300 seconds;

$$I_1 = 0.60 \text{ mcal/s, conversion of [TMPTA]}_1 = 2.80 \text{ mol/l}$$

$$I_2 = 0.34 \text{ mcal/s, conversion of [TMPTA]}_2 = 2.18 \text{ mol/l}$$

The overall rate of polymerisation,  $R_p$ , is proportional to the light intensity,  $I_0$ , by the equation;

$$R_p \propto \sqrt{I_0} \quad \text{From the two experiments it follows that,}$$

$$\frac{\sqrt{I_1}}{\sqrt{I_2}} = \frac{[\text{TMPTA}]_1}{[\text{TMPTA}]_2}$$

From the experimental values measured for the light intensity,

$$\frac{\sqrt{I_1}}{\sqrt{I_2}} = \frac{\sqrt{0.60}}{\sqrt{0.34}} = 1.33$$

and from the calculated values of the degree of conversion,

$$\frac{[\text{TMPTA}]_1}{[\text{TMPTA}]_2} = \frac{2.80}{2.18} = 1.28$$

The two results are within reasonable experimental error and confirm the predictions that can be made when using the theoretical equations.

### 2.5.3 UV curing results of naphthyl compounds (and higher)

A number of naphthylsilanes and stannanes were synthesised in order to increase the conjugation and extend the wavelength range for direct irradiation compared to the corresponding benzylic derivatives. Taking this idea further a pyrene derivative, which is a pale yellow colour, was synthesised and tested. The results are presented below in table 2.10.

Table 2.10 UV curing results of naphthyl (and higher) compounds incorporated at 5% w/w in TMPTA

E X P T	INITIATOR	NUMBER OF PASSES			
		Touching Quartz	Touching Glass	In Air	Glass Filter
1	1-NpCH <sub>2</sub> SiMe <sub>3</sub>	4	7	30	*
2	2-NpCH <sub>2</sub> SiMe <sub>3</sub>	3	5	*	*
3	1-NpCH <sub>2</sub> SnBu <sub>3</sub>	1	1	(*)	*
4	"	1 <sup>a</sup>	1 <sup>a</sup>	-	-
5	2-NpCH <sub>2</sub> SnBu <sub>3</sub>	1	1	(*)	*
6	"	1 <sup>a</sup>	1 <sup>a</sup>	-	-
7	2-NpCH <sub>2</sub> SnMe <sub>3</sub>	1	2	*	*
8	1-pyreneCH <sub>2</sub> SiMe <sub>3</sub>	1	4	*	*
9	TMPTA	6	40	*	*

\* = curing not detected after 30 passes

(\*) = curing observed but not tack-free after 30 passes

- = experiment not performed

a = belt speed 230 ft/min

Belt speed = 10 ft/min for all other experiments

The results again bear out the relationship that the rate of polymerisation is in the order:  $\text{NpCH}_2\text{SnBu}_3 > \text{NpCH}_2\text{SnMe}_3 > \text{NpCH}_2\text{SiMe}_3$

which is in agreement with the previous results (see section 2.5.2).

The pyrene derivative (EXPT 8) shows an improvement in rate of cure when compared to the naphthylsilanes (EXPT's 1 and 2), which is probably due to, the enhanced absorption properties of the pyrene moiety.

#### 2.5.4 UV curing results of allylsilanes

A number of allylsilanes were tested (5% w/w) in the presence of a monomer, TMPTA, using the UV Colordry apparatus described earlier (see section 1.7.1). This was in order to assess the free radical-initiating properties of the compounds under test. The results are presented below in table 2.11.

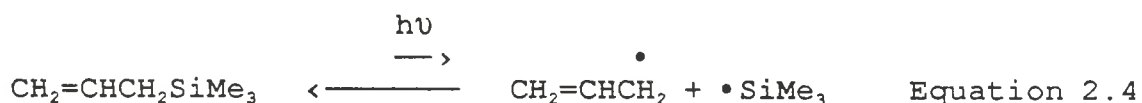
Table 2.11 UV curing results of allylsilanes incorporated at 5% w/w in TMPTA

E X P T	INITIATOR	NUMBER OF PASSES			
		Touching Quartz	Touching Glass	In Air	Glass Filter
1	CH <sub>2</sub> =CHCH <sub>2</sub> SiMe <sub>3</sub>	3	20	*	*
2	Me <sub>2</sub> C=CHCH <sub>2</sub> SiMe <sub>3</sub>	3	13	*	*
3	CH <sub>2</sub> =CHCH <sub>2</sub> SiPh <sub>3</sub>	6	*	*	*
4	TMPTA	6	40	*	*

\* = no curing observed after 30 passes

Belt speed = 10 ft/min for all experiments

The results indicate that the allylsilanes will initiate radical polymerisation by homolytic cleavage. The situation is similar to benzylsilanes where the equilibrium in equation 2.4 lies well to the left.



### 2.5.5 UV curing results of allylstannanes

A number of allylstannanes were tested (5% w/w) in the presence of a monomer, TMPTA, using the UV Colordry apparatus described earlier (see section 1.7.1). This was in order to assess the free radical-initiating properties of the compounds under test. The results are presented below in table 2.12. For comparison the result of

allyltrimethylsilane is included (EXPT 1, table 2.12).

Table 2.12 UV curing results of allylstannanes incorporated at 5% w/w in TMPTA

EXPT	INITIATOR	NUMBER OF PASSES			
		Touching Quartz	Touching Glass	In Air	Glass Filter
1	$\text{CH}_2=\text{CHCH}_2\text{SiMe}_3$	3	20	*	*
2	$\text{CH}_2=\text{CHCH}_2\text{SnBu}_3$	2	14	*	*
3	$\text{CH}_2=\text{C}(\text{Me})\text{CH}_2\text{SnBu}_3$	2	13	*	*
4	$\text{MeCH}=\text{CHCH}_2\text{SnBu}_3$	2	11	*	*
5	$\text{Me}_2\text{C}=\text{CHCH}_2\text{SnBu}_3$	1	6	*	*
6	TMPTA	6	40	*	*

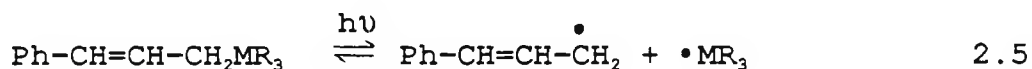
\* = no polymerisation detected after 30 passes

Belt speed = 10 ft/min for all experiments

The allylstannanes are more reactive than the allylsilanes in initiating photopolymerisation, which is probably due to the weaker bond strength, and thus easier homolytic cleavage, of the C-Sn bond when compared to the C-Si bond. In the case of the tri-*n*-butylstannanes (EXPT's 2 to 5) it is the more substituted allylstannane that shows greater reactivity towards photopolymerisation. This can be explained in terms of the stability of the allylic radical produced upon homolytic cleavage.

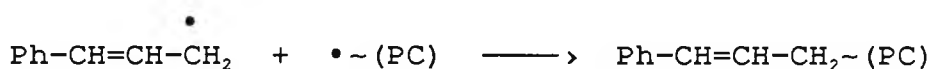


uncharacteristic for the majority of the allylic, benzylic, and naphthyllic silanes and stannanes previously tested. It is believed that the curing in air is related to the function of the cinnamyl radical formed on photolysis (equation 2.5).



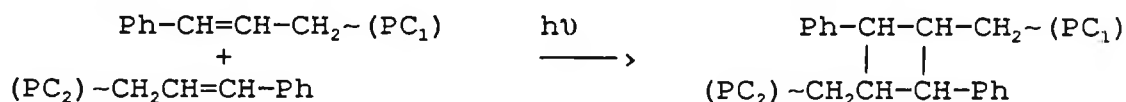
The cinnamyl radical can react with a growing polymer chain radical to give the cinnamyl functionality attached to the polymer backbone as in scheme 2.1.

Scheme 2.1 Cinnamylation of the polymer chain (PC)



If the cinnamyl group attached encounters another cinnamyl functionality attached to a different polymer backbone then it is possible that a reaction between the two cinnamyl groups via a [2+2] cycloaddition process may occur as in scheme 2.2.

Scheme 2.2 [2 + 2] cycloaddition of cinnamyl groups



Cycloaddition polymerisation, in contrast to free radical polymerisation, is a non-radical process and does not exhibit a marked oxygen inhibition effect on the rate of polymerisation. This could explain why the cinnamylstannane (EXPT 1) gave curing in air in contrast to the analogous allyl and benzyl stannanes which showed no evidence of curing in air.

This prompted the synthesis of the styrylsilane to see if a similar effect was possible. It was shown that polymerisation was not detected for the styrylsilane in air (EXPT 2) although for a more appropriate comparison the styrylstannane is required.

#### 2.5.7 Photoinduced electron transfer reactions

There has been a lot of interest in the electron transfer reactions of allylic and benzylic silanes and stannanes. This can be attributed to the low oxidation potentials of these compounds which render them effective electron donors (see table 5.1: Appendix). Early work indicated that benzyltri-*n*-butylstannane could be used as an activator in the dye sensitised free radical polymerisation of vinylic monomers (Eaton, 1979). This was proposed to be via a mechanism similar to that of the dye/amine reaction proposed earlier (Davidson and Trethewey, 1975). The same author reported on the one electron transfer reaction of benzyltrialkylstannanes with tetracyanoethylene (Eaton,

1980a). The radical cation formed was shown to fragment by dual modes in which the partition ratio depended on the substituent on the aromatic ring of the benzylstannane.

Other evidence was presented for electron transfer reactions of allylic and benzylic silanes and stannanes via the product studies of the photoreactions with a number of cyanoaromatic compounds. These include 9,10-dicyanoanthracene (Eaton, 1980b; Eaton, 1981; Mizuno *et al*, 1985b), *p*-dicyanobenzene (Mizuno *et al*, 1985a; Mizuno *et al*, 1988c), and 1,4-dicyanonaphthalene (Mizuno *et al*, 1988a; Sulpizio *et al*, 1989). Other electron acceptors that have been used include the aryldicyanoethylenes (Mizuno *et al*, 1987; Mizuno *et al*, 1988b).

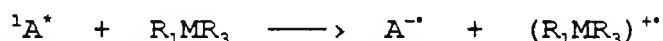
The photoaddition of allyl- and benzylsilanes to iminium salts via electron transfer has been extensively studied by Mariano and co-workers (Ohga and Mariano, 1982; Chen *et al*, 1983; Lan *et al*, 1984; Lan *et al*, 1987; Tu and Mariano, 1987).

Evidence has also been reported for electron transfer photoadditions of allylstannanes to pyrrolinium perchlorates (Borg and Mariano, 1986) and another report on the photoallylation of quinones via photoinduced electron transfer using allylstannanes (Maruyama *et al*, 1986). The proposed mechanism of photoinduced electron transfer from an allylstannane to a quinone was later confirmed by the same workers using CIDNP studies (Maruyama and Imahori, 1989). The photoinduced electron transfer addition reaction of trimethylallylstannane to benzophenone has also been

described (Takuwa et al, 1987) whereas in a later report by the same group the photoreaction of benzophenone with trimethylallylsilane no electron transfer products were reported (Takuwa et al, 1989). Later work showed that other carbonyl derivatives, including a variety of diketones, such as benzil derivatives and acenaphthenequinone, could be used to sensitise the photoinduced electron transfer reactions with allyl, benzyl, and cinnamylstannanes (Takuwa et al, 1990).

#### 2.5.8 UV Curing: sensitisation using DCA

As was mentioned earlier (see section 2.5.7) cyanoaromatics have been used effectively as sensitisers in photoreactions involving electron transfer in the presence of allylic and benzylic silanes and stannanes. A schematic representation of the proposed mechanism via the photoinduced single electron transfer pathway is given below:

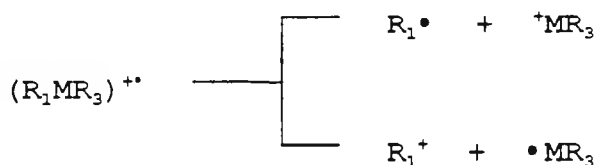


$R_1$  = allyl, benzyl, naphthyl

R = Me, n-Bu, Ph

M = Si, Sn

The radical cation so produced in the above scheme may fragment via two different routes:



The interesting route from the UV curing point of view is the one that produces the metal-centred radical which is capable of initiating polymerisation. This hypothesis was tested experimentally by irradiating a formulation of the sensitiser, DCA, and the organometallic donor in the presence of a free radical polymerisable monomer, TMPTA. The UV spectra of the sensitiser, DCA, and a number of representative silanes and stannanes are shown in the Appendix (Figure 5.1). The results of the testing carried out using the UV Colordry apparatus (see section 1.7.1) are presented below.

2.5.9 UV curing results of benzylsilanes with DCA

Table 2.14 UV curing of TMPTA with benzylsilanes (1% w/w) sensitised using DCA (0.25% w/w)

EXPT	INITIATING SYSTEM	BELT SPEED ft/min	NUMBER OF PASSES			
			Touching Quartz	Touching Glass	In Air	Glass Filter
1	PhCH <sub>2</sub> SiMe <sub>3</sub> + DCA	10	1	1	*	*
2	"	80	2	3	-	-
3	PhCH <sub>2</sub> SiMe <sub>3</sub>	10	6	20	*	*
4	4-PhC <sub>6</sub> H <sub>4</sub> CH <sub>2</sub> -SiMe <sub>3</sub> +DCA	10	1	2	30	*
5	"	80	2	4	-	-
6	4-PhC <sub>6</sub> H <sub>4</sub> CH <sub>2</sub> -SiMe <sub>3</sub>	10	3	6	*	*
7	Ph <sub>2</sub> CHSiMe <sub>3</sub> + DCA	10	1	1	*	*
8	"	230	2	5	-	-
9	Ph <sub>2</sub> CHSiMe <sub>3</sub>	10	3	9	*	*
10	DCA	10	6	15	*	*

\* = polymerisation not detected after 30 passes

- = experiment not performed

Sensitisation in the presence of DCA occurs for all the benzylsilanes tested when touching quartz and touching glass

as evidenced by the reduced number of passes required to achieve tack-free cure. This is proposed to be via an electron transfer mechanism with the ground state benzylsilane donating an electron to the excited singlet state of the sensitiser. This results in the formation of  $\text{Me}_2\text{Si}^\bullet$  radicals which enhance the rate of polymerisation.

#### 2.5.10 UV curing results of benzylstannanes with DCA

Table 2.15 UV curing of TMPTA with benzylstannanes (1% w/w) sensitised using DCA (0.25% w/w)

E X P T	INITIATING SYSTEM	BELT SPEED ft/min	NUMBER OF PASSES			
			Touching Quartz	Touching Glass	In Air	Glass Filter
1	$\text{PhCH}_2\text{SnBu}_3$ + DCA	10	1	2	*	*
2	"	80	2	4	-	-
3	$\text{PhCH}_2\text{SnBu}_3$	10	1	3	*	*
4	"	80	2	-	-	-
5	$4\text{-MeC}_6\text{H}_4\text{CH}_2$ $\text{-SnBu}_3$ DCA	10	1	1	*	*
6	"	80	1	3	-	-
7	$4\text{-MeC}_6\text{H}_4\text{CH}_2$ $\text{-SnBu}_3$	10	1	3	*	*
8	"	80	2	-	-	-
9	DCA	10	6	15	*	*

\* = polymerisation not detected after 30 passes

- = experiment not performed

The effect of sensitisation is much reduced for the benzylstannanes (table 2.15) when compared to the benzylsilanes (table 2.14). This is undoubtedly due in part to the greater lability of the C-Sn (benzylic) bond to homolytic cleavage via photolysis compared to that of the C-Si (benzylic) bond. This homolytic process for the benzylstannanes probably dominates in the touching quartz experiments since the whole Hg lamp spectrum is available. There is a small effect of sensitisation in the touching glass experiments due to the filter effect of the glass cut off. Another feature of note is that the energy of the light corresponding to the UV spectrum of these compounds is greater than the bond strength.

#### 2.5.11 UV curing results of naphthylsilanes with DCA

Table 2.16 UV curing of TMPTA with naphthylsilanes (1% w/w) sensitised by DCA (0.25% w/w)

E X P T	INITIATING SYSTEM	NUMBER OF PASSES			
		Touching Quartz	Touching Glass	In Air	Glass Filter
1	1-NpCH <sub>2</sub> SiMe <sub>3</sub> + DCA	2	4	*	*
2	1-NpCH <sub>2</sub> SiMe <sub>3</sub>	4	7	*	*
3	2-NpCH <sub>2</sub> SiMe <sub>3</sub> + DCA	2	4	*	*
4	2-NpCH <sub>2</sub> SiMe <sub>3</sub>	3	6	*	*
5	DCA	6	15	*	*

Belt speed = 10 ft/min for all experiments

\* = polymerisation not detected after 30 passes

There is a small effect of sensitisation and this is probably due to competitive absorption of the sensitiser and the naphthylsilanes. Thus sensitisation is not as effective as in the case of the benzylic compounds.

#### 2.5.12 UV curing results of allylsilanes with DCA

Table 2.17 UV curing of TMPTA with allylsilanes (1% w/w) sensitised by DCA (0.25% w/w)

E X P T	INITIATING SYSTEM	NUMBER OF PASSES			
		Touching Quartz	Touching Glass	In Air	Glass Filter
1	$\text{CH}_2=\text{CHCH}_2\text{SiMe}_3$ + DCA	5	9	*	*
2	$\text{CH}_2=\text{CHCH}_2\text{SiMe}_3$	4	14	*	*
3	$\text{CH}_2=\text{CHCH}_2\text{SiPh}_3$ + DCA	6	13	*	*
4	$\text{CH}_2=\text{CHCH}_2\text{SiPh}_3$	6	18	*	*
5	DCA	6	15	*	*
6	TMPTA	6	40	*	*

Belt speed = 10 ft/min for all experiments

\* = polymerisation not detected after 30 passes

The sensitisation of the allylsilanes using DCA (Table 2.17)

is much reduced when compared to the sensitisation of benzylsilanes by DCA (Table 2.14). This is thought to be due to the higher oxidation potentials of the allylsilanes when compared to the benzylsilanes (see Table 5.1: Appendix) which render them less useful, on energetic grounds, in electron transfer schemes.

### 2.5.13 UV curing results of allylstannanes with DCA

Table 2.18 UV curing of TMPTA with allylstannanes (1% w/w) sensitised by DCA (0.25% w/w)

E X P T	INITIATING SYSTEM	NUMBER OF PASSES			
		Touching Quartz	Touching Glass	In Air	Glass Filter
1	$\text{CH}_2=\text{CHCH}_2\text{SnBu}_3$ + DCA	2	5	*	*
2	$\text{CH}_2=\text{CHCH}_2\text{SnBu}_3$	3	11	*	*
3	$\text{CH}_2=\text{C}(\text{Me})\text{CH}_2\text{SnBu}_3$ + DCA	2	4	*	*
4	$\text{CH}_2=\text{C}(\text{Me})\text{CH}_2\text{SnBu}_3$	3	8	*	*
5	$\text{Me}_2\text{C}=\text{CHCH}_2\text{SnBu}_3$ + DCA	1	1	*	*
6	"	2 <sup>a</sup>	4 <sup>a</sup>	*	*
7	$\text{Me}_2\text{C}=\text{CHCH}_2\text{SnBu}_3$	1	5	*	*
8	DCA	6	15	*	*

a = belt speed 80 ft/min

Belt speed = 10 ft/min for all other experiments

\* = polymerisation not detected after 30 passes

The sensitisation of the allylstannanes using DCA (Table 2.18) appears to be related to the relative oxidation potentials of the prospective electron donors (see Table 5.1: Appendix). Thus it is the allylstannane that is expected to have the lowest oxidation potential, which shows the greatest effect of sensitisation (EXPT 5).

#### 2.5.14 Sensitisation of polymerisation with aromatic ketones

A number of aromatic ketone triplet photosensitisers exist, with the classical example being benzophenone. The related cyclic aromatic ketones xanthone and thioxanthone and 1,2-diketones such as benzil, as well as both 1,4- and 1,2-quinones, behave in a similar manner. All these compounds can be used as triplet sensitisers and will abstract hydrogen from a suitable H-donor through an encounter complex. One reaction of this type that has received considerable attention is the photoreduction of aromatic ketones with *t*-amines possessing  $\alpha$ -hydrogen atoms (Cohen et al, 1973; Davidson, 1975; Davidson, 1983). It was shown by several workers that an electron transfer mechanism was operative with the transfer occurring from the nitrogen lone-pair to the carbonyl oxygen in the excited complex (exciplex). The exciplex can proceed to a ketyl radical and

an  $\alpha$ -amino alkyl radical, which can then go on and initiate radical polymerisation. The rates of polymerisation of various monomers using *t*-amine/ketone combinations have been determined (see Hageman, 1985 and references within). The major factor in determining the efficiency of the photoreduction was shown to be the ionisation potential of the amine. It was shown that there exists a rough correlation between the ionisation potential of the amine and the rate of quenching of the excited carbonyl for amines with an ionisation potential of  $< 9\text{eV}$  (Turro, 1978).

Since the prepared silanes and stannanes have low oxidation potentials there is the possibility that these compounds undergo electron transfer reactions with ketones. It was decided to test this hypothesis and see whether these organometallics would form such exciplexes with aromatic carbonyl compounds which would lead to an increase in the rate of polymerisation. Early reports in the literature indicated that these organometallics would undergo photoinduced electron transfer reactions with suitable aromatic carbonyl sensitisers. The first report in this area was the photoreaction of quinones with allylstannanes to give allylated quinones (Maruyama *et al*, 1986). Formation of these products indicated the involvement of an electron transfer process. Later work by the same group reported on the photoallylation of benzophenone and benzaldehyde derivatives by allylic stannanes and these reactions were proposed as occurring via an electron

transfer mechanism (Takuwa et al, 1987).

Interestingly no photoinduced electron transfer reaction occurred with benzophenone when allyltrimethylsilane was used instead of allyltributylstannane. According to a later report the reason for this behaviour is understandable on the basis of the free energy of the electron transfer process between the allylsilane and the photoexcited triplet of benzophenone which was estimated to be positive (Takuwa et al, 1989). Further work was documented of the photoreaction of allyl and benzyl stannanes with a quinone and the values for the free energy of this reaction were calculated to be negative which is indicative of the feasibility of an electron transfer pathway (Maruyama and Imahori, 1989). The photoreaction of allylic stannanes with triplet carbonyl sensitizers was extended to include benzil derivatives and acenaphthenequinone (Takuwa et al, 1990). The free energy changes from the Rehm-Weller equation for the reaction of allyltrimethylstannane ( $E_{ox} = 1.06V$ ) and 3-methyl-2-butenyltrimethylstannane ( $E_{ox} = 0.68V$ ) with benzil were calculated to be  $-5.5$  and  $-17.5$  kcal mol<sup>-1</sup> respectively. The same workers also looked at the conjugate addition of allylic groups, including allylic and cinnamyl stannanes, to a variety of  $\alpha,\beta$ -unsaturated ketones via an electron transfer pathway (Takuwa et al, 1991). An elegant experiment from this work illustrated the importance of the reduction potential of the sensitizer in electron transfer schemes. Irradiation of 1,3-diphenyl-2-propen-1-one ( $E_{red} = -$

1.45V) with allyltrimethylstannane gave only [2 + 2] cycloaddition products without the formation of any allylated products. On the other hand, chalcones having a cyano group on the phenyl ring yielded allylated products presumably via an electron transfer mechanism which is rendered possible due to their lower reduction potentials.

2.5.15 UV curing results of benzylsilanes and stannanes with benzanthrone

The aromatic ketone sensitiser looked at was benzanthrone which showed good absorption characteristics in the UV region. UV spectra of benzanthrone and a number of representative silanes and stannanes are given in the Appendix.

Table 2.19 UV curing of TMPTA with benzylsilanes and stannanes (both 5% w/w) sensitised by benzanthrone (1% w/w)

E X P T	INITIATING SYSTEM	NUMBER OF PASSES			
		Touching Quartz	Touching Glass	In Air	Glass Filter
1	PhCH <sub>2</sub> SiMe <sub>3</sub> + Benzanthrone	4	8	21	*
2	PhCH <sub>2</sub> SiMe <sub>3</sub>	4	28	*	*
3	4-PhC <sub>6</sub> H <sub>4</sub> CH <sub>2</sub> SiMe <sub>3</sub> + Benzanthrone	4	7	15	*
4	4-PhC <sub>6</sub> H <sub>4</sub> CH <sub>2</sub> SiMe <sub>3</sub>	2	11	*	*
5	Ph <sub>2</sub> CHSiMe <sub>3</sub> + Benzanthrone	3	7	21	*
6	Ph <sub>2</sub> CHSiMe <sub>3</sub>	3	9	*	*
7	PhCH <sub>2</sub> SnBu <sub>3</sub> + Benzanthrone	2	6	18	*
8	PhCH <sub>2</sub> SnBu <sub>3</sub>	1	3	*	*
9	Benzanthrone	4	10	25	*

Belt speed = 10 ft/min for all experiments

\* = polymerisation not detected after 30 passes

There is some evidence of an improvement in the cure rate when using benzanthrone with the benzylsilanes and the stannane. This could be due to sensitisation of polymerisation when using benzanthrone, or via a combination of different initiation pathways from the sensitiser and the silane/stannane. Further experiments are required to elucidate the mechanism of initiation.

UV curing results of allylsilanes and stannanes  
with benzanthrone

Table 2.20 UV curing of TMPTA with allylsilanes and stannanes (both at 5% w/w) sensitised by benzanthrone (1% w/w)

E X P T	INITIATING SYSTEM	NUMBER OF PASSES			
		Touching Quartz	Touching Glass	In Air	Glass Filter
1	CH <sub>2</sub> =CHCH <sub>2</sub> SiMe <sub>3</sub> + Benzanthrone	4	10	25	*
2	CH <sub>2</sub> =CHCH <sub>2</sub> SiMe <sub>3</sub>	3	20	*	*
3	CH <sub>2</sub> =CHCH <sub>2</sub> SiPh <sub>3</sub> + Benzanthrone	6	12	25	*
4	CH <sub>2</sub> =CHCH <sub>2</sub> SiPh <sub>3</sub>	6	*	*	*
5	CH <sub>2</sub> =CHCH <sub>2</sub> SnBu <sub>3</sub> + Benzanthrone	8	11	<b>20</b>	*
6	CH <sub>2</sub> =CHCH <sub>2</sub> SnBu <sub>3</sub>	2	14	*	*
7	Benzanthrone	4	10	25	*

Belt speed = 10 ft/min for all experiments

\* = polymerisation not detected after 30 passes

There appears to be little benefit of using benzanthrone to 'sensitise' the polymerisation of TMPTA using the allylic derivatives. Thus the allylic compounds (Table 20) are not sensitised by benzanthrone to the same extent as the benzylic compounds (Table 19). This suggests that there is some exciplex formation between benzanthrone and the

organometal which will be favoured by lower oxidation potentials of the organometal. In general the benzylic compounds have lower oxidation potentials than the allylic compounds which supports this argument and the allylstannane (EXPT 5; table 20), which has the lowest oxidation potential of the allylic compounds tested, shows a small improvement in cure rate in air.

2.5.17 UV curing results of naphthylsilanes and stannanes with benzanthrone

Table 2.21 UV curing of TMPTA with naphthylsilanes and stannanes (both at 5% w/w) sensitised by benzanthrone (1% w/w)

E X P T	INITIATING SYSTEM	NUMBER OF PASSES			
		Touching Quartz	Touching Glass	In Air	Glass Filter
1	1-NpCH <sub>2</sub> SiMe <sub>3</sub> + Benzanthrone	5	8	<b>15</b>	*
2	1-NpCH <sub>2</sub> SiMe <sub>3</sub>	4	7	30	*
3	1-NpCH <sub>2</sub> SnBu <sub>3</sub> + Benzanthrone	1	1	<b>11</b>	<b>30</b>
4	"	2 <sup>a</sup>	2 <sup>a</sup>	-	-
5	1-NpCH <sub>2</sub> SnBu <sub>3</sub>	1	1	30	*
6	"	2 <sup>a</sup>	2 <sup>a</sup>	-	-
7	Benzanthrone	4	10	25	*

a = belt speed 80 ft/min

Belt speed = 10 ft/min for all other experiments

\* = polymerisation not detected after 30 passes

- = experiment not performed

The results for the naphthyl compounds indicate that there may be sensitisation taking place when benzanthrone is used. This effect with the naphthyl compounds could be due to the lower oxidation potentials of these derivatives. This would explain why there is little effect of sensitisation when using the benzylic (Table 2.19) and allylic (Table 2.20) derivatives, which have higher oxidation potentials than the naphthyl derivatives (see Table 5.1: Appendix). The 'sensitisation' with the naphthyl derivatives, could also be due to the combined separate initiating properties of benzanthrone and the naphthyl derivative.

#### 2.5.18 UV curing results using 4,4'-dimethylbenzil (DMB) as a sensitiser

The first report on the photochemical reactions of a number of allylstannanes and benzyltrimethylstannane with benzil derivatives appeared recently (Takuwa et al, 1990). Irradiation (400-480nm) of the benzil derivatives in the presence of the respective stannane gave the allylated or benzylated product. The reaction was proposed to proceed via a photoinduced electron transfer mechanism. It was decided to test a number of silanes and stannanes prepared in view of this mechanistic conjecture since

radicals produced could effect polymerisation. The silane or stannane was incorporated along with the sensitiser, 4,4'-dimethylbenzil, in the monomer, TMPTA, and tested using the UV Colordry apparatus described earlier (see section 1.7.1). The UV spectra of 4,4'-dimethylbenzil and a number of representative silanes and stannanes are given in the Appendix. The UV curing results are given in table 2.22 below.

Table 2.22 UV curing results for the sensitisation of polymerisation of TMPTA using 4,4'-dimethylbenzil (1% w/w) with silanes (1% w/w) and stannanes (5% w/w)

E X P T	INITIATOR	NUMBER OF PASSES			
		Touching Quartz	Touching Glass	In Air	Glass Filter
1	$\text{Me}_2\text{C}=\text{CHCH}_2\text{SnBu}_3$ + DMB	1	1	5	10
2	$\text{Me}_2\text{C}=\text{CHCH}_2\text{SnBu}_3$	1	6	*	*
3	$4\text{-MeC}_6\text{H}_4\text{CH}_2\text{SnBu}_3$ + DMB	1	1	4	9
4	$4\text{-MeC}_6\text{H}_4\text{CH}_2\text{SnBu}_3$	1	3	*	*
5	DMB + $\text{CH}_2=\text{CHCH}_2\text{SiPh}_3$	2 <sup>a</sup>	4 <sup>a</sup>	-	-
6	DMB + $\text{Me}_3\text{Si-SiMe}_3$	1 <sup>a</sup>	3 <sup>a</sup>	-	-
7	DMB	1	1	17	*
8	"	3 <sup>a</sup>	6 <sup>a</sup>	-	-

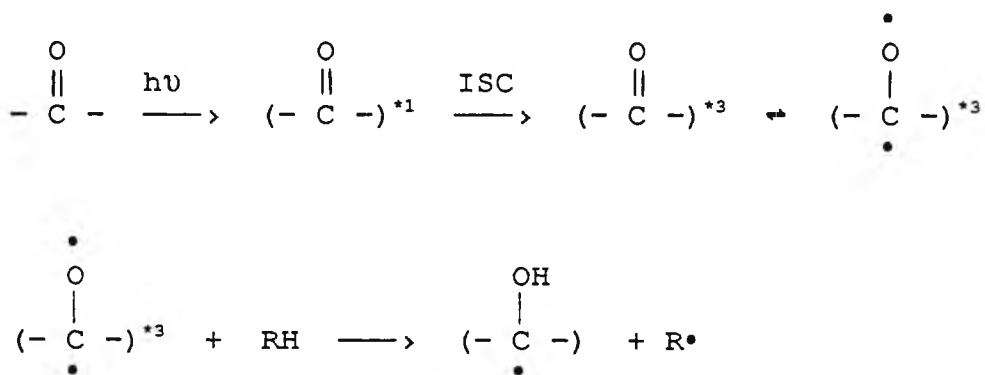
\* = polymerisation not detected after 30 passes

a = belt speed 230 ft/min

Belt speed = 10 ft/min for all other experiments

- = experiment not performed

These preliminary results, especially when using the stannanes, looked promising since curing in air (both in air and with glass cover) was observed. One important point to note is that 4,4'-dimethylbenzil will effect polymerisation when it is used on it's own (EXPT's 7 and 8). This type of aromatic ketone will act as a photoinitiator by an intermolecular hydrogen abstraction from donor molecules by the following illustrative mechanism:



It is thought that the donor RH could originate from either the monomer or from the activated CH<sub>3</sub> group on the benzil derivative.

It was also noticed that on irradiation the films in EXPT's 1 and 3 (when the stannanes were used) underwent a colour change from light yellow to a much darker yellow/orange. This is discussed further in the RTIR results where testing

of a wide range of silanes and stannanes was carried out (see section 2.6.10).

#### 2.5.19 UV curing results using thiopyrylium salts as sensitisers

The photocuring of epoxides using thiopyrylium salts with anions derived from Lewis acids has been described (Ketley and Tsao, 1979) and patented (US 4,139,655). In all cases the UV cure rates of the epoxides were shown to be considerably lower for the thiopyrylium salts than for sulphonium salts under comparable conditions. In a different role 2,4,6-triphenylpyrylium salts were used as electron acceptors in photoinduced charge transfer schemes with pinacolic donors (Sankararaman and Kochi, 1989). The pyrylium salts were found to rival more conventional singlet sensitisers such as the cyanoarenes. In the light of this work it appeared that the pyrylium/thiopyrylium salts could be effective as sensitisers for free radical photopolymerisation when used in conjunction with suitable electron donors such as allyl and benzyl silanes and stannanes. This led to the testing of this idea using formulations of a thiopyrylium salt with an organometallic donor in the presence of a radically polymerisable monomer, TMPTA. The results of the tests using the UV Colordry apparatus (see section 1.7.1) are given below in tables 2.23, 2.24, and 2.25.

Table 2.23 UV curing results of 2,4,6-triphenylthiopyrylium tetrafluoroborate (thiopyrylium A) (0.25%) with benzylic silanes and stannane (all at 1% w/w) in the presence of TMPTA

E X P T	INITIATING SYSTEM	NUMBER OF PASSES			
		Touching Quartz	Touching Glass	In Air	Glass Filter
1	PhCH <sub>2</sub> SiMe <sub>3</sub> + Thiopyrylium A	2	3	*	*
2	PhCH <sub>2</sub> SiMe <sub>3</sub>	4	28	*	*
3	4-PhC <sub>6</sub> H <sub>4</sub> CH <sub>2</sub> SiMe <sub>3</sub> + Thiopyrylium A	2	3	*	*
4	4-PhC <sub>6</sub> H <sub>4</sub> CH <sub>2</sub> SiMe <sub>3</sub>	3	6	*	*
5	PhCH <sub>2</sub> SnBu <sub>3</sub> + Thiopyrylium A	1	3	*	*
6	PhCH <sub>2</sub> SnBu <sub>3</sub>	4	20	*	*
7	Thiopyrylium A	7	23	*	*

Belt speed = 10 ft/min for all experiments

\* = polymerisation not detected after 30 passes

It is noticeable that sensitisation of polymerisation occurs in all the touching quartz and touching glass examples of results of 2,4,6-triphenylthiopyrylium tetrafluoroborate with benzylic silanes and stannane. Sensitisation is more evident in the touching glass experiments. This is probably

because in the case of the touching glass experiments the thiopyrylium salt absorbs virtually all of the available light since the benzylic organometals do not absorb to any great extent beyond the glass cut-off point (>310nm).

Table 2.24 UV curing results of 2,4,6-triphenylthiopyrylium tetrafluoroborate (thiopyrylium A) (0.25% w/w) with allylic stannanes and silane (all at 1% w/w) in the presence of TMPTA

E X P T	INITIATING SYSTEM	NUMBER OF PASSES			
		Touching Quartz	Touching Glass	In Air	Glass Filter
1	$\text{CH}_2=\text{CHCH}_2\text{SiPh}_3$ Thiopyrylium A	6	10	*	*
2	$\text{CH}_2=\text{CHCH}_2\text{SiPh}_3$	6	18	*	*
3	$\text{CH}_2=\text{CHCH}_2\text{SnBu}_3$ + Thiopyrylium A	3	6	*	*
4	$\text{CH}_2=\text{CHCH}_2\text{SnBu}_3$	2	14	*	*
5	$\text{Me}_2\text{C}=\text{CHCH}_2\text{SnBu}_3$ + Thiopyrylium A	2	5	*	*
6	$\text{Me}_2\text{C}=\text{CHCH}_2\text{SnBu}_3$	2	7	*	*
7	Thiopyrylium A	7	23	*	*

Belt speed = 10 ft/min for all experiments

\* = polymerisation not detected after 30 passes

It is apparent that the allylic organometallic compounds

(Table 2.24) are not sensitised to the same extent as the benzylic compounds (table 2.23) when using the same thiopyrylium salt. This may be due to the fact that in general the allylic compounds have higher ionisation potentials (see Table 5.1: Appendix) than benzylic compounds and are consequently less able to undergo electron transfer reactions. In order to discover the general applicability of this sensitised photopolymerisation another thiopyrylium salt was used in conjunction with a variety of allylic and benzylic organometallic compounds of silicon and tin. The results are presented below.

Table 2.25 UV curing results of 4-*n*-butoxyphenyl-2,6-bis(4-methoxyphenyl)thiopyrylium tetrafluoroborate (1% w/w) with benzylic and allylic silanes and stannanes (all 5% w/w)

E X P T	INITIATOR	NUMBER OF PASSES			
		Touching Quartz	Touching Glass	In Air	Glass Filter
1	PhCH <sub>2</sub> SiMe <sub>3</sub> + Thiopyrylium B	1	3	*	*
2	PhCH <sub>2</sub> SiMe <sub>3</sub>	4	28	*	*
3	4-PhC <sub>6</sub> H <sub>4</sub> CH <sub>2</sub> SiMe <sub>3</sub> + Thiopyrylium B	1	2	29	*
4	4-PhC <sub>6</sub> H <sub>4</sub> CH <sub>2</sub> SiMe <sub>3</sub>	2	11	*	*
5	PhCH <sub>2</sub> SnBu <sub>3</sub> + Thiopyrylium B	1	4	*	*
6	PhCH <sub>2</sub> SnBu <sub>3</sub>	1	5	*	*

Table 2.25 continued

7	4-MeC <sub>6</sub> H <sub>4</sub> CH <sub>2</sub> SnBu <sub>3</sub> + Thiopyrylium B	1	3	*	*
8	4-MeC <sub>6</sub> H <sub>4</sub> CH <sub>2</sub> SnBu <sub>3</sub>	1	3	*	*
9	CH <sub>2</sub> =CHCH <sub>2</sub> SnBu <sub>3</sub> + Thiopyrylium B	1	2	*	*
10	CH <sub>2</sub> =CHCH <sub>2</sub> SnBu <sub>3</sub>	2	14	*	*
11	Thiopyrylium B	3	6	*	*

Belt speed = 10 ft/min for all experiments

\* = polymerisation not detected after 30 passes

Sensitisation of polymerisation is seen in the case of the benzylic silanes (EXPT'S 1 and 3) and the allylstannane (EXPT 9) but little effect is observed with the benzylic stannanes (EXPT'S 5 and 7). This could be due to the competition in the case of the benzylstannane of sensitisation by the thiopyrylium salt with homolytic cleavage of the C-Sn bond. This would be dependent on the relevant absorption properties in the desired wavelength range of the benzylstannane and the thiopyrylium salt.

At the same time another group was working in the same area and an article was published concerned with the photoalkylation of a pyrylium salt with group 14 donors via electron transfer (Kyushin *et al*, 1990). The electron donors used included allylstannanes and benzylstannanes. It was concluded from the published work that the radical

cation of the group 14 organometallic compound releases the group which is the most stable as a radical in the following order;

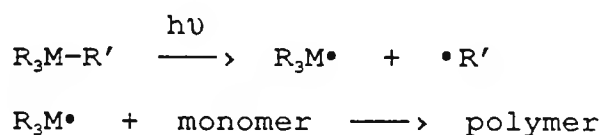


## 2.6 Real-time infrared spectroscopy (RTIR) results

### 2.6.1 Introduction

The maximum rate of polymerisation,  $R_{p(\text{max})}$ , and the degree of conversion have been evaluated at various time intervals utilising the technique of RTIR spectroscopy, which has been described previously (see section 1.7.2). The results of the initiator under test may then be compared to the situation where a sensitiser has been incorporated into the formulation. The efficiency of the sensitisation can be inferred from the comparison of the rates of polymerisation in the situations with and without the use of a sensitiser.

The RTIR results of the initiators used on their own gives an indication of the ease of cleavage of the M-C bond since the proposed mechanism of initiation is via homolytic cleavage of the M-C bond.



It is also worth noting that a number of the initiators tested using the RTIR spectroscopy apparatus did not show any signs of polymerisation which is believed to be due to the lack of absorption of the light source since a cover slip of polyethylene was used in all the experiments which absorbed in the UV region (see Figure 5.1: Appendix). A number of the compounds tested absorb in the same region as the cover-slip and hence the observed kinetic trace showed no evidence of polymerisation. For these compounds in particular the UV curing results obtained using the UV Colordry apparatus are useful since an indication of the effectiveness of these compounds in initiation can be deduced and compared to the remainder of the initiators.

### 2.6.2 RTIR results of benzylsilanes

Table 2.26 RTIR results of the photopolymerisation of TMPTA using benzylsilanes

E X P T	INITIATOR	UV/ $\lambda_{max}$ ( $\epsilon$ )	% initiator		Rp (max) / mol/l/s	% Conv/ at 1 min
			w/w	mol		
1	PhCH <sub>2</sub> SiMe <sub>3</sub>	274 (750)	1.6	2.9	-	-
2	4-MeC <sub>6</sub> H <sub>4</sub> CH <sub>2</sub> - SiMe <sub>3</sub>	273 (650)	5.0	8.3	-	-
3	4-MeOC <sub>6</sub> H <sub>4</sub> CH <sub>2</sub> - SiMe <sub>3</sub>	283 (1850)	5.0	7.6	0.579	43.0
4	4-PhC <sub>6</sub> H <sub>4</sub> CH <sub>2</sub> - SiMe <sub>3</sub>	278 (3500)	1.0	1.2	0.196	16.0

- = no polymerisation detected

The results indicate that under the conditions tested only experiments 3 and 4 show evidence of polymerisation, which is probably related to the greater values of the extinction coefficients and the longer wavelength absorbance of these compounds compared to those in experiments 1 and 2. The results also reflect a similar outcome depicted by the UV curing results shown in table 2.4.

### 2.6.3 RTIR results of benzylic silanes

Table 2.27 RTIR results of the photopolymerisation of TMPTA using benzylic silanes

EXPT	INITIATOR	UV/ $\lambda_{max}$ ( $\epsilon$ )	% initiator		Rp (max) / mol/l/s	% Conv/ at 1 min
			w/w	mol		
1	PhCH <sub>2</sub> SiMe <sub>3</sub>	274 (750)	1.6	2.9	-	-
2	Ph <sub>2</sub> CHSiMe <sub>3</sub>	272 (1400)	1.0	1.2	0.021	5.8
3	9-(SiMe <sub>3</sub> )- fluorene	296 (6500)	1.0	1.2	0.382	28.2
4	9-(SiMe <sub>3</sub> )- thioxanthene	280 (4500)	5.0	5.5	0.224	36.7

- = no polymerisation detected

The first observation is that on going from benzyltrimethylsilane (EXPT 1) to diphenylmethyltrimethylsilane (EXPT 2) there is an approximate two-fold increase in the extinction coefficient when comparing the  $\lambda_{max}$  values of 274nm and 272nm

respectively. This improvement in absorption properties may explain the result of an observed kinetic trace for the diphenylmethyltrimethylsilane (EXPT 2), albeit at a relatively low rate of polymerisation and degree of conversion, compared to the case of benzyltrimethylsilane (EXPT 1) where no polymerisation was detected.

On moving to more conjugated benzylic silanes in experiments 3 and 4 a large increase in the extinction coefficients is realised and this is also illustrated by the increased rate of polymerisation (over 10-fold) and in the degree of conversion when compared to experiment 2.

#### 2.6.4 RTIR results of benzylstannanes

Table 2.28 RTIR results of the photopolymerisation of TMPTA using benzylstannanes

E X P T	INITIATOR	UV/ $\lambda_{\max}$ ( $\epsilon$ )	% initiator		Rp (max) / mol/l/s	% Conv/ at 1 min
			w/w	mol		
1	PhCH <sub>2</sub> SiMe <sub>3</sub>	274 (750)	1.6	2.9	-	-
2	PhCH <sub>2</sub> SnMe <sub>3</sub>	273 (700)	5.0	5.8	0.605	27.7
3	PhCH <sub>2</sub> SnBu <sub>3</sub>	265 (860)	1.2	0.9	0.335	21.7
4	4-MeC <sub>6</sub> H <sub>4</sub> CH <sub>2</sub> - SnBu <sub>3</sub>	279 (850)	1.8	1.4	0.298	19.3
5	4-MeOC <sub>6</sub> H <sub>4</sub> CH <sub>2</sub> - SnBu <sub>3</sub>	281 (2250)	5.0	3.6	1.960	36.9

- = no polymerisation detected

A comparison of the ease of cleavage of the benzylic C-Sn bond compared to the benzylic C-Si bond can be made when comparing the results of benzyltrimethylstannane (EXPT 2) to those of benzyltrimethylsilane (EXPT 1). Both the  $\lambda_{\max}$  values and the extinction coefficients are similar for each of the compounds. The result using benzyltrimethylstannane indicates that light is interacting with the initiator to give cleavage of the C-Sn bond. It must be concluded that light is also being absorbed by benzyltrimethylsilane and that the process of C-Si homolytic cleavage in this case is not an efficient process. When the three Me groups in benzyltrimethylstannane (EXPT 2) are replaced with three *n*-Bu groups (EXPT 3) initiation is again shown to be more efficient via homolytic cleavage than for benzyltrimethylsilane (EXPT 1). When a 4-MeO substituent is incorporated (EXPT 5) a marked red shift in absorption occurs as well as an increase in the extinction coefficient when compared to the parent compound (EXPT 3). This is reflected in the ability of this compound to initiate polymerisation as depicted by the  $R_{p(\max)}$  value and the degree of conversion.

## 2.6.5

RTIR results of naphthyl (and higher) silanes  
and stannanesTable 2.29 RTIR results of the photopolymerisation of  
TMPTA using naphthyl (and higher) silanes and  
stannanes

E X P T	INITIATOR	UV/ $\lambda_{\max}$ ( $\epsilon$ )	% initiator		Rp(max) / mol/l/s	% Conv/ at 1 min
			w/w	mol		
1	1-NpCH <sub>2</sub> SiMe <sub>3</sub>	321 (700)	6.0	8.3	0.195	28.1
2	2-NpCH <sub>2</sub> SiMe <sub>3</sub>	324 (1000)	5.0	6.9	0.187	26.2
3	1-NpCH <sub>2</sub> SnBu <sub>3</sub>	334 (1000)	5.0	3.4	3.78	43.2
4	2-NpCH <sub>2</sub> SnBu <sub>3</sub>	333 (1200)	1.0	0.7	3.91	33.3
5	2-NpCH <sub>2</sub> SnMe <sub>3</sub>	335 (1000)	1.0	1.0	1.60	30.7
6	1-pyreneCH <sub>2</sub> - SiMe <sub>3</sub>	379 (2400) 358 (6200) 347 (17800) 331 (17600)	1.0	1.0	0.202	28.0

The absorption spectra of all of the compounds in table 2.29 show a red shift in absorbance compared to the corresponding benzylic derivatives in tables 2.26, 2.27 and 2.28, as would be expected. Although there is little change in the extinction coefficients when comparing benzyltrimethylsilane (EXPT 1; table 2.26) versus 1- (and 2)naphthylmethyltrimethylsilane (EXPT's 1 and 2 respectively; table 2.29), benzyltrimethylstannane (EXPT 2;

table 2.28) versus 2-naphthylmethyltrimethylstannane (EXPT 5; table 2.29), and benzyltri-*n*-butylstannane (EXPT 3; table 2.28) versus 1-(and 2-)naphthylmethyltri-*n*-butylstannane (EXPT's 3 and 4 respectively; table 2.29), the red shift in the absorption spectra is enough to yield more active initiators in all cases compared here.

It also appears that for the naphthylstannanes the (*n*-Bu)<sub>3</sub>Sn group in experiments 3 and 4 has a greater effect on the rate of polymerisation and the degree of conversion than the Me<sub>3</sub>Sn group in experiment 5. This suggests that the rate of reaction is in the order (*n*-Bu)<sub>3</sub>Sn > Me<sub>3</sub>Sn, a point which has been observed previously (see section 2.5.2).

When increasing the absorption using the 1-pyrenylmethyltrimethylsilane (EXPT 6) compared to the corresponding naphthylmethyltrimethylsilanes (EXPT 1 and 2) there is little change in either the rate of polymerisation or the degree of conversion. This indicates that there is a limiting factor, namely that C-Si bond scission reaches a maximum rate irrespective of the absorption properties of the molecule. It is concluded that other factors need to be introduced to the molecular structure to induce a greater rate of photopolymerisation utilising the homolytic cleavage of the C-Si bond as a mechanism of initiation.

## 2.6.6 RTIR results of allylic silanes and stannanes

Table 2.30 RTIR results of the photopolymerisation of TMPTA using allylic silanes and stannanes

E X P T	INITIATOR	UV/ $\lambda_{max}$ ( $\epsilon$ )	% initiator		Rp (max) / mol/l/s	% Conv/ at 1 min
			w/w	mol		
1	CH <sub>2</sub> =CHCH <sub>2</sub> - SiMe <sub>3</sub>	271 (100)	5.0	13.0	-	-
2	CH <sub>2</sub> =CHCH <sub>2</sub> - SnBu <sub>3</sub>	240 (5000)	1.5	2.2	0.010	3.8
3	Me <sub>2</sub> C=CHCH <sub>2</sub> - SnBu <sub>3</sub>	270 (50)	1.5	1.9	0.080	9.5
4	Ph-CH=CHCH <sub>2</sub> SnBu <sub>3</sub>	268	5.0	3.6	0.660	35.0

- = polymerisation not detected

The results show that these compounds are relatively ineffective UV initiators in their own right and must be sensitised to be of potential interest. Again it is shown that C-Sn homolytic cleavage is more facile than C-Si homolytic cleavage for the allylic systems tested here.

### RTIR results of a cinnamyllic stannane (EXPT 4; Table 2.30)

This compound does not show a particularly high rate of polymerisation but it does show a relatively high degree of conversion which may be related to the fact that [2 + 2] cycloaddition may be involved.

2.6.7 RTIR results of benzylsilanes with DCA

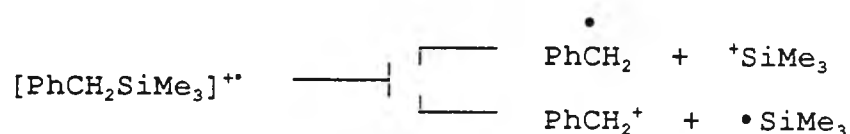
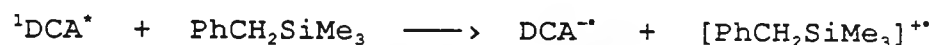
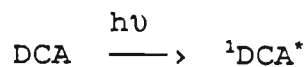
Table 2.31 RTIR spectroscopy results for the photopolymerisation of TMPTA using benzylsilanes sensitised by DCA

EXPT	INITIATING SYSTEM	UV/ $\lambda_{\max}$ ( $\epsilon$ )	% initiator		Rp(max) / mol/l/s	% Conv/ at 1 min
			w/w	mol		
1	PhCH <sub>2</sub> SiMe <sub>3</sub> + DCA	274 (750) see expt 9	1.5 0.25	2.7 0.3	0.77	11.1
2	PhCH <sub>2</sub> SiMe <sub>3</sub>	274 (750)	1.6	2.9	-	-
3	Ph <sub>2</sub> CHSiMe <sub>3</sub> + DCA	272 (1400) see expt 9	2.5 0.25	3.0 0.3	1.00	19.6
4	Ph <sub>2</sub> CHSiMe <sub>3</sub>	272 (750)	1.0	1.2	0.02	5.8
5	4-PhC <sub>6</sub> H <sub>4</sub> CH <sub>2</sub> - SiMe <sub>3</sub> + DCA	278 (3500) see expt 9	1.0 0.25	1.2 0.3	0.34	24.0
6	4-PhC <sub>6</sub> H <sub>4</sub> CH <sub>2</sub> - SiMe <sub>3</sub>	278 (3500)	1.0	1.2	0.20	16.0
7	9-(Me <sub>3</sub> Si)-fl- uorene + DCA	296 (6500) see expt 9	1.0 0.25	1.2 0.3	0.11	32.3
8	9-(Me <sub>3</sub> Si)-fl- uorene	296 (6500)	1.0	1.2	0.38	28.2
9	DCA	424 (13000) 376 (11000) 312 (1000)	0.25	0.3	0.003	2.3

- = polymerisation not detected

The results show that there is definite sensitisation occurring for all the benzylic silanes tested when used in conjunction with DCA (apart from the fluorene derivative [EXPT 7] which is a special case and is discussed later). These results fully support the evidence that sensitisation

occurs in the UV curing results for these initiating systems discussed earlier. A most convincing case for sensitisation is obtained when comparing the result where benzyltrimethylsilane is sensitised by DCA (EXPT 1) to those of benzyltrimethylsilane on its own (EXPT 2) and the sensitiser, DCA, on its own (EXPT 9). As has been previously mentioned benzyltrimethylsilane is not an efficient initiator due to both the low homolysis rate on irradiation and the low extinction coefficient for this compound. Thus in the experimental apparatus no polymerisation is observed when benzyltrimethylsilane is used in the absence of any sensitiser (EXPT 2). To act as a standard for comparison, the RTIR spectrum of the sensitiser, DCA, was recorded and it showed a small degree of polymerisation (EXPT 9). When the combination of benzyltrimethylsilane and the sensitiser, DCA, was used (EXPT 1) a large increase in both  $R_{p(max)}$  and the degree of conversion resulted, giving conclusive evidence for sensitisation. The mechanism of sensitisation is believed to occur via photoinduced electron transfer and is outlined below.



Similarly when DCA was used with diphenylmethyltrimethylsilane (EXPT 3) and 1,1'-biphenylmethyltrimethylsilane (EXPT 5) sensitisation is noticed and both  $R_{p(max)}$  and the degree of conversion are increased when compared to the corresponding experiments without the presence of sensitiser (EXPT 4 and EXPT 6 respectively). This analysis is not applicable to the 'sensitisation' of fluorenyltrimethylsilane (EXPT 7). When comparing the  $R_{p(max)}$  for the sensitised case (EXPT 7;  $R_{p(max)} = 0.11$ ) to the value obtained without sensitiser (EXPT 8;  $R_{p(max)} = 0.38$ ) it would appear that DCA has a detrimental effect on the rate of polymerisation. The explanation of this phenomenon lies in an earlier observation regarding the mechanism of initiation of the fluorene derivative in the absence of any sensitiser. It is proposed that fluorenone is formed on photolysis of the fluorenyltrimethylsilane, which consumes oxygen, hence reducing oxygen inhibition of polymerisation, and thus increasing the rate of initiation (usually  $R_{p(max)}$ ). In the presence of the sensitiser, DCA, the two compounds compete for the available light with the net result that less light is absorbed by the fluorenyltrimethylsilane. This reduces the rate of the reaction of the fluorenyltrimethylsilane with oxygen, with a resultant increase in oxygen inhibition, and thus reduces the value of  $R_{p(max)}$  in the 'sensitised' case (EXPT 7) compared to the absence of sensitiser (EXPT 8). In contrast the degree of conversion (at 1 minute) for the sensitised case (EXPT 7; degree of conversion = 32.3) compared to the

degree of conversion (at 1 minute) for the sensitised case (EXPT 7; degree of conversion = 32.3) compared to the absence of sensitiser (EXPT 8; degree of conversion = 28.2) indicates that there is some sensitisation of polymerisation occurring. It seems that this sensitisation has been masked by the competing reaction of the fluorenyltrimethylsilane with oxygen which gives a relatively high  $R_{p(max)}$ .

#### 2.6.8 RTIR results of benzyl and naphthylstannanes with DCA

Table 2.32 RTIR spectroscopy results for the photopolymerisation of TMPTA using benzylic stannanes sensitised by DCA

EXPT	INITIATING SYSTEM	UV/ $\lambda_{max}$ ( $\epsilon$ )	% initiator		$R_p(max)$ / mol/l/s	% Conv/ at 1 min
			w/w	mol		
1	PhCH <sub>2</sub> SnBu <sub>3</sub> + DCA	265 (860) see expt 7	1.2 0.25	0.9 0.3	0.80	35.1
2	PhCH <sub>2</sub> SnBu <sub>3</sub>	265 (860)	1.2	0.9	0.34	21.7
3	4-MeC <sub>6</sub> H <sub>4</sub> CH <sub>2</sub> - SnBu <sub>3</sub> + DCA	279 (850) see expt 7	1.2 0.25	0.9 0.3	0.77	31.6
4	4-MeC <sub>6</sub> H <sub>4</sub> CH <sub>2</sub> - SnBu <sub>3</sub>	279 (850)	1.8	1.4	0.30	19.3
5	2-NpCH <sub>2</sub> SnMe <sub>3</sub> + DCA	335 (1000) see expt 7	1.0 0.25	1.0 0.3	1.51	31.9
6	2-NpCH <sub>2</sub> SnMe <sub>3</sub>	335 (1000)	1.0	1.0	1.60	30.7
7	DCA	424 (13000) 376 (10000) 312 (1000)	0.25	0.3	0.003	2.3

photosensitisation of polymerisation occurring when using DCA with benzyltri-*n*-butylstannane (EXPT 1) and the 4-methyl analogue (EXPT 3) when compared to the stannanes in the absence of sensitiser (EXPT 2 and EXPT 4, respectively). In the case of these two benzylstannanes the increase in the  $R_{p(max)}$  value (both gave a 2.5 fold increase) is not as marked as was observed in the benzylsilanes (250 fold increase for benzyltrimethylsilane [EXPT 1 compared to EXPT 9; table 2.31], 50 fold increase for diphenylmethyltrimethylsilane [EXPT 3 compared to EXPT 4; table 2.31]) as shown below in table 2.33.

Table 2.33      The effect of sensitisation on the  $R_{p(max)}$  value of photopolymerisation of TMPTA using DCA with benzylsilanes and stannanes

COMPOUND	$R_{p(max)}$ / mol/l/s		Improvement Ratio A/B
	No DCA (B)	With DCA (A)	
PhCH <sub>2</sub> SiMe <sub>3</sub>	0.003	0.77	250
Ph <sub>2</sub> CHSiMe <sub>3</sub>	0.02	1.00	50
PhCH <sub>2</sub> SnBu <sub>3</sub>	0.34	0.80	2.5
4-MeC <sub>6</sub> H <sub>4</sub> CH <sub>2</sub> SnBu <sub>3</sub>	0.30	0.77	2.5

This contrast in behaviour is due to the fact that the benzylstannanes are effective initiators in the absence of

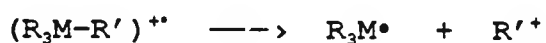
sensitiser whereas the benzylsilanes are relatively poor initiators in the absence of sensitiser. This behaviour reflects the greater tendency of the Sn-C (benzylic) bond to undergo homolytic cleavage compared to the Si-C (benzylic) bond. For the benzylstannanes in the presence of the sensitiser the process of homolytic cleavage will compete with that of sensitisation. The preference of one pathway over the other will depend on both the light available from the source and on the amount of light absorbed from that source.

What is noticeable is that for both the benzylsilanes and the benzylstannanes the effect of introducing the sensitiser, DCA, is to increase the degree of conversion by approximately the same amount as illustrated below.

Table 2.34 The effect of sensitisation on the degree of conversion value of photopolymerisation of TMPTA using DCA with benzylsilanes and stannanes

COMPOUND	% conversion /1 min		Improvement
	No DCA (B)	With DCA (A)	
PhCH <sub>2</sub> SiMe <sub>3</sub>	0.0	11.1	11.1
Ph <sub>2</sub> CHSiMe <sub>3</sub>	5.8	19.6	13.8
PhCH <sub>2</sub> SnBu <sub>3</sub>	21.7	35.1	13.4
4-MeC <sub>6</sub> H <sub>4</sub> CH <sub>2</sub> SnBu <sub>3</sub>	19.3	31.6	12.3

Therefore, there must be further radical species being produced in the presence of DCA that are capable of initiating polymerisation. This suggests that sensitisation takes place and this is proposed to be via an electron transfer mechanism. This also implies that the fragmentation of the radical cation of the organometallic species produced gives rise to initiating radicals, which are likely to be  $R_3M^\bullet$  radicals as depicted below.



In the case of the sensitisation of the 2-naphthylmethyltrimethylstannane (Table 2.32; EXPT 5) there was little evidence to suggest that DCA had any effect on either  $R_{p(\max)}$  or the degree of conversion compared to the situation without sensitiser (Table 2.32; EXPT 6). This is probably due to the competitive absorption of the initiator and the sensitiser in this case.

## 2.6.9 RTIR results of an allylstannane with DCA

Table 2.35 RTIR spectroscopy results for the photopolymerisation of TMPTA using an allylstannane sensitised by DCA

E X P T	INITIATING SYSTEM	UV/ $\lambda_{\max}$ ( $\epsilon$ )	% initiator		Rp (max) / mol/l/s	% Conv/ at 1 min
			w/w	mol		
1	Me <sub>2</sub> C=CHCH <sub>2</sub> - SnBu <sub>3</sub> + DCA	271 (100) see expt 3	1.8 0.25	1.5 0.3	0.08	17.4
2	Me <sub>2</sub> C=CHCH <sub>2</sub> - SnBu <sub>3</sub>	271 (100)	1.5	1.2	0.08	9.5
3	DCA	424 (13000) 376 (11000) 312 (1000)	0.25	0.3	0.003	2.3

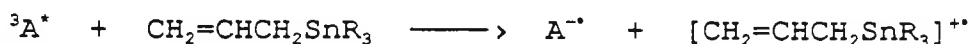
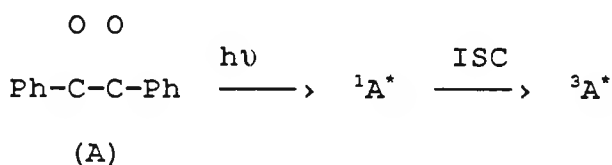
Sensitisation is seen to occur for the allylstannane in table 2.35 with regard to the degree of conversion. There is not a similar effect with other allylsilanes and stannanes which is attributed to the relatively high oxidation potentials of the allylic organometals in general (see Table 5.1; Appendix).

## 2.6.10 RTIR results using 4,4'-dimethylbenzil (DMB) as a sensitiser

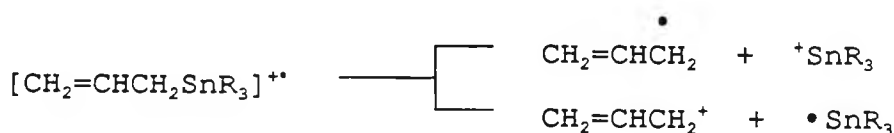
### 2.6.11 Introduction

It has been reported previously that carbonyl compounds such as benzophenone can be successfully allylated using allylstannanes under photochemical conditions via an

electron transfer mechanism (Takuwa et al, 1987). Later work showed that diphenylethanediones (benzils) afforded  $\alpha$ -allylbenzoins in high yield when photolysed in the presence of allylstannanes which were again proposed to be formed via a one electron transfer pathway (Takuwa et al, 1990). The reaction scheme is shown below.



First the benzil derivative is excited to the singlet state. On intersystem crossing the excited triplet state is arrived at. The ground state allylstannane then interacts with the excited triplet state sensitiser which gives rise to an exciplex. Electron transfer then occurs from the allylstannane to the benzil derivative giving rise to a radical cation in the case of the allylstannane, and a radical anion in the case of the benzil derivative. It is then possible that the radical cation of the allylstannane will fragment. This has been shown to occur by two different pathways.

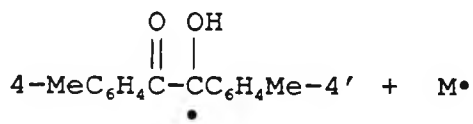


It is known that trialkyltin radicals are effective at initiating free radical polymerisation (Neumann et al, 1961; Davies, 1977).

In an attempt to harness the free radical produced in this way a free radical polymerisable monomer, TMPTA, was used as the 'solvent' for photolysis and the ensuing photopolymerisation was followed using the technique of RTIR spectroscopy described earlier (see section 1.7.2).

This reaction scheme has been further extended to include the use of naphthyl stannanes and silanes in the photopolymerisation of TMPTA.

It is important to mention that the sensitiser used, 4,4'-dimethylbenzil, will initiate photopolymerisation of TMPTA when used on its own without the incorporation of a co-initiator. This is presumably free radical initiation of polymerisation via H-abstraction by the sensitiser from the monomer as shown below.



2.6.12 RTIR results of benzylsilanes with DMB

Table 2.36 RTIR spectroscopy results for the photopolymerisation of TMPTA using benzylsilanes sensitised by DMB

E X P T	INITIATING SYSTEM	UV/ $\lambda_{\max}$ ( $\epsilon$ )	mol %	Rp(max) / mol/l/s	% Conv/ at 1 min
1	PhCH <sub>2</sub> SiMe <sub>3</sub> + DMB	274 (750) see expt 5	8.2 1.2	1.03	36.8
2	PhCH <sub>2</sub> SiMe <sub>3</sub>	274 (750)	2.9	-	-
3	4-MeO-C <sub>6</sub> H <sub>4</sub> CH <sub>2</sub> SiMe <sub>3</sub> + DMB	283 (1850) see expt 5	7.6 1.2	2.08	47.3
4	4-MeO-C <sub>6</sub> H <sub>4</sub> CH <sub>2</sub> SiMe <sub>3</sub>	283 (1850)	7.6	0.58	43.0
5	DMB	269 (29000)	1.2	0.40	32.4

- = no polymerisation detected

It is clear that there is a synergistic effect of the benzylsilanes on the rate of polymerisation in both cases. There is also an improvement in the degree of conversion for both silanes. This is not the case for other benzylic silanes shown below in table 2.37.

### 2.6.13 RTIR results of benzylic silanes with DMB

Table 2.37 RTIR spectroscopy results for the photopolymerisation of TMPTA using benzylic silanes sensitised by DMB

EXPT	INITIATING SYSTEM	UV/ $\lambda_{\max}$ ( $\epsilon$ )	mol %	$R_p(\max)$ / mol/l/s	% Conv/ at 1 min
1	9-Me <sub>3</sub> Si-fluorene + DMB	296 (6500)	1.2 1.2	0.30	30.2
2	9-Me <sub>3</sub> Si-fluorene	296 (6500)	1.2	0.38	28.2
3	9-Me <sub>3</sub> Si-thioxanthen + DMB	280 (4500)	1.1 1.2	0.04	13.4
4	9-Me <sub>3</sub> Si-thioxanthen	280 (4500)	5.5	0.22	36.7
5	DMB	269 (29000)	1.2	0.40	32.4

It is apparent that both the  $R_{p(\max)}$  and the degree of conversion (1 min) are reduced when the fluorene derivative is tested with 4,4'-dimethylbenzil (EXPT 1) when compared to the situation with 4,4'-dimethylbenzil on its own (EXPT 5). There is also a reduction in the  $R_{p(\max)}$  value (EXPT 1) when compared to the fluorene derivative on its own (EXPT 2). A similar situation occurs for the combination of the thioxanthene derivative and 4,4-dimethylbenzil (EXPT 3) except that the reduction in both the  $R_{p(\max)}$  and the degree of conversion (1 min) is much more evident when compared to the thioxanthene derivative on its own (EXPT 4) and 4,4'-dimethylbenzil on its own (EXPT 5).

One explanation why the  $R_{p(max)}$  and the degree of conversion (1 min) results in the 'sensitised' experiments of the fluorene derivative (EXPT 1) and the thioxanthene derivative (EXPT 3) are not as high as the results of the benzylic silanes in the absence of 'sensitiser' (EXPT's 2 and 4 respectively) could be due to the reaction of these compounds with oxygen discussed earlier (see section 2.5.1). Thus the 'sensitiser' preferentially absorbs the available light which reduces the absorption of light by the benzylic silane. This means that the benzylic silane does not react with oxygen under photolytic conditions to both reduce oxygen inhibition and increase the  $R_{p(max)}$  and the degree of conversion (1 min). In the case of the thioxanthene derivative there could also be triplet quenching of the sensitiser since sulphur compounds can act in this way. This would explain the marked reduction in the  $R_{p(max)}$  and the degree of conversion (1 min) values in EXPT 3.

### 2.6.14 RTIR results of benzylstannanes with DMB

Table 2.38 RTIR spectroscopy results for the photopolymerisation of TMPTA using benzylstannanes sensitised by DMB

EXPT	INITIATING SYSTEM	UV/ $\lambda_{\max}$ ( $\epsilon$ )	mol %	$R_p(\max)$ / mol/l/s	% Conv/ at 1 min
1	PhCH <sub>2</sub> SnBu <sub>3</sub> + DMB	265 (860) see expt 5	4.0 1.2	1.66	37.2
2	PhCH <sub>2</sub> SnBu <sub>3</sub>	265 (860)	0.9	0.34	21.7
3	4-Me-C <sub>6</sub> H <sub>4</sub> CH <sub>2</sub> SnBu <sub>3</sub> + DMB	279 (850) see expt 5	3.8 1.2	4.54	47.6
4	4-Me-C <sub>6</sub> H <sub>4</sub> CH <sub>2</sub> SnBu <sub>3</sub>	279 (850)	1.4	0.30	19.3
5	DMB	269 (29000)	1.2	0.40	32.4
6	Irgacure 907	-	<b>0.9</b>	6.52	32.4



It is evident that both the benzylstannanes show an improvement in both the  $R_{p(\max)}$  and the degree of conversion (1 min) values in the presence of sensitiser (EXPT's 1 and 3) when compared to the results of the benzylstannanes in the absence of sensitiser (EXPT's 2 and 4 respectively) and the sensitiser on it's own (EXPT 5). In particular the result with 4-Me-C<sub>6</sub>H<sub>4</sub>CH<sub>2</sub>SnBu<sub>3</sub> (EXPT 3) shows a high  $R_{p(\max)}$  value and compares with the measured value of Irgacure 907, a commercial photoinitiator.

2.6.15 RTIR results of naphthylsilanes and stannanes with DMB

Table 2.39 RTIR spectroscopy results for the photopolymerisation of TMPTA using naphthyl silanes and stannanes sensitised by DMB

EXPT	INITIATING SYSTEM	UV/ $\lambda_{max}$ ( $\epsilon$ )	mol %	$R_p$ (max) / mol/l/s	% Conv/ at 1 min
1	1-NpCH <sub>2</sub> SiMe <sub>3</sub> + DMB	321 (700) see expt 10	8.5 1.2	0.45	36.8
2	1-NpCH <sub>2</sub> SiMe <sub>3</sub>	321 (700)	10.9	0.20	28.1
3	2-NpCH <sub>2</sub> OSiMe <sub>3</sub> + DMB	see expt 10	1.6 1.2	0.16	25.8
4	2-NpCH <sub>2</sub> SnMe <sub>3</sub> + DMB	335 (1000) see expt 10	1.0 1.2	3.95	34.6
5	2-NpCH <sub>2</sub> SnMe <sub>3</sub>	335 (1000)	1.0	1.60	30.7
6	2-NpCH <sub>2</sub> SnBu <sub>3</sub> + DMB	333 (1200) see expt 10	3.5 1.2	3.99	52.6
7	2-NpCH <sub>2</sub> SnBu <sub>3</sub>	333 (1200)	0.7	3.91	33.3
8	1-NpCH <sub>2</sub> SnBu <sub>3</sub> + DMB	334 (1000) see expt 10	3.5 1.2	3.70	37.9
9	1-NpCH <sub>2</sub> SnBu <sub>3</sub>	334 (1000)	3.5	3.78	43.2
10	DMB	269 (29000)	1.2	0.40	32.4

1-NpCH<sub>2</sub>SiMe<sub>3</sub> shows a small improvement in the  $R_{p(max)}$  and the degree of conversion (1 min) values when sensitised (EXPT 1), when compared to the situation on its own (EXPT 2) and the sensitiser on its own (EXPT 10). This could be related to the competitive absorption with the sensitiser. The

silyl ether (EXPT 3) does not show any improvement when sensitised (EXPT 3), when compared to the sensitiser on its own (EXPT 10). When 2-NpCH<sub>2</sub>SnMe<sub>3</sub> was tested with the sensitiser (EXPT 4) there is a noticeable increase in the R<sub>p(max)</sub> and the degree of conversion (1 min) values when compared to the stannane on it's own (EXPT 5) and the sensitiser on its own (EXPT 10). The other naphthylstannanes did not show a similar trend, probably due to the higher % levels of these compounds, which means that they compete effectively with the sensitiser for the available light. This means that homolytic cleavage of the stannane will form a part of the overall mechanism of polymerisation as well as the sensitisation process.

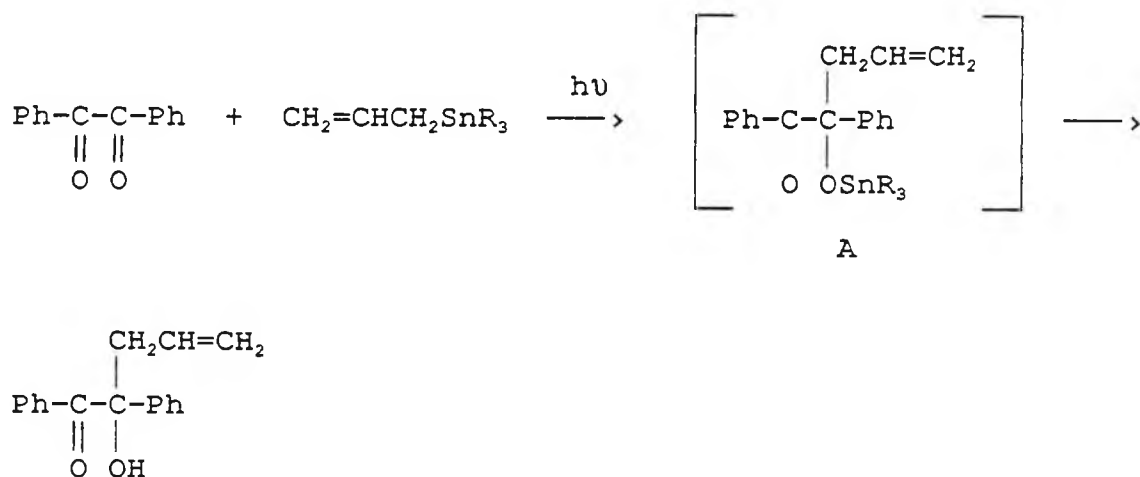
#### 2.6.16 RTIR results of allylsilanes and stannanes with DMB

Table 2.40 RTIR spectroscopy results for the photopolymerisation of TMPTA using allylic silanes and stannanes sensitised by DMB

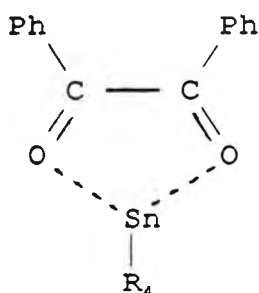
EXPT	INITIATING SYSTEM	UV/ λ <sub>max</sub> (ε)	mol %	R <sub>p</sub> (max) / mol/l/s	% Conv/ at 1 min
1	CH <sub>2</sub> =CHCH <sub>2</sub> SiPh <sub>3</sub> + DMB	see expt 4	1.0 1.2	0.42	30.2
2	Me <sub>2</sub> C=CHCH <sub>2</sub> SnBu <sub>3</sub> + DMB	270 (50) see expt 4	6.3 1.2	0.98	39.0
3	Me <sub>2</sub> C=CHCH <sub>2</sub> SnBu <sub>3</sub>	270 (50)	1.9	0.08	9.5
4	DMB	269 (29000)	1.2	0.40	32.4

The allylstannane shows an improvement in the  $R_{p(max)}$  and the degree of conversion (1 min) values when compared to the stannane on its own (EXPT 3) and the sensitiser on its own (EXPT 4). It appears that the allylsilane has little effect on the polymerisation, which is probably related to its higher oxidation potential than that for the allylstannane, rendering it less effective in an electron transfer mechanism.

One general observation from the results is that the sensitiser has a much greater effect when used with the stannanes than with the silanes. During this work a further report on the photoallylation of benzil with allylstannanes appeared (Takuwa et al, 1991). This gave an insight into the mechanistic details of the photoreaction.



It is proposed that there is a further precursor to species A involving the coordination of the Sn to both the carbonyl groups in a charge transfer complex as depicted below.



This type of complex could be important for symmetrical benzil derivatives with each carbonyl group being equally reactive. This is not the case for the photoreaction of unsymmetrical diketones with allylstannanes where a preferential addition product has been observed (Takuwa et al, 1990).

This could explain the earlier observation during the UV Colordry experiments that films incorporating 4,4-dimethylbenzil and the stannanes gave rise to a colour change on irradiation from light yellow to dark yellow/orange.

The ability of tin to increase its coordination is much greater than for silicon and would explain the apparent difference of behaviour of the silanes and the stannanes with the sensitiser, 4,4'-dimethylbenzil.

## 2.7 Experimental section

All chemicals were purchased from Aldrich and used as received without further purification. Melting points were recorded using a Griffin melting point apparatus and are uncorrected. IR spectra were run on a Perkin-Elmer 983 instrument.  $^1\text{H}$  NMR spectra were recorded using either a Jeol MH 100 instrument or a Jeol PMX 60 spectrometer with TMS as the internal standard. UV/vis absorption spectra were obtained using either a Perkin-Elmer Lambda 5 or a Perkin-Elmer Lambda 16 spectrophotometer. Mass spectra were recorded on either a VG Masslab Biotech Trio-2 instrument or a VG Zab-2F spectrometer. GLC was performed on a Perkin-Elmer Sigma 5 gas chromatograph fitted with a flame ionisation detector. The column (internal diameter 2mm, length 2m) contained liquid phase 5% SE 30. The flow rate of  $\text{N}_2$  was 25mls/min, and the oven temperature was  $100^\circ\text{C}$ . CHN were performed on a Carlo Erba 1106 CHN simultaneous analyser. Photolysis was carried out on solutions in quartz cuvettes (1cm) placed in a circular array of 10x8W lamps having a maximal emission of 300nm. UV curing was performed using a Colordry UV curing unit which housed a medium pressure Hg lamp mounted above a conveyor belt system (lamp 15cm above moving belt; lamp  $80\text{Wcm}^{-1}$  and 23cm in length). Films were coated onto Gateway Natural Tracing (GNT) paper using Meyer bar coater number 3 (thickness  $25\mu$ ). The RTIR spectroscopy apparatus comprised of a Perkin-Elmer 597 spectrophotometer coupled to a Wotan 100W medium

pressure Hg source (Oriel). Kinetic traces were recorded with the spectrophotometer in the time-drive mode. A polyethylene cover slip, in contact with the film under test, was used in all the experiments (for UV see figure 5.1; Appendix). Photo-DSC experiments were run on a modified Perkin-Elmer DSC-4 calorimeter. The two ends of a two-branch UV light conducting fibre were inserted on the cover of the DSC-4 directly above the sample and reference holders. The two-branch flexible UV light guides (50cm long each) ended on a ferrule connector which was plugged into one side of an extended aluminium cylinder. Into this aluminium cylinder were placed a manual shutter to block the incident light on the input end, an interference 365nm filter (International Light NB-365), a solid IR filter (Schott KG-1) and neutral density filters. The extended cylinder assembly was joined to the water-cooling house of a Hanovia Uvitron irradiation system provided with a quartz lens and a 100W high pressure mercury lamp.

## 1. Trimethyl (phenylmethyl) silane

### Method 1

A.

Refluxing and stirring a mixture of benzyl chloride (50.6g; 0.4 mol), trichlorosilane (81.6g; 0.6mol) and tri-*n*-propylamine (57.4g; 0.4mol) at 56-90°C for 20h afforded on work up (ether precipitation of the amine hydrochloride, filtration, and fractionation of the filtrate) 40.0g (40%) of phenylmethyltrichlorosilane with bp 95-96°C/10mm (lit bp 100-102°C/15mm; Benkeser et al, 1969).

B.

A mixture of phenylmethyltrichlorosilane (4.1g; 18mmol) in anhydrous ether (20ml) was added slowly to an ice cooled stirred solution of MeMgBr (20ml; 3M solution in ether; 60mmol) The mixture was stirred at room temperature overnight. The ether was removed and the residue was microdistilled under vacuum to give 1.0g (35%) yield with bp 29°C/0.8mm (lit bp 191.2-191.4/759.5mm; Bygden, 1912)

### Method 2

Trichlorosilane (50g; 0.369mol) was added dropwise under argon with stirring to a mixture of benzaldehyde

(13.1g;0.123mol) and tri-*n*-propylamine (17.6g;0.123mol) in anhydrous ether (100ml). A vigorously exothermic reaction was observed. The mixture was then refluxed for 2h, cooled, and then excess pentane was added until all the amine hydrochloride precipitated. The precipitate was then filtered off. Distillation of the filtrate gave 15.0g (74%) yield of phenylmethyltrichlorosilane with bp 200°C (lit bp 100-102°C/15mm; Benkeser et al, 1969).

B.

MeMgBr (100ml;3M solution in ether;0.30mol) was added dropwise with stirring under argon to phenylmethyltrichlorosilane (15g;0.09mol) in anhydrous ether (100ml). On complete addition the reaction mixture was stirred at room temperature overnight. The reaction mixture was then refluxed for 3h. The reaction was cooled, and quenched with saturated ammonium chloride solution. The mixture was extracted with ether, dried (MgSO<sub>4</sub>), and concentrated. Distillation of the crude product gave 10.0g (32%) yield with bp 188-189°C (lit bp 191.2-191.4°C/759.5mm; Bygden, 1912).

#### Analysis

<sup>1</sup>H NMR:            0.40 (s,9H), 2.20 (s,2H), 6.90-7.50 (m,5H)

IR:                3061 (s), aromatic C-H stretch

2955 (s), aliphatic C-H stretch  
1601 (s), C=C stretch  
1249 (vs), Si-CH<sub>3</sub> stretch  
738 (s), 698 (s), monosubstituted aromatic

UV (EtOH):  $\lambda_{\max}$  274nm ( $\epsilon=750$ )

MS: M<sup>+</sup> 164, 73 (SiMe<sub>3</sub><sup>+</sup>; base peak)

CHN: Calculated for C<sub>10</sub>H<sub>16</sub>Si  
Required C 73.09 H 9.81  
Found C 73.47 H 10.06

## 2. Trimethyl[(4-methylphenyl)methyl]silane

Magnesium turnings (1.95g; 0.08mol) and anhydrous ether (30ml) were placed under argon. The dropping funnel was charged with  $\alpha$ -bromo-p-xylene (10g; 0.055mol) in anhydrous ether (30ml). Stirring was started and a 1-2ml portion of the  $\alpha$ -bromo-p-xylene solution was added into the reaction flask. The resulting temperature rise and cloudiness indicated that the reaction had started. The remainder of the  $\alpha$ -bromo-p-xylene solution was added at such a rate as to maintain a gentle reflux. After complete addition the reaction mixture was refluxed for 1.5h. During reflux the dropping funnel was charged with chlorotrimethylsilane

(6.0g;0.055mol) in anhydrous ether (30ml). After reflux, heating was stopped and the chlorotrimethylsilane solution was added at such a rate as to maintain gentle reflux (36-38°C). After complete addition the reaction mixture was refluxed for 1.5h. The reaction mixture was then quenched with ice-cold saturated ammonium chloride solution to lower the temperature below 35°C. The ether layer was separated, dried (magnesium sulphate), and concentrated. Distillation gave 4.7g (48%) yield of trimethyl[(4-methylphenyl)methyl]silane with bp 212°C (lit bp 211.5°C; Eaborn and Parker, 1955).

#### Analysis

<sup>1</sup>H NMR: relative to SiMe<sub>3</sub>; 0.00 (s,9H), 2.05 (s,2H),  
2.30 (s,3H), 7.00 (s,4H)

IR: 3045 (m), aromatic C-H stretching  
2954 (s), aliphatic C-H stretching  
1510 (s), C=C stretching  
1248 (vs), Si-C stretching  
814 (s), 1,4-disubstituted aromatic

MS: M<sup>+</sup> 178, 105 (C<sub>8</sub>H<sub>9</sub><sup>+</sup>), 73 (base peak, SiMe<sub>3</sub><sup>+</sup>)

UV (EtOH): λ<sub>max</sub> = 280nm (ε=600), 273nm (ε=650)

CHN: Calculated for C<sub>11</sub>H<sub>18</sub>Si

Required	C 74.08	H 10.17
Found	C 74.76	H 11.22

### 3. Trimethyl[(4-methoxyphenyl)methyl]silane

4-Methoxybenzyl chloride (5.00g;0.032mol) in anhydrous THF (15ml) was added dropwise at room temperature under argon, with external irradiation of ultrasound, to a mixture of chlorotrimethylsilane (2.93g;0.027mol), magnesium turnings (0.83g;0.034mol) and 1,2-dibromoethane (0.5ml) in anhydrous THF (20ml). After 3.5h irradiation the reaction mixture was quenched with saturated aqueous  $\text{NH}_4\text{Cl}$  solution and then extracted with ether. The combined organic extracts were dried (magnesium sulphate), and concentrated. Bulb to bulb distillation gave 5.2g (98%) yield of trimethyl([4-methoxyphenyl)methyl)silane with bp 74-75°C/0.1mm (lit bp 238°C; Eaborn and Parker, 1955).

#### Analysis

$^1\text{H}$  NMR: relative to  $\text{SiMe}_3$ ; 0.00 (s,9H), 2.10 (s,2H), 3.90 (s,3H), 6.90-7.20 (m,4H)

IR: 3029, aromatic C-H stretching  
2953, 2896, 2833, aliphatic C-H stretching  
1609, 1580, C=C stretching  
1248, Ar-O stretching

1039, Me-O stretching

830, 1,4-disubstituted benzene

MS:  $M^+$  194, 121 ( $\text{MeO}(\text{C}_6\text{H}_4)\text{CH}_2^+$ ), 73 ( $\text{SiMe}_3^+$ )

UV (EtOH):  $\lambda_{\text{max}} = 283\text{nm}$  ( $\epsilon=1850$ ),  $258\text{nm}$  ( $\epsilon=600$ )

CHN: Calculated for  $\text{C}_{11}\text{H}_{18}\text{OSi}$

Required C 67.98 H 9.34

Found C 68.23 H 9.49

#### 4. (Diphenylmethyl)trimethylsilane

A.

Making sure equipment was dry, trichlorosilane (30.2ml;0.3mol) was added dropwise to a stirred mixture of benzophenone (18.2g,;0.1mol) and tri-*n*-propylamine (19.0ml;0.1mol) at 0°C. After complete addition the reaction mixture was refluxed at 55-75°C for 1 hour. Excess pentane was then added to the cold reaction mixture until complete precipitation of tri-*n*-propylamine hydrochloride occurred. The precipitate was then filtered off and the excess pentane was removed. The crude product was vacuum distilled with bp 109°C/0.5mm (lit bp 141-145°C/2.5mm; Benkeser and Smith, 1969) to give 15.0g (50%) yield of (diphenylmethyl)trichlorosilane with mp 40-42°C (lit mp 48-49°C; Benkeser and Smith, 1969).

B.

A mixture of diphenylmethyltrichlorosilane (2.75g; 9mmol) in anhydrous ether (20ml) was added slowly to an ice cooled stirred solution of MeMgBr (10ml; 3M solution in ether; 30mmol). The mixture was stirred at room temperature overnight. The ether was removed and the residue was microdistilled under vacuum with bp 91°C/0.3mm (lit bp 135°C/4mm; Hauser and Hance, 1951). The product obtained was purified on a silica gel column using cyclohexane as eluent ( $R_f=0.5$ ) to give 0.4g (20%) yield of (diphenylmethyl)trimethylsilane with mp 74-75°C (lit mp 74.5-75.5°C; Hauser and Hance, 1951).

#### Analysis

$^1\text{H NMR}$ : 0.40 (s, 9H), 3.80 (s, 1H), 7.60 (m, 10H)

$\text{IR}$ : 3057 (m), aromatic C-H stretch  
2951 (m), aliphatic C-H stretch  
1594 (m), C=C stretch  
1249 (s), Si-CH<sub>3</sub> stretch  
748 (s), 698 (s), monosubstituted aromatic

$\text{MS}$ :  $M^+$  240, 73 (base peak; SiMe<sub>3</sub><sup>+</sup>)

$\text{UV (EtOH)}$ :  $\lambda_{\text{max}} = 272\text{nm}$  ( $\epsilon=1400$ )

5. Trimethyl(1,1'-biphenyl-4-ylmethyl)silane (Hayashi et al, 1981)

A.

NaH (4.4g; 60% dispersion in oil; 0.11mol) was placed in anhydrous THF (20ml) under argon. A solution of 4-phenylphenol (17g; 0.1mol) in anhydrous THF (50ml) was added dropwise with stirring. After complete addition the mixture was stirred for 0.5h. Diethylphosphorchloridate (17.2g; 0.1mol) was then added in one portion and stirring was continued overnight. The mixture was diluted with ether (500ml) and washed with NaOH (10%; 3x100ml). The combined ethereal extracts were dried (magnesium sulphate), filtered and concentrated to give 15.0g (49%) yield of 1,1'-biphenyl-4-diethylphosphate.

#### Analysis

$^1\text{H}$  NMR: 1.35 (t, 6H), 4.25 (m, 4H), 7.40 (m, 9H)

B.

1,1'-biphenyl-4-diethylphosphate (5.0g; 0.016mol) in anhydrous ether (15ml) was added under argon, to a stirred mixture of  $\text{Ni}(\text{acac})_2$  (0.22g; 0.0008mol) and trimethylsilylmethylmagnesium chloride (50ml; 1M solution in ether; 0.05mol). The mixture was then stirred overnight at room temperature and hydrolysed with dilute HCl. The ether

layer was separated, dried (magnesium sulphate), and evaporated to yield a crude brown solid which was purified on a silica gel column with hexane as the eluent ( $R_f=0.55$ ) to give 0.5g (25%) yield, which was recrystallised from MeOH to give colourless crystals with mp 51-52°C.

### Analysis

$^1\text{H NMR}$ : relative to  $\text{SiMe}_3$ ; 0.00 (s, 9H), 2.07 (s, 2H), 6.90-7.60 (m, 9H)

IR (KBr): 3055 (m), 3032 (m), aromatic C-H stretching  
2955 (m), aliphatic C-H stretching  
1610 (m), 1599 (m), C=C stretching  
1247 (vs), Si-C stretching of  $\text{SiMe}_3$  group

MS:  $M^+$  240, 73 ( $\text{SiMe}_3^+$ ; base peak), 28 ( $\text{Si}^+$ )

UV (EtOH):  $\lambda_{\text{max}} = 278\text{nm}$  ( $\epsilon=3500$ )

CHN: Calculated for  $\text{C}_{16}\text{H}_{20}\text{Si}$   
Required C 79.93 h 8.38  
Found C 80.04 H 8.42

6. (9H-Fluoren-9-yl)trimethylsilane (Bey and Weyenberg, 1966)

A solution of *n*-BuLi in hexane (0.15mol) was added under argon during 3h at 25-32°C to fluorene (8.31g;0.05mol) in anhydrous THF (125ml). The resulting orange/brown solution was added via a syringe to rapidly stirring trimethylchlorosilane (97.4g;0.90mol) under argon. The temperature was maintained at 10-20°C during the 1h addition. After complete addition the solvent was removed by distillation. The residue was dissolved in chloroform (150ml) and the LiCl filtered off. The filtrate was concentrated on a rotary evaporator. Crystallisation from EtOH (150ml) gave a crude orange product. Further concentration of EtOH gave additional orange/brown product. The crude product was purified on a silica gel column with hexane as the eluent to give a yield of 5.0g (43%) which was recrystallised from methanol to give a crystalline solid with mp 96-97°C (lit mp 97.5°C; Earborn and Shaw, 1955).

#### Analysis

<sup>1</sup>H NMR: relative to SiMe<sub>3</sub>; 0.00 (s,9H), 3.80 (s,1H),  
7.00-7.30 (m,8H)

IR: 3055 (w), aromatic C-H stretch  
2956 (m), aliphatic C-H stretch  
1606 (w), C=C stretching  
1250 (s), Si-C stretching  
740 (s), 1,2-disubstituted aromatic

UV (EtOH):  $\lambda_{\text{max}} = 296\text{nm}$  ( $\epsilon=6500$ )

MS:  $m^+$  238, 222 (base peak,  $\text{C}_{15}\text{H}_{14}\text{Si}^+$ ), 73 ( $\text{SiMe}_3^+$ )

7. (9H-Thioxanthen-9-yl)trimethylsilane

A.

Trichlorosilane (28.5g;210mmol) was added dropwise under argon, with stirring, to a mixture of thioxanthone (15.0g;70mmol) and tri-*n*-propylamine (10.1g;70mmol) in anhydrous THF (150ml). After complete addition the reaction mixture was refluxed for 4h and cooled. Excess pentane was added to the reaction mixture to precipitate the amine hydrochloride. The mixture was then filtered and the filtrate was rapidly transferred to a distillation flask. The filtrate was first distilled at atmospheric pressure to remove solvent and then under vacuum with the collecting flask immersed in liquid nitrogen to give 15.0g (64%) of the desired (9-trichlorosilyl)thioxanthene with bp 220°C/2mmHg.

B.

Anhydrous THF (50ml) was added to (9-trichlorosilyl)thioxanthene (15.0g;0.045mol) under argon. MeMgBr (50ml;3M solution in ether;0.150mol) was then added dropwise with stirring. On complete addition the reaction mixture was left stirring overnight. The mixture was then

refluxed for 6h, cooled, and quenched with saturated ammonium chloride solution. It was then extracted with ether, dried ( $\text{MgSO}_4$ ), and concentrated. The white solid product was recrystallised from ethanol to give 8.0g (48%) yield of colourless needles with mp 107-108°C.

### Analysis

$^1\text{H}$  NMR: relative to  $\text{SiMe}_3$ ; 0.00 (s, 9H), 3.70 (s, 1H),  
7.70 (m, 8H)

IR (KBr): 3055 (m), aromatic C-H stretch  
2960 (m), aliphatic C-H stretch  
1589 (m), C=C stretch  
1246 (vs), Si-C stretch of  $\text{SiMe}_3$  group  
744 (vs), 1,2-disubstituted aromatic

UV (EtOH):  $\lambda_{\text{max}} = 280\text{nm}$  ( $\epsilon=4500$ )

MS:  $M^+$  270, 197 (base peak;  $\text{C}_{13}\text{H}_9\text{S}^+$ ), 73 ( $\text{SiMe}_3^+$ )

CHN: Calculated for  $\text{C}_{16}\text{H}_{18}\text{SSi}$   
Required C 71.05 H 6.71  
Found C 72.01 H 7.15

### 8. Tri-n-butyl(phenylmethyl)stannane

This compound was prepared by the method described in

experiment 3, using benzyl chloride (5.5ml;0.048mol), chlorotri-*n*-butylstannane (10.8ml;0.040mol), magnesium turnings (1.25g;0.052mol), and 1,2-dibromoethane (0.5ml) with irradiation of ultrasound for 1h. Bulb to bulb distillation gave 13.0g (86%) yield with bp 141°C/0.5mm (lit bp 105°C/0.2mm; Eaton, 1981).

### Analysis

<sup>1</sup>H NMR: 0.50-1.70 (m,27H), 2.24 (s,2H), 6.72-7.32 (m,5H)

IR: 2956 (s), C-H asymmetric stretch of CH<sub>3</sub> group  
2923 (s), C-H asymmetric stretch of CH<sub>2</sub> group  
2871 (s), C-H symmetric stretch of CH<sub>3</sub> group  
2853 (s), C-H symmetric stretch of CH<sub>2</sub> group  
1599 (m), 1489 (m), 1462 (m), C=C stretching  
753 (s), 696 (s), monosubstituted benzene

MS:

M<sup>+</sup> 382, 380, 378; (<sup>120</sup>Sn, <sup>118</sup>Sn, <sup>116</sup>Sn respectively)  
291,289,287; Sn(*n*-butyl)<sub>3</sub><sup>+</sup> (<sup>120</sup>Sn, <sup>118</sup>Sn, <sup>116</sup>Sn respectively)  
235,233,231; SnH(*n*-butyl)<sub>2</sub><sup>+</sup> (<sup>120</sup>Sn, <sup>118</sup>Sn, <sup>116</sup>Sn respectively)  
177,175,173; Sn(*n*-butyl)<sup>+</sup> (<sup>120</sup>Sn, <sup>118</sup>Sn, <sup>116</sup>Sn respectively)  
121,119,117; SnH<sup>+</sup> (<sup>120</sup>Sn, <sup>118</sup>Sn, <sup>116</sup>Sn respectively)  
91; PhCH<sub>2</sub><sup>+</sup>

UV (EtOH): λ<sub>max</sub> = 265nm (ε=860)

<sup>13</sup>C NMR:

5	4	3	2	1	Sn	a	b	c	d
122.8	128.2	127.0	143.7	18.1		9.4	29.2	27.4	13.8

CHN:

Calculated for C<sub>19</sub>H<sub>34</sub>Sn

Required C 59.87 H 8.99

Found C 60.16 H 9.50

### 9. Tri-*n*-butyl[(4-methylphenyl)methyl]stannane

This compound was prepared by the method described in experiment 3, using  $\alpha$ -bromo-*p*-xylene (12.0g;0.065mol), chlorotri-*n*-butylstannane (21.6ml;0.080mol), magnesium turnings (2.50g;0.104mol), and 1,2-dibromoethane (0.5ml) with irradiation of ultrasound for 1h. Bulb to bulb distillation gave 11.5g (45%) yield with bp 144°C/0.3mm (lit bp 101-105°C; Eaton, 1981).

#### Analysis

<sup>1</sup>H NMR: 0.60-1.50 (m,27H), 2.22 (2 singlets,5H),  
6.60-7.00 (m,4H)

IR: 2955 (s), C-H asymmetric stretch of CH<sub>3</sub> group  
2924 (s), C-H asymmetric stretch of CH<sub>2</sub> group  
2871 (s), C-H symmetric stretch of CH<sub>3</sub> group  
2853 (s), C-H symmetric stretch of CH<sub>2</sub> group

1611 (w), 1507 (s), 1461 (s), C=C stretching  
812 (s), 1,4-disubstituted benzene

MS:

M<sup>+</sup> 396, 394, 392 (<sup>120</sup>Sn, <sup>118</sup>Sn, <sup>116</sup>Sn respectively)  
291, 289, 287; Sn(*n*-butyl)<sub>3</sub><sup>+</sup> (<sup>120</sup>Sn, <sup>118</sup>Sn, <sup>116</sup>Sn respectively)  
235, 233, 231; SnH(*n*-butyl)<sub>2</sub><sup>+</sup> (<sup>120</sup>Sn, <sup>118</sup>Sn, <sup>116</sup>Sn respectively)  
177, 175, 173; Sn(*n*-butyl)<sup>+</sup> (<sup>120</sup>Sn, <sup>118</sup>Sn, <sup>116</sup>Sn respectively)  
121, 119, 117; SnH<sup>+</sup> (<sup>120</sup>Sn, <sup>118</sup>Sn, <sup>116</sup>Sn respectively)  
105, [Me(C<sub>6</sub>H<sub>4</sub>)CH<sub>2</sub><sup>+</sup>]

UV (EtOH):  $\lambda_{\text{max}}$  = 279nm ( $\epsilon=850$ ), 264nm ( $\epsilon=935$ )

<sup>13</sup>C NMR:

6	5	4	3	2	1	Sn	a	b	c	d
20.9	132.1	129.0	127.0	140.4	17.6		9.4	29.2	27.4	13.8

CHN:

Calculated for C<sub>20</sub>H<sub>36</sub>Sn

Required C 60.78 H 9.18

Found C 60.92 H 9.28

#### 10. Tri-*n*-butyl[(4-methoxyphenyl)methyl]stannane

This compound was prepared by the method described in experiment 3, using 4-methoxybenzyl chloride (5.0g;0.032mol), chlorotri-*n*-butylstannane (8.7g;0.027mol), magnesium turnings (0.83g;0.035mol), and 1,2-dibromoethane (0.5ml) with irradiation of ultrasound for 3.5h. Bulb to

bulb distillation gave 11.0g (100%) yield with bp 44°C/0.02mm (lit bp 125-126°C/0.1mm; Eaton, 1981).

### Analysis

<sup>1</sup>H NMR: 0.50-1.60 (m, 27H), 2.24 (s, 2H), 3.68 (s, 3H),  
6.53-6.91 (m, 4H)

IR: 2956 (s), C-H asymmetric stretch of CH<sub>3</sub> group  
2925 (s), C-H asymmetric stretch of CH<sub>2</sub> group  
2871 (s), C-H symmetric stretch of CH<sub>3</sub> group  
2854 (s), C-H symmetric stretch of CH<sub>2</sub> group  
1601 (s), C=C stretching  
1247 (s), Ph-O stretch  
1037 (m), Me-O stretch  
830 (m), 1,4-disubstituted benzene

MS:

M<sup>+</sup> 412, 410, 408; (<sup>120</sup>Sn, <sup>118</sup>Sn, <sup>116</sup>Sn respectively)  
291, 289, 287; Sn(n-butyl)<sub>3</sub><sup>+</sup> (<sup>120</sup>Sn, <sup>118</sup>Sn, <sup>116</sup>Sn respectively)  
235, 233, 231; SnH(n-butyl)<sub>2</sub><sup>+</sup> (<sup>120</sup>Sn, <sup>118</sup>Sn, <sup>116</sup>Sn respectively)  
177, 175, 173; Sn(n-butyl)<sup>+</sup> (<sup>120</sup>Sn, <sup>118</sup>Sn, <sup>116</sup>Sn respectively)  
121; MeO(C<sub>6</sub>H<sub>4</sub>)CH<sub>2</sub><sup>+</sup> (base peak)

UV (EtOH): λ<sub>max</sub> = 281nm (ε=2250), 273nm (ε=2260)

CHN: Calculated for C<sub>20</sub>H<sub>36</sub>OSn  
Required C 67.98 H 9.34

**11. Trimethyl(phenylmethyl)stannane**

Chlorotrimethyltin (5.0g; 0.025mol) in anhydrous THF (30ml) was added dropwise with stirring at room temperature under argon to a solution of benzylmagnesium chloride (12.5ml; 2M solution in THF; 0.025mol). On complete addition the mixture was refluxed for 4h, cooled, and quenched with saturated aqueous  $\text{NH}_4\text{Cl}$  solution. The resultant solution was extracted with ether and the combined organic extracts were dried (magnesium sulphate) and concentrated. Bulb to bulb distillation gave 4.0g (63%) yield with bp  $56^\circ\text{C}/1.4\text{mm}$  (lit bp  $89-90^\circ\text{C}/9\text{mm}$ ; Bullpit et al, 1976).

Analysis

$^1\text{H}$  NMR: relative to  $\text{SnMe}_3$ ; 0.00 (s, 9H), 2.20 (s, 2H),  
7.00-7.20 (m, 5H)

IR: 3070 (m), 3022 (s), aromatic C-H stretching  
2979 (s), 2915 (s), aliphatic C-H stretching  
1600 (s), C=C stretch  
754 (s), Sn-C stretch of  $\text{SnMe}_3$  group

MS:

$\text{M}^+$  256, 254, 252 ( $^{120}\text{Sn}$ ,  $^{118}\text{Sn}$ ,  $^{116}\text{Sn}$  respectively)

165, 163, 161;  $\text{Sn}(\text{CH}_3)_3^+$  ( $^{120}\text{Sn}$ ,  $^{118}\text{Sn}$ ,  $^{116}\text{Sn}$  respectively)

91, PhCH<sub>2</sub><sup>+</sup>

UV (EtOH):  $\lambda_{\text{max}} = 273\text{nm}$  ( $\epsilon=700$ )

CHN: Calculated for C<sub>10</sub>H<sub>16</sub>Sn  
Required C 47.12 H 6.33  
Found C 47.15 H 6.34

## 12. Trimethyl(1-naphthalenylmethyl)silane

This compound was prepared by the method described in experiment 3, using 1-bromomethylnaphthalene (2.5g;0.011mol), chlorotrimethylsilane (1.0g;0.009mol), magnesium turnings (0.29g;0.012mol), and 1,2-dibromoethane (0.5ml) with irradiation of ultrasound for 10h. Bulb to bulb distillation gave 1.2g (62%) yield with bp 48°C/0.02mm (lit bp 143°C/11mm; Bock and Alt, 1969).

### Analysis

<sup>1</sup>H NMR: relative to SiMe<sub>3</sub>; 0.00 (s,9H), 3.00 (s,2H),  
7.00-7.80 (m,7H)

IR: 3062 (m), aromatic C-H stretch  
2954 (s), aliphatic C-H stretch  
1594 (m), 1508 (m), C=C stretching  
1249 (s), Si-C stretch of SiMe<sub>3</sub> group  
798 (s), 777 (s), C-H deformation for 1-

substituted naphthalene

MS:  $M^+$  214, 141 ( $\text{NpCH}_2^+$ ), 73 ( $\text{SiMe}_3^+$ ; base peak)

UV (EtOH):  $\lambda_{\text{max}} = 321\text{nm}$  ( $\epsilon=700$ ),  $287\text{nm}$  ( $\epsilon=6000$ )

CHN: Calculated for  $\text{C}_{14}\text{H}_{10}\text{Si}$   
Required C 78.44 H 8.46  
Found C 78.48 H 8.64

13. Trimethyl(2-naphthalenylmethyl)silane

This compound was prepared by the method described in experiment 3, using 2-bromomethylnaphthalene (2.5g; 0.011mol), chlorotrimethylsilane (1.0g; 0.009mol), magnesium turnings (0.29g; 0.012mol), and 1,2-dibromoethane (0.5ml) with irradiation of ultrasound for 10h. Recrystallisation (EtOH) gave 1.7g (88%) yield with mp  $61^\circ\text{C}$  (lit mp  $61^\circ\text{C}$ ; Bock and Alt, 1969).

Analysis

$^1\text{H}$  NMR: relative to  $\text{SiMe}_3$ ; 0.00 (s, 9H), 2.30 (s, 2H),  
7.10-7.90 (m, 7H)

IR: 3055 (m), aromatic C-H stretch  
2955 (m), 2892 (m), aliphatic C-H stretching  
1625 (m), 1596 (m), 1501 (m), C=C stretching

865 (s), 825 (s), 743 (s), C-H out of plane deformation for 2-substituted naphthalene

MS:  $M^+$  214, 141 ( $NpCH_2^+$ ), 73 ( $SiMe_3^+$ ; base peak)

UV (EtOH):  $\lambda_{max}$  = 324nm ( $\epsilon=1000$ ), 309nm ( $\epsilon=900$ ), 280nm ( $\epsilon=4800$ )

CHN: Calculated for  $C_{14}H_{18}Si$   
Required C 78.44 H 8.46  
Found C 78.69 H 8.82

#### 14. Tri-*n*-butyl(1-naphthalenylmethyl) stannane

This compound was prepared by the method described in experiment 3, using 1-bromomethylnaphthalene (3.5g; 0.016mol), chlorotri-*n*-butylstannane (4.23g; 0.013mol), magnesium turnings (0.40g; 0.017mol), and 1,2-dibromoethane (0.5ml) with irradiation of ultrasound for 5h. Bulb to bulb distillation gave 3.5g (63%) yield with bp 110°C/0.04mm.

#### Analysis

$^1H$  NMR: 0.60-1.90 (m, 27H), 2.80 (s, 2H), 7.30-8.20 (m, 7H)

IR: 3051 (m), aromatic C-H stretch  
2955 (s), C-H asymmetric stretch of  $CH_3$  group

2922 (s), C-H asymmetric stretch of CH<sub>2</sub> group  
2870 (s), C-H symmetric stretch of CH<sub>3</sub> group  
2852 (s), C-H symmetric stretch of CH<sub>2</sub> group  
1596 (m), 1501 (m), 1462 (m), aromatic C=C  
stretching  
791 (s), 774 (s), 1-substituted naphthalene

MS:

M<sup>+</sup> 432 (<sup>120</sup>Sn)

291, 289, 287; Sn(*n*-butyl)<sub>3</sub><sup>+</sup> (<sup>120</sup>Sn, <sup>118</sup>Sn, <sup>116</sup>Sn respectively)

235, 233, 231; SnH(*n*-butyl)<sub>2</sub><sup>+</sup> (<sup>120</sup>Sn, <sup>118</sup>Sn, <sup>116</sup>Sn respectively)

179, 177, 175; SnH<sub>2</sub>(*n*-butyl)<sup>+</sup> (<sup>120</sup>Sn, <sup>118</sup>Sn, <sup>116</sup>Sn respectively)

141 (base peak) NpCH<sub>2</sub><sup>+</sup>

UV (EtOH): λ<sub>max</sub> = 290nm (ε=7500)

CHN: Calculated for C<sub>23</sub>H<sub>36</sub>Sn

Required C 64.06 H 8.42

Found C 63.89 H 8.68

#### 15. Tri-*n*-butyl(2-naphthalenylmethyl)stannane

This compound was prepared by the method described in experiment 3, using 2-bromomethylnaphthalene (3.1g; 0.014mol), chlorotri-*n*-butylstannane (4.23g; 0.013mol), magnesium turnings (0.40g; 0.017mol), and 1,2-dibromoethane (0.5ml) with irradiation of ultrasound for 5h. Bulb to bulb distillation gave 4.2g (78%) yield, bp 110°C/0.04mm.

## Analysis

$^1\text{H}$  NMR: 0.50-1.70 (m, 27H), 2.40 (s, 2H), 7.10-8.00 (m, 7H)

IR: 2955 (s), C-H asymmetric stretch of  $\text{CH}_3$  group  
2922 (s), C-H asymmetric stretch of  $\text{CH}_2$  group  
2870 (s), C-H symmetric stretch of  $\text{CH}_3$  group  
2852 (s), C-H symmetric stretch of  $\text{CH}_2$  group  
1629 (m), 1596 (m), 1501 (m), C=C stretching  
850 (m), 815 (m), 744 (m), C-H out of plane deformation for 2-substituted naphthalene

MS:

$\text{M}^+$  432 ( $^{120}\text{Sn}$ )

291, 289, 287;  $\text{Sn}(n\text{-butyl})_3^+$  ( $^{120}\text{Sn}$ ,  $^{118}\text{Sn}$ ,  $^{116}\text{Sn}$  respectively)

235, 233, 231;  $\text{SnH}(n\text{-butyl})_2^+$  ( $^{120}\text{Sn}$ ,  $^{118}\text{Sn}$ ,  $^{116}\text{Sn}$  respectively)

179, 177, 175;  $\text{SnH}_2(n\text{-butyl})^+$  ( $^{120}\text{Sn}$ ,  $^{118}\text{Sn}$ ,  $^{116}\text{Sn}$  respectively)

141; (base peak)  $\text{NpCH}_2^+$

UV (EtOH):  $\lambda_{\text{max}} = 333\text{nm}$  ( $\epsilon=1200$ )

CHN: Calculated for  $\text{C}_{23}\text{H}_{36}\text{Sn}$

Required C 64.06 H 8.42

Found C 65.04 H 9.09

## 16. Trimethyl(2-naphthalenylmethyl) stannane

This compound was prepared by the method described in experiment 3, using 2-bromomethylnaphthalene (6.60g;0.030mol), chlorotrimethylstannane (5.00g;0.025mol), magnesium turnings (0.78g;0.033mol), and 1,2-dibromoethane (0.5ml) with irradiation of ultrasound for 2h. The resultant solid was recrystallised from ethanol to give 3.5g (46%) yield with mp 60°C (lit mp 59-60°C; Bullpit et al, 1976).

### Analysis

<sup>1</sup>H NMR: relative to SnMe<sub>3</sub>; 0.00 (s, 9H), 2.40 (s, 2H), 7.2-7.6 (m, 7H)

IR: 3048 (m), aromatic C-H stretch  
2981 (m), 2917 (m), aliphatic C-H stretching  
1626 (m), 1595 (s), C=C stretching  
860 (m), 825 (s), 719 (m), 2-substituted naphthalene

MS:

M<sup>+</sup> 306, 304, 302 (<sup>120</sup>Sn, <sup>118</sup>Sn, <sup>116</sup>Sn respectively)  
165, 163, 161; Sn(CH<sub>3</sub>)<sub>3</sub><sup>+</sup> (<sup>120</sup>Sn, <sup>118</sup>Sn, <sup>116</sup>Sn respectively)  
141, NpCH<sub>2</sub><sup>+</sup>

UV (MeOH): λ<sub>max</sub> = 335nm (ε=1000), 318nm (ε=1000)

CHN:	Calculated for $C_{14}H_{18}Sn$		
	Required	C 55.13	H 5.95
	Found	C 55.48	H 5.90

17. Trimethyl(1-pyrenylmethyl)silane

A.

Trichlorosilane (17.7g;0.130mol) was added dropwise with stirring to a mixture of 1-pyrenecarboxaldehyde (10.0g;0.043mol) and tri-*n*-propylamine (6.2g;0.043mol) in anhydrous THF (50ml). On complete addition the mixture was refluxed for 2h, cooled, and excess pentane was added. The precipitated amine hydrochloride was filtered off and the filtrate was transferred rapidly and distilled, firstly at atmospheric pressure to remove undesired pentane/THF/trichlorosilane and then under vacuum to obtain the desired product. This was collected in a flask immersed in liquid nitrogen to give 6.0g (40%) yield of trichloro(1-methylpyrene)silane with bp 220°C/3mm.

B.

MeMgBr (20ml;3M solution in ether;0.06mol) was added dropwise with stirring under argon to trichloro(1-methylpyrene)silane (6.0g;0.017mol) in anhydrous ether (50ml). The mixture was stirred overnight and then refluxed for 3h. The reaction mixture was cooled and then quenched

with saturated aqueous  $\text{NH}_4\text{Cl}$  solution, extracted with ether, dried (magnesium sulphate), and concentrated to give a pale yellow solid. The crude product was recrystallised (EtOH) to give 1.8g (37%) of pale yellow crystals with mp 69–70°C.

### Analysis

$^1\text{H}$  NMR: relative to  $\text{SiMe}_3$ ; 0.00 (s, 9H), 2.70 (s, 2H), 7.40–8.10 (m, 9H)

IR: 3039 (m), aromatic C-H stretch  
2953 (m), aliphatic C-H stretch  
1602 (m), C=C stretch  
1247 (s), Si-C stretch of  $\text{SiMe}_3$  group

MS:  $\text{M}^+$  288, 215 ( $\text{pyreneCH}_2^+$ ), 73 ( $\text{SiMe}_3^+$ ; base peak)

UV (MeOH):  $\lambda_{\text{max}}$  = 379nm ( $\epsilon=2400$ ), 358nm ( $\epsilon=6200$ ), 347nm ( $\epsilon=17800$ ), 331nm ( $\epsilon=17600$ )

CHN: Calculated for  $\text{C}_{20}\text{H}_{20}\text{Si}$   
Required C 83.28 H 6.99  
Found C 83.52 H 7.54

### 18. Trimethyl-2-propenylsilane

Magnesium turnings (2.60g; 0.11mol) and anhydrous ether

(30ml) were placed under argon. A solution of allyl bromide (8.60ml; 0.10mol) in anhydrous ether (30ml) was added dropwise with stirring and on complete addition the mixture was refluxed for 1.5h. On cooling chlorotrimethylsilane (10.90g; 0.10mol) was added dropwise with stirring and after complete addition the mixture was refluxed for a further 1.5h. The reaction mixture was then cooled and quenched with cold saturated ammonium chloride solution. The solution was extracted with ether, dried (magnesium sulphate), and concentrated. Distillation of the crude product gave 4.8g (42%) yield with bp 86°C (lit bp 86-87°C; Koizumi et al, 1989).

#### Analysis

<sup>1</sup>H NMR: Relative to SiMe<sub>3</sub>; 0.00 (s, 9H), 1.50 (d, 2H), 4.80 (d, 2H), 5.75 (m, 1H)

IR: 3079 (m), C-H stretch of =CH<sub>2</sub> group  
2957 (s), 2900 (m), aliphatic C-H stretching  
1630 (s), C=C stretch  
1251 (s), Si-C stretch of SiMe<sub>3</sub> group  
894 (s), =CH<sub>2</sub> out of plane bending

MS: M<sup>+</sup> 114, 73 (SiMe<sub>3</sub><sup>+</sup>; base peak), 41 (C<sub>3</sub>H<sub>5</sub><sup>+</sup>)

UV (MeOH): λ<sub>max</sub> = 271nm (ε=100), 213nm (ε=1150)

## 19. Triphenyl-2-propenylsilane

Triphenylchlorosilane (13.25g; 0.045mol) dissolved in anhydrous THF (30ml) was added dropwise with stirring under argon to allylmagnesium bromide (50ml; 1M solution in Et<sub>2</sub>O; 0.050mol). After stirring at room temperature overnight the reaction mixture was quenched by pouring into cold ammonium chloride solution. The separated organic layer was dried (sodium sulphate) and the solvent was evaporated to give 10g (74%) of triphenyl-2-propenylsilane which was recrystallised from ethanol with mp 81-82°C (lit mp 84-84°C; Henry and Noltes, 1960).

### Analysis

<sup>1</sup>H NMR:            2.40 (d, 2H), 4.90 (d, 2H), 5.90 (m, 1H), 7.10-  
                      7.70 (m, 15H)

IR:                    1626 (m), C=C stretch  
                      1426 (s), 1112 (s), Ph-Si stretching  
                      893 (s), =CH<sub>2</sub> out of plane bending  
                      733 (s), 699 (s), monosubstituted benzene

UV (EtOH):         $\lambda_{\max} = 270\text{nm}$  ( $\epsilon=650$ )

MS:                    M<sup>+</sup> 300

CHN:                    Calculated for C<sub>21</sub>H<sub>20</sub>Si

Required	C 83.94	H 6.71
Found	C 83.87	H 6.75

## 20. Tri-*n*-butyl-2-propenylstannane

Magnesium turnings (3.6g;0.14mol) and anhydrous ether (50ml) were placed under argon. A solution of allyl bromide (8ml;0.09mol) in anhydrous ether (15ml) was placed in the dropping funnel. A 1-2ml portion of the allyl bromide solution was added into the reaction flask. A temperature rise and cloudiness indicated that the reaction had commenced. The remainder of the allyl bromide solution was added dropwise with continued stirring at such a rate as to maintain a gentle reflux. After complete addition which required approximately 1.5h, the mixture was refluxed for a further 1.5h. During reflux the dropping funnel was charged with bis(tri-*n*-butyltin)oxide (18g;0.03mol) in anhydrous ether (30ml). After reflux, heating was stopped and the bis(tri-*n*-butyltin)oxide solution was added at such a rate as to maintain the temperature between 36-38°C. The reaction mixture was refluxed for 1.5h and then stirred at room temperature overnight. The reaction mixture was cooled in an ice bath and quenched with saturated ammonium chloride solution. The supernatant solution was decanted through glass wool on to 20g of ice in a separating funnel. The residual solids were washed with three portions of hexane and the washes were decanted into the separating funnel.

After the phases were separated the aqueous phase was washed with an additional portion of hexane. The combined organic extracts were washed with saturated ammonium chloride solution (50ml) and then with brine (50ml). The organic layer was dried (magnesium sulphate) filtered, and concentrated. Bulb to bulb distillation gave 11.0g (56%) yield with bp 50°C/0.02mm (lit bp 89°C/0.3mm; Schwartz and Post, 1964).

### Analysis

<sup>1</sup>H NMR: 0.50-1.70 (m, 29H), 5.00-5.60 (m, 3H)

IR: 3076 (w), C-H stretch of =CH<sub>2</sub> group  
2956 (s), C-H asymmetric stretch of CH<sub>3</sub> group  
2924 (s), C-H asymmetric stretch of CH<sub>2</sub> group  
2871 (s), C-H symmetric stretch of CH<sub>3</sub> group  
2854 (s), C-H symmetric stretch of CH<sub>2</sub> group  
1620 (m), C=C stretch  
877 (m), =CH<sub>2</sub> out of plane bending

UV (EtOH):  $\lambda_{\max} = 240\text{nm}$  ( $\epsilon=5000$ )

MS:

M<sup>+</sup> 332, 330, 328 (<sup>120</sup>Sn, <sup>118</sup>Sn, <sup>116</sup>Sn respectively)  
291, 289, 287; Sn(*n*-butyl)<sub>3</sub><sup>+</sup> (<sup>120</sup>Sn, <sup>118</sup>Sn, <sup>116</sup>Sn respectively)  
235, 233, 231; SnH(*n*-butyl)<sub>2</sub><sup>+</sup> (<sup>120</sup>Sn, <sup>118</sup>Sn, <sup>116</sup>Sn respectively)  
177, 175, 173; Sn(*n*-butyl)<sup>+</sup> (<sup>120</sup>Sn, <sup>118</sup>Sn, <sup>116</sup>Sn respectively)

121, 119, 117; SnH<sup>+</sup> (<sup>120</sup>Sn, <sup>118</sup>Sn, <sup>116</sup>Sn respectively)

41; C<sub>3</sub>H<sub>5</sub><sup>+</sup>

<sup>13</sup>C NMR:

3	2	1	Sn	a	b	c	d
109.1	138.2	16.2		9.1	29.1	27.4	13.7

### 21. 2-butenyltri-*n*-butylstannane

This compound was prepared by the method described in experiment 3, using crotylchloride (4.34g; 4.70ml; 0.048mol), chlorotri-*n*-butylstannane (13.0g; 10.8ml; 0.040mol), magnesium turnings (1.25g; 0.052mol), and 1,2-dibromoethane (0.5ml) with irradiation of ultrasound for 2h. Bulb to bulb distillation gave 9.5g (69%) yield of the trans isomer with bp 90°C/0.05mm.

#### Analysis

<sup>1</sup>H NMR: 0.40-2.10 (m, 32H), 4.90-5.70 (m, 2H)

IR: 2959 (s), C-H asymmetric stretch of CH<sub>3</sub> group  
2923 (s), C-H asymmetric stretch of CH<sub>2</sub> group  
2871 (s), C-H symmetric stretch of CH<sub>3</sub> group  
2854 (s), C-H symmetric stretch of CH<sub>2</sub> group  
1594 (m), C=C stretching  
1462 (m), 1376 (m), C-H deformation

UV (EtOH):  $\lambda_{\text{max}} = 264\text{nm}$  ( $\epsilon=70$ )

MS:  $M^+$  346 ( $^{120}\text{Sn}$ )

291,289,287;  $\text{Sn}(n\text{-butyl})_3^+$  ( $^{120}\text{Sn}$ ,  $^{118}\text{Sn}$ ,  $^{116}\text{Sn}$  respectively)

235,233,231;  $\text{SnH}(n\text{-butyl})_2^+$  ( $^{120}\text{Sn}$ ,  $^{118}\text{Sn}$ ,  $^{116}\text{Sn}$  respectively)

177,175,173;  $\text{Sn}(n\text{-butyl})^+$  ( $^{120}\text{Sn}$ ,  $^{118}\text{Sn}$ ,  $^{116}\text{Sn}$  respectively)

121,119,117;  $\text{SnH}^+$  ( $^{120}\text{Sn}$ ,  $^{118}\text{Sn}$ ,  $^{116}\text{Sn}$  respectively)

55;  $\text{C}_4\text{H}_7^+$

## 22. Tri-*n*-butyl(2-methyl-2-propenyl)stannane

This compound was prepared by the method described in experiment 3, using 3-chloro-2-methylpropene (4.34g; 4.70ml; 0.048mol), chlorotri-*n*-butylstannane (13.0g; 10.8ml; 0.040mol), magnesium turnings (1.25g; 0.052mol), and 1,2-dibromoethane (0.5ml) with irradiation of ultrasound for 2h. Bulb to bulb distillation gave 8.5g (62%) yield with bp 89°C/0.10mm (lit bp 121-122°C/4mm; Naruta, 1980).

### Analysis

$^1\text{H}$  NMR: 0.50-2.10 (m, 35H), 5.20 (t, 1H)

IR: 3072 (m), C-H stretch of =CH<sub>2</sub> group  
2955 (s), C-H asymmetric stretch of CH<sub>3</sub> group  
2921 (s), C-H asymmetric stretch of CH<sub>2</sub> group  
2871 (s), C-H symmetric stretch of CH<sub>3</sub> group

2853 (s), C-H symmetric stretch of CH<sub>2</sub> group  
 1627 (m), C=C stretching  
 1461 (m), 1375 (m), C-H deformation  
 860 (m), CH<sub>2</sub> out of plane deformation

UV (EtOH):  $\lambda_{\max} = 245\text{nm}$  ( $\epsilon=6000$ )

MS:

$M^+$  346 (<sup>120</sup>Sn)  
 291, 289, 287; Sn(*n*-butyl)<sub>3</sub><sup>+</sup> (<sup>120</sup>Sn, <sup>118</sup>Sn, <sup>116</sup>Sn respectively)  
 235, 233, 231; SnH(*n*-butyl)<sub>2</sub><sup>+</sup> (<sup>120</sup>Sn, <sup>118</sup>Sn, <sup>116</sup>Sn respectively)  
 179, 177, 175; SnH<sub>2</sub>(*n*-butyl)<sup>+</sup> (<sup>120</sup>Sn, <sup>118</sup>Sn, <sup>116</sup>Sn respectively)  
 121, 119, 117; SnH<sup>+</sup> (<sup>120</sup>Sn, <sup>118</sup>Sn, <sup>116</sup>Sn respectively)  
 55; CH<sub>2</sub>=C(CH<sub>3</sub>)CH<sub>2</sub><sup>+</sup>

<sup>13</sup>C NMR:

4	3	2	1	Sn	a	b	c	d
25.0	105.6	146.3	20.6		9.4	29.1	27.4	13.7

### 23. Tri-*n*-butyl(3-methyl-2-butenyl) stannane

This compound was prepared by the method described in experiment 3, using 1-chloro-3-methyl-2-butene (5.0g; 0.048mol), chlorotri-*n*-butylstannane (13.0g; 10.8ml; 0.040mol), magnesium turnings (1.25g; 0.052mol), and 1,2-dibromoethane (0.5ml) with irradiation of ultrasound for 2h. Bulb to bulb distillation

gave 11.0g (77%) yield with bp 93°C/0.01mm (lit bp 114-116°C/1mm; Naruta, 1980).

### Analysis

<sup>1</sup>H NMR: 0.70-1.70 (m, 35H), 5.30 (m, 1H)

IR: 2957 (s), C-H asymmetric stretch of CH<sub>3</sub> group  
2921 (s), C-H asymmetric stretch of CH<sub>2</sub> group  
2871 (s), C-H symmetric stretch of CH<sub>3</sub> group  
2852 (s), C-H symmetric stretch of CH<sub>2</sub> group  
1659 (w), C=C stretching  
1462 (m), 1375 (m), C-H deformation

MS:

M<sup>+</sup> 360, 358, 356 (<sup>120</sup>Sn, <sup>118</sup>Sn, <sup>116</sup>Sn respectively)  
291, 289, 287; Sn(n-butyl)<sub>3</sub><sup>+</sup> (<sup>120</sup>Sn, <sup>118</sup>Sn, <sup>116</sup>Sn respectively)  
235, 233, 231; SnH(n-butyl)<sub>2</sub><sup>+</sup> (<sup>120</sup>Sn, <sup>118</sup>Sn, <sup>116</sup>Sn respectively)  
179, 177, 175; SnH<sub>2</sub>(n-butyl)<sup>+</sup> (<sup>120</sup>Sn, <sup>118</sup>Sn, <sup>116</sup>Sn respectively)  
121, 119, 117; SnH<sup>+</sup> (<sup>120</sup>Sn, <sup>118</sup>Sn, <sup>116</sup>Sn respectively)  
69; C<sub>5</sub>H<sub>9</sub><sup>+</sup>

UV (EtOH): λ<sub>max</sub> = 263nm (ε=160)

<sup>13</sup>C NMR:

5 4 3 2 1 Sn a b c d

10.7 26.0 125.3 123.0 17.4 9.5 29.3 27.4 13.7

24. Tri-*n*-butyl(3-phenyl-2-propenyl)stannane

Cinnamyl chloride (7.3g;0.048mol) in anhydrous THF (15ml) was added dropwise under argon with external irradiation of ultrasound to a mixture of chlorotri-*n*-butylstannane (13g;10.8ml;0.040mol), magnesium turnings (0.25g;0.052mol), and 1,2-dibromoethane (0.5ml) in anhydrous THF (20ml). After 2h irradiation the reaction was quenched with saturated aqueous ammonium chloride solution. The resultant solution was washed with ether and the combined organic extracts were dried (magnesium sulphate) and evaporated. Bulb to bulb distillation gave 7.3g (44%) yield of the trans isomer with bp 162°C/0.5mm (lit bp 163-166/0.4mm; Naruta, 1980).

Analysis

<sup>1</sup>H NMR: 0.70-2.10 (m,29H), 4.20 (d,2H), 7.30 (s,5H)

IR: 2957 (s), C-H asymmetric stretch of CH<sub>3</sub> group  
2921 (s), C-H asymmetric stretch of CH<sub>2</sub> group  
2871 (s), C-H symmetric stretch of CH<sub>3</sub> group  
2852 (s), C-H symmetric stretch of CH<sub>2</sub> group  
1640 (m), C=C stretching of allyl group  
1600 (m), 1496 (m), C=C stretching (aromatic)  
957 (s), *trans* CH=CH

UV (MeOH):  $\lambda_{\max} = 268\text{nm}$

MS:  $M^+ = 408$  ( $^{120}\text{Sn}$ )

291, 289, 287;  $\text{Sn}(n\text{-butyl})_3^+$  ( $^{120}\text{Sn}$ ,  $^{118}\text{Sn}$ ,  $^{116}\text{Sn}$  respectively)

235, 233, 231;  $\text{SnH}(n\text{-butyl})_2^+$  ( $^{120}\text{Sn}$ ,  $^{118}\text{Sn}$ ,  $^{116}\text{Sn}$  respectively)

179, 177, 175;  $\text{SnH}_2(n\text{-butyl})^+$  ( $^{120}\text{Sn}$ ,  $^{118}\text{Sn}$ ,  $^{116}\text{Sn}$  respectively)

121, 119, 117;  $\text{SnH}^+$  ( $^{120}\text{Sn}$ ,  $^{118}\text{Sn}$ ,  $^{116}\text{Sn}$  respectively)

## 25. [(4-ethenylphenyl)methyl]trimethylsilane

Lithium diisopropylamide (10.7g; 0.1 mol) was obtained as a solid and transferred to a reaction vessel under nitrogen in an Atmosbag (Aldrich). THF (80ml) was added under nitrogen and the mixture was stirred for a few minutes. Then 4-methylstyrene (11.8g; 0.1 mol) was added dropwise, when the mixture turned yellow. After complete addition chlorotrimethylsilane (10.9g; 0.1 mol) in anhydrous THF (60ml) was dropped slowly into the stirred mixture for 3h at room temperature. On complete addition the mixture was stirred for a further 1h. The THF was evaporated and the residue was distilled to give 6.7g (35%) yield with bp  $55^\circ\text{C}/0.3\text{mm}$  (lit bp  $48^\circ\text{C}/0.15\text{mm}$ ; Reynolds et al, 1977).

### Analysis

$^1\text{H}$  NMR: relative to  $\text{SiMe}_3$ ; 0.00 (s, 9H), 2.20 (s, 2H),

5.00-5.70 (m, 2H), 6.40-6.70 (m, 1H), 7.00-7.30  
(m, 4H)

IR: 3088 (w), C-H stretching of =CH<sub>2</sub> group  
3050 (w), C-H stretching of =CH- group  
2956 (s), C-H asymmetric stretch of CH<sub>3</sub> group  
  
2899 (m), C-H symmetric stretch of CH<sub>3</sub> group  
1629 (m), 1608 (m), C=C stretching (lit 1633  
and 1608; Reynolds et al, 1977)  
1252 (vs), Si-C stretch of SiMe<sub>3</sub> group

MS: M<sup>+</sup> 190, 117 (CH<sub>2</sub>=CH-C<sub>6</sub>H<sub>4</sub>CH<sub>2</sub><sup>+</sup>), 73 (SiMe<sub>3</sub><sup>+</sup>; base  
peak)

## 26. Hexamethyldisilane

To a suspension of lithium in oil (58.14g; 30% dispersion containing 1% sodium; 2.50mol) was added anhydrous THF (98ml). The resulting mixture was degassed with nitrogen through a gas dispersion tube for 15min. The condenser was charged with dry ice/acetone. A slow stream of nitrogen was passed through the reaction mixture and chlorotrimethylsilane (161.2ml; 1.25mol) was added in one portion via a funnel. The reaction mixture was stirred at room temperature for 15min and then refluxed for 8h. Diatomaceous earth was added to the cooled reaction mixture and the resultant mixture was filtered through the

additional diatomaceous earth. The filter cake was washed well with ether (unreacted lithium was destroyed by cautious addition of methanol prior to discarding the filter cake.) The combined filtrate and ether washings were washed with water, dried with magnesium sulphate, and decanted into a flask fitted with a receiver cooled in a bath of dry ice/acetone. The mixture was distilled at 160°C (bath temperature) and atmospheric pressure until the mineral oil residue was shown to be free of product by glc analysis.

#### Analysis

<sup>1</sup>H NMR: 0.05 (s)

IR: 2952 (vs), C-H asymmetric stretch  
2894 (s), C-H symmetric stretch  
1246 (vs), Si-C stretch of SiMe<sub>3</sub> group  
834 (s), Si-C stretch of SiMe<sub>3</sub> group

UV (MeOH):  $\lambda_{\max}$  = 270nm ( $\epsilon=50$ ), 209nm ( $\epsilon=500$ )

#### **27. Trimethyl[(2-naphthalenyloxy)methyl]silane**

Dimethylsulphoxide (100ml; anhydrous) was added to NaH (4.0g; 60% in oil; 0.1mol; obtained by washing with anhydrous ether [3 times 50ml] under argon). To this suspension was added 2-naphthol (14.4g; 0.1mol) in anhydrous DMSO (100ml)

and the mixture was stirred at room temperature overnight. Then chloromethyltrimethylsilane (13.9ml; 0.1mol) was added and stirring was continued for 8h. After hydrolysis with water and extraction with ether, the ether layer was washed several times with water, dried ( $\text{MgSO}_4$ ), and concentrated. Recrystallisation of the residue from ethanol gave 14.0g (61%) yield with mp  $35^\circ\text{C}$ .

### Analysis

$^1\text{H}$  NMR: relative to  $\text{SiMe}_3$ ; 0.00 (s, 9H), 3.40 (s, 2H),  
6.95-7.40 (m, 7H)

IR: 3059 (s), aromatic C-H stretch  
2957 (s), 2895 (s), 2820 (m), aliphatic C-H  
stretching  
1250 (s), Si-C stretch of  $\text{SiMe}_3$  group  
1118 (s), C-O stretch

MS:  $\text{M}^+$  230, 141 (base peak;  $\text{C}_{11}\text{H}_9^+$ ), 73 ( $\text{SiMe}_3^+$ )

UV (EtOH):  $\lambda_{\text{max}} = 325\text{nm}$  ( $\epsilon=1600$ )

### 28. Diphenyliodonium hexafluorophosphate

(Crivello and Lam, 1978; Crivello and Lam, 1979)

A mixture of  $\text{KIO}_3$  (100g; 0.46 mol), acetic anhydride (200

ml), and benzene (90 ml; 1.0 mol), was placed into a flask equipped with a mechanical stirrer and a condenser and cooled to  $-5^{\circ}\text{C}$  (dry ice/acetone). Then conc.  $\text{H}_2\text{SO}_4$  (70 ml) was added dropwise with stirring over a period of 3h during which time the temperature was maintained at  $-5^{\circ}\text{C}$ . When the addition was complete the mixture was stirred for a further 2.5h at  $-5^{\circ}$  to  $0^{\circ}\text{C}$  and then allowed to reach room temperature and left standing overnight. Distilled water (400 ml) was slowly added to hydrolyse the remaining acetic anhydride. Then a slight excess of  $\text{KPF}_6$  in water (200 ml) was added and the mixture was stirred for 1h to complete the double decomposition. The organic layer was separated and the aqueous layer was washed with benzene (2 x 100ml). The organic layers were combined and the product was precipitated by the addition of ether, filtered off, and recrystallised twice from IPA to give 49.0g (25%) yield with mp  $191-192^{\circ}\text{C}$ .

### Analysis

$^1\text{H}$  NMR: 7.60-8.40 (m)

IR: 3095 (m), 3058 (m), aromatic C-H stretching  
1580 (m), 1564 (s), C=C stretching  
741 (s), 700 (w), monosubstituted benzene

UV (EtOH):  $\lambda_{\text{max}} = 266\text{nm}$  ( $\epsilon=2400$ )

MS: 204 (PhI<sup>+</sup>), 127 (I<sup>+</sup>), 77 (C<sub>6</sub>H<sub>5</sub><sup>+</sup>)

CHN: Calculated for C<sub>12</sub>H<sub>10</sub>F<sub>6</sub>IP

Required C 33.83 H 2.37

Found C 33.59 H 2.38

### 29. Triphenylsulphonium hexafluorophosphate

(Crivello and Lam, 1978)

A mixture of diphenyliodonium hexafluorophosphate (10.15g; 0.025 mol), diphenylsulphide (4.66g; 0.025 mol), and copper (II) benzoate (0.2g; 0.0006 mol) was heated with stirring under argon for 3h (oil bath temperature 120°C). On cooling the crystalline material was collected by filtration and washed several times with ether to remove iodobenzene and then air-dried. The fawn coloured crystals were recrystallised from 95% ethanol/water to give 6.1g (60%) yield of colourless needles with mp 193-194°C.

#### Analysis

<sup>1</sup>H NMR: 7.85 (s)

IR: 3099 (w), aromatic C-H stretch

1585 (w), C=C stretch

752 (s), 704 (w), monosubstituted benzene

UV (EtOH):  $\lambda_{\max}$  = 275nm ( $\epsilon=2900$ ), 268nm ( $\epsilon=3900$ )

MS: 186 ( $\text{Ph}_2\text{S}^+$ ), 77 ( $\text{C}_6\text{H}_5^+$ ), 32 ( $\text{S}^+$ )

CHN: Calculated for  $\text{C}_{18}\text{H}_{15}\text{F}_6\text{PS}$

Required	C	52.94	H	3.70
----------	---	-------	---	------

Found	C	53.17	H	3.84
-------	---	-------	---	------

## 2.8 References

Bach, R.D., and Scherr, P.A., (1973). *Tet.Lett.*, 1099

Benkesser, R.A., and Smith, W.E., (1969). *J.Am.Chem.Soc.*,  
91, 1556

Benkeser, R.A., Gaul, J.M., and Smith, W.E., (1969).  
*J.Am.Chem.Soc.*, 91, 3666

Bey, A.E., and Weyenberg, D.R., (1966). *J.Org.Chem.*, 31,  
2036

Bock, H., and Alt, H., (1969). *Chem.Ber.*, 102, 1534

Bock, H., Mollère, P., Becker, G., and Fritz, G., (1972).  
*J.Organomet.Chem.*, 46, 89

Borg, R.M., and Mariano, P.S., (1986). *Tet.Lett.*, 27, 2821

Boschi, R., Lappert, M.F., Pedley, J.B., Schmidt, W., and  
Wilkins, B.T., (1973). *J.Organomet.Chem*, 50, 69

Bowser, R., & Davidson, R.S., (1992) 'Current Trends in  
*Sonochemistry*', Royal Society of Chemistry, Ed. G.J. PRICE,  
50-58

Bullpitt, M., Kitching, W., Adcock, W., and Doddrell, D.,  
(1976). *J.Organomet.Chem.*, 116, 187

Butcher, E., Rhodes, C.J., Standing, M., Davidson, R.S., and Bowser, R., (1992). *J.Chem.Soc., Perkin II*, 1469

Bygden, A., (1912). *Berichte*, **45**, 707

Calas, R., and Dunogués, J., (1976). *J.Organomet.Chem.Rev.*, **2**, 277

Chan, T.H., and Fleming, I., (1979). *Synthesis*, 761

Chen, S., Ullrich, J.W., and Mariano, P.S., (1983). *J.Am.Chem.Soc.*, **105**, 6160

Cohen, S.G., Parola, A.H., and Parsons, G.H., (1973). *Chem.Rev.*, **73**, 141

Colvin, E., (1981). "Silicon in Organic Synthesis", Butterworths, London

Crivello, J.V., and Lam, J.H.W., (1978). *J.Org.Chem.*, **43**, 3055

Crivello, J.V., and Lam, J.H.W., (1979). *J.Polym.Sci., Polym.Chem.Edn.*, **17**, 977

Davidson, R.S., (1975). "Molecular Association", (ed) Foster, R., Academic Press, London, **1**, 216

Davidson, R.S., and Trethewey, K.R., (1975). *Chem.Commun.*,

- Davidson, R.S., (1983). "Advances in Physical Organic Chemistry", (eds.) Bethel, D., and Gold, V., Academic Press, London, 19, 1
- Davies, A.G., Roberts, B.P., and Smith, J.M., (1970). *Chem. Commun.*, 557
- Davies, A.G., Roberts, B.P., and Smith, J.M., (1972). *J. Chem. Soc., Perkin II*, 2221
- Davies, A.G., (1977). *Proceedings A.M.P.E.R.E. Colloq. CNRS, Organic Free Radicals, Aix-en-Provence*
- Dinnocenzo, J.P., Farid, S., Goodman, J.L., Gould, I.R., Todd, W.P., and Mattes, S.L., (1989). *J. Am. Chem. Soc.*, 111, 8973
- Eaborn, C., and Parker, S.H., (1955). *J. Chem. Soc.*, 126
- Eaborn, C., and Shaw, R.A., (1955). *J. Chem. Soc.*, 1420
- Eaborn, C., (1956). *J. Chem. Soc.*, 4858
- Eaton, D.F., (1979). *Photog. Sci. Eng.*, 23, 150
- Eaton, D.F., (1980a). *J. Am. Chem. Soc.*, 102, 3278

- Eaton, D.F., (1980b). *J.Am.Chem.Soc.*, **102**, 3280
- Eaton, D.F., (1981). *J.Am.Chem.Soc.*, **103**, 7235
- Egorov, Yu.P., Leites, L.A., Tolstikova, N.G., and Tschernyshev, E.A., (1961). *Izv.Akad.Nauk USSR, Ser.Khim.*, 445
- Evans, S., Green, J.C., Joachim, P.J., Orchard, A.F., Turner, D.W., and Maier, J.P., (1979). *J.Chem.Soc., Faraday Trans.2*, **68**, 905
- Gatechair, L.R., and Pappas, S.P., (1983). *ACS Symposium Series*, **212**, 173
- George, M.V., Peterson, D.J., and Gilman, H., (1960). *J.Am.Chem.Soc.*, **82**, 403
- Hageman, H.J., (1985). *Progress in Organic Coatings*, **13**, 123
- Hanstein, W., Berwin, H.J., and Traylor, T.G., (1970a). *J.Amer.Chem.Soc.*, **92**, 829
- Hanstein, W., Berwin, H.J., and Traylor, T.G., (1970b). *J.Amer.Chem.Soc.*, **92**, 7476
- Hauser, C.R., and Hance, C.R., (1951). *J.Am.Chem.Soc.*, **73**, 5846

- Hayashi, T., Katsuro, Y., Okamoto, Y., and Kumada, M., (1981). *Tet.Lett.*, **22**, 4449
- Henry, M.C., and Noltes, J.G., (1960). *J.Am.Chem.Soc.*, **82**, 555
- Hilinski, E.F., Huppert, D., Kelley, D.F., Milton, S.V., and Rentzepis, P.M., (1984). *J.Amer.Chem.Soc.*, **106**, 1951
- Hosomi, A., and Traylor, T.G., (1975). *J.Amer.Chem.Soc.*, **97**, 3682
- Hudrilik, P.F., Waugh, M.A., & Hudrilik, A.M., (1984) *J. Organomet. Chem.*, **271**, 69
- Johnston, L.J., and Scaiano, J.C., (1985). *J.Amer.Chem.Soc.*, **107**, 6368
- Ketley, A.D., and Tsao, J-H, (1979). *J.Rad.Curing*, **22**
- Kira, M., Yoshida, H., and Sakurai, H., (1985). *J.Amer.Chem.Soc.*, **107**, 7767
- Koizumi, T., Fuchigami, T., and Nonaka, T., (1989). *Bull.Chem.Soc.Jpn.*, **62**, 219
- Kyushin, S., Nakadaira, Y., & Ohashi, M., (1990) *Chem.Letts.*, 2191

Lan, A.J.Y., Quillen, S.L., Heuckeroth, R.O., and Mariano, P.S., (1987). *J.Am.Chem.Soc.*, **106**, 6439

Lan, A.J.Y., Heuckeroth, R.O., and Mariano, P.S., (1984). *J.Am.Chem.Soc.*, **109**, 2738

Leites, L.A., (1963). *Izv.Akad.Nauk USSR, Ser.Khim.*, 1525

Lyons, A.R., and Symons, M.C.R., (1971). *Chem.Comm.*, 1068

Maruyama, K., Imahori, H., Osuka, A., Takuwa, A., and Tagawa, H., (1986). *Chem.Lett.*, 1719

Maruyama, K., and Imahori, H., (1989). *Bull.Chem.Soc.Jpn.*, **62**, 816

Mizuno, K., Ikeda, M., and Otsuji, Y., (1985a). *Tet.Lett.*, **26**, 461

Mizuno, K., Terasaka, K., Ikeda, M., and Otsuji, Y., (1985b). *Tet.Lett.*, **26**, 5819

Mizuno, K., Toda, S., and Otsuji, Y., (1987). *Chem.Lett.*, 203

Mizuno, K., Terasaka, K., Yasueda, M., and Otsuji, Y., (1988a). *Chem.Lett.*, 145

Mizuno, K., Ikeda, M., and Otsuji, Y., (1988b). *Chem.Lett.*,

Mizuno, K., Nakanishi, K., and Otsuji, Y., (1988c).  
*Chem.Lett.*, 1833

Moore, C.J., and Kitching, W., (1973). *J.Organomet.Chem.*,  
59, 225

Naruta, Y., (1980). *J.Am.Chem.Soc.*, 102, 3774

Naruta, Y., Nishigaichi, Y., and Maruyama, K., (1986).  
*Chem.Lett.*, 1857

Nesmeyanov, A.N., and Kritskaya, I.I., (1958).  
*Dokl.Akad.Nauk SSSR*, 121, 447

Neumann, W.P., Niermann, H., and Sommer, R., (1961).  
*Angew.Chem.*, 73, 768

Ohga, K., and Mariano, P.S., (1982). *J.Am.Chem.Soc.*, 104,  
617

Petrov, A.D., Egorov, Yu.P., Mironov V.F., Nikishkin, G.I.,  
and Bulgakova, A.A., (1956). *Izv.Akad.Nauk USSR, Ser.Khim.*,  
50

Pitt, C.G., (1970). *J.Organomet.Chem.*, 23, C35

Pitt, C., and Bock, H., (1972). *J.Chem.Soc., Chem.Commun.*,

Reynolds, W.F., Hamer, G.K., and Bassindale, A.R., (1977).  
*J.Chem.Soc., Perkin II*, 971

Roberts, R.M.G., and Kaissi, F.El, (1968).  
*J.Organomet.Chem.*, 12, 79

Sankararaman, S., & Kochi, J.K., (1989). *J.Chem.Soc., Chem. Commun.* , 1800

Sarkar, T.K., (1990a). *Synthesis*, 969

Sarkar, T.K., (1990b). *Synthesis*, 1101

Schwartz, W.T., and Post, H.W., (1964). *J.Organomet.Chem.*,  
2, 357

Schweig, A., Weidner, U., and Manuel, G., (1973a).  
*J.Organomet.Chem.*, 67, C4

Schweig, A., Weidner, U., and Manuel, G., (1973b).  
*J.Organomet.Chem.*, 54, 145

Seyferth, D., and Weiner, M.A., (1961). *J.Org.Chem.*, 26,  
4797

Sirimanne, S.R., Li, Z., Vander Veer, D.R., and Talbot,  
L.M., (1991). *J.Am.Chem.Soc*, 113, 1766

- Slocum, G.H., Kaufmann, K., and Schuster, G.B., (1981).  
*J.Amer.Chem.Soc.*, 103, 4625
- Soundararajan, N., and Platz, M.S., (1987). *Tet.Letts.*, 28,  
2813
- Still, W.C., (1976). *J.Org.Chem.*, 41, 3063
- Sulpizio, A., Albini, A., Alessandro, N.D., Fasani, E., and  
Pietra, S., (1989). *J.Am.Chem.Soc.*, 111, 5773
- Takuwa, A., Tagawa, H., Iwamoto, H., Soga, O., and Maruyama,  
K., (1987). *Chem.Lett.*, 1091
- Takuwa, A., Fujii, N., Tagawa, H., and Iwamoto, H., (1989).  
*Bull.Chem.Soc.Jpn.*, 62, 336
- Takuwa, A., Nishigaichi, Y., Yamashita, K., and Iwamoto,  
H., (1990). *Chem.Lett.*, 639
- Takuwa, A., Nishigaichi, Y., and Iwamoto, H., (1991).  
*Chem.Lett.*, 1013
- Tamborski, C., Ford, F.E., and Soloski, E.J., (1963).  
*J.Org.Chem.*, 28, 237
- Traylor, T.G., and Ware, J.C., (1967). *J.Amer.Chem.Soc.*,  
89, 2304

Tu, C.L., and Mariano, P.S., (1987). *J.Am.Chem.Soc.*, **109**, 5287

Turro, N.J., (1978). "*Modern Molecular Photochemistry*", Benamin Cummings, Menlo Park, California

Valkovich, P.B., Ito, T.J., and Weber, W.P., (1974). *J.Org.Chem.*, **39**, 3543

Vedeneyev, V.I., Gurvich, L.V., Kondrat'yev, V.N., Medvedev, V.A., and Frankevich, Ye.L., (1966). "*Bond Energies, Ionisation Potentials and Electron Affinities*", Arnold, London

Weidner, U., and Schweig, A., (1972a). *J.Organomet.Chem.*, **39**, 261

Weidner, U., and Schweig, (1972b). *Angew.Chem.,Internat.Edit.Engl.*, **11**, 146

Wilkinson, G., Stone, F.G.A., and Abel, E.W. (eds) (1982). "*Comprehensive Organometallic Chemistry*", Pergamon Press

## **Chapter 3.**

# **PHOTOINITIATION OF FREE RADICAL POLYMERISATION USING ORGANOMETALLIC AMINES OF SILICON AND TIN**

### 3.1 Introduction

A number of organometallic amines of the general formula:



(where  $R' = \text{Me, Et}$ ;  $M = \text{Si, Sn}$ ;  $R = \text{Me, } n\text{-Bu, Ph}$ ;  $n = 1, 2, 3$ )

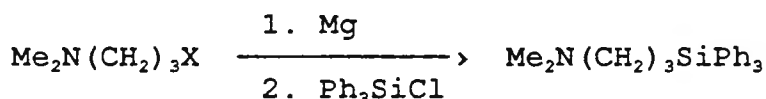
have been synthesised and tested for use as photoinitiators in free radical polymerisation reactions. It was of interest to determine how these electron donors behaved both on their own and in conjunction with sensitisers, such as electron acceptors, in free radical photopolymerisations. The rates of polymerisation have been determined using the technique of RTIR spectroscopy which has been described earlier (see section 1.7.2). From a mechanistic point of view both the formation and the subsequent fragmentation of the radical cations, formed in charge transfer schemes, were of interest and were probed using EPR spectroscopy (see section 1.7.4).

### 3.2 Previous synthetic routes

A number of routes exist for the synthesis of these compounds, but most of them require a multi-step procedure (Sato et al, 1976; Suggs and Lee, 1986). The most direct route for synthesising the stannylalkylamines involves the lithiation of tri-*n*-butyltin chloride at 0°C, followed by

reaction with an  $\alpha$ -dimethylamino- $\omega$ -haloalkane (Sato et al, 1976). Using this method 3-(N,N-dimethylamino)propyltri-*n*-butyltin was obtained in 18% yield.

It was decided to search for a more convenient synthetic route for a number of these compounds to obviate the necessity for the multi-step preparations which often involved the preparation of air and moisture sensitive intermediates. It was noted that a synthesis of  $\text{Ph}_3\text{Si}(\text{CH}_2)_3\text{NMe}_2$  using a Grignard reagent had been reported (US 3,853,994).

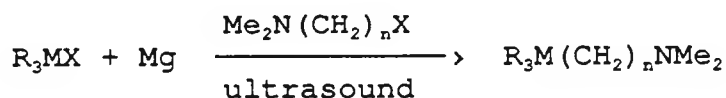


A similar procedure involving a Grignard reagent has also been reported for the synthesis of the analogous stannane  $\text{Me}_2\text{N}(\text{CH}_2)_3\text{SnPh}_3$  (Meganem, 1980). In a separate finding it had been reported that ultrasound could be used to effect the Barbier reaction (a modified Grignard procedure) for the preparation of allylstannanes (Naruta et al, 1986).

### 3.2.1 Synthetic routes used

This reaction was extended to prepare a number of allylic, benzylic, and naphthyllic silanes and stannanes, reported herein, and similar methodology was applied in the synthesis of aminoalkylsilanes and stannanes to illustrate further possibilities of ultrasound in synthetic organic chemistry (Bowser and Davidson, 1992). Using this procedure it has

been found that  $\alpha$ -dimethylamino- $\omega$ -chloroalkanes react with chlorotrimethylsilane and chlorotri-*n*-butylstannane to give reasonable yields of dimethylaminoalkyl-silanes and stannanes respectively in the presence of magnesium and with the application of ultrasound at room temperature.



R = Me, Bu, Ph; M = Si, Sn ; X = halogen ; n = 2, 3

This route has been employed to synthesise a number of silylalkylamines and stannylalkylamines using a 'one-pot' procedure with relatively short reaction times and reasonable yields as outlined below in table 3.1.

Table 3.1 The reaction times and yields of the synthesis of a number of dimethylaminoalkylsilanes and stannanes using ultrasound

COMPOUND	REACTION TIME <sup>a</sup> / hours	YIELD/ %
Me <sub>2</sub> N(CH <sub>2</sub> ) <sub>3</sub> SiMe <sub>3</sub>	4	37
Me <sub>2</sub> N(CH <sub>2</sub> ) <sub>3</sub> SnBu <sub>3</sub>	2	35
Me <sub>2</sub> N(CH <sub>2</sub> ) <sub>2</sub> SiPh <sub>3</sub>	4	40
Me <sub>2</sub> N(CH <sub>2</sub> ) <sub>2</sub> SnPh <sub>3</sub>	4	35
Me <sub>2</sub> N(CH <sub>2</sub> ) <sub>3</sub> SiPh <sub>3</sub>	4	30
Me <sub>2</sub> N(CH <sub>2</sub> ) <sub>2</sub> SnMe <sub>3</sub>	2	45

<sup>a</sup>= all reactions carried out at 25°C with THF as solvent.

What is immediately apparent from table 1 is that although the reaction yields are moderate the reaction times are significantly reduced when compared to the multi-step procedures mentioned earlier. The mechanism of the reaction is of interest since using the Barbier ultrasound route there is no prior formation of the alkyl metal halide unlike traditional Grignard procedures. In this case the haloalkylamine is added slowly to a solution of the trisubstituted metal halide and magnesium turnings. The haloalkylamine is added at such a rate as to form an *in-situ* Grignard reagent with the magnesium which immediately reacts with the excess trisubstituted metal halide to complete the reaction. In practice one cannot be sure if the sequence of events begins with the metallation of the silyl/stannyl chloride or whether the alkyl metal halide is formed and then reacts rapidly with the silyl/stannyl chloride. There is no doubt, however, that the success of the synthetic strategy depends upon the activation of magnesium by ultrasound.

### 3.3 Applications of alkylaminosilanes and stannanes

One area that these compounds have been investigated is in the base promoted reactions of quaternary ammonium salts, which include the Stevens rearrangement, the Sommelet-Hauser rearrangement, and the Hoffmann elimination (Pine, 1970). An early report on this type of reaction involved the



Later work has shown an improved Sommelet-Hauser rearrangement in non-basic media with the minimum formation of the Stevens rearrangement products (Nakano and Sato, 1985; Nakano and Sato, 1987). A number of these compounds, including  $\text{Bu}_3\text{Sn}(\text{CH}_2)_3\text{NMe}_2$ , have been found to exhibit fungicidal and bacteriological properties (Ger Offen 2,801,700). A similar claim was made of aminoalkylsilane derivatives which can be used as hypotensive agents (US 3,853,994). The aminoalkylsilanes and both their acid addition and quaternary ammonium salts have been shown to be useful since they possess pharmacological activity. In particular these compounds, such as  $\text{Ph}_3\text{Si}(\text{CH}_2)_3\text{NMe}_2$ , can act as mild tranquillisers when applied in a capsule or tablet form.

Another interesting application of these compounds that was investigated involved their use as antiknock additives in the combustion of engine fuels (Cullis et al, 1985).

### 3.4 Electron paramagnetic resonance (EPR) spectroscopy results

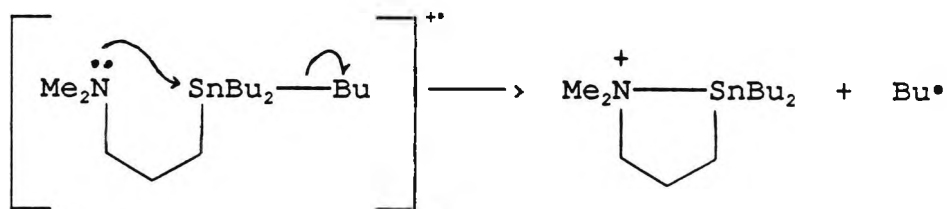
It is known that *t*-amines will form charge transfer complexes with suitable acceptors. This readiness to form such complexes can be attributed, in part, to the low oxidation potentials of *t*-amines. Similarly the organometallic amines synthesised are expected to be effective in charge transfer schemes due to the low oxidation potentials of these *t*-amines. Thus the oxidation

potential for  $\text{Me}_2\text{NCH}_2\text{SiMe}_3$ , has been calculated to be 8.20 eV (Bock et al, 1979) which renders this organometallic amine potentially useful in charge transfer schemes. It is expected that with a suitable acceptor charge transfer from the amine to the acceptor gives rise to the amine radical cations. It is of particular interest from a mechanistic point of view on determining the fragmentation pathways available to the radical cations so produced. This information can then be applied in the design of new photoactive compounds. One method that has been used to assess the role of the radical cations produced is epr spectroscopy. Epr spectroscopy was used in order to detect the formation and monitor the subsequent fragmentation of the radical cations of  $\text{Me}_2\text{N}(\text{CH}_2)_3\text{SnBu}_3$  and  $\text{Me}_2\text{N}(\text{CH}_2)_3\text{SiMe}_3$ . These compounds, in a solid fluorotrichloromethane matrix (77K), were exposed to  $\gamma$ -irradiation (1Mrad) using a  $^{60}\text{Co}$  source. Following the recording of the spectra at 77K the temperature of the matrix was gradually increased to the melting point of the matrix (160K) and spectra were recorded, wherever possible, of the breakdown products (Butcher et al, 1992a; Butcher et al, 1992b).

The epr spectra recorded at 77K for  $[\text{Me}_2\text{N}(\text{CH}_2)_3\text{SnBu}_3]^+$  can be assigned to *n*-butyl radicals as the sole paramagnetic product. This is a rather interesting contrast to the behaviour of the radical cation derived from tetra-*n*-butylstannane which under similar conditions, gave a stable radical cation and only a minor yield of *n*-butyl radicals. The functional change on going from the tetra-*n*-

butylstannane to  $\text{Me}_2\text{N}(\text{CH}_2)_3\text{SnBu}_3$  is formally remote with respect to the metal centre and yet the radical cation of the latter must be highly unstable to give fragmentation at 77K. This radical cation is probably not an energy minimum inferring that reorganisation of the molecular geometry occurs after ionisation and prior to the dissociation pathway. Consideration of the ionisation potential data (Vedeneyev et al, 1966) for  $\text{R}_3\text{N}$  and  $\text{R}_4\text{Sn}$  ( $\text{R} = \text{alkyl}$ ) compounds favours the electron loss as being from the tin unit and so the structure of the primary radical cation would be expected to be similar to that of  $[(n\text{-Bu})_4\text{Sn}^{+\cdot}]$ . It is proposed, therefore, that scheme 3.1 accounts for the behaviour and observed C-Sn bond cleavage of the radical cation giving rise to *n*-butyl radicals.

Scheme 3.1 The proposed fragmentation of  $[\text{Me}_2\text{N}(\text{CH}_2)_3\text{SnBu}_3]^{+\cdot}$  at 77K from epr spectroscopic evidence



Results for  $[\text{Me}_2\text{N}(\text{CH}_2)_3\text{SiMe}_3]^{+\cdot}$  indicate that the radical cation is observed as a normal nitrogen centred  $\pi$ -radical (Eastland et al, 1984) and is entirely stable up to the melting point of the matrix (160K). This result is in agreement with the ionisation potential data for  $\text{R}_3\text{N}$  and  $\text{R}_4\text{Si}$  compounds (Eastland et al, 1984) and with previous

mechanistic conjecture from the photochemical studies of compounds of this type (Hasegawa et al, 1988b).

### 3.5 UV curing results

#### 3.5.1 UV curing results of Et<sub>2</sub>NCH<sub>2</sub>SiMe<sub>3</sub>

Initially Et<sub>2</sub>NCH<sub>2</sub>SiMe<sub>3</sub> was synthesised and evaluated for potential use as an initiator of free radical polymerisation. The free radical initiating properties of this amine were tested by incorporation into a suitable monomer, TMPTA, both on its own and in conjunction with sensitisers. The results are presented below in table 3.2.

Table 3.2 UV curing results of the polymerisation of TMPTA using Et<sub>2</sub>NCH<sub>2</sub>SiMe<sub>3</sub> in the presence and absence of sensitisers

E X P T	INITIATING SYSTEM	% w/w in TMPTA	NUMBER OF PASSES
			In Air
1	Et <sub>2</sub> NCH <sub>2</sub> SiMe <sub>3</sub>	1.7	* <sup>a</sup>
2	Et <sub>2</sub> NCH <sub>2</sub> SiMe <sub>3</sub> + ITX	1.7 1.8	8 <sup>a</sup>
3	ITX	1.8	8 <sup>a</sup>
4	Et <sub>2</sub> NCH <sub>2</sub> SiMe <sub>3</sub> + DMC	1.9 0.8	35 <sup>b</sup>
5	DMC	0.8	55 <sup>b</sup>

ITX = mixture of 1-(and 2-)isopropylthioxanthone

DMC = 3-benzoyl-5,7-dimethoxycoumarin

a Belt speed = 10 ft/min

b Belt speed = 230 ft/min

When used on its own (EXPT 1) the amine did not effect polymerisation of TMPTA when tested in air in the UV Colordry apparatus. The incorporation of a sensitiser such as ITX did not give an enhanced cure rate (EXPT 2) when compared to the curing using ITX on its own (EXPT 3). When DMC was used as a sensitiser there was a small synergistic effect (EXPT 4) when compared to the result of DMC on its own (EXPT 5). This evidence is substantiated by an earlier claim that the photoaddition of  $\text{Et}_2\text{NCH}_2\text{SiMe}_3$  to 9,10-dicyanoanthracene (DCA) is inefficient (Hasegawa et al, 1988a). It was demonstrated that the photoaddition gave a variety of different products in low yields. It was proposed that the low efficiency of adduct formation might be due to a low rate of coupling of the  $\alpha$ -amino radical,  $\text{Et}_2\text{NCH}_2^\bullet$ , to a DCA-derived radical based on steric and electronic effects.

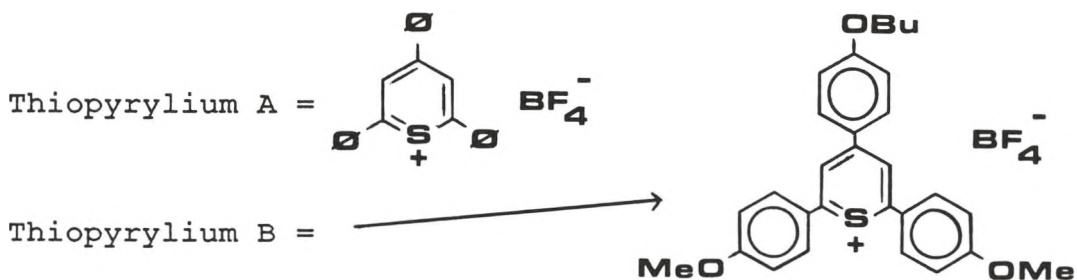
### 3.5.2 UV curing results of dimethylaminoalkylsilanes

In an attempt to reduce the steric bulk around the nitrogen two further amines,  $\text{Me}_2\text{NCH}_2\text{SiPh}_3$  and  $\text{Me}_2\text{N}(\text{CH}_2)_3\text{SiMe}_3$  were subsequently synthesised. Testing of the above compounds both with and without sensitisers showed that they could be effective in free radical polymerisation as seen from the

results in table 3.3.

**Table 3.3** UV curing results of dimethylaminoalkylsilanes in the presence and absence of sensitisers

E X P T	INITIATOR	NUMBER OF PASSES			
		Touching Quartz	Touching Glass	In Air	Glass Filter
1	Me <sub>2</sub> NCH <sub>2</sub> SiPh <sub>3</sub>	1	2	*	*
2	Me <sub>2</sub> N(CH <sub>2</sub> ) <sub>3</sub> SiMe <sub>3</sub>	1	11	*	*
3	Me <sub>2</sub> N(CH <sub>2</sub> ) <sub>3</sub> SiMe <sub>3</sub> + thiopyrylium A	1	5	*	*
4	thiopyrylium A	7	23	*	*
5	Me <sub>2</sub> N(CH <sub>2</sub> ) <sub>3</sub> SiMe <sub>3</sub> + thiopyrylium B	1	3	*	*
6	thiopyrylium B	3	6	*	*
7	Me <sub>2</sub> N(CH <sub>2</sub> ) <sub>3</sub> SiMe <sub>3</sub> + DCA	4	15	*	*
8	DCA	6	15	*	*

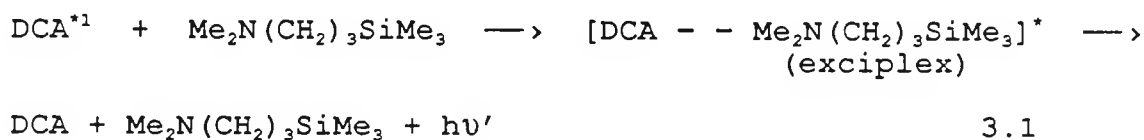


DCA = 9,10-dicyanoanthracene

Belt speed = 10 ft/min for all experiments

The results indicate that these compounds could be effective in radical polymerisations as evidenced by the sensitised polymerisation using the thiopyrylium salts (EXPT's 3 & 5).

When the amine  $\text{Me}_2\text{N}(\text{CH}_2)_3\text{SiMe}_3$  was used with DCA (EXPT 7) a decrease in the rate of polymerisation was noticed when compared to the amine in the absence of any sensitiser (EXPT 2). This can be explained by the collapse of the exciplex formed during irradiation with regeneration of the starting materials as depicted in equation 3.1.



Thus the amine quenches the fluorescence of DCA without formation of any reactive intermediates. This explanation would also support the fact that Mariano and co-workers observed a low yield of photoaddition products in the reaction of  $\text{Et}_2\text{NCH}_2\text{SiMe}_3$  with DCA (Hasegawa *et al*, 1988a).

### 3.5.3 UV curing results of dimethylaminoalkylsilanes and stannanes

An investigation into the initiating properties of the amines used on their own in a free radical polymerisable monomer, TMPTA, was investigated using the UV Colordry apparatus described earlier. The results are presented below in table 3.4.

Table 3.4 UV curing results for a number of dimethylaminoalkyl- silanes and stannanes (1% w/w) in TMPTA

E X P E R I M E N T	INITIATOR	NUMBER OF PASSES			
		Touching Quartz	Touching Glass	In Air	Glass Filter
1	Me <sub>2</sub> NCH <sub>2</sub> SiPh <sub>3</sub>	1	2	*	*
2	Me <sub>2</sub> N(CH <sub>2</sub> ) <sub>3</sub> SiMe <sub>3</sub>	1	2	*	*
3	"	2 <sup>a</sup>	8 <sup>a</sup>	-	-
4	Me <sub>2</sub> N(CH <sub>2</sub> ) <sub>3</sub> SiPh <sub>3</sub>	4	12	*	*
5	Me <sub>2</sub> N(CH <sub>2</sub> ) <sub>3</sub> SnBu <sub>3</sub>	1	3	*	*
6	"	7 <sup>a</sup>	24 <sup>a</sup>	-	-
7	Me <sub>2</sub> N(CH <sub>2</sub> ) <sub>2</sub> SnMe <sub>3</sub>	1	1	*	*
8	"	6 <sup>a</sup>	15 <sup>a</sup>	-	-
9	TMPTA	6	40	*	*

\* = no polymerisation detected after 30 passes

- = experiment not performed

a = belt speed = 160 ft/min

Belt speed = 10 ft/min for all other experiments

When air is excluded the amines have initiating properties during the photopolymerisation process. This occurs for all the compounds tested when a cover slide of either quartz or

glass is used. The amines may form a charge transfer complex with the monomer which would result in the production of some  $\alpha$ -aminoalkyl radicals, which could then initiate polymerisation. The amines do not show evidence of polymerisation when air is present during photolysis.

#### 3.5.4 Sensitisation of polymerisation using benzanthrone

It is well established that carbonyl/amine initiating systems are of value in free radical photopolymerisation. The photoreduction of aromatic ketones with amines has been shown to occur via the formation of an excited complex (exciplex) (Sander et al, 1972). It is the excited triplet of the carbonyl group which forms an exciplex with the amine. The exciplex is stabilised to a certain extent by the formation of a weak charge transfer complex due to the low ionisation potential of the amine. Thus the formation of the exciplex will depend on both the ionisation potential of the amine and the reduction potential of the carbonyl compound. The exciplex can collapse by a number of different routes including:

1. Efficient quenching of the excited triplet of the carbonyl group resulting in regeneration of the starting materials.
2. Electron transfer from the amine to the ketone in which radical ions are produced.
3. Hydrogen-abstraction from the amine by the ketone in which ketyl and amine radicals are produced.

Generally *t*-amines are favoured since the relative reactivity is related to the ease with which the amine is oxidised which is tertiary > secondary > primary. Also *t*-amines are good hydrogen donors since they have a hydrogen atoms which are situated in an  $\alpha$ -position to the nitrogen and are activated. This is important when considering the hydrogen abstraction mechanism which is strongly dependent on the C-H bond strength and will be related to the activation energy for the process.

The photoreduction of the ketone depends on the nature of the excited state (Hutchinson and Ledwith, 1973). Aromatic ketones have two different types of chromophore which can produce the excited triplet state. These are derived from:

1. The aromatic nucleus:  $\pi, \pi^*$  transition
2. The carbonyl group:  $n, \pi^*$  transition

Both types of excited state have been photoreduced by *t*-amines. As a result of the photoreduction free radicals are produced which are efficient photoinitiators of free radical polymerisation. The rates of polymerisation of various ketone/*t*-amine hybrid systems have previously been determined (Ledwith and Purbrick, 1973; Davidson and Goodin, 1982). It has been shown that it is the  $\alpha$ -aminoalkyl radical that is efficient at initiating polymerisation (Block et al, 1971; Hutchinson et al, 1973). Another added bonus is that the  $\alpha$ -aminoalkyl radical so produced is

effective at reducing oxygen inhibition of free radical polymerisation (see section 1.4.5).

### 3.5.5 UV curing results of dimethylaminoalkylsilanes and stannanes with benzanthrone

From the results presented previously it was proposed to test a number of the dimethylaminoalkyl- silanes and stannanes with an aromatic ketone, benzanthrone, in order to test the free radical initiating properties of these hybrid systems. The UV curing results of the combinations tested in the monomer TMPTA are presented in table 3.5.

Table 3.5 Sensitisation of polymerisation of TMPTA using dimethylaminoalkyl- silanes and stannanes (1% w/w) with benzanthrone (1% w/w)

E X P T	INITIATING SYSTEM	NUMBER OF PASSES			
		Touching Quartz	Touching Glass	In Air	Glass Filter
1	Me <sub>2</sub> N(CH <sub>2</sub> ) <sub>2</sub> SnMe <sub>3</sub> + benzanthrone	1 (1)	1 (1)	5 (*)	15 (*)
2	"	1 (6)	1 (15)	12 (-)	* (-)
3	Me <sub>2</sub> N(CH <sub>2</sub> ) <sub>3</sub> SiMe <sub>3</sub> + benzanthrone	1 (1)	1 (2)	16 (*)	* (*)
4	"	1 (3)	2 (8)	- (-)	- (-)
5	Me <sub>2</sub> N(CH <sub>2</sub> ) <sub>3</sub> SiPh <sub>3</sub> + benzanthrone	3 (4)	6 (12)	27 (*)	* (*)
6	benzanthrone	5	12	26	*

( ) = UV curing results for dimethylaminoalkylsilane/stannane in the absence of sensitiser

\* = no polymerisation detected after 30 passes

- = experiment not performed

Belt speed = 160 ft/min in EXPT's 2 & 4

Belt speed = 10 ft/min in all other experiments

The results in table 3.5 give evidence of sensitisation of the amines  $\text{Me}_2\text{N}(\text{CH}_2)_2\text{SnMe}_3$  (EXPT's 1 and 2) and  $\text{Me}_2\text{N}(\text{CH}_2)_3\text{SiMe}_3$  (EXPT's 3 and 4) when used in conjunction with benzanthrone in the polymerisation of TMPTA. For  $\text{Me}_2\text{N}(\text{CH}_2)_2\text{SnMe}_3$  (EXPT's 1 and 2) sensitisation occurs for all four experimental conditions of polymerisation tested. Thus an increase in the rate of polymerisation as evidenced in the reduced number of passes when compared to the amine on its own [EXPT's 1 and 2: figures in brackets ( )] and benzanthrone on its own (EXPT 6) was realised. The results in EXPT 1 show that there is polymerisation observed when air is present (both in air and with a glass cover slide).

### 3.6 Real-time infrared (RTIR) spectroscopy results

#### 3.6.1 RTIR results of dimethylaminoalkylsilanes and stannanes

The RTIR spectra of the photopolymerisation of TMPTA using the organometallic amines were recorded in order to give an indication of the role of homolytic cleavage in the

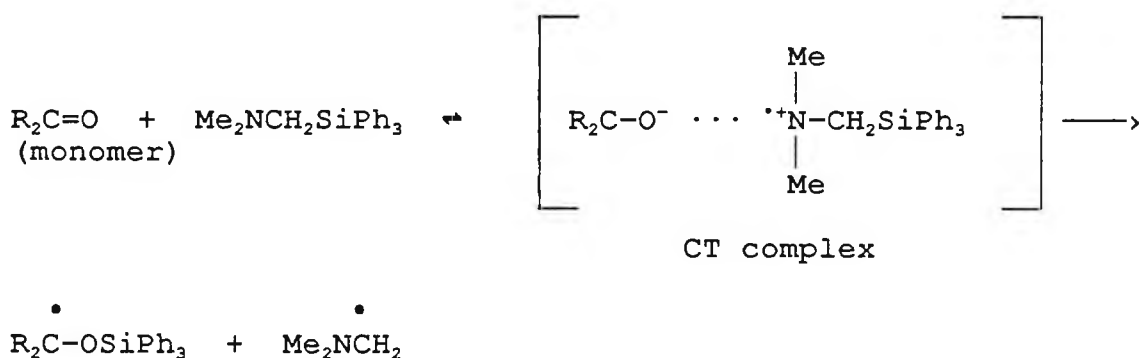
polymerisation mechanism. The situation is complicated by the fact that TMPTA absorbs in the UV region ( $\lambda$  (sh) = 240nm [ $\epsilon=300$ ]). Thus it cannot be ruled out that a charge transfer (CT) complex may be formed between the amine and the monomer resulting in a different mechanism of initiation to that of homolytic cleavage of the amine. The results are shown below in table 3.6.

Table 3.6 RTIR spectroscopy results for the photopolymerisation of TMPTA using organometallic amines

EXPT	INITIATOR	UV/ $\lambda_{max}$ ( $\epsilon$ )	% mol in TMPTA	$R_p$ (max) / mol/l/s	% Conv/ at 1 min
1	$Me_2NCH_2SiPh_3$	271 (1100)	0.9	0.167	14.8
2	$Me_2N(CH_2)_2SiPh_3$	265 (1400)	0.9	0.053	5.0
3	$Me_2N(CH_2)_3SiPh_3$	270 (1350)	0.9	0.075	5.8
4	$Me_2N(CH_2)_3SiMe_3$	273 (100)	1.9	0.095	6.4
5	$Me_2N(CH_2)_3SnBu_3$	270 (100)	0.8	0.065	6.9
6	$Me_2N(CH_2)_2SnMe_3$	269 (100)	1.2	0.342	18.0
7	$Me_2N(CH_2)_2SnPh_3$	257 (1800)	0.7	0.077	13.3

For the series  $Me_2N(CH_2)_nSiPh_3$  (where  $n = 1, 2, 3$ ) it is shown that when  $n = 1$  (EXPT 1) there is a relatively high degree of conversion and  $R_{p(max)}$  value obtained when compared to the other amines in this series (where  $n = 2$  & 3: EXPT's 2 and

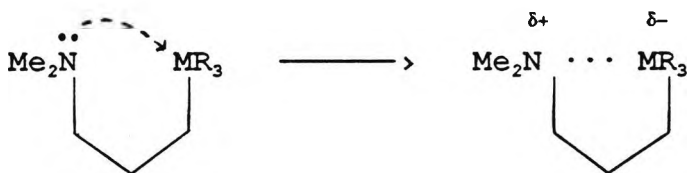
3 respectively). This is thought to be related to the expected hyperconjugative effect which operates between the Si and the  $\beta$ -N via the alkyl link ( $n = 1$ ). When the alkyl link is increased to  $-(\text{CH}_2)_2-$  or  $-(\text{CH}_2)_3-$  (EXPT's 2 and 3 respectively) in this series the hyperconjugative effect is minimised resulting in the reduced degree of conversion and  $R_{p(\text{max})}$  values obtained. It is expected that this  $\beta$ -effect will stabilise the formation of a radical cation formed via a CT complex with the monomer resulting in reactive  $\alpha$ -aminoalkyl radicals shown below.



A similar mechanism can be proposed to account for the relatively high values of the degree of conversion and  $R_{p(\text{max})}$  for the stannanes,  $\text{Me}_2\text{N}(\text{CH}_2)_2\text{SnR}_3$  (where  $\text{R} = \text{Me}, \text{Ph}$  in EXPT's 6 & 7 respectively). The CT complex formation is likely to be linked to the oxidation potentials of the amine donors which could explain why the silane in this series  $\text{Me}_2\text{N}(\text{CH}_2)_2\text{SiPh}_3$  (EXPT 2) does not exhibit a similar reactivity to the above stannanes.

It is apparent that in the series  $\text{Me}_2\text{N}(\text{CH}_2)_3\text{MR}_3$  (EXPT's 3, 4, & 5) there is a reduced activity towards polymerisation when

compared to the other amines. This could be due to structural features that have been noted earlier which involve the coordination of the nitrogen lone pair into the available d orbitals of the metal as shown below.



This would stop these compounds forming exciplexes to any great extent and could explain the reduction in the degree of conversion and  $R_{p(\max)}$  values. It is anticipated that this type of structure is more important for tin compounds than silicon compounds due to the greater ability of tin to extend coordination through the use of d-orbitals in bonding.

### 3.6.2 RTIR results of dimethylaminoalkylsilanes and stannanes with benzanthrone

RTIR spectroscopy was used to substantiate the earlier work carried out using the UV Colordry apparatus for the sensitisation of polymerisation of TMPTA using benzanthrone with the organometallic amines. The results are presented below in table 3.7.

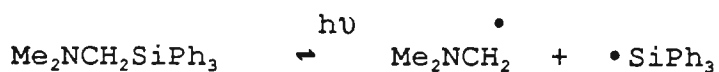
Table 3.7 RTIR spectroscopy results for the photopolymerisation of TMPTA using organometallic amines sensitised using benzanthrone

EXPT	INITIATING SYSTEM	UV/ $\lambda_{\max}$ ( $\epsilon$ )	% mol in TMPTA	Rp(max) / mol/l/s	% Conv/ at 1 min
1	Benzanthrone + $\text{Me}_2\text{NCH}_2\text{SiPh}_3$	see expt 6 271 (1100)	1.3 0.9	0.679	32.2
2	Benzanthrone + $\text{Me}_2\text{N}(\text{CH}_2)_3\text{SiMe}_3$	see expt 6 273 (100)	1.3 1.9	1.395	40.2
3	Benzanthrone + $\text{Me}_2\text{N}(\text{CH}_2)_3\text{SnBu}_3$	see expt 6 270 (100)	1.3 0.8	0.435	30.9
4	Benzanthrone + $\text{Me}_2\text{N}(\text{CH}_2)_2\text{SnMe}_3$	see expt 6 269 (100)	1.3 1.2	1.366	35.3
5	Benzanthrone + $\text{Me}_2\text{N}(\text{CH}_2)_2\text{SnPh}_3$	see expt 6 257 (1800)	1.3 0.7	0.581	45.8
6	Benzanthrone	395 (10000) 305 (8000)	1.3	0.052	22.7

The results show that the sensitisation of polymerisation of TMPTA using benzanthrone with the organometallic amines is very efficient. The mechanism of sensitisation is likely to involve the formation of an exciplex between the sensitiser and the amine which subsequently collapses to give an  $\alpha$ -aminoalkyl radical which can initiate polymerisation.

One interesting feature is observed when comparing the values of the degree of conversion and  $R_{p(max)}$  for  $Me_2N(CH_2)_3SiMe_3$  (EXPT 2) and  $Me_2N(CH_2)_3SnBu_3$  (EXPT 3). The silane shows a greater increase in the values of the degree of conversion and  $R_{p(max)}$  when compared to the stannane. This could be explained by the earlier observation that the N is coordinated to the Sn in the stannane which effectively reduces the possibility of forming an exciplex with the sensitiser and thus reduces the effect of sensitisation as demonstrated. The silicon compound does not undergo this coordination to any great extent and thus the N is free to form an exciplex with the sensitiser resulting in sensitisation of polymerisation.

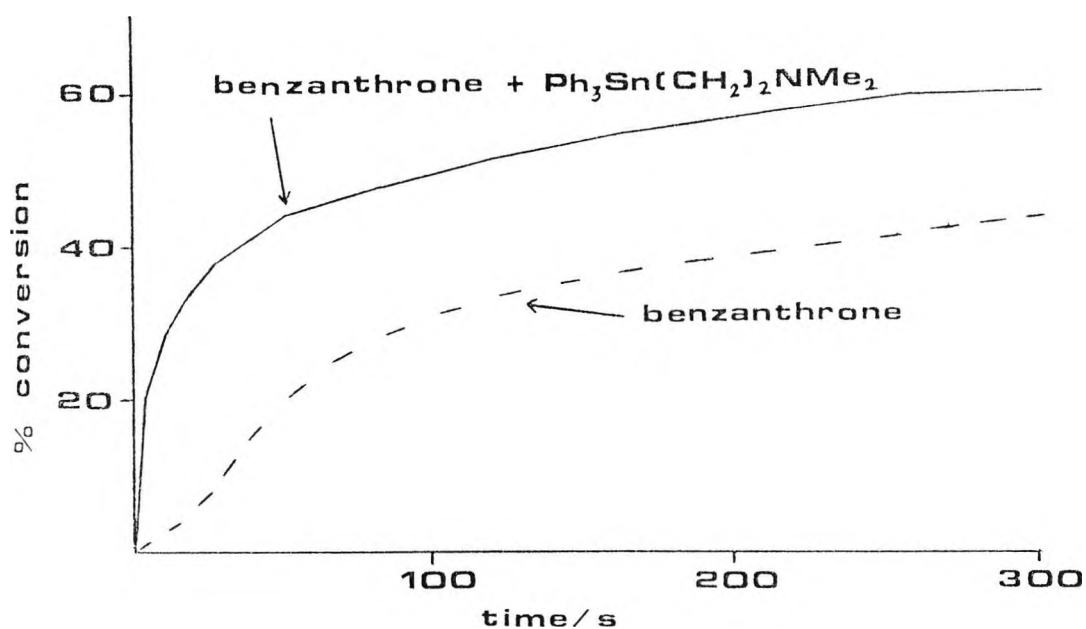
The effect of sensitisation in the case of  $Me_2NCH_2SiPh_3$  (EXPT 1) is not as evident as for the other amines since there may be some homolytic cleavage of this compound, which competes with the sensitisation process.



Another interesting feature is seen when comparing the kinetic curves of the RTIR spectra of benzanthrone (EXPT 6) with the situation of benzanthrone + amine (EXPT's 1 to 5). In the former case excited state benzanthrone presumably abstracts a hydrogen from the resin to yield a monomer radical capable of initiating polymerisation. In the latter case polymerisation occurs via sensitisation with the production of  $\alpha$ -aminoalkyl radicals which are extremely

efficient at initiating polymerisation. The rates of polymerisation via the two different routes may be compared when viewing the RTIR kinetic traces shown below in figure 3.1.

Figure 3.1 A plot of the degree of conversion versus time obtained from the RTIR spectroscopy results of the curing of TMPTA for an organometallic amine in the presence and absence of a sensitiser (benzanthrone)



Other evidence for the formation of  $\alpha$ -aminoalkyl radicals being formed in the sensitised experiment is that under the conditions tested no observable induction period was noticed. It is well documented that  $\alpha$ -aminoalkyl radicals are good scavengers of oxygen which effectively reduces the

oxygen inhibition of polymerisation (see section 1.4.5). Thus in this case, RTIR spectroscopy has been used to calculate different rates of polymerisation for the situations with benzanthrone in the presence and in the absence of amines. From the results it can be inferred that a different mechanism of polymerisation occurs for the two situations described. This points to the value of RTIR spectroscopy as a diagnostic technique which, when used with other evidence, may be used to infer reaction mechanisms.

### 3.7 Experimental section

See section 2.7 for general experimental details. All  $^1\text{H}$  NMR were run in  $\text{CDCl}_3$  with TMS as the internal standard, where used. IR spectra were recorded using neat films or KBr discs. Methanol was used as the solvent for UV spectra.

### 30. Triphenyl(N,N-dimethylaminomethyl)silane

A.

Equipment was dried overnight at  $160^\circ\text{C}$ . Trimethylsilyl iodide was supplied in a 5g ampoule. Trimethylsilyl iodide (5g;0.025mol) in anhydrous ether (10ml) was added to the flask. At  $0^\circ\text{C}$  2-methyl-2-butene (0.15ml) was added followed by dropwise addition of N,N,N',N'-tetramethylenediamine (2.56g;0.025mol) in anhydrous ether (10ml). A white precipitate formed immediately and this mixture was allowed to stir for 20 min. The precipitate was collected by vacuum filtration and washed with anhydrous ether (3 x 20ml), air-dried, and rapidly transferred to a vacuum desiccator to give 3.35g (72%) of dimethyl(methylene)ammonium iodide (Bryson et al, 1980).

#### Analysis

$^1\text{H}$  NMR: 3.60 (s,6H), 8.20 (s,2H)

B.

Thiophenol (2g;18mmol) was added at room temperature to a

stirred suspension of NaH (0.8g; 60%; 20mmol) under nitrogen. After 0.5h dimethyl(methylene)ammonium iodide (3.35g; 80mmol) was added as a solid and the resulting solution was stirred overnight. Following the addition of water (40ml) the resulting mixture was extracted with ether (3 x 40ml) and the combined organic extracts were washed successively with a saturated NaHCO<sub>3</sub> solution, water, and brine, dried over MgSO<sub>4</sub>, filtered, and concentrated in vacuo, leaving 2.4g (80%) of a yellow oil of dimethylaminomethylphenylsulphide (Bryson et al, 1980).

#### Analysis

<sup>1</sup>H NMR: 2.20 (s, 6H), 4.40 (s, 2H), 7.00-7.50 (m, 5H)

C.

THF (25ml) was slowly added under nitrogen, with stirring to a mixture of chlorotriphenylsilane (2.95g; 0.01mol) and Li (30% dispersion in mineral oil; 0.92g; 0.04mol). A few minutes after the addition of the solvent a white precipitate was noticed. Within 20 min the reaction mixture turned light yellow; the colour gradually turned orange-brown and finally black-brown, after 3h stirring at room temperature. This solution of triphenylsilyllithium was added under nitrogen to an ice-cold solution of dimethylaminophenyl sulphide (1.18g; 7mmol) in anhydrous THF (10ml). After addition the mixture was stirred at room temperature for 3h and hydrolysed with saturated ammonium chloride solution. The THF layer was separated and the

aqueous layer was extracted with ether. The combined organic extracts were concentrated and the residue was extracted with 10% HCl solution. The acid extract was neutralised and extracted with ether, dried ( $\text{MgSO}_4$ ), and concentrated. The solid residue was recrystallised from pet ether to give 1.0g (35%) with mp 111-112°C (lit mp 111-113°C; Sato et al, 1976).

### Analysis

$^1\text{H NMR}$ : 2.20 (s, 6H), 2.70 (s, 2H), 7.20-7.70 (m, 15H)

IR: 3064 (m), aromatic C-H stretch  
2926 (m), aliphatic C-H stretch  
2810 (s), C-H asymmetric stretch of  $\text{NCH}_3$  group  
2763 (s), C-H symmetric stretch of  $\text{NCH}_3$  group  
1426 (m), C-H bending  
1109 (m), Ph-Si stretch  
784 (m), 700 (m), monosubstituted benzene

UV:  $\lambda_{\text{max}} = 271\text{nm}$  ( $\epsilon=1100$ )

MS:  $\text{M}^+$  317, 259 ( $\text{Ph}_3\text{Si}^+$ ), 77 ( $\text{C}_6\text{H}_5^+$ ), 58 ( $\text{Me}_2\text{NCH}_2^+$ )

### 31. N-(Trimethylsilylmethyl)-N,N'-diethylamine

A solution of diethylamine (58.5ml; 0.55mol) and iodomethyltrimethylsilane (12.0g; 0.05mol) in anhydrous



ether. The combined organic extracts were dried (magnesium sulphate) and concentrated. The solid residue was purified initially by column chromatography (CCl<sub>4</sub>/alumina; R<sub>f</sub>=0.80) and then recrystallisation (EtOH) to give 2.1g (30%) yield with mp 75-76°C.

### Analysis

<sup>1</sup>H NMR: 1.30-1.90 (m, 4H), 2.20-2.60 (m, 8H), 7.20-7.70 (m, 15H)

IR: 3050 (m), aromatic C-H stretch  
2930 (m), aliphatic C-H stretch  
2810 (m), C-H asymmetric stretch of NCH<sub>3</sub> group  
2765 (m), C-H symmetric stretch of NCH<sub>3</sub> group  
1425 (m), C-H bending  
1100 (m), Ph-Si stretch  
740 (s), 700 (s), monosubstituted benzene

UV:  $\lambda_{\max}$  = 270nm ( $\epsilon$  = 1350)

MS: M<sup>+</sup> 345, 259 (Ph<sub>3</sub>Si<sup>+</sup>), 77 (C<sub>6</sub>H<sub>5</sub><sup>+</sup>), 58 (Me<sub>2</sub>NCH<sub>2</sub><sup>+</sup>)

### 33. 2-N,N'-Dimethylamino-1-triphenylsilylethane

This compound was prepared by the method described in

experiment 32, using 2-dimethylaminoethylchloride (2.2g;0.02mol), chlorotriphenylsilane (5.0g;0.017mol), magnesium turnings (0.53g;0.022mol), and 1,2-dibromoethane (0.5ml) with irradiation of ultrasound for 4h. The solid residue was purified initially by column chromatography (CCl<sub>4</sub>/alumina; R<sub>f</sub>=0.80) and then recrystallisation (EtOH) which gave 2.2g (40%) yield with mp 61°C (lit mp 66-72°C; Sato et al, 1976).

### Analysis

<sup>1</sup>H NMR: 1.25 (t,2H), 2.10 (s,6H), 2.60 (t,2H), 7.20-7.70 (m,15H)

IR: 3055 (m), aromatic C-H stretch  
2930 (m), aliphatic C-H stretch  
2810 (m), C-H asymmetric stretch of NCH<sub>3</sub> group  
2764 (m), C-H symmetric stretch of NCH<sub>3</sub> group  
1424 (s), C-H bending  
1105 (s), Ph-Si stretch  
750 (s), 700 (s), monosubstituted benzene

UV:  $\lambda_{max} = 265\text{nm}$  ( $\epsilon=1400$ )

MS: 259 (Ph<sub>3</sub>Si<sup>+</sup>), 77 (C<sub>6</sub>H<sub>5</sub><sup>+</sup>), 58 (Me<sub>2</sub>NCH<sub>2</sub><sup>+</sup>)

#### 34. 2-N,N'-Dimethylamino-1-triphenylstannylethane

This compound was prepared by the method described in experiment 32, using 2-dimethylaminoethylchloride (2.2g;0.02mol), chlorotriphenylstannane (6.6g;0.017mol), magnesium turnings (0.53g;0.022mol), and 1,2-dibromoethane (0.5ml) with irradiation of ultrasound for 4h. The solid residue was purified initially by column chromatography (CCl<sub>4</sub>/silica; R<sub>f</sub>=0.50) and then recrystallisation (EtOH) which gave 2.5g (35%) yield with mp 80-81°C (lit mp 81-83°C; Sato and Ban, 1973).

#### Analysis

<sup>1</sup>H NMR: 1.70 (t,2H), 2.10 (s,6H), 2.60 (t,2H), 7.20-7.70 (m,15H)

IR: 3045 (m), aromatic C-H stretch  
2940 (m), aliphatic C-H stretch  
2810 (m), C-H asymmetric stretch of NCH<sub>3</sub> group  
2765 (m), C-H symmetric stretch of NCH<sub>3</sub> group  
1425 (s), C-H bending  
726(s), 695 (s), monosubstituted benzene

UV:  $\lambda_{\max} = 257\text{nm}$  ( $\epsilon=1800$ )

MS: 351 (Ph<sub>3</sub><sup>120</sup>Sn<sup>+</sup>), 120 (<sup>120</sup>Sn<sup>+</sup>), 58 (Me<sub>2</sub>NCH<sub>2</sub><sup>+</sup>)

### 35. 3-N,N'-Dimethylamino-1-trimethylsilylpropane

This compound was prepared by the method described in experiment 32, using 3-dimethylaminopropylchloride (5.0g;0.041mol), chlorotrimethylsilane (3.7g;0.034mol), magnesium turnings (1.07g;0.045mol), and 1,2-dibromoethane (0.5ml) with irradiation of ultrasound for 4h. The residue was purified by column chromatography (CHCl<sub>3</sub>/silica; R<sub>f</sub>=0.65) which gave 2.0g (37%) yield.

#### Analysis

<sup>1</sup>H NMR: Relative to SiMe<sub>3</sub>: 0.00 (s, 9H), 0.40-0.50 (m, 2H),  
1.30-1.50 (m, 2H), 2.20-2.60 (m, 8H)

IR: 2953 (s), 2896 (m), C-H stretching  
2815 (m), C-H asymmetric stretch of NCH<sub>3</sub> group  
2765 (m), C-H symmetric stretch of NCH<sub>3</sub> group  
1463 (m), C-H deformation  
1248 (s), Si-C stretch

MS: M<sup>+</sup> 159, 73 (SiMe<sub>3</sub><sup>+</sup>), 58 (Me<sub>2</sub>NCH<sub>2</sub><sup>+</sup>)

UV:  $\lambda_{\max}$  = 273nm ( $\epsilon$  = 100)

### 36. 3-N,N'-Dimethylamino-1-tri-n-butylstannylpropane

This compound was prepared by the method described in experiment 32, using 3-dimethylaminopropylchloride (3.0g;0.025mol), chlorotri-*n*-butylstannane (6.7g;0.021mol), magnesium turnings (0.65g;0.027mol), and 1,2-dibromoethane (0.5ml) with irradiation of ultrasound for 2h. Bulb to bulb distillation of the residue gave 2.8g (35%) yield with bp 95°/0.01mm (lit bp 120°C/0.1mm; Suggs and Lee, 1986)

#### Analysis

<sup>1</sup>H NMR: 0.70-1.70 (m, 31H), 2.20 (m, 8H)

IR: 2955 (s), C-H asymmetric stretch of CH<sub>3</sub> group  
2923 (s), C-H asymmetric stretch of CH<sub>2</sub> group  
2871 (s), C-H symmetric stretch of CH<sub>3</sub> group  
2854 (s), C-H symmetric stretch of CH<sub>2</sub> group  
2813 (m), C-H asymmetric stretch of NCH<sub>3</sub> group  
2764 (m), C-H symmetric stretch of NCH<sub>3</sub> group  
2720 (w), C-H asymmetric stretch of NCH<sub>2</sub> group  
1461 (m), 1375 (m), C-H bending

MS: M<sup>+</sup> 376, 374, 372 (<sup>120</sup>Sn, <sup>118</sup>Sn, <sup>116</sup>Sn respectively)  
291, 289, 287; Sn(*n*-butyl)<sub>3</sub><sup>+</sup> (<sup>120</sup>Sn, <sup>118</sup>Sn, <sup>116</sup>Sn respectively)  
235, 233, 231; SnH(*n*-butyl)<sub>2</sub><sup>+</sup> (<sup>120</sup>Sn, <sup>118</sup>Sn, <sup>116</sup>Sn respectively)  
177, 175, 173; Sn(*n*-butyl)<sup>+</sup> (<sup>120</sup>Sn, <sup>118</sup>Sn, <sup>116</sup>Sn respectively)  
121, 119, 117; SnH<sup>+</sup> (<sup>120</sup>Sn, <sup>118</sup>Sn, <sup>116</sup>Sn respectively)

58;  $\text{Me}_2\text{NCH}_2^+$

UV:  $\lambda_{\text{max}} = 270\text{nm}$  ( $\epsilon=100$ )

### 37. 2-Dimethylaminoethyltrimethylstannane

This compound was prepared by the method described in experiment 32, using 2-dimethylaminoethylchloride (1.3g;0.012mol), chlorotrimethylstannane (2.0g;0.010mol), magnesium turnings (0.31g;0.013mol), and 1,2-dibromoethane (0.5ml) with irradiation of ultrasound for 2h. Bulb to bulb distillation of the residue gave 1.1g (45%) yield with bp  $82^\circ\text{C}$ .

#### Analysis

$^1\text{H}$  NMR: relative to  $\text{SnMe}_3$ ; 0.00 (s,9H), 0.70 (t,2H), 2.10 (m,8H)

IR: 2974 (s), 2937 (s), 2856 (s), C-H stretching  
2814 (s), C-H asymmetric stretch of  $\text{NCH}_3$  group  
2766 (s), C-H symmetric stretch of  $\text{NCH}_3$  group  
2721 (m), C-H asymmetric stretch of  $\text{NCH}_2$  group  
1460 (m), 1371 (m), C-H bending  
766 (s), Sn-C stretching of  $\text{SnMe}_3$

MS:

$M^+$  236, 234, 232 ( $^{120}\text{Sn}$ ,  $^{118}\text{Sn}$ ,  $^{116}\text{Sn}$  respectively)  
 165, 163, 161;  $\text{Sn}(\text{Me})_3^+$  ( $^{120}\text{Sn}$ ,  $^{118}\text{Sn}$ ,  $^{116}\text{Sn}$  respectively)  
 150, 148, 146;  $\text{Sn}(\text{Me})_2^+$  ( $^{120}\text{Sn}$ ,  $^{118}\text{Sn}$ ,  $^{116}\text{Sn}$  respectively)  
 135, 133, 131;  $\text{Sn}(\text{Me})^+$  ( $^{120}\text{Sn}$ ,  $^{118}\text{Sn}$ ,  $^{116}\text{Sn}$  respectively)  
 120;  $\text{Sn}$  ( $^{120}\text{Sn}$ )  
 58;  $\text{Me}_2\text{NCH}_2^+$

UV:  $\lambda_{\text{max}} = 269\text{nm}$  ( $\epsilon=100$ )

### 3.8 References

- Block, H., Ledwith, A., and Taylor, A.R., (1971). *Polymer*, **12**, 271
- Bock, H., Kaim, W., Kira, M., Osawa, H., and Sakurai, H., (1979). *J.Organomet.Chem.*, **164**, 295
- Bowser, R., and Davidson, R.S., (1992). "The use of Ultrasound in Organic Synthesis", Price, G.J. (Ed.), Royal Society of Chemistry, 50-58
- Bryson, T.A., Bonitz, G.H., Reichel, C.J., and Dardis, R.E., (1980). *J.Org.Chem.*, **45**, 524
- Butcher, E., Rhodes, C.J., Standing, M., Bowser, R., and Davidson, R.S., (1992a). *J.Chem.Soc., Perkin Trans. 2*, 1469
- Butcher, E., Rhodes, C.J., Bowser, R., and Davidson, R.S., (1992b). *J.Organomet.Chem.*, **436**, C5
- Cullis, C.F., Herron, D., and Hirschler, M.M., (1985). *Combustion and Flame*, **59**, 151
- Davidson, R.S., and Goodin, J.W., (1982). *Europ.Polym.J.*, **18**, 597
- Eastland, G.W., Rao, D.N.R., and Symons, M.C.R., (1984).

*J.Chem.Soc., Perkin Trans. II*, 1551

Hasegawa, E., Brumfield, M.A., Mariano, P.S., and Yoon, U.C., (1988a). *J.Org.Chem.*, **53**, 5435

Hasegawa, E., Xu, W., Mariano, P.S., Yoon, U.C., and Kim, K.U., (1988b). *J.Am.Chem.Soc.*, **110**, 8099

Hutchinson, J., Lambert, M.C., and Ledwith, A., (1973). *Polymer*, **14**, 250

Hutchinson, J., and Ledwith, A., (1973). *Polymer*, **14**, 405

Ledwith, A., and Purbrick, M.D., (1973). *Polymer*, **14**, 521

Meganem, F., (1980). *J.Soc.Chim.Tunis.*, (3), 13

Nakano, M., and Sato, Y., (1985). *J.Chem.Soc., Chem.Commun.*, 1684

Nakano, M., and Sato, Y., (1987). *J.Org.Chem.*, **52**, 1844

Naruta, Y., Nishigaichi, Y., and Maruyama, K., (1986). *Chem.Lett.*, 1857

Pine, S.H., (1970). "Org.Reactions", **18**, 403, Wiley, NY

Sander, M.R., Osborn, C.L., and Trecker, D.J., (1972).

*J.Polym.Sci, A1, 10, 3173*

Sato, Y., Ban, Y., (1973). *J.Org.Chem., 38, 4373.*

Sato, Y., Ban, Y., and Shirai, H., (1974). *J.Chem.Soc., Chem.Commun., 182*

Sato, Y., Toyo'oka, T., Aoyama, T., and Shirai, H., (1975). *J.Chem.Soc., Chem.Commun., 640*

Sato, Y., Ban, Y., and Shirai, H., (1976). *J.Organomet.Chem., 113, 115*

Sato, Y., and Sakakibara, H., (1979). *J.Organomet.Chem., 166, 303*

Suggs, J.W., and Lee, K.S., (1986). *J.Organomet.Chem., 299, 297*

Vedeneyev, V.I., Gurvich, L.V., Kondrat'yev, V.N., Medvedev, V.A., and Frankevich, Ye.L., (1966). "Bond Energies, Ionisation Potentials and Electron Affinities", Arnold, London

Wardell, J.L., (1978). *Inorg.Chim.Acta, 26, L18*

Ger.Offen. 2,801,700

US 3,853,994

## **Chapter 4.**

# **PHOTOINITIATION OF FREE RADICAL AND CATIONIC POLYMERISATION USING IRON-ARENE COMPLEXES**

#### 4.1 Introduction

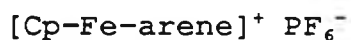
The first example of a transition metal sandwich complex that involved coordination of both a cyclopentadienyl and a benzenoid ring to the central metal atom was reported by Coffield *et al* in 1957 who prepared the iodide salt of  $\eta^6$ -mesitylene- $\eta^5$ -cyclopentadienyliron(II) (Coffield *et al*, 1957). The  $\eta^6$ -benzene analogue was prepared in 1960 by Green *et al* (Green *et al*, 1960). Extensive work by Nesmeyanov *et al* led to the development of a synthetic route of general applicability for a number of  $\eta^6$ -benzenoid- $\eta^5$ -cyclopentadienyl iron(II) complexes. The earliest example of this route reported in 1963 involved the reaction of ferrocene and benzene in the presence of aluminium chloride and aluminium powder as shown in equation 4.1 (Nesmeyanov *et al*, 1963).



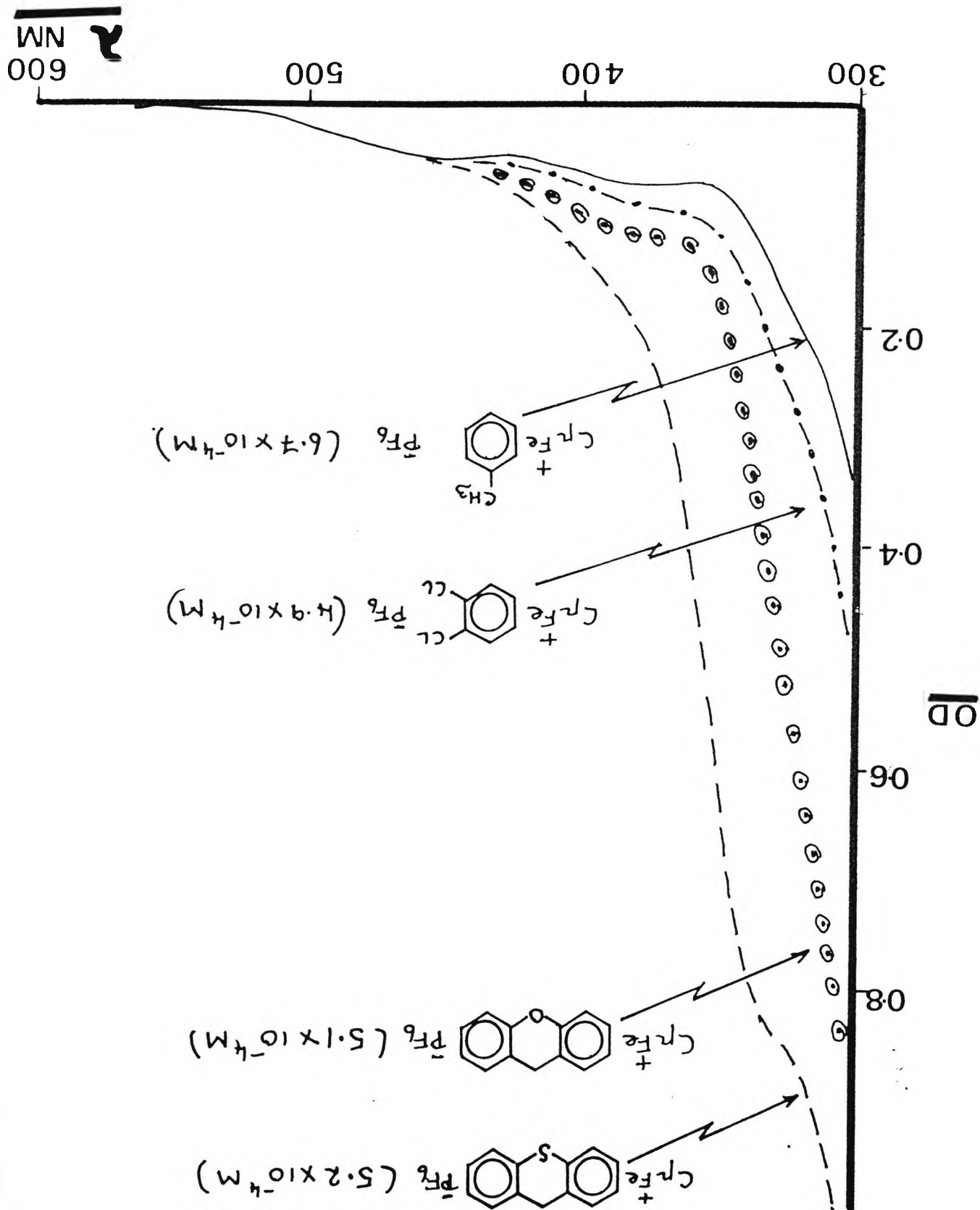
The iron-arene complexes are commonly isolated as either the hexafluorophosphate or the tetrafluoroborate salts. Various complexes were synthesised which contained electron-donating or electron-accepting substituents on either the arene or the cyclopentadienyl rings (Nesmeyanov *et al*, 1965; Nesmeyanov *et al*, 1966; Nesmeyanov *et al*, 1967). When polyaromatics such as biphenyl, naphthalene, and fluorene

were used in the ferrocene cyclopentadienyl ring replacement reaction Nesmeyanov et al discovered that only one of the rings took part in the ligand exchange with ferrocene (Nesmeyanov et al, 1966). It was also shown by Lee et al that the  $\pi$ -arene bis( $[\pi$ -cyclopentadienyl]iron) dications could be synthesised by reacting the corresponding monocations with excess ferrocene to substitute the remaining aromatic rings (Lee et al, 1972).

A number of iron arene salts were synthesised using the general procedure of Nesmeyanov outlined in equation 4.1. All the salts prepared were isolated as the hexafluorophosphate derivatives and may be represented by the general formulae:

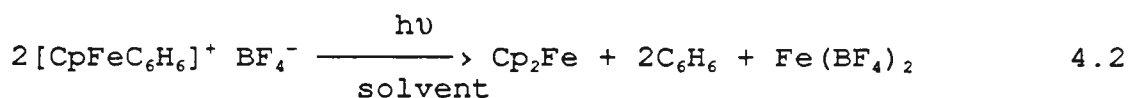


where the arene may be toluene, 4-chlorotoluene, 1,2-dichlorobenzene, fluorene, thioxanthene, or xanthene. In the case of the latter three derivatives only one of the available benzene rings is coordinated to iron which gives rise to the monocationic species. The compounds synthesised exhibit good absorption properties in the UV region which renders them useful for initiation of polymerisation. Examples of a number of the UV spectra of the iron-arene complexes are shown below.



## 4.2 Photochemistry of iron-arene complexes

In 1970 Nesmeyanov et al reported on the photolysis of benzene cyclopentadienyliron(II) tetrafluoroborate (Nesmeyanov et al, 1970). Irradiation in a variety of organic solvents gave ferrocene, the free arene, and the inorganic ion as outlined in equation 4.2.

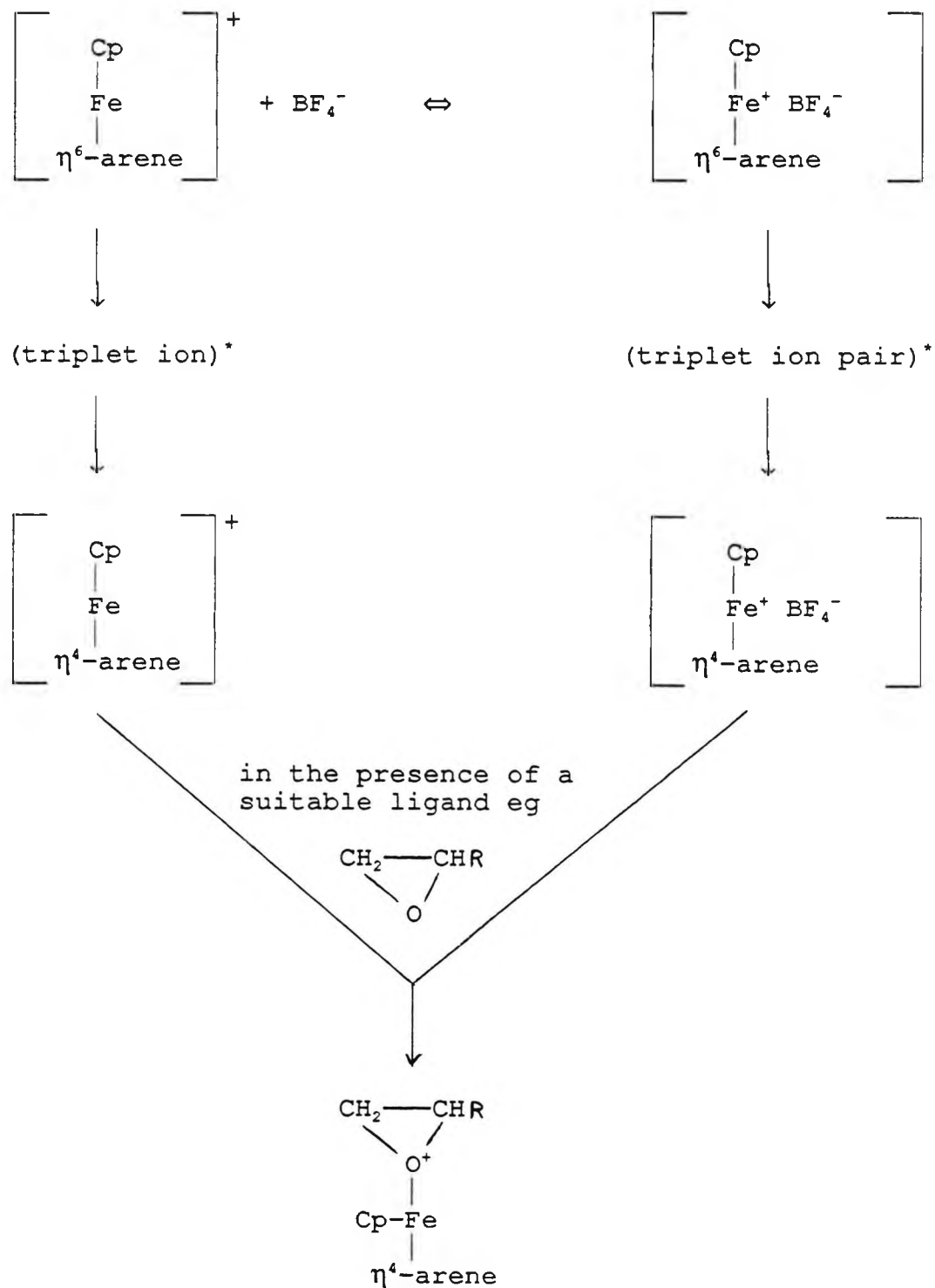


In the mid 1970's the electronic structure of  $[\text{CpFe-arene}]^+\text{X}^-$  complexes was investigated (Morrison et al, 1974; Morrison et al, 1975). This work showed by analogy to ferrocene that the low energy optical absorptions are spin allowed d-d transitions leading to  $a^1E_{1g}$ ,  $^1E_{2g}$ , and  $b^1E_{1g}$  states. Analysis of these states using molecular orbital theory leads to the prediction that excitation of the iron-arene complex will labilise the ligands (Albright, 1982; Zink, 1974). This prediction is supported by the experimental data. In 1980 Gill and Mann reported on the photochemically induced arene ligand replacement reactions of the cyclopentadienyl (p-xylene)iron(II) cation (Gill and Mann, 1980). Thus irradiation (436nm) of the ligand field bands of the cyclopentadienyl (p-xylene)iron(II) cation in dichloromethane gave a ligand field excited state which resulted, in the presence of suitable ligands such as CO, in products arising from metal-ligand bond scission including

cyclopentadienyliron(II) (CO)<sub>3</sub><sup>+</sup>. In 1983 the same workers extended the earlier work by Nesmeyanov *et al* (Nesmeyanov *et al*, 1970) when they reinvestigated the photolysis of an iron-arene complex in acetonitrile (Gill and Mann, 1983). They discovered that on photolysis of the cyclopentadienyl (p-xylene)iron(II) cation in acetonitrile a purple species characterised as the cyclopentadienyliron(II) (CH<sub>3</sub>CN)<sub>3</sub> cation was isolated at -40°C. This intermediate was then used to synthesise a number of iron(II)cyclopentadienyl complexes with a wide range of ligand substitution. In the same year Mann *et al* reported on the solvent and ion-pairing effects on the photochemical arene replacement reactions of the cyclopentadienyl (p-xylene)iron(II) cation (Schrenk *et al*, 1983). They suggested that the arene replacement reaction is consistent with nucleophilic attack of the medium on a ligand field excited state of iron. This can occur through pathways involving solvent assisted steps (in polar, nucleophilic solvents) or anion assisted steps (in non polar, weakly nucleophilic solvents). These experiments and others led Mann to propose that the photoactive species in these reactions is the a<sup>3</sup>E<sub>1g</sub> ligand field state with a triplet energy of 42kcal/mol and a short triplet lifetime of < 1.5ns (McNair *et al*, 1984). More recently further advances have been made on the mechanism of photolysis of the iron-arene complexes (Chrisope *et al*, 1989). The mechanism of photolysis was shown to proceed via a multistep process in which the replacement of the arene is controlled by the identity of the counterion and the concentration of the

attacking ligands. A summary of the mechanism is given below in scheme 4.1.

Scheme 4.1 Photochemistry of iron-arene complexes

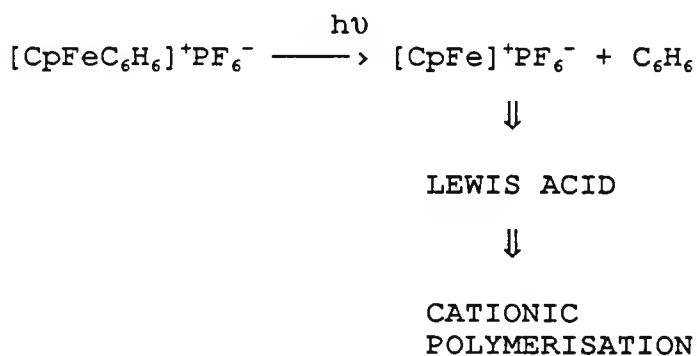


It is this reaction with epoxides that has received much attention in the field of photoimaging discussed in the next section.

#### 4.3 Photoimaging using iron-arene complexes

On photolysis of the iron-arene complexes the uncharged ligand is removed resulting in an unsaturated cation, a Lewis acid, which is capable of initiating cationic polymerisation (EP 0094915, 1984; EP 0126712; Zweifel and Meier, 1985) as shown in scheme 4.2.

Scheme 4.2 Mechanism of cationic polymerisation of epoxides using iron-arene salts



The photolysis of the iron-arene complexes was sensitised with the use of anthracene derivatives (Meier and Zweifel, 1985).

The spectral response of the iron-arene initiators was

altered by varying the arene ligand and in some cases the initiators were suitable for laser applications (Meier and Zweifel, 1986). Photolysis in the presence of ethylene oxide yielded white crystalline iron crown ether complexes whose structure was determined by X-ray analysis (Meier and Rhis, 1985), indicating that iron-arene complexes form Lewis acids on irradiation. The initial UV absorption of these initiators changes on irradiation with a gradual reduction in UV absorbance as irradiation proceeds. This leads to a bleachable system so that light penetration is possible throughout the film thickness. It was found that heat treatment was required to complete the polymerisation to a fully crosslinked resin. It was noted that the oxidation state of the iron in these photoinitiators is +2, before and after irradiation. Oxidation of the iron to the +3 state was only possible after irradiation. If the irradiation was carried out in the presence of an oxidant, such as cumene hydroperoxide, the iron +3 species, a stronger Lewis acid, was obtained with increased reactivity in epoxide polymerisation. As a result of electron exchange interactions in the iron complex/oxidant system, radical species were formed (in addition to Lewis acid) and mixed radical/cationic polymerisations are possible.

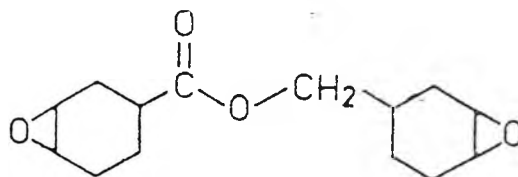
From DSC experiments it was shown that the iron-arene photoinitiators are less reactive than Brønsted acids obtained from triarylsulphonium salts. A heat treatment (around 100°C) was required to complete polymerisation. The

DSC trace showed a narrow enthalpy peak which has been interpreted mechanistically as a uniform reaction pathway (Lohse and Zweifel, 1986). DSC evidence was also presented to show that in the presence of oxidant an iron +3 species was more reactive (heat treatment 50°C) than the iron +2 species in the absence of any oxidant. The photoinitiating properties of several iron arene complexes used in the polymerisation of epoxides have been reviewed in a number of articles (Curtis *et al*, 1986; Roloff *et al*, 1986; Klingert *et al*, 1988).

#### 4.4 UV curing results for iron-arene complexes in cationic polymerisation

A number of the iron-arene salts prepared have been investigated for their use as photoinitiators in the presence of a typical cycloaliphatic difunctional epoxide, 3,4-epoxycyclohexylmethyl-3',4'-epoxycyclohexane carboxylate (Degacure K126 from Degussa) shown below.

Structural Formula



The photoinitiators were incorporated at 1% w/w in the above monomer and tested on the UV Colordry moving belt system described earlier (see section 1.7.1). Since the monomer molecule contains two epoxy groups, chain propagation will

develop in three dimensions to yield ultimately a highly crosslinked polymer network. The results are presented below in table 4.1.

Table 4.1 UV curing results for the cationic polymerisation of 3,4-epoxycyclohexylmethyl-3',4'-epoxycyclohexane carboxylate using iron-arene photoinitiators

E X P T	INITIATOR	NUMBER OF PASSES			
		Touching Quartz #	Touching Glass #	In Air	Glass Filter
1	[CpFe-fluorene] <sup>+</sup>	14	18	3	7
2	[CpFe-xanthene] <sup>+</sup>	19	19	4	10
3	[CpFe-toluene] <sup>+</sup>	11	11	2	4
4	[CpFe-thioxanth- ene] <sup>+</sup>	*	*	*	*

All above iron complexes isolated as their PF<sub>6</sub><sup>-</sup> salts

(Moving belt speed = 10ft/min, Coating thickness = 25μ)

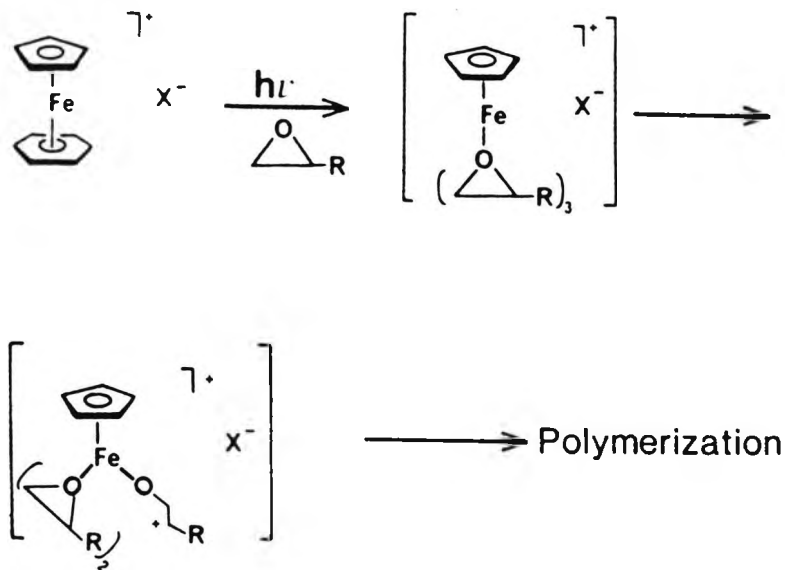
\* curing observed, but not to tack-free state after 30 passes

# curing observed at edges first

The first general point to note is that the rate of cure in air and under glass filter is greater than the corresponding touching quartz or touching glass experiment. Thus the polymerisation proceeds at a greater rate for cationic polymerisation using these initiators when air is present. This is in marked contrast to free radical polymerisation

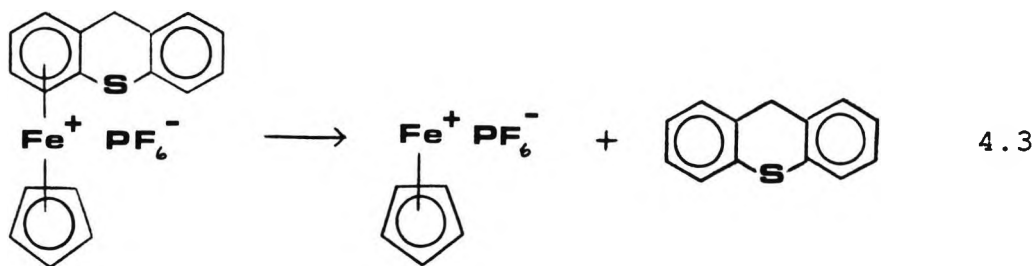
where the reverse is normally true due to the oxygen inhibition effect. It is proposed that oxygen actually enhances the cure rate for these compounds in cationic polymerisation. The oxidation state of the iron in these complexes is +2. The proposed role of oxygen is to oxidise the compounds with iron in the +2 oxidation state to the +3 oxidation state. Iron in the +3 oxidation state is a better Lewis acid than the +2 oxidation state. This effectively means that the better Lewis acid (+3 oxidation state) will be more reactive towards an epoxide, a Lewis base, and hence require a lower number of passes, indicating a greater rate of polymerisation, to achieve a tack-free cure. This process is outlined in scheme 4.3.

Scheme 4.3 A general mechanism for the polymerisation of epoxides using iron-arene salts



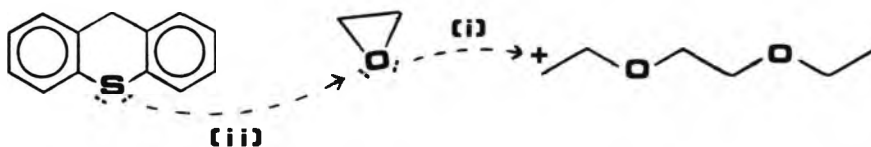
This also explains why the results with touching quartz and touching glass cure is always noticed at the edges first since oxygen is present here and the above scheme may operate.

The second point to note is that the thioxanthene derivative (EXPT 4, Table 4.1) was observed to cure well initially but does not reach a tack free cure after 30 passes. This could be due to the nucleophilic character of sulphur and its ability to increase its coordination. On photolysis a Lewis acid is released, which can initiate polymerisation, along with the thioxanthene group as shown in equation 4.3.



As polymerisation proceeds the sulphur atom of the thioxanthene group can act as a nucleophile to attack the growing polymer chain terminating polymerisation as shown in scheme 4.4.

Scheme 4.4 The nucleophilic character of sulphur in the cationic polymerisation of an epoxide



This would result in a large number of low molecular weight polymers which could explain the observed phenomenon.

Attempts were made to increase the rate of cationic polymerisation using the iron-arene compounds in conjunction with co-initiators. The approach used was to incorporate electron acceptors into the formulation in order that the oxidation of the iron-arene complexes from the +2 oxidation state to the +3 oxidation state would be accelerated giving rise to a greater rate of polymerisation. The iron-arene complexes (1% w/w) were used in conjunction with;

(1)  $\text{Ph}_2\text{I}^+\text{PF}_6^-$  (1% w/w)

(2)  $\text{Ph}_3\text{S}^+\text{PF}_6^-$  (1% w/w)

which were incorporated into the above monomer. The results indicated no beneficial effect of adding either of the above compounds. Previous studies indicated that the reactivity of the iron-arene complexes in cationic polymerisation can be enhanced

in the presence of the oxidant cumene hydroperoxide (Meier and Zweifel, 1986). This suggests that the role of oxygen is crucial in the electron exchange on going from the iron (II) to the iron (III) species.

#### 4.5 UV curing results for iron-arene complexes in free radical polymerisation

Although there have been several reports on the initiation of cationic polymerisation using the iron-arene salts relatively little attention has been given to the free radical initiating properties of these complexes. One recent report gave details of the related ferrocene sensitised photopolymerisations of vinyl monomers by means of kinetic and spectroscopic analyses (Tsubakiyama *et al*, 1991).

It was decided to investigate the possible free radical initiating properties of the iron-arene complexes.

The iron-arene complexes (1% w/w) were tested in both tripropyleneglycol diacrylate (TPGDA) and trimethylolpropane triacrylate (TMPTA) using the UV Colordry apparatus described earlier (see section 1.7.1). The results using the difunctional monomer, TPGDA, are presented in table 4.2, and the results using the trifunctional monomer, TMPTA, are given in table 4.3.

Table 4.2 UV curing results for the free radical polymerisation of TPGDA initiated by iron-arene complexes

E X P T	INITIATOR	NUMBER OF PASSES			
		Touching Quartz	Touching Glass	In Air	Glass Filter
1	[CpFe-thioxanthene] <sup>+</sup>	9	20	28	*
2	[CpFe-xanthene] <sup>+</sup>	12	*	*	*
3	[CpFe-1,2-dichlorobenzene] <sup>+</sup>	6	25	*	*
4	[CpFe-toluene] <sup>+</sup>	10	19	*	*
5	[CpFe-fluorene] <sup>+</sup>	11	25	*	*
6	[CpFe-4-chlorotoluene] <sup>+</sup>	9	(*)	*	*
7	TPGDA	*	*	*	*

All above iron complexes isolated as their PF<sub>6</sub><sup>-</sup> salts

(Moving belt speed = 10ft/min, Coating thickness = 25μ)

\* curing not observed after 30 passes

(\*) curing observed but not tack-free after 30 passes

Table 4.3 UV curing results for the free radical polymerisation of TMPTA initiated by iron-arene complexes

E X P T	INITIATOR	NUMBER OF PASSES			
		Touching Quartz	Touching Glass	In Air	Glass Filter
1	[CpFe-4-chloro- toluene] <sup>+</sup>	5	10	*	*
2	[CpFe-1,2-dichl- orobenzene] <sup>+</sup>	4	7	*	*
3	[CpFe-thioxanth- ene] <sup>+</sup>	4	9	*	*
4	[CpFe-fluorene] <sup>+</sup>	4	8	*	*
5	[CpFe-xanthene] <sup>+</sup>	6	13	*	*
6	[CpFe-toluene] <sup>+</sup>	3	6	*	*
7	TMPTA	6	*	*	*

All above iron complexes isolated as their PF<sub>6</sub><sup>-</sup> salts  
 Moving belt speed = 10ft/min, \* = curing not observed after  
 30 passes

The results in tables 4.2 and 4.3 indicate that the iron-arene complexes will initiate the polymerisation of acrylate monomers, presumably via a free radical pathway. The results also show that the rate of polymerisation is greater for the triacrylate (TMPTA) than for the diacrylate (TPGDA) as evidenced by the reduced number of passes for the complexes in table 4.3 when compared to table 4.2.

One interesting result in TPGDA is that the thioxanthene derivative (EXPT 1, Table 4.2) cures when touching glass (20 passes) and also in air (28 passes). It is proposed that this is due to the special nature of the thioxanthene group in reducing the inhibitive effect of oxygen on the polymerisation rate (see section 2.5.1).

#### 4.5.1 UV curing results for iron-arene complexes with N-methyldiethanolamine in free radical polymerisation

An attempt was made to reduce the oxygen inhibition effect for the free radical polymerisation of TPGDA using the iron-arene complexes. Thus N-methyldiethanolamine (5% w/w), which has been shown to act as an efficient oxygen scavenger (see section 1.4.5), was incorporated into the formulation along with the corresponding iron-arene initiator (1% w/w). The UV curing results are presented below in table 4.4.

Table 4.4 UV curing results for the free radical polymerisation of TPGDA initiated by iron-arene complexes (1% w/w) in the presence of N-methyldiethanolamine (5 %w/w)

EXPT	INITIATING SYSTEM	NUMBER OF PASSES			
		Touching Quartz	Touching Glass	In Air	Glass Filter
1	[CpFe-thioxanthene] <sup>+</sup> + Am	4 (9)	7 (20)	24 (28)	* (*)
2	[CpFe-xanthene] <sup>+</sup> + Am	9 (12)	* (*)	* (*)	* (*)
3	[CpFe-1,2-dichlorobenzene] <sup>+</sup> + Am	10 (6)	* (25)	* (*)	* (*)
4	[CpFe-toluene] <sup>+</sup> + Am	3 (10)	16 (19)	* (*)	* (*)
5	[CpFe-fluorene] <sup>+</sup> + Am	14 (11)	* (25)	* (*)	* (*)
6	[CpFe-4-chlorotoluene] <sup>+</sup> + Am	25 (9)	* (*)	* (*)	* (*)
7	Am	1	3	30	*

All above iron complexes isolated as their PF<sub>6</sub><sup>-</sup> salts

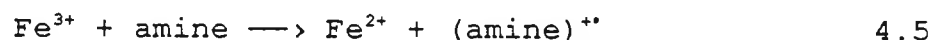
Am = N-methyldiethanolamine incorporated at 5% w/w TPGDA

(Moving belt speed = 10ft/min, Coating thickness = 25μ)

\* curing not observed after 30 passes

The amine used, N-methyldiethanolamine, will initiate polymerisation when it is used on its own (EXPT 7, table 4.4). The mechanism of this polymerisation is probably one of H-abstraction by the monomer from the amine to give α-aminoalkyl radicals which are capable of both (i) initiating polymerisation and (ii) reducing the effect of oxygen

inhibition. In comparison to this result all the other experiments in table 4.4 show a decrease in the rate of polymerisation. A possible explanation for this phenomenon is that the amine is being consumed in other reactions which reduce its effectiveness in its dual role. It is proposed that the amine reacts with the iron (III) species (produced in a photocatalysed oxidative process from the iron (II) species) which reduces the effectiveness of both the iron (III) species and the amine in initiating polymerisation as outlined in equations 4.4 and 4.5 below.



When the original photoactive iron (II) species in equation 4.4 has been consumed, producing the photoinactive iron (II) species in equation 4.5, then the amine can go on to initiate polymerisation via the  $\alpha$ -aminoalkyl radicals. Due to competitive absorption with the iron species and arene fragments the efficiency of this process is somewhat reduced in all cases when compared to the case where the amine is used on its own. It would appear that it is not beneficial to use electron donors as co-initiators in radical polymerisation in conjunction with iron-arene complexes.

## 4.6 Real-Time Infrared (RTIR) Spectroscopy results for iron-arene complexes

### 4.6.1 Introduction

The iron-arene compounds have been tested utilising the technique of RTIR Spectroscopy which has been described earlier (see section 1.7.2). The compounds have been irradiated using a medium pressure mercury lamp for a period of five minutes during which time the polymerisation kinetic curve was recorded. It is possible to calculate both the degree of conversion and the rate of polymerisation,  $R_p$ , at any time during the experiment.

### 4.6.2 RTIR results of iron-arene complexes in free radical polymerisation

A summary of the results is given below in table 4.5.

Table 4.5 RTIR spectroscopy results of the free radical polymerisation of TMPTA initiated by iron-arene complexes

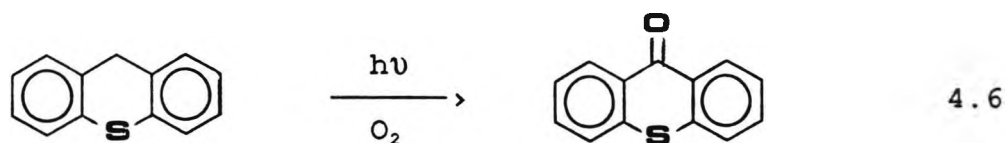
E X P T	INITIATOR	Induction Period/ seconds	R <sub>p</sub> (max) / 10 <sup>-2</sup> mol/l/s	Degree of Conversion (5 minutes) / %
1	[CpFe-toluene] <sup>+</sup>	36	0.9	16
2	[CpFe-4-chloro- toluene] <sup>+</sup>	18	0.9	18
3	[CpFe-1,2-dich- lorobenzene] <sup>+</sup>	15	1.3	20
4	[CpFe-thioxanth- ene] <sup>+</sup>	1	1.9	34
5	[CpFe-fluorene] <sup>+</sup>	18	1.3	25
6	[CpFe-xanthene] <sup>+</sup>	6	1.5	24

All above complexes isolated as their PF<sub>6</sub><sup>-</sup> salts and formulated at 0.5% w/w in TMPTA

The first point to make is that the iron-arene compounds are capable of initiating the free radical polymerisation of an acrylate monomer. This is evidenced by the reduction in the 810cm<sup>-1</sup> absorption in the IR spectrum corresponding to the disappearance of the C=C stretching vibration for all the compounds tested. A general trend that appears from table 4.5 is that the R<sub>p</sub>(max) value is related to the degree of conversion which in turn is related to the induction period observed.

Thus the toluene derivative (EXPT 1, Table 4.5) shows the longest induction period (36s), has the lowest degree of conversion (16%), and the lowest rate of polymerisation ( $0.9 \times 10^{-2}$  mol/l/s). In contrast to this the thioxanthene derivative (EXPT 4, Table 4.5) has the shortest induction period (1s), with the highest degree of polymerisation (34%), and the highest rate of polymerisation ( $1.9 \times 10^{-2}$  mol/l/s).

A further point of interest is the particularly short induction period of 1 second shown for the thioxanthene derivative. This is thought to be due to the role of the thioxanthene moiety in the polymerisation mechanism. The induction period is primarily due to the effect of oxygen inhibition of polymerisation. It is believed that the thioxanthene group has an effect on reducing the effect of oxygen inhibition on the polymerisation process. The thioxanthene group can react with oxygen present to yield thioxanthone thus reducing oxygen inhibition of polymerisation as shown below in equation 4.6.



4.6.3 UV curing results for cationic polymerisation using an iron-arene salt sensitised with a diphenyliodonium salt

It is known that thioxanthone sensitises diphenyliodonium

salts in cationic polymerisation (Gatechair and Pappas, 1982). This sensitisation was proposed to be via an electron transfer mechanism and model calculations showed that the free energy for this process,  $\Delta G = -22\text{Kcal/mol}$ , which is in accordance with a diffusion controlled reaction (Rehm and Weller, 1969; Arnold and Maroulis, 1976). Therefore, it was decided to test  $\eta^6$ -thioxanthene- $\eta^5$ -cyclopentadienyliron hexafluorophosphate (1% w/w) in the presence of diphenyliodonium hexafluorophosphate (1% w/w) and the cycloaliphatic diepoxide monomer, 3,4-epoxycyclohexylmethyl-3',4'-epoxycyclohexane carboxylate, to see if any sensitisation of polymerisation occurred. The formulation was tested using the UV Colordry moving belt system (see section 1.7.1) the results are given in table 4.6.

Table 4.6 Cationic polymerisation of an epoxide using diphenyliodonium hexafluorophosphate sensitised with an iron arene salt

E X P T	INITIATOR	NUMBER OF PASSES			
		Touching Quartz	Touching Glass	In Air	Glass Filter
1	[CpFe-thioxanthene] <sup>+</sup>	(*)	(*)	(*)	(*)
2	Ph <sub>2</sub> I <sup>+</sup> PF <sub>6</sub> <sup>-</sup>	4	*	4	*
3	[CpFe-thioxanthene] <sup>+</sup> + Ph <sub>2</sub> I <sup>+</sup> PF <sub>6</sub> <sup>-</sup>	2	13	1	9
4	"	-	-	3	-

[CpFe-thioxanthene]<sup>+</sup> isolated as the PF<sub>6</sub><sup>-</sup> salt.

(Coating thickness = 25μ for all experiments, moving belt speed = 10ft/min for all experiments except EXPT 4 = 80ft/min)

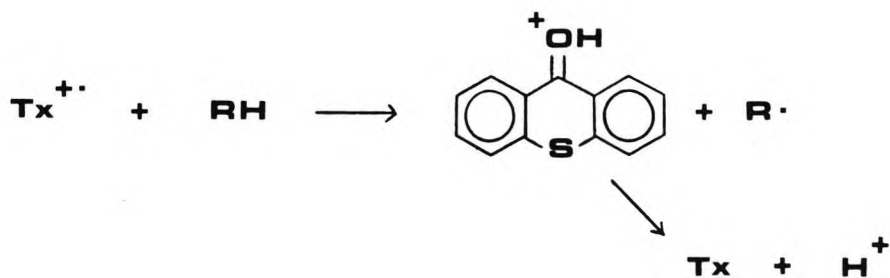
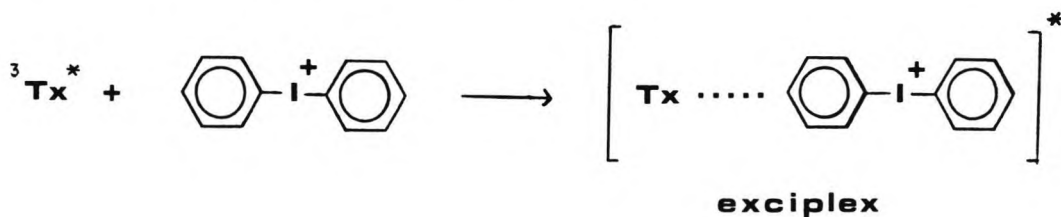
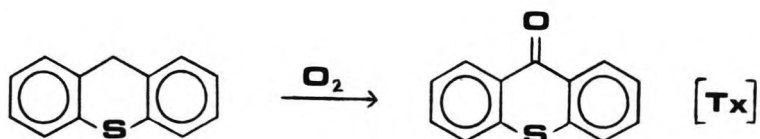
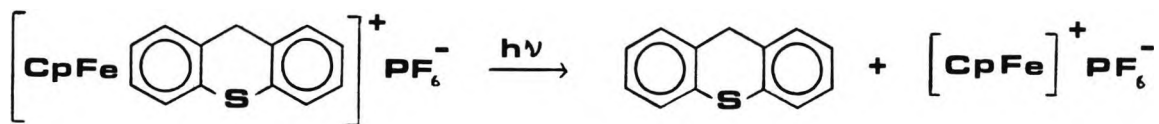
(\*) = curing observed but not to tack-free state

\* = curing not observed after 30 passes

- = experiment not performed

The results indicate a definite sensitisation for all four experimental conditions. What can be seen from table 4.6 is that the polymerisation proceeds at a greater rate when atmospheric oxygen is present than when it is excluded by the use of a touching slide (EXPT 3, Table 4.6). This can be seen when comparing the results of touching quartz (2 passes) versus in air (1 pass, or 3 passes at faster belt speed) where both experiments receive the full output of the lamp. This effect can also be seen when comparing the results of touching glass (13 passes) versus glass filter (9 passes) where both experiments receive the same amount of filtered light. This indicates that the presence of oxygen is important in the mechanism of polymerisation and the following sequence in scheme 4.5 is proposed to account for the above observations.

Scheme 4.5 The role of oxygen in the sensitisation of diphenyliodonium hexafluorophosphate in cationic polymerisation using  $\eta^6$ -thioxanthene- $\eta^5$ -cyclopentadienyliron hexafluorophosphate

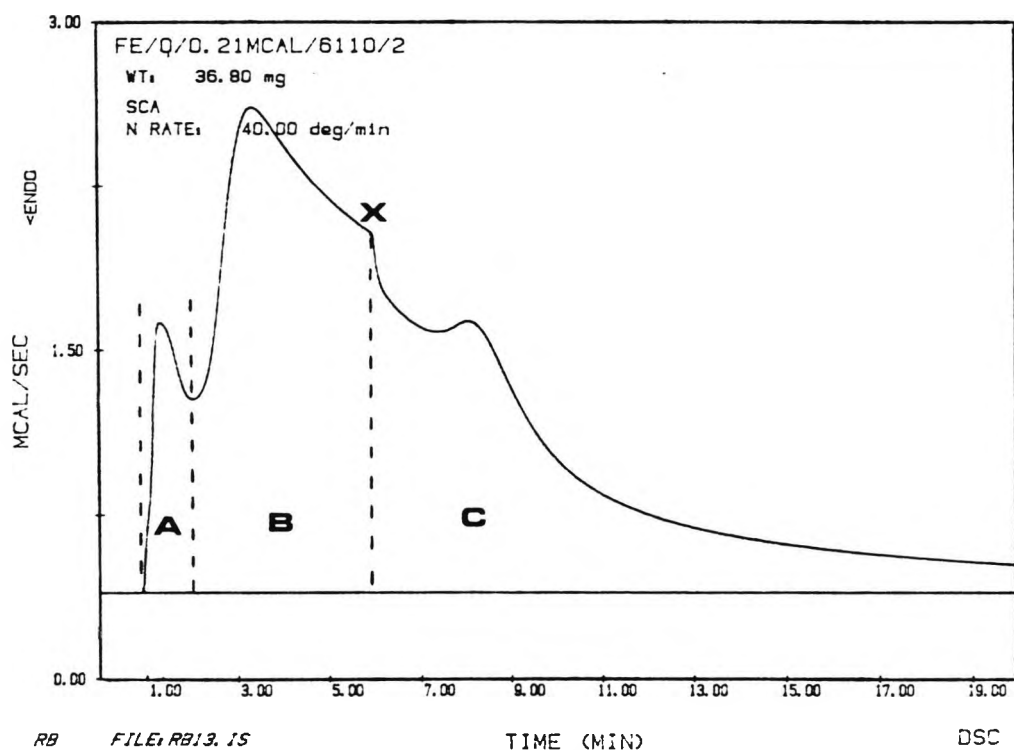


4.7 Photo-differential scanning calorimetry (Photo-DSC)  
results of iron-arene complexes

An iron arene complex has been tested using the technique of Photo-DSC described earlier (see section 1.7.3).

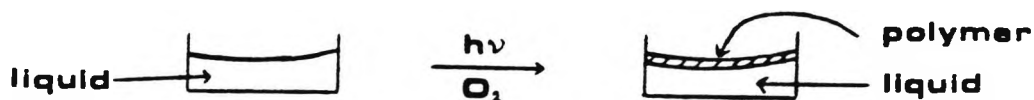
4.7.1 Photo-DSC results of iron-arene complexes in  
cationic polymerisation

Figure 4.1 The Photo-DSC results for the cationic polymerisation of an epoxide initiated by an iron-arene complex



A sample of  $\eta^6$ -fluorene- $\eta^5$ -cyclopentadienyliron hexafluorophosphate (1% w/w) in 3,4-epoxycyclohexylmethyl-3',4'-epoxycyclohexane carboxylate was irradiated in the presence of air to give the polymerisation trace in figure 4.1. The trace may be visualised in three different sections represented by;

A. The liquid sample initially forms a solid polymeric meniscus in the DSC sample pan as the initiator reacts with oxygen present at the air/liquid interface to effect polymerisation. This is represented below.



This gives rise to the sharp exothermic peak shown in A.

B. The remainder of the bulk in the DSC sample pan is polymerised in part B. The rate reaches a maximum and then slowly decreases.

C. At point X the light source was turned off as the rate of polymerisation is declining. The rate continues to decline and then proceeds to reach another maximum. This is thought to be due to the Tromsdorff Effect in which autoacceleration of polymerisation takes place. After the maximum the polymerisation rate gradually declines. It is noticeable that this decline is much more gradual than for a trace of a free radical polymerisation. This emphasises

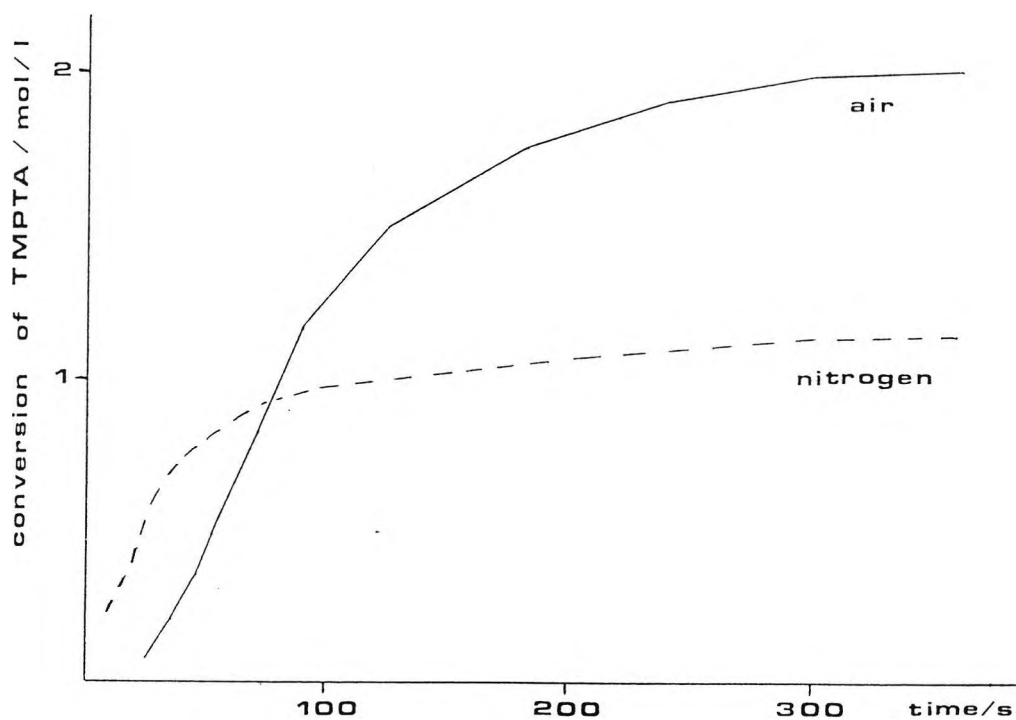
the 'living polymer' nature so often exhibited by cationic polymerisations.

A similar experiment was performed but this time the sample was irradiated in the presence of nitrogen instead of in air. During the same time period of irradiation no polymerisation was detected and the sample remained liquid in the DSC sample pan. This same sample was then irradiated in the presence of air (oxygen) and again no polymerisation was detected and the sample remained liquid after the same time period of irradiation. A possible explanation for this observation is that in the presence of nitrogen the initiator was photolysed giving rise to only iron II species which are not reactive at this light intensity and wavelength under isothermal conditions to initiate polymerisation. When air is readmitted into the DSC chamber the photoinitiator concentration has been depleted to a much lower level so that there is virtually no original photoinitiator present. This in effect means that no iron III species can be formed and explains why no polymerisation was observed. Therefore, to be of use this initiator must be photolysed in the presence of an oxidant (in this case oxygen) so that a beneficial effect on the rate of polymerisation may be seen.

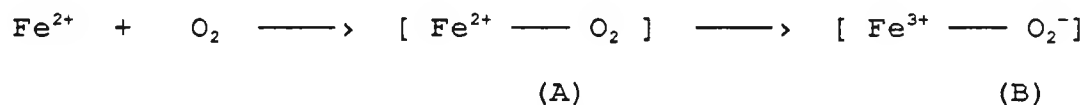
4.7.2 Photo-DSC results of iron-arene complexes in free radical polymerisation

Photo-DSC has been used to look at the free radical polymerisation of  $\eta^6$ -fluorene- $\eta^5$ -cyclopentadienyliron hexafluorophosphate (1% w/w) in the presence of TMPTA. Figure 4.2 shows the effect of irradiation of the complex in the presence of air and under nitrogen.

Figure 4.2 The Photo-DSC results for the free radical polymerisation of TMPTA, in air and under nitrogen, initiated by an iron-arene complex



As for cationic polymerisation it is proposed that the iron II species reacts with oxygen to produce an iron III species. The precise mechanism of this reaction is in some doubt but an initial step is likely to be:



The electronic possibilities of A include one-electron acceptance by O<sub>2</sub> so that there is effectively a coordinated superoxide ion (and Fe<sup>3+</sup>) as shown in (B). This gives rise to a possibility of a radical species which could go on to initiate polymerisation.

In a nitrogen atmosphere there is virtually no induction period observed and polymerisation ensues. When air is present the polymerisation curve shows a noticeable induction period which is gradually overcome as the rate of polymerisation increases. This is presumably due to the reaction above occurring and giving rise to more free radical species. In the presence of air the degree of conversion is much greater than when nitrogen is present. This indicates that a certain amount of air is beneficial to the radical polymerisation using this initiator, though presumably there will be a balance between the beneficial effect, as it is used to oxidise the initiator, and the detrimental effect of oxygen inhibition of polymerisation.

A further experiment involved the use of an electron donor, benzyltri-*n*-butylstannane, with the fluorene derivative. Independent experiments were performed in air (oxygen) to give DSC results of;

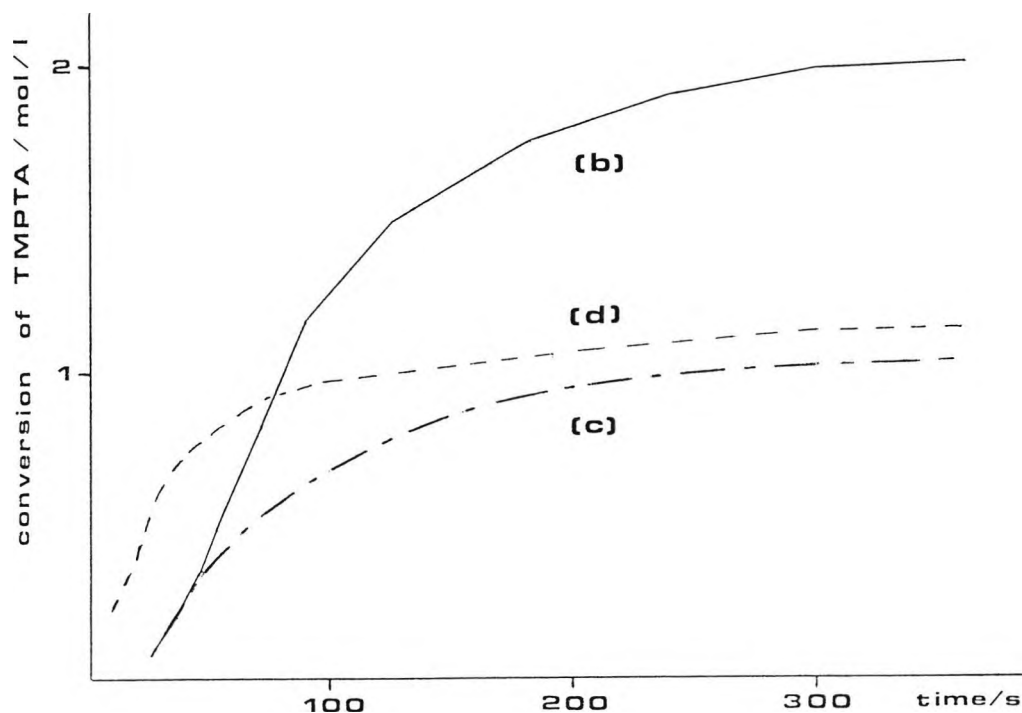
- (a) Benzyltri-*n*-butylstannane (1% w/w) in TMPTA
- (b) Fluorene derivative (1%w/w) in TMPTA
- (c) Fluorene derivative (1%w/w) + benzyltri-*n*-butylstannane (1% w/w) in TMPTA

It was found that;

- (a) did not polymerise in air
- (b) & (c) showed polymerisation in air

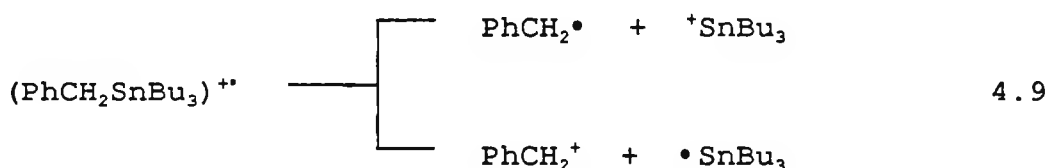
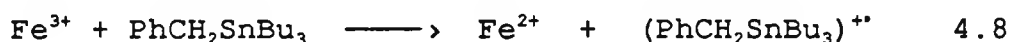
The resultant DSC traces for experiments (b) and (c) are shown in figure 4.3 below along with trace (d) which represents the polymerisation of the fluorene derivative (1% w/w) in TMPTA under a nitrogen atmosphere.

Figure 4.3 The Photo-DSC results for the free radical polymerisation of TMPTA initiated by an iron-arene complex (on it's own in air [b] and nitrogen [d], and in the presence of  $\text{PhCH}_2\text{SnBu}_3$  in air [c])



The results show that the overall degree of conversion is lower when the two compounds are tested together, ie. curve (c), than when the fluorene derivative is tested on its own, ie. curve (b). This could be due to a combination of electron transfer reactions and the depletion of oxygen by any tin radicals produced as outlined in scheme 4.6 below.

Scheme 4.6 Proposed reaction scheme for the photopolymerisation of TMPTA in air using  $\eta^6$ -fluorene- $\eta^5$ -cyclopentadienyliron hexafluorophosphate (1% w/w) with benzyltri-*n*-butylstannane (1% w/w)



Consider curve (c) which represents the formulation of the stannane + fluorene derivative. Initially the predominant reaction is that shown in equation 4.7. This gives rise to the production of iron (III) species which can then react with the stannane as shown in equation 4.8. The radical cation of the stannane, so formed, in equation 4.8 may then fragment as depicted in equation 4.9 to yield a tri-*n*-butyltin radical which is known to react with oxygen as shown in equation 4.10 (Bennett and Howard, 1972). This depletes the available oxygen level for the reaction with the original iron-arene, shown in equation 4.7, and thus reduces the reactivity towards polymerisation.

Another interesting feature is observed when comparing the DSC traces of the formulation of the stannane + fluorene

derivative in air (curve c) with the formulation of the fluorene derivative in nitrogen (curve d). The combination in air (curve c) exhibits a reactivity that is similar to the iron (II) species on its own in nitrogen (curve d). This is further evidence to support the reaction scheme 4.6 shown above. The two curves (c and d) show a remarkably similarity with the main difference being the oxygen inhibition of the mixture (c) giving an induction period and a slightly lower overall percentage conversion.

#### 4.8 Experimental Section

See section 2.7 for general experimental details. All  $^1\text{H}$  NMR were run in acetone- $d^6$  with TMS as the internal standard. All IR spectra were recorded using KBr discs. Methanol was used as the solvent for all UV spectra.

#### 38. $\eta^6$ -methylbenzene- $\eta^5$ -cyclopentadienyliron hexafluorophosphate

A mixture of ferrocene (15.0g; 81 mmol), powdered anhydrous  $\text{AlCl}_3$  (21.3g; 162 mmol), and Al powder (size  $20\mu$ ; 2.1g; 81 mg-atom), in toluene (300 ml) was refluxed overnight (bath temperature  $140^\circ\text{C}$ ). The colour of the solution changed from orange through light-green to red-brown. The mixture was cooled, and added to iced-water (400ml) carefully, and then stirred vigorously for a few minutes. The mixture was filtered prior to washing with ether. The aqueous layer was then treated with a slight excess of  $\text{KPF}_6$ . The pale-yellow precipitate was filtered off and purified by reprecipitation from acetone by addition of ether, followed by recrystallisation from ethanol to give 14.5g (50%) yield with mp  $164\text{--}165^\circ\text{C}$  (lit mp  $165^\circ\text{C}$ ; Astruc and Dabard, 1975).

#### Analysis

$^1\text{H}$  NMR: 6.40 (m, 5H), 5.15 (s, 5H), 2.50 (s, 3H)

IR: 3121 (m), aromatic C-H stretch

1464 (m), 1421 (m), C=C stretch

1114 (w), 1011 (w), Cp

UV:  $\lambda_{\text{max}}$  = 460nm ( $\epsilon=60$ ), 360nm ( $\epsilon=100$ ), 320nm ( $\epsilon=300$ )

MS: 213 (tolueneFeCp<sup>+</sup>), 186 (Cp<sub>2</sub>Fe<sup>+</sup>), 92 (toluene<sup>+</sup>), 65 (Cp<sup>+</sup>)

CHN: calculated for C<sub>12</sub>H<sub>13</sub>F<sub>6</sub>FeP

required C 40.25 H 3.66

found C 39.97 H 3.69

39.  $\eta^6$ -4-Chloro (methylbenzene) - $\eta^5$ -cyclopentadienyliron hexafluorophosphate

The title compound was synthesised by the same procedure used to obtain compound 38, using 4-chlorotoluene (100ml) as the refluxing solvent (bath temperature 190°C) with ferrocene (6.0g; 32mmol), AlCl<sub>3</sub> (8.0g; 60mmol), and Al powder (0.7g; 26mg-atom) to give 6.4g (45%) yield with mp 200°C (decomp.).

Analysis

<sup>1</sup>H NMR: 6.60 (m, 4H), 5.20 (s, 5H), 2.50 (s, 3H)

IR: 3122 (w), 3093 (w), aromatic C-H stretching  
2925 (w), aliphatic C-H stretch  
1456 (m), 1421 (m), C=C stretching

1096 (m), 1013 (w), Cp  
874 (s), 1,4-disubstituted benzene  
474 (s), Ph-Cl stretch

UV:  $\lambda_{\text{max}}$  = 460nm ( $\epsilon=84$ ), 380nm ( $\epsilon=184$ ), 320nm ( $\epsilon=480$ )

MS: 128, 127, 126, 125 (Cl-C<sub>6</sub>H<sub>4</sub>-Me<sup>+</sup>), 91 (C<sub>6</sub>H<sub>4</sub>-Me<sup>+</sup>)

CHN: Calculated for C<sub>12</sub>H<sub>12</sub>ClF<sub>6</sub>FeP  
required C 36.72 H 3.08  
found C 36.86 H 3.01

40.  $\eta^6$ -1,2-Dichlorobenzene- $\eta^5$ -cyclopentadienyliron  
hexafluorophosphate

The title compound was synthesised by the same procedure used to obtain compound 38, using 1,2-dichlorobenzene (100ml) as the refluxing solvent (bath temperature 190°C) with ferrocene (6.0g; 32mmol), AlCl<sub>3</sub> (8.0g; 60mmol), and Al powder (0.7g; 26mg-atom) to give 6.6g (50%) yield with mp 200°C (decomp).

Analysis

<sup>1</sup>H NMR: 6.90 (m, 4H), 5.41 (s, 5H)

IR: 3123 (s), 3092 (s), aromatic C-H stretch  
1426 (s), 1397 (s), C=C stretch  
1109 (m), 1012 (m), Cp

746 (s), 1,2-disubstituted benzene

UV:  $\lambda_{max} = 450\text{nm}$  ( $\epsilon=82$ ),  $380\text{nm}$  ( $\epsilon=164$ ),  $320\text{nm}$  ( $\epsilon=600$ )

MS: 186 ( $\text{Cp}_2\text{Fe}^+$ ), 146 (dichlorobenzene<sup>+</sup>), 65 ( $\text{Cp}^+$ ), 56 ( $\text{Fe}^+$ )

CHN: Calculated for  $\text{C}_{11}\text{H}_9\text{Cl}_2\text{F}_6\text{FeP}$   
required C 32.00 H 2.20  
found C 31.89 H 2.18

**41.  $\eta^6$ -Thioxanthene- $\eta^5$ -cyclopentadienyliron hexafluorophosphate**

A.

Thioxanthone (5.0g; 0.024 mol) was dissolved in anhydrous THF (300ml). Borane (48ml; 1M solution in THF; 0.048 mol) was added at room temperature with stirring under argon. The mixture was stirred for 1h and then refluxed for 3h. After cooling excess borane was decomposed by addition of ice-chips. The solution was diluted with an equal volume of water and the THF was removed. The resulting precipitate was filtered off in quantitative yield.

B.

A mixture of ferrocene (5.5g; 30 mmol),  $\text{AlCl}_3$  (16.0g; 120mmol), Al powder (0.81g; 30 mmol), and thioxanthene (4.7g; 24 mmol) was heated with mechanical stirring in decalin (75 ml) for 4h (bath temperature  $190^\circ\text{C}$ ). After

cooling slightly the reaction mixture was poured onto iced-water (500 ml) with stirring. Any residual solid was washed out of the reaction flask with water and ether. After stirring for 10 min the solid material was filtered off. The aqueous layer was washed with ether and then treated with a slight excess of  $KPF_6$ . The precipitate was filtered off and purified by reprecipitation from acetone by addition of ether, followed by recrystallisation from ethanol to give 4.5g (40%) yield with mp 127-128°C.

#### Analysis

$^1H$  NMR: 7.60 (m, 4H), 6.60 (m, 4H), 4.70 (s, 5H), 4.1 (q, 2H)

IR: 3114 (w), aromatic C-H stretch  
1439 (m), 1418 (m), C=C stretching  
1104 (w), 1013 (w), Cp  
754 (m), 1,2-disubstituted benzene

UV:  $\lambda_{max} = 460nm$  ( $\epsilon=77$ ),  $400nm$  ( $\epsilon=270$ ),  $330nm$  ( $\epsilon=1600$ )

MS: 319 (thioxanthene $FeCp^+$ ), 198 (thioxanthene $^+$ ), 186 (Cp $_2Fe^+$ ), 121 (Cp $Fe^+$ ), 56 (Fe $^+$ )

CHN: Calculated for C $_{18}$ H $_{15}$ F $_6$ FePS  
required C 46.60 H 3.26  
found C 46.47 H 3.20

#### 42. $\eta^6$ -Fluorene- $\eta^5$ -cyclopentadienyliron hexafluorophosphate

The title compound was synthesised by a similar procedure used to obtain compound 41, (part B) using fluorene (16.6g; 0.1mol), ferrocene (18.6g; 0.1mol), AlCl<sub>3</sub> (64.0g; 0.48mol), and Al powder (3.6g; 0.12mol) heated in decalin overnight (bath temperature 160°C) to give 23.0g (53%) yield with mp 161-162°C (decomp) (lit mp 163-165°C [decomp]; Helling and Hendrickson, 1977).

#### Analysis

<sup>1</sup>H NMR: 7.40-8.20 (m, 4H), 6.40-7.30 (m, 4H), 5.20 (s, 5H), 4.5 (s, 1H), 4.20 (s, 1H)

IR: 3130 (w), aromatic C-H stretch  
1435 (m), 1421 (m), C=C stretching  
1108 (w), 1014 (w), Cp  
775 (s), 1,2-disubstituted benzene

UV:  $\lambda_{max}$  = 460nm ( $\epsilon=100$ ), 400nm ( $\epsilon=160$ ), 320nm ( $\epsilon=600$ )

MS: 287 (fluoreneFeCp<sup>+</sup>), 186 (Cp<sub>2</sub>Fe<sup>+</sup>), 166 (fluorene<sup>+</sup>)

CHN: calculated for C<sub>18</sub>H<sub>15</sub>F<sub>6</sub>FeP  
required C 50.03 H 3.50  
found C 50.02 H 3.43

#### 43. $\eta^6$ -Xanthene- $\eta^5$ -cyclopentadienyliron hexafluorophosphate

The title compound was synthesised by a similar procedure

used to obtain compound 41 (part B), using xanthene (10.0g; 55mmol), ferrocene (10.0g; 55mmol), AlCl<sub>3</sub> (29.3g; 220mmol), and Al powder (1.5g; 55mmol) heated in decalin for 5h (bath temperature 140°C) to give 11.0g (45%) yield with mp 114-115°C.

Analysis

<sup>1</sup>H NMR: 7.40 (m, 4H), 6.40 (m, 4H), 5.00 (s, 5H), 4.30 (s, 2H)

IR: 3125 (w), aromatic C-H stretch  
1457 (s), C=C stretch  
1263 (s), Ph-O stretch  
1110 (w), 1012 (w), Cp  
764 (s), 1,2-disubstituted benzene

UV:  $\lambda_{\text{max}}$  = 460nm ( $\epsilon=78$ ), 390nm ( $\epsilon=196$ ), 320nm ( $\epsilon=1176$ )

MS: 182 (xanthene<sup>+</sup>)

CHN: calculated for C<sub>18</sub>H<sub>15</sub>F<sub>6</sub>FeOP  
required C 48.24 H 3.37  
found C 48.13 H 3.25

#### 4.9 References

- Albright, T.A., (1982). *Tetrahedron*, **38**, 1339
- Arnold, D.R., and Maroulis, A.J., (1976). *J.Am.Chem.Soc.*, **98**, 5931
- Astruc, D., and Dabard, R., (1975). *Bull.Soc.Chem.France*, 2571
- Bennett, J.E., and Howard, J.A., (1972). *J.Am.Chem.Soc.*, **94**, 8244
- Chrisope, D.R., Kyung, M.P., and Schuster, G.B., (1989). *J.Am.Chem.Soc.*, **111**, 6195
- Coffield, T.H., Sandel, V., and Closson, R.D., (1957). *J.Am.Chem.Soc.*, **79**, 5826
- Curtis, H., Irving, E., and Johnson, B.F.G., (1986). *Chem.Brit.*, 327
- Gatechair, L.R., and Pappas, S.P., (1982). *Org.Coat.Appl.Polym.Sci.Proc.*, **46**, 183 ACS Meeting, Las Vegas, March 25 - April 2
- Gill, T.P., and Mann, K.R., (1980). *Inorg.Chem.*, **19**, 3007

- Gill, T.P., and Mann, K.R., (1983). *Inorg.Chem.*, **22**, 1986
- Green, M.L.H., Pratt, L., and Wilkinson, G., (1960).  
*J.Chem.Soc. A*, 989
- Helling, J.F., and Hendrickson, W.A., (1977).  
*J.Organomet.Chem.*, **141**, 99
- Klingert, B., Riediker, M., and Roloff, A., (1988).  
*Comments Inorg. Chem.*, **7**, 109
- Lee, C.C., Sutherland, R.G., and Thomson, B.J., (1972).  
*J.Chem.Soc.Chem.Comm.*, 907
- Lohse, F., and Zweifel, H., (1986). *Adv.Polym.Sci.*, **78**, 61
- McNair, A.N., Schrenk, J.L., and Mann, K.R., (1984).  
*Inorg.Chem.*, **23**, 2633
- Meier, K., and Rhis, G., (1985). *Angew.Chem.*, **97**, 879
- Meier, K., and Zweifel, H., (1985). *EP* 152 377
- Meier, K., and Zweifel, H., (1986). *J.Rad.Curing*, 26
- Morrison, W.H., Ho, E.Y., and Hendrickson, D.N., (1974).  
*J.Am.Chem.Soc.*, **96**, 3603

- Morrison, W.H., Ho, E.Y., and Hendrickson, D.N., (1975).  
*Inorg.Chem.*, **14**, 500
- Nesmeyanov, A.N., Vol'kenau, N.A., and Bolesova, I.N.,  
(1963). *Tet.Lett.*, 1725
- Nesmeyanov, A.N., Vol'kenau, N.A., and Bolesova, I.N.,  
(1965). *Dokl.Akad.Nauk SSSR*, **160**, 1327
- Nesmeyanov, A.N., Vol'kenau, N.A., and Bolesova, I.N.,  
(1966). *Dokl.Akad.Nauk SSSR*, **166**, 607
- Nesmeyanov, A.N., Vol'kenau, N.A., Sirotkina, E.I., and  
Deryabin, V.V., (1967). *Dokl.Akad.Nauk SSSR*, **177**, 1110
- Nesmeyanov, A.N., Vol'kenau, N.A., and Shilovtseva, L.S.,  
(1970). *Dokl.Akad.Nauk SSSR*, **190**, 857
- Rehm, D., and Weller, A., (1969). *Ber.Bunsenges.*  
*Phys.Chem.*, **73**, 834
- Roloff, A., Meier, K., and Riediker, M., (1986). *Pure &*  
*Appl. Chem.*, **58**, 1267
- Schrenk, J.L., Palazzotto, M.C., Mann, K.R., (1983).  
*Inorg.Chem.*, **22**, 4047
- Tsubakiyama, K., Fujisaki, S., Tabata, E., and Nakahara, S.,

(1991). *J.Macromol.Sci., Chem.A*, 28, 557

Zink, J.I., (1974). *J.Am.Chem.Soc.*, 96, 4464

Zweifel, H., and Meier, K., (1985). *Polym.Prepr.*, 26, 347

EP 094915 (1984) Ciba Geigy AG

EP 126712

# APPENDIX

## 5.1 Introduction

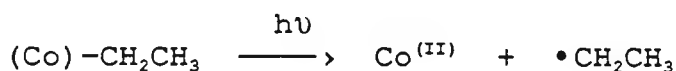
A preliminary investigation into some visible photoinitiators was carried out. Reports in the literature indicated that it could be of benefit to utilise cobaloximes and porphyrins as sources of alkyl radicals. It was proposed that the alkyl radicals, produced on irradiation of these complexes, could be used to initiate free radical polymerisation. The reaction mechanism in both the cobaloximes involves the cleavage of a metal-carbon bond which is in keeping with the theme of this work.

## 5.2 Cobaloximes

The photodealkylation of organocobalt derivatives of vitamin B<sub>12</sub> and of bisdimethylglyoximato-cobalt compounds ("cobaloximes") yields cobalt (II) derivatives of the parent chelates and alkyl radicals as the initial products (Shrauzer et al, 1968). The photolysis of alkylcobaloximes is initiated by excitation of the Co-C bond and proceeds by a mechanism related to charge-transfer (CT) induced photoreduction reactions of Co (III) complexes. The rate of Co-C bond photolysis depends essentially on the energy and intensity of the Co-C CT transition, both of which vary with the axial base attached to cobalt.

The photochemical reactions of alkylcobaloximes have been extensively studied (Dolphin, 1982). Golding et al (Golding et al, 1977) showed conclusively that for aqueous solutions

homolysis of the Co-C bond was the major primary process. Shrauzer et al (Shrauzer et al, 1968) drew similar conclusions. The methyl derivative gave both methane and ethane as photolysis products, the latter being formed by dimerisation. However, olefins were the major product for other alkylcobaloximes. An interesting mechanism has been proposed to explain this result (Shrauzer et al, 1968).



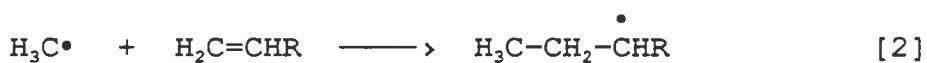
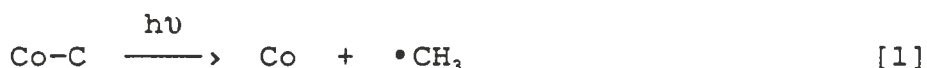
The aim of this work was to produce alkyl radicals in the presence of a free radical polymerisable monomer, TMPTA, to initiate polymerisation. What was not clear was the extent to which the alkyl radicals, produced on irradiation, would undergo initiation reactions in preference to other reactions such as recombination or disproportionation. In order to gain more information on the photoinitiating properties of these complexes the cobaloximes were incorporated into a polymerisable monomer, TMPTA, and tested using the UV Colordry apparatus described earlier (see section 1.7.1). The results are presented below.

E X P T	"COBALOXIME"	% w/w in TMPTA	NUMBER OF PASSES IN AIR
1	Me-Cobaloxime	1.0	19
2	Br(CH <sub>2</sub> ) <sub>4</sub> -Cobaloxime	1.0	*

2 lamps used for irradiation in both cases

\* = polymerisation not detected after 30 passes

The results indicate that the methyl-cobaloxime will initiate free radical polymerisation in air. This indicates that Co-C bond homolysis occurs on photolysis producing a methyl radical as shown below [1].



The methyl radical produced in [1] exists independently and must compete effectively with the dimerisation reaction [3] to initiate polymerisation [2].

In the case of the Br(CH<sub>2</sub>)<sub>4</sub> derivative it appears that either the extent of photolysis of the Co-C bond is low, or that on photolysis the recombination/disproportionation reactions

occur preferentially to the reaction initiating polymerisation.

These preliminary studies indicate some promise for further investigations of the methylcobaloxime derivative.

### 5.3 Porphyryns

The photochemistry of metalloporphyrins is of much interest in connection with the role of chlorophyll in photosynthesis. One report indicated that there was photoactivation of the metal-axial bond in aluminium porphyrins by visible light (Hirai et al, 1988). It has been known that photoactivation of a transition metal-axial ligand bond in metalloporphyrins brings about free radical dissociation, leading to the change in valence of the central metal (Imamura et al, 1985; Hendrickson et al, 1987).

In order to evaluate if this reaction could be used to produce free radicals capable of initiating polymerisation a porphyrin derivative was synthesised. First the free base porphyrin was synthesised using the procedure of Adler et al (Adler et al, 1970). This was reacted further with  $\text{CrCl}_2$  to yield the desired porphyrin  $\text{Cr}(\text{TPP})\text{Cl}$ , using the method described previously (Hoffmann and Basolo, 1977).

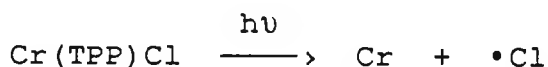
In order to determine the free radical-initiating properties of  $\text{Cr}(\text{TPP})\text{Cl}$  the porphyrin was incorporated (1% w/w) into

the free radically polymerisable monomer, TMPTA, and tested using the UV Colordry apparatus described earlier (see section 1.7.1). The result is presented below.

E X P T	"PORPHYRIN"	% w/w in TMPTA	NUMBER OF PASSES IN AIR
1	Cr (TPP)Cl	1.0	14

2 lamps used for irradiation

From the result it can be inferred that free radicals are produced from the photolysis of Cr(TPP)Cl, presumably via the following reaction:



The Cl• produced can then initiate free radical polymerisation. It may be of interest to replace the Cl with other ligands, eg. alkyl groups, to investigate this reaction further.

#### 5.4 Experimental section

##### (4-Bromo-n-butyl)bis[(2,3-butanedionedioximato)(1-)-N,N'](pyridine)cobalt

A suspension of cobalt (II) chloride ( 6.50g, 0.05 mol ) and dimethylglyoxime ( 11.6g, 0.10 mol) in methanol ( 190ml ) was stirred until all the cobalt chloride had dissolved. After adding sodium hydroxide ( 4g, 0.10 mol ) in water ( 12.5 ml ) the suspension was stirred under nitrogen for 10 min. Next 1,4-dibromobutane ( 7.50g ) was added, followed by sodium hydroxide ( 2.0g, 0.05 mol ). After 10 minutes the reaction mixture was filtered and diluted with water (500 ml). Excess dibromobutane was removed in an air stream. On adding pyridine (4.0g, 0.05 mol) a yellow precipitate formed which was washed , dried, and recrystallised (methanol). On cooling and standing crystals of 1,4-tetramethylenebis(pyridinatoncobaloxime) formed. From the filtrate (methanol), on dilution with water (4-bromo-n-butyl)bis[(2,3-butanedionedioximato)(1-)-N,N'](pyridine)cobalt was obtained (2.1g, 17%) : mp 175-176°C

##### Analysis

$^1\text{H}$  NMR: 1.10 (m,2H), 1.60 (m,4H), 2.20 (s,12H), 3.40 (m,2H), 7.30 (m,3H), 8.60 (m,2H)

IR: 3438 (broad), O-H stretch  
3109 (w), 3041 (w), 3000 (w), aromatic C-H stretching  
2951 (m), 2911 (m), 2853 (w), aliphatic C-H stretching  
1602 (m), 1560 (m), C=C stretching

UV:  $\lambda_{(\text{max})}$  = 430nm (sh) [ $\epsilon=2500$ ], 380nm (sh) [ $\epsilon=2800$ ],  
266nm [ $\epsilon=11,000$ ]

CHN: Calculated for  $\text{C}_{17}\text{H}_{27}\text{N}_5\text{O}_4\text{BrCo}$

Theory	C	40.48	H	5.39	N	13.88
Found	C	40.47	H	5.40	N	13.59

(Methyl)bis[(2,3-butanedionedioximato)(1-)-N,N'](pyridine)cobalt

A suspension of dimethylglyoxime (13.8g; 0.12mol) and cobalt(II)chloride (7.12g; 0.06mol) in methanol (100ml) was stirred until all the cobalt chloride had dissolved. Then NaOH (4.8g; 50%; 0.12mol) and pyridine (5.0g; 0.06mol) were added. The stirred suspension was cooled ( $-10^{\circ}\text{C}$ ) and stirred for 15 min. after adding NaOH (2.4g; 50%; 0.06mol) and sodium borohydride (0.40g; 0.01mol). Next dimethylsulphate (8.1g; 0.06mol) was added and the solution was gradually warmed to room temperature under an air stream. The mixture was stirred with water (32ml) and pyridine (1.7g; 0.02mol). The orange crystals were

collected and dried to give 10.5g (46% yield) (Shrauzer & Windgassen, 1966)

### Analysis

IR: 3448 (broad), O-H stretch  
2896 (w), aliphatic C-H stretching  
1599 (m), 1556 (m), C=C stretching

UV:  $\lambda_{(max)}$  = 440nm (sh) [ $\epsilon=2000$ ], 415nm (sh) [ $\epsilon=2500$ ],  
375nm (sh) [ $\epsilon=2800$ ], 266nm [ $\epsilon=11,000$ ]

CHN: Calculated for  $C_{14}H_{22}N_5O_4Co$

Theory	C	43.86	H	5.78	N	18.26
Found	C	42.95	H	5.66	N	17.89

### 5,10,15,20-Tetraphenyl-21H,23H-porphine

Pyrrole (28ml, 0.40 mol) and benzaldehyde (40ml, 0.40 mol) were added to refluxing propionic acid (400ml) and the mixture was refluxed for 30 min. The resulting mixture was filtered, washed (methanol and then water) and dried to give purple crystals (5.8g, 9%).

### Chloro(5,10,15,20-tetraphenyl-21H,23H-porphinato(2-)-N21,N23,N24)Chromium (Cr(TPP)Cl)

Tetraphenylporphyrin (2.5g) was dissolved in refluxing N,N'-

dimethylformamide (250ml). After complete solution had occurred chromous chloride (0.5g) was added. After a few minutes completion of reaction was checked using UV spectrophotometry. If the reaction was not complete another 0.25g of chromous chloride was added, the reaction allowed to proceed for another 10 minutes, and then rechecked for completion. This procedure was continued until completion of reaction. The reaction mixture was cooled and chilled, and distilled water (250ml) was added. The resultant precipitate was washed with water and dried in a vacuum oven for 1 hr at 100°C; yield of crude Cr(TPP)Cl, 1.5g.

#### Purification of Cr(TPP)Cl

Crude Cr(TPP)Cl (1.5g) was dissolved in chloroform (50ml) and applied to a dry alumina column (neutral Brockman Grade 1). Elution with chloroform gave a reddish band with the solvent front. This was followed by a light green band followed by a darker green band, (containing the Cr(TPP)Cl) After the Cr(TPP)Cl was eluted from the column (200ml) aqueous HCl (12M, 2ml) was added to the chloroform solution and left stirring overnight. The chloroform was removed and the solid was recrystallised from chloroform and dried in a vacuum desiccator to give Cr(TPP)Cl.

#### ANALYSIS

IR: 3053 (w), aromatic C-H stretch  
1641 (w), C=N stretch

1595 (m), C=C stretch

752 (s), 703 (s), monosubstituted benzene

UV:  $\lambda_{(max)}$  = 600nm, 560nm, 520nm, 448nm, 394nm

5.5 Table 5.1:      The oxidation and ionisation potentials  
for a number of silanes and stannanes

Allylic compounds	Oxidation potential/V	Ionisation potential/eV
$\text{CH}_2=\text{CHCH}_2\text{CMe}_3$		9.5 [1]
$\text{CH}_2=\text{CHCH}_2\text{SiMe}_3$	1.58 [2]	9.0 [1]
$\text{CH}_2=\text{C}(\text{Me})\text{CH}_2\text{SiMe}_3$	1.28 [2]	
$\text{Me}_2\text{C}=\text{CHCH}_2\text{SiMe}_3$	0.92 [2]	
$\text{CH}_2=\text{CHCH}_2\text{SnMe}_3$	1.06 [3]	
$\text{Me}_2\text{C}=\text{CHCH}_2\text{SnMe}_3$	0.68 [3]	
$\text{CH}_2=\text{CHCH}_2\text{SnBu}_3$		8.4 [4]
Benzylic compounds		
$\text{PhCH}_3$	1.98 [5]	
$\text{PhCH}_2\text{CMe}_3$		8.7 [1]
$\text{PhCH}_2\text{SiMe}_3$	1.38 [5]	8.4 [1]
4-Me-C <sub>6</sub> H <sub>4</sub> -Me	1.70 [5]	
4-Me-C <sub>6</sub> H <sub>4</sub> CH <sub>2</sub> SiMe <sub>3</sub>	1.17 [5]	
$\text{PhCH}_2\text{SnMe}_3$		8.1 [1]
$\text{PhCH}_2\text{SnBu}_3$	0.85 [6]	7.9 [1]

Table 5.1 continued overleaf

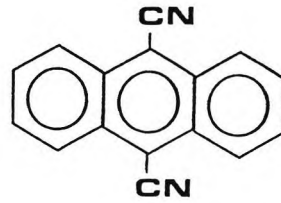
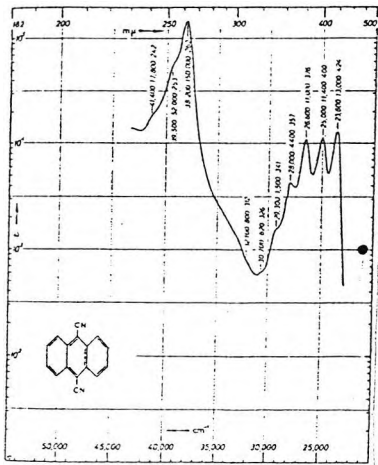
Table 5.1 continued

Naphthyllic compounds	Oxidation potential/V	Ionisation potential/eV
1-NpCH <sub>2</sub> SiMe <sub>3</sub>	0.96 [6]	7.8 [8]
2-NpCH <sub>2</sub> SiMe <sub>3</sub>	0.96 [6]	
2-NpCH <sub>2</sub> SnBu <sub>3</sub>	0.60 [6]	
Others		
Ph-CH=CHCH <sub>2</sub> SiMe <sub>3</sub>	0.91 [6]	
Me <sub>3</sub> Si-SiMe <sub>3</sub>	1.88 [7]	8.7 [7]

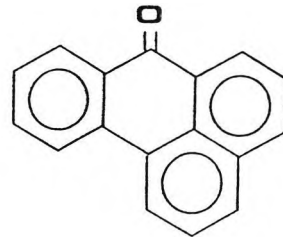
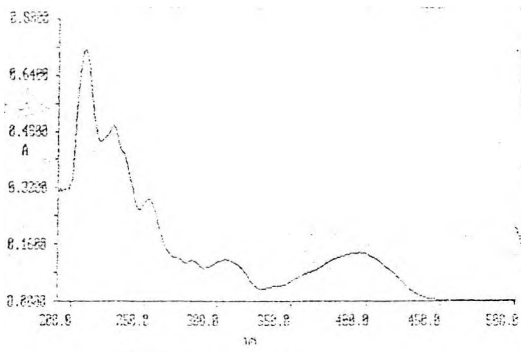
[1] = (Schweig et al, 1967), [2] = (Mizuno et al, 1985), [3] = (Takuwa et al, 1990), [4] = (Schweig et al, 1973), [5] = (Koizumi et al, 1989), [6] = (Mizuno et al, 1988), [7] = (Fukuzumi et al, 1990), [8] = (Pitt, 1973)

5.6

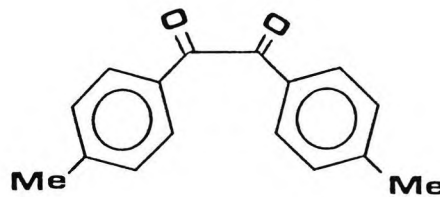
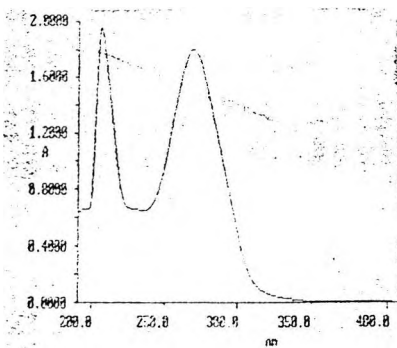
Figure 5.1 UV spectra



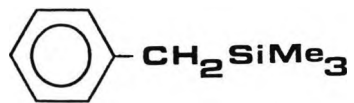
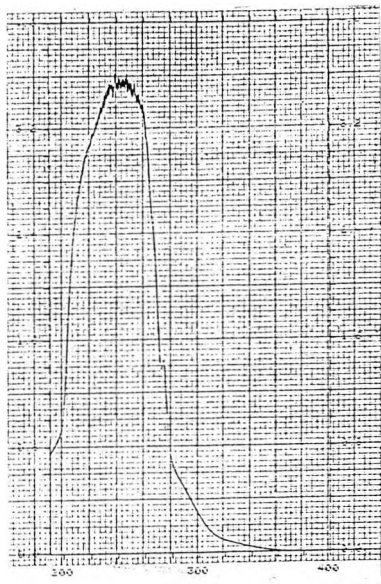
$$C = 1.1 \times 10^{-4} \text{ M}$$



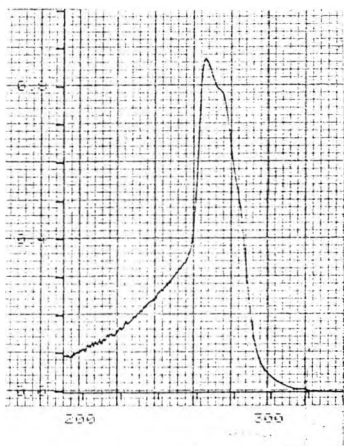
$$C = 7.2 \times 10^{-6} \text{ M}$$



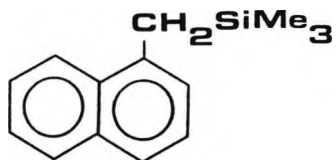
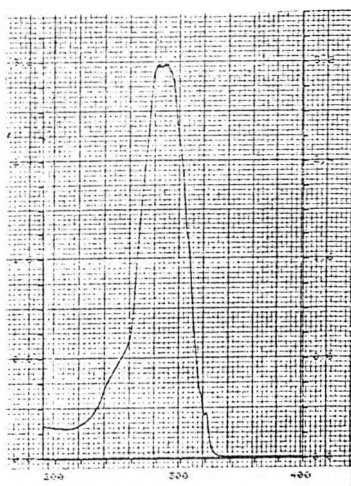
$$C = 6.2 \times 10^{-5} \text{ M}$$



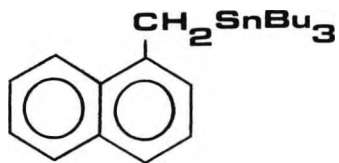
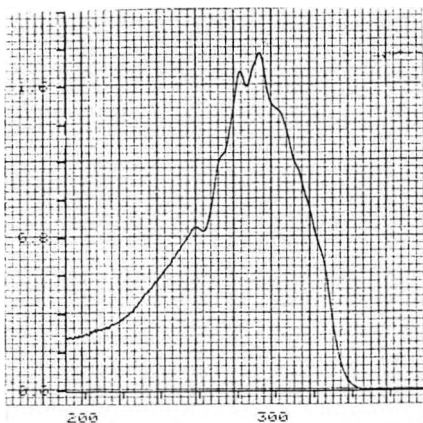
$$C = 1.9 \times 10^{-3} \text{ M}$$



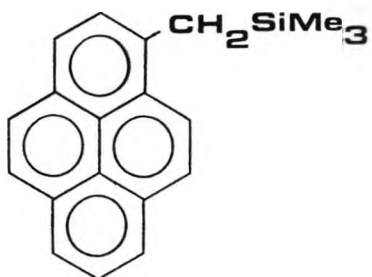
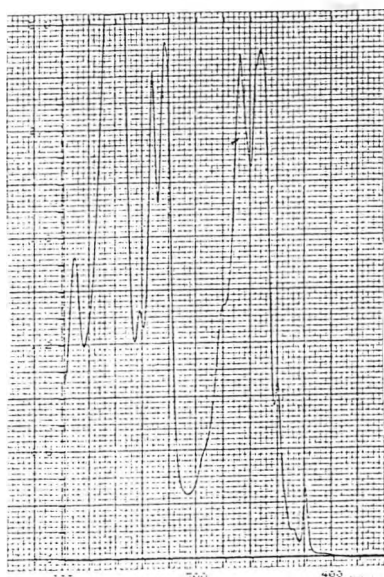
$$C = 1.0 \times 10^{-3} \text{ M}$$



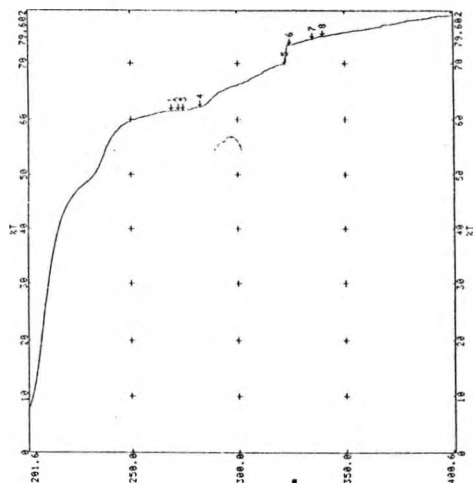
$$C = 5.3 \times 10^{-4} \text{ M}$$



$$C = 2.4 \times 10^{-4} \text{ M}$$



$$C = 1.6 \times 10^{-4} \text{ M}$$



polyethylene cover  
slip used in RTIR  
experiments

References

Adler, A.D., Longo, F.R., Kampas, F., and Kim, J., (1970).  
*J.Inorg.Nucl.Chem.*, 32, 2443

Dolphin, D, (ed.), (1982). "B12", Wiley, New York, Volume  
1

Fukuzumi, S., Kitano, T., and Mochida, K., (1990).  
*Chem.Lett.*, 1741

Golding, B.T., Kemp, T.J., Sellers, P.J., and Nocchi, E.,  
(1977). *J.Chem.Soc., Dalton Trans.*, 1266

Hendrickson, D.N., Kinnaird, M.G., and Suslick, K.S.J.,  
(1987). *J.Am.Chem.Soc.*, 109, 1243

Hirai, Y., Maruyama, H., Aida, T., and Inoue, S., (1988).  
*J.Am.Chem.Soc.*, 110, 7387

Hoffmann and Basolo, (1977). *J.Am.Chem.Soc.*, 99, 8195

Imamura, T., Jin, T., Suzuki, T., and Fujimoto, M., (1985).  
*Chem.Lett.*, 847

Koizumi, T., Fuchigami, T., and Nonaka, T., (1989).  
*Bull.Soc.Chem.Jpn.* 62, 219

Mizuno, K., Ikeda, M., and Otsuji, Y., (1985). *Tet.Lett.*  
26, 5819

Mizuno, K., Yasueda, M., and Otsuji, Y., (1988).  
*Chem.Lett.*, 229

Pitt, C.G., (1973). *J.Organomet.Chem.* 61, 49

Shrauzer, G.N., and Windgassen, R.J., (1966).  
*J.Amer.Chem.Soc.*, 88, 3738

Schweig, A., Weidner, U., and Manuel, G., (1967).  
*J.Organomet.Chem.* 67, C4

Schweig, A., Weidner, U., and Manuel, G., (1973).  
*J.Organomet.Chem.* 54, 145

Shrauzer, G.N., Sibert, J.W., and Windgassen, R.J., (1968).  
*J.Amer.Chem.Soc.*, 90, 6681

Takuwa, A., Nishigaichi, Y., and Yamashita, K., (1990).  
*Chem.Lett.*, 639